NOVEL STRATEGIES TARGETING OBESITY AND METABOLIC DISEASES

EDITED BY: Xinran Ma, Dechun Feng, Yan Lu, Nuo Sun, Jiqiu Wang and Lingyan Xu
PUBLISHED IN: Frontiers in Physiology

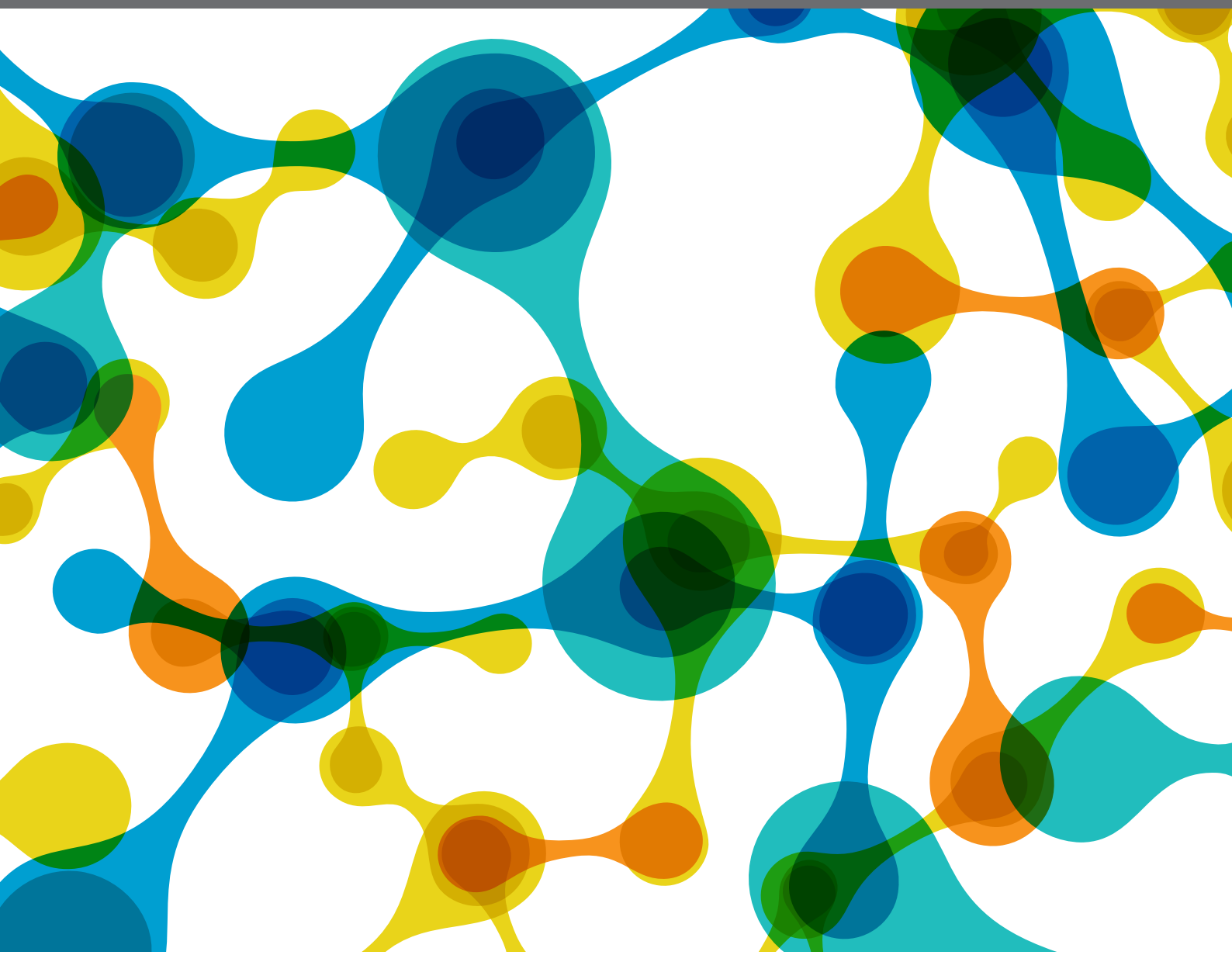

frontiers Research Topics

ISSN 1664-8714
ISBN 978-2-88963-041-7
DOI 10.3389/978-2-88963-041-7

About Frontiers

Frontiers is more than just an open-access publisher of scholarly articles: it is a pioneering approach to the world of academia, radically improving the way scholarly research is managed. The grand vision of Frontiers is a world where all people have an equal opportunity to seek, share and generate knowledge. Frontiers provides immediate and permanent online open access to all its publications, but this alone is not enough to realize our grand goals.

Frontiers Journal Series

The Frontiers Journal Series is a multi-tier and interdisciplinary set of open-access, online journals, promising a paradigm shift from the current review, selection and dissemination processes in academic publishing. All Frontiers journals are driven by researchers for researchers; therefore, they constitute a service to the scholarly community. At the same time, the Frontiers Journal Series operates on a revolutionary invention, the tiered publishing system, initially addressing specific communities of scholars, and gradually climbing up to broader public understanding, thus serving the interests of the lay society, too.

Dedication to Quality

Each Frontiers article is a landmark of the highest quality, thanks to genuinely collaborative interactions between authors and review editors, who include some of the world's best academicians. Research must be certified by peers before entering a stream of knowledge that may eventually reach the public - and shape society; therefore, Frontiers only applies the most rigorous and unbiased reviews.
Frontiers revolutionizes research publishing by freely delivering the most outstanding research, evaluated with no bias from both the academic and social point of view. By applying the most advanced information technologies, Frontiers is catapulting scholarly publishing into a new generation.

What are Frontiers Research Topics?

Frontiers Research Topics are very popular trademarks of the Frontiers Journals Series: they are collections of at least ten articles, all centered on a particular subject. With their unique mix of varied contributions from Original Research to Review Articles, Frontiers Research Topics unify the most influential researchers, the latest key findings and historical advances in a hot research area! Find out more on how to host your own Frontiers Research Topic or contribute to one as an author by contacting the Frontiers Editorial Office: researchtopics@frontiersin.org

NOVEL STRATEGIES TARGETING OBESITY AND METABOLIC DISEASES

Topic Editors:
Xinran Ma, East China Normal University, China
Dechun Feng, National Institutes of Health, United States
Yan Lu, Fudan University, China
Nuo Sun, The Ohio State University, United States
Jiqiu Wang, Shanghai Jiao Tong University School of Medicine, China
Lingyan Xu, East China Normal University, China

Citation: Ma, X., Feng, D., Lu, Y., Sun, N., Wang, J., Xu, L., eds. (2019). Novel Strategies Targeting Obesity and Metabolic Diseases. Lausanne: Frontiers Media.
doi: 10.3389/978-2-88963-041-7

Table of Contents

frontiers in Physiology

EDITORIAL
published: 29 May 2019
doi: 10.3389/fphys.2019.00668

Editorial: Novel Strategies Targeting Obesity and Metabolic Diseases

Xinran Ma[1], *Dechun Feng*[2], *Yan Lu*[3], *Nuo Sun*[4], *Jiqiu Wang*[5] *and Lingyan Xu*[1]*

[1] *Shanghai Key Laboratory of Regulatory Biology, Institute of Biomedical Sciences and School of Life Sciences, East China Normal University, Shanghai, China,* [2] *National Institute on Alcohol Abuse and Alcoholism, National Institutes of Health, Bethesda, MD, United States,* [3] *Department of Endocrinology and Metabolism, Zhongshan Hospital, Fudan University, Shanghai, China,* [4] *Wexner Medical Center, The Ohio State University, Columbus, OH, United States,* [5] *National Key Laboratory for Medical Genomes, Department of Endocrinology and Metabolism, China National Research Center for Metabolic Diseases, Ruijin Hospital, Shanghai Jiao Tong University School of Medicine, Shanghai, China*

Keywords: obesity, metabolic disease, pathophysiology, treatment, diagnosis

Editorial on the Research Topic

Novel Strategies Targeting Obesity and Metabolic Diseases

The obesity pandemic poses one of the most serious problems threatening public health with its staggering morbidity/mortality rate and its close link to multiple diseases including diabetes, cardiovascular disease, hypertension, non-alcoholic hepatic steatosis, and certain types of cancer. The imbalance of energy intake/expenditure and the genetic susceptibility of the individual both impact obesity development. With the prevalent sedentary life style in modern society, the obesity incidence soars yet efficient pharmacotherapeutic solutions targeting appetite or energy expenditure are limited and often with undesired side effects. Nowadays, it is urgent to seek better understandings of obesity to seek effective strategies that target obesity and related metabolic diseases. With the opportunity of the current Frontiers Research Topic, we focus on obesity and discuss analytic tools for obese phenotypes, potential therapeutic gene targets, as well as novel strategies against obesity and over-nutrition induced metabolic derangements, with the hope to provide a comprehensive summary of the latest metabolic studies.

Obesity features excessive lipid accumulation in adipose tissues. As the saying goes, "a handy tool makes a handyman," it makes good sense to start this research topic with handy tools accessing the obese phenotypes. Zhi et al. present a novel adipocyte counting system, AdipoCount, which provides automatic quantification of the number and diameter of adipocytes with higher accuracy and supports manual correction compared to existing tools. It serves as a necessary step to accurately access the obese phenotype in humans and animal models for further scientific studies.

Secondly, we discuss advances in our understanding in the development of obesity and potential therapeutic targets against it. Research article from Wang et al. reveals novel functions of GPR54, a family member of G protein-coupled receptors (GPCRs), in promoting adipocyte differentiation and triglyceride accumulation by regulating lipogenic genes including PPARγ via ERK1/2 phosphorylation. GPR54 deficient mice are resistant to central obesity, insulin resistance, and inflammation under high fat diet (HFD). Thus, it would be worthwhile to develop GPR54 inhibitors as potential treatment for obesity and metabolic diseases.

Unlike GPR54, a relatively novel player in the metabolic field, the functions of AMP-Activated Protein Kinase (AMPK) are extensively studied in many metabolic organs. However, how AMPK regulates energy metabolism in adipose tissues is not fully understood. Using Adipose tissue-specific AMPK α1/α2 KO (AKO) mice, Wu et al. demonstrate that AMPKα deficiency in adipocytes causes impairment in the browning capability in inguinal fat (iWAT, mainly consists of beige adipocytes).

Edited by:
Johannes Van Lieshout, University of Amsterdam, Netherlands

Reviewed by:
Markus Niessen, University of Zürich, Switzerland
Dick C. Chan, University of Western Australia, Australia

***Correspondence:**
Lingyan Xu
lyxu@bio.ecnu.edu.cn

Specialty section:
This article was submitted to Clinical and Translational Physiology, a section of the journal Frontiers in Physiology

Received: *04 September 2018*
Accepted: *10 May 2019*
Published: *29 May 2019*

Citation:
Ma X, Feng D, Lu Y, Sun N, Wang J and Xu L (2019) Editorial: Novel Strategies Targeting Obesity and Metabolic Diseases. Front. Physiol. 10:668. doi: 10.3389/fphys.2019.00668

AMPKα KO mice are cold intolerant and poised to obesity, whereas chronic AMPK activation by its allosteric activator A-769662 promotes iWAT browning and protects mice against diet-induced obesity and related metabolic dysfunction. It is well established that beige fat plays a vital role in promoting thermogenesis and energy expenditure, as well as in maintaining glucose and lipid homeostasis as metabolic sinks in both rodents and human. Thus, Wu et al's. report lends strong support to implicating AMPK agonists as potential therapeutics for obesity and metabolic diseases.

Meanwhile, in the review article from Kuang et al., spotlight is focused on another key regulator in obesity and metabolic diseases, Sirt6. As an important member of the Sirtuin family, Sirt6 impacts multiple physiological and pathological processes including aging, cancer, obesity, and energy metabolism. Sirt6 level and function decrease under aging and over nutrition, resulting in abnormal glucose and lipid metabolism. *In vivo* studies indicate that Sirt6 deficiency promotes diet-induced obesity, insulin resistance and liver steatosis, suggesting a protective role of Sirt6 activation of in obesity and diabetes.

Thirdly, in the everlasting quest for effective therapeutic leads targeting obesity and metabolic diseases, we discuss novel inspirations emerging from areas both new and old. Gut microbiota, a relatively new yet critical player in the battle against obesity, has been shown to actively contribute to the pathogenesis and intervention of obesity through their interaction with the host, a myriad of metabolites they produce, or their dynamic composition, all of which are in turn influenced by diet. In the systematic review from Zhang et al. the impacts of dietary substrates and host genotype/enterotype on microbiota composition and metabolites are discussed. These factors contribute to the maintenance of a health commensal homeostasis between gut microbiota and the host, which is vital for host metabolic fitness and obesity prevention. In addition, Madsen et al. focus on the impact of different dietary protein sources on gut microbiota. Different dietary protein sources vary in amino acid composition and other factors such as fatty acids and pollutions, which could modulate the composition of gut microbiota and thereby affect energy efficiency and obesity development. These studies emphasize the importance of gut microbiota on metabolic health, while at the same time offer dietary intervention as a promising strategy in combating obesity and metabolic diseases.

In the original study from Sun's lab, a daily supplement, branched-chain amino acid (BCAA), is highlighted. BCAA (including essential amino acids leucine, isoleucine, and valine) has been shown to be beneficial for metabolic fitness by regulating lipid and glucose homeostasis in liver and adipose tissues, as well as protein synthesis and degradation in skeleton muscle. In this regard, Liu et al. demonstrate that BCAA negatively targeting Krüppel-like factor 15, a master regulator of glucose, lipid, and amino acids metabolism, via PI3K-AKT signaling, which offer new mechanistic insights underlying BCAA's multiple functions in metabolic regulation.

On the other hand, two articles explore the possibility of finding effective therapeutic strategies from traditional Chinese medicine. Zhao et al. examine the effects of Er-Miao-Fang, a traditional Chinese Medical prescription, on HFD-induced adipose tissue dysfunction and find that its extracts reduce fatty acids and glycerol release from adipose tissue, thus block fatty acids and inflammatory molecules trafficking from adipose tissues to the liver, which in the end inhibits adipose tissue inflammation and ameliorates hepatic steatosis and insulin resistance under HFD. Likewise, Du et al. find that Astragaloside IV, the main active ingredient in the medicinal herb *Astragalus membranaceus*, suppresses adipocyte HSL activity through cAMP/Akt/PDE3B signaling, which results in reduced lipolysis and decreased circulating free fatty acid levels, thus limits hepatic lipid deposition and restrains excessive hepatic glucose production.

Last but not least, obesity and its associated metabolic derangements, i.e., chronic low-grade inflammation, insulin resistance, abnormal lipid profiles, often lead to a range of diseases and complications including diabetes, cardiovascular diseases, renal pathological changes etc., which are our next focus of discussion. For example, diabetic cardiomyopathy (DCM) is partially initiated by prolonged disturbances in energy substrates in diabetes. With ultra-high-performance liquid chromatography coupled to a quadruple time of flight mass spectrometer (UPLC/Q-TOF/MS) approach, Dong et al. reveal lipidomic biomarkers in the rat model of diabetic cardiomyopathy including 17 potential biomarkers of phosphatidylcholines, phosphatidylethanolamines, and sphingolipids. They also offer berberine administration as an effective treatment in the protection against cardiac diastolic and systolic dysfunctions partially via reversing the lipid profiles. With similar strategy, Li et al. evaluate lipid metabolites in endometriosis and indicate phosphatidylcholine (18:1/22:6), (20:1/14:1), (20:3/20:4), and phosphatidylserine (20:3/23:1) and increased phosphatidic acid (25:5/22:6) as early diagnostic biomarkers for endometriosis.

Prolonged diabetes may lead to the development of diabetic nephropathy (DN). Zhang et al. report the inhibition of (pro)renin receptor (PRR) contributes to renoprotection against DN by Angiotensin II type 1 receptor (AT1R) blockade. They thus highlight a potential therapeutics for renoprotection using combined blockade of AT1R with losartan, and PRR with a decoy peptide of prorenin.

Additionally, the study from Fan et al. links male subfertility with obesity-induced chronic inflammatory status in male genital tract, while Yang et al. show that immune status impacts insulin sensitivity in Hashimoto's Thyroiditis (HT) patients and HT mice. In HT mice, reinfusion of regulatory T cells (Tregs) from peripheral blood of normal mice improves insulin sensitivity and decreases inflammation. They also report increased resident Tregs and enhanced cytokine production in visceral adipose tissues (VAT) in HT mice, suggesting a critical role of VAT resident Tregs in HT associated insulin resistance.

In conclusion, the current research topic provides comprehensive and in depth understandings on various aspects of the researches on obesity, offering novel quantitative methods, diagnostic biomarkers, targeting molecules, and their action of mechanisms, as well as potential therapeutics toward obesity and metabolic diseases. Together, these studies would

facilitate future development of effective prevention, diagnosis, and personalized therapeutic strategies to combat obesity and other metabolic diseases.

AUTHOR CONTRIBUTIONS

XM and LX conceived and drafted the editorial. DF, YL, NS, and JW critically revised the work and approved its version to be submitted.

Conflict of Interest Statement: The authors declare that the research was conducted in the absence of any commercial or financial relationships that could be construed as a potential conflict of interest.

frontiers in Physiology

ORIGINAL RESEARCH
published: 14 August 2018
doi: 10.3389/fphys.2018.01041

Er-Miao-Fang Extracts Inhibits Adipose Lipolysis and Reduces Hepatic Gluconeogenesis via Suppression of Inflammation

Wenjun Zhao[1,2], Xin Feng[1], Baolin Liu[3], Jiechen Xian[4] and Ning Zhang[1]**

[1] Experiment Center for Science and Technology, Shanghai University of Traditional Chinese Medicine, Shanghai, China, [2] Shanghai Key Laboratory of Regulatory Biology, Institute of Biomedical Sciences and School of Life Sciences, East China Normal University, Shanghai, China, [3] Clinical Metabolomics Centre, China Pharmaceutical University, Nanjing, China, [4] Engineering Research Center of Modern Preparation Technology of Traditional Chinese Medicine, Shanghai University of Traditional Chinese Medicine, Shanghai, China

High-fat-diet (HFD) feeding induces adipose dysfunction. This study aims to explore whether the Traditional Chinese Medical prescription Er-Miao-Fang could ameliorate adipose dysfunction and prevent hepatic glucose output. Short-term HFD feeding induced adipose lipolysis accompanied with enhanced hepatic glucose output in mice. Adipose lipolysis is initiated by cyclic adenosine monophosphate (cAMP)/protein kinase A (PKA) signaling. Oral administration Er-Miao-Fang inhibited inflammation in adipose tissue by dephosphorylation of JNK and reducing TNF-α and IL-1β production, and thus preserved phosphodiesterase 3B (PDE3B) induction, contributing to preventing cAMP accumulation. As a result, from suppression of PKA activation, Er-Miao-Fang reduced fatty acids and glycerol release from adipose tissue due to the inhibition hormone-sensitive lipase (HSL). By blocking the traffic of fatty acids and inflammatory mediators from adipose tissue to the liver, Er-Miao-Fang attenuated hepatic cAMP/PKA signaling by protecting phosphodiesterase 4B (PDE4B) induction from inflammatory insult, and thereby reduced hepatic glucose production by suppression of hepatic glucagon response in HFD-fed mice. In conclusion, Er-Miao-Fang prevented adipose lipolysis by suppression of inflammation, contributing to reducing excessive hepatic glucose output. These findings present a new view of regulating gluconeogenesis and provide the guiding significance for the regulation of multi-link targets with Traditional Chinese Medicine.

Keywords: Er-Miao-Fang, inflammation, PDE3B, PDE4B, glucagon, gluconeogenesis

OPEN ACCESS

Edited by:
Yan Lu,
Fudan University, China

Reviewed by:
Jiejie Zhao,
Shanghai Jiao Tong University School of Medicine, China
Bin Liu,
Hubei Polytechnic University, China

****Correspondence:***
Jiechen Xian
xjc_1983@126.com
Ning Zhang
ningzh18@yeah.net

Specialty section:
This article was submitted to Clinical and Translational Physiology, a section of the journal Frontiers in Physiology

Received: *06 November 2017*
Accepted: *12 July 2018*
Published: *14 August 2018*

Citation:
Zhao W, Feng X, Liu B, Xian J and Zhang N (2018) Er-Miao-Fang Extracts Inhibits Adipose Lipolysis and Reduces Hepatic Gluconeogenesis via Suppression of Inflammation. Front. Physiol. 9:1041. doi: 10.3389/fphys.2018.01041

INTRODUCTION

Adipose tissue functions as a site of fat storage, while adipose dysfunction in obesity and diabetes induces lipolysis and increases circulating free fatty acids to promote ectopic fat deposits. It is generally accepted that lipid accumulation in the liver and muscle is the main cause for insulin resistance (Lafontan and Girard, 2008; Kowalski et al., 2015; Zhao et al., 2016). The action of insulin

Abbreviations: cAMP, cyclic adenosine monophosphate; CREB, cAMP-response element binding protein; G6pase, glucose-6-phosphatase; HSL, hormone-sensitive lipase; PA, palmitic acid; PDE3B, phosphodiesterase 3B; PDE4B, phosphodiesterase 4B; PEPCK, phosphoenolpyruvate carboxykinase; PGC-1α, PPARγ coactivator 1α.

in liver is to suppress hepatic glucose production and lipolysis-induced lipid accumulation in the liver is shown to attenuate insulin sensitivity and increase hepatic glucose production, responsible for hyperglycemia during fasting in diabetes (Perry et al., 2014). These events suggest the functional interaction between adipose lipolysis and abnormal hepatic gluconeogenesis.

Several hormones and effectors can induce lipolysis in adipose tissue though the activation of cAMP-dependent protein kinase A (PKA), in which hormone-sensitive lipase (HSL), a key enzyme in the mobilization of fatty acids from stored triacylglyceride (TG), is activated (Greenberg et al., 2001; Greenberg et al., 2011; Schweiger et al., 2014). Insulin regulates post-prandial glucose levels by promoting glucose disposal, while maintains glucose homeostasis during fasting conditions by promoting hepatic glucose output. Several lines of evidence demonstrate that enhanced hepatic glucagon response is responsible for hyperglycemia during fasting (Unger and Cherrington, 2012). In liver, hepatic gluconeogenesis responded to glucagon is also initiated by cAMP/PKA signaling, transcriptionally regulating gene encoding to gluconeogenesis enzymes, including G6Pase and PEPCK (Leahy et al., 1999; Streeper et al., 2001; Yang and Yang, 2016). Blocking cAMP/PKA signaling suppresses HSL activation to inhibit lipolysis (Zhao et al., 2016). Hepatic glucagon response is restrained by blocking cAMP/PKA signaling and inhibiting transcriptional regulation of G6Pase and PEPCK (He et al., 2009). All these well elucidate that cAMP/PKA signaling plays a vital role in regulation of lipid and glucose metabolism.

As a second messenger, cAMP is synthesized by adenylate cyclase (AC) while phosphodiesterases (PDEs) could prevent cAMP accumulation through degradation. PDEs are invariably diverse, for instance, PDE3 and PDE4 provide the major portion of cAMP hydrolyzing activity in most cells (Francis et al., 2011). PDE3B is proposed to be the predominant isoform of PDEs in adipose tissue. Inflammation is demonstrated to regulate PDE3B induction. TNF-α inhibited PDE3B activity with suppression of PDE3B induction and thus increases lipolysis, indicative of the involvement of inflammation in lipolysis (Mei et al., 2002). In the liver, the members of the PDE3 and PDE4 subfamilies are both expressed. While PDE4B is the predominant regulator for hepatic cAMP degradation (Miller et al., 2013). Similarly, it is documented that inhibiting cAMP accumulation by preserving PDE4B activity contributes to suppress hepatic glucagon response (Xiao et al., 2017). So, decreased PDEs expression is associated with the dysfunction in adipose and liver, and these events emphasize the possible relevance of inflammation in the regulation of fatty acid and hepatic glucagon response.

Er-Miao-Fang is a famous Traditional Chinese Medical prescription first recorded in Dan Xi Xin Fa in 1481. It is composed of two medicinal herbs: *Phellodendron chinense* Schneid and *Atractylodes lancea* (Thunb.) DC or *Atractylodes chinensis* (DC.) Koidz and it has been widely used to treat arthritis, urinary tract infections, and diarrhea for decades. Studies about the pharmacological mechanism of this ancient prescription are performed mainly focused on its anti-inflammatory activity (Chen et al., 2014; Bae et al., 2015). The alkaloids are the main components in the Er-Miao-Fang extracts with abundant berberine (4.019%) and phellodendrine (0.371%), the main effective ingredients (Feng et al., 2017). Berberine was documented to reduce lipid droplet accumulation and improve insulin sensitivity (Lee et al., 2006). Treatment of berberine reduces the levels of fasting blood glucose and inhibits the expression of G6Pase and PEPCK (Wei et al., 2016). Phellodendrine ameliorated oxidative stress by downregulating NF-κB phosphorylation (Li et al., 2016). These studies suggest the potential role of Er-Miao-Fang extracts in the metabolism disorder. Hence, in this study, we explored the possible pharmacological action of Er-Miao-Fang extracts in regulation of lipolysis and hepatic gluconeogenesis by inhibiting adipose inflammation.

MATERIALS AND METHODS

Preparation of Er-Miao-Fang

Phellodendron chinense Schneid and *A. lancea* (Thunb.) DC. were purchased from Shanghai Kangqiao Chinese Medicine Yinpian Co., Ltd. (Shanghai, China) and authenticated by Yan Ke (Experiment Center for Teaching and Learning, Shanghai University of Traditional Chinese Medicine). Qualities of the crude drugs meet the standards of "Pharmacopoeia of the People's Republic of China" (2015 edition). *P. chinense* Schneid with the same weight of *A. lancea* (Thunb.) DC. was boiled three times with 10 times the volume (*v/w*) of 70% ethanol for 2 h each time after soaking 30 min. The extracts were filtered, concentrated and decompression vacuum drying fewer than 65°C was adopted. Er-Miao-Fang extracts were prepared and the yield was 24.7%. The chemical components of Er-Miao-Fang extracts were analyzed by UPLC-MS/MS, and the followings are the chief six components and contents tested in the extracts: berberine, 4.019%; phellodendrine, 0.371%; chlorogenic acid, 0.158%; ferulic acid, 0.141%; magnoflorine, 0.107 %; and palmatine, 0.039% (Feng et al., 2017).

Reagents

Metformin (purity ≥ 99%) was purchased from Sangon Biotech (Shanghai, China) and dissolved in 0.3% (*w/v*) sodium carboxymethylcellulose (CMC-Na) for animal administration or in dimethyl sulfoxide (DMSO) for cell experiment [the final concentration of DMSO was 0.1% (*v/v*)]. Glucagon (purity ≥ 98%) was obtained from Kinase Chemicals Ltd. (Suffolk, United Kingdom). Sodium pyruvate (purity ≥ 99%) was provided by Sigma-Aldrich (Shanghai, China). Palmitate (PA, Sinopharm, Shanghai, China) was dissolved in ethanol to prepare 200 mM stock solution, and then diluted with medium containing 10% non-esterified fatty acid (NEFA)-free bovine serum albumin (BSA) before use (*v/v*, 1:19). Mouse cAMP, AMP, TNF-α, and IL-1β ELISA kits were provided by Shuojia Biotechnology Co., Ltd. (Shanghai, China). The following items were purchased from the cited commercial sources: anti-phospho-(Ser/Thr) PKA substrate (9621), anti-phospho-HSL (Ser660) (4126), anti-HSL (4107), anti-phospho-SAPK/JNK (Thr183/Tyr185) (4668), anti-SAPK/JNK (9252), anti-β-actin (4970), Cell Signaling Technology (Beverly, MA, United States);

anti-TNF-α (ab6671), anti-CREB (phospho S133) (ab32096), anti-CREB (ab32515), goat anti-rabbit IgG H&L (Alexa Fluor®488) (ab150077), Abcam (Cambridge, MA, United States); PDE3B (H-300) (sc-20793), PDE4B (H-56) (sc-25812), Santa Cruz Biotechnology (Dallas, TX, United States); peroxidase-conjugated affinipure goat anti-Rabbit IgG (H&L) (111-035-003), Jackson ImmunoResearch Laboratories Inc. (West Grove, PA, United States); mouse IL-1β (AF-401-NA), R&D System (Minneapolis, MN, United States); RNAiso Plus (9108), RT Reagent Kit (RR037A), SYBR® Premix Ex Taq (RR420A), Takara Bio Inc. (Dalian, China).

Animals

Male ICR mice (6 weeks) were purchased from Sino-British Sippr/BK Lab. Animal Ltd. (Shanghai, China, production license: SCXK (Shanghai) 2013-0016). Mice were housed with 12 h light/dark cycles under a constant temperature (22 ± 2°C) and free access to water and food. This study was carried out in accordance with the recommendations of Provision and General Recommendation of Chinese Experimental Animals Administration Legislation. The protocol was approved by Animal Ethics Committee of Shanghai University of Traditional Chinese Medicine.

Mice were fed a regular chow diet or high-fat-diet (HFD) (10% yolk, 10% Lard, 0.2% cholate, 1% cholesterol and 78.8% standard diet, 36.45% Kcal fat) for 10 days (Wang et al., 2016; Zhao et al., 2016) with oral administration of saline, Er-Miao-Fang extracts (1 g/kg) or metformin (200 mg/kg), respectively every day. Blood was collected after 8 h fasting and blood glucose was assayed with commercial kits (Jiancheng, Nanjing, China). Levels of insulin and glucagon in blood were tested using ELISA kits (Shuojia, Shanghai, China). Mice were sacrificed after fasting for 8 h and the epididymis adipose tissue and liver tissue were isolated or cultured for assay. Epididymal adipose tissue or liver tissue was grinded in RIPA lysis buffer (Beyotime, Haimen, China). The lysates were centrifuged for collection of supernatants. The contents of cAMP, AMP, TNF-α, and IL-1β in the supernatant were measured by commercial ELISA Kits. The results were normalized by the amount of protein.

Preparation of Conditioned Medium (CM) of Adipose Tissue From HFD-fed Mice

Epididymis adipose tissue was collected from chow-fed or HFD-fed mice and cut into small pieces, then incubated with the same weight in 2 mL DMEM (25 mM glucose, Gibco, Grand Island, NY, United States) containing 10% FBS, 100 U/mL penicillin and 100 μg/mL streptomycin) for 24 h at 37°C in a 5% CO_2 incubator (Wang et al., 2016; Zhao et al., 2016). Collected the DMEM, centrifuged at 3,000 *g* for 5 min at 4°C and the supernatant was harvested as conditioned medium (CM). For the preparation of glucose-free CM, the chow-fed or HFD-fed mice adipose tissue was incubated in Krebs-Ringer phosphate-HEPES buffer (KRH buffer, containing 118 mM NaCl, 5 mM KCl, 1.3 mM $CaCl_2$, 1.2 mM $MgSO_4$, 1.2 mM KH_2PO_4, and 30 mM HEPES, containing 0.5% BSA, pH 7.4). The CM was used to culture hepatocytes to explore the crosstalk between adipose and liver. The levels of free fatty acids and glycerol in CM were detected with commercial kits following the manufacturer's instructions (Jiancheng, Nanjing, China).

Isolated Adipose Tissue Treatment

To study the pathway whereby Er-Miao-Fang inhibits lipolysis *in vitro*, epididymis adipose tissue was collected from sacrificed normal male mice, cut into small pieces, and then incubated in DMEM. Isolated adipose tissue was treated with Er-Miao-Fang (100 μg/mL), TNF-α antibody (1 μg/mL), or IL-1β antibody (0.6 μg/mL) for 30 min before challenged with PA (100 μM) for 24 h. The adipose tissue was homogenized in PBS and cAMP contents in the suspension were measured by ELISA kits. The PDE3B in the isolated adipose tissue was extracted with RIPA lysis buffer (Beyotime, Haimen, China). The lysates were centrifuged and the expression of PDE3B in the supernatant was determined by Western blot.

Glucose and Pyruvate Tolerance Tests

Oral glucose tolerance testing (GTT) was performed in mice using glucose (2 g/kg) after overnight fasting. For pyruvate tolerance test (PTT), mice were injected intraperitoneally with pyruvate (2 g/kg) after fasting for 16 h. Blood was collected at regular intervals for the assay of glucose contents and calculated blood glucose area under the curve (AUC-G) with the methods mentioned before (Zhao et al., 2014).

Hepatocytes Culture and Measurement of Cellular cAMP

BNL CL.2 hepatocytes (Cell storeroom of Chinese Academy of Sciences, Shanghai, China) were cultured in DMEM and maintained at 37°C in a 5% CO_2 incubator. The cells were treated with adipose-derived CM or TNF-α antibody (1 μg/mL) and IL-1β antibody (0.6 μg/mL) in the presence or absent of glucagon (100 nM) for 24 h. After treatment, cells were collected and extracted with RIPA lysis buffer. The lysates were centrifuged and the contents of cAMP in the supernatant were measured by commercial ELISA Kits.

Hepatocytes Glucose Output

BNL CL.2 hepatocytes were cultured with glucose-free adipose-derived CM or TNF-α antibody (1 μg/mL) and IL-1β antibody (0.6 μg/mL) for 24 h. After washing, the cells were incubated in KRH buffer supplemented with 20 mM pyruvate, with or without 100 nM glucagon for 6 h. The supernatant was collected for glucose analysis with commercial kits.

Quantitative Real Time RT-PCR

Total mRNA was extracted from tissue or cells using RNAiso plus following the manufacture's protocol and cDNA synthesis were preformed using RT reagent kit. Relative cDNA levels were determined using the SYBR Premix Ex Taq and amplified with ABI 7500 system. Target mRNA was normalized by ribosomal 18s RNA, an endogenous control. PCR primers were used as follows: mouse *PGC-1α* (134 bp), Forward Primer: 5′-TATGGA GTGACATAGAGTGTGCT-3′, Reverse Primer: 5′-CCACTTC

AATCCACCCAGAAAG-3′; mouse *Pepck* (159 bp), Forward Primer: 5′-CTGCATAACGGTCTGGACTTC-3′, Reverse Primer: 5′-CAGCAACTGCCCGTACTCC-3′; mouse G6pase (*G6pc*, 173 bp), Forward Primer: 5′-CGACTCGCTATCTCCAA GTGA-3′, Reverse Primer: 5′-GTTGAACCAGTCTCCGACC A-3′; mouse 18s RNA (151 bp), Forward Primer: 5′-GTAACCC GTTGAACCCCATT-3′, Reverse Primer: 5′-CCATCCAATCG GTAGTAGCG-3′. Relative quantification was calculated based on the following equation: relative quantification = $2\xi^{-\Delta\Delta C_t}$. Ct is the threshold cycle to detect fluorescence.

Western Blot Analysis

Tissue or cells were homogenized in RIPA lysis buffer with PMSF (RIPA: PMSF = 100:1, v/v). The lysates were centrifuged for collection of supernatants. Bicinchoninic acid (BCA) Protein Assay Kit (Beyotime, Haimen, China) was used to test the supernatant proteins contents. The protein samples were separated by 10% SDS–PAGE, transferred to PVDF membranes (Millipore Co., Ltd. MA, United States), blocked with 5% BSA/TBST buffer (5 mM Tris-base, pH 7.6, 136 mM NaCl, 0.05% Tween-20), immunoblotted with primary and secondary antibody. ECL Western Blotting Detection System and Image-Pro Plus 6.0 software (IPP 6.0, IPWIN Applicaton, Inc., Rrockville, MD, United States) was applied to analysis antibody-antigen complexes. The original images are provided as **Supplementary Image 1**.

Statistical Analysis

All the results were expressed as mean ± SD and were subjected to one-way ANOWA analysis of variance followed by Student-Newman-Keuls multiple comparison test if significant (IBM SPSS Statistics 21.0, SPSS Inc., Chicago, IL, United States). $p < 0.05$ was considered statistically significant.

RESULTS

Er-Miao-Fang Attenuated Lipolysis in Adipose Tissue

Short-term HFD feeding induced lipolysis from adipose tissue in mice, demonstrated by increased free fatty acids and glycerol released from isolated epididymal adipose

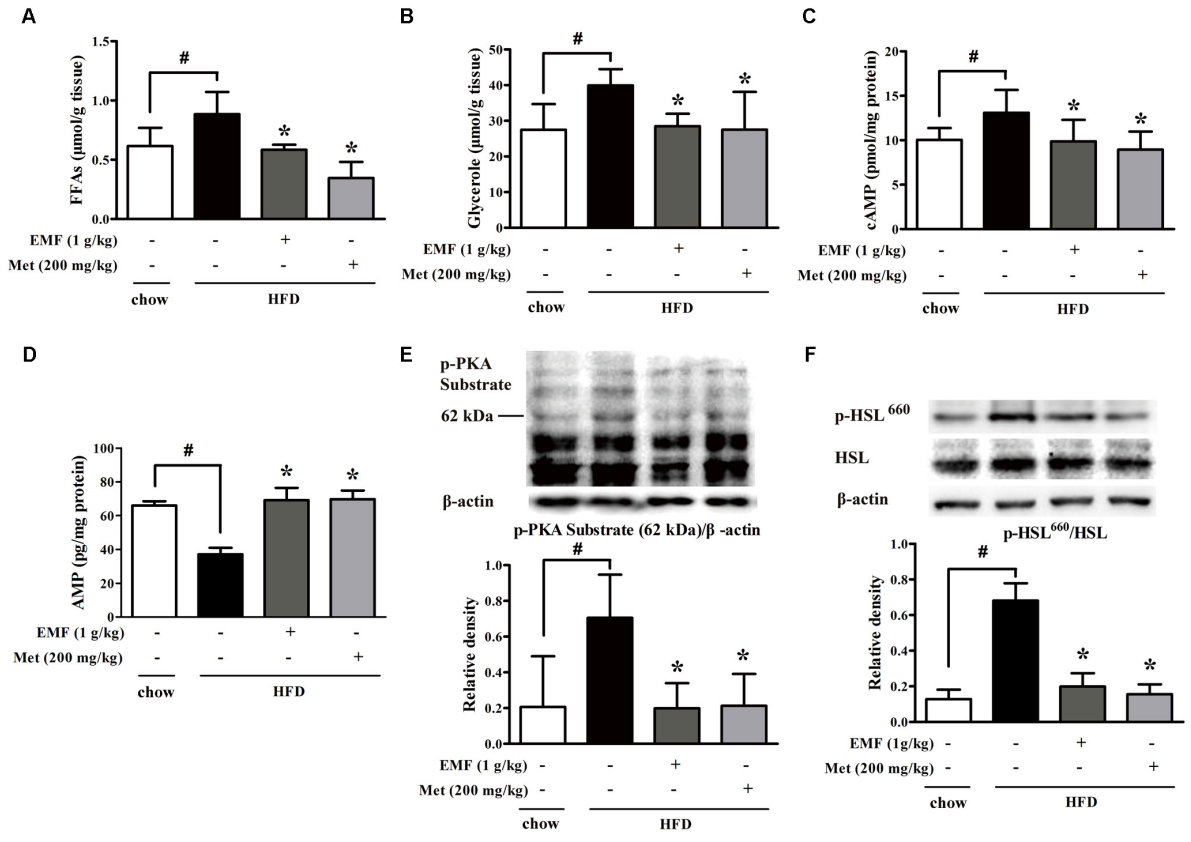

FIGURE 1 | Er-Miao-Fang attenuated lipolysis in adipose tissue. Mice were fed with chow diet or HFD for 10 days with oral administration of Er-Miao-Fang extracts (EMF, 1 g/kg) or metformin (Met, 200 mg/kg). **(A,B)** Adipose tissue from chow diet fed or HFD fed mice were incubated in DMEM for 24 h. The fat-derived CM in DMEM was collected and detected the contents of free fatty acids (FFAs) and glycerol released from adipose tissue. The results were expressed as the mean ± SD (n = 5∼6). **(C,D)** cAMP and AMP in epididymal adipose tissue were determined by ELISA kits (mean ± SD, n = 5∼6). **(E)** Phosphorylation of PKA substrate and **(F)** Ser-660 motif of HSL in epididymal adipose tissue were detected by Western blot. The results were showed as the mean ± SD from four independent experiments. *$p < 0.05$ vs. HFD feeding only treatment, #$p < 0.05$ vs. the indicated treatment.

tissue, whereas the increased lipolysis was inhibited by oral administration of Er-Miao-Fang extracts during HFD feeding (**Figures 1A,B**). Because adipose lipolysis is mediated by cAMP/PKA signaling, we examined the effects of Er-Miao-Fang in adipose tissue, and found that HFD feeding increased cAMP accumulation with reducing AMP contents in adipose tissue, whereas the changes were reversed by oral administration of Er-Miao-Fang (**Figures 1C,D**). HFD feeding induced PKA activation, but Er-Miao-Fang treatment inactivated PKA by dephosphorylation of PKA 62KDa substrate (**Figure 1E**). These results suggested that Er-Miao-Fang prevented PKA activation by downregulation of cAMP. The phosphorylation of PKA substrate at 62 KDa corresponds to the molecular weight of perilipin. As the major substrate for phosphorylation of PKA, perilipin facilitates lipolysis by HSL hydrolyzing triacylglycerol and diacylglycerol to induce fatty acid release (Miyoshi et al., 2006; Brasaemle, 2007; Gauthier et al., 2008). We found that oral administration of Er-Miao-Fang suppressed HSL activation by dephosphorylation (**Figure 1F**). These results suggested that Er-Miao-Fang prevented adipose lipolysis by blocking cAMP/PKA signaling. Anti-diabetic agent metformin also effectively reduced lipolysis from adipose tissue in HFD-fed mice.

Er-Miao-Fang Inhibited Inflammation in Adipose Tissue

Adipose dysfunction is associated with inflammation. HFD feeding evoked inflammatory response, whereas Er-Miao-Fang and metformin inhibited inflammation in adipose tissue by attenuating JNK phosphorylation and reducing TNF-α and IL-1β production (**Figures 2A–C**). The protein expression of PDE3B was decreased in adipose tissue of HFD-fed mice. Nevertheless, administration of Er-Miao-Fang and metformin preserved PDE3B induction (**Figure 2D**). To investigate the impact of inflammation on lipolysis, we isolated adipose tissue from normal mice and treated with saturated fatty acid palmitate (PA). PA stimulation inhibited PDE3B expression and increased

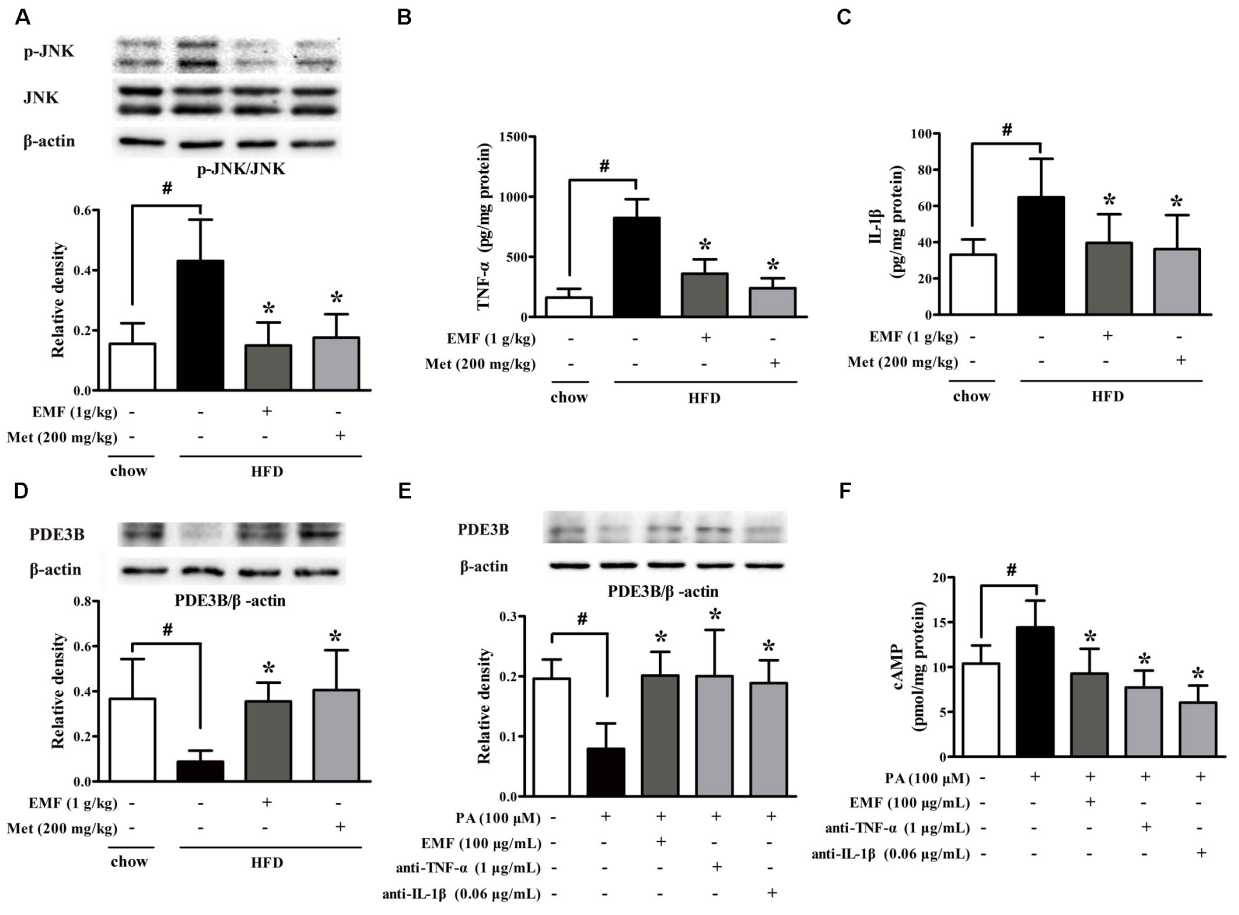

FIGURE 2 | Er-Miao-Fang inhibited inflammation in adipose tissue. Mice were fed with chow diet or HFD for 10 days with oral administration of Er-Miao-Fang extracts (EMF, 1 g/kg) or metformin (Met, 200 mg/kg). **(A)** JNK protein expression was assessed by Western blot ($n = 4$). **(B,C)** TNF-α ($n = 6$) and IL-1β ($n = 8$∼10) were measured by ELISA kits. **(D)** PDE3B protein expression was determined by Western blot ($n = 4$). **(E,F)** Isolated adipose tissue from normal mice were cultured in DMEM and treated with Er-Miao-Fang (EMF, 100 μg/mL), TNF-α antibody (1 μg/mL), or IL-1β antibody (0.6 μg/mL) for 30 min before challenged with PA (100 μM) for 24 h. PDE3B expression and cAMP contents in isolated adipose tissue were determined by Western blot ($n = 4$) or ELISA ($n = 5$∼6), respectively. The results were expressed as the mean ± SD. *$p < 0.05$ vs. HFD feeding or PA challenge only treatment, #$p < 0.05$ vs. the indicated treatment.

cAMP accumulation, but these alternations were reversed by Er-Miao-Fang treatment at concentration of 100 μg/ml (**Figures 2E,F**). Neutralizing pro-inflammatory cytokines TNF-α and IL-1β with special antibodies preserved PDE3B protein expression and decreased cAMP accumulation in adipose tissue (**Figures 2E,F**).

Er-Miao-Fang Improved Pyruvate Tolerance in HFD-fed Mice

High-fat-diet feeding increased fasting blood glucose with glucose intolerance in mice. Oral administration of Er-Miao-Fang and metformin reduced fasting blood glucose with improved glucose tolerance in HFD-fed mice (**Figures 3A,B**). Meanwhile, we observed that Er-Miao-Fang decreased the levels of blood glucagon without affecting insulin contents in the blood (**Figures 3C,D**). Pyruvate tolerance test is an indicator of endogenous glucose production since pyruvate load provides the substrate for hepatic glucose production through gluconeogenesis. The changes in glucose levels after a challenge with pyruvate revealed higher glucose levels in HFD-fed mice when compared with chow-fed mice, indicative of impaired pyruvate tolerance (**Figure 3E**). Oral administration of Er-Miao-Fang and metformin reversed pyruvate intolerance in HFD-fed mice (**Figure 3E**). Consistent with inhibitory effect on adipose lipolysis, Er-Miao-Fang downregulated the elevated levels of blood free fatty acids and glycerol without affecting other biochemical parameters in the blood (**Supplementary Figure 1**). These results suggested the inhibitory effect on endogenous glucose production.

Er-Miao-Fang Blocked Hepatic cAMP and PKA Induction

Next, we examined hepatic gluconeogenesis in HFD-fed mice, and found that HFD feeding attenuated PDE4B protein expression with cAMP accumulation in the liver (**Figures 4A,B**). Er-Miao-Fang and metformin preserved PDE4B protein

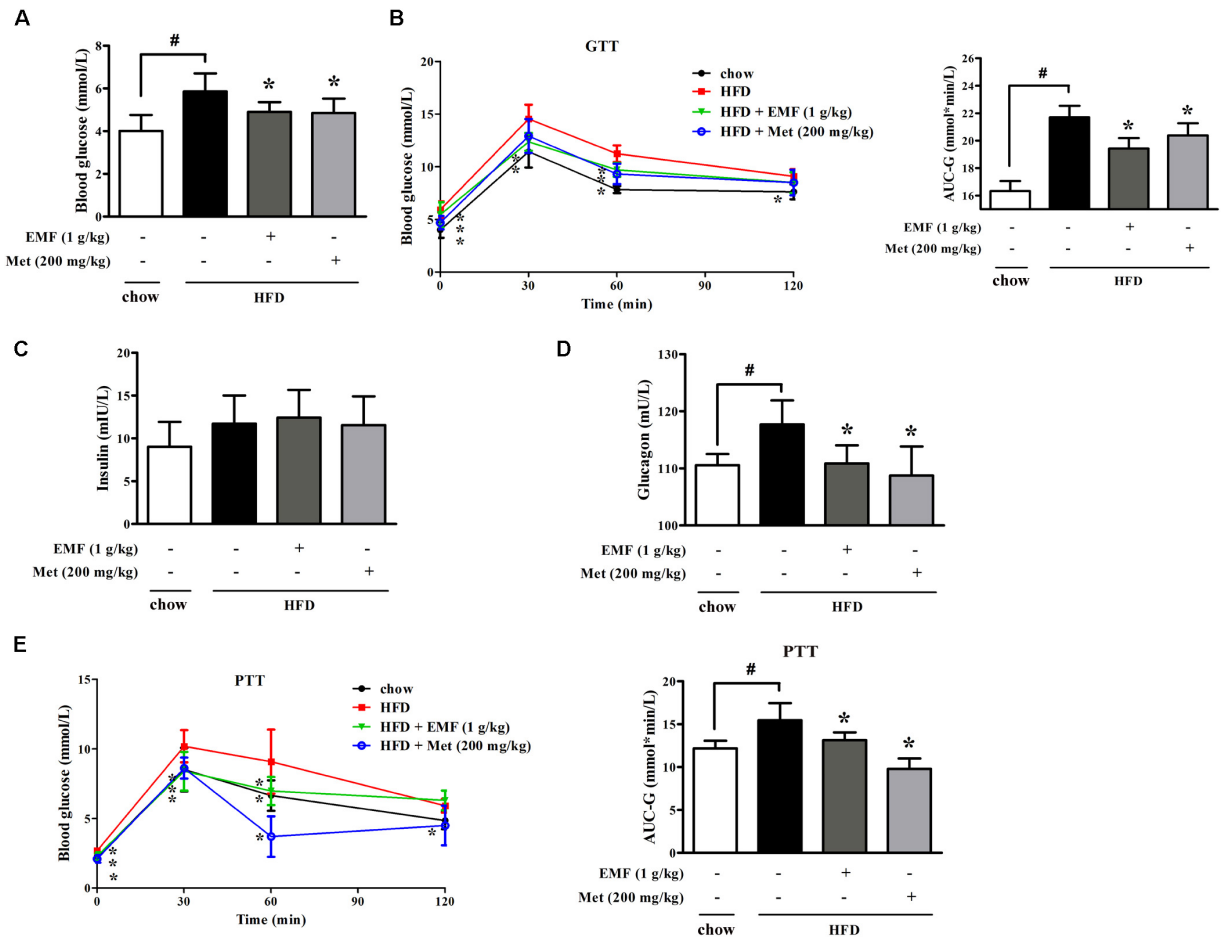

FIGURE 3 | Oral administration of Er-Miao-Fang inhibited endogenous glucose production in HFD-fed mice. Mice were fed with chow diet or HFD for 10 days with oral administration of Er-Miao-Fang extracts (EMF, 1 g/kg) or metformin (Met, 200 mg/kg). **(A)** Fasting blood glucose levels were determined by biochemical kits. **(B)** Blood glucose levels and AUC during the oral glucose tolerance test **(C,D)** Blood insulin and glucagon contents were detected by ELISA. **(E)** Blood glucose levels and AUC during the pyruvate tolerance test. Data were expressed as the mean ± SD (n = 10). *$p < 0.05$ vs. HFD feeding only treatment, #$p < 0.05$ vs. the indicated treatment. GTT, glucose tolerance test; PTT, pyruvate tolerance test.

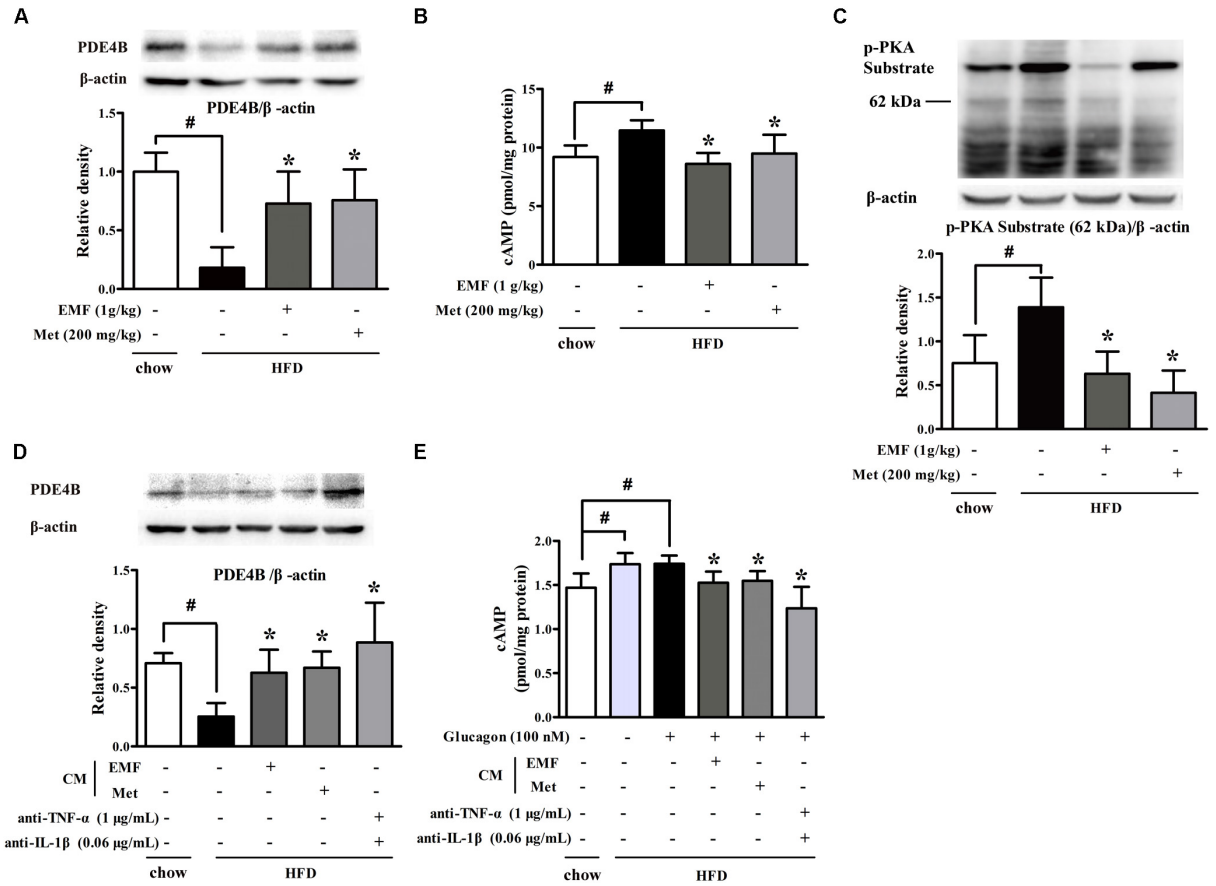

FIGURE 4 | Er-Miao-Fang blocked hepatic cAMP and PKA induction. Mice were fed with chow diet or HFD for 10 days with oral administration of Er-Miao-Fang extracts (EMF, 1 g/kg) or metformin (Met, 200 mg/kg). BNL CL.2 hepatocytes were cultured in fat-derived CM from chow or HFD feeding mice or TNF-α antibody (1 μg/mL) and IL-1β antibody (0.6 μg/mL) treated with or without glucagon (100 nM) for 24 h. **(A)** PDE4B expression in liver tissue were detected by Western blot. The results were showed as the mean ± SD from four independent experiments. **(B)** cAMP in liver tissue were determined by ELISA kits (mean ± SD, $n = 9$∼10). **(C)** Phosphorylation of PKA substrate in liver tissue was detected by Western blot. The results were showed as the mean ± SD from four independent experiments. **(D)** PDE4B expression in hepatocytes were determined by Western blot ($n = 3$) and **(E)** cAMP contents in the present of glucagon (100 nM) were measured by ELISA kits ($n = 6$). The results were expressed as the mean ± SD. $^{*}p < 0.05$ vs. HFD feeding or HFD-CM or HFD-CM with glucagon treatment, $^{\#}p < 0.05$ vs. the indicated treatment. CM, conditioned medium.

expression and then effectively reduced cAMP accumulation by preserving PDE4B induction, resultantly inhibiting PKA activity (**Figures 4A–C**). In view of the contribution of adipose dysfunction to hepatic gluconeogenesis (Perry et al., 2014), we prepared CM by incubation of adipose tissue of chow or HFD feeding mice and then incubated with hepatocytes. BNLCL.2 hepatocytes treated with HFD feeding mice-derived CM decreased PDE4B expression and increased glucagon-mediated cAMP accumulation in hepatocytes, but these effects were attenuated by co-treatment with TNF-α and IL-1β antibodies, suggesting that adipose dysfunction-derived inflammatory mediators impaired hepatic PDE4B to prevent cAMP degradation (**Figures 4D,E**). As expected, Er-Miao-Fang or metformin-derived CM effectively restored PDE4B protein expression and thus reduced cAMP accumulation in response to glucagon (**Figures 4D,E**). These results provided evidence that hepatic PDE4B induction was also impaired by inflammation partly and amelioration of adipose dysfunction might have the potential contribution to attenuate hepatic glucagon signaling.

Er-Miao-Fang Restrained Hepatic Glucagon Response

In response to cAMP/PKA signaling, the transcription factor cAMP-response element binding protein (CREB) is activated indicated by increased phosphorylation. Consistently, we observed CREB activation in liver of HFD-fed mice; however, oral administration of Er-Miao-Fang and metformin inhibited CREB activation by dephosphorylation (**Figure 5A**). To confirm the involvement of inflammation in CREB activation and downstream gene regulation, we co-incubated hepatocytes with adipose-derived CM. Glucagon promoted phosphorylated CREB translocation into the nucleus and this action was enhanced by co-treatment with CM derived from HFD-fed mice, but the increased phosphorylated CREB in the nucleus

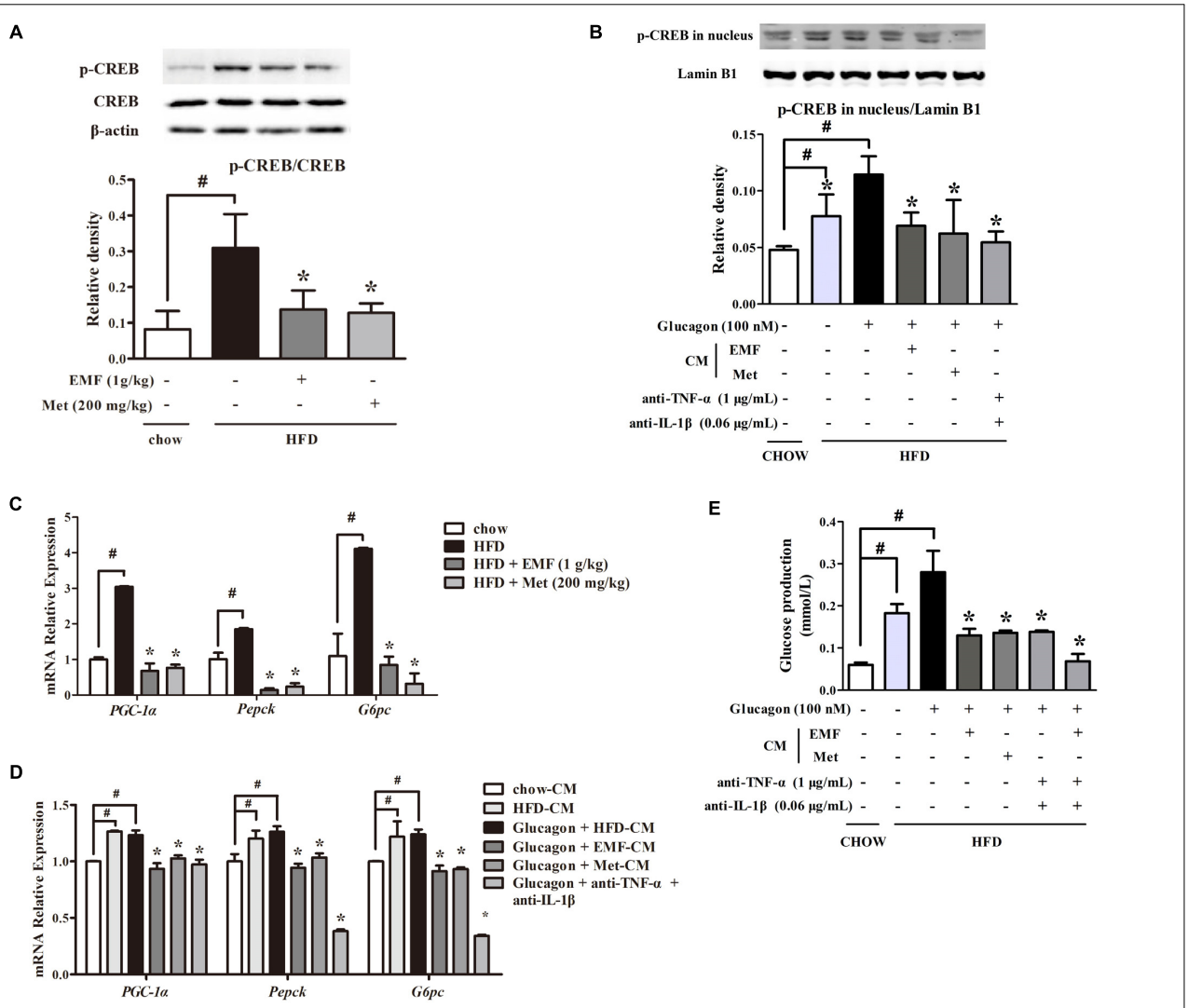

FIGURE 5 | Er-Miao-Fang restrained hepatic glucagon response. Mice were fed with chow diet or HFD for 10 days with oral administration of Er-Miao-Fang (EMF, 1 g/kg) or metformin (Met, 200 mg/kg). BNL CL.2 hepatocytes were cultured in fat-derived CM from chow or HFD feeding mice or TNF-α antibody (1 μg/mL) and IL-1β antibody (0.6 μg/mL) treated with glucagon (100 nM) for 24 h. **(A,B)** CREB protein expression in liver tissue and the phosphorylation of CREB in hepatic nucleus were determined by Western blot (mean ± SD, $n = 3$) **(C,D)** mRNA expressions of *PGC-1α*, *Pepck*, and *G6pc* in liver tissue or hepatocytes were measured by quantitative real time RT-PCR (Q-PCR). Data were mean ± SD of triplicate determinations, which were repeated three times with similar results. **(E)** Hepatic glucose production in response to glucagon in BNL CL.2 hepatocytes treated with fat-derived CM with or without TNF-α antibody (1 μg/mL) and IL-1β antibody (0.6 μg/mL) in the presence or absent of glucagon (100 nM). The results were showed as the mean ± SD ($n = 6$). *$p < 0.05$ vs. HFD feeding or HFD-CM with glucagon treatment, #$p < 0.05$ vs. the indicated treatment. CM, conditioned medium.

was reduced by neutralizing TNF-α and IL-1β with special antibodies (**Figure 5B**). CREB transcriptionally upregulates gene encoding gluconeogenesis. HFD feeding increased gene expressions of *PGC-1α, Pepck*, and *G6pc* in the liver, but the increased gene expressions were inhibited by Er-Miao-Fang and metformin administration (**Figure 5C**). When hepatocytes were exposed adipose-derived CM, Er-Miao-Fang and metformin, or TNF-α and IL-1β antibodies, suppressed gluconeogenetic gene expression (**Figure 5D**). We next showed that when hepatocytes were incubated with adipose-derived CM and antibodies of inflammatory factors at the same time, reduced hepatic glucose production in response to glucagon (**Figure 5E**). Together, these results might suggest that Er-Miao-Fang inhibited hepatic glucagon response in HFD-fed mice through inhibiting adipose inflammation.

DISCUSSION

Adipose dysfunction is closely related to metabolic diseases. Inflammatory mediators, including pro-inflammatory cytokines and FFAs, increase in the contents of FFAs in the blood circulation, linking adipose dysfunction and systemic insulin resistance in diabetes (Unger, 1995; Boden, 1999; Kim et al., 2001;

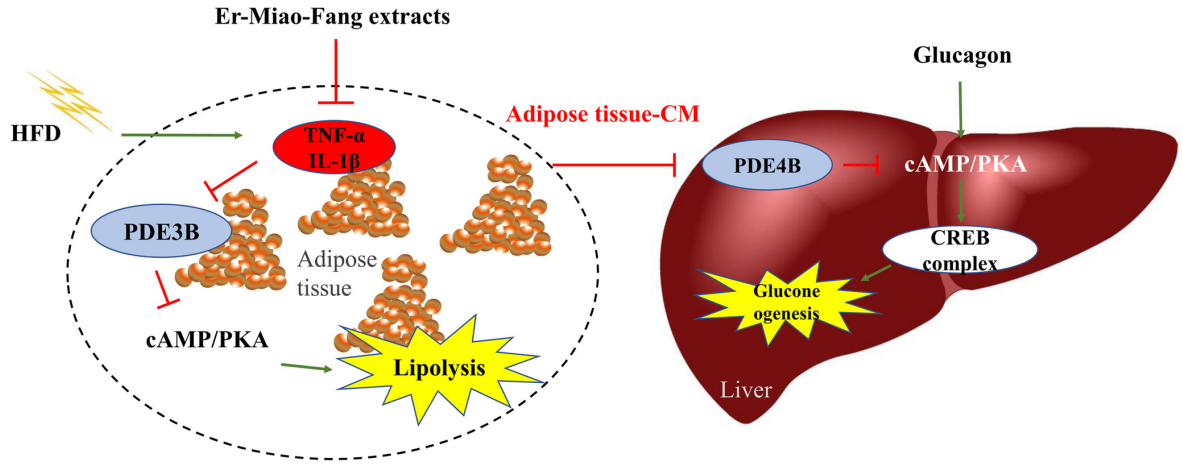

FIGURE 6 | The working pathway for Er-Miao-Fang inhibiting inflammation and blocking hepatic gluconeogenesis. HFD feeding induced inflammation and increased hepatic glucagon response, which leading to endogenous glucose production. Er-Miao-Fang inhibited inflammation and improved adipose dysfunction by preserving PDE3B and decreasing the accumulation of cAMP to prevent lipolysis. By blocking the traffic of fatty acids and inflammatory mediators from adipose tissue to the liver, Er-Miao-Fang inhibited the effect on hepatic gluconeogenesis through preserving PDE4B and reducing cAMP/PKA signaling.

Frayn, 2002). Herein, our work showed that Er-Miao-Fang might prevent adipose lipolysis by suppression of inflammation in adipose tissue, contributing to reducing excessive hepatic glucose output. This provides new insight into the role of Er-Miao-Fang in regulation of hepatic gluconeogenesis and presents the guiding significance for the regulation of multi-link targets with Traditional Chinese Medicine.

In the chief six components of prepared Er-Miao-Fang extracts, the main ingredients are alkaloids (Feng et al., 2017). Berberine and phellodendrine were reported to have the anti-inflammation activation. Short-term HFD induces adipose inflammation and adipose dysfunction, which is the upstream of crosstalk between adipose and liver. We found that berberine or phellodendrine inhibited the release of fatty acids from adipose tissue, while Er-Miao-Fang extracts prevented lipolysis even well. This suggested the potential advantages of Er-Miao-Fang extracts compared to berberine or phellodendrine in inhibiting lipolysis (**Supplementary Figure 2**), and it might be worth to discuss the superiority of Traditional Chinese Medical prescription in further study.

High-fat-diet feeding causes metabolic disorders. Actually, in our studies, lipolysis was induced by activating cAMP/PKA signaling. HFD-feeding enhanced PKA activation with an increase in cAMP accumulation and AMP reduction in adipocytes. As it has been known, cAMP is synthesized by AC and degraded by PDEs. Adenosine nucleosides are shown to inhibit AC activity (Fain et al., 1972). Er-Miao-Fang reduced cAMP accumulation with elevated levels of AMP in the fat of HFD-feeding mice, indicating that Er-Miao-Fang inhibited the expression of PKA and HSL phosphorylation to decreased lipolysis *via* attenuating cAMP/PKA signaling.

Phosphodiesterases activity was attenuated with cAMP accumulation, which was increased by pro-inflammatory cytokine TNF-α and NF-κB inflammatory signaling (Zhang et al., 2002; Degerman et al., 2011; Ke et al., 2015). So, it is necessary to investigate the relation of cAMP/PKA lipolysis signaling and inflammation in HFD-fed mice. cAMP is an important regulator of immune and inflammatory response, and turnover of intracellular cyclic nucleotides is dependent on the activity of PDEs (Oldenburger et al., 2012). In adipose tissue of obesity, TNF-α is found to impair the activity of PDE3B (Mei et al., 2002). Downregulation of PDE3B contributes to the mechanism whereby TNF-α induces lipolysis and excess release of FFAs (Rahn Landström et al., 2000). In our work, inflammation in adipose tissue of HFD-feeding mice was distinct, with the decrease of PDE3B expression. However, the decrease was removed by adding the TNF-α or IL-1β antibodies, indicating the contribution of inflammation to the activation of cAMP/PKA signaling. Er-Miao-Fang inhibited JNK activation with reduced inflammatory TNF-α and IL-1β release, and effectively preserved PDE3B activity. Also, Er-Miao-Fang showed the same effects with the neutralizing antibodies of inflammation factors, presenting that Er-Miao-Fang prevented lipolysis by inhibiting inflammation.

Obesity is characterized by low-grade inflammation, and chronic or continuous inflammation activates NF-κB signaling in adipose tissue and liver (Arkan et al., 2005; Cai et al., 2005; Donath and Shoelson, 2011). PEDs express not only in adipose, but also in liver (Abdollahi et al., 2003; Ke et al., 2015), and hepatic cAMP degradation is predominantly caused by PDE4B (Miller et al., 2013; Johanns et al., 2016). Recent studies demonstrated that PDE4B expression was associated with enhanced NF-κB activation and transcriptional activity. Indeed, we observed that expression of PDE4B was reduced in liver with adipose dysfunction. So, we next demonstrated that TNF-α and IL-1β antibodies preserved the PDE4B expression in BNL CL.2 hepatocytes, which was decreased by HFD fat-derived CM. Simultaneously, TNF-α and IL-1β antibodies decreased cAMP accumulation in hepatocytes activated by glucagon and HFD fat-derived CM. This data implied that adipose inflammation might

link to the PDE4B expression, which induced hepatic cAMP degradation.

Er-Miao-Fang improved pyruvate tolerance in the HFD-fed mice, demonstrating its inhibitory effect on endogenous glucose production. Glucagon increases hepatic glucose output through gluconeogenesis mediated by activating cAMP/PKA signaling, which phosphorylates CREB protein. Phosphorylated CREB, together with different co-activators, translocases into the nucleus and stimulates transcription of gluconeogenic genes (Gonzalez and Montminy, 1989; Ravnskjaer et al., 2007). Metformin, which is the first line therapeutic drug for diabetes to decrease blood glucose, triggers the dissociation of the CREB transcription complex and reduces gluconeogenic enzyme gene expression (He et al., 2009). For this, we observed the effect of Er-Miao-Fang on the glucagon response. Similar to metformin, Er-Miao-Fang decreased the phosphorylation status of CREB, the translocation to nucleus, gluconeogenic enzyme gene expression and glucose production in HFD-feeding mice liver tissue and hepatocytes stimulated by glucagon. Studies documented that overactivation of liver NF-κB-inducing kinase (NIK) enhanced hyperglycemia by increasing CREB stability in obese mice (Sheng et al., 2012). Interestingly, we further demonstrated that TNF-α and IL-1β antibodies lowered that effect, partly indicating the potential pathway that Er-Miao-Fang decreased hepatic cAMP/PKA gluconeogenesis signaling through inhibiting inflammation in HFD-feeding mice. However, this is should be further confirmed by blocking adipose inflammation or adopting adipose-specific PDE3B mutant mice in the future study.

It is noteworthy that inflammation-associated lipolysis occurred in short-term feeding and this could be the potential cause of insulin resistance and hepatic glucose production (Li et al., 2017). Also, our work showed that lipolysis occurred by inhibiting PDE3B and increasing cAMP activity in adipose, and this gives rise to suggesting that the product FFAs may have an effluence to glucose metabolism through other pathways to be proved. Overall, these may partly support the relevance of adipose inflammation and hepatic glucose production. However, the possibility that Er-Miao-Fang ameliorates inflammation in liver could not be excluded. Given that the feature of Traditional Chinese Medical may be of multi-link, it will be worth to pay attention to the explicit pathway that mediating glucose and lipid metabolism in the future study.

In summary, inflammation in adipose tissue might act as an important mediator to induce lipolysis and hepatic gluconeogenesis. Traditional Chinese Medical prescription Er-Miao-Fang prevented inflammation in adipose tissue and subsequent inhibited hepatic cAMP accumulation in liver contributing to restraint of the hepatic glucagon response (**Figure 6**). This study presents a new view of inhibiting inflammation to ameliorate glucose homeostasis and provides the guiding significance for the regulation of multi-link targets with Traditional Chinese Medicine.

AUTHOR CONTRIBUTIONS

NZ, BL, and JX designed the research. WZ performed experiments, analyzed, interpreted data, and drafted the manuscript. XF collected the data and reviewed the manuscript. NZ and JX edited the manuscript. BL contributed to the discussion of the manuscript. All authors approved the final version of the paper.

SUPPLEMENTARY MATERIAL

The Supplementary Material for this article can be found online at: https://www.frontiersin.org/articles/10.3389/fphys.2018.01041/full#supplementary-material

REFERENCES

Abdollahi, M., Chan, T. S., Subrahmanyam, V., and O'Brien, P. J. (2003). Effects of phosphodiesterase 3,4,5 inhibitors on hepatocyte cAMP levels, glycogenolysis, gluconeogenesis and susceptibility to a mitochondrial toxin. *Mol. Cell. Biochem.* 252, 205–211.

Arkan, M. C., Hevener, A. L., Greten, F. R., Maeda, S., Li, Z. W., Long, J. M., et al. (2005). IKK-β links inflammation to obesity-induced insulin resistance. *Nat. Med.* 11, 191–198. doi: 10.1038/nm1185

Bae, S., Jung, Y., Choi, Y. M., and Li, S. (2015). Effects of er-miao-san extracts on TNF-alpha-induced MMP-1 expression in human dermal fibroblasts. *Biol. Res.* 48:8. doi: 10.1186/0717-6287-48-8

Boden, G. (1999). Free fatty acids, insulin resistance, and type 2 diabetes mellitus. *Proc. Assoc. Am. Physicians* 111, 241–248. doi: 10.1046/j.1525-1381.1999.99220.x

Brasaemle, D. L. (2007). Thematic review series: adipocyte biology. The perilipin family of structural lipid droplet proteins: stabilization of lipid droplets and control of lipolysis. *J. Lipid Res.* 48, 2547–2559. doi: 10.1194/jlr.R700014-JLR200

Cai, D., Yuan, M., Frantz, D. F., Melendez, P. A., Hansen, L., Lee, J., et al. (2005). Local and systemic insulin resistance resulting from hepatic activation of IKK-β and NF-κB. *Nat. Med.* 11, 183–190. doi: 10.1038/nm1166

Chen, G., Li, K., Fung, C., Liu, C., Wong, H., Leung, P., et al. (2014). Er-Miao-San, a traditional herbal formula containing Rhizoma Atractylodis and Cortex Phellodendri inhibits inflammatory mediators in LPS-stimulated RAW264.7 macrophages through inhibition of NF-κB pathway and MAPKs activation. *J. Ethnopharmacol.* 154, 711–718. doi: 10.1016/j.jep.2014.04.042

Degerman, E., Ahmad, F., Chung, Y. W., Guirguis, E., Omar, B., Stenson, L., et al. (2011). From PDE3B to the regulation of energy homeostasis. *Curr. Opin. Pharmacol.* 11, 676–682. doi: 10.1016/j.coph.2011.09.015

Donath, M. Y., and Shoelson, S. E. (2011). Type 2 diabetes as an inflammatory disease. *Nat. Rev. Immunol.* 11, 98–107. doi: 10.1038/nri2925

Fain, J. N., Pointer, R. H., and Ward, W. F. (1972). Effects of adenosine nucleosides on adenylate cyclase, phosphodiesterase, cyclic adenosine monophosphate accumulation, and lipolysis in fat cells. *J. Biol. Chem.* 247, 6866–6872.

Feng, X., Zhao, W., Hou, T., and Zhang, N. (2017). Simultaneous determination of 14 compounds in Er Miao San extracts by UPLC-MS/MS. *Zhongguo Shi Yan Fang Ji Xue Za Zhi* 23, 116–122.

Francis, S. H., Blount, M. A., and Corbin, J. D. (2011). Mammalian cyclic nucleotide phosphodiesterases: molecular mechanisms and physiological functions. *Physiol. Rev.* 91, 651–690. doi: 10.1152/physrev.00030.2010

Frayn, K. N. (2002). Adipose tissue as a buffer for daily lipid flux. *Diabetologia* 45, 1201–1210. doi: 10.1007/s00125-002-0873-y

Gauthier, M. S., Miyoshi, H., Souza, S. C., Cacicedo, J. M., Saha, A. K., Greenberg, A. S., et al. (2008). AMP-activated protein kinase is activated as a consequence of lipolysis in the adipocyte: potential mechanism and physiological relevance. *J. Biol. Chem.* 283, 16514–16524. doi: 10.1074/jbc.M708177200

Gonzalez, G. A., and Montminy, M. R. (1989). Cyclic AMP stimulates somatostatin gene transcription by phosphorylation of CREB at serine 133. *Cell* 59, 675–680. doi: 10.1016/0092-8674(89)90013-5

Greenberg, A. S., Coleman, R. A., Kraemer, F. B., McManaman, J. L., Obin, M. S., Puri, V., et al. (2011). The role of lipid droplets in metabolic disease in rodents and humans. *J. Clin. Invest.* 121, 2102–2110. doi: 10.1172/JCI46069

Greenberg, A. S., Shen, W. J., Muliro, K., Patel, S., Souza, S. C., Roth, R. A., et al. (2001). Stimulation of lipolysis and hormone-sensitive lipase via the extracellular signal-regulated kinase pathway. *J. Biol. Chem.* 276, 45456–45461. doi: 10.1074/jbc.M104436200

He, L., Sabet, A., Djedjos, S., Miller, R., Sun, X., Hussain, M. A., et al. (2009). Metformin and insulin suppress hepatic gluconeogenesis through phosphorylation of CREB binding protein. *Cell* 137, 635–646. doi: 10.1016/j.cell.2009.03.016

Johanns, M., Lai, Y. C., Hsu, M. F., Jacobs, R., Vertommen, D., Van Sande, J., et al. (2016). AMPK antagonizes hepatic glucagon-stimulated cyclic AMP signalling via phosphorylation-induced activation of cyclic nucleotide phosphodiesterase 4B. *Nat. Commun.* 7:10856. doi: 10.1038/ncomms10856

Ke, B., Zhao, Z., Ye, X., Gao, Z., Manganiello, V., Wu, B., et al. (2015). Inactivation of NF-κB p65 (RelA) in liver improves insulin sensitivity and inhibits cAMP/PKA pathway. *Diabetes Metab. Res. Rev.* 64, 3355–3362. doi: 10.2337/db15-0242

Kim, J. K., Fillmore, J. J., Chen, Y., Yu, C., Moore, I. K., Pypaert, M., et al. (2001). Tissue-specific overexpression of lipoprotein lipase causes tissue-specific insulin resistance. *Proc. Natl. Acad. Sci. U.S.A.* 98, 7522–7527. doi: 10.1073/pnas.121164498

Kowalski, G. M., De Souza, D. P., Burch, M. L., Hamley, S., Kloehn, J., Selathurai, A., et al. (2015). Application of dynamic metabolomics to examine in vivo skeletal muscle glucose metabolism in the chronically high-fat fed mouse. *Biochem. Biophys. Res. Commun.* 462, 27–32. doi: 10.1016/j.bbrc.2015.04.096

Lafontan, M., and Girard, J. (2008). Impact of visceral adipose tissue on liver metabolism. Part I: heterogeneity of adipose tissue and functional properties of visceral adipose tissue. *Diabetes Metab.* 34, 317–327. doi: 10.1016/j.diabet.2008.04.001

Leahy, P., Crawford, D. R., Grossman, G., Gronostajski, R. M., and Hanson, R. W. (1999). CREB binding protein coordinates the function of multiple transcription factors including nuclear factor I to regulate phosphoenolpyruvate carboxykinase (GTP) gene transcription. *J. Biol. Chem.* 274, 8813–8822. doi: 10.1074/jbc.274.13.8813

Lee, Y. S., Kim, W. S., Kim, K. H., Yoon, M. J., Cho, H. J., Shen, Y., et al. (2006). Berberine, a natural plant product, activates AMP-activated protein kinase with beneficial metabolic effects in diabetic and insulin-resistant states. *Diabetes Metab. Res. Rev.* 55, 2256–2264. doi: 10.2337/db06-0006

Li, L., Huang, T., Tian, C., Xiao, Y., Kou, S., Zhou, X., et al. (2016). The defensive effect of phellodendrine against AAPH-induced oxidative stress through regulating the AKT/NF-κB pathway in zebrafish embryos. *Life Sci.* 157, 97–106. doi: 10.1016/j.lfs.2016.05.032

Li, L. Z., Zhang, T., Yang, L., Zhang, L., Wang, L., Liu, B., et al. (2017). Inhibition of lipolysis by ilexgenin A via AMPK activation contributes to the prevention of hepatic insulin resistance. *Eur. J. Pharmacol.* 813, 84–93. doi: 10.1016/j.ejphar.2017.07.038

Mei, J., Holst, L. S., Landström, T. R., Holm, C., Brindley, D., Manganiello, V., et al. (2002). C(2)-ceramide influences the expression and insulin-mediated regulation of cyclic nucleotide phosphodiesterase 3B and lipolysis in 3T3-L1 adipocytes. *Diabetes Metab. Res. Rev.* 51, 631–637. doi: 10.2337/diabetes.51.3.631

Miller, R. A., Chu, Q., Xie, J., Foretz, M., Viollet, B., and Birnbaum, M. J. (2013). Biguanides suppress hepatic glucagon signalling by decreasing production of cyclic AMP. *Nature* 494, 256–260. doi: 10.1038/nature11808

Miyoshi, H., Souza, S. C., Zhang, H. H., Strissel, K. J., Christoffolete, M. A., Kovsan, J., et al. (2006). Perilipin promotes hormone-sensitive lipase-mediated adipocyte lipolysis via phosphorylation-dependent and -independent mechanisms. *J. Biol. Chem.* 281, 15837–15844. doi: 10.1074/jbc.M601097200

Oldenburger, A., Roscioni, S. S., Jansen, E., Menzen, M. H., Halayko, A. J., Timens, W., et al. (2012). Anti-inflammatory role of the cAMP effectors Epac and PKA: implications in chronic obstructive pulmonary disease. *PLoS One* 7:e31574. doi: 10.1371/journal.pone.0031574

Perry, R. J., Samuel, V. T., Petersen, K. F., and Shulman, G. I. (2014). The role of hepatic lipids in hepatic insulin resistance and type 2 diabetes. *Nature* 510, 84–91. doi: 10.1038/nature13478

Rahn Landström, T., Mei, J., Karlsson, M., Manganiello, V., and Degerman, E. (2000). Down-regulation of cyclic-nucleotide phosphodiesterase 3B in 3T3-L1 adipocytes induced by tumour necrosis factor alpha and cAMP. *Biochem. J.* 346(Pt 2), 337–343. doi: 10.1042/bj3460337

Ravnskjaer, K., Kester, H., Liu, Y., Zhang, X., Lee, D., Yates, J. R. III, et al. (2007). Cooperative interactions between CBP and TORC2 confer selectivity to CREB target gene expression. *EMBO J.* 26, 2880–2889. doi: 10.1038/sj.emboj.7601715

Schweiger, M., Eichmann, T. O., Taschler, U., Zimmermann, R., Zechner, R., and Lass, A. (2014). Measurement of lipolysis. *Methods Enzymol.* 538, 171–193. doi: 10.1016/B978-0-12-800280-3.00010-4

Sheng, L., Zhou, Y., Chen, Z., Ren, D., Cho, K. W., Jiang, L., et al. (2012). NF-κB-inducing kinase (NIK) promotes hyperglycaemia and glucose intolerance in obesity by augmenting glucagon action. *Nat. Med.* 18, 943–949. doi: 10.1038/nm.2756

Streeper, R. S., Hornbuckle, L. A., Svitek, C. A., Goldman, J. K., Oeser, J. K., and O'Brien, R. M. (2001). Protein kinase A phosphorylates hepatocyte nuclear factor-6 and stimulates glucose-6-phosphatase catalytic subunit gene transcription. *J. Biol. Chem.* 276, 19111–19118. doi: 10.1074/jbc.M101442200

Unger, R. H. (1995). Lipotoxicity in the pathogenesis of obesity-dependent NIDDM. Genetic and clinical implications. *Diabetes* 44, 863–870. doi: 10.2337/diab.44.8.863

Unger, R. H., and Cherrington, A. D. (2012). Glucagonocentric restructuring of diabetes: a pathophysiologic and therapeutic makeover. *J. Clin. Invest.* 122, 4–12. doi: 10.1172/JCI60016

Wang, L., Zhang, B., Huang, F., Liu, B., and Xie, Y. (2016). Curcumin inhibits lipolysis via suppression of ER stress in adipose tissue and prevents hepatic insulin resistance. *J. Lipid Res.* 57, 1243–1255. doi: 10.1194/jlr.M067397

Wei, S., Zhang, M., Yu, Y., Lan, X., Yao, F., Yan, X., et al. (2016). Berberine attenuates development of the hepatic gluconeogenesis and lipid metabolism disorder in type 2 diabetic mice and in palmitate-incubated HepG2 cells through suppression of the HNF-4α miR122 pathway. *PLoS One* 11:e0152097. doi: 10.1371/journal.pone.0152097

Xiao, N., Lou, M., Lu, Y., Yang, L., Liu, Q., Liu, B., et al. (2017). Ginsenoside Rg5 attenuates hepatic glucagon response via suppression of succinate-associated HIF-1α induction in HFD-fed mice. *Diabetologia* 60, 1084–1093. doi: 10.1007/s00125-017-4238-y

Yang, H., and Yang, L. (2016). Targeting cAMP/PKA pathway for glycemic control and type 2 diabetes therapy. *J. Mol. Endocrinol.* 57, R93–R108. doi: 10.1530/JME-15-0316

Zhang, H. H., Halbleib, M., Ahmad, F., Manganiello, V. C., and Greenberg, A. S. (2002). Tumor necrosis factor-α stimulates lipolysis in differentiated human adipocytes through activation of extracellular signal-related kinase and elevation of intracellular cAMP. *Diabetes* 51, 2929–2935. doi: 10.1152/ajpendo.00228.2012

Zhao, W., Li, A., Feng, X., Hou, T., Liu, K., Liu, B., et al. (2016). Metformin and resveratrol ameliorate muscle insulin resistance through preventing lipolysis and inflammation in hypoxic adipose tissue. *Cell. Signal.* 28, 1401–1411. doi: 10.1016/j.cellsig.2016.06.018

Zhao, W., Wang, M., Shao, L., Liao, M., Liu, K., Huang, F., et al. (2014). The total phenolic fraction of Anemarrhena asphodeloides inhibits inflammation and reduces insulin resistance in adipocytes via regulation of AMP-kinase activity. *Planta Med.* 80, 146–152. doi: 10.1055/s-0033-1360197

Conflict of Interest Statement: The authors declare that the research was conducted in the absence of any commercial or financial relationships that could be construed as a potential conflict of interest.

frontiers in Physiology

ORIGINAL RESEARCH
published: 02 August 2018
doi: 10.3389/fphys.2018.01042

Berberine Could Ameliorate Cardiac Dysfunction via Interfering Myocardial Lipidomic Profiles in the Rat Model of Diabetic Cardiomyopathy

Shifen Dong[1], Shuofeng Zhang[1], Zhirong Chen[1], Rong Zhang[1], Linyue Tian[1], Long Cheng[1], Fei Shang[2] and Jianning Sun[1]**

[1] School of Chinese Materia Medica, Beijing University of Chinese Medicine, Beijing, China, [2] Department of Pharmacology, Analysis and Testing Center, Beijing University of Chemical Technology, Beijing, China

OPEN ACCESS

Edited by:
Xinran Ma,
East China Normal University, China

Reviewed by:
Qun Liu,
China Pharmaceutical University, China
Lin Li,
Xuanwu Hospital, Capital Medical University, China

***Correspondence:**
Shifen Dong
tedong4444@gmail.com
Jianning Sun
jn_sun@sina.com

Specialty section:
This article was submitted to Clinical and Translational Physiology, a section of the journal Frontiers in Physiology

Received: 05 April 2018
Accepted: 12 July 2018
Published: 02 August 2018

Citation:
Dong S, Zhang S, Chen Z, Zhang R, Tian L, Cheng L, Shang F and Sun J (2018) Berberine Could Ameliorate Cardiac Dysfunction via Interfering Myocardial Lipidomic Profiles in the Rat Model of Diabetic Cardiomyopathy. Front. Physiol. 9:1042. doi: 10.3389/fphys.2018.01042

Background: Diabetic cardiomyopathy (DCM) is considered to be a distinct clinical entity independent of concomitant macro- and microvascular disorders, which is initiated partly by disturbances in energy substrates. This study was to observe the dynamic modulations of berberine in DCM rats and explore the changes of lipidomic profiles of myocardial tissue.

Methods: Sprague-Dawley (SD) rats were fed high-sucrose and high-fat diet (HSHFD) for totally 22 weeks and intraperitoneally (i.p.) injected with 30 mg/kg of streptozotocin (STZ) at the fifth week to induce DCM. Seventy-two hours after STZ injection, the rats were orally given with berberine at 10, 30 mg/kg and metformin at 200 mg/kg, respectively. Dynamic changes of cardiac function, heart mass ratios and blood lipids were observed at f 4, 10, 16, and 22, respectively. Furthermore, lipid metabolites in myocardial tissue at week 16 were profiled by the ultra-high-performance liquid chromatography coupled to a quadruple time of flight mass spectrometer (UPLC/Q-TOF/MS) approach.

Results: Berberine could protect against cardiac diastolic and systolic dysfunctions, as well as cardiac hypertrophy, and the most effective duration is with 16-week of administration. Meanwhile, 17 potential biomarkers of phosphatidylcholines (PCs), phosphatidylethanolamines (PEs) and sphingolipids (SMs) of DCM induced by HSFD/STZ were identified. The perturbations of lipidomic profiles could be partly reversed with berberine intervention, i.e., PC (16:0/20:4), PC (18:2/0:0), PC (18:0/18:2), PC (18:0/22:5), PC (20:4/0:0), PC (20:4/18:0), PC (20:4/18:1), PC (20:4/20:2), PE (18:2/0:0), and SM (d18:0/16:0).

Conclusions: These results indicated a close relationship between PCs, PEs and SMs and cardiac damage mechanisms during development of DCM. The therapeutic effects of berberine on DCM are partly caused by interferences with PCs, PEs, and SMs metabolisms.

Keywords: diabetic cardiomyopathy, myocardial tissue, lipidomic profiles, berberine, UPLC/Q-TOF/MS

INTRODUCTION

Diabetes mellitus (DM) is among the most prevalent and morbid chronic diseases, and the worldwide prevalence of diabetic people is predicted to dramatically increase from 415 million to 642 million by 2040 (Boles et al., 2017; Ingelfinger and Jarcho, 2017; Ruiz et al., 2018). In China, there also be a rapid increase in the prevalence of DM associated with recent economic development, and the current diabetic subjects were ∼113.9 million, and a further 493.4 million persons with prediabetes (Xu et al., 2013; Chan et al., 2014). And the type 2 DM that closely related to obesity is the main contributor to the increase of DM prevalence (Ma et al., 2017).

Diabetes mellitus and prediabetes status increase all cause and cardiovascular mortality (Huang et al., 2017). Diabetic cardiomyopathy (DCM) is considered to be a distinct clinical entity independent of concomitant macro- and microvascular disorders (Huynh et al., 2014; Jia et al., 2018), and occurs in the absence of coronary artery disease, valvular disease, and other conventional cardiovascular risk factors, which could induce direct damage to myocardium and lead to heart failure (Loffroy et al., 2009; Trachanas et al., 2014; Jia et al., 2018). Various potential molecular and cellular mechanisms are involved in the pathophysiological process of DCM (Ruiz et al., 2018), such as disturbances in myocardial energy utilization, calcium signaling pathway, as well as mitochondrial dysfunction (Palomer et al., 2013).

The metabolic disturbances in DCM are mainly characterized by triglycerides (TGs) accumulation in the myocardial tissue, excessive lipid oxidation, and reduced glucose utilization (Bakshi et al., 2015), which may lead to the exceeding oxidative stress, mitochondrial dysfunction and apoptosis of cardiomyocytes (Palomer et al., 2013; Bakshi et al., 2015). In addition, the lipidomic profiling extends far beyond detection of total cholesterol (TCH) and TGs, which is becoming increasingly useful to clarify the interactions between lipid metabolism, diet, and metabolic diseases (Meikle and Summers, 2017).

Berberine is a kind of isoquinoline alkaloids that can be extracted from various plants, such as Coptis chinensis (Chinese goldthread), Berberis vulgaris (barberry), and Phellodendron amurense (Amur corktree), which is widely used in traditional Chinese medicine (Cicero and Baggioni, 2016). The current clinical and experimental research have suggested a potential effect of berberine on regulation of lipid and glucose homeostasis, as well as inhibiting inflammation and cancer growth (Wang et al., 2018). Oral administration of berberine could improve hypercholesterolemic patients and reduce serum TCH, TG, and low-density lipoprotein (LDL)—cholesterol (Kong et al., 2004). Berberine could also improve nonalcoholic fatty liver disease patients and alter circulating ceramides (Chang et al., 2016). The lowering lipid effect of berberine was related to the activation of adenosine monophosphate (AMP)-activated protein kinase (AMPK) pathway (Jiang et al., 2016) and regulation of LDL receptor (LDLR) post-transcription, as well as ameliorating abnormal lipid deposition and reducing oxidative stress (Sun et al., 2017). However, little is known about the effect of berberine on lipidomic profiling in DCM subjects (Li et al., 2015).

The recent studies in DCM animal models suggested the important role of phospholipids (e.g., phosphatidylcholine and phosphatidylethanolamine) in the development of cardiac dysfunction and remodeling of DCM (Dong et al., 2017). We also found that berberine could protect against cardiac dysfunction induced by high caloric diet via promoting glucose transport and inhibiting cardiac lipid accumulation (Dong et al., 2011). The purpose of this study was to observe the dynamic pathogenesis changes of DCM and the effect of berberine on changes of myocardial lipidomic profiles in DCM rats, in order to explore novel targets for further research.

MATERIALS

Chemicals and Reagents

Streptozotocin (STZ), berberine chloride, and metformin were obtained from Sigma-Aldrich (St Louis, MO, USA). The STZ was dissolved in 0.1 M citrate buffer (pH = 4.5), and berberine was suspended in 0.5% sodium carboxymethyl cellulose (CMC) solution. Liquid chromatography tandem mass spectrometry (LC-MS)-grade methanol, chloroform, and acetonitrile were obtained from Thermo Fisher Scientific (Pittsburgh, PA, USA). Biochemical kits of plasma samples were purchased from Nanjing Jiancheng Bioengineering Institute (Nanjing, China) (Dong et al., 2011).

Animal Care

Male Sprague-Dawley rats [Grade II, certificate No. SCXK (jing) 2012-0001], weighing 180 ± 20 g, were purchased from Beijing Vital River Laboratory Animal Technology Co., Ltd. (Beijing, China). All animals were maintained under specific pathogen free conditions. Regular housing temperatures were maintained between 21 and 23°C with a 12 h light−12 h dark cycle. Water and various diets (regular chow diet or HSFD) were given to animals *ad libitum*. All studies involving animals were in accordance with ethics standards of the Animal Care and Welfare Committee of Beijing University of Chinese Medicine [Certificate No. BUCM-04-2015090201-3008].

Three 100 rats were randomly divided into five groups, with 60 rats in each group. Rats in the control group (CON) were given with regular chow diet and 0.5% sodium CMC (Dong et al., 2011). Other rats were fed high-sucrose and high-fat diet (HSHFD, 2920 Kcal/kg) provided by Ke'ao Cooperation Co., Ltd. (Beijing, China), and i.p. injected with 30 mg/kg of streptozotocin (STZ) following a 12 h fast at the fifth week of HSFD feeding to induce diabetic cardiomyopathy (DCM). Seventy-two hours following STZ injection, fasting blood glucose (FBG) levels were determined and the rats with high FBG (≥11.1 mmol/L) were recruited for further research. In addition, rats in treated groups were i.g. administered with berberine at 10, 30 mg/kg and metformin at 200 mg/kg, respectively. And rats in DCM model group were just orally given with vehicle.

Dynamic Assessment of Cardiac Function

Parameters of cardiac function were observed at 4 time points. After administered with berberine and metformin for 4, 10, 16, and 22 weeks, respectively, the rats were intraperitoneally

anesthetized with 35 mg/kg pentobarbital sodium following a 12 h fast. A 20 G catheter was placed in the left ventricle via the right common carotid artery for detection of cardiac function, i.e., left ventricular end diastolic pressure (LVEDP), and left ventricular systolic pressure (LVSP). Data were detected by MP150 system (BIOPAC Systems, Ins., CA, USA).

Dynamic Assessment of Blood Lipids

Following detection of cardiac function at each time point, the whole blood was collected from the right carotid artery of rats, and transferred to tubes with anticoagulant (sodium heparin). Plasma samples were prepared by centrifuging whole blood at 2,000 g for 10 min. Levels of plasma TCH and TG were determined by ultraviolet spectrophotometric approach according to the manufacturer's protocol.

Measurement of the Whole Heart Mass and Left Ventricular Mass

After blood collection, the rats were euthanized by cervical dislocation (Reis et al., 2005). The hearts were excised and weighed. And the heart weight index (BWI) and left ventricular weight index (LVWI) were calculated, respectively (Bai et al., 2018).

BWI=heart weight (HW) / body weight (BW).

LVWI=left ventricular weight (LVW) / body weight (BW).

UPLC/QTOF/MS Analysis

The ultra-high-performance liquid chromatography coupled to a quadruple time of flight mass spectrometer (UPLC/Q-TOF/MS, Waters MS Technologies, Manchester, UK) was applied for data collection. And the procedures were performed as described (Dunn et al., 2011; Want et al., 2013). Freeze samples of myocardial tissue were thawed at room temperature, and 100 mg of each sample was accurately weighed and homogenized in homogenization tubes by a Speed Mill Plus (Analytik Jena, Jena, Germany). One milliliter of chloroform/methanol (3:1) were added to tissue containing in the 1.5-mL centrifuge tube (Axygen MCT-150-C, Corning, NY, USA) and thoroughly mixed on a vortex mixer for 30 min, and then the protein precipitate was pelleted in a centrifuge at 4°C and 12,000 rpm for 10 min. After centrifuge, 400 μL of subnatant was carefully collected and dried in a Savant™ SpeedVac™ High Capacity Concentrators (Thermo Fisher, Pittsburgh, USA). And then 400 μL of isopropyl alcohol/acetonitrile (1:1) was added into each tube and dissolved in ultrasound. The dissolved matter was centrifuged at 12,000 rpm for 10 min, and the supernatant (100 μL) was transferred to a vial insert (200 μL) for liquid chromatography-mass spectrometry analysis.

For C_{18} separation, mobile phase A was acetonitrile/water (60/40) and mobile phase B was isopropanol/ acetonitrile (90/10), and both A and B contained 0.1% formic acid and 10 mM ammonium acetate. The gradient conditions for reversed phase C_{18} separation were shown in **Table 1**.

A Waters Acquity UPLC CSH C_{18} column (2.1 × 100 mm, 1.7 μm) was operated at 45°C and 300 μL/min flow rate. And the injection volume was 2 μL. Samples were analyzed in positive and negative electrospray ionization (ESI) using Waters xevo G2 QTOF Mass Spectrometer. And conditions of ESI^+ and ESI^- were showed in **Table 2**.

TABLE 1 | The gradient conditions for reversed phase C_{18} separation for lipids.

Time (min)	A (v%)	B (v%)
0	80	20
2	70	30
5	55	45
6.5	40	60
12	35	65
14	15	85
17.5	0	100
18	0	100
18.1	80	20
19.5	80	20

TABLE 2 | Analysis condition of positive and negative electrospray ionization.

Parameter	ESI^+	ESI^-
Capillary voltage	3,200 V	2,300 V
Sampling cone	30 V	30 V
Desolvation temperature	400°C	400°C
Desolvation gas flow	800 L/h	800 L/h
Cone gas flow	30 L/h	40 L/h
Source temperature	120°C	120°C

Statistical Methods

All of the MS data were processed by Progenesis QI software (Nonlinear Dynamics, Newcastle, UK). And the steps that carried out to conduct a sample analysis, included imputing raw data, peak alignment, picking, and normalization to produce peak intensities for retention time (t_R) and mass-to-charge ratio (m/z) data pairs (Saigusa et al., 2018). The range of automatic peak picking was 0.7 ∼19 min. Databases including our database containing more than 600 metabolite standards and the online databases such as LIPID MAPS (http://www.Lipidmaps.org/tools/index.html) were used to identify the lipid metabolites (Saigusa et al., 2016). For example, in positive mode the ion of m/z 544.34034 (t_R, 1.3903 min) was speculated as $C_{28}H_{50}NO_7P$ by analyzing the elemental composition and the fractional isotope abundance (Qian et al., 2017). Then, this metabolite was identified as PC (20:4/0:0) after comparing the tandem mass spectrometry (MS/MS) data with Lipid Standards MS/MS spectra in LIPID MAPS.

A multivariate analysis was performed using the SIMCA 14.1 software (Meikle et al., 2014) (Umetrics AB, Umea, Sweden). An unsupervised model of principal component analysis (PCA) with unit variance scaling was used to assess the holistic metabolome alterations among groups and monitor the stability of this study. A supervised model of orthogonal projection to latent structures discriminant analysis (OPLS-DA) with unit variance scaling was performed to maximize the distance between groups and identify important variables with an important contribution to

the classification according to the variable important in the projection (VIP) values. The permutation test was conducted for 200 times to evaluate the risk of over-fitting for the OPLS-DA model.

Additional data are shown as mean ± SD. In each experiment, *n* defines the number of rats. Statistical significance between multiple groups was evaluated by one-way analysis of variance (ANOVA) followed by least significant difference (LSD) *post-hoc* tests using SPSS version 17.0. $P < 0.05$ was considered as statistically significant.

RESULTS

Berberine Improved Cardiac Diastolic Function in DCM Rats

In this study, the dynamic changes of cardiac function in rats were observed at week 4, 10, 16, and 22, respectively. When compared with the normal rats, LVEDP values in DCM rats increased from week 10 to week 22 and showed significant changes at week 16 ($P < 0.05$) and week 22 ($P < 0.05$), respectively. In addition, only after 16-week administration with berberine at 10, 30 mg/kg and metformin at 200 mg/kg, respectively, values of LVEDP showed remarkable reduction ($P < 0.01$), when compared with the DCM rats (**Figure 1**). These results indicated that berberine could protect against cardiac diastolic dysfunction, and the most effective duration is with 16-week administration.

Berberine Improved Cardiac Systolic Function in DCM Rats

When compared with control rats, values of LVSP were significantly decreased at week 10 ($P < 0.01$), week 16 ($P < 0.05$), and week 22 ($P < 0.05$). After administration with berberine at 30 mg/kg and metformin at 200 mg/kg, respectively, LVSP levels were increased significantly at week 10 and week 16 ($P < 0.05$) compared to DCM group (**Figure 2**). These results indicated that berberine could protect against cardiac systolic dysfunction, and the most effective duration is with 10–16 weeks of administration.

Berberine Decreased the Ratios of HW/BW and LVW/BW in DCM Rats

When compared with the control rats, values of both LVW/BW and HW/BW were remarkably increased from week 4 to week 22 ($P < 0.05$ or $P < 0.01$) in DCM model rats, which indicated a cardiac hypertrophy status. Berberine at 30 mg/kg caused a significant reduction in HW/BW at week 16 ($P < 0.05$), when compared with DCM rats (**Figure 3**).

Blood Lipid Parameters

Levels of plasma TCH and TG of DCM rats were increased significantly from week 4 to week 22 ($P < 0.05$ or $P < 0.01$). Berberine 30 mg/kg caused a significant reduction in TCH levels at week 16 ($P < 0.05$), when compared with DCM rats (**Figure 4**).

Taken in concert, all above experimental results manifested protection effects of berberine on DCM rats. Berberine could protect against cardiac diastolic and systolic dysfunction, as well as cardiac hypertrophy, and the most effective duration is around 16-week administration. Therefore, the samples at this time point were selected for the subsequent lipidomic profiles analysis.

Lipidomic Profiles Analysis of Myocardial Tissue

Metabolic profiles of the myocardial tissue were acquired by UPLC/Q-TOF/MS approach in ESI^+ and ESI^- modes. Totally, 66390 positive ion peaks and 9030 negative ion peaks were obtained.

The quality control (QC) samples were used to monitor the stability and performance of LC-MS system and the reproducibility of the samples. The pretreatment of QC samples was in the same manner as the test samples. In this study, five QC samples of myocardial tissue were inserted at regular intervals (6∼8 samples) into the run sequence in order to assess the repeatability of data (Want et al., 2013). The features were selected according to their coefficients of variation (CVs) with quality control, and features with CVs over 15% were eliminated (Saigusa et al., 2016). As shown in **Figure 5**, the cluster of the QC samples in the principal component analysis (PCA) scores scatter plot exhibited stability and repeatability of this lipidomic analysis system (Xu et al., 2017).

Identification of Potential Biomarkers

The PCA was applied to analyze all acquired observations in order to investigate the global lipidomics metabolism variations. The lipid metabolic phenotypes based on all imported samples could be classified by the approach of PCA method (Xu et al., 2017). An overviews of all samples in the data and a clear grouping trend (R^2X, 0.861; Q^2, 0.752) between the control group, DCM group, DCM +Metformin 200 mg/kg group, DCM + Berberine 10 mg/kg group and DCM + Berberine 30 mg/kg group could be observed. The DCM group *vs.* control group exhibited an improved separation. This observation indicated that DCM status may disturb the metabolism of the lipids, when compared to control group. Berberine at 10, 30 mg/kg and metformin at 200 mg/kg showed interferences in the DCM rats, although the trajectory of the drug-treated groups did not return to the normal state (**Figure 6**).

To further confirm the certain lipids used as selective and sensitive biomarkers for pathogenesis of diabetic cardiomyopathy, the OPLS-DA approach was used to compare the changes of lipid metabolites between the DCM and the control rats (Xu et al., 2017). A clear separation of the control rats and the DCM rats was observed as demonstrated by OPLS-DA scores scatter plot (**Figure 7A**). In the OPLS-DA model, the cumulative R^2Y and Q^2 are 0.966 and 0.901, respectively. No over-fitting was observed according to results of chance permutation (**Figure 7B**). Afterwards, the significant changed lipid metabolites of the DCM group compared to the normal group were filtered out based on variable important in the projection (VIP) values (VIP > 1) and *t*-test ($P < 0.05$).

Subsequently, total 17 potential lipids biomarkers of DCM models, including 12 PCs, 3 PEs, and 2 SMs were further studied (**Table 3**).

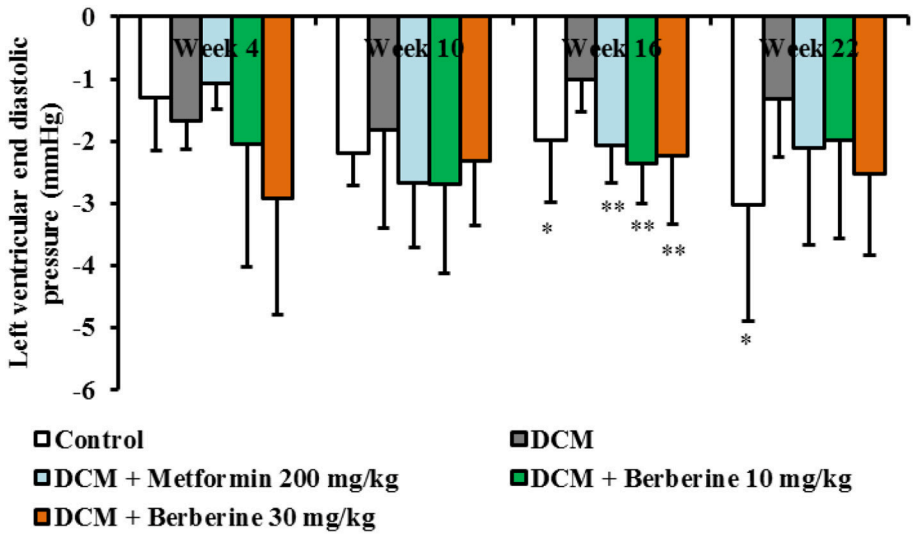

FIGURE 1 | Berberine improved cardiac diastolic function in DCM rats. Diabetic cardiomyopathy (DCM) model rats were established by feeding with high-sucrose and high-fat diet (HSHFD) consisting of regular diet (66.5%), lard (10%), sucrose (20%), cholesterol (2.5%), and bile salt (1%) and intraperitoneally (i.p.) injected with 30 mg/kg of streptozotocin (STZ) at the fifth week. Seventy-two hours after STZ injection, berberine at the dosage of 10, 30 mg/kg, and metformin at 200 mg/kg were orally given to DCM rats, respectively, for consecutive 4, 10, 16, and 22 weeks. The dynamic changes of cardiac function were measured by invasive left ventricular catheterization in anesthetized rats. DCM, diabetic cardiomyopathy. Data were shown as mean ± SD, with $n = 7 \sim 12$. Statistical significance was determined by one-way analysis of variance (ANOVA) followed by least significant difference (LSD) *post-hoc* test. $^{*}P < 0.05$, $^{**}P < 0.01$ vs. DCM group.

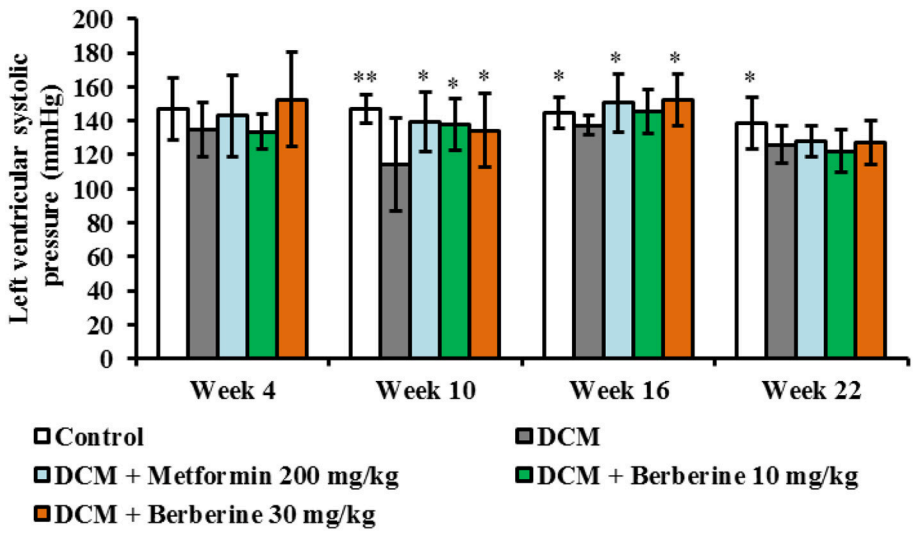

FIGURE 2 | Berberine improved cardiac systolic function in DCM rats. DCM, diabetic cardiomyopathy. Data were shown as mean ± SD, with $n = 7 \sim 12$. Statistical significance was determined by one-way ANOVA followed by LSD *post-hoc* test. $^{*}P < 0.05$, $^{**}P < 0.01$ vs. DCM group.

The changed levels and names of selected biomarkers were shown in **Figure 8**. Specifically, the lipid levels of 2 PCs, 2 PEs, and 2 SMs, including PC (18:0/18:2), PC (18:2/0:0), PE (P-18:0/0:0), PE (18:2/0:0), SM (d18:0/16:0), and SM (d18:1/18:1) were significantly up-regulated in the DCM rats, when compared with normal rats ($P < 0.05$ or $P < 0.001$). Meanwhile, lipid levels of 10 PCs and 1 PE, including PC (16:0/14:0), PC (16:0/16:0), PC (16:0/20:4), PC (18:0/22:5), PC (20:4/0:0), PC (20:4/18:0), PC (20:4/18:1), PC (20:4/18:2), PC (20:4/20:2), PC (20:4/20:4), and PE (20:4/16:0) were remarkably reduced in the DCM rats, when compared with normal rats ($P < 0.05$ or $P < 0.001$).

After administered with berberine, lipid levels of 8 PCs, 1 PE, and 1 SM were significantly altered and exhibited a normal-level tendency ($P < 0.05$), i.e., PC (18:0/18:2), PC (18:2/0:0), PC (16:0/20:4), PC (18:0/22:5), PC (20:4/0:0), PC (20:4/18:0), PC (20:4/18:1), PC (20:4/20:2), PE (18:2/0:0), and SM (d18:0/16:0).

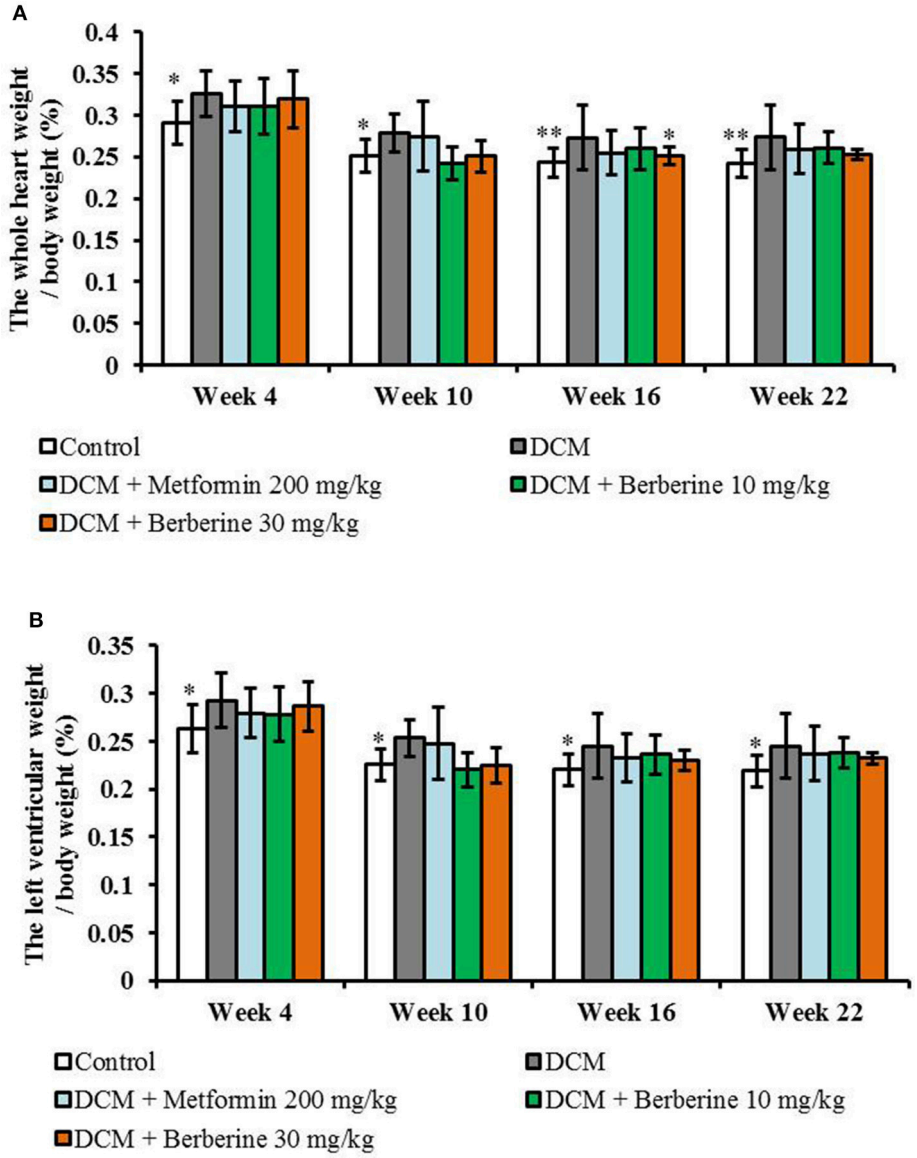

FIGURE 3 | Berberine decreased the heart weight index and left ventricular weight index in DCM rats. **(A)** Heart weight index: the whole heart weight / body weight. **(B)** Left ventricular weight index: the left ventricular weight / body weight. DCM, diabetic cardiomyopathy. Data are presented as mean ± SD, with $n = 7 \sim 12$. Statistical significance was determined by one-way ANOVA followed by LSD *post-hoc* test. $^{*}P < 0.05$, $^{**}P < 0.01$ vs. DCM group.

DISCUSSION

Dyslipidemia is a major contributor to the pathological process of DCM, and the main therapeutic methods involve lowering lipid (Meikle and Summers, 2017). In the present study, we explored the association between altered lipidomic profiling and cardiac dysfunction in the diabetic rats, as well as the regulation of berberine.

Current lipid parameters commonly used clinically are including TG, TCH, high-density lipoprotein and low-density lipoprotein cholesterol, which provide a relative narrow snapshot of the dynamic processes of lipid metabolism (Wong et al., 2013; Meikle et al., 2014). The application of lipidomics analyzed approach has been greatly expanding our understanding of the extent and complexity of lipid dysregulation in diabetes and its complications (Meikle and Summers, 2017). Lipidomics has been used to explore the physiological functions of lipid molecules (Hu and Zhang, 2018), and it was also applied to discover the biomarkers for diagnosis and therapy of metabolic disease (Meikle et al., 2014; Hu and Zhang, 2018).

The use of HPLC increases the sensitivity for low abundance lipids and their metabolites (Zhao et al., 2015). Identification of lipid metabolites in this method is achieved on the basis of searching for accurate mass-to-charge ratios from databases

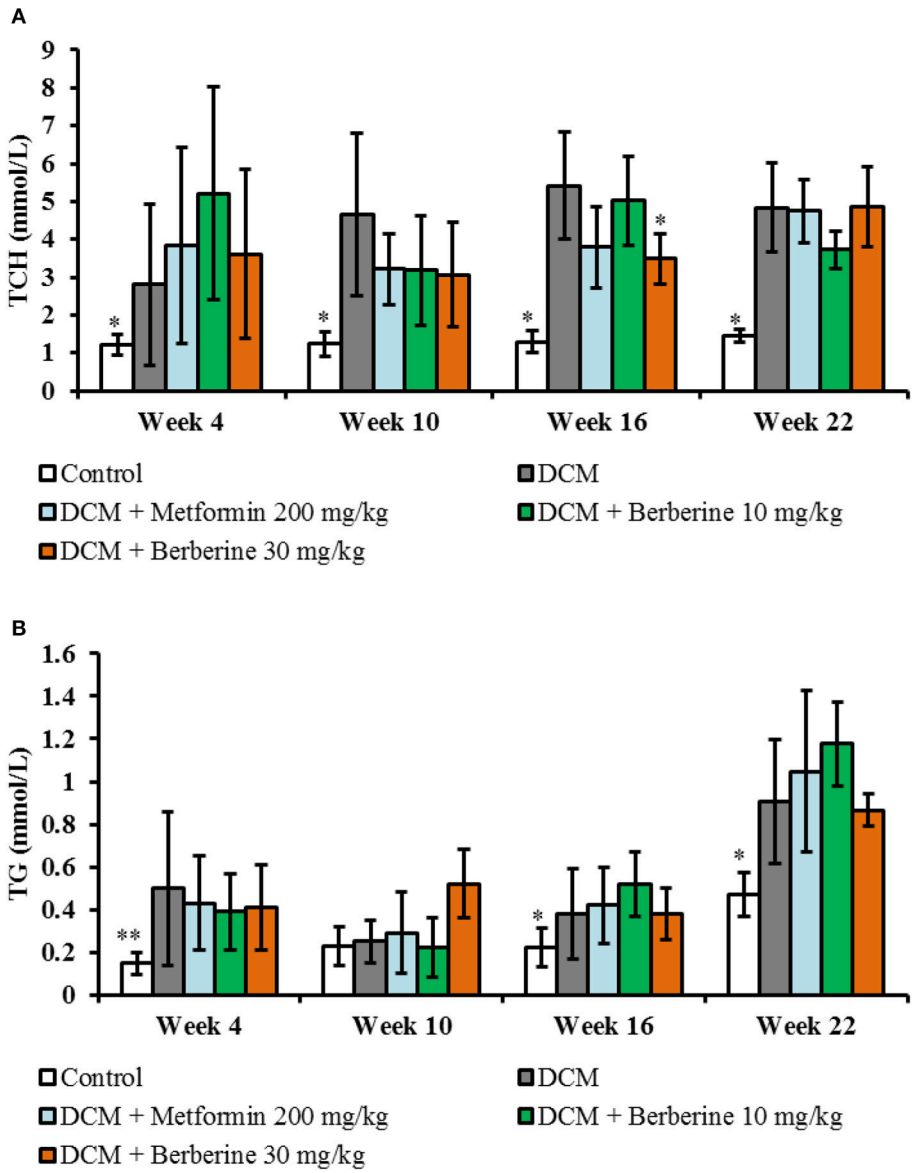

FIGURE 4 | Blood lipid parameters. **(A)** Dynamic changes of total cholesterol. **(B)** Dynamic changes of triglyceride. TCH, total cholesterol; TG, triglyceride; DCM, diabetic cardiomyopathy. Data are presented as mean ± SD, with $n = 7\sim12$. Statistical significance was evaluated by one-way ANOVA followed by LSD *post-hoc* test. $^{*}P < 0.05$, $^{**}P < 0.01$ vs. DCM model group.

of known lipids and further tandem mass spectrometry based experiments (Nygren et al., 2011; Meikle et al., 2014). This approach has been applied for the analysis of plasma and serum in depicting the pathophysiological mechanism of disease (Laaksonen et al., 2006; Yetukuri et al., 2011; Meikle et al., 2014). Furthermore, when investigating the molecular mechanisms of diseases, and the metabolic changes induced by pathophysiological stress are considered to be more concentrated in some specific organs of localized diseases such as DCM, the use of related organs in this platform are useful (Nam et al., 2017; Hu and Zhang, 2018).

Our previous research indicated that berberine at 30 mg/kg orally administered for 6 weeks could attenuate cardiac dysfunction and cardiac hypertrophy in rats induced by feeding high-sucrose/fat diet plus i.p. injection with streptozotocin (30 mg/kg) through alleviating cardiac lipid accumulation and promoting glucose transport (Dong et al., 2011). Then, we used UPLC/Q-TOF/MS analyzed approach to explore the changes of myocardial lipidomic profiles in diabetic rats. And the results manifested that the cardiac lipid metabolites have remarkable correlation with changes of cardiac function and heart mass ratio (Dong et al., 2017).

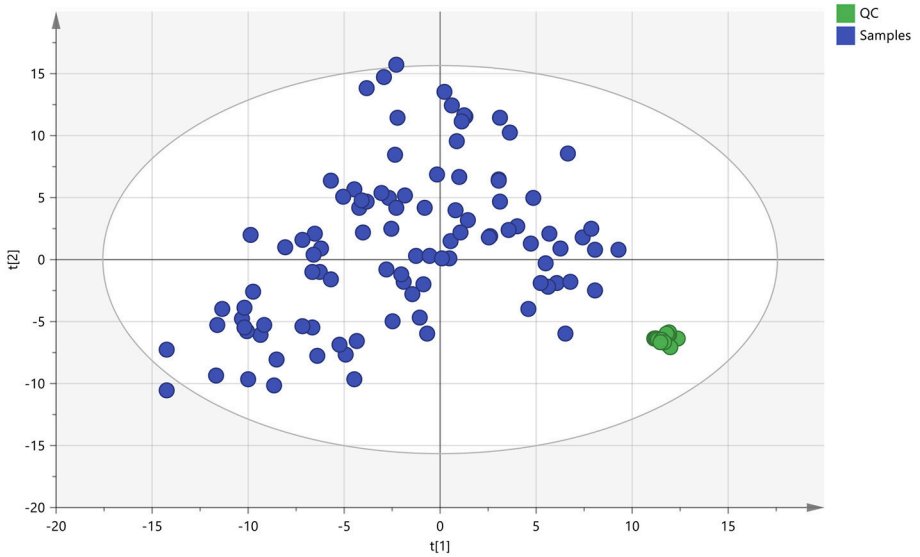

FIGURE 5 | The PCA scores plot of QC and On-test Samples. Quality control (QC) samples were applied to exhibit the stability of the liquid chromatography-mass spectrometer (LC-MS) system. The cluster of the quality control samples in the principal component analysis scores scatter plot showed a satisfactory stability and repeatability of this lipidomic analysis approach. The colors display the subjects from different groups. ●: QC, quality control; ●, Test samples.

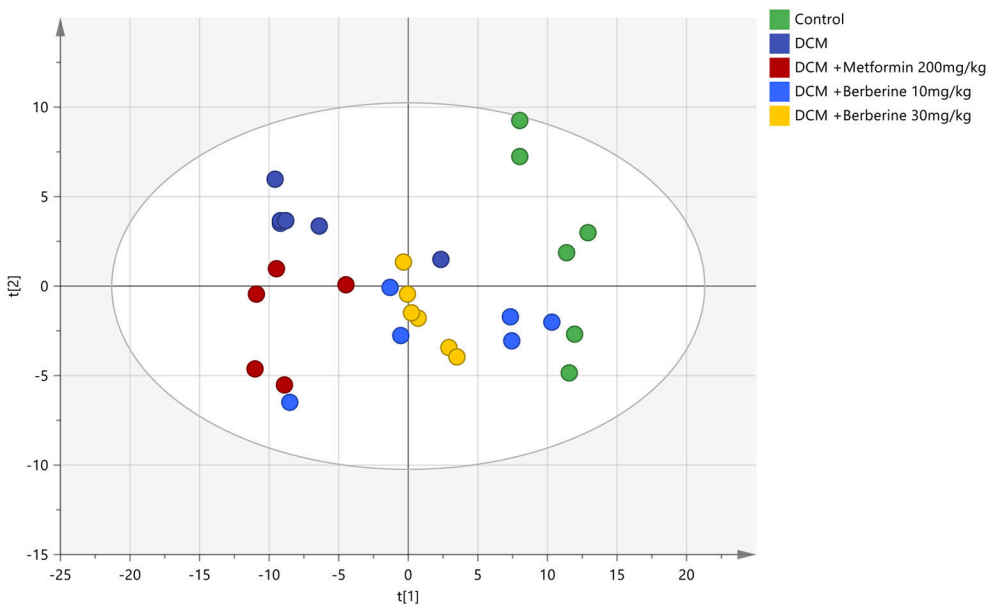

FIGURE 6 | The PCA scores plot of five groups. DCM, diabetic cardiomyopathy. The colors display the subjects from different groups. ●, Control; ●, DCM; ●, DCM + Metformin 200 mg/kg; ●, DCM + Berberine 10 mmg/kg; ●, DCM + Berberine 30 mg/kg.

In this study, we observed dynamic changes of cardiac functions, heart mass ratios and blood lipids at week 4, 10, 16, and 22, respectively. And the results demonstrated that berberine could protect against cardiac diastolic and systolic dysfunctions, as well as cardiac hypertrophy, and the most effective duration is with 16-week administration. In addition, 17 potential biomarkers of phosphatidylcholines (PCs), phosphatidylethanolamine (PEs) and sphingolipid (SMs) of DCM induced by HSFD/STZ have been identified. Furthermore, our results manifested that the perturbations could be partly reversed by berberine intervention, i.e., PC (18:0/18:2), PC (18:2/0:0), PC (16:0/20:4), PC (18:0/22:5), PC (20:4/0:0), PC (20:4/18:0), PC (20:4/18:1), PC (20:4/20:2), PE (18:2/0:0), and SM (d18:0/16:0).

Many phospholipid and sphingolipid metabolites have been proved to be important components linking obesity to type

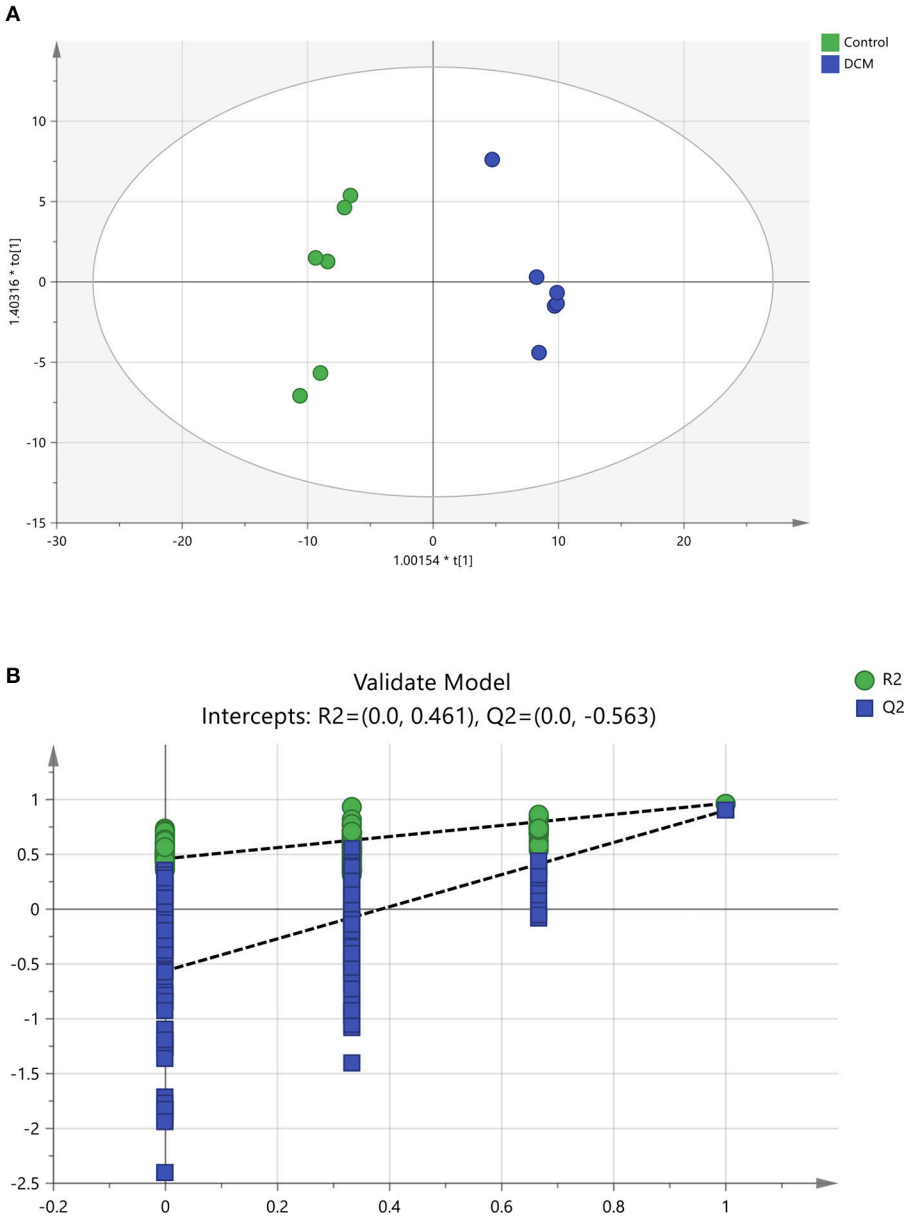

FIGURE 7 | The OPLS-DA scores scatter plot and validation plot. **(A)** The orthogonal projection to latent structures discriminant analysis (OPLS-DA) scores scatter plot obtained from the diabetic cardiomyopathy (DCM) group vs. control group. **(B)** Validation plot for OPLS-DA model. The permutation test was conducted for 200 times to evaluate the risk of over-fitting for the OPLS-DA model. DCM, diabetic cardiomyopathy. **(A)** ●, Control, ●, DCM model group; **(B)** ●, R^2, ■, Q^2.

2 DM and cardiovascular diseases (Meikle and Summers, 2017). The major components of the phospholipids involve the phosphatidylcholines (PCs) and phosphatidylethanolamines (PEs).

As the major constituents of the biologic membranes, the phospholipids can prevent the stability of cell membrane degeneration and promote recovery via improving cell membrane, protecting cells and mitochondria membrane against injury, promoting synthesis of lipoproteins, and increasing membrane fluidity and enzyme activities (Morrison et al., 2012; Zhang et al., 2014). Phospholipids also allow selected molecules to diffuse or move across the cell membrane into cells (Bishop and Bell, 1988; Zhang et al., 2014). And the membrane phospholipids are also the reservoir of lipid mediators and signaling molecules such as arachidonic acid (AA), prostaglandins, inositol triphosphate, endocannabinoids, and diacylglycerol (Lamari et al., 2013).

Besides important role involved in many cell processes, the phospholipids are the probable modulators of cardiac muscle insulin resistance rather than diacyglycerol or triacyglycerol

TABLE 3 | Identification of potential biomarkers related to development of diabetic cardiomyopathy rats.

No.	t_R (min)	Mass-to-charge (m/z) ratios	Metabolites	DCM vs. CON			MET 200 vs. DCM		BER 10 vs. DCM		BER 30 vs. DCM	
				VIP values	*P*-values	FC values	*P*-values	FC values	*P*-values	FC values	*P*-values	FC values
1	12.0796	786.60079	PC(18:0/18:2)	3.006781	1.32E-07	3.0068	0.327604	1.0807	0.013098	0.7619	0.027139	0.6058
2	1.5160	520.34032	PC(18:2/0:0)	2.690564	0.000507	2.6906	0.555070	1.1357	0.016675	0.5969	0.025931	0.5989
3	3.0185	466.32977	PE(P-18:0/0:0)	3.347361	1.62E-06	3.3474	0.307410	0.8457	0.005106	0.7163	0.450433	0.9335
4	1.5517	478.29289	PE(18:2/0:0)	2.142614	0.022380	2.1426	0.767972	1.0863	0.029045	0.4881	0.024280	0.4366
5	8.7803	705.59059	SM(d18:0/16:0)	3.805205	1.21E-06	3.8052	0.245808	0.8385	0.000135	0.5423	0.000020	0.3671
6	8.3575	729.59056	SM(d18:1/18:1)	2.043793	5.34E-05	2.0438	0.163162	0.8610	0.603399	0.9569	0.416094	0.9196
7	8.1461	706.53886	PC(16:0/14:0)	3.403970	3.14E-06	0.2938	0.000664	0.5270	0.609048	1.0346	0.796824	1.4075
8	10.8241	734.57009	PC(16:0/16:0)	2.064071	2.48E-06	0.4845	0.011311	0.7546	0.394074	0.9302	0.746697	1.0889
9	8.7446	782.56980	PC(16:0/20:4)	3.218626	3.24E-05	0.3107	0.197687	0.6865	0.048580	1.3616	0.211812	1.5514
10	11.8139	836.61668	PC(18:0/22:5)	2.477047	0.000951	0.4037	0.144162	0.5809	0.018528	1.6424	0.074504	2.3522
11	1.3903	544.34034	PC(20:4/0:0)	4.333849	7.64E-05	0.2307	0.736446	0.8593	0.017967	1.8425	0.077411	3.1387
12	11.6239	810.60078	PC(20:4/18:0)	2.534677	0.000301	0.3945	0.327411	0.7201	0.007459	1.7659	0.128390	1.7546
13	9.0317	808.58519	PC(20:4/18:1)	2.578941	0.000242	0.3878	0.218952	0.6849	0.035153	1.4237	0.197382	1.6132
14	7.3106	806.56949	PC(20:4/18:2)	2.010264	0.001226	0.4974	0.153197	0.6732	0.153344	1.2372	0.917770	1.0087
15	10.8527	834.60065	PC(20:4/20:2)	3.423473	0.000324	0.2921	0.124597	0.5275	0.010437	1.8687	0.100724	2.6785
16	6.8407	830.56954	PC(20:4/20:4)	2.833827	8.79E-05	0.3529	0.031543	0.5630	0.052507	1.3728	0.225158	1.6431
17	9.2859	740.52268	PE(20:4/16:0)	1.919220	8.79E-05	0.5210	0.059134	0.7180	0.207394	1.1066	0.781551	1.1054

t_R, retention time; VIP, variable important in the projection; FC, folder change; PC, phosphatidylcholine; PE, phosphatidylethanolamine; SM, sphingolipid; CON, control group; DCM, diabetic cardiomyopathy model group; MET 200, DCM + Metformin 200 mg/kg group; BER 10, DCM + Berberine 10 mg/kg group; BER 30, DCM + Berberine 30 mg/kg group.

(Quehenberger et al., 2010). Lots of evidences indicated the significance of impaired phospholipid-mediated signaling systems in DCM, heart failure and cardiac hypertrophy (Tabbi-Anneni et al., 2003). Also, *in vitro* and *in vivo* studies have confirmed the association between dysregulated phospholipid metabolism and cardiac lipotoxicity in DCM (Lim et al., 2011).

A plasma lipidomic study in humans indicated a relationship of PC species with risk measures of metabolic diseases, and PC (32:1) and PC (38:3) were associated with a high risk of metabolic syndrome (Kulkarni et al., 2013). There were 45 glycerophospholipid and sphingolipid (SM) species observed reduced in the coronary artery disease (Sutter et al., 2016). A population-based research indicated that serum PC (18:2/0:0) was associated with several cardiovascular disease-risk factors in adolescents (Syme et al., 2016). Serum lipid metabolites PC (18:0/18:2) and PC (16:0/14:0) were observed reduced from pre-diabetes to diabetes (Zeng et al., 2017). A clinical observation showed a persistent lipid signature with higher levels of plasma TGs, and diacylphospholipids as well as lower levels of alkylacyl phosphatidylcholines in progress to type 2 DM (Suvitaival et al., 2018). And plasma SM (d18:1/18:1) was significantly decreased in type 1 diabetic patients relative to controls (Sorensen et al., 2010). The myocardial phosphatidylinositol mass increased by 46%, and 1-stearoyl-2-arachidonoyl phosphatidylethanolamine decreased

FIGURE 8 | continued.

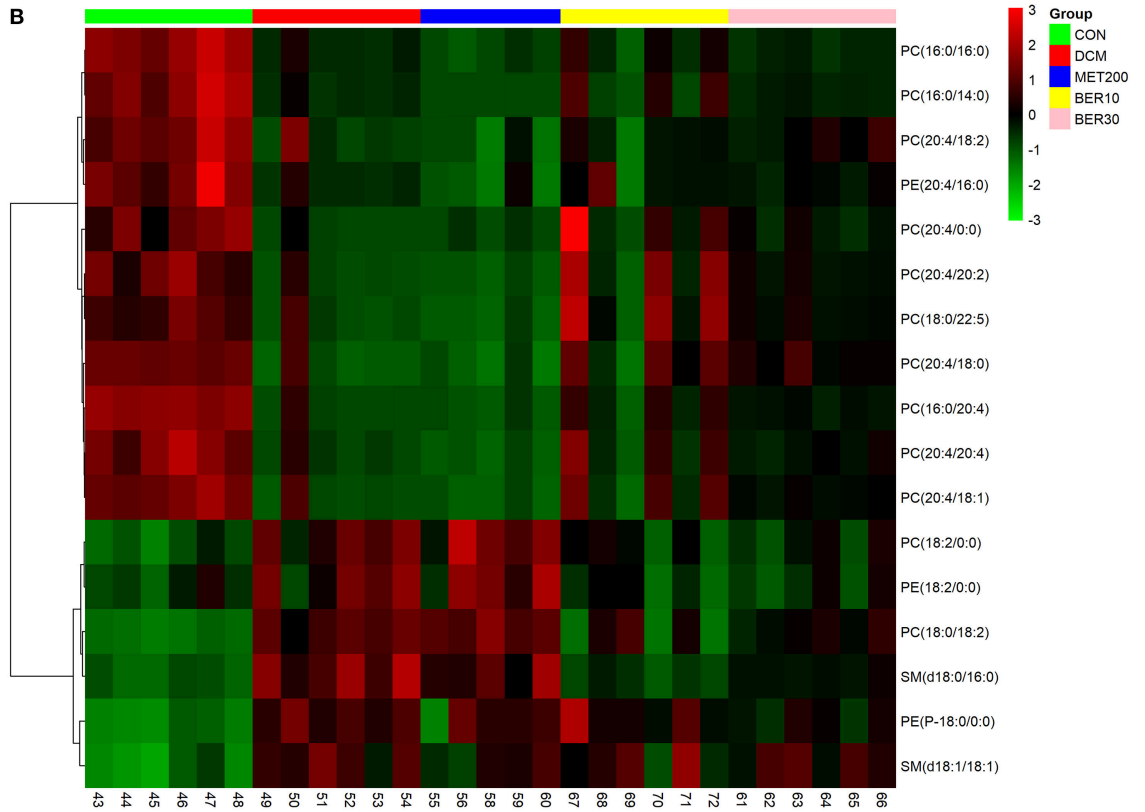

FIGURE 8 | Identification of potential biomarkers related to diabetic cardiomyopathy development. **(A)** Metabolic changes of lipids in the five test groups. **(B)** Heat map. Only metabolites with VIP > 1 and P <0.05 were selected, and different shades of color present the concentration (red, black, and green presented the high, normal, and low concentration, respectively). CON, control group; DCM, diabetic cardiomyopathy model group; MET 200, DCM + Metformin 200 mg/kg group; BER 10, DCM + Berberine 10 mg/kg group; BER 30, DCM + Berberine 30 mg/kg group; PC, phosphatidylcholine; PE, phosphatidylethanolamine; SM, sphingolipid. Statistical significance was evaluated by one-way ANOVA followed by LSD *post-hoc* test. $^{*}P < 0.05$, $^{**}P < 0.01$, and $^{***}P < 0.001$ vs. DCM group.

by 22% in diabetic rats induced by STZ (Han et al., 2000). The *easily shocked* (*eas*) mutant heart in *Drosophila* exhibited defects in cardiac physiology, including reduction in diastolic and systolic diameters, as well as heartbeat length and the absolute volume output, and exhibited increased concentrations of TG, and low levels of PE, which suggested that lipid metabolism and cardiac function could be regulated by phospholipid homeostasis (Lim et al., 2011).

And it has been confirmed that the maintenance of the balance of the PC: PE ratio has important health potentials (Korematsu et al., 2017). Blood-based lipidomic studies in humans showed a strong association of reduced PC: PE ratio with obesity, type 2 DM and prediabetes (Meikle et al., 2013; Weir et al., 2013; Henstridge et al., 2015).

In terms of diabetic cardiomyopathy, the cardiomyopathic status such as cardiac hypertrophy, fibrosis, and cell death induced by both hyperglycemia and cardiac metabolic imbalance can lead to abnormal Ca^{2+} transients and contractile activity. The cellular ion homeostasis imbalance and changes of contractile proteins can impair the excitation-contraction coupling, and potential of autonomic responsiveness and autonomic neuropathy. Also, the structural abnormalities occur (Tappia, 2007). The lipid metabolites, especially the main components of cardiomyocytes membrane such as phosphatidylcholine and phosphatidylethanolamine are closely related to intracellular ion homeostasis, which may contribute to the structural and functional alterations in the diabetic heart (Ussher et al., 2016; Meikle and Summers, 2017). Insulin treatment of diabetic rats could restore the species profile of phosphatidylethanolamines and overcorrect the changes in molecular species of phosphatidylcholines (Vecchini et al., 2000), which suggested that the abnormal in molecular species of glycerophospholipids may play an important role in membrane dysfunction and defective contractility of the diabetic heart (Vecchini et al., 2000; Tappia, 2007).

CONCLUSIONS

Our results indicated a close relationship between PCs, PEs, and SMs and cardiac damage mechanisms during development of DCM. And the therapeutic effects of berberine on DCM are partly due to interferences with PC, PE, and SM metabolisms.

AVAILABILITY OF DATA AND SUPPORTING MATERIALS

The datasets used and analyzed during the current study available from the corresponding author or the first author on reasonable request.

AUTHOR CONTRIBUTIONS

JS and SD designed experiments. RZ, SZ, LC, ZC, and SD performed experiments. FS and RZ performed UPLCQ-TOF/MS analysis. LT and SD conducted statistical analysis. SD wrote this paper. And all authors read and approved the final manuscript.

FUNDING

This paper was supported by the National Natural Science Foundation of China (Grant No. 81503287, 81430094), Natural Science Foundation of Beijing Municipality (Grant No. 7174312, 7144222), and Doctoral Program Foundation of Institutions of Higher Education of China (Grant No. 20130013 120002).

REFERENCES

Bai, X. J., Hao, J. T., Wang, J., Zhang, W. F., Yan, C. P., Zhao, J. H., et al. (2018). Curcumin inhibits cardiac hypertrophy and improves cardiovascular function via enhanced Na^{+}/Ca^{2+} exchanger expression after transverse abdominal aortic constriction in rats. *Pharmacol. Rep.* 70, 60–68. doi: 10.1016/j.pharep.2017.07.014

Bakshi, M. V., Azimzadeh, O., Barjaktarovic, Z., Kempf, S. J., Merl-Pham, J., Hauck, S. M., et al. (2015). Total body exposure to low-dose ionizing radiation induces long-term alterations to the liver proteome of neonatally exposed mice. *J. Proteome Res.* 14, 366–373. doi: 10.1021/pr500890n

Bishop, W. R., and Bell, R. M. (1988). Assembly of phospholipids into cellular membranes: biosynthesis, transmembrane movement and intracellular translocation. *Annu. Rev. Cell Biol.* 4, 579–610. doi: 10.1146/annurev.cb.04.110188.003051

Boles, A., Kandimalla, R., and Reddy, P. H. (2017). Dynamics of diabetes and obesity: epidemiological perspective. *Biochim. Biophys. Acta* 1863, 1026–1036. doi: 10.1016/j.bbadis.2017.01.016

Chan, J. C., Zhang, Y., and Ning, G. (2014). Diabetes in China: a societal solution for a personal challenge. *Lancet Diabetes Endocrinol.* 2, 969–979. doi: 10.1016/S2213-8587(14)70144-5

Chang, X., Wang, Z., Zhang, J., Yan, H., Bian, H., Xia, M., et al. (2016). Lipid profiling of the therapeutic effects of berberine in patients with nonalcoholic fatty liver disease. *J. Transl. Med.* 14:266. doi: 10.1186/s12967-016-0982-x

Cicero, A. F., and Baggioni, A. (2016). Berberine and its role in chronic disease. *Adv. Exp. Med. Biol.* 928, 27–45. doi: 10.1007/978-3-319-41334-1_2

Dong, S. F., Hong, Y., Liu, M., Hao, Y. Z., Yu, H. S., Liu, Y., et al. (2011). Berberine attenuates cardiac dysfunction in hyperglycemic and hypercholesterolemic rats. *Eur. J. Pharmacol.* 660, 368–374. doi: 10.1016/j.ejphar.2011.03.024

Dong, S., Zhang, R., Liang, Y., Shi, J., Li, J., Shang, F., et al. (2017). Changes of myocardial lipidomics profiling in a rat model of diabetic cardiomyopathy using UPLC/Q-TOF/MS analysis. *Diabetol. Metab. Syndr.* 9:56. doi: 10.1186/s13098-017-0249-6

Dunn, W. B., Broadhurst, D., Begley, P., Zelena, E., Francis-Mcintyre, S., Anderson, N., et al. (2011). Procedures for large-scale metabolic profiling of serum and plasma using gas chromatography and liquid chromatography coupled to mass spectrometry. *Nat. Protoc.* 6, 1060–1083. doi: 10.1038/nprot.2011.335

Han, X., Abendschein, D. R., Kelley, J. G., and Gross, R. W. (2000). Diabetes-induced changes in specific lipid molecular species in rat myocardium. *Biochem. J.* 352(Pt 1), 79–89. doi: 10.1042/bj3520079

Henstridge, D. C., Estevez, E., Allen, T. L., Heywood, S. E., Gardner, T., Yang, C., et al. (2015). Genetic manipulation of cardiac Hsp72 levels does not alter substrate metabolism but reveals insights into high-fat feeding-induced cardiac insulin resistance. *Cell Stress Chaperones* 20, 461–472. doi: 10.1007/s12192-015-0571-6

Hu, T., and Zhang, J. L. (2018). Mass-spectrometry-based lipidomics. *J. Sep. Sci.* 41, 351–372. doi: 10.1002/jssc.201700709

Huang, D., Refaat, M., Mohammedi, K., Jayyousi, A., Al Suwaidi, J., and Abi Khalil, C. (2017). Macrovascular complications in patients with diabetes and prediabetes. *Biomed. Res. Int.* 2017:7839101. doi: 10.1155/2017/7839101

Huynh, K., Bernardo, B. C., McMullen, J. R., and Ritchie, R. H. (2014). Diabetic cardiomyopathy: mechanisms and new treatment strategies targeting antioxidant signaling pathways. *Pharmacol. Ther.* 142, 375–415. doi: 10.1016/j.pharmthera.2014.01.003

Ingelfinger, J. R., and Jarcho, J. A. (2017). Increase in the incidence of diabetes and its implications. *N. Engl. J. Med.* 376, 1473–1474. doi: 10.1056/NEJMe1616575

Jia, G., Hill, M. A., and Sowers, J. R. (2018). Diabetic cardiomyopathy: an update of mechanisms contributing to this clinical entity. *Circ. Res.* 122, 624–638. doi: 10.1161/CIRCRESAHA.117.311586

Jiang, D., Wang, D., Zhuang, X., Wang, Z., Ni, Y., Chen, S., et al. (2016). Berberine increases adipose triglyceride lipase in 3T3-L1 adipocytes through the AMPK pathway. *Lipids Health Dis.* 15:214. doi: 10.1186/s12944-016-0383-4

Kong, W., Wei, J., Abidi, P., Lin, M., Inaba, S., Li, C., et al. (2004). Berberine is a novel cholesterol-lowering drug working through a unique mechanism distinct from statins. *Nat. Med.* 10, 1344–1351. doi: 10.1038/nm1135

Korematsu, S., Yamada, H., Miyahara, H., and Ihara, K. (2017). Increased levels of anti-phosphatidylcholine and anti-phosphatidylethanolamine antibodies in pediatric patients with cerebral infarction. *Brain Dev.* 39, 542–546. doi: 10.1016/j.braindev.2017.01.010

Kulkarni, H., Meikle, P. J., Mamtani, M., Weir, J. M., Barlow, C. K., Jowett, J. B., et al. (2013). Variability in associations of phosphatidylcholine molecular species with metabolic syndrome in Mexican-American families. *Lipids* 48, 497–503. doi: 10.1007/s11745-013-3781-7

Laaksonen, R., Katajamaa, M., Paiva, H., Sysi-Aho, M., Saarinen, L., Junni, P., et al. (2006). A systems biology strategy reveals biological pathways and plasma biomarker candidates for potentially toxic statin-induced changes in muscle. *PLoS ONE* 1:e97. doi: 10.1371/journal.pone.0000097

Lamari, F., Mochel, F., Sedel, F., and Saudubray, J. M. (2013). Disorders of phospholipids, sphingolipids and fatty acids biosynthesis: toward a new category of inherited metabolic diseases. *J. Inherit. Metab. Dis.* 36, 411–425. doi: 10.1007/s10545-012-9509-7

Li, X. X., Li, C. B., Xiao, J., Gao, H. Q., Wang, H. W., Zhang, X. Y., et al. (2015). Berberine attenuates vascular remodeling and inflammation in a rat model of metabolic syndrome. *Biol. Pharm. Bull.* 38, 862–868. doi: 10.1248/bpb.b14-00828

Lim, H. Y., Wang, W., Wessells, R. J., Ocorr, K., and Bodmer, R. (2011). Phospholipid homeostasis regulates lipid metabolism and cardiac function through SREBP signaling in Drosophila. *Genes Dev.* 25, 189–200. doi: 10.1101/gad.1992411

Loffroy, R., Bernard, S., Serusclat, A., Boussel, L., Bonnefoy, E., D'athis, P., et al. (2009). Noninvasive assessment of the prevalence and characteristics of coronary atherosclerotic plaques by multidetector computed tomography in asymptomatic type 2 diabetic patients at high risk of significant coronary artery disease: a preliminary study. *Arch. Cardiovasc. Dis.* 102, 607–615. doi: 10.1016/j.acvd.2009.04.007

Ma, R. C. W., Tsoi, K. Y., Tam, W. H., and Wong, C. K. C. (2017). Developmental origins of type 2 diabetes: a perspective from China. *Eur. J. Clin. Nutr.* 71, 870–880. doi: 10.1038/ejcn.2017.48

Meikle, P. J., and Summers, S. A. (2017). Sphingolipids and phospholipids in insulin resistance and related metabolic disorders. *Nat. Rev. Endocrinol.* 13, 79–91. doi: 10.1038/nrendo.2016.169

Meikle, P. J., Wong, G., Barlow, C. K., and Kingwell, B. A. (2014). Lipidomics: potential role in risk prediction and therapeutic monitoring for diabetes and cardiovascular disease. *Pharmacol. Ther.* 143, 12–23. doi: 10.1016/j.pharmthera.2014.02.001

Meikle, P. J., Wong, G., Barlow, C. K., Weir, J. M., Greeve, M. A., Macintosh, G. L., et al. (2013). Plasma lipid profiling shows similar associations with prediabetes and type 2 diabetes. *PLoS ONE* 8:e74341. doi: 10.1371/journal.pone.0074341

Morrison, K., Witte, K., Mayers, J. R., Schuh, A. L., and Audhya, A. (2012). Roles of acidic phospholipids and nucleotides in regulating membrane binding and activity of a calcium-independent phospholipase A2 isoform. *J. Biol. Chem.* 287, 38824–38834. doi: 10.1074/jbc.M112.391508

Nam, M., Jung, Y., Ryu, D. H., and Hwang, G. S. (2017). A metabolomics-driven approach reveals metabolic responses and mechanisms in the rat heart following myocardial infarction. *Int. J. Cardiol.* 227, 239–246. doi: 10.1016/j.ijcard.2016.11.127

Nygren, H., Seppanen-Laakso, T., Castillo, S., Hyotylainen, T., and Oresic, M. (2011). Liquid chromatography-mass spectrometry (LC-MS)-based lipidomics for studies of body fluids and tissues. *Methods Mol. Biol.* 708, 247–257. doi: 10.1007/978-1-61737-985-7_15

Palomer, X., Salvado, L., Barroso, E., and Vazquez-Carrera, M. (2013). An overview of the crosstalk between inflammatory processes and metabolic dysregulation during diabetic cardiomyopathy. *Int. J. Cardiol.* 168, 3160–3172. doi: 10.1016/j.ijcard.2013.07.150

Qian, Y., Peng, Y., Shang, E., Zhao, M., Yan, L., Zhu, Z., et al. (2017). Metabolic profiling of the hepatotoxicity and nephrotoxicity of Ginkgolic acids in rats using ultra-performance liquid chromatography-high-definition mass spectrometry. *Chem. Biol. Interact.* 273, 11–17. doi: 10.1016/j.cbi.2017.05.020

Quehenberger, O., Armando, A. M., Brown, A. H., Milne, S. B., Myers, D. S., Merrill, A. H., et al. (2010). Lipidomics reveals a remarkable diversity of lipids in human plasma. *J. Lipid Res.* 51, 3299–3305. doi: 10.1194/jlr.M009449

Reis, F., Rocha, L., Ponte, L., Alcobia, T., Almeida, L., Costa-Almeida, C., et al. (2005). Effect of preventive and regressive isosorbide 5-mononitrate treatment on catecholamine levels in plasma, platelets, adrenals, left ventricle and aorta in cyclosporin a-induced hypertensive rats. *Life Sci.* 77, 2514–2528. doi: 10.1016/j.lfs.2005.01.032

Ruiz, M., Coderre, L., Allen, B. G., and Des Rosiers, C. (2018). Protecting the heart through MK2 modulation, toward a role in diabetic cardiomyopathy and lipid metabolism. *Biochim. Biophys. Acta* 1864, 1914–1922. doi: 10.1016/j.bbadis.2017.07.015

Saigusa, D., Okamura, Y., Motoike, I. N., Katoh, Y., Kurosawa, Y., Saijyo, R., et al. (2016). Establishment of protocols for global metabolomics by LC-MS for biomarker discovery. *PLOS ONE* 11:e0160555. doi: 10.1371/journal.pone.0160555

Saigusa, D., Suzuki, N., Matsumoto, Y., Umeda, K., Tomioka, Y., Koshiba, S., et al. (2018). Detection of novel metabolite for Roxadustat doping by global metabolomics. *J. Biochem.* 163:e1. doi: 10.1093/jb/mvy036

Sorensen, C. M., Ding, J., Zhang, Q., Alquier, T., Zhao, R., Mueller, P. W., et al. (2010). Perturbations in the lipid profile of individuals with newly diagnosed type 1 diabetes mellitus: lipidomics analysis of a Diabetes antibody standardization program sample subset. *Clin. Biochem.* 43, 948–956. doi: 10.1016/j.clinbiochem.2010.04.075

Sun, Y., Yuan, X., Zhang, F., Han, Y., Chang, X., Xu, X., et al. (2017). Berberine ameliorates fatty acid-induced oxidative stress in human hepatoma cells. *Sci. Rep.* 7:11340. doi: 10.1038/s41598-017-11860-3

Sutter, I., Klingenberg, R., Othman, A., Rohrer, L., Landmesser, U., Heg, D., et al. (2016). Decreased phosphatidylcholine plasmalogens–a putative novel lipid signature in patients with stable coronary artery disease and acute myocardial infarction. *Atherosclerosis* 246, 130–140. doi: 10.1016/j.atherosclerosis.2016.01.003

Suvitaival, T., Bondia-Pons, I., Yetukuri, L., Poho, P., Nolan, J. J., Hyotylainen, T., et al. (2018). Lipidome as a predictive tool in progression to type 2 diabetes in finnish men. *Metabolism* 78, 1–12. doi: 10.1016/j.metabol.2017.08.014

Syme, C., Czajkowski, S., Shin, J., Abrahamowicz, M., Leonard, G., Perron, M., et al. (2016). Glycerophosphocholine metabolites and cardiovascular disease risk factors in adolescents: a cohort study. *Circulation* 134, 1629–1636.doi: 10.1161/CIRCULATIONAHA.116.022993

Tabbi-Anneni, I., Helies-Toussaint, C., Morin, D., Bescond-Jacquet, A., Lucien, A., and Grynberg, A. (2003). Prevention of heart failure in rats by trimetazidine treatment: a consequence of accelerated phospholipid turnover? *J. Pharmacol. Exp. Ther.* 304, 1003–1009. doi: 10.1124/jpet.102.042143

Tappia, P. S. (2007). Phospholipid-mediated signaling systems as novel targets for treatment of heart disease. *Can. J. Physiol. Pharmacol.* 85, 25–41. doi: 10.1139/y06-098

Trachanas, K., Sideris, S., Aggeli, C., Poulidakis, E., Gatzoulis, K., Tousoulis, D., et al. (2014). Diabetic cardiomyopathy: from pathophysiology to treatment. *Hellenic J. Cardiol.* 55, 411–421.

Ussher, J. R., Elmariah, S., Gerszten, R. E., and Dyck, J. R. (2016). The emerging role of metabolomics in the diagnosis and prognosis of cardiovascular disease. *J. Am. Coll. Cardiol.* 68, 2850–2870. doi: 10.1016/j.jacc.2016.09.972

Vecchini, A., Del Rosso, F., Binaglia, L., Dhalla, N. S., and Panagia, V. (2000). Molecular defects in sarcolemmal glycerophospholipid subclasses in diabetic cardiomyopathy. *J. Mol. Cell. Cardiol.* 32, 1061–1074. doi: 10.1006/jmcc.2000.1140

Wang, H., Zhu, C., Ying, Y., Luo, L., Huang, D., and Luo, Z. (2018). Metformin and berberine, two versatile drugs in treatment of common metabolic diseases. *Oncotarget* 9, 10135–10146. doi: 10.18632/oncotarget.20807

Want, E. J., Masson, P., Michopoulos, F., Wilson, I. D., Theodoridis, G., Plumb, R. S., et al. (2013). Global metabolic profiling of animal and human tissues via UPLC-MS. *Nat. Protoc.* 8, 17–32. doi: 10.1038/nprot.2012.135

Weir, J. M., Wong, G., Barlow, C. K., Greeve, M. A., Kowalczyk, A., Almasy, L., et al. (2013). Plasma lipid profiling in a large population-based cohort. *J. Lipid Res.* 54, 2898–2908. doi: 10.1194/jlr.P035808

Wong, G., Barlow, C. K., Weir, J. M., Jowett, J. B., Magliano, D. J., Zimmet, P., et al. (2013). Inclusion of plasma lipid species improves classification of individuals at risk of type 2 diabetes. *PLoS ONE* 8:e76577. doi: 10.1371/journal.pone.0076577

Xu, J., Tang, L. Y., Zhang, Q., Wei, J. Y., Xian, M. H., Zhao, Y., et al. (2017). Relative quantification of neuronal polar lipids by UPLC-MS reveals the brain protection mechanism of Danhong injection. *Rsc Adv.* 7, 45746–45756. doi: 10.1039/C7RA09245H

Xu, Y., Wang, L., He, J., Bi, Y., Li, M., Wang, T., et al. (2013). Prevalence and control of diabetes in Chinese adults. *JAMA* 310, 948–959. doi: 10.1001/jama.2013.168118

Yetukuri, L., Huopaniemi, I., Koivuniemi, A., Maranghi, M., Hiukka, A., Nygren, H., et al. (2011). High density lipoprotein structural changes and drug response in lipidomic profiles following the long-term fenofibrate therapy in the FIELD substudy. *PLoS ONE* 6:e23589. doi: 10.1371/journal.pone.0023589

Zeng, H., Tong, R., Tong, W., Yang, Q., Qiu, M., Xiong, A., et al. (2017). Metabolic biomarkers for prognostic prediction of pre-diabetes: results from a longitudinal cohort study. *Sci. Rep.* 7:6575. doi: 10.1038/s41598-017-06309-6

Zhang, Y., Zou, W., Cui, F., Wang, N., Zhang, D., Cui, Y., et al. (2014). Protective effect of phosphatidylcholine on restoration of ethanol-injured hepatocytes related with caveolin-1. *J. Membr. Biol.* 247, 73–80. doi: 10.1007/s00232-013-9613-0

Zhao, Y. Y., Miao, H., Cheng, X. L., and Wei, F. (2015). Lipidomics: novel insight into the biochemical mechanism of lipid metabolism and dysregulation-associated disease. *Chem. Biol. Interact.* 240, 220–238. doi: 10.1016/j.cbi.2015.09.005

Conflict of Interest Statement: The authors declare that the research was conducted in the absence of any commercial or financial relationships that could be construed as a potential conflict of interest.

frontiers in Physiology

ORIGINAL RESEARCH
published: 13 March 2018
doi: 10.3389/fphys.2018.00209

Kisspeptin Receptor GPR54 Promotes Adipocyte Differentiation and Fat Accumulation in Mice

Tongtong Wang[1†], Xueqin Cui[1†], Ling Xie[1], Roumei Xing[1], Panpan You[1], Yongliang Zhao[1], Yiqing Yang[1], Yongqian Xu[1], Li Zeng[2], Huaqing Chen[1] and Mingyao Liu[1,3*]*

[1] Shanghai Key Laboratory of Regulatory Biology, Institute of Biomedical Sciences, School of Life Sciences, East China Normal University, Shanghai, China, [2] Bioray Laboratories Incorporation, Shanghai, China, [3] Department of Molecular and Cellular Medicine, Institute of Biosciences and Technology, Texas A&M University Health Science Center, Houston, TX, United States

GPR54, Kisspeptin-1 receptor (KISS1R), a member of rhodopsin family, plays a critical role in puberty development and has been proposed to be involved in regulation of energy metabolism. This study aims to explore the function of GPR54 in adipogenesis, lipid metabolism, and obesity in addition to its effect through hormones. Results showed that when fed a high-fat diet, the weight growth of castrated or ovariectomized *Gpr54*$^{-/-}$ mice was significantly slower than that of WT control, together with a lower triglyceride concentration. The ratio of white adipose tissue was lower, and average size of adipocytes was smaller in *Gpr54*$^{-/-}$ mice. Meanwhile, there were less adipose tissue macrophages (ATMs), especially pro-inflammatory macrophages. Expression of inflammatory related genes also indicated that inflammatory response caused by obesity was not as drastic in *Gpr54*$^{-/-}$ mice as in WT mice. Liver triglyceride in *Gpr54*$^{-/-}$ mice was reduced, especially in female mice. On the other hand, oil drop formation was accelerated when hepatocytes were stimulated by kisspeptin-10 (Kp-10). Primary mesenchymal stem cells (MSCs) of *Gpr54*$^{-/-}$ mice were less likely to differentiate into adipocytes. When stimulated by Kp-10, 3T3-L1 cell differentiation into adipocytes was accelerated and triglyceride synthesis was significantly promoted. These data indicated that GPR54 could affect obesity development by promoting adipocyte differentiation and triglyceride accumulation. To further elucidate the mechanism, genes related to lipid metabolism were analyzed. The expression of genes involved in lipid synthesis including PPARγ, ACC1, ADIPO, and FAS was significantly changed in *Gpr54*$^{-/-}$ mice. Among them PPARγ which also participate in adipocyte differentiation displayed a marked reduction. Moreover, phosphorylation of ERK, which involved in GPR54 signaling, was significantly decreased in *Gpr54*$^{-/-}$ mice, suggesting that GPR54 may promote lipid synthesis and obesity development by activating MAP kinase pathway. Therefore, in addition to the involvement in hormone regulation, our study demonstrated that GPR54 directly participates in obesity development by promoting adipocyte differentiation and fat accumulation. This provided evidence of involvement of GPR54 in lipid metabolism, and revealed new potentials for the identification and development of novel drug targets for metabolic diseases.

Keywords: GPR54, energy metabolism, obesity, adipocyte differentiation, MAP kinase

OPEN ACCESS

Edited by:
Jiqiu Wang,
School of Medicine, Shanghai Jiao Tong University, China

Reviewed by:
Markus Niessen,
University of Zurich, Switzerland
Mikael Rydén,
Karolinska Institute (KI), Sweden
Yao Li,
Fudan University, China

****Correspondence:***
Huaqing Chen
hqchen@bio.ecnu.edu.cn
Mingyao Liu
myliu@bio.ecnu.edu.cn

† These authors have contributed equally to this work as first authors.

Specialty section:
This article was submitted to Clinical and Translational Physiology, a section of the journal Frontiers in Physiology

Received: *24 October 2017*
Accepted: *23 February 2018*
Published: *13 March 2018*

Citation:
Wang T, Cui X, Xie L, Xing R, You P, Zhao Y, Yang Y, Xu Y, Zeng L, Chen H and Liu M (2018) Kisspeptin Receptor GPR54 Promotes Adipocyte Differentiation and Fat Accumulation in Mice. Front. Physiol. 9:209. doi: 10.3389/fphys.2018.00209

INTRODUCTION

Nowadays, obesity has become a global burden that seriously impairs the health and quality of people's life. Overweight or obesity is associated with abnormal fat accumulation, which is caused by imbalanced energy metabolism. Energy homeostasis is a complicated system involving many aspects of glucose or lipid metabolism including lipogenesis and lipolysis, glycolysis, and gluconeogenesis. When energy intake exceeds energy expenditure, the surplus energy will be stored as lipid and the body will become overweight. In addition to life style and eating habit, genetic factors such as mutations in genes like *ob* (Farooqi et al., 1998) and *MC4R* (You et al., 2016) were found to be involved in some of obesity development. More new genes related to obesity were identified (Locke et al., 2015; Liu et al., 2017). Chronic metabolic disturbance is directly associated with increasing prevalence of metabolic diseases including diabetes and cardiovascular diseases. It is urgent to identify key players in the metabolic pathways in order to develop potential targets that can be utilize as candidates for obesity treatment.

Kiss1 gene was identified when investigating metastasis of human melanoma cells (Lee et al., 1996). The product of *Kiss1*, kisspeptin, is a 54-aa peptide also known as metastin. It could split into smaller peptides including kisspeptin-10 (Kp-10), Kp-13, and Kp-14. The peptide share similar functions and activities. The specific receptor of kisspeptins, GPR54, belongs to the rhodopsin family (Ohtaki et al., 2001). The critical function of GPR54/KISS1 system in nervous-gonadal axis was first reported in 2003 (de Roux et al., 2003). Since then, more studies have demonstrated that GPR54/KISS1 plays an important role in puberty development (Gutiérrez-Pascual et al., 2007; Kauffman et al., 2007; Sonigo and Binart, 2012). Interestingly, in addition to high expression in pituitary gland and placenta (Kotani et al., 2001), GPR54 is also expressed in pancreas, brain, liver, and skeletal muscle (Kalamatianos et al., 2008). This indicates that GPR54 also play roles in other biological processes, especially in energy metabolism. Previous studies on GPR54/KISS1's function in metabolic system were mostly performed *in vitro*. Studies were focused on demonstrating differential expression of *Kiss1* gene in adipose tissue or hypothalamus under different situations or stimulations in an effort to show the potential involvement of *Kiss1* in energy metabolism. The results, however, were inconclusive. For example, adult rats showed a reduction in *Kiss1* mRNA and a decreased luteinizing hormone after fasting (Castellano et al., 2005; Brown et al., 2008). GPR54 expression was reduced in adult rats when fasted for 12–48 h, but increased in pubertal rats when fasted for 72 h (Castellano et al., 2005; Luque et al., 2007). Early in 1996, *Kiss1* gene was found highly expressed in pancreas and implied kisspeptins involvement in pancreativ activity (Lee et al., 1996). A series of studies showed that kisspeptins and their receptor co-localized in alpha and beta cells of pancreas (Hauge-Evans et al., 2006). It was also shown that Kp-54 and Kp-10 could stimulate primary pancreas cells to secret insulin (Hauge-Evans et al., 2006; Wahab et al., 2011). Yet, other studies reported that kisspeptins inhibited insulin secretion in a concentration dependent manner (Bowe et al., 2009; Vikman and Ahren, 2009). Data from *in vivo* studies were limited. A recent report stated that $Gpr54^{-/-}$ female mice displayed a heavier body weight and an impaired glucose tolerance (Tolson et al., 2014). On the contrary, another paper in the same year reported inhibition of *Kiss1* attenuated hyperglycemia. Increased kisspeptins were detected in both liver and serum of type 2 diabetes patients and mice (Song et al., 2014). This kind of variations in data from *in vitro* as well as *in vivo* studies implied that GPR54/KISS1 signaling might play a complex role, exerting different functions at different tissues, different stages, and under different biological conditions. Further investigations need to be carried out to help elucidating and understanding the different functions and mechanisms of GPR54/KISS1 signaling. In this study we mainly used castrated or ovariectomized $Gpr54^{-/-}$ mice in order to minimize hormone effects, and evaluated the direct functions of GPR54 in lipid metabolism, and the possible mechanism for the signaling pathway in adipose tissue. Results showed that GPR54 deficiency in mice led to slower body weight increase and reduced adipocyte differentiation. In *in vitro* cell system, GPR54/KISS1 activation led to enhanced adipocyte differentiation and triglyceride accumulation, suggesting involvement of GPR54/KISS1 signaling in adipogenesis, lipid metabolism, and obesity development, through a mechanism independent of sex hormone signaling.

MATERIALS AND METHODS

Animals

GPR54 deficient C57BL/6 mice were obtained from Dr. Eric L. Gustafson at Schering-Plow Research Institute (Kenilworth, NJ, USA). Genotyping was conducted by PCR as described previously (Funes et al., 2003). The genotypes of all animals were verified as correct (Supplementary Figure 1). Mice were bred and maintained at 4–5 per cage, in a constant room temperature (25°C) and photoperiod cycle (12 h light/12 h dark) in specific pathogen-free (SPF) level Laboratory at Animal Center of East China Normal University, with free access to water and food. To minimize hormone influence, mice were castrated (female ovariectomized) at 20–21 post-natal days under avertin anesthetization. This study was carried out in accordance with the recommendations of NIH guidelines. All protocols were approved by the institutional Animal Ethics Committee (permit No. m20140704).

Histological Analysis of Adipose Tissues

Mice were euthanized by cervical dislocation. Adipose tissue was excised and fixed overnight in 4% paraformaldehyde and embedded in paraffin. Sections at 4 μm were cut and stained by Hematoxylin and eosin (HE) for histological analysis. Digital images (200×) were captured from five random field per section using a Leica microscope, then analyzed using ImageJ software. To evaluate adipocyte size, a minimum of 100 independent mature adipocytes per mouse was measured. Number of adipocytes was assessed from at least three samples of three mouse.

Flow Cytometry Analysis of Adipose Tissue Macrophages (ATMs)

Inguinal adipose tissue was dissected and lymph nodes were removed. Adipocytes and stromal vascular cells were separated by conventional method using type II collagenase (Sigma-Aldrich) digestion (Cho et al., 2014; Kitada et al., 2016). Antibodies were purchased from Biolegend, including APC anti-mouse F4/80 monoclonal antibody (Clone BM8, Cat. No. 123115), FITC anti-mouse CD206 antibody (Clone C068C2, Cat. No. 141703). Analysis of ATMs was first gated on living cells, followed by analysis for F4/80 and CD206 by flow cytometry (FACSCalibur, Becton Dickinson, USA).

RT-PCR and Real-Time PCR Analysis

Total RNA was isolated from homogenated tissues using Trizol (Invitrogen). cDNA was synthesized using PrimeScript^{TM} RT kit (Takara). RT-PCR products were analyzed on 1.5% agarose gel. Real-time PCR was conducted using SYBR Green PCR Master Mix (Takara) according to the manufacturer's instruction and run on real-time PCR system (MX3005p, Stratagene, USA) and analyzed using MXProv 4.1. Primers (listed in Supplementary Table 1) were synthesized by Shanghai Biosune (Shanghai, China).

Adipocyte Differentiation Models

3T3-L1 system: mouse 3T3-L1 preadipocytes (from The National Center for Drug Screening, Shanghai, China) were maintained in complete high-glucose Dulbecco's modified Eagle's medium (DMEM, GIBCO, USA) supplemented with 10% fetal bovine serum (FBS) at 37°C, in a humidified incubator with 5% CO_2. For induction of adipose differentiation, 30,000 cells in 300 ml per well were seeded in 48-well plates and incubated until confluence. After incubated for another day, cells were exposed to inducer A (complete medium with 0.5 mM isobutylmethylxanthine, 1 μM dexamethasone, 0.2 mM indometacin, and 10 μg/ml insulin). After 3 days, the medium was changed to inducer B (complete medium containing 10 μg/ml insulin) and incubated for another 3 days. After that cells were cultured in complete medium for 2 days. As for Kp-10 stimulation, different concentrations of Kp-10 were added together with inducer A and B, with DMSO as control. Insulin-dependent glucose uptake experiment was conducted as usual. Briefly, after induction, 3T3-L1 cells were starved then stimulated with 0.6 μg/ml insulin for 30 min. The uptake of the fluorescent glucose homolog 2-NBDG (Invitrogen) was measured by incubation cells with 80 nM 2-NBDG for 15 min. After wash, fluorescence was measured on a FLUOstar Omega (BMG LABTECH).

Mesenchymal stem cell (MSC) system: MSCs were separated from bone marrow. Femurs and tibiae were removed after mice were euthanized. All connective tissue were cleaned and the ends of each tibia and femur were clipped. The marrow was blown into a 10 cm dish by a 5 ml syringe, and cultured in 8 ml complete high-glucose DMEM medium for overnight. Non-adherent cells were removed and adherent cells were washed. Fresh complete medium was then added and cultured for 2–4 days. The cells were lifted by incubation with trypsin/EDTA for 2–3 min, plated at 100,000 cells per well in 48-well plates. Induction for adipose differentiation and Kp-10 stimulation was conducted as described in 3T3-L1 system.

Kp-10 peptide was synthesized according to reference (Asami et al., 2012) in which analog 13 showed not only high metabolic stability but also excellent GPR54 agonistic activity to human and mouse.

The Cellular Non-Alcoholic Fatty Liver Disease (NAFLD) Model

The cellular steatosis model suitable for investigation of the impact of GPR54 on fat accumulation in liver was established in a human normal liver cell line LO_2. LO_2 cells were purchased from the Cell Bank of Type Culture Collection of Chinese Academy of Science (Shanghai, China), and cultured in complete high-glucose DMEM medium. For steatosis induction, cells were exposed to a mixture of free fatty acids (0.25 mM sodium oleate and 0.125 mM palmitate) for 12 h. Different concentrations of Kp-10 were added together with the free fatty acids, with DMSO as normal control.

Immunoblotting

Adipose tissue was homogenated in Ripa lysis buffer (with 1mM PMSF, Merck Millipore). Proteins were extracted and separated on 10% SDS-PAGE gel, and electroblotted onto a nitrocellulose membrane (Schleicher and Schuell MicroScience) using a Mini trans-blot apparatus (Bio-Rad). The membrane was blocked with 5% skim milk-PBS (pH 7.4) for 1 h at room temperature, then incubated with primary antibody for overnight at 4°C. After washed in PBS-1‰ Tween-20, the membrane was incubated in secondary antibody for 2 h at room temperature, then analyzed on the Odyssey infrared imaging system (LI-COR). All the antibodies were purchased from Cell Signaling Technology except rabbit anti-PPARγ polyclonal antibody (Proteintech, USA, Cat. No. 16643-1-AP, Dilution: 1:1,000). These included P44/42 MAPK (Erk1/2) antibody (Cat. No. 9102, Dilution: 1:1,000), Phospho-p44/42 MAPK (Erk 1/2) monoclonal antibody (Clone 197G2, Cat. No. 4377, Dilution: 1:1,000), p38 MAPK rabbit polyclonal antibody (Cat. No. 9212, Dilution: 1:1,000) and phospho-p38 MAPK rabbit monoclonal antibody (Clone D3F9, Cat. No. 9211, Dilution: 1:1,000).

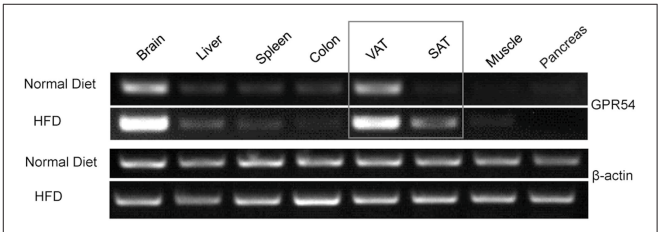

FIGURE 1 | GPR54 mRNA level in metabolism related tissues. RT-PCR analysis for GPR54 in different tissues of 10-week old WT mice fed on normal diet or HFD. Total RNA was extracted using TRIzol. β-actin was used as control.

Statistics

All data were presented as mean ± SD. Statistical analysis was performed using Graphpad Prism. Student's *t*-test was used for comparison of two groups and one way ANOVA was used for multiple comparison. p-value < 0.05 were considered as statistically significant.

RESULTS

HFD Induction Enhanced GPR54 Expression in Adipose Tissues

In order to explore the possibility of GPR54 involvement in metabolism, GPR54 expression profile in metabolism related tissues was assessed by RT-PCR. Data showed that GPR54 was highly expressed in brain and visceral adipose tissue (VAT). Moreover, GPR54 expression increased significantly in brain, VAT as well as subcutaneous adipose tissues (SAT) of HFD-fed mice (**Figure 1**). These data suggested that, in addition to the involvement in central nervous system, GPR54 may play a direct role in adipose tissues and participate in lipid metabolism.

Effect of GPR54 on Obesity Development

To study the direct function of GPR54 on metabolism, $Gpr54^{+/+}$ (WT) and $Gpr54^{-/-}$ mice were castrated or ovariectomized at 20–21 post-natal days to equalize sex hormones. Mice were maintained on normal diet until 6 weeks old, then transferred to HFD (noted as day 0) for 6 weeks. During the HFD period, consumption of water and food was measured every 2 days, and body weight was measured every week. Body weight in $Gpr54^{-/-}$ mice was significantly lower than that in WT. This phenomenon was manifested in both male and female mice (**Figure 2A**). Meanwhile, female $Gpr54^{-/-}$ mice displayed significantly lower triglyceride (TG) content in blood than female WT mice. Male mice showed the same trend but did not reach significance (**Figure 2B**). There was no significant difference in food intake between $Gpr54^{-/-}$ and WT mice (**Figure 2C**), indicating that the less severe obesity induced in $Gpr54^{-/-}$ mice was not a result of difference in food consumption.

Unaltered Glucose Metabolism in GPR54 Deficient Mice

Obesity development could lead to insulin resistance and impaired glucose tolerance. Regulation of blood glucose in $Gpr54^{-/-}$ and WT mice was examined using oral glucose tolerance test (OGTT). As shown in **Figures 3A,B** both WT and $Gpr54^{-/-}$ mice displayed a higher than normal level of fasting blood-glucose (>7.0 mM), suggesting impaired glucose tolerance by HFD induction. This was quite different from mice kept on normal diet which showed a normal fasting blood-glucose (**Figure 3F**). However, $Gpr54^{-/-}$ mice did not showed significant

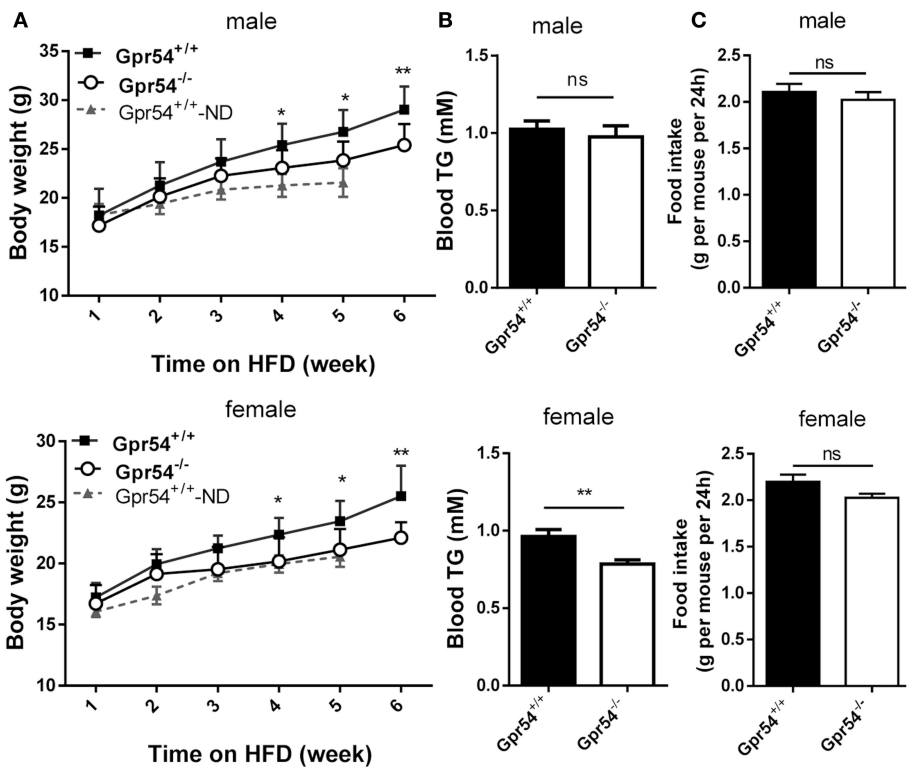

FIGURE 2 | Effect of GPR54 deficiency on body weight, blood TG and food intake after HFD induction. **(A)** Body weight after HFD induction, compare with normal diet (ND)-fed WT mice. **(B)** Blood TG and **(C)** food intake of WT and $Gpr54^{-/-}$ mice. Data were expressed as mean ± *SD* ($n = 10$–12), $^{*}p < 0.05$, $^{**}p < 0.01$.

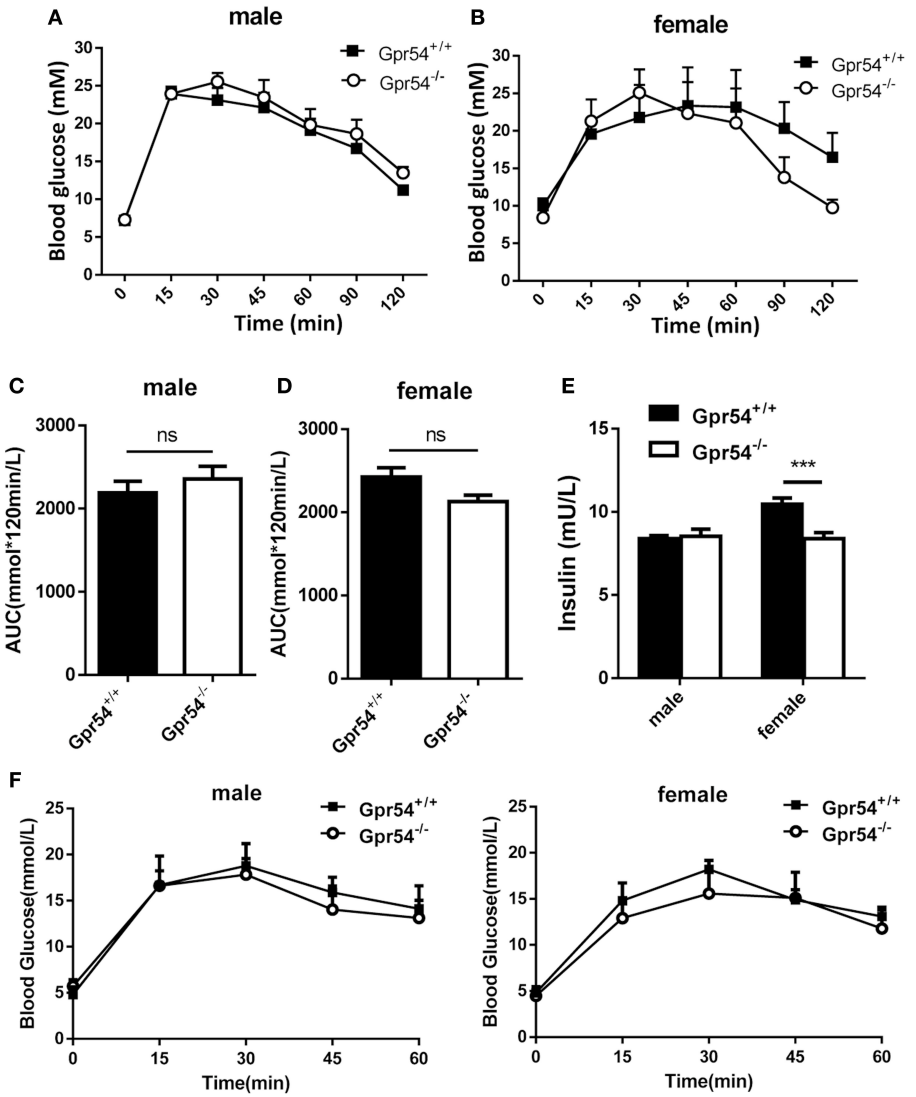

FIGURE 3 | Effect of GPR54 deficiency on glucose metabolism. **(A,B)** OGTT time course and **(C,D)** respective AUC values of the HFD-fed mice ($n = 7$–10). **(E)** Insulin levels of serum from two genotypes fed on HFD. **(F)** OGTT of mice kept on normal diet ($n = 6$). Mice were fasted 12 h before the test, followed by oral glucose challenge at 2 g/kg. Data were expressed as mean ± *SD*, ***$p < 0.001$.

difference in glucose tolerance as compared to WT control, no matter fed on a HFD or normal diet (**Figures 3A–D,F**). In other hand, significant reduction of insulin was only found in female *Gpr54*$^{-/-}$ mice (**Figure 3E**). Altogether, GPR54 did not play a very important role in glucose metabolism in this study.

GPR54 Regulation on Adiposity and Adipose Tissue Macrophages

In order to investigate whether the reduced weight growth was associated with alteration in adipose tissue, we measured body fat of mice. After HFD induction, GPR54 deficient mice demonstrated significantly reduced VAT as compared to WT littermates. Male *Gpr54*$^{-/-}$ mice displayed a significantly lower relative VAT percentage than WT, while female mice had the same trend but did not reach significance (**Figure 4A**). Consistent with this result, histology analysis by HE staining showed that adipocytes from both female and male *Gpr54*$^{-/-}$ mice had smaller size and higher adipocyte density than WT control, close to the normal phenotype of adipocytes from normal diet-fed WT mice (**Figures 4B–E**). These data suggested that GPR54 deficiency attenuated HFD-induced adipocyte hypertrophy and lipid accumulation in mice, resulting in slower body weight growth.

It was reported that obesity increased ATM accumulation in visceral adipose depots, and was associated with qualitative changes of ATMs (Weisberg et al., 2003; Harman-Boehm et al., 2007). To this end ATMs in fat were analyzed.

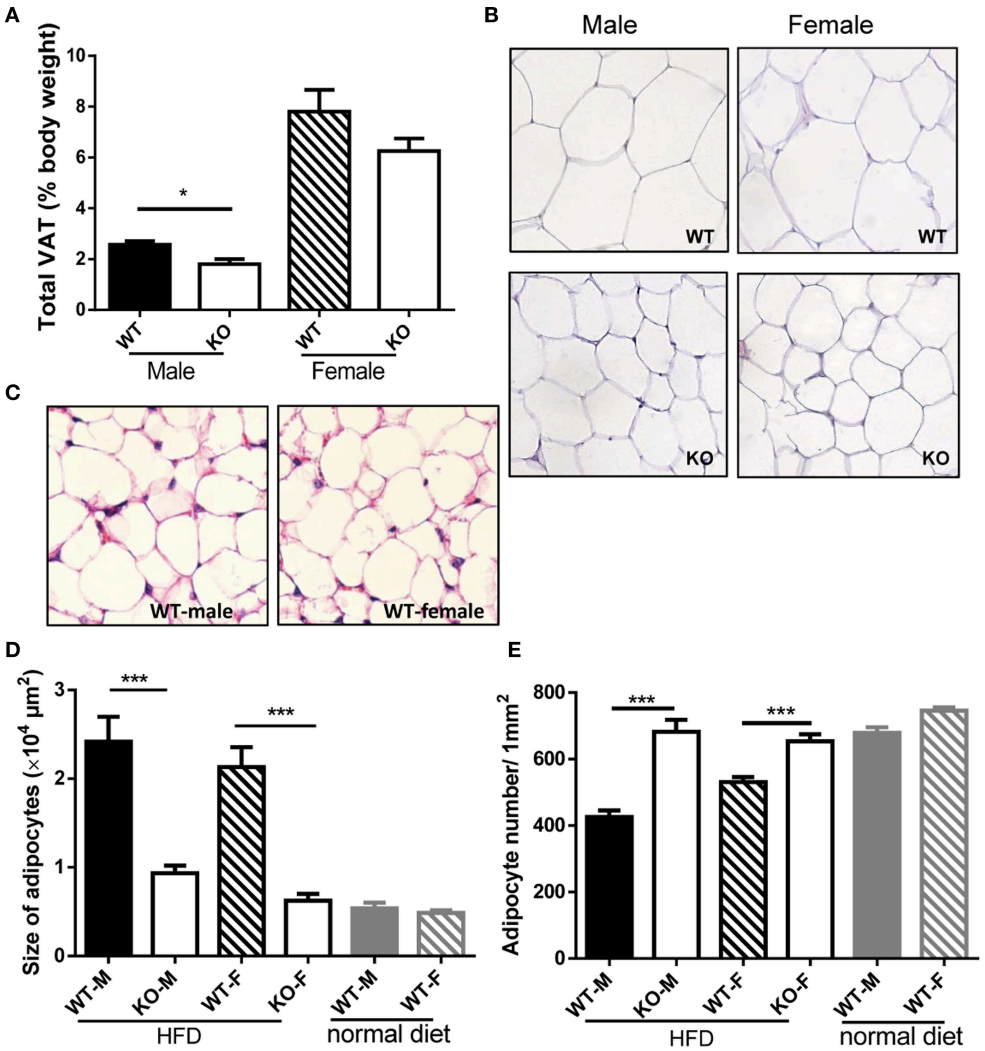

FIGURE 4 | VAT percentage and HE staining of adipose tissue. **(A,B)** VAT percentage to body weight of WT (*Gpr54*$^{+/+}$) and KO (*Gpr54*$^{-/-}$) mice after HFD induction ($n = 5$), and representative image of adipocytes (magnification ×200). **(C)** Representative image of adipocytes from WT mice kept on normal diet. **(D,E)** Statistical results for average adipocyte size and adipocyte density. M, male; F, female. Data were expressed as mean ± *SD*, $^{*}p < 0.05$, $^{***}p < 0.001$ vs. respective WT control.

Adipocytes and stromal vascular fractions (SVF) were separated from WT mice. Data showed that GPR54 expression was increased in HFD-fed mice as compared to that in normal diet-fed mice (**Figure 5A**). SVFs were then separated from WT and *Gpr54*$^{-/-}$ obese littermates. Cells were stained by F4/80 and CD206 antibody, and analyzed by FACS analysis. Results showed that *Gpr54*$^{-/-}$ mice presented less ATMs than WT littermates, together with significantly more M2-like (F4/80^{+}CD206^{+}) anti-inflammatory macrophages (**Figures 5B,C**). In addition, a trend of reduced inflammation was also manifested in reduced expression of IL-6 and adiponectin (ADIPO), as well as increased IL-10 and arginase 1 (Arg1) in *Gpr54*$^{-/-}$ VAT (**Figure 5D**). These data suggested that inflammatory response caused by obesity in *Gpr54*$^{-/-}$ mice was not as drastic as that in WT mice.

Effect of GPR54 Deficiency on Liver

Livers of different groups of mice were examined. Relative liver weight in *Gpr54*$^{-/-}$ female mice was significantly lower than that in WT littermates (**Figure 6A**). No significant difference in liver weight was revealed in male counterparts. TG content in *Gpr54*$^{-/-}$ liver of both sexes was significantly reduced as compared to that in respective WT counterparts (**Figure 6B**).

To further confirm regulatory function of GPR54 in steatosis, normal human hepatocytes LO_2 were used to establish the NAFLD model. The shortest kisspeptin Kp-10 stimulation accelerated adipose accumulation, with peak stimulation at 1 nM. In addition, TG synthesis in the cells was found to be enhanced by Kp-10. The peak enhancement also appeared at 1 nM (**Figures 6C,D**). Therefore, it can be concluded that Kp-10 stimulation promoted TG synthesis and adipose accumulation of liver cells. The pattern of Kp-10

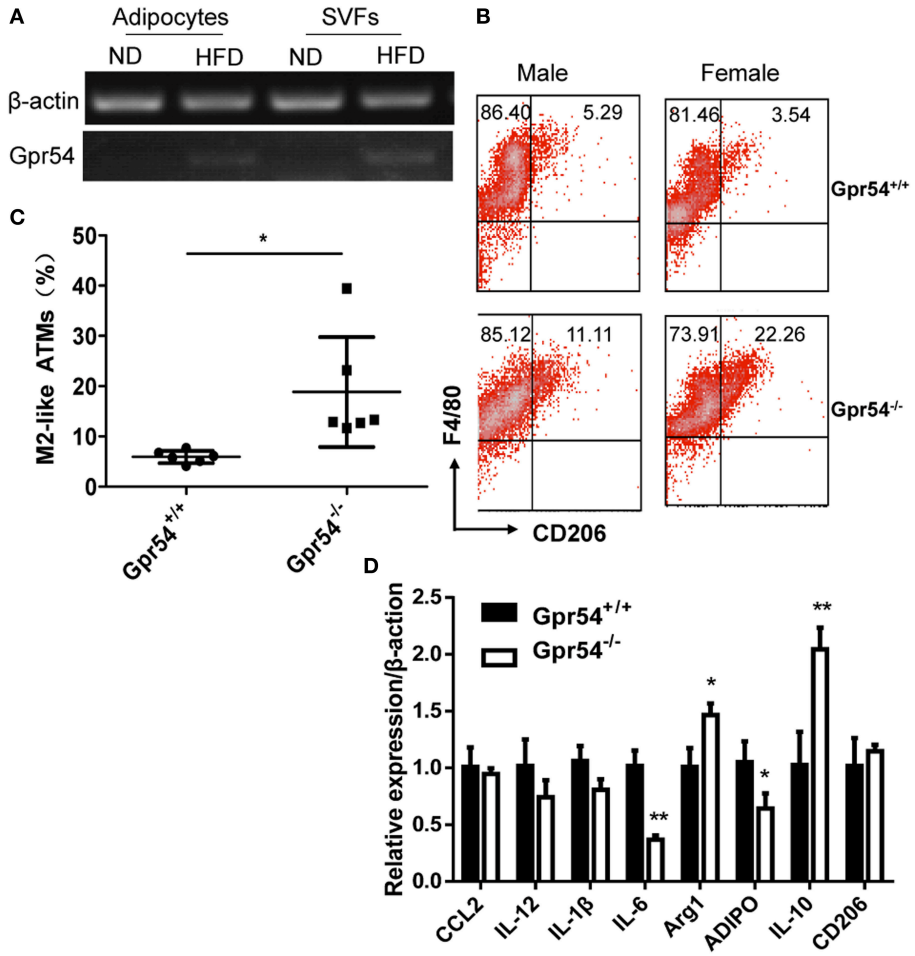

FIGURE 5 | GPR54 deficiency led to alteration of ATMs in obese mice. **(A)** GPR54 mRNA expression in mature adipocytes and stromal vascular fractions (SVF) of normal diet (ND) and HFD-fed WT mice. **(B)** Representative FACS histogram for SVFs from *Gpr54*$^{-/-}$ and WT littermates. F4/80^{+}: total macrophages. CD206^{+}: M2-like macrophages. **(C)** Different percentage of M2-like in total macrophages. Data were expressed as mean ± *SD* (Total six pairs of mice with three male and three female), $^{*}p < 0.05$. **(D)** Expression of pro-inflammatory and anti-inflammatory genes in VAT of two genotypes. Arginase 1 (Arg1); Adiponectin (ADIPO). $^{**}p < 0.01$.

stimulation did not show typical concentration gradient effect, which was consistent with previous report that Kp-10 may exert opposite effect at higher concentrations (Olbrich et al., 2010).

GPR54 Promoted Adipocyte Differentiation

We next established adipocyte differentiation models with both bone marrow-derived MSCs and 3T3-L1 cells. MSCs from WT mice were found to express GPR54 (**Figure 7A**). When MSCs separated from three-week old *Gpr54*$^{-/-}$ and WT mice were induced, Oil Red O staining showed that MSCs from *Gpr54*$^{-/-}$ mice displayed a lower differentiation as compared to that from WT littermates (**Figure 7B**). At the same time, intracellular TG in the differentiated cells from *Gpr54*$^{-/-}$ mice was lower than that from WT mice (**Figure 7C**).

The above results were confirmed in 3T3-L1 system in which GPR54 mRNA expression displayed an upregulated trend in the differentiation process (**Figure 7D**). In this system, Kp-10 stimulation promoted adipose differentiation (**Figure 7E**), accompanied by the increased TG in cells (**Figure 7F**). In addition, Kp-10 stimulation enhanced insulin-dependent glucose uptake in 3T3-L1 cells (**Figure 7G**). Altogether, these data clearly demonstrated that Kp-10 stimulation of GPR54 promoted adipocyte differentiation and metabolic function.

Mechanism of GPR54 Regulation of Adipocyte Differentiation

In order to gain more insight into GPR54 signaling in lipogenesis and lipid metabolism, key lipid metabolic genes including FAS and ACC1 were assessed in experimental *Gpr54*$^{-/-}$ and WT littermates by real-time PCR analysis. In adipose tissue of *Gpr54*$^{-/-}$ mice, reduction was shown in adipogenic markers such as FAS, ACC1, and PPARγ, with PPARγ presenting the largest reduction (one-fifth). No change was detected in the level of SREBP (**Figure 8A**). UCP-1 expression was increased but no significant increase was found in other browning related genes. DIO2 even displayed a marked reduction (**Figure 8B**). These data suggest that there was no browning effect associated with

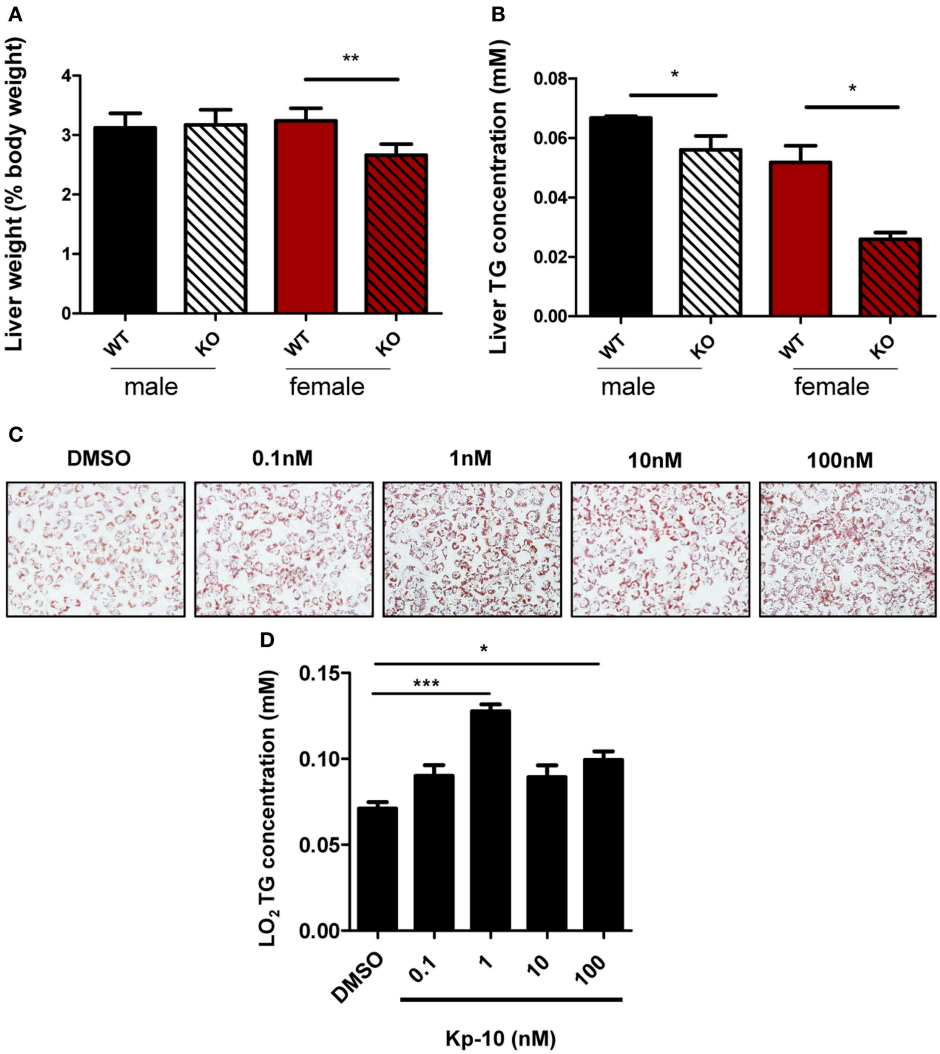

FIGURE 6 | Alteration of liver in GPR54 deficient mice. **(A)** Relative liver weight (as percentage of body weight) of KO (*Gpr54*$^{-/-}$) and WT (*Gpr54*$^{+/+}$) littermates after HFD induction. **(B)** TG content in liver. Data were expressed as mean ± SD ($n = 4$–6), $^{*}p < 0.05$, $^{**}p < 0.01$ vs. respective WT control. **(C)** Kp-10 stimulation promoted lipid accumulation in LO2 cells. Different concentrations of Kp-10 were added in the NAFLD model of LO2 induced by free fatty acids. Cells were stained by Oil Red O solution (magnification ×200). **(D)** TG content in LO2 cells. Data were expressed as mean ± SD ($n = 3$), $^{*}p < 0.05$, $^{***}p < 0.001$ vs. DMSO control.

GPR54 deficiency. In addition, mRNA level of the lipid droplet-associated protein, perilipin (PLIN), was analyzed and significant reduction was found in PLIN1 of liver and PLIN3 of adipose tissue of GPR54 deficient mice (Supplementary Figure 2).

The marked alteration in PPARγ prompted us to analyze its protein level, as it is a master regulator of adipocyte differentiation (Ahmadian et al., 2013). Reduction of PPARγ expression in GPR54 deficient mice was confirmed in Western blotting using adipose tissue extracts. It was previously demonstrated that mitogen-activated protein kinases (MAPK) p38 and ERK1/2 were markers of GPR54 activation (Castaño et al., 2009; Cvetkovic et al., 2013). Moreover, inhibition of MAPK/ERK signaling pathway could suppress adipogenesis and down regulate PPARγ expression (Wang et al., 2009). We proposed that MAPK might be a convergence point for GPR54 signaling and adipogenesis signaling. By checking these MAP kinases in adipose tissues, western blot analysis was carried out. Data showed a, reduced phosphorylation of ERK (**Figures 8C–E**). In addition, insulin responsiveness of adipocytes is important, Akt-PI3K signaling pathway, and no significant alteration was found in expression and phosphorylation of AKT or PI3K (**Figure 8C**). Therefore, it was concluded that GPR54 deficiency inhibited ERK phosphorylation and reduced PPARγ expression.

DISCUSSION

This study investigated functions of GPR54 on lipid metabolism. GPR54 deficiency substantially attenuated body weight gain and TG level in HFD-induced castrated/ovariectomized

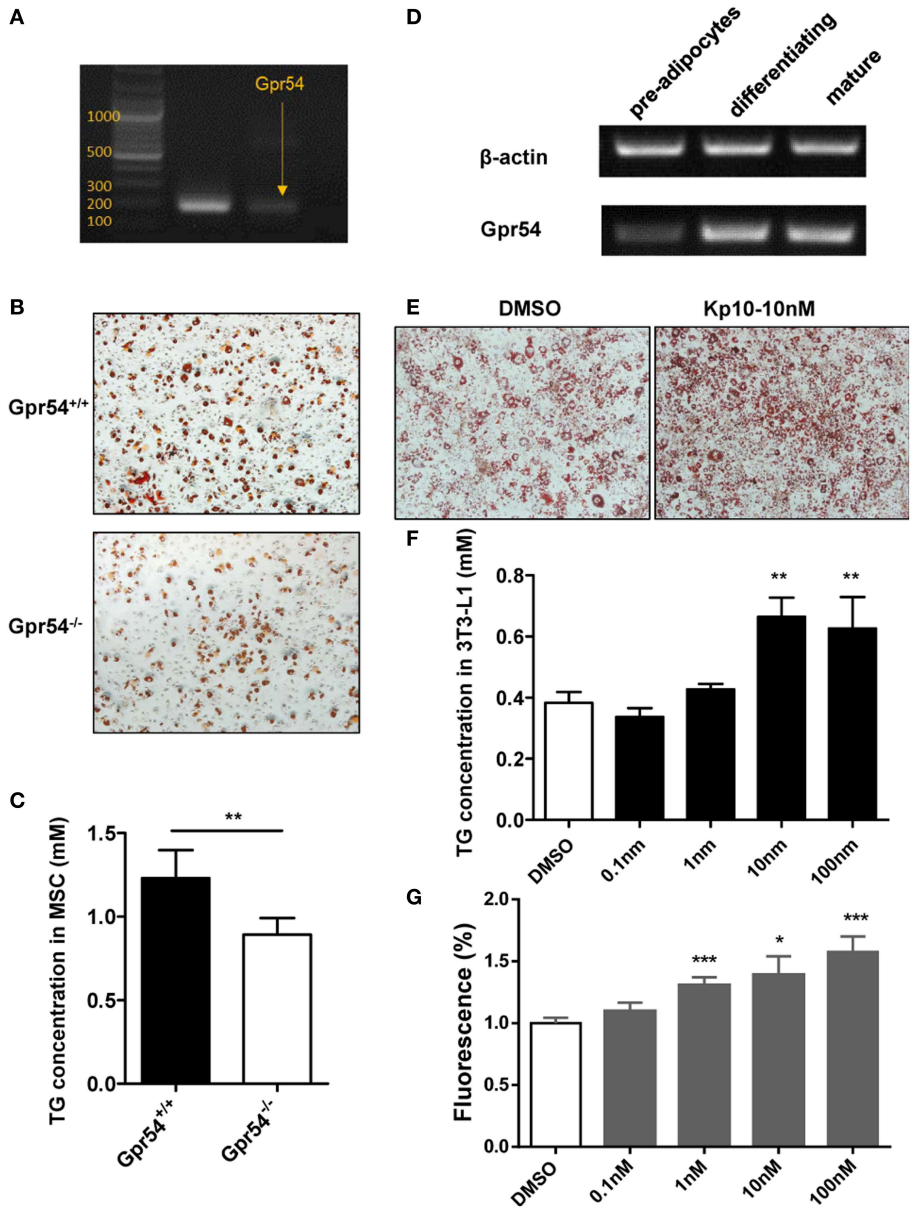

FIGURE 7 | Kp-10 stimulation of GPR54 promoted adipocyte differentiation. **(A)** GPR54 expression in MSCs. **(B)** Oil Red O staining of MSC differentiation into adipocytes (magnification ×100). **(C)** Cellular TG contents of MSCs ($n = 6$). **(D)** GPR54 expression in different stages of differentiated 3T3-L1 cells. **(E)** Oil Red O staining of 3T3-L1 cells stimulated by 10 nM Kp-10 vs. DMSO control (magnification ×100). **(F)** Cellular TG of 3T3-L1 cells ($n = 3$). **(G)** Insulin-dependent glucose uptake in 3T3-L1 cells stimulated by Kp-10 ($n = 12$). Data were expressed as mean ± *SD*, $^{*}p < 0.05$, $^{**}p < 0.01$, $^{***}p < 0.001$ vs. DMSO control.

mice. These findings were consistent with the observation in adipose tissue, as GPR54 deficient mice presented a reduced adipose tissue percentage and smaller adipocyte size, as well as reduced pro-inflammatory ATMs. Meanwhile, GPR54 agonist Kp-10 upregulated TG synthesis and lipid accumulation in normal liver cells, as well as increased TG synthesis and adipose differentiation in both MSC and 3T3-L1 systems. These results suggested that anti-obesity effect of GPR54 deletion in HFD-fed mice was mediated via inhibition of adipocyte differentiation and lipogenesis, reducing serum TG level by altering hepatic lipid metabolism.

GPR54 is highly expressed in placental tissue and central nervous system, and expression had also been reported in peripheral tissues such as adipose, thymus (Kotani et al., 2001; Muir et al., 2001; Funes et al., 2003; Herbison et al., 2010) and peripheral blood lymphocytes (Xing et al., 2018). Here we manifested GPR54 expression in adipose tissues which was markedly increased in HFD-induced mice. Increased expression was also found in mature adipocytes and SVFs. In addition,

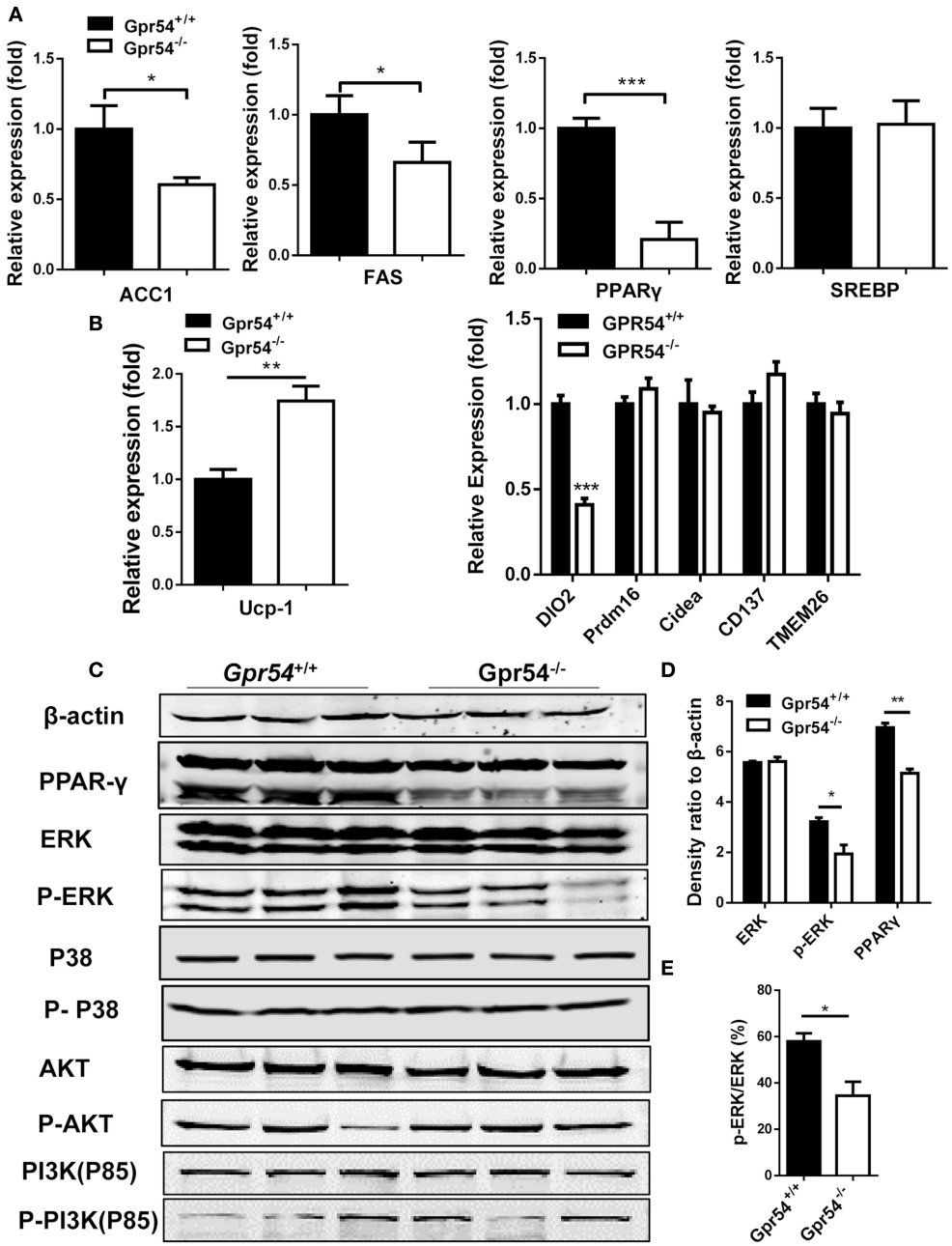

FIGURE 8 | GPR54 regulatory effects on key genes related to lipid metabolism. **(A)** Expression of key genes in white adipose tissue of HFD-induced mice, analyzed by real-time PCR analysis (triplicates). ACC1, acetyl-CoA carboxylase 1; FAS, fatty acid synthase; SREBP, sterol regulatory element-binding protein; PPAR, peroxisome proliferator activated receptor; **(B)** Expression of browning genes. UCP, uncoupling protein; PRDM16, PR domain containing 16. **(C)** Effects of GPR54 on PPARγ, MAPK, and AKT/PI3K pathways in adipose tissue of HFD-induced mice. **(D)** Density ratio of different genes. **(E)** Percentage of phosphorylated ERK. PI3K, Phosphatidylinositol 3-kinase. Data were expressed as mean ± *SD*, $^{*}p < 0.05$, $^{**}p < 0.01$, $^{***}p < 0.001$ vs. WT control.

GPR54 expression was exhibited in MSCs and 3T3-L1 pre-adipocytes, and expression increased when cells were induced and differentiated into mature adipocytes. The wide distribution in adipocytes and adipose tissues suggest that GPR54 plays a direct role in lipid metabolism. Since GPR54/KISS1 system is crucial in puberty development and sex hormone secretions which have effects on lipid metabolism and body weight (Butera, 2010; Lizcano and Guzman, 2014). We used castrated or ovariectomized WT and *Gpr54*$^{-/-}$ mice in order to equalize sex hormones. While intact *Gpr54*$^{-/-}$ mice showed an increased body weight as compared to WT partly due to reduced sex hormones (data not shown), we found quite different phenotypes in castrated or ovariectomized mice. Our result indicate that in addition to its involvement in reproduction, GPR54 could

influence body weight growth and lipid metabolism through a pathway that was independent of sex steroids.

Although no GPR54 expression was reported in macrophages, ATMs are predominant leukocytes in fat and key contributors to obesity associated inflammation. Previous observations supported the general model that ATMs undergo a phenotypic switch from an anti-inflammatory M2 state to a pro-inflammatory M1 state when animals develop obesity (Lumeng et al., 2007; Chawla et al., 2011). In our experiment, the phenotype of ATM polarization was consistent with overall results including body weight and VAT percentage. Less M1-type and more M2-type macrophages presented in less obese *Gpr54*$^{-/-}$ mice as compared to WT.

Many studies on GPR54/KISS1 expression related to energy metabolism had been carried out which mainly via *in vitro* systems. Results were unclear and hard to reach a conclusion (Hauge-Evans et al., 2006; Luque et al., 2007; Brown et al., 2008; Vikman and Ahren, 2009). Only a few reports about GPR54 deficiency on energy metabolism were available. Earlier data came from studies regarding hypogonadism associated with *Kiss1* or *Gpr54* knockout mice. It was shown that GPR54 or KISS1 deficient mice displayed almost no body weight difference except that GPR54 deficient males weighted slightly less than WT males (Lapatto et al., 2007). Recently a report in JCI stated that *Gpr54* knockout mice displayed a sexually-dimorphic metabolic phenotype, with male *Gpr54*$^{-/-}$ showed no alteration, but normal diet fed female *Gpr54*$^{-/-}$ mice ovariectomized at two weeks old developed obesity by 4–5 months of age. In addition, female *Gpr54*$^{-/-}$ mice ovariectomized at adulthood then directly transferred to HFD also displayed a mildly enhanced body weight increase (Tolson et al., 2014). However, they reported glucose intolerance in normal diet-fed *Gpr54*$^{-/-}$ mice, but not in HFD-induced *Gpr54*$^{-/-}$ mice. Also it was very difficult to explain the huge difference between male and female mice. Moreover, no obesity phenotype was reported in studies on human subjects with *Gpr54* or *Kiss1* mutations (de Roux et al., 2003; Seminara et al., 2003; Topaloglu et al., 2012). Later in young animals (6 weeks old), it was found that female *Gpr54*$^{-/-}$ mice fed on normal diet had normal body weights, normal feeding and glucose tolerance as compared to female WT, although some alteration in adiposity was exhibited (Tolson et al., 2016). Another study in Cell Metabolism reported that inhibition to *Kiss1* led to attenuated hyperglycemia but no change in body weight. Higher kisspeptin levels in diabetic patients as well as diabetic/obesity mice were observed, while kisspeptin knockdown led to insulin secretion and improved glucose intolerance (Song et al., 2014). Their work in some way agreed with our result, but they emphasized more on effect of glucose metabolism of liver kisspeptin, while our study investigated effect of GPR54/KiSS1 system on lipid metabolism, mostly in adipose tissues. Both observed that inhibition of GPR54/KiSS1 signaling could prevent obesity or diabetes. Variations in above study results may come from different experiment design. For example the JCI paper kept their ovariectomized (at 2 weeks) mice in normal diet, whereas in our experiment, we castrated mice at 3 weeks then accustomed them in normal diet for 3 weeks before transferred to HFD. On the other hand these variations may be a reflection of the complex roles of GPR54/KISS1 pathway, including distinctive regulatory function at different ages of the animals and under different situations. It was reported that KISS1 had varying roles across the reproductive lifespan including conception, puberty, menopause, and aging (Clarke and Dhillo, 2016).

According to the expression profile, the regulatory mechanisms of GPR54 might reflect GPR54 signaling impairment in the brain or adipose tissues. Kisspeptin neurons in brain were reported to regulate POMC and NPY neurons (Backholer et al., 2010). However, no significant change in food intake was observed in our *Gpr54*$^{-/-}$ mice, indicating there might be other pathways involved, possibly through dysregulated GPR54 signaling in adipose tissues. As some of the metabolic phenotypes in *Gpr54*$^{-/-}$ mice were more prominent in females than in males in our experiment, the preliminary study for the regulatory mechanism of GPR54 in adipose tissue was conducted in female mice. ERK and p-38 activation have been previously established as part of GPR54 signaling (Castaño et al., 2009; Cvetkovic et al., 2013), On the other hand, inhibition of MAPK/ERK signaling pathway was reported to suppress adipogenesis and down regulation of PPARγ (Wang et al., 2009). Our result confirmed that deficiency of GPR54 signaling in adipose tissue led to inhibition of ERK phosphorylation, suggesting that GPR54 signaling may converge with lipogenesis signaling at the level of MAPK. The inhibited MAPK activation probably lead to reduction in PPARγ expression and adipogensis.

In conclusion, we demonstrated that GPR54 played a direct pro-obesity role by promoting adipocyte differentiation and lipid accumulation in addition to its previously established role in reproductive regulation. These results help to elucidate the complex biological functions of GPR54/KISS1 system, and will be beneficial for further identification and development of potential drug targets for metabolic diseases.

AUTHOR CONTRIBUTIONS

TW, HC, and ML: Conceived the experiments; TW, XC, LX, RX, PY, YZ, YY, and YX: Conducted the experiments; HC, LZ, TW, XC, LX, RX, PY, YZ, YY, and YX: Analyzed the results; TW and XC: Drafted the work; HC, LZ, and ML: Wrote and revised the manuscript. All authors reviewed and approved the manuscript.

ACKNOWLEDGMENTS

This work was supported by grant funding from the National Natural Science Foundation of China (31271468). We are grateful to Dr. Eric L. Gustafson at Schering-Plow Research Institute for providing the male and female *GPR54*$^{+/-}$ mouse lines.

SUPPLEMENTARY MATERIAL

The Supplementary Material for this article can be found online at: https://www.frontiersin.org/articles/10.3389/fphys.2018.00209/full#supplementary-material

REFERENCES

Ahmadian, M., Suh, J. M., Hah, N., Liddle, C., Atkins, A. R., Downes, M., et al. (2013). PPARgamma signaling and metabolism: the good, the bad and the future. *Nat. Med.* 19, 557–566. doi: 10.1038/nm.3159

Asami, T., Nishizawa, N., Ishibashi, Y., Nishibori, K., Nakayama, M., Horikoshi, Y., et al. (2012). Serum stability of selected decapeptide agonists of KISS1R using pseudopeptides. *Bioorg. Med. Chem. Lett.* 22, 6391–6396. doi: 10.1016/j.bmcl.2012.08.069

Backholer, K., Smith, J. T., Rao, A., Pereira, A., Iqbal, J., Ogawa, S., et al. (2010). Kisspeptin cells in the ewe brain respond to leptin and communicate with neuropeptide Y and proopiomelanocortin cells. *Endocrinology* 151, 2233–2243. doi: 10.1210/en.2009-1190

Bowe, J. E., King, A. J., Kinsey-Jones, J. S., Foot, V. L., Li, X. F., O'Byrne, K. T., et al. (2009). Kisspeptin stimulation of insulin secretion: mechanisms of action in mouse islets and rats. *Diabetologia* 52, 855–862. doi: 10.1007/s00125-009-1283-1

Brown, R. E., Imran, S. A., Ur, E., and Wilkinson, M. (2008). KiSS-1 mRNA in adipose tissue is regulated by sex hormones and food intake. *Mol. Cell. Endocrinol.* 281, 64–72. doi: 10.1016/j.mce.2007.10.011

Butera, P. C. (2010). Estradiol and the control of food intake. *Physiol. Behav.* 99, 175–180. doi: 10.1016/j.physbeh.2009.06.010

Castaño, J. P., Martínez-Fuentes, A. J., Gutiérrez-Pascual, E., Vaudry, H., Tena-Sempere, M., and Malagón, M. M. (2009). Intracellular signaling pathways activated by kisspeptins through GPR54: do multiple signals underlie function diversity? *Peptides* 30, 10–15. doi: 10.1016/j.peptides.2008.07.025

Castellano, J. M., Navarro, V. M., Fernández-Fernández, R., Nogueiras, R., Tovar, S., Roa, J., et al. (2005). Changes in hypothalamic KiSS-1 system and restoration of pubertal activation of the reproductive axis by kisspeptin in undernutrition. *Endocrinology* 146, 3917–3925. doi: 10.1210/en.2005-0337

Chawla, A., Nguyen, K. D., and Goh, Y. P. (2011). Macrophage-mediated inflammation in metabolic disease. *Nat. Rev. Immunol.* 11, 738–749. doi: 10.1038/nri3071

Cho, K. W., Morris, D. L., and Lumeng, C. N. (2014). Flow cytometry analyses of adipose tissue macrophages. *Methods Enzymol.* 537, 297–314. doi: 10.1016/B978-0-12-411619-1.00016-1

Clarke, S. A., and Dhillo, W. S. (2016). Kisspeptin across the human lifespan:evidence from animal studies and beyond. *J. Endocrinol.* 229, R83–R98. doi: 10.1530/JOE-15-0538

Cvetković, D., Babwah, A. V., and Bhattacharya, M. (2013). Kisspeptin/KISS1R system in breast cancer. *J. Cancer* 4, 653–661. doi: 10.7150/jca.7626

de Roux, N., Genin, E., Carel, J. C., Matsuda, F., Chaussain, J. L., and Milgrom, E. (2003). Hypogonadotropic hypogonadism due to loss of function of the KiSS1-derived peptide receptor GPR54. *Proc. Natl. Acad. Sci. U.S.A.* 100, 10972–10976. doi: 10.1073/pnas.1834399100

Farooqi, S., Rau, H., Whitehead, J., and O'Rahilly, S. (1998). ob gene mutations and human obesity. *Proc. Nutr. Soc.* 57, 471–475. doi: 10.1079/PNS19980067

Funes, S., Hedrick, J. A., Vassileva, G., Markowitz, L., Abbondanzo, S., Golovko, A., et al. (2003). The KiSS-1 receptor GPR54 is essential for the development of the murine reproductive system. *Biochem. Biophys. Res. Commun.* 312, 1357–1363. doi: 10.1016/j.bbrc.2003.11.066

Gutiérrez-Pascual, E., Martínez-Fuentes, A. J., Pinilla, L., Tena-Sempere, M., Malagón, M. M., and Castaño, J. P. (2007). Direct pituitary effects of kisspeptin: activation of gonadotrophs and somatotrophs and stimulation of luteinising hormone and growth hormone secretion. *J. Neuroendocrinol.* 19, 521–530. doi: 10.1111/j.1365-2826.2007.01558.x

Harman-Boehm, I., Blüher, M., Redel, H., Sion-Vardy, N., Ovadia, S., Avinoach, E., et al. (2007). Macrophage infiltration into omental versus subcutaneous fat across different populations: effect of regional adiposity and the comorbidities of obesity. *J. Clin. Endocrinol. Metab.* 92, 2240–2247. doi: 10.1210/jc.2006-1811

Hauge-Evans, A. C., Richardson, C. C., Milne, H. M., Christie, M. R., Persaud, S. J., and Jones, P. M. (2006). A role for kisspeptin in islet function. *Diabetologia* 49, 2131–2135. doi: 10.1007/s00125-006-0343-z

Herbison, A. E., de Tassigny, X. D., Doran, J., and Colledge, W. H. (2010). Distribution and postnatal development of Gpr54 gene expression in mouse brain and gonadotropin-releasing hormone neurons. *Endocrinology* 151, 312–321. doi: 10.1210/en.2009-0552

Kalamatianos, T., Grimshaw, S. E., Poorun, R., Hahn, J. D., and Coen, C. W. (2008). Fasting reduces KiSS-1 expression in the anteroventral periventricular nucleus (AVPV): effects of fasting on the expression of KiSS-1 and neuropeptide Y in the AVPV or arcuate nucleus of female rats. *J. Neuroendocrinol.* 20, 1089–1097. doi: 10.1111/j.1365-2826.2008.01757.x

Kauffman, A. S., Clifton, D. K., and Steiner, R. A. (2007). Emerging ideas about kisspeptin-GPR54 signaling in the neuroendocrine regulation of reproduction. *Trends Neurosci.* 30, 504–511. doi: 10.1016/j.tins.2007.08.001

Kitada, Y., Kajita, K., Taguchi, K., Mori, I., Yamauchi, M., Ikeda, T., et al. (2016). Blockade of sphingosine 1-phosphate receptor 2 signaling attenuates high-fat diet-induced adipocyte hypertrophy and systemic glucose intolerance in mice. *Endocrinology* 157, 1839–1851. doi: 10.1210/en.2015-1768

Kotani, M., Detheux, M., Vandenbogaerde, A., Communi, D., Vanderwinden, J. M., Le Poul, E., et al. (2001). The metastasis suppressor gene KiSS-1 encodes kisspeptins, the natural ligands of the orphan G protein-coupled receptor GPR54. *J. Biol. Chem.* 276, 34631–34636. doi: 10.1074/jbc.M104847200

Lapatto, R., Pallais, J. C., Zhang, D., Chan, Y. M., Mahan, A., Cerrato, F., et al. (2007). Kiss1$^{-/-}$ mice exhibit more variable hypogonadism than Gpr54$^{-/-}$ mice. *Endocrinology* 148, 4927–4936. doi: 10.1210/en.2007-0078

Lee, J. H., Miele, M. E., Hicks, D. J., Phillips, K. K., Trent, J. M., Weissman, B. E., et al. (1996). KiSS-1, a novel human malignant melanoma metastasis-suppressor gene. *J. Natl. Cancer Inst.* 88, 1731–1737. doi: 10.1093/jnci/88.23.1731

Liu, R., Zou, Y., Hong, J., Cao, M., Cui, B., Zhang, H., et al. (2017). Rare loss-of-function variants in NPC1 predispose to human obesity. *Diabetes* 66, 935–947. doi: 10.2337/db16-0877

Lizcano, F., and Guzmán, G. (2014). Estrogen deficiency and the origin of obesity during menopause. *Biomed. Res. Int.* 2014:757461. doi: 10.1155/2014/757461

Locke, A. E., Kahali, B., Berndt, S. I., Justice, A. E., Pers, T. H., Day, F. R., et al. (2015). Genetic studies of body mass index yield new insights for obesity biology. *Nature* 518, 197–206. doi: 10.1038/nature14177

Lumeng, C. N., Bodzin, J. L., and Saltiel, A. R. (2007). Obesity induces a phenotypic switch in adipose tissue macrophage polarization. *J. Clin. Invest.* 117, 175–184. doi: 10.1172/JCI29881

Luque, R. M., Kineman, R. D., and Tena-Sempere, M. (2007). Regulation of hypothalamic expression of KiSS-1 and GPR54 genes by metabolic factors: analyses using mouse models and a cell line. *Endocrinology* 148, 4601–4611. doi: 10.1210/en.2007-0500

Muir, A. I., Chamberlain, L., Elshourbagy, N. A., Michalovich, D., Moore, D. J., Calamari, A., et al. (2001). AXOR12, a novel human G protein-coupled receptor, activated by the peptide KiSS-1. *J. Biol. Chem.* 276, 28969–28975. doi: 10.1074/jbc.M102743200

Ohtaki, T., Shintani, Y., Honda, S., Matsumoto, H., Hori, A., Kanehashi, K., et al. (2001). Metastasis suppressor gene KiSS-1 encodes peptide ligand of a G-protein-coupled receptor. *Nature* 411, 613–617. doi: 10.1038/35079135

Olbrich, T., Ziegler, E., Türk, G., Schubert, A., Emons, G., and Gründker, C. (2010). Kisspeptin-10 inhibits bone-directed migration of GPR54-positive breast cancer cells: evidence for a dose-window effect. *Gynecol. Oncol.* 119, 571–578. doi: 10.1016/j.ygyno.2010.08.018

Seminara, S. B., Messager, S., Chatzidaki, E. E., Thresher, R. R., Acierno, J. S. Jr., Shagoury, J. K., et al. (2003). The GPR54 gene as a regulator of puberty. *N. Engl. J. Med.* 349, 1614–1627. doi: 10.1056/NEJMoa035322

Song, W. J., Mondal, P., Wolfe, A., Alonso, L. C., Stamateris, R., Ong, B. W., et al. (2014). Glucagon regulates hepatic kisspeptin to impair insulin secretion. *Cell Metab.* 19, 667–681. doi: 10.1016/j.cmet.2014.03.005

Sonigo, C., and Binart, N. (2012). Overview of the impact of kisspeptin on reproductive function. *Ann. Endocrinol.* 73, 448–458. doi: 10.1016/j.ando.2012.07.680

Tolson, K. P., Garcia, C., Delgado, I., Marooki, N., and Kauffman, A. S. (2016). Metabolism and energy expenditure, but not feeding or glucose tolerance, are impaired in young Kiss1r KO female mice. *Endocrinology* 157, 4192–4199. doi: 10.1210/en.2016-1501

Tolson, K. P., Garcia, C., Yen, S., Simonds, S., Stefanidis, A., Lawrence, A., et al. (2014). Impaired kisspeptin signaling decreases metabolism and promotes glucose intolerance and obesity. *J. Clin. Invest.* 124, 3075–3079. doi: 10.1172/JCI71075

Topaloglu, A. K., Tello, J. A., Kotan L. D., Ozbek, M. N., Yilmaz, M. B., Erdogan, S., et al. (2012). Inactivating KISS1 mutation and hypogonadotropic hypogonadism. *N. Engl. J. Med.* 366, 629–635. doi: 10.1056/NEJMoa1111184

Vikman, J., and Ahrén, B. (2009). Inhibitory effect of kisspeptins on insulin secretion from isolated mouse islets. *Diabetes Obes. Metab.* 11(Suppl. 4), 197–201. doi: 10.1111/j.1463-1326.2009.01116.x

Wahab, F., Riaz, T., and Shahab, M. (2011). Study on the effect of peripheral kisspeptin administration on basal and glucose-induced insulin secretion under fed and fasting conditions in the adult male rhesus monkey (*Macaca mulatta*). *Horm. Metab. Res.* 43, 37–42. doi: 10.1055/s-0030-1268458

Wang, M., Wang, J. J., Li, J., Park, K., Qian, X., Ma, J. X., et al. (2009). Pigment epithelium-derived factor suppresses adipogenesis via inhibition of the MAPK/ERK pathway in 3T3-L1 preadipocytes. *Am. J. Physiol. Endocrinol. Metab.* 297, E1378–E1387. doi: 10.1152/ajpendo.00252.2009

Weisberg, S. P., McCann, D., Desai, M., Rosenbaum, M., Leibel, R. L., and Ferrante, A. W. Jr. (2003). Obesity is associated with macrophage accumulation in adipose tissue. *J. Clin. Invest.* 112, 1796–1808. doi: 10.1172/JCI200319246

Xing, R., Liu, F., Yang, Y., Cui, X., Wang, T., Xie, L., et al. (2018). GPR54 deficiency reduces the treg population and aggravates experimental autoimmune encephalomyelitis in mice. *Sci China Life Sci.* 61, 1–13. doi: 10.1007/s11427-017-9269-8

You, P., Hu, H., Chen, Y., Zhao, Y., Yang, Y., Wang, T., et al. (2016). Effects of melanocortin 3 and 4 receptor deficiency on energy homeostasis in rats. *Sci. Rep.* 6:34938. doi: 10.1038/srep34938

Conflict of Interest Statement: The authors declare that the research was conducted in the absence of any commercial or financial relationships that could be construed as a potential conflict of interest.

frontiers in Physiology

ORIGINAL RESEARCH
published: 28 February 2018
doi: 10.3389/fphys.2018.00136

Depletion of Regulatory T Cells in Visceral Adipose Tissues Contributes to Insulin Resistance in Hashimoto's Thyroiditis

Min Yang[1†], *Li Su*[2†], *Qin Tao*[1], *Chenxi Zhang*[2], *Yueyue Wu*[1] *and Jun Liu*[1*]

[1] *Department of Endocrinology, The Fifth People's Hospital of Shanghai, Fudan University, Shanghai, China,* [2] *Testing and Analysis Center, School of Pharmacy, Second Military Medical University, Shanghai, China*

OPEN ACCESS

Edited by:
Dechun Feng,
National Institute on Alcohol Abuse and Alcoholism, United States

Reviewed by:
Hua Wang,
Anhui Medical University, China
Ying Lu,
National Cancer Institute (NIH), United States

***Correspondence:**
Jun Liu
liujun@5thhospital.com

[†] *These authors have contributed equally to this work.*

Specialty section:
This article was submitted to Clinical and Translational Physiology, a section of the journal Frontiers in Physiology

Received: *06 December 2017*
Accepted: *12 February 2018*
Published: *28 February 2018*

Citation:
Yang M, Su L, Tao Q, Zhang C, Wu Y and Liu J (2018) Depletion of Regulatory T Cells in Visceral Adipose Tissues Contributes to Insulin Resistance in Hashimoto's Thyroiditis. Front. Physiol. 9:136. doi: 10.3389/fphys.2018.00136

Hashimoto's Thyroiditis (HT) is a common organ-specific autoimmune disorder associated with a high incidence, and insulin resistance is highly related to autoimmune. Here, we examined the insulin sensitivity in HT patients and found decreased insulin sensitivity occurred in HT patients. To explore the relationship between impaired insulin sensitivity and immune status, we established HT model mice which showed similar pathological features and immune features to HT patients. In HT model mice, reinfusion of regulatory T cells (Tregs) from peripheral blood of normal mice could improve insulin sensitivity and decrease the inflammation. Anti-CD25 antibodies blocked beneficial effects from reinfusion of Tregs, but delayed administration of anti-CD25 antibodies could not abolished the effect from Tregs. Delayed administration of anti-CD25 antibodies abolished exogenous Tregs in peripheral blood, but there were increased exogenous Tregs located to visceral adipose tissues (VATs) which modulated the expression of cytokines in VATs. These findings suggest that insulin resistance exists in HT patients and it associates with the decreased Tregs and increased inflammation in the VATs.

Keywords: Hashimoto's Thyroiditis, regulatory T cells, insulin resistance, cytokines, visceral adipose tissues

INTRODUCTION

Hashimoto's Thyroiditis (HT), a common organ-specific autoimmune disorder, presents the infiltration of the thyroid gland by inflammatory cells and the production of autoantibodies to thyroid-specific antigens (Ajjan and Weetman, 2015). HT is associated with the destruction of thyroid cells, and hypothyroidism is the main clinical manifestation (Işgüven et al., 2016). Hypothyroidism is associated with the susceptibility of insulin resistance and metabolic syndromes (Fernandez-Real et al., 2006; Roos et al., 2007; Jornayvaz et al., 2012). So HT should be connected to insulin resistance directly. But the reason that induces insulin resistance in HT patients is not clear.

Regulatory T cells (Tregs) are an important class of T cells maintaining immune self-tolerance (Yu et al., 2017). Tregs help to prevent the immune response against self-antigens (Perdigoto et al., 2015). In HT, T cells destruct the thyroid epithelial cells and thyroid epithelial structure (Stassi and De Maria, 2002). The role of Tregs in HT has been reported by many researchers that the thyroid damage in HT relating to Tregs/Th17 cell imbalance (Kristensen, 2016). Foxp3$^+$ Tregs have the characteristic phenotype (CD4$^+$CD25^{bright}) and the suppressive effect through the synthesis of TGF, IL-10, and IL-35 (Rodriguez-Munoz et al., 2016). Decreased level of CD4$^+$CD25^{bright}Foxp3$^+$ Tregs associates with increased autoimmune response in HT patients, and the decease of Tregs is also determined in the peripheral blood mononuclear cells (PBMCs) in HT patients in comparison to healthy individuals (Rodriguez-Munoz et al., 2016). It means that the level of Tregs is changed not only in thyroid. Abnormal level of Tregs is another important factor relating to insulin resistance. The percentage of peripheral CD4$^+$CD25$^+$Foxp3$^+$ Tregs is decreased in the patients with type 2 diabetes mellitus and the accumulation of Tregs in adipose tissue plays an important role in reducing obesity related insulin resistance in mice (Yuan et al., 2018). Thus, further researches are required to investigate the relationship between abnormal level of Tregs in HT and insulin resistance.

Experimental autoimmune thyroiditis (EAT) can be induced by the injection of thyroglobulin and adjuvant, and high iodide ingestion can also accelerate the incidence and severity of EAT (Lira et al., 2005; Fang et al., 2007). CBA/J mice are susceptible to EAT (Fang et al. 2007), and the thyroid lesions in this model are similar to the HT.

In this study, we elucidated the role of CD4$^+$CD25$^+$Foxp3$^+$ Tregs to insulin resistance in a CBA/J mice model of HT is established by the administration of iodine and induction of immune response to thyroid globulin. We also investigated the mechanism by which CD4$^+$CD25$^+$Foxp3$^+$ Tregs decreases insulin resistance.

MATERIALS AND METHODS

Animals

Female CBA/J mice (6 week aged) were purchased from Shanghai SLAC Laboratory Animal Co., Ltd. (Shanghai, China). Mice were maintained in a specific pathogen-free facility and were cared for in accordance with animal guidelines. The study was approved by the Institutional Animal Care and Use Committee in Second Military Medical University.

Human Serum

For human serum samples, written informed consent was obtained from all participants, and the study was approved and supervised by the Ethics Committee of our hospital. HT patients were first diagnosed and they had not received treatment when we collected the serum. Other basic information of patients is listed in schedule 1.

HT Model of Mice

Twenty-three female CBA/J mice of were randomly divided into the control group ($n = 8$) and the high iodine feeding group ($n = 45$) after 1 week of adaptive feeding. The high iodine group was fed with iodine containing 0.05% sodium iodide (1000HI, equivalent to 1,000 times that of the iodine intake of the normal mice), the control group was fed with sterile distilled water. Iodine is immediately used to avoid light preservation. The first immunization and repeated immunization: high iodine group was treated porcine thyroglobulin (mTg) (200 μg/mouse) subcutaneous injection in d0 and d14. The first immunization was used complete Freund's adjuvant (CFA) and repeated immunization was used incomplete Freund adjuvant (IFA).

Sodium iodide was purchased from Shanghai Xinping Fine Chemicals Co. Ltd. Incomplete Freund adjuvant and complete Freund's adjuvant was purchased from Shanghai Tongyi Biotechnology Company. Porcine thyroglobulin (mTg) was purchased from Nanjing Jiancheng Biological Engineering Institute.

Cytokines Assay

TNF-α, IFN-γ, IL1, IL6, IL10, and IL17 was analyzed by a LEGEND plexTM kit (Biolegend, San Diego, CA) according to the manufacturer's protocol.

Separation of Visceral Adipose Tissue Cells

Visceral adipose tissue (VAT) separated and digested with 2 mg/mL collagenase type V in Hanks' balanced salt solution for 30 min at 37°C. Digests were passed through a 40-μm cell strainer.

Flow Cytometry

T cells were stained with fluorochrome-conjugated monoclonal antibodies: anti-mouse CD3, CD4, CD8, IFN-γ, IL-4, IL-17a, CD25, Foxp3 (eBioscience, USA).

PBMC were separated from blood of participants, and then treated with PMA (50 ng/ml), ionomycin (1 μg/ml), BFA (3 μg/ml), and monensin (1.4 μg/ml) for 5 h. Then, those samples were stained with antibodies to different markers for flow cytometry.

Cells were analyzed with the FACS Calibur flow cytometer (BD Biosciences, USA).

Glucose Tolerance Assay and Insulin Assay

At 16 weeks, mice were fasted for 8 h and received intraperitoneal injection of glucose. Serum levels of glucose and insulin in mice were measured at 30, 60, 90, 120 min after the intraperitoneal injection of 20% glucose solution (0.2 ml/10 g weight). Glucose assay kits and mice insulin ELISA kits were purchased from Shanghai Tongyi Biotechnology Company and the analysis was accord to the manufacturer's protocols. Glucose was purchased from Sinopharm Chemical Reagent Company.

Histological Analysis

Sections (5 μm) of formalin-fixed tissue sections were stained with hematoxylin and eosin according to standard procedures. Sections were incubated in 0.3% H_2O_2, and followed by another 30 min in 1% BSA. Then, sections were incubated with anti-myeloperoxidase (MPO) (Biocare Medical, USA) primary antibodies overnight at 4°C. Vectastain Elite ABC Staining Kit and DAB Peroxidase Substrate Kit (Vector Laboratories,

USA) were used to visualize the staining according to the manufacturer's instructions.

Thyroid Globulin Antibodies and Anti-Thyroid Microsomal Antibodies Assay

The ELISA kits of thyroid globulin antibody (TGAb) and anti-thyroid microsomal antibody (TMAb) were purchased from the Institute of bioengineering in Nanjing.

Treg Cells Preparation and Injection

At first, B cells, macrophages, $CD8^+$ T cells, NK cells, dendritic cells, erythrocytes, and granulocytes were removed from plasma of normal mice by mouse $CD4^+$ negative selection kit (Dynal Biotech). Purified $CD4^+$ T cells were incubated with phycoerythrin-labeled anti-CD25 anti-body and anti-phycoerythrin magnetic beads and isolated using a MACS separation column (Miltenyi Biotec) to obtain $CD4^+CD25^+$ T cells. Cell purity was assessed by fluorescence-activated cell sorter and was consistently higher than 90% with an average purity of 96% for caudal vein injection (10^6 cells per mouse). Flow cytometry analysis also confirmed that about 85% purified cells were $Foxp3^+$.To mark transferred cells, we mixed lentivirus expressing GFP with purified Tregs (MOI = 6) for 4 h at 37°C in cell culture incubator, and washed with PBS before the injection.

Treg Cells Depletion

To deplete Treg cells, mice were given anti-CD25 (Bio X cell (West Lebanon, NH), 50 μg/kg) intravenously 1 h after the reinfusion of Tregs.

Statistical Analysis

The data are shown as mean ± SEM. Data from two groups were compared with an unpaired *t*-test. Data from three or more groups were analyzed with one-way ANOVA with Tukey's multiple comparisons test. *p*-values < 0.05 and *p*-values < 0.01 were considered as statistically significant.

RESULTS

Abnormal Insulin Sensitivity and Peripheral Immune Status Are Associated With HT Patients

To confirm our hypothesis, we analyzed indexes of insulin sensitivity in HT patients (**Table 1**). These patients had normal thyroid function, but they had enlarged thyroid and increased autoantibodies to thyroid peroxidase and thyroid globulin (**Figure 1A**, $p < 0.05$). In these patients, fasting blood glucose was raised significantly compared with normal control, and they also had higher postprandial plasma insulin after 30 min or 120 min (**Figure 1B**, $p < 0.05$). Rates of impaired fasting glucose and impaired glucose tolerance were also significantly higher than normal control (**Figure 1B**). All the results implied that insulin resistance occurred in HT patients. Serum total triglyceride, total cholesterol, high density lipoprotein (HDL), low density lipoprotein (LDL), apolipoprotein A, apolipoprotein B, and lipoprotein A showed not difference between HT patients and normal control (**Figure 1C**, $p > 0.05$), which meant the insulin resistance should not relate to fat or lipid metabolism in HT patients.

TABLE 1 | Basic information of participants.

	HT group	Control	*P*
n	61	38	
Sex (Female/male)	59/2	37/1	NS
Age (year)	47.2 ± 14.7	40.6 ± 16.9	NS
Hypertension (%)	1.6	0	NS
FT_3 (pg/ml)	2.9 ± 0.6	2.9 ± 0.7	NS
FT_4 (ng/dl)	1.1±0.3	1.1±0.1	NS
TT_3 (ng/ml)	1.1±0.4	1.4±1.5	NS
TT_4 (ug/dL)	8.5 ± 3.0	9.3 ± 1.7	NS
TSH (ulU/ml)	2.1 ± 1.2	2.2 ± 1.3	NS
TPOAb (U/ml)	790.1 ± 572.3	30.3 ± 16.6	<0.0001
TGAb (U/ml)	216.5 ± 29.3	16.1 ± 9.7	<0.0001

Production of cytokines and subsets of T cell subsets were also measured in peripheral blood from HT patients. Inflammatory cytokines, such as TNF-α, IL-1β, and IL-6 (**Figure 1D**, $p < 0.05$), were increased in HT patients. IL-10, an important anti-inflammatory cytokine was also changed significantly (**Figure 1D**, $p < 0.05$). Increased $CD4^+$ T cells and decreased $CD8^+$T cells were found compared with normal control (**Figure 2A**). Although Th2 cells did not significantly changed (**Figure 2C**), Th1 cells and Th17 cells increased in HT patients (**Figures 2B,D**, $p < 0.05$). $CD25^+Foxp3^+$ Tregs were also decreased in HT patients (**Figure 2E**, $p < 0.05$).

So insulin resistance and Tregs decrease occurred in HT patients.

Peripheral $CD25^+Foxp3^+$ Tregs From Normal Mice Decreased Symptoms of HT in HT Model Mice

Figure 3A is the progress of experiment design.

In HT model mice, autoantibodies to thyroid globulin and thyromicrosome were significantly induced (**Figures 3F,G**, $p < 0.05$). Infiltration of inflammatory cells to the thyroid gland was also observed in HT model mice in comparison with control mice (**Figure 4**). So the HT model mice established by us shown the similar pathological features in clinic. Beside the change in the thyroid gland, pathological changes in VATs were also decreased (**Figure 4**).

The reinfusion of peripheral $CD25^+Foxp3^+$ Tregs from normal mice significantly decreased autoantibodies to thyroid globulin and thyromicrosome and thyroid weight (**Figures 3C,F,G**). Exogenous $CD25^+Foxp3^+$ Tregs also decreased the infiltration of inflammatory cells to the thyroid gland (**Figure 4**). These effects could be blocked by the administration of anti-CD25 antibodies (**Figures 3C,F,G**, **4**). It shown the fact that recovery of Tregs in HT model mice modulated the immune system and decreased severity of decrease.

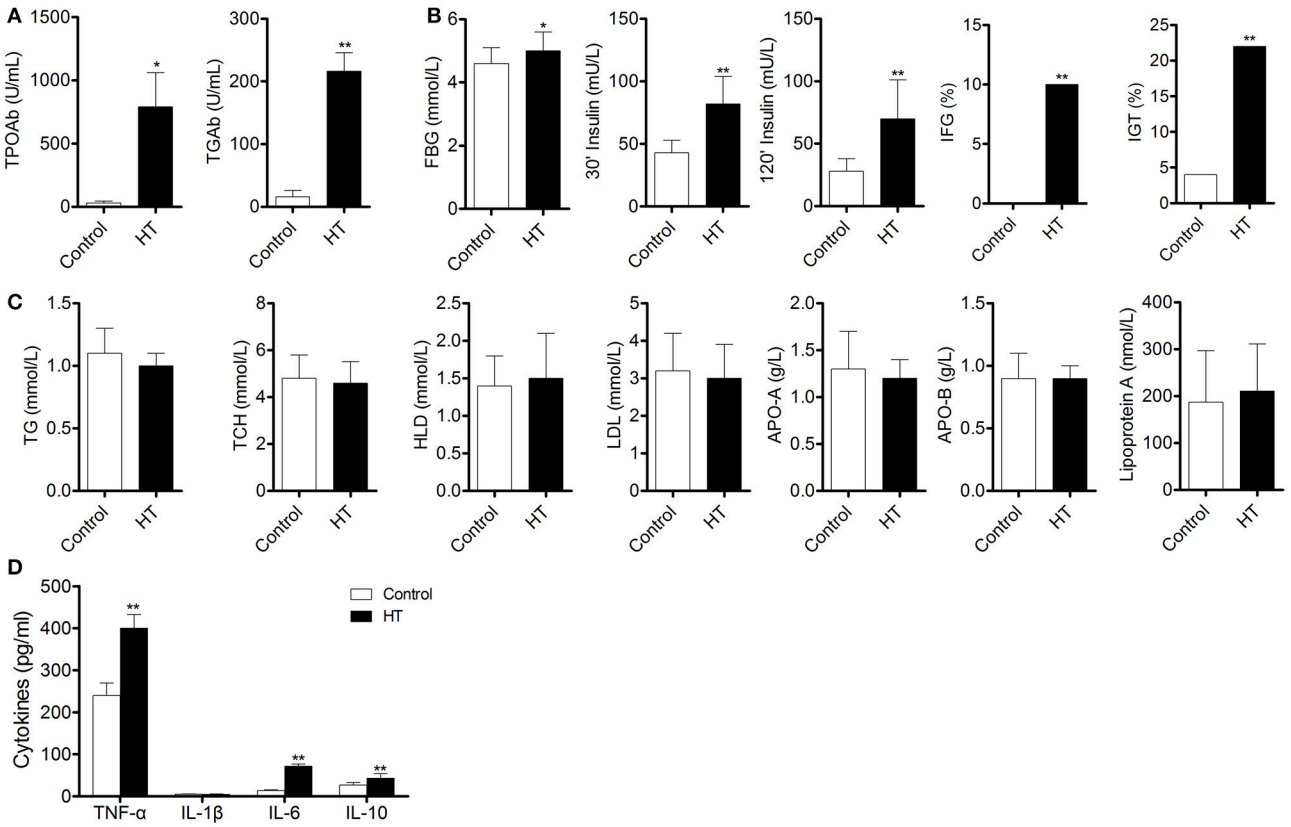

FIGURE 1 | Abnormal insulin sensitivity and peripheral immune status are associated with HT patients. **(A)** Autoantibodies to thyroid peroxidase and thyroid globulin increased in HT patients (*$p < 0.05$; **$p < 0.01$ compared with normal control). **(B)** Insulin sensitivity decreased in HT patients compared with normal control (*$p < 0.05$; **$p < 0.01$ compared with normal control). **(C)** Lipid metabolism was not changed between HT patients and normal control. **(D)** Expression pattern of cytokines was changed between HT patients and normal control (**$p < 0.01$ compared with normal control).

Changed β-Cell Function and Insulin Sensitivity Were Detected in HT Model Mice

Although similar glucose concentrations were found between HT model mice and control mice (**Figure 3D**), higher insulin levels at 30 and 120 min during oral glucose tolerance test were presented in HT model mice comparing with control mice (**Figure 3E**, $p < 0.05$). High levels of InsAUC30/GluAUC30 and InsAUC120/GluAUC120 were detected in HT model mice (**Figures 3D,E**, $p < 0.05$), which meant the early phase insulin release and total insulin release were both significantly changed in comparison with control mice. In each group, body weight was not significantly changed (**Figure 3B**), and it meant the change of insulin sensitivity should not be the result of weight/fat. Thyroid weight increased significantly in HT model mice (**Figure 3C**), and it might exclude the influence of hypothyroidism which was reported to relate to insulin resistance. These results suggested that the sensitivity of insulin resistance was lacked in HT model mice.

T Cell Subsets in Peripheral Blood and Visceral Adipose Tissues Were Changed in HT Model Mice

As an autoimmune disease, abnormal distribution of T cell subsets is important to HT disease. We analyzed T cells in peripheral blood by flow cytometry, and we found the $CD3^+$ cells were not changed between HT model mice and control mice (**Figure 5A**). The ratio of $CD4^+/CD8^+$ T cells was significantly increased in HT model mice (**Figure 5B**), which reflects the abnormal immune reaction in HT model mice, and decreased $CD25^+Foxp3^+$ Tregs was also found in peripheral blood of HT model mice (**Figure 5C**). And these changes were similar to the results of HT patients.

Visceral adipose tissues (VATs) are important to insulin sensitivity in physiological condition. We separated the VATs from both of HT model mice and control mice, and the abnormal distribution of T cell subsets was also found in adipose tissues from HT model mice (**Figure 6**). Increased ratio of $CD4^+/CD8^+$ T cells (**Figure 6B**) and decreased $CD25^+Foxp3^+$ Tregs (**Figure 6C**) meant that

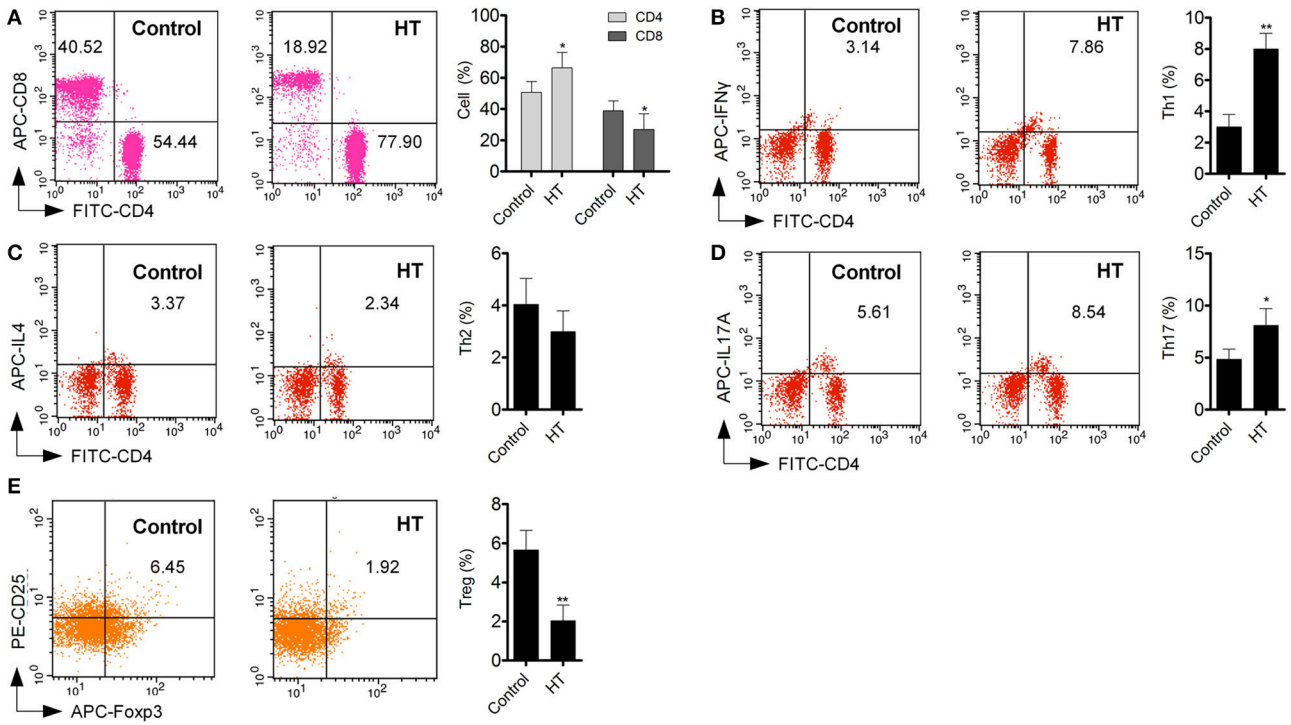

FIGURE 2 | T cell subsets in peripheral blood were different between HT patients and normal control. **(A)** Increased $CD4^+$ T cell and deceased $CD8^+$ T cells were found in peripheral blood from HT patients (*$p < 0.05$ compared with normal control). **(B–E)** Increased Th1 and Th17 cells were found in HT patients, but Tregs were decreased in HT patients (*$p < 0.05$; **$p < 0.01$ compared with normal control).

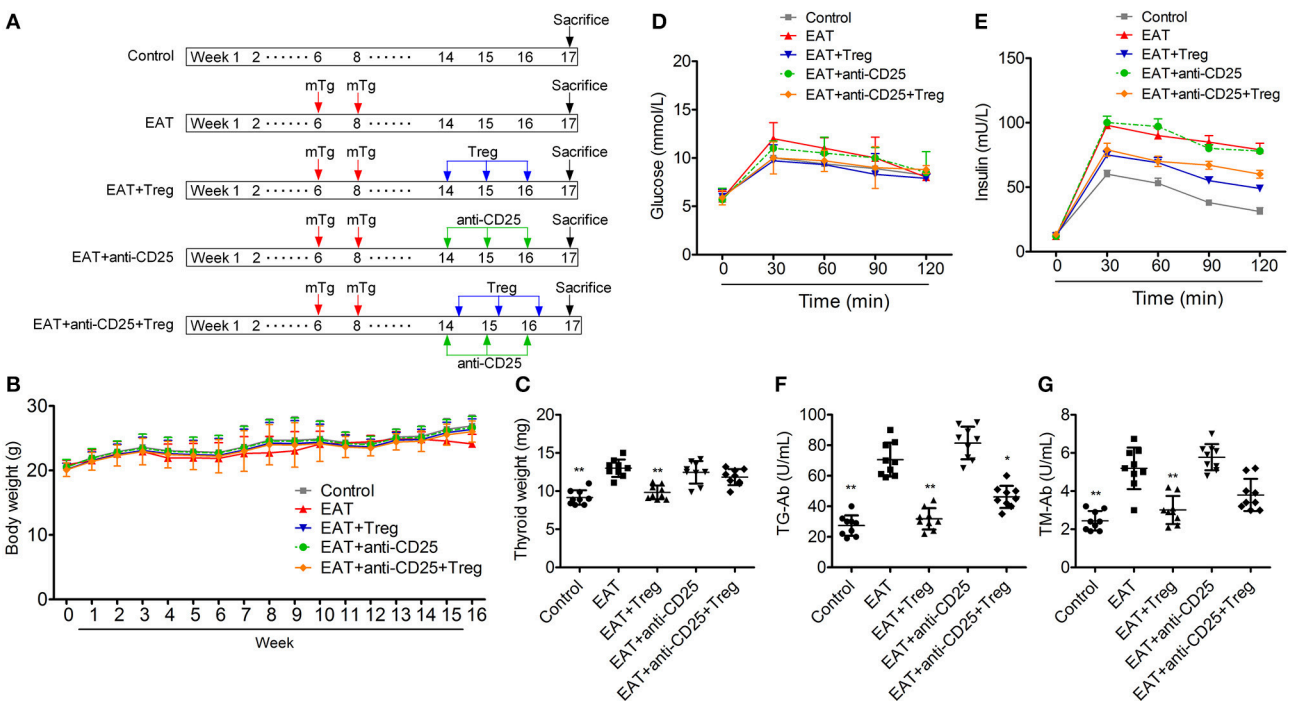

FIGURE 3 | Establishment of HT model mice and the insulin sensitivity of HT model mice was changed. **(A)** The progress of experiment design. **(B)** Bodies weight did not change between groups. **(C,F,G)** Thyroid weight was increased in HT model mice, and the reinfusion of Tregs improved the pathological changes (*$p < 0.05$; **$p < 0.01$ compared with EAT group). **(D,E)** Insulin sensitivity of HT model mice was impaired compared with control mice.

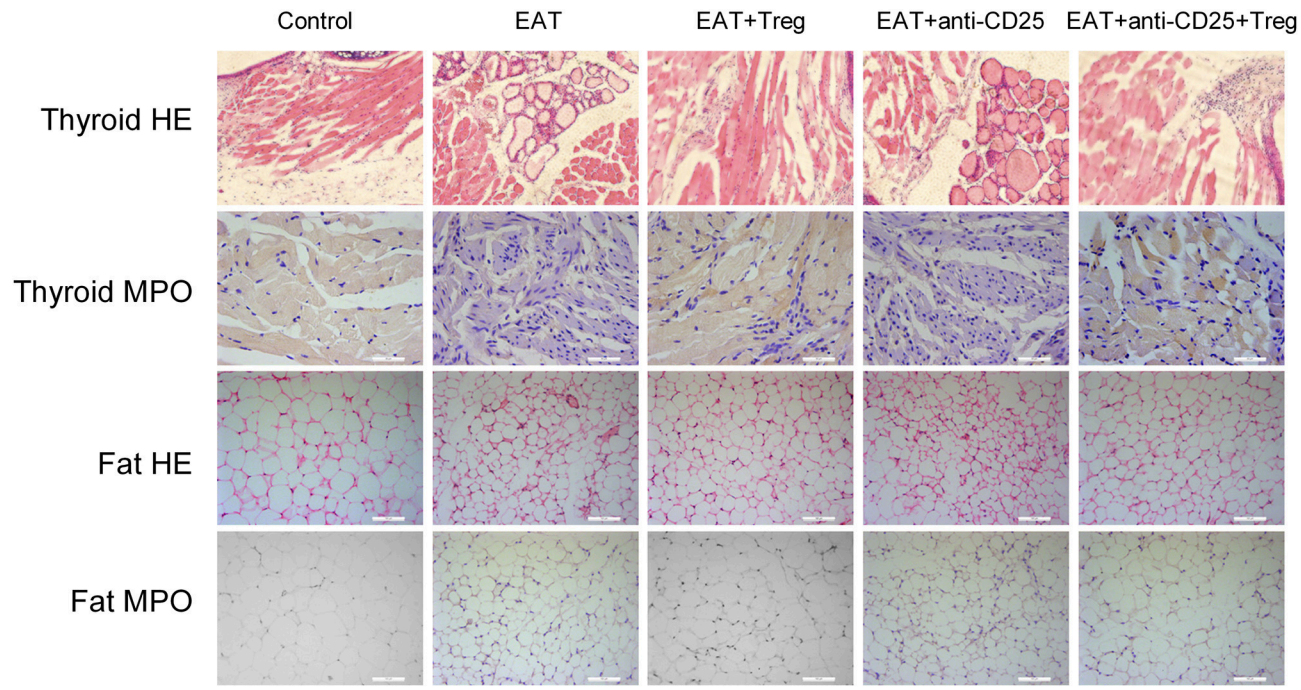

FIGURE 4 | Pathological changes were observed in HT model mice and the reinfusion of Tregs showed beneficial effects to HT model mice.

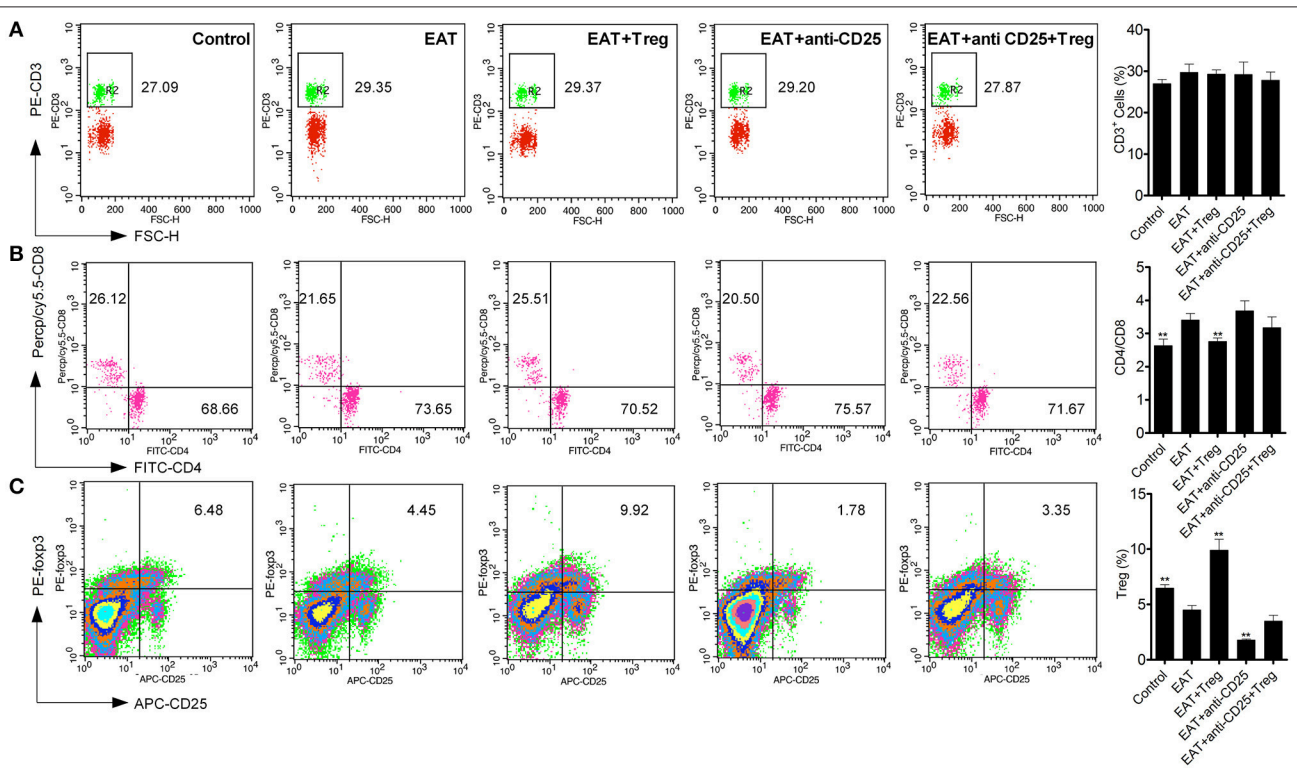

FIGURE 5 | T cell subsets were changed in peripheral blood from HT model mice. **(A)** $CD3^+$ cells were not changed in each groups. **(B)** Higher ratio of $CD4^+/CD8^+$ was found in HT model mice and the reinfusion of Tregs rescued imbalance of $CD4^+/CD8^+$ (**$p < 0.01$ compared with EAT group). This beneficial effect was blocked by anti-CD25 antibodies. **(C)** $CD25^+Foxp3^+$ Tregs decreased in peripheral blood from HT model mice and they were rescued by the reinfusion of Tregs, but it was abolished by anti-CD25 antibodies (**$p < 0.01$ compared with EAT group).

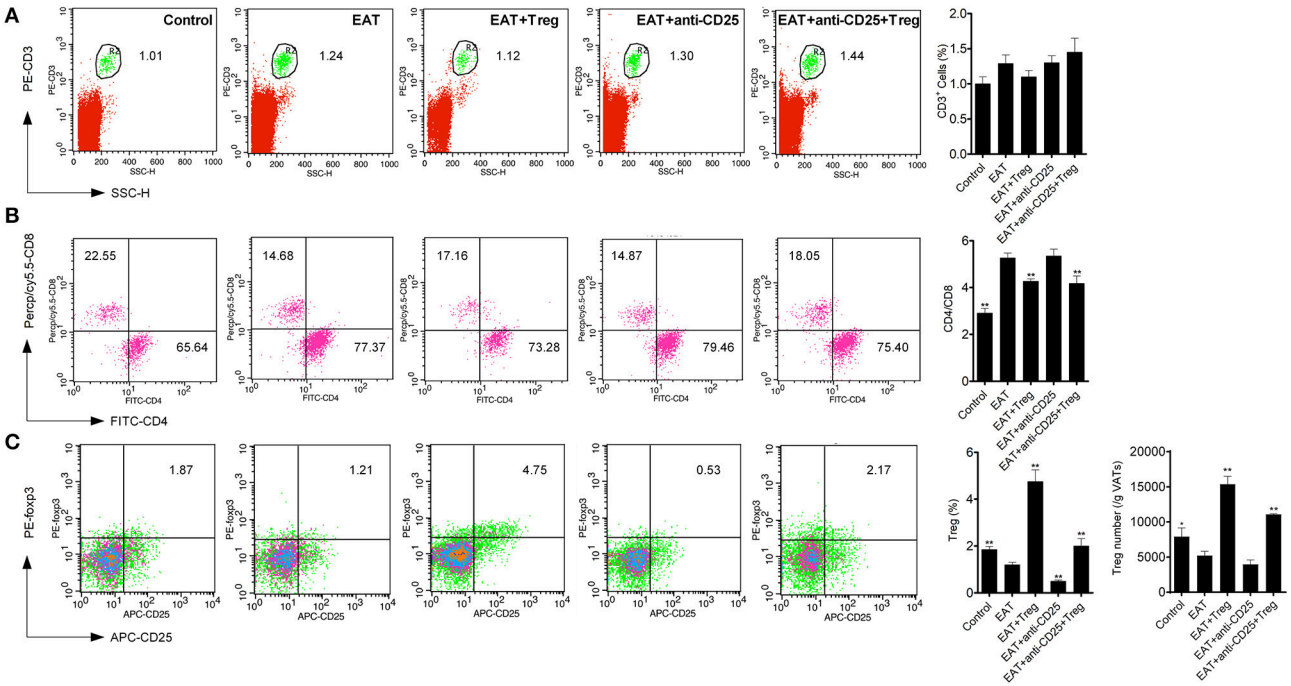

FIGURE 6 | T cell subsets were changed in visceral adipose tissues from HT model mice. **(A)** $CD3^+$ cells were not changed in each groups. **(B)** Higher ratio of $CD4^+/CD8^+$ was found in HT model mice and the reinfusion of Tregs rescued imbalance of $CD4^+/CD8^+$ (**$p < 0.01$ compared with EAT group). This beneficial effect was blocked by anti-CD25 antibodies. **(C)** $CD25^+Foxp3^+$ Tregs decreased in visceral adipose tissues from HT model mice and they were rescued by the reinfusion of Tregs, and it was partly abolished by anti-CD25 antibodies (**$p < 0.01$ compared with EAT group; *$p < 0.01$ compared with EAT group).

HT might induce abnormal immune reaction not only in thyroid gland, periphery but also VATs. VATs Tregs are necessary for restore the insulin sensitivity in type-2 diabetes, so decreased VATs Tregs in HT model might associate with the decrease of insulin sensitivity in HT model mice.

Peripheral $CD25^+Foxp3^+$ Tregs From Normal Mice Restored the Insulin Sensitivity in HT Model Mice

In HT model mice, $CD25^+Foxp3^+$ Tregs were decreased significantly in both of peripheral blood and VATs when compared with the control group (**Figure 6C**), and Tregs in VATs are important to insulin sensitivity. Therefore, we separated and transfused peripheral blood $CD25^+Foxp3^+$ Tregs from normal mice into HT model mice, and the treatment significantly increased $CD25^+Foxp3^+$ Tregs in both of peripheral blood and VATs (**Figures 5C**, **6C**). In HT model mice, the transfusion of $CD25^+Foxp3^+$ Tregs decreased the level of InsAUC30/GluAUC30 and InsAUC120/GluAUC120 (**Figures 3D,E**). All of these results showed that increased level of $CD25^+Foxp3^+$ Tregs not only improved the state of HT but also the sensitivity of insulin. These beneficial effects were abolished by anti-CD25 antibodies (**Figure 3E**). So $CD25^+Foxp3^+$Tregs related to the insulin resistance in HT model mice.

Increased $CD25^+Foxp3^+$ Tregs in Visceral Adipose Tissues Restored the Insulin Sensitivity in HT Model Mice

To confirm the mechanism of $CD25^+Foxp3^+$ Tregs increased insulin sensitivity, we adopted $CD25^+Foxp3^+$ Tregs to HT model mice and administered mice with anti-CD25 antibodies after 3 days (**Figure 7A**). Administration of anti-CD25 antibodies just partly abolished beneficial effects from $CD25^+Foxp3^+$ Tregs (**Figure 7B**), so we hypothesized that $CD25^+Foxp3^+$ Tregs in VATs might more important to insulin resistance in HT. To confirm the hypothesis, we expressed GFP in separated $CD25^+Foxp3^+$ Tregs (named GFP-$CD25^+Foxp3^+$ Tregs), and we transfused these GFP-$CD25^+Foxp3^+$ Tregs into HT model mice. After 3 days, mice were treated with anti-CD25 antibodies, and we found almost no GFP-$CD25^+Foxp3^+$ Tregs were detected in peripheral blood after the administration of anti-CD25 antibodies (**Figure 7C**). But amount of GFP-$CD25^+Foxp3^+$ Tregs could still be detected in VATs (**Figure 7C**). These adoptive transferred Tregs trafficked to adipose tissue and might played roles in local tissues.

Cytokines in Visceral Adipose Tissues Played Important Roles in Insulin Sensitivity in HT Model Mice

In previous researches, cytokines and inflammation in adipose tissue are important to insulin resistance in T2DM, so changed

level of $CD25^+Foxp3^+$ Tregs might relate to insulin resistance through cytokines in HT. we measured the cytokines in peripheral blood and VATs, and significantly increased IFN-γ, IL-1β, IL17A, IL6, and TNF-α were found in HT model mice (**Figure 8A**, $p < 0.05$ compared with control mice). After the transfusion of $CD25^+Foxp3^+$ Tregs, IFN-γ, IL-1β, IL17A, IL6, and TNF-α were decreased and IL-10 was increased significantly (**Figure 8A**, $p < 0.05$). Combined with anti-CD25 antibodies, the transfusion of $CD25^+Foxp3^+$ Tregs could not induce beneficial effects on the production of cytokines in peripheral blood (**Figure 8A**).Anti-CD25 antibodies abolished changes of cytokines in VATs when combined anti-CD25 antibodies with $CD25^+Foxp3^+$ Tregs (**Figure 8B**), but changes of cytokines in VATs still existed when anti-CD25 antibodies were administrated

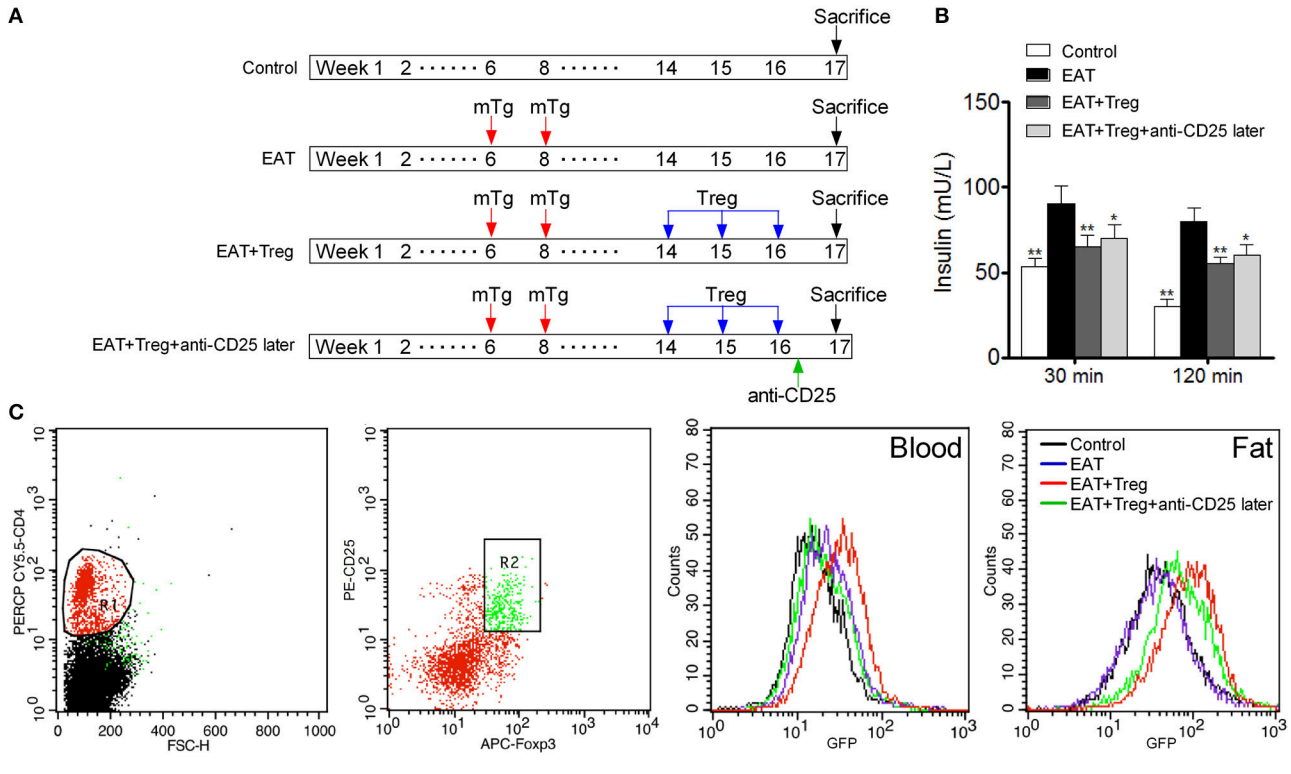

FIGURE 7 | Administration of anti-CD25 antibodies after the reinfusion did not abolished the beneficial effects from exogenous Tregs. **(A)** Design of the experiment. **(B)** Insulin sensitivity was rescued even combined with anti-CD25 antibodies (*$p < 0.05$; **$p < 0.01$ compared with EAT group). **(C)** We analyzed T cell subsets which were $CD4^+CD25^+Foxp3^+$ Tregs, and delayed administration of anti-CD25 antibodies decreased exogenous Tregs in peripheral blood but not in visceral adipose tissues.

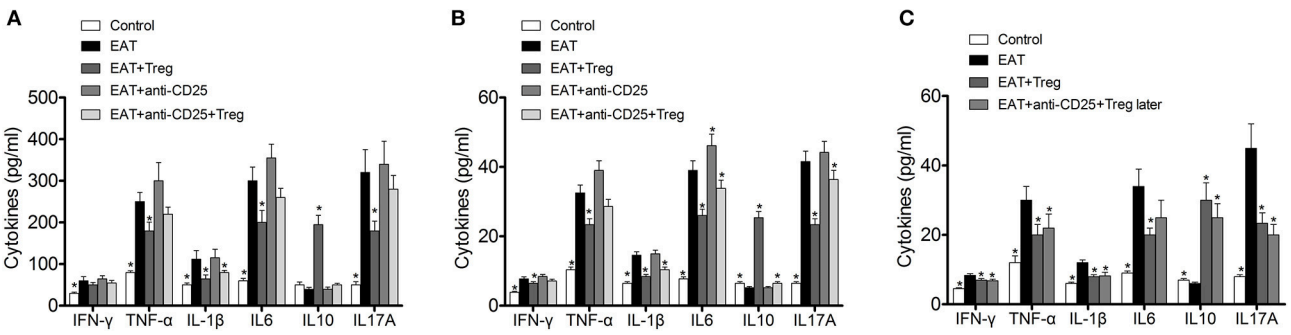

FIGURE 8 | Reinfusion of Tregs changed the pattern of cytokines in both of peripheral blood and visceral adipose tissues. **(A)** Exogenous Tregs normalized the pattern of cytokines in peripheral blood of HT model mice, but it could be blocked by anti-CD25 antibodies (*$p < 0.05$ compared with EAT group). **(B)** Exogenous Tregs normalized the pattern of cytokines in visceral adipose tissues of HT model mice, but it could be blocked by anti-CD25 antibodies (*$p < 0.05$ compared with EAT group). **(C)** Exogenous Tregs normalized the pattern of cytokines in visceral adipose tissues of HT model mice, and it could not be blocked by delayed administration of anti-CD25 antibodies (*$p < 0.05$ compared with EAT group).

3 days after the reinfusion (**Figure 8C**). The production of cytokines was consistent with insulin sensitivity in mice. So Tregs from donor mice should move to VATs and suppressed the local inflammation, which leaded to the reversal of insulin resistance.

DISCUSSION

HT is an autoimmune disease, and there are growing evidences that autoimmune links to insulin resistance. Although hypothyroidism is thought the major reason that links HT to insulin resistance (Fernandez-Real et al., 2006), the abnormal immune in HT might relate to insulin resistance directly. In this study, we provided that decreased level of $CD25^+Foxp3^+$ Tregs in HT model mice related to increased early phase and total insulin secretion, and the reinfusion of $CD25^+Foxp3^+$ Tregs separated from peripheral blood of normal mice restored the insulin sensitivity in HT model mice. It indicated that decreased Tregs in HT patients might be a critical factor for insulin resistance. We also depleted the peripheral $CD25^+Foxp3^+$ Tregs after the reinfusion, but the effect of insulin sensitivity was still retained. We found the administration of anti-CD25 antibodies depleted $CD25^+Foxp3^+$ Tregs effectively in peripheral blood but not in VATs, and the change of cytokines in peripheral blood and VATs were similar to the results of $CD25^+Foxp3^+$ Tregs. Thus, HT is connected with insulin resistance which relates to the depletion of Tregs in VATs.

Insulin resistance is the excessive insulin accumulation in blood with normal blood glucose levels (Reilly and Saltiel, 2017). Various diseases are associated with insulin resistance, such as type 2 diabetes, metabolic syndromes, obesity, and so on. Most of these diseases are related to abnormal immune responses, and chronic inflammation is an important factor of insulin resistance (Samuel and Shulman, 2012). In type 2 diabetes, it is clear that inflammation in adipose tissue is important to insulin resistance and the pathogenesis, and induction of Tregs alleviates insulin resistance in T2DM mice(Ilan et al., 2010; Nekoua et al., 2016). In HT, auto-reactive $CD4^+$ T cells are activated and induced cytotoxic T cells to destruct thyroid cells, and HT is regarded as primarily a T-cell mediated disease (Kristensen, 2016).Tregs are reduced in HT and the existence of Tregs is important to induce tolerance to autoimmune thyroiditis (Xue et al., 2015; Li et al., 2016). But the relationship between abnormal Tregs and insulin resistance in HT has not been reported in HT. The findings of the current study are similar with previous researches. Tregs were decreased significantly in peripheral blood of HT model mice, and the decrease of Tregs in VATs revealed the involvement of Tregs in HT model mice with insulin resistance. Fat-reside Tregs and the chronic adipose inflammatory are related to insulin resistance in patients with type 2 diabetes, and Tregs are important negative regulators of VAT inflammation and insulin resistance (Bapat et al., 2015; Sepehri et al., 2017). Increased level of inflammatory cytokines, such as IFN-γ, IL-1β, IL17A, IL6, and TNF-α, is also related to insulin resistance, and increased anti-inflammatory cytokines can improve glucose metabolism which regulates insulin sensitivity (Winer et al., 2009; Chng et al., 2015). Th1 and Th2 CD4 cells, as well as IFN-γ+CD8 T cells, present in the adipose tissue and the balance of these subsets is associated with not only the responses to antigenic stimulation but also the insulin resistance (McLaughlin et al., 2014; Stafeev et al., 2017).

In conclusion, insulin resistance exists in both of HT patients and HT model mice, and the abnormal distribution of T cell subsets especially in VATs contributes to the insulin resistance in HT.

AUTHOR CONTRIBUTIONS

All authors have seen and approved the final version of the manuscript. JL conceived and designed the experiments. MY and LS contributed equally to the paper. MY performed the animal experiments and staining of tissues. LS and CZ separated and analyzed T cells from peripheral blood and visceral adipose tissues. YW and QT analyzed cytokines and data. JL wrote the paper. MY and LS also contributed to the writing of the paper.

FUNDING

This study was funded by the Scientific Research Plan Project of Health and Family Planning Commission of Shanghai (grant no. 20174Y0118), Natural Science Foundation of Minghang District (2016MHZ17).

REFERENCES

Ajjan, R. A., and Weetman, A. P. (2015). The pathogenesis of Hashimoto's Thyroiditis: further developments in our understanding. *Horm. Metab. Res.* 47, 702–710. doi: 10.1055/s-0035-1548832

Bapat, S. P., Myoung Suh, J., Fang, S., Liu, S., Zhang, Y., Cheng, A., et al. (2015). Depletion of fat-resident Treg cells prevents age-associated insulin resistance. *Nature* 528, 137–141. doi: 10.1038/nature16151

Chng, M. H., Alonso, M. N., Barnes, S. E., Nguyen, K. D., and Engleman, E. G. (2015). Adaptive immunity and antigen-specific activation in obesity-associated insulin resistance. *Mediators Inflamm.* 2015:593075. doi: 10.1155/2015/593075

Fang, Y., DeMarco, V. G., Sharp, G. C., and Braley-Mullen, H. (2007). Expression of transgenic FLIP on thyroid epithelial cells inhibits induction and promotes resolution of granulomatous experimental autoimmune thyroiditis in CBA/J mice. *Endocrinology* 148, 5734–5745. doi: 10.1210/en.2007-0939

Fernández-Real, J. M., Lopez-Bermejo, A., Castro, A., Casamitjana, R., and Ricart, W. (2006). Thyroid function is intrinsically linked to insulin sensitivity and endothelium-dependent vasodilation in healthy euthyroid subjects. *J. Clin. Endocrinol. Metab.* 91, 3337–3343. doi: 10.1210/jc.2006-0841

Ilan, Y., Maron, R., Tukpah, A. M., Maioli, T. U., Murugaiyan, G., Yang, K., et al. (2010). Induction of regulatory T cells decreases adipose inflammation and alleviates insulin resistance in ob/ob mice. *Proc. Natl. Acad. Sci. U.S.A.* 107, 9765–9770. doi: 10.1073/pnas.0908771107

Işgüven, P., Gündüz, Y., and Kiliç, M. (2016). Effects of thyroid autoimmunity on early atherosclerosis in euthyroid girls with Hashimoto's Thyroiditis. *J. Clin. Res. Pediatr. Endocrinol.* 8, 150–156. doi: 10.4274/jcrpe.2145

Jornayvaz, F. R., Lee, H. Y., Jurczak, M. J., Alves, T. C., Guebre-Egziabher, F., Guigni, B. A., et al. (2012). Thyroid hormone receptor-alpha gene knockout

mice are protected from diet-induced hepatic insulin resistance. *Endocrinology* 153, 583–591. doi: 10.1210/en.2011-1793

Kristensen, B. (2016). Regulatory B and T cell responses in patients with autoimmune thyroid disease and healthy controls. *Dan. Med. J.* 63:B5177.

Li, C., Yuan, J., Zhu, Y. F., Yang, X. J., Wang, Q., Xu, J., et al. (2016). Imbalance of Th17/Treg in different subtypes of autoimmune thyroid diseases. *Cell. Physiol. Biochem.* 40, 245–252. doi: 10.1159/000452541

Lira, S. A., Martin, A. P., Marinkovic, T., and Furtado, G. C. (2005). Mechanisms regulating lymphocytic infiltration of the thyroid in murine models of thyroiditis. *Crit. Rev. Immunol.* 25, 251–262. doi: 10.1615/CritRevImmunol.v25.i4.10

McLaughlin, T., Liu, L. F., Lamendola, C., Shen, L., Morton, J., Rivas, H., et al. (2014). T-cell profile in adipose tissue is associated with insulin resistance and systemic inflammation in humans. *Arterioscler. Thromb. Vasc. Biol.* 34, 2637–2643. doi: 10.1161/ATVBAHA.114.304636

Nekoua, M. P., Fachinan, R., Atchamou, A. K., Nouatin, O., Amoussou-Guenou, D., Amoussou-Guenou, M. K., et al. (2016). Modulation of immune cells and Th1/Th2 cytokines in insulin-treated type 2 diabetes mellitus. *Afr. Health Sci.* 16, 712–724. doi: 10.4314/ahs.v16i3.11

Perdigoto, A. L., Chatenoud, L., Bluestone, J. A., and Herold, K. C. (2015). Inducing and administering tregs to treat human disease. *Front. Immunol.* 6:654. doi: 10.3389/fimmu.2015.00654

Reilly, S. M., and Saltiel, A. R. (2017). Adapting to obesity with adipose tissue inflammation. *Nat. Rev. Endocrinol.* 13, 633–643. doi: 10.1038/nrendo.2017.90

Rodríguez-Muñoz, A., Vitales-Noyola, M., Ramos-Levi, A., Serrano-Somavilla, A., González-Amaro, R., and Marazuela, M. (2016). Levels of regulatory T cells $CD69^{+}NKG2D^{+}IL\text{-}10^{+}$ are increased in patients with autoimmune thyroid disorders. *Endocrine* 51, 478–489. doi: 10.1007/s12020-015-0662-2

Roos, A., Bakker, S. J., Links, T. P., Gans, R. O., and Wolffenbuttel, B. H. (2007). Thyroid function is associated with components of the metabolic syndrome in euthyroid subjects. *J. Clin. Endocrinol. Metab.* 92, 491–496. doi: 10.1210/jc.2006-1718

Samuel, V. T., and Shulman, G. I. (2012). Mechanisms for insulin resistance: common threads and missing links. *Cell* 148, 852–871. doi: 10.1016/j.cell.2012.02.017

Sepehri, Z., Kiani, Z., Afshari, M., Kohan, F., Dalvand, A., and Ghavami, S. (2017). Inflammasomes and type 2 diabetes: an updated systematic review. *Immunol. Lett.* 192, 97–103. doi: 10.1016/j.imlet.2017.10.010

Stafeev, I. S., Vorotnikov, A. V., Ratner, E. I., Menshikov, M. Y., and Parfyonova, Y. V. (2017). Latent inflammation and insulin resistance in adipose tissue. *Int. J. Endocrinol.* 2017:5076732. doi: 10.1155/2017/5076732

Stassi, G., and De Maria, R. (2002). Autoimmune thyroid disease: new models of cell death in autoimmunity. *Nat. Rev. Immunol.* 2, 195–204. doi: 10.1038/nri750

Winer, S., Chan, Y., Paltser, G., Truong, D., Tsui, H., Bahrami, J., et al. (2009). Normalization of obesity-associated insulin resistance through immunotherapy. *Nat. Med.* 15, 921–929. doi: 10.1038/nm.2001

Xue, H., Yu, X., Ma, L., Song, S., Li, Y., Zhang, L., et al. (2015). The possible role of $CD4^{+}CD25$(high)$Foxp3^{+}/CD4^{+}IL\text{-}17A^{+}$ cell imbalance in the autoimmunity of patients with Hashimoto thyroiditis. *Endocrine* 50, 665–673. doi: 10.1007/s12020-015-0569-y

Yu, H., Paiva, R., and Flavell, R. A. (2017). Harnessing the power of regulatory T cells to control autoimmune diabetes: overview and perspective. *Immunology* 153, 161–170. doi: 10.1111/imm.12867

Yuan, N., Zhang, H. F., Wei, Q., Wang, P., and Guo, W. Y. (2018). Expression of $CD4^{+}CD25^{+}Foxp3^{+}$ regulatory T cells, interleukin 10 and transforming growth factor beta in newly diagnosed type 2 diabetic patients. *Exp. Clin. Endocrinol. Diabetes*. 126, 96–101. doi: 10.1055/s-0043-113454

Conflict of Interest Statement: The authors declare that the research was conducted in the absence of any commercial or financial relationships that could be construed as a potential conflict of interest.

frontiers in Physiology

MINI REVIEW
published: 27 February 2018
doi: 10.3389/fphys.2018.00135

The Role of Sirt6 in Obesity and Diabetes

Jiangying Kuang[1,2], *Lei Chen*[1,3], *Qin Tang*[1,3], *Jinhang Zhang*[1,3], *Yanping Li*[1,3] *and Jinhan He*[1,3]*

[1] State Key Laboratory of Biotherapy, Department of Pharmacy, West China Hospital, Sichuan University, Chengdu, China, [2] Department of Cardiology, The Second Hospital of Shandong University, Shandong University, Jinan, China, [3] Laboratory of Clinical Pharmacy and Adverse Drug Reaction, West China Hospital, Sichuan University, Chengdu, China

Sirt6 is one of the sirtuin family members, a kind of NAD+-dependent histone deacetylase and ADP-ribose transferase enzyme. It has an important role in physiological and pathological processes, regulating aging, cancer, obesity, insulin resistance, inflammation, and energy metabolism. Recent studies have suggested that reduced Sirt6 action is related to obesity and diabetes. Aging and overnutrition, two major risk factors for obesity and diabetes, lead to decreased Sirt6 level and function, which results in abnormal glucose and lipid metabolism. Whole-body ablation of Sirt6 in mice results in severe hypoglycemia. Sirt6 deficiency leads to liver steatosis and promotes diet-induced obesity and insulin resistance. Sirt6 has a protective effect on obesity and diabetes. This review surveys evidence for an emerging role of Sirt6 as a regulator of metabolism in mammals and summarizes its major functions in obesity and diabetes.

Keywords: Sirt6, obesity, diabetes mellitus, type 2, LiPo, gluconeogenesis

OPEN ACCESS

Edited by:
Dechun Feng,
National Institute on Alcohol Abuse and Alcoholism, United States

Reviewed by:
Hua Wang,
Anhui Medical University, China
Zlyi Liu,
National Institutes of Health (NIH), United States

***Correspondence:**
Jinhan He
jinhanhe@scu.edu.cn

Specialty section:
This article was submitted to Clinical and Translational Physiology, a section of the journal Frontiers in Physiology

Received: *07 January 2018*
Accepted: *12 February 2018*
Published: *27 February 2018*

Citation:
Kuang J, Chen L, Tang Q, Zhang J, Li Y and He J (2018) The Role of Sirt6 in Obesity and Diabetes. Front. Physiol. 9:135. doi: 10.3389/fphys.2018.00135

INTRODUCTION

The sirtuins are a highly conserved family of NAD^+-dependent deacetylases and ADP-ribosyltransferases that play an important regulatory role in the physiological and pathological processes of the organism. They participate in regulating the life span and aging, cancer, obesity, insulin resistance, inflammatory response and energy metabolism (Michan and Sinclair, 2007). The founding member of the sirtuin family, Sirt2, was originally discovered in *Saccharomyces cerevisiae*. Currently, seven sirtuins (Sirt1-7) have been found in mammals, each containing the conserved sirtuin core domain that confers NAD^+-dependent deacetylase activity (Frye, 1999).

Each member has distinct subcellular localizations, targets and functions. Sirt1 and Sirt2 were found in both the nucleus and cytoplasm; Sirt3, Sirt4, and Sirt5 were found in mitochondria, and Sirt6 and Sirt7 were found in the nucleus (Michishita et al., 2005). Sirt1-3 have strong deacetylase activity, whereas Sirt4 has ADP-ribosyltransferase activity (Michishita et al., 2005). Sirt5 has weak NAD^+-dependent deacetylase, desuccinylase and demalonylase activity (Michishita et al., 2005). Sirt7 was recently shown to be a highly specific deacetylase (Michishita et al., 2005). Sirt6 has several enzymatic activities, including NAD^+-dependent deacetylase activity and mono-ADP-ribosyl transferase activity of acetyl groups and long-chain acyl groups. The most well-studied sirtuin is Sirt1, and the study of Sirt6 is still in its infancy.

As one of NAD^+-dependent deacetylases, Sirt6 was first cloned from a human spleen cDNA library (Liszt et al., 2005). Recent studies have suggested reduced Sirt6 activity related to obesity and diabetes. Aging and overnutrition, two major risk factors for obesity and diabetes, lead to decreased Sirt6 level and function and result in abnormal glucose and lipid metabolism. Whole-body ablation

of Sirt6 in mice resulted in severe hypoglycemia (Kanfi et al., 2008, 2010; Kuang et al., 2017; Yao et al., 2017). Hepatic-specific ablation of Sirt6 increased liver steatosis (Kim et al., 2010). Fat-specific deletion of Sirt6 increased blood glucose levels and hepatic steatosis and promoted diet-induced obesity and insulin resistance (Kuang et al., 2017; Xiong et al., 2017; Yao et al., 2017). Neural-specific deletion of Sirt6 in mice promoted diet-induced obesity and insulin resistance (Schwer et al., 2010). In contrast, Sirt6 overexpression protected against diet-induced obesity and insulin resistance (Kanfi et al., 2010).

These recent studies showed that Sirt6 plays an important role in lipid and glucose metabolism. This review summarizes the role of Sirt6 in obesity and diabetes.

Sirt6 AND GLUCOSE METABOLISM

Glucose is an essential energy source needed by all cells and organs of our bodies. Therefore, blood glucose should be kept at a certain level to maintain tissue and organ energy requirements. The imbalance of glucose homeostasis is an important pathogenic factor of diabetes, obesity and other metabolic diseases. Sirt6 plays an important role in glucose production and metabolism (**Figure 1**). Mice with whole-body Sirt6 deficiency showed severe hypoglycemia (Mostoslavsky et al., 2006). Subsequent studies found that Sirt6 affects both gluconeogenesis and glycolysis (Zhong et al., 2010; Dominy et al., 2012; Zhang et al., 2014). Moreover, recent reports suggested that Sirt6 regulates pancreatic β-cell function, an important organ for maintaining blood glucose level (Kugel et al., 2016; Demir et al., 2017).

Sirt6 and Blood Glucose

The first clue that Sirt6 might play a role in glucose metabolism came from a severe hypoglycemia phenotype observed in Sirt6-deficient mice (Mostoslavsky et al., 2006). Mice with whole-body Sirt6 deficiency showed increased glucose uptake and enhanced insulin signaling (Xiao et al., 2010). Sirt6-deficient mice, although small, appear normal in the first 2 weeks, then show a series of acute degenerative phenotypes, dying at about age 1 month (Mostoslavsky et al., 2006). The phenotypes include lymphopenia, osteopenia, lordokyphosis and loss of subcutaneous fat (Mostoslavsky et al., 2006). The most striking phenotype is severe hypoglycemia, which could be the main factor killing the mice before age 1 month. However, the severe hypoglycemia phenotype may be not triggered by the abnormal insulin level, because blood insulin levels are even lower than in wild-type mice (Xiao et al., 2010). When the mice were fed water containing 10% glucose, blood glucose was increased and about 83% of the mice with whole-body Sirt6 deficiency survived, indicating the hypoglycemia was a main factor in the postnatal lethality (Xiao et al., 2010).

Xiao et al. found that Sirt6 negatively regulates Akt phosphorylation at Thr 308 and Ser 473 by inhibiting multiple upstream molecules, insulin receptors, and insulin receptor substrate 1 and 2 (Xiao et al., 2010). With Sirt6 deficiency, insulin signaling is activated and Akt phosphorylation is increased (Xiao et al., 2010). Then, glucose uptake is increased, which may cause hypoglycemia. In contrast, Sirt6 deficiency does not affect intestinal glucose absorption and does not lead to higher glucose secretion in the kidney (Zhong et al., 2010). *In vivo* study by ^{18}F-fluorodeoxyglucose-positron emission tomography (FDG-PET) in Sirt6-deficient mice showed increased glucose uptake in both brown adipose tissue and muscle but not liver, brain or heart, which could further explain the hypoglycemic phenotype (Zhong et al., 2010). The increased glucose uptake in these tissues could be explained by higher expression of glucose transporter 1 (Glut1), one of main glucose transporters that modulates basal uptake of glucose, independent of insulin or growth factor (Zhong et al., 2010). The central nervous system also plays an important role in regulating glucose metabolism. Growth hormone and insulin-like growth factor 1 (IGF-1) levels were lower in mice with brain-specific Sirt6 knockout than control mice, similar to mice with whole-body Sirt6 knockout (Schwer et al., 2010). Thus, under certain physiological conditions, Sirt6 may affect glucose metabolism and insulin sensitivity via growth hormone/IGF-1 signaling.

Sirt6 and Glycolysis

With sufficient oxygen, glucose is metabolized to pyruvate, which is further converted to ATP in mitochondria. However, in the absence of nutrients or during hypoxia, cells undergo anaerobic respiration and pyruvate is converted to lactic acid (Aragonés et al., 2009; Vander Heiden et al., 2009). In understanding the hypoglycemia seen in Sirt6-deficient mice, Zhong et al. demonstrated that Sirt6 regulates glucose homoeostasis by suppressing the expression of multiple glycolytic genes (Zhong et al., 2010). This suppression results in efficient ATP production via mitochondrial oxidative phosphorylation instead of glycolysis. Loss of Sirt6 increases glycolysis and diminishes mitochondrial respiration (Aragonés et al., 2009). The role of Sirt6 in glycolysis is mediated by hypoxia-inducible factor 1α (Hif-1α), known to regulate glycolysis and mitochondrial respiration in a coordinated manner (Zhong et al., 2010). Sirt6 deficiency induced Hif-1α activity and then increased the expression of glycolysis-related genes such as Glut1, lactate dehydrogenase (LDH), phosphoglycerate kinase (PGK1), glucose-6-phosphate isomerase (GPI), and phosphofructokinase

Abbreviations: ACC1, acetyl CoA carboxylase 1; ACOX1, acyl-coenzyme A oxidase 1; AMPK, AMP-activated protein kinase; ATF2, activating transcription factor 2; Bmal1, aryl Hydrocarbon Receptor Nuclear Translocator Like; C/EBPα/β/δ, CCAAT/enhancer-binding protein α, β, and δ; CCGs, clock control gene; CK2, enhancing casein kinase 2; CPT1α, carnitine palmitoyltransferase 1; DGAT1, diacylglycerol acyltransferase 1; FAS, fatty acid synthase; FoxO1, Forkhead box protein O1; G6p, glucose-6-phosphatase; GCN5, general control non-repressed protein 5; Glut1, glucose transporter 1; GPI, glucose-6-phosphate isomerase; HFD, high-fat diet; Hif-1α, hypoxia-inducible factor-1α; IGF-1, insulin-like growth factor 1; KIF5C, kinesin family member 5C; LDH, lactate dehydrogenase; PCSK9, proprotein convertase subtilisin/kexin type 9; PDK, dehydrogenase kinase; Pepck, phosphoenolpyruvate carboxykinase; PFK-1, phosphofructokinase-1; PGC-1α, peroxisome proliferator activated receptor γ coactivator 1-α; PGK1, phosphoglycerate kinase; PPARγ, peroxisome proliferator-activated receptor gamma; SCD1, stearoyl-CoA desaturase-1; SREBP 1/2, sterol regulatory element binding proteins 1/2; UCP1, uncoupling protein 1; ATGL, adipose triglyceride lipase; CR, calorie restriction; WAT, white adipose tissue; TG, triglycerides; LDL, low-density lipoprotein; TNFα, tumor necrosis factor α; IL-8, interleukin 8.

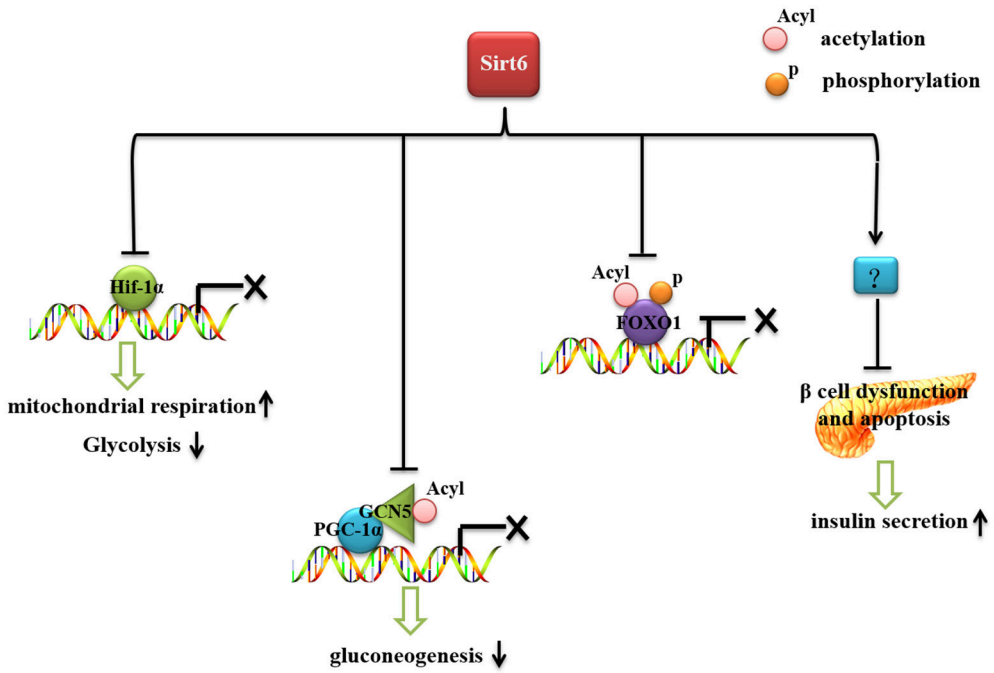

FIGURE 1 | The role of Sirt6 in glucose metabolism. Sirt6 inhibits recruitment of Hif-1α to its target gene promoters, increases mitochondrial respiration and inhibits glycolysis. Sirt6 binds to and activates GCN5, inhibits the acetylation of PGC-1α, and decreases the expression of gluconeogenic genes. Sirt6 can specifically interact with FoxO1, decrease FoxO1 acetylation and phosphorylation level, and inhibit the interaction between FoxO1 and its downstream gene promoters, thereby reducing the expression of gluconeogenic genes. Sirt6 protects against β-cell dysfunction and apoptosis and increases insulin secretion.

1 (PFK-1), and promoted glycolysis (Hu et al., 2006; Zhong et al., 2010). Simultaneously, activated Hif-1α directly inhibited mitochondrial respiration by increasing the expression of dehydrogenase kinase (PDK) (Kim et al., 2006; Papandreou et al., 2006). Moreover, when mice with Sirt6 deficiency were treated with an Hif-1α inhibitor, the hypoglycemia phenotype was rescued, which suggests that increased activity of Hif-1α contributes to the impaired glucose metabolism in these mice (Zhong et al., 2010).

Further study revealed that Sirt6 could regulate Hif-1α via two plausible scenarios: (1) Sirt6 inhibits recruitment of Hif-1α (accelerating its degradation) to its target gene promoters, or (2) Hif-1α could already localize to the promoters under normoglycemia, but the presence of Sirt6 would inhibit its transcriptional activity (Zhong et al., 2010).

Sirt6 and Gluconeogenesis

In addition to regulating glycolysis, Sirt6 affects gluconeogenesis. In the absence of Sirt6, hepatic gluconeogenesis was significantly elevated, which suggests a compensatory response to hypoglycemia (Dominy et al., 2012). Gluconeogenesis is tightly controlled by various cellular signaling pathways and transcription factors (Magnusson et al., 1992). Peroxisome proliferator-activated receptor γ coactivator 1-α (PGC-1α) is a key transcriptional regulator for gluconeogenesis. PGC-1α increases the expression of gluconeogenic enzymes such as glucose-6-phosphatase (G6p) and phosphoenolpyruvate carboxykinase (Pepck) (Puigserver et al., 2003). The transcriptional activity of PGC-1α is negatively regulated by its acetylation level. General control non-repressed protein 5 (GCN5) increased the acetylation level of PGC-1α and decreased PGC-1α transcriptional activity (Lerin et al., 2006). Sirt6 could directly bind to and activate GCN5 (Dominy et al., 2012). With knockout of Sirt6, GCN5 activity is decreased, the acetylation level of PGC-1α is reduced and PGC-1α controls the expression of gluconeogenic genes (Dominy et al., 2012).

Forkhead box protein O1 (FoxO1) also plays an important role in regulating gluconeogenesis. FoxO1 activates gluconeogenesis by directly binding the promoter regions of G6p and Pepck (Schilling et al., 2006). With mutation of the FoxO1 transcriptional activation domain and activity abolished, gluconeogenesis was significantly diminished (Nakae et al., 2001). FoxO1 deficiency significantly impaired the fasting-induced expression of G6p and Pepck (Matsumoto et al., 2007). The transcriptional activity of FoxO1 is mainly regulated by its phosphorylation and acetylation (Brunet et al., 2004; Yamagata et al., 2008; Zhao et al., 2010). In Sirt6-deleted cardiomyocytes, FoxO1 phosphorylation was increased (Sundaresan et al., 2012). The phosphorylation of FoxO1 promotes the translocation of FoxO1 from the nucleus to the cytoplasm, thereby reducing its transcriptional activity. Subsequent studies found that Sirt6 can specifically interact with FoxO1, thereby inhibiting the interaction between FoxO1 and its downstream genes G6p and Pepck, to reduce the expression of gluconeogenic genes (Zhang et al., 2014).

Sirt6 and Pancreatic β-Cell Function

The connection between Sirt6 and glucose metabolism is strengthened by the critical role of Sirt6 in promoting glucose-stimulated insulin secretion and ATP production in pancreatic β-cells (Xiong et al., 2016). These effects might be related to evidence of mitochondria damage (mitochondrial function and Ca^{2+} dynamic regulation in β cells impaired in Sirt6-deficient mice) and lower rate of oxygen consumption seen in Sirt6-deficient pancreatic β cells (Xiong et al., 2016). Sirt6 ablation also increases cell apoptosis and impairs insulin secretion in response to glucose in MIN6 cells (β-cell lines). Conversely, Sirt6 overexpression protects against palmitate-induced β-cell dysfunction and apoptosis (Song et al., 2016; Xiong et al., 2016). Recently, a new study found that Sirt6 is critical for pancreatic β-cell function and survival in mice (Qin et al., 2018). Sirt6 deficiency does not affect endocrine morphology, β-cell mass or insulin production but did result in glucose intolerance and defective glucose-stimulated insulin secretion in mice (Qin et al., 2018). β-cell specific deletion of Sirt6 reproduced the defect in insulin secretion. Loss of Sirt6 increases acetylation of histone H3K9Ac, H3K56Ac, and activates RNA polymerase II at the promoter region of thioredoxin-interacting protein (TXNIP) (Qin et al., 2018). TXNIP expression is negatively associated with glucose-stimulated insulin secretion in β-cells and that overexpression of TXNIP inhibits insulin secretion (Rani et al., 2010; Yoshihara et al., 2010; Luo et al., 2014). Sirt6-deficiency in β-cells exhibited a time-dependent increase in H3K9Ac, H3K56Ac, and TXNIP levels. Finally, β-cell specific Sirt6-deficient mice showed increased sensitivity to streptozotocin induced β-cell apoptosis (Qin et al., 2018). Together, this report indicates that Sirt6 has a key role in pancreatic function.

Sirt6 AND CALORIE RESTRICTION

Calorie restriction (CR) reduces cellular NADH concentration, thereby increasing the NAD+/NADH ratio and promoting Sirt2 activity (Tasselli et al., 2016a). Sirt6 activity is significantly modulated by CR. It is increased by nutrient depletion or long-term CR in the brain, white adipose tissue (WAT), muscle, liver and kidney in mice (Kanfi et al., 2008; Kuang et al., 2017). Sirt6 also mediates the effects of CR, which is known to delay the onset of age-associated diseases, including diabetes and cardiovascular diseases. Sirt6 ablation abolished CR-induced life extension. Moreover, CR-activated Sirt6 suppressed NF-κB signaling and delayed aging (Zhang et al., 2013). Transgenic mice overexpressing Sirt6 showed multiple phenotypes resembling CR, including reduced body weight, enhanced metabolic activity, and reduced serum levels of cholesterol, adipokines, insulin, and glucose, which further demonstrates the regulatory role of Sirt6 in energy metabolism (Kanfi et al., 2010, 2012).

Sirt6 AND LIPID METABOLISM

Recent reports have shown that Sirt6 is an important regulator of lipid metabolism (**Figure 2**). Sirt6 regulates the hepatic accumulation of triglycerides (TG), which is associated with fatty liver disease (Kugel and Mostoslavsky, 2014; Vitiello et al., 2017). Sirt6 deficiency promotes lipogenesis and fatty acid uptake but inhibits β-oxidation (Kim et al., 2010). Cholesterol synthesis is also negatively regulated by Sirt6 (Elhanati et al., 2013). Sirt6 positively regulates lipid mobilization and thermogenesis in adipose tissue (Chen et al., 2017; Kuang et al., 2017; Xiong et al., 2017; Yao et al., 2017). Moreover, Sirt6 regulates circadian metabolic programs, accompanied by changes in lipid metabolism (Masri et al., 2014).

Sirt6 and Hepatic Lipid Metabolism

The liver is a key metabolic organ controlling aspects of lipid metabolism in response to hormonal or nutritional signals. Under starvation, the liver converts lipid stores into available energy via fatty acid oxidation. In the fed condition, metabolic programs in the liver are switched on to store energy in the form of lipid droplets via the process of lipogenesis (Puigserver et al., 2003).

In addition to its critical regulatory role in glucose metabolism, Sirt6 plays an important regulatory role in hepatic lipid metabolism. Hepatic-specific disruption of Sirt6 in mice resulted in fatty liver formation (Kim et al., 2010). Hepatic TG accumulation in liver is mainly regulated by fatty acid uptake, β-oxidation, and TG synthesis and secretion. Deletion of Sirt6 increased the expression of hepatic fatty acid transport genes and reduced that of fatty acid β-oxidation genes (carnitine palmitoyltransferase 1 [CPT1α], acyl-coenzyme A oxidase 1 [ACOX1]). Genetic deletion of Sirt6 in mice increased the mRNA levels of lipogenic genes such as acetyl CoA carboxylase 1 (ACC1), fatty acid synthase (FAS), and stearoyl-CoA desaturase-1 (SCD1) (Kim et al., 2010).

Rosiglitazone (RGZ), an agonist of peroxisome proliferator-activated receptor gamma (PPARγ), plays an important role in protecting against fatty liver disease. Activation of PPARγ by RGZ increased Sirt6 expression (Yang et al., 2011). RGZ treatment ameliorated hepatic lipid accumulation and increased the expression of Sirt6, PGC-1α, and FoxO1 in rat liver (Yang et al., 2011). In addition, AMP-activated protein kinase (AMPK) phosphorylation was increased by RGZ. Sirt6 knockdown increased hepatocyte lipid accumulation and abolished the effect of RGZ on hepatic steatosis (Yang et al., 2011). Sirt6 knockdown also abolished the effect of RGZ on the mRNA and protein expression of PGC1-α and FoxO1 and phosphorylation levels of AMPK, which suggests that Sirt6 is involved in the RGZ-mediated metabolic effects (Yang et al., 2011). However, this result contradicts a report that Sirt6 inhibits the activity of PGC-1a by increasing GCN5 expression (Dominy et al., 2012), so Sirt6 may have different regulatory roles in different models. MicroRNA-122 (miR-122), a microRNA (miRNA) highly expressed in liver, constitutes 70% of the total miRNA pool in liver (Chang et al., 2004; Bhattacharyya et al., 2006; Jopling, 2012). MiR-122 plays an important regulatory role in many metabolic processes, including cholesterol synthesis and fatty acid oxidation (Krützfeldt et al., 2005; Esau et al., 2006). Sirt6 and miR-122 are reciprocally regulated to control the gene expression of fatty

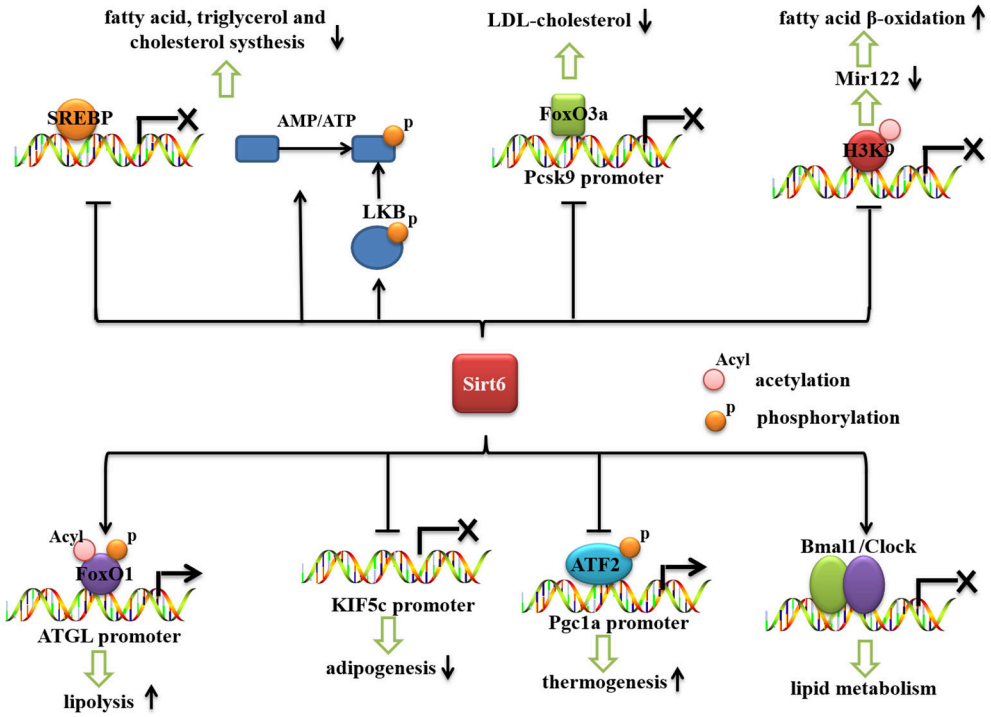

FIGURE 2 | The role of Sirt6 in lipid metabolism. Sirt6 represses the mRNA expression of SREBP1/2 and inhibits the cleavage of SREBPs into their active forms. Sirt6 activates AMPK (by increasing the AMP/ATP ratio and activating LKB), which phosphorylates and inactivates SREBP. Sirt6 can be recruited by FoxO3a to the Pcsk9 promoter, suppress its gene expression and decrease the level of LDL-cholesterol. Sirt6 downregulates miR-122 by deacetylating H3K56, reduces miR-122 expression, and increases fatty acid β-oxidation. Sirt6 also specifically interacts with FoxO1, decreases FoxO1 acetylation and phosphorylation, and promotes the interaction between FoxO1 and the promoter of its downstream gene, ATGL, thereby increasing ATGL expression and inducing lipolysis in adipose tissue. Sirt6 inhibits KIF5C gene expression and impairs adipogenesis. Sirt6 regulates phospho-ATF2 (p-ATF2) binding to the PGC-1α promoter and subsequently affects the thermogenic program. Sirt6 regulates the circadian rhythm in the liver by maintaining a proper cyclic recruitment of CLOCK/BMAL1.

acid oxidation (Elhanati et al., 2016). Sirt6 downregulates miR-122 by deacetylating H3K56. MiR-122 binds to three sites on the Sirt6 3' untranslated region and reduces its levels. Overexpression of Sirt6 in mouse liver reduced miR-122 expression and increased that of fatty acid β-oxidation genes (Elhanati et al., 2016).

Sirt6 also regulates low-density lipoprotein (LDL)-cholesterol levels (Kanfi et al., 2010). Sirt6 regulates cholesterol level via the lipogenic transcription factors sterol regulatory element binding proteins 1/2 (SREBP1/2) and AMPK (Elhanati et al., 2013). It represses the expression of SREBP1/2 and by three mechanisms: it represses the transcription levels of SREBP1/2 and inhibits their cleavage into their active forms (Elhanati et al., 2013) and it activates AMPK (by increasing the AMP/ATP ratio and activating LKB), which phosphorylates and inactivates SREBP1 (Elhanati et al., 2013). Proprotein convertase subtilisin/kexin type 9 (PCSK9) is a crucial gene regulating LDL-cholesterol (Tao et al., 2013). Sirt6 plays a critical role in regulating Pcsk9 gene expression. Sirt6 can be recruited by FoxO3a to the Pcsk9 gene promoter and deacetylate histone H3 at Lys 9 and 56, thereby suppressing the gene expression (Tao et al., 2013).Conversely, overexpression of Sirt6 decreased LDL-cholesterol level in high-fat diet (HFD)-fed mice (Kanfi et al., 2010).

Sirt6 and Adipose Tissue Lipolysis

Sirt6 regulates the lipid metabolism of adipose tissues. Sirt6 ablation mediated by ap2-CRE or adiponectin-CRE in adipose tissue increased HFD-induced obesity and insulin resistance (Kuang et al., 2017; Yao et al., 2017), and Sirt6 overexpression inhibited HFD-induced obesity and insulin resistance (Kanfi et al., 2010). Sirt6 ablation increased diet-induced obesity via adipocyte hypertrophy rather than abnormal adipocyte differentiation (Kuang et al., 2017). Adipocyte hypertrophy in Sirt6-deficient mice might be attributed to impaired lipolytic activity, which causes fat storage synthesis exceeding lipolysis and results in obesity. Adipose TG lipase (ATGL) is the key lipase that hydrolyzes TG into diglycerides (Zimmermann et al., 2004; Kuang et al., 2017); Sirt6 ablation suppressed ATGL expression. Sirt6 physically interacts with FoxO1, and Sirt6 deficiency increased the acetylation and phosphorylation of FoxO1, thereby promoting its nuclear exclusion and decreasing its transcriptional activity, which downregulated ATGL expression (Kuang et al., 2017). The role of Sirt6 in regulating FoxO1 is contradictory in liver and adipose tissue (Zhang et al., 2014; Kuang et al., 2017), which indicates that the regulatory function of Sirt6 is tissue-specific. Sirt6 overexpression protects against HFD-induced physiological damage by blocking the lipotoxicity of

obesity and restoring glucose homeostasis via specific reduction of PPARγ signaling and level of diacylglycerol acyltransferase 1 (DGAT1), a key regulator of TG synthesis (Kanfi et al., 2010).

Sirt6 and Adipogenesis

Adipose tissue, differentiated from pre-adipocytes, is regulated by multiple transcriptional factors, including PPARγ and CCAAT/enhancer-binding protein α, β, and δ (C/EBPα/β/δ). Recently, Chen et al found that Sirt6 deficiency in preadipocytes blocks their adipogenesis (Chen et al., 2017). Sirt6 deficiency impairs adipogenesis, and Sirt6 is an essential factor for mitotic clonal expansion during adipogenesis by inhibiting the expression of kinesin family member 5C (KIF5C) and enhancing casein kinase 2 (CK2) activity. KIF5C is negatively regulated by Sirt6. Moreover, this study showed that KIF5C is a negative factor for adipogenesis by interacting with CK2a, a catalytic subunit of CK2 (Chen et al., 2017).

Sirt6 and Thermogenesis

Obesity is due to a chronic imbalance between energy intake and energy expenditure. WAT is essential for TG storage and insulin resistance, whereas brown adipose tissue (BAT) generates heat by dissipating energy via uncoupled respiration mediated by uncoupling protein 1 (UCP1) (Lowell and Spiegelman, 2000; Nedergaard and Cannon, 2010). WAT could be converted into brown-like adipocytes (beige cells). Cells undergoing a browning process have been suggested to have strong anti-diabetic or anti-obesity benefit (Cypess et al., 2009; Barbatelli et al., 2010; Petrovic et al., 2010; Wu et al., 2012). Recent studies show that Sirt6 has a critical role in regulating the thermogenesis of fat (Yao et al., 2017). Cold exposure and a β-adrenergic agonist markedly induced Sirt6 expression in fat. Fat-specific ablation of Sirt6 mediated by Ap2-CRE impairs the thermogenic function of brown adipocytes, thereby causing a morphological "whitening" of brown fat, and decreased oxygen consumption, core body temperature and cold sensitivity (Yao et al., 2017). PGC-1α is highly expressed in BAT and is a central regulator of brown fat thermogenesis (Puigserver et al., 1998). White fat cells overexpressing PGC-1α show mitochondrial oxidation phosphorylation and expression of thermogenesis genes (Puigserver et al., 1998). Sirt6 depletion markedly decreased the expression of PGC-1α and other thermogenic genes (Yao et al., 2017). Sirt6-depleted adipocytes also decreased basal mitochondrial respiration and maximal mitochondrial respiratory capacity. Mitochondrial oxidative phosphorylation and the expression of biogenesis genes are decreased significantly in primary brown adipocytes with Sirt6 deletion (Yao et al., 2017). Decreased PGC-1α expression in brown fat was not attributed to changes in acetylation levels of H3K9 or H3K56 in its promoter region in Sirt6-deficient mice (Yao et al., 2017). Activating transcription factor 2 (ATF2) is recruited to the PGC-1α promoter after β-adrenergic receptor activation in BAT (Herzig et al., 2001; Cao et al., 2004). Sirt6 depletion reduced phosphorylated ATF2 binding to the PGC-1α promoter and subsequently decreased the thermogenic program of brown fat and led to obesity (Yao et al., 2017).

Sirt6 AND CIRCADIAN RHYTHM

Circadian rhythm refers to changes in the life cycle during 24 h. Circadian rhythms play an important role in regulating body metabolism (Kohsaka et al., 2007; Barnea et al., 2009). In mice with circadian rhythm disruption, energy metabolism, especially glucose metabolism, was disturbed. Both behavioral and molecular circadian rhythms were changed in mice with metabolic disorders caused by an HFD (Kohsaka et al., 2007; Barnea et al., 2009). The clock has a central role in the circadian rhythm (Feng and Lazar, 2012). Bmal1 gene (also called aryl hydrocarbon receptor nuclear translocator-like [ARNTL]) is the central part of the biological clock transcription and translation feedback loop (Kiyohara et al., 2006). These two genes, encoding the protein together to form a Clock/Bmal1 isomer, play an important role in the feedback loop. Sirt6 is the only constitutive chromatin-associated sirtuin and is prominently present at transcriptionally active genomic loci (Masri et al., 2014). Sirt6 interacts with CLOCK/BMAL1 and, differently from SIRT1, governs their chromatin recruitment to gene promoters (Masri et al., 2014). Sirt6 contributes to chromatin recruitment of both the circadian machinery as well as SREBP-1 (Masri et al., 2014). Liver-specific deletion of Sirt6 downregulates hepatic rhythmic transcription, accompanied by changes in lipid metabolism (Masri et al., 2014). Deletion of Sirt6 leads to decreased binding of Clock/Bmal to the clock control gene (CCG) promoter and the binding of SREBP1 with its downstream gene promoters, thereby affecting lipid metabolism in the organism (Masri et al., 2014). The relationship between Sirt6 and fatty acid metabolism remains unclear. Sirt6 regulation of the circadian metabolic programs sheds new light on how the enzyme couples chromatin dynamics to metabolism (Masri et al., 2014; Tasselli et al., 2016b).

Sirt6 AND INFLAMMATION

Sirt6 deficiency increases the inflammatory response in many tissues. In adipose tissue, Sirt6 deficiency increases macrophage infiltration and adipose tissue inflammation and promotes HFD-induced insulin resistance (Kuang et al., 2017; Xiong et al., 2017). Sirt6 deficiency in mouse immune cells leads to liver inflammation and fibrosis (Xiao et al., 2012). In particular, in pancreatic cancer cells, Sirt6 induces the expression of proinflammatory cyto-/chemokines [interleukin 8 and tumor necrosis factor α (TNFα)] (Lappas, 2012). In endothelial cells, Sirt6 deficiency increased the expression of proinflammatory cytokines, extracellular matrix remodeling enzymes and adhesion molecules (Lappas, 2012). Loss of Sirt6 increased the expression of NF-κB, whereas overexpression of Sirt6 decreased NF-κB transcriptional activity (Lappas, 2012). Sirt6 interacts with the NF-κB subunit, deacetylates histone H3 lysine 9 (H3K9) at NF-kB target gene promoters, and inhibits the expression of downstream target genes, thus inhibiting the inflammatory reaction (Kawahara et al., 2009). In Sirt6-deficient cells, RELA promoter occupancy was increased; it enhanced hyperacetylation of NF-κB target gene promoters and induced NF-κB–dependent gene expression, cellular senescence and apoptosis (Kawahara et al., 2009). Sirt6 also binds to c-Jun and decreases the expression

of its downstream target genes IL-6, monocyte chemoattractant protein 1, TNFα and H3K9, thereby inhibiting the expression of these genes (Xiao et al., 2012; Kuang et al., 2017).

Sirt6 AND DNA DAMAGE AND DIABETES

DNA damage is a permanent change of nucleotide sequence during DNA replication, resulting in the change of corresponding genetic characteristics (Shimizu et al., 2014). It is also related to the occurrence and development of chronic diseases, such as cancer and diabetes (Blasiak et al., 2004; Grindel et al., 2016). Sirt6 has been characterized as a histone deacetylase (HDAC) that targets specific sites (Michishita et al., 2008, 2009; Yang et al., 2009; Tasselli et al., 2016a). Sirt6 deacetylates the histone H3 on acetylated K9, K56 (Michishita et al., 2008, 2009) and the more recently identified K18 residue (Yang et al., 2009), causing the repression of many genes involved in inflammation, aging, genome stability, metabolic pathways and telomere integrity (Vitiello et al., 2017). Loss of Sirt6 affects the pathway of ATM/CHK2 and recruitment of repair factors to sites of DNA damage (Cagnetta et al., 2018). Sirt6 interacts, deacetylates and affects telomere repeat binding factor 2 (TRF2) stability, which may be part of a higher order complex with functional impacts on DNA damage response (DDR), cancer and aging (Rizzo et al., 2017). Moreover, following DNA damage, Sirt6 is recruited to double-strand breaks ensuring the proper activation of downstream DDR factors leading to an efficient DNA repair. Studies in diabetic patients showed greater oxidative damage to DNA. This indicates that the role of Sirt6 in DNA damage may as a new therapeutic pathway for cancer and diabetes related disorders.

CONCLUSION

Excessive intake of carbohydrates or fat can lead to a range of metabolic syndromes, such as obesity, fatty liver and diabetes. With evidence that plays an important regulatory role in energy metabolism, it may be a potential therapeutic target for obesity and diabetes mellitus. Clinical trials investigating the use of sirtuin activators for treating diabetes are under way; such activators show promise as alternatives to current diabetes therapies. Thus, further research of sirtuin activators may result in a new class of safe, effective diabetes treatments.

AUTHOR CONTRIBUTIONS

JK designed and wrote the manuscript. LC, QT, JZ, and YL contributed to the discussion and review of the manuscript. JH obtained funding and wrote the manuscript.

ACKNOWLEDGMENTS

This work was supported by the National Natural Science Foundation of China (81471068 and 81270926), Distinguished Young Scientists of Sichuan Province (2014JQ0034) and Young Scientist Fellowship of Sichuan University (2013SCU04A17).

REFERENCES

Aragonés, J., Fraisl, P., Baes, M., and Carmeliet, P. (2009). Oxygen sensors at the crossroad of metabolism. *Cell Metab.* 9, 11–22. doi: 10.1016/j.cmet.2008.10.001

Barbatelli, G., Murano, I., Madsen, L., Hao, Q., Jimenez, M., Kristiansen, K., et al. (2010). The emergence of cold-induced brown adipocytes in mouse white fat depots is determined predominantly by white to brown adipocyte transdifferentiation. *Am. J. Physiol. Endocrinol. Metab.* 298, E1244–E1253. doi: 10.1152/ajpendo.00600.2009

Barnea, M., Madar, Z., and Froy, O. (2009). High-fat diet delays and fasting advances the circadian expression of adiponectin signaling components in mouse liver. *Endocrinology* 150, 161–168. doi: 10.1210/en.2008-0944

Bhattacharyya, S. N., Habermacher, R., Martine, U., Closs, E. I., and Filipowicz, W. (2006). Relief of microRNA-mediated translational repression in human cells subjected to stress. *Cell* 125, 1111–1124. doi: 10.1016/j.cell.2006.04.031

Blasiak, J., Arabski, M., Krupa, R., Wozniak, K., Zadrozny, M., Kasznicki, J., et al. (2004). DNA damage and repair in type 2 diabetes mellitus. *Mutat. Res.* 554, 297–304. doi: 10.1016/j.mrfmmm.2004.05.011

Brunet, A., Sweeney, L. B., Sturgill, J. F., Chua, K. F., Greer, P. L., Lin, Y., et al. (2004). Stress-dependent regulation of FOXO transcription factors by the SIRT1 deacetylase. *Science* 303, 2011–2015. doi: 10.1126/science.1094637

Cagnetta, A., Soncini, D., Orecchioni, S., Talarico, G., Minetto, P., Guolo, F., et al. (2018). Depletion of SIRT6 enzymatic activity increases acute myeloid leukemia cells' vulnerability to DNA-damaging agents. *Haematologica* 103, 80–90. doi: 10.3324/haematol.2017.176248

Cao, W., Daniel, K. W., Robidoux, J., Puigserver, P., Medvedev, A. V., Bai, X., et al. (2004). p38 mitogen-activated protein kinase is the central regulator of cyclic AMP-dependent transcription of the brown fat uncoupling protein 1 gene. *Mol. Cell. Biol.* 24, 3057–3067. doi: 10.1128/MCB.24.7.3057-3067.2004

Chang, J., Nicolas, E., Marks, D., Sander, C., Lerro, A., Buendia, M. A., et al. (2004). miR-122, a mammalian liver-specific microRNA, is processed from hcr mRNA and may downregulate the high affinity cationic amino acid transporter CAT-1. *RNA Biol.* 1, 106–113. doi: 10.4161/rna.1.2.1066

Chen, Q., Hao, W., Xiao, C., Wang, R., Xu, X., Lu, H., et al. (2017). SIRT6 is essential for adipocyte differentiation by regulating mitotic clonal expansion. *Cell Rep.* 18, 3155–3166. doi: 10.1016/j.celrep.2017.03.006

Cypess, A. M., Lehman, S., Williams, G., Tal, I., Rodman, D., Goldfine, A. B., et al. (2009). Identification and importance of brown adipose tissue in adult humans. *N. Engl. J. Med.* 360, 1509–1517. doi: 10.1056/NEJMoa0810780

Demir, I. E., Ceyhan, G. O., and Friess, H. (2017). Epigenomic therapies: the potential of targeting SIRT6 for the treatment of pancreatic cancer. *Expert Opin. Ther. Targets* 21, 1–3. doi: 10.1080/14728222.2017.1265507

Dominy, J. E. Jr., Lee, Y., Jedrychowski, M. P., Chim, H., Jurczak, M. J., Camporez, J. P., et al. (2012). The deacetylase Sirt6 activates the acetyltransferase GCN5 and suppresses hepatic gluconeogenesis. *Mol. Cell* 48, 900–913. doi: 10.1016/j.molcel.2012.09.030

Elhanati, S., Ben-Hamo, R., Kanfi, Y., Varvak, A., Glazz, R., Lerrer, B., et al. (2016). Reciprocal regulation between SIRT6 and miR-122 controls liver metabolism and predicts hepatocarcinoma prognosis. *Cell Rep.* 14, 234–242. doi: 10.1016/j.celrep.2015.12.023

Elhanati, S., Kanfi, Y., Varvak, A., Roichman, A., Carmel-Gross, I., Barth, S., et al. (2013). Multiple regulatory layers of SREBP1/2 by SIRT6. *Cell Rep.* 4, 905–912. doi: 10.1016/j.celrep.2013.08.006

Esau, C., Davis, S., Murray, S. F., Yu, X. X., Pandey, S. K., Pear, M., et al. (2006). miR-122 regulation of lipid metabolism revealed by *in vivo* antisense targeting. *Cell Metab.* 3, 87–98. doi: 10.1016/j.cmet.2006.01.005

Feng, D., and Lazar, M. A. (2012). Clocks, metabolism, and the epigenome. *Mol. Cell* 47, 158–167. doi: 10.1016/j.molcel.2012.06.026

Frye, R. A. (1999). Characterization of five human cDNAs with homology to the yeast SIR2 gene: Sir2-like proteins (sirtuins) metabolize NAD and may have protein ADP-ribosyltransferase activity. *Biochem. Biophys. Res. Commun.* 260, 273–279. doi: 10.1006/bbrc.1999.0897

Grindel, A., Guggenberger, B., Eichberger, L., Poppelmeyer, C., Gschaider, M., Tosevska, A., et al. (2016). Oxidative stress, DNA damage and DNA repair in female patients with diabetes mellitus type 2. *PLoS ONE* 11:e0162082. doi: 10.1371/journal.pone.0162082

Herzig, S., Long, F., Jhala, U. S., Hedrick, S., Quinn, R., Bauer, A., et al. (2001). CREB regulates hepatic gluconeogenesis through the coactivator PGC-1. *Nature* 413, 179–183. doi: 10.1038/35093131

Hu, C. J., Iyer, S., Sataur, A., Covello, K. L., Chodosh, L. A., and Simon, M. C. (2006). Differential regulation of the transcriptional activities of hypoxia-inducible factor 1 alpha (HIF-1alpha) and HIF-2alpha in stem cells. *Mol. Cell. Biol.* 26, 3514–3526. doi: 10.1128/MCB.26.9.3514-3526.2006

Jopling, C. (2012). Liver-specific microRNA-122: biogenesis and function. *RNA Biol.* 9, 137–142. doi: 10.4161/rna.18827

Kanfi, Y., Naiman, S., Amir, G., Peshti, V., Zinman, G., Nahum, L., et al. (2012). The sirtuin SIRT6 regulates lifespan in male mice. *Nature* 483, 218–221. doi: 10.1038/nature10815

Kanfi, Y., Peshti, V., Gil, R., Naiman, S., Nahum, L., Levin, E., et al. (2010). SIRT6 protects against pathological damage caused by diet-induced obesity. *Aging Cell* 9, 162–173. doi: 10.1111/j.1474-9726.2009.00544.x

Kanfi, Y., Shalman, R., Peshti, V., Pilosof, S. N., Gozlan, Y. M., Pearson, K. J., et al. (2008). Regulation of SIRT6 protein levels by nutrient availability. *FEBS Lett.* 582, 543–548. doi: 10.1016/j.febslet.2008.01.019

Kawahara, T. L., Michishita, E., Adler, A. S., Damian, M., Berber, E., Lin, M., et al. (2009). SIRT6 links histone H3 lysine 9 deacetylation to NF-kappaB-dependent gene expression and organismal life span. *Cell* 136, 62–74. doi: 10.1016/j.cell.2008.10.052

Kim, H. S., Xiao, C., Wang, R. H., Lahusen, T., Xu, X., Vassilopoulos, A., et al. (2010). Hepatic-specific disruption of SIRT6 in mice results in fatty liver formation due to enhanced glycolysis and triglyceride synthesis. *Cell Metab.* 12, 224–236. doi: 10.1016/j.cmet.2010.06.009

Kim, J. W., Tchernyshyov, I., Semenza, G. L., and Dang, C. V. (2006). HIF-1-mediated expression of pyruvate dehydrogenase kinase: a metabolic switch required for cellular adaptation to hypoxia. *Cell Metab.* 3, 177–185. doi: 10.1016/j.cmet.2006.02.002

Kiyohara, Y. B., Tagao, S., Tamanini, F., Morita, A., Sugisawa, Y., Yasuda, M., et al. (2006). The BMAL1 C terminus regulates the circadian transcription feedback loop. *Proc. Natl. Acad. Sci. U.S.A.* 103, 10074–10079. doi: 10.1073/pnas.0601416103

Kohsaka, A., Laposky, A. D., Ramsey, K. M., Estrada, C., Joshu, C., Kobayashi, Y., et al. (2007). High-fat diet disrupts behavioral and molecular circadian rhythms in mice. *Cell Metab.* 6, 414–421. doi: 10.1016/j.cmet.2007.09.006

Krützfeldt, J., Rajewsky, N., Braich, R., Rajeev, K. G., Tuschl, T., Manoharan, M., et al. (2005). Silencing of microRNAs *in vivo* with 'antagomirs'. *Nature* 438, 685–689. doi: 10.1038/nature04303

Kuang, J., Zhang, Y., Liu, Q., Shen, J., Pu, S., Cheng, S., et al. (2017). Fat-specific Sirt6 ablation sensitizes mice to high-fat diet-induced obesity and insulin resistance by inhibiting lipolysis. *Diabetes* 66, 1159-1171. doi: 10.2337/db16-1225

Kugel, S., and Mostoslavsky, R. (2014). Chromatin and beyond: the multitasking roles for SIRT6. *Trends Biochem. Sci.* 39, 72–81. doi: 10.1016/j.tibs.2013.12.002

Kugel, S., Sebastian, C., Fitamant, J., Ross, K. N., Saha, S. K., Jain, E., et al. (2016). SIRT6 suppresses pancreatic cancer through control of Lin28b. *Cell* 165, 1401–1415. doi: 10.1016/j.cell.2016.04.033

Lappas, M. (2012). Anti-inflammatory properties of sirtuin 6 in human umbilical vein endothelial cells. *Mediators Inflamm.* 2012:597514. doi: 10.1155/2012/597514

Lerin, C., Rodgers, J. T., Kalume, D. E., Kim, S. H., Pandey, A., and Puigserver, P. (2006). GCN5 acetyltransferase complex controls glucose metabolism through transcriptional repression of PGC-1alpha. *Cell Metab.* 3, 429–438. doi: 10.1016/j.cmet.2006.04.013

Liszt, G., Ford, E., Kurtev, M., and Guarente, L. (2005). Mouse Sir2 homolog SIRT6 is a nuclear ADP-ribosyltransferase. *J. Biol. Chem.* 280, 21313–21320. doi: 10.1074/jbc.M413296200

Lowell, B. B., and Spiegelman, B. M. (2000). Towards a molecular understanding of adaptive thermogenesis. *Nature* 404, 652–660. doi: 10.1038/35007527

Luo, Y., He, F., Hu, L., Hai, L., Huang, M., Xu, Z., et al. (2014). Transcription factor Ets1 regulates expression of thioredoxin-interacting protein and inhibits insulin secretion in pancreatic beta-cells. *PLoS ONE* 9:e99049. doi: 10.1371/journal.pone.0099049

Magnusson, I., Rothman, D. L., Katz, L. D., Shulman, R. G., and Shulman, G. I. (1992). Increased rate of gluconeogenesis in type II diabetes mellitus. A 13C nuclear magnetic resonance study. *J. Clin. Invest.* 90, 1323-1327. doi: 10.1172/JCI115997

Masri, S., Rigor, P., Cervantes, M., Ceglia, N., Sebastian, C., Xiao, C., et al. (2014). Partitioning circadian transcription by SIRT6 leads to segregated control of cellular metabolism. *Cell* 158, 659–672. doi: 10.1016/j.cell.2014.06.050

Matsumoto, M., Pocai, A., Rossetti, L., Depinho, R. A., and Accili, D. (2007). Impaired regulation of hepatic glucose production in mice lacking the forkhead transcription factor Foxo1 in liver. *Cell Metab.* 6, 208–216. doi: 10.1016/j.cmet.2007.08.006

Michan, S., and Sinclair, D. (2007). Sirtuins in mammals: insights into their biological function. *Biochem. J.* 404, 1–13. doi: 10.1042/BJ20070140

Michishita, E., McCord, R. A., Berber, E., Kioi, M., Padilla-Nash, H., Damian, M., et al. (2008). SIRT6 is a histone H3 lysine 9 deacetylase that modulates telomeric chromatin. *Nature* 452, 492–496. doi: 10.1038/nature06736

Michishita, E., McCord, R. A., Boxer, L. D., Barber, M. F., Hong, T., Gozani, O., et al. (2009). Cell cycle-dependent deacetylation of telomeric histone H3 lysine K56 by human SIRT6. *Cell Cycle* 8, 2664–2666. doi: 10.4161/cc.8.16.9367

Michishita, E., Park, J. Y., Burneskis, J. M., Barrett, J. C., and Horikawa, I. (2005). Evolutionarily conserved and nonconserved cellular localizations and functions of human SIRT proteins. *Mol. Biol. Cell* 16, 4623–4635. doi: 10.1091/mbc.E05-01-0033

Mostoslavsky, R., Chua, K. F., Lombard, D. B., Pang, W. W., Fischer, M. R., Gellon, L., et al. (2006). Genomic instability and aging-like phenotype in the absence of mammalian SIRT6. *Cell* 124, 315–329. doi: 10.1016/j.cell.2005.11.044

Nakae, J., Kitamura, T., Silver, D. L., and Accili, D. (2001). The forkhead transcription factor Foxo1 (Fkhr) confers insulin sensitivity onto glucose-6-phosphatase expression. *J. Clin. Invest.* 108, 1359–1367. doi: 10.1172/JCI200112876

Nedergaard, J., and Cannon, B. (2010). The changed metabolic world with human brown adipose tissue: therapeutic visions. *Cell Metab.* 11, 268–272. doi: 10.1016/j.cmet.2010.03.007

Papandreou, I., Cairns, R. A., Fontana, L., Lim, A. L., and Denko, N. C. (2006). HIF-1 mediates adaptation to hypoxia by actively downregulating mitochondrial oxygen consumption. *Cell Metab.* 3, 187–197. doi: 10.1016/j.cmet.2006.01.012

Petrovic, N., Walden, T. B., Shabalina, I. G., Timmons, J. A., Cannon, B., and Nedergaard, J. (2010). Chronic peroxisome proliferator-activated receptor gamma (PPARgamma) activation of epididymally derived white adipocyte cultures reveals a population of thermogenically competent, UCP1-containing adipocytes molecularly distinct from classic brown adipocytes. *J. Biol. Chem.* 285, 7153–7164. doi: 10.1074/jbc.M109.053942

Puigserver, P., Rhee, J., Donovan, J., Walkey, C. J., Yoon, J. C., Oriente, F., et al. (2003). Insulin-regulated hepatic gluconeogenesis through FOXO1-PGC-1alpha interaction. *Nature* 423, 550–555. doi: 10.1038/nature01667

Puigserver, P., Wu, Z., Park, C. W., Graves, R., Wright, M., and Spiegelman, B. M. (1998). A cold-inducible coactivator of nuclear receptors linked to adaptive thermogenesis. *Cell* 92, 829–839. doi: 10.1016/S0092-8674(00)81410-5

Qin, K., Zhang, N., Zhang, Z., Nipper, M., Zhu, Z., Leighton, J., et al. (2018). SIRT6-mediated transcriptional suppression of Txnip is critical for pancreatic beta cell function and survival in mice. *Diabetologia* doi: 10.1007/s00125-017-4542-6. [Epub ahead of print]

Rani, S., Mehta, J. P., Barron, N., Doolan, P., Jeppesen, P. B., Clynes, M., et al. (2010). Decreasing Txnip mRNA and protein levels in pancreatic MIN6 cells reduces reactive oxygen species and restores glucose regulated insulin secretion. *Cell. Physiol. Biochem.* 25, 667–674. doi: 10.1159/000315086

Rizzo, A., Iachettini, S., Salvati, E., Zizza, P., Maresca, C., D'angelo, C., et al. (2017). SIRT6 interacts with TRF2 and promotes its degradation in response to DNA damage. *Nucleic Acids Res.* 45, 1820–1834. doi: 10.1093/nar/gkw1202

Schilling, M. M., Oeser, J. K., Boustead, J. N., Flemming, B. P., and O'brien, R. M. (2006). Gluconeogenesis: re-evaluating the FOXO1-PGC-1alpha connection. *Nature* 443, E10–E11. doi: 10.1038/nature05288

Schwer, B., Schumacher, B., Lombard, D. B., Xiao, C., Kurtev, M. V., Gao, J., et al. (2010). Neural sirtuin 6 (Sirt6) ablation attenuates somatic growth and causes obesity. *Proc. Natl. Acad. Sci. U.S.A.* 107, 21790–21794. doi: 10.1073/pnas.1016306107

Shimizu, I., Yoshida, Y., Suda, M., and Minamino, T. (2014). DNA damage response and metabolic disease. *Cell Metab.* 20, 967–977. doi: 10.1016/j.cmet.2014.10.008

Song, M. Y., Wang, J., Ka, S. O., Bae, E. J., and Park, B. H. (2016). Insulin secretion impairment in Sirt6 knockout pancreatic beta cells is mediated by suppression of the FoxO1-Pdx1-Glut2 pathway. *Sci. Rep.* 6:30321. doi: 10.1038/srep30321

Sundaresan, N. R., Vasudevan, P., Zhong, L., Kim, G., Samant, S., Parekh, V., et al. (2012). The sirtuin SIRT6 blocks IGF-Akt signaling and development of cardiac hypertrophy by targeting c-Jun. *Nat. Med.* 18, 1643–1650. doi: 10.1038/nm.2961

Tao, R., Xiong, X., Depinho, R. A., Deng, C. X., and Dong, X. C. (2013). FoxO3 transcription factor and Sirt6 deacetylase regulate low density lipoprotein (LDL)-cholesterol homeostasis via control of the proprotein convertase subtilisin/kexin type 9 (Pcsk9) gene expression. *J. Biol. Chem.* 288, 29252–29259. doi: 10.1074/jbc.M113.481473

Tasselli, L., Xi, Y., Zheng, W., Tennen, R. I., Odrowaz, Z., Simeoni, F., et al. (2016a). SIRT6 deacetylates H3K18ac at pericentric chromatin to prevent mitotic errors and cellular senescence. *Nat. Struct. Mol. Biol.* 23, 434–440. doi: 10.1038/nsmb.3202

Tasselli, L., Zheng, W., and Chua, K. F. (2016b). SIRT6: novel mechanisms and links to aging and disease. *Trends Endocrinol. Metab.* 28, 168–185. doi: 10.1016/j.tem.2016.10.002

Vander Heiden, M. G., Cantley, L. C., and Thompson, C. B. (2009). Understanding the warburg effect: the metabolic requirements of cell proliferation. *Science* 324, 1029–1033. doi: 10.1126/science.1160809

Vitiello, M., Zullo, A., Servillo, L., Mancini, F. P., Borriello, A., Giovane, A., et al. (2017). Multiple pathways of SIRT6 at the crossroads in the control of longevity, cancer, and cardiovascular diseases. *Ageing Res. Rev.* 35, 301–311. doi: 10.1016/j.arr.2016.10.008

Wu, J., Boström, P., Sparks, L. M., Ye, L., Choi, J. H., Giang, A. H., et al. (2012). Beige adipocytes are a distinct type of thermogenic fat cell in mouse and human. *Cell* 150, 366–376. doi: 10.1016/j.cell.2012.05.016

Xiao, C., Kim, H. S., Lahusen, T., Wang, R. H., Xu, X., Gavrilova, O., et al. (2010). SIRT6 deficiency results in severe hypoglycemia by enhancing both basal and insulin-stimulated glucose uptake in mice. *J. Biol. Chem.* 285, 36776–36784. doi: 10.1074/jbc.M110.168039

Xiao, C., Wang, R. H., Lahusen, T. J., Park, O., Bertola, A., Maruyama, T., et al. (2012). Progression of chronic liver inflammation and fibrosis driven by activation of c-JUN signaling in Sirt6 mutant mice. *J. Biol. Chem.* 287, 41903–41913. doi: 10.1074/jbc.M112.415182

Xiong, X., Sun, X., Wang, Q., Qian, X., Zhang, Y., Pan, X., et al. (2016). SIRT6 protects against palmitate-induced pancreatic beta-cell dysfunction and apoptosis. *J. Endocrinol.* 231, 159–165. doi: 10.1530/JOE-16-0317

Xiong, X., Zhang, C., Zhang, Y., Fan, R., Qian, X., and Dong, X. C. (2017). Fabp4-Cre-mediated Sirt6 deletion impairs adipose tissue function and metabolic homeostasis in mice. *J. Endocrinol.* 233, 307–314. doi: 10.1530/JOE-17-0033

Yamagata, K., Daitoku, H., Takahashi, Y., Namiki, K., Hisatake, K., Kako, K., et al. (2008). Arginine methylation of FOXO transcription factors inhibits their phosphorylation by Akt. *Mol. Cell* 32, 221–231. doi: 10.1016/j.molcel.2008.09.013

Yang, B., Zwaans, B. M., Eckersdorff, M., and Lombard, D. B. (2009). The sirtuin SIRT6 deacetylates H3 K56Ac *in vivo* to promote genomic stability. *Cell Cycle* 8, 2662–2663. doi: 10.4161/cc.8.16.9329

Yang, S. J., Choi, J. M., Chae, S. W., Kim, W. J., Park, S. E., Rhee, E. J., et al. (2011). Activation of peroxisome proliferator-activated receptor gamma by rosiglitazone increases sirt6 expression and ameliorates hepatic steatosis in rats. *PLoS ONE* 6:e17057. doi: 10.1371/journal.pone.0017057

Yao, L., Cui, X., Chen, Q., Yang, X., Fang, F., Zhang, J., et al. (2017). Cold-inducible SIRT6 Regulates thermogenesis of brown and beige fat. *Cell Rep.* 20, 641–654. doi: 10.1016/j.celrep.2017.06.069

Yoshihara, E., Fujimoto, S., Inagaki, N., Okawa, K., Masaki, S., Yodoi, J., et al. (2010). Disruption of TBP-2 ameliorates insulin sensitivity and secretion without affecting obesity. *Nat. Commun.* 1:127. doi: 10.1038/ncomms1127

Zhang, H. J., Zhang, X. F., Ma, Z. M., Pan, L. L., Chen, Z., Han, H. W., et al. (2013). Irisin is inversely associated with intrahepatic triglyceride contents in obese adults. *J. Hepatol.* 59, 557–562. doi: 10.1016/j.jhep.2013.04.030

Zhang, P., Tu, B., Wang, H., Cao, Z., Tang, M., Zhang, C., et al. (2014). Tumor suppressor p53 cooperates with SIRT6 to regulate gluconeogenesis by promoting FoxO1 nuclear exclusion. *Proc. Natl. Acad. Sci. U.S.A.* 111, 10684–10689. doi: 10.1073/pnas.1411026111

Zhao, Y., Yang, J., Liao, W., Liu, X., Zhang, H., Wang, S., et al. (2010). Cytosolic FoxO1 is essential for the induction of autophagy and tumour suppressor activity. *Nat. Cell Biol.* 12, 665–675. doi: 10.1038/ncb2069

Zhong, L., D'urso, A., Toiber, D., Sebastian, C., Henry, R. E., Vadysirisack, D. D., et al. (2010). The histone deacetylase Sirt6 regulates glucose homeostasis via Hif1alpha. *Cell* 140, 280–293. doi: 10.1016/j.cell.2009.12.041

Zimmermann, R., Strauss, J. G., Haemmerle, G., Schoiswohl, G., Birner-Gruenberger, R., Riederer, M., et al. (2004). Fat mobilization in adipose tissue is promoted by adipose triglyceride lipase. *Science* 306, 1383–1386. doi: 10.1126/science.1100747

Conflict of Interest Statement: The authors declare that the research was conducted in the absence of any commercial or financial relationships that could be construed as a potential conflict of interest.

frontiers in Physiology

ORIGINAL RESEARCH
published: 21 February 2018
doi: 10.3389/fphys.2018.00122

AMP-Activated Protein Kinase (AMPK) Regulates Energy Metabolism through Modulating Thermogenesis in Adipose Tissue

Lingyan Wu[1,2†], *Lina Zhang*[1†], *Bohan Li*[1,2†], *Haowen Jiang*[3], *Yanan Duan*[3], *Zhifu Xie*[1,2], *Lin Shuai*[1,2], *Jia Li*[1] *and Jingya Li*[1*]

[1] State Key Laboratory of Drug Research, Shanghai Institute of Materia Medica, Chinese Academy of Sciences, Shanghai, China, [2] University of Chinese Academy of Sciences, Beijing, China, [3] Shanghai Engineering Research Center of Molecular Therapeutics and New Drug Development, East China Normal University, Shanghai, China

OPEN ACCESS

Edited by:
Xinran Ma,
East China Normal University, China

Reviewed by:
Yu-Chiang Lai,
University of Dundee, United Kingdom
Claudio de Lucia,
Temple University, United States

***Correspondence:**
Jingya Li
jyli@simm.ac.cn

[†] These authors have contributed equally to this work.

Specialty section:
This article was submitted to Clinical and Translational Physiology, a section of the journal Frontiers in Physiology

Received: 15 November 2017
Accepted: 06 February 2018
Published: 21 February 2018

Citation:
Wu L, Zhang L, Li B, Jiang H, Duan Y, Xie Z, Shuai L, Li J and Li J (2018) AMP-Activated Protein Kinase (AMPK) Regulates Energy Metabolism through Modulating Thermogenesis in Adipose Tissue. Front. Physiol. 9:122. doi: 10.3389/fphys.2018.00122

Obesity occurs when excess energy accumulates in white adipose tissue (WAT), whereas brown adipose tissue (BAT), which is specialized in dissipating energy through thermogenesis, potently counteracts obesity. White adipocytes can be converted to thermogenic "brown-like" cells (beige cells; WAT browning) under various stimuli, such as cold exposure. AMP-activated protein kinase (AMPK) is a crucial energy sensor that regulates energy metabolism in multiple tissues. However, the role of AMPK in adipose tissue function, especially in the WAT browning process, is not fully understood. To illuminate the effect of adipocyte AMPK on energy metabolism, we generated Adiponectin-Cre-driven adipose tissue-specific AMPK α1/α2 KO mice (AKO). These AKO mice were cold intolerant and their inguinal WAT displayed impaired mitochondrial integrity and biogenesis, and reduced expression of thermogenic markers upon cold exposure. High-fat-diet (HFD)-fed AKO mice exhibited increased adiposity and exacerbated hepatic steatosis and fibrosis and impaired glucose tolerance and insulin sensitivity. Meanwhile, energy expenditure and oxygen consumption were markedly decreased in the AKO mice both in basal conditions and after stimulation with a β3-adrenergic receptor agonist, CL 316,243. In contrast, we found that in HFD-fed obese mouse model, chronic AMPK activation by A-769662 protected against obesity and related metabolic dysfunction. A-769662 alleviated HFD-induced glucose intolerance and reduced body weight gain and WAT expansion. Notably, A-769662 increased energy expenditure and cold tolerance in HFD-fed mice. A-769662 treatment also induced the browning process in the inguinal fat depot of HFD-fed mice. Likewise, A-769662 enhanced thermogenesis in differentiated inguinal stromal vascular fraction (SVF) cells via AMPK signaling pathway. In summary, a lack of adipocyte AMPKα induced thermogenic impairment and obesity in response to cold and nutrient-overload, respectively, whereas chronic AMPK activation by A-769662 promoted WAT browning in inguinal WAT

and protected against HFD-induced obesity and related metabolic dysfunction. These findings reveal a vital role for adipocyte AMPK in regulating the browning process in inguinal WAT and in maintaining energy homeostasis, which suggests that the targeted activation of adipocyte AMPK may be a promising strategy for anti-obesity therapy.

Keywords: AMP-activated protein kinase, thermogenesis, energy metabolism, A-769662, white adipose browning, PGC-1α

INTRODUCTION

Obesity, which has reached epidemic proportions globally (Finucane et al., 2011), is associated with disorders, including type II diabetes, cardiovascular disease, and some cancer. The main cause of obesity is a chronic imbalance between energy intake and energy expenditure. For many years, it was believed that two main types of adipose tissue exist in mammals: white adipose tissue (WAT) and brown adipose tissue (BAT). The primary function of WAT is to store excess energy as triglycerides, whereas BAT is responsible for dissipating chemical energy as heat through thermogenesis (Berry et al., 2013). BAT and skeletal muscle are two well-described thermogenic tissues that utilize different mechanisms to generate heat for maintaining normal core body temperature in cold environment (Rowland et al., 2015; Bal et al., 2017a). Skeletal muscle employs both shivering and nonshivering thermogenesis via various mechanisms including mitochondrial metabolism and futile ATP hydrolysis, while BAT-mediated nonshivering thermogenesis is extremely dependent on mitochondrial metabolism (Bal et al., 2012, 2017b). Recent studies have discovered another type of thermogenic adipose tissue called beige fat and have demonstrated that both classic brown adipocyte and beige adipocyte coexist in adult humans (van Marken Lichtenbelt et al., 2009; Wu et al., 2012; Rosen and Spiegelman, 2014). However, beige adipocytes possess some distinct characteristics over classic brown adipocytes. First, beige adipocytes have a relatively low basal level of uncoupling protein 1 (UCP1) but express a high level of UCP1 in response to cold and adrenergic stimulation. Second, beige adipocytes are not derived from the myf5$^+$ lineage from which classic brown adipocytes originate. Third, beige adipocytes are readily induced by various environmental cues, such as chronic cold stimulation, exercise and agonists of pro-adipogenic or pro-thermogenic transcription factors that regulate beige adipogenesis or thermogenesis (Kajimura et al., 2015; Inagaki et al., 2016).

Evidence has shown that augmenting the activity or content of brown and beige fat is beneficial for boosting energy expenditure (Bartelt and Heeren, 2014). Therefore, therapeutics that target brown fat or remodel white fat into beige fat (referred to as WAT browning) for the treatment of obesity and its related metabolic diseases have gained clinical interest. In rodents, a number of tissues and cell types have been found to secrete factors that regulate WAT browning or thermogenesis in brown and beige adipose tissue, such as orexin (Sellayah et al., 2011), bone morphogenetic protein 7 (BMP7) (Tseng et al., 2008), catecholamine hormones such as norepinephrine (NE) secreted from sympathetic neurons (Collins, 2011), natriuretic peptides secreted from cardiac tissue (Bordicchia et al., 2012), fibroblast growth factor 21 (FGF21) secreted from the liver and BAT (Lee et al., 2014), PGC-1α-dependent myokine irisin (Boström et al., 2012), T4 secreted from the thyroid, and BMP8b and vascular endothelial growth factor (VEGF) secreted from BAT (Whittle et al., 2012; Bagchi et al., 2013). In addition to secreted factors, several small molecules have also been shown to induce WAT browning, such as a transient receptor potential cation channel subfamily V member 4 (TRPV4) antagonist that upregulates PGC-1α (Ye et al., 2012).

AMPK, a ubiquitously distributed serine/threonine protein kinase, regulates cellular energy homeostasis, acting as a central energy sensor and monitor by turning on catabolic pathways to generate ATP and turning off energy-consuming anabolic pathways (Zhang et al., 2009). AMPK generally functions as an indispensable heterotrimeric complex that is composed of a catalytic subunit (α1 and α2) and two regulatory subunits (β and γ; Carling, 2004). The direct metabolic substrates of

Abbreviations: ACC, acetyl-CoA carboxylase; Acot2, acyl-CoA thioesterase 2; Acta2, smooth muscle actin alpha 2; AICAR, 5-aminoimidazole-4-carboxamide-1-β-D-ribofuranoside; AKT, protein Kinase B; ALT, alanine aminotransferase; AMP, adenosine monophosphate; AMPK, AMP-activated protein kinase; AST, aspartate transaminase; ATP, adenosine triphosphate; BAT, brown adipose tissue; BMI, Body Mass Index; BMP7, bone morphogenetic protein 7; BMP8b, bone morphogenetic protein 8b; Cidea, cell death-inducing DFFA-like effector a; Col1a1, collagen type I alpha 1 chain; Cox5b, cytochrome c oxidase polypeptide 5b; Cox7a1, cytochrome c oxidase polypeptide 7a1; Cox8b, cytochrome c oxidase polypeptide 8b; CPT1, carnitine palmitoyltransferase 1; Ctgf, connective tissue growth factor; Dio2, type II iodothyronine deiodinase; EE, energy expenditure; Elovl3, elongation of very long chain fatty acids protein 3; eWAT, epididymal white adipose tissue; FAO, fatty acid oxidation; Fasn, fatty acid synthase; FBG, fasting blood glucose; Fbxo31, f-box only protein 31; FCCP, carbonyl cyanide 4-(trifluoromethoxy) phenylhydrazone; FGF21, fibroblast growth factor 21; Fndc5, fibronectin type III domain-containing protein 5; Gck, glucose kinase; GTT, glucose tolerance test; hADMSC, human adipose-derived mesenchymal stem cell; HDL-C, high-density lipoprotein cholesterol; H&E, hematoxylin and eosin; HFD, High-fat-diet; Hspb7, heat shock protein family, member 7; IBMX, 3-Isobutyl-1-methylxanthine; IR, insulin receptor; ITT, insulin tolerance test; iWAT, inguinal white adipose tissue; Lcad, long chain acyl-CoA dehydrogenase; LC-MS/MS, liquid chromatography-mass spectrometry/mass spectrometry; LDL-C, low-density lipoprotein cholesterol; Me1, malic enzyme; Mmp2, matrix metallopeptidase 2; mtDNA, mitochondrial DNA; Myf5, myogenic factor 5; NE, norepinephrine; NEFA, nonesterified fatty acid; NMR, 1H-nuclear magnetic resonance; OCR, oxygen consumption rates; Oplah, 5-Oxoprolinase (ATP-Hydrolysing); OXPHOS, oxidative phosphorylation; PGC-1α, Peroxisome proliferator-activated receptor gamma coactivator 1-alpha; Ppargc1b, Peroxisome proliferator-activated receptor gamma coactivator beta; PRDM16, PR domain containing 16; pWAT, perirenal WAT; RER, respiratory exchange rate; Slc29a1, solute carrier family 29 member 1; SVF, stromal vascular fraction; T3, 3,3′,5-Triiodo-L-thyronine; T4, thyroxin; TC, total cholesterol; TG, triglyceride; Timp1, tissue inhibitor of metalloproteinases 1; TRPV4, transient receptor potential cation channel subfamily V member 4; UCP1, uncoupling protein 1; VEGF, vascular endothelial growth factor; WAT, white adipose tissue; ZMP, 5-aminoimidazole-4-carboxamide ribonucleoside monophosphate.

AMPK are related to almost all branches of cellular metabolism (Hoffman et al., 2015; Schaffer et al., 2015). AMPK is widely implicated in diverse biological processes including cell growth, cell polarity and migration, autophagy and energy metabolism (Mihaylova and Shaw, 2011). Importantly, AMPK plays a critical role in regulating fatty acid metabolism, thermogenesis and the development of adipose tissue (O'Neill et al., 2013; Day et al., 2017). AMPK activation is known to inhibit fatty acid synthesis and to promote fatty acid oxidation by phosphorylating acetyl-CoA carboxylase (ACC) and by decreasing malonyl-CoA level, thereby reinstating the activity of carnitine palmitoyltransferase 1 (CPT1) (Carlson and Kim, 1973; Carling et al., 1987; Fullerton et al., 2013). Acute treatment with A-769662, an allosteric AMPK activator that depends on the existence of AMPK β1, lowers the liver malonyl-CoA level and enhances fatty acid oxidation in Sprague Dawley rats, and chronic A-769662 treatment decreases plasma and liver triglyceride levels in *ob/ob* mice (Cool et al., 2006). AMPK also regulates mitochondria biogenesis by phosphorylating and activating PGC-1α (Jager et al., 2007). The natural compound berberine has been shown to promote thermogenesis in brown and WAT via the AMPK-PGC-1α pathway (Zhang et al., 2014). Regarding the development of adipose tissue, several studies have suggested that AMPK plays an inhibitory role in white adipocyte differentiation (Habinowski and Witters, 2001; Dagon et al., 2006; Zhou et al., 2009). Some other studies have shown that AMPK activation promotes brown adipocyte differentiation *in vitro* and that AMPK positively regulates brown adipogenesis and BAT development via epigenetically decreasing the DNA methylation of the PRDM16 promotor (Yang et al., 2016). Most studies on adipocyte AMPK are mainly based on the use of indirect pharmacological AMPK activators, which may cause off-target effects (Cool et al., 2006). For example, pharmacological, chronic activation of AMPK by 5-aminoimidazole-4-carboxamide-1-β-D-ribofuranoside (AICAR) has been reported to enhance energy dissipation in white adipocytes (Gaidhu et al., 2009). When AICAR is converted to 5-aminoimidazole-4-carboxamide ribonucleoside monophosphate (ZMP), it mimics the effects of AMP and activates AMPK (Corton et al., 1995; Carling et al., 2012). However, this mechanism causes other effects, such as the stimulation of glycogen phosphorylase and inhibition of fructose-1,6-bisphosphatase (Cool et al., 2006), and it is unclear whether the metabolic effects seen with AICAR administration are mediated entirely through AMPK stimulation. Therefore, alternative methods for directly and more specifically activating AMPK are needed to study the role of AMPK in adipose metabolism.

Recently, a study reported that adipose tissue-specific deletion of both AMPK β1 and β2 subunits exacerbated high-fat diet (HFD)-induced insulin resistance and hepatic steatosis due to compromised BAT and WAT function (Mottillo et al., 2016). Meanwhile, another study showed that genetic deletion of both AMPK α1 and α2 subunits in adipose reduced adiposity due to an increase in lipolysis and fatty acid oxidation in adipose tissue (Kim et al., 2016). Despite the different genetic knockout strategies used in these two studies, the phenotypes in genotypes with adipocyte AMPK abrogation are quite controversial. In this study, we focus on elucidating the role of AMPK in adipose tissue metabolism by generating a mouse model with the adipocyte AMPK catalytic subunits (α1 and α2) ablated (AKO) and by investigating the metabolic effects of the chronic, direct activation of AMPK by A-769662 on a HFD-fed obese mouse model. Similar to adipose tissue-specific double AMPK β1/β1 KO mice (Mottillo et al., 2016), the AKO mice were prone to HFD-induced obesity and hepatic steatosis and fibrosis, and displayed impaired glucose and lipid metabolism. Consistent with this result, cold-induced adaptive thermogenesis and both basal and β3-adrenergic-activated energy expenditure were significantly blunted in AKO mice. Furthermore, we demonstrated that chronic AMPK activation by A-769662 reduced body weight gain and WAT expansion in HFD-fed mice. Notably, A-769662 enhanced cold-induced thermogenesis and induced browning in the inguinal fat depot. Collectively, our findings indicate that AMPK plays a critical role in the regulation of energy homeostasis and chronic AMPK activation may provide promising therapeutics for treating of obesity and related metabolic diseases through promoting energy expenditure.

MATERIALS AND METHODS

Materials

Antibody sources are as follows: UCP-1 (alpha diagnostic, UCP11-A, 1:1,000, 32 kDa), PGC-1a (Calbiochem, ST1202, 1:1,000, 113 kDa); IR (Santa Cruz, sc-711, 1:1,000, 95 kDa), AMPKα1 (#ab3759, 1:1,000, 63 kDa), AMPKα2 (#ab3760, 1:1,000, 63 kDa) (abcam); AMPKγ2 (#AP51709, 1:1000, 38 kDa), β-actin (AM1021B, 1:10,000, 42 kDa) (Abgent); AMPKα (#2532, 1:1,000, 62 kDa), AMPKβ1 (#12063, 1:1,000, 38 kDa), AMPKβ2 (#4148, 1:1,000, 30 kDa), AMPKγ2 (#2536, 1:1,000, 75 kDa), phospho-AMPKα (Thr172) (#2535, 1:1,000, 62 kDa), ACC (#3662, 1:1,000, 280 kDa), phospho-ACC (Ser79) (#3661, 1:1,000, 280 kDa), AKT (#4691, 1:1,000, 60 kDa), phospho-AKT (Ser473) (#4060, 1:1,000, 60 kDa), phospho-IR (Tyr1162) (#3918, 1:1,000, 95 kDa) (Cell Signaling Technology). A-769662, CL 316,243, norepinephrine, rosiglitazone, dexamethasone, 3-Isobutyl-1-methylxanthine (IBMX), 3,3′,5-Triiodo-L-thyronine (T3), indomycine, oligomycin, carbonyl cyanide 4-(trifluoromethoxy) phenylhydrazone (FCCP), rotenone and antimycin A were purchased from Sigma-Aldrich. Recombinant human Insulin (Eli Lily) was purchased from Changzheng Hospital (Shanghai, China). ELISA kits used in measurement of plasma parameters are as follows: TG (Shanghai Fosun Long March, 1.02.1801), TC (Shanghai Fosun Long March, 1.02.0401), HDL-C (XinJianKangCheng Bio, E0303), LDL-C (XinJianKangCheng Bio, E0403), NFEA (WAKO, 294-63601), Insulin (Millipore, EZRMI-13K), Irisin (Phoenix, EK-067-29), Leptin (Millipore, EZML-82K), Adiponectin (abcam, ab108785), Glucagon (BIOSWAMP, MU30638), Epinephrine (CUSABIO, CSB-E08679m), Norepinephrine (CUSABIO, CSB-E07870m), ALT (Sysmex, 290703, 290704), AST (Sysmex, 290705, 290706).

Animal Model

All animal experiments were approved by the Animal Care and Use Committee of the Shanghai Institute of Materia Medica,

where the experiments were conducted. All animals were housed in a temperature-controlled room (22 ± 2°C) with a light/dark cycle of 12 h. To obtain adipose tissue-specific AMPKα1/α2 double-KO mice (referred to as AKO mice), AMPKα1/α2-floxed mice were first generated by mating homozygous AMPKα1-floxed mice (stock No: 014141, Prkaa1^{fl}, Jackson Laboratory, Bar Harbor, Maine, USA) with AMPKα2-floxed (stock No: 014142, Prkaa2^{fl}, Jackson Laboratory, Bar Harbor, Maine, USA). Next, AMPK α1/α2-floxed mice were crossed with Adiponectin-Cre mice (stock No: 010803, Jackson Laboratory, Bar Harbor, Maine, USA) to generate adipose tissue-specific AKO mice. Male AKO mice and age-matched AMPKα1/α2-floxed littermates were randomly divided into two groups and starting from 8 weeks of age for 34 weeks fed either a normal chow diet or a HFD (60% calories from fat, 20% calories from protein, 20% calories from carbohydrate; Research Diets). Body weight and food intake were recorded weekly. Cold exposure experiments were performed at 8 weeks of age. Glucose tolerance tests and insulin tolerance tests were conducted at 20 and 30 weeks of age, respectively. Metabolic analysis and body composition analysis were performed at 40 weeks of age. For chronic anti-obesity studies, beginning at 6 weeks of age, male C57BL/6J mice (Shanghai SLAC Laboratory Animal Co., Shanghai, China) were fed a HFD. At 14 weeks of age, HFD-fed mice and chow-fed mice were randomly assigned to treatment groups. Mice received either vehicle [1% DMSO, 2% castor oil and 0.9% NaCl, q.d., intraperitoneally (i.p.)] or A-769662 (30 mg/kg/day q.d. i.p.) for 6 weeks. Body weight and food intake were recorded daily. Glucose tolerance tests and calorimetry metabolic analysis were conducted during the 4th week of treatment. The blood samples were collected during the 5th week of treatment and the plasma parameters were determined using the indicated kits according to the manufacturers' instructions. Cold exposure experiments were performed at 4°C during the 6th week of treatment. At the end of the study, the tissues were dissected, weighed, immediately frozen in liquid nitrogen and stored at −80°C.

Cold Exposure

For chronic cold exposure, mice were singly housed at 4°C for 24 h. Food and water were available *ad libitum*. For acute cold exposure, mice were individually housed at 4°C for 8 h without food but with free access to water. Body temperature was measured every hour with a BAT-12 microprobe digital thermometer and RET-3 mouse rectal probe (Physitemp Instruments, Clifton, USA).

Metabolic Analysis

Mouse O_2 consumption, CO_2 production, heat production and locomotor activity were measured using a sixteen-chamber indirect calorimeter (TSE PhenoMaster, TSE system) according to manufacturer's instructions. Mice were acclimated to the chambers for 24 h before the measurements began. Food and water were fed *ad libitum* throughout the experiment. Basal metabolic parameters were measured during the following 12-h light/dark cycle and the CL 312,643-stimulated metabolic parameters were measured for 10 h after the i.p. injection of CL 312,643 (1 mg/kg). Whole-body fat mass, lean mass and fluid mass were determined by ^{1}H-nuclear magnetic resonance (NMR) spectroscopy (Minispec LF90 II, Bruker).

Glucose Tolerance Test (GTT) and Insulin Tolerance Test (ITT)

After fasting for 6 h, mice were i.p. injected with either glucose (2 g/kg) or insulin (0.75 U/kg). Glucose concentrations were measured before and 15, 30, 60, 90, and 120 min after the injection of glucose or insulin.

Quantitative RT-PCR

Total RNA was isolated from cells or homogenized tissues using TRIzol reagent (Invitrogen). One microgram of total RNA was reverse transcribed using PrimeScript Reverse Transcriptase (Takara). The resulting cDNAs were amplified using 2 × SYBR Green qPCR Master Mix (Vazyme) and a Stratagene Mx3005P instrument (Agilent Technologies). Expression was normalized to that of indicated control gene. Primer sequence details are shown in Supplementary Table 1.

Mitochondrial DNA (mtDNA) Quantification

Adipose tissues were cut into small pieces, and total DNA was extracted using a DNeasy Blood & Tissue Kit (Qiagen, 69506) according to the manufacturer's instructions. Quantitative (Q) PCR was performed using mitochondrial DNA-specific primer (16S rRNA)and genomic DNA-specific primer (hexokinase 2 gene, intron 9). Primer sequence details are shown in Supplementary Table 1.

Immunoblotting

Total protein from the tissues or cells was prepared in RIPA buffer (50 mM Tris-HCl (pH 8.0), 150 mM NaCl, 1% NP-40, 1 mM Na_3VO_4, 1 mM DTT, 1 mM EDTA, and 1 mM EGTA) containing complete protease inhibitors (Roche). After boiling for 10 min in SDS loading buffer, equal amounts of protein for each sample were electrophoresed through SDS-PAGE gels.

Histology

Mouse tissues were fixed in 4% neutral-buffered formalin and embedded in paraffin. Sections (5-μm thick) were stained with hematoxylin and eosin (H&E) and Sirius red according to standard protocols. Microscopy analysis was performed by using a Leica DM6 B microscope at the indicated magnification, and images were captured by a sCMOS camera under the same parameter setting. The average adipocyte size and lipid droplet area in adipose tissue sections [expressed as the average cross-sectional area per cell (μm^2)] was determined by using ImageJ software (National Institutes of Health) according to the method described in Parlee et al. (2014). Fibrosis was evaluated by calculating the proportional area of picrosirius red-stained matrix using image analysis (Quant center, 3D HISTECH, Hungary).

Tissue Hydroxyproline Measurement

Frozen liver samples (100–105 mg) were weighed and acid-hydrolyzed with 5M HCl at 110°C for 18–22 h. Hydroxyproline contents were measured using a hydroxyproline colorimetric

assay kit (BioVison, K555-100) according to the manufacturer's instructions.

Liver Triglyceride and Cholesterol Measurement

The liver triacylglycerol and cholesterol content were measured following a Folch extraction (Folch et al., 1957). The dried lipid residues were then resuspended in 800 μl ethanol with 1% triton for follow-up TG and TC assays. The Liver TG and TC levels were determined with the same kit as used in the plasma analysis.

Transmission Electron Microscopy

The adipose tissues were cut into 1 mm^3 and fixed in 2.5% glutaraldehyde (pH 7.4) for 24 h. Then the sample was washed with 0.1 M phosphate buffer for three times and fixed in osmic acid for 3 h in 4°C. The sample was flushed again, dehydrated with ethanol step by step, and displaced with epoxy propane. Finally, the block was embedded in Spurr resin (Spi-Chem, USA) and polymerization at 70°C. Thin sections were cut on a Leica EM UC6 ultramicrotome and counter stained with uranyl acetate and lead citrate. Then samples were observed with a JEM1230 transmission electron microscope (JEOL, Japan). For each sample, total mitochondria and mitochondria bearing cristae disruption were quantified, and percentage of mitochondria with disrupted cristae was calculated. Criteria for disrupted cristae included any observable disorganization, vacuolization, or dissolution of cristae within mitochondria (Mottillo et al., 2016; Bal et al., 2017a).

Stromal Vascular Fraction (SVF) Cells Isolation and Differentiation

SVF cells were isolated as described previously (Wang et al., 2013). In brief, adipose tissue was minced and digested with 10 mg/ml collagenase D (Roche) and 2.4 mg/ml Dispase II (Roche) in PBS supplemented with 1% bovine serum albumin for 45 min at 37°C, followed by quenching with complete medium. The digested tissue suspensions were centrifuged, washed and successively filtered through 100 and 40 μm strainer (BD Biosciences), and then, the cells were plated onto 10 cm dishes. SVFs were cultured in DMEM/F12 supplemented with 10% FBS (Gibco), 1% penicillin/streptomycin (Invitrogen). SVF cells were plated onto 24-well plates to reach confluence. Once cells reached confluency, adipocyte differentiation was carried out in growth medium supplemented with 850 nM insulin, 0.5 mM IBMX, 1 μM dexamethasone, 125 nM indomethacin and 1 nM T3 for 48 h and then in growth medium supplemented with 850 nM insulin and 1 nM T3 for an additional 6 days. To investigate the effect of AMPKα knockdown on NE-induced thermogenic, iWAT-SVF cells were isolated from 5 week-old AMPK α1/α2-floxed mice and induced to differentiate toward beige adipocytes. Cells were infected with NC and Cre adenovirus on day 6 and were treated with NE (10 μM) on day 8 for 6 h. To investigate the effect of A-769662 on thermogenesis, differentiated SVF cells (day 7) were cultured with serum-free DMEM/F12 medium for 2 h and treated with DMSO or A-769662 at the indicated concentration for 6 h in quantitatvie RT-PCR, for 12 h in the measurement of oxygen consumption rates (OCRs) and for 24 h in western blot analysis. To confirm whether A-769662-induced thermogenesis *in vitro* via AMPK signaling pathway, iWAT-SVF cells isolated from the floxed mice were differentiated into beige adipocytes followed by infected with NC and Cre lentivirus on day 6, and were treated with A-769662 at the indicated concentration on day 8.

Measurement of OCRs

SVF cells were plated in a 96-well XF microplate (Seahorse Bioscience) and differentiated for 7 days, OCR was measured at 37°C using a 96 Extracellular Flux Analyzer (Seahorse Bioscience) in accordance with the manufacturer's instructions. Uncoupled respiration was detected by treating cells with oligomycin (2 μM).

Tissue Distribution Assay

HFD-fed mice were i.p. injected with A-769662 (30 mg/kg). After 1 h, the animals were sacrificed, and the plasma, liver, and various adipose depots and muscles were collected and preserved at −80°C. Tissue samples were analyzed with a liquid chromatography-mass spectrometry/mass spectrometry (LC-MS/MS) system (an Agilent 1200 HPLC coupled to an Agilent 6460 Triple Quad instrument, Agilent Technologies, USA) to detect the concentration of A-769662. Data were analyzed by MassHunter Quantitative Analysis (version B.02.01, Agilent Technologies, USA).

Statistical Analysis

The results are presented as the means ± SEM. Differences between the groups were analyzed using Student's *t*-test or one-way ANOVA followed by Dunnett's multiple comparisons test by GraphPad Prism version 7.00 for Windows (GraphPad Software, La Jolla California USA). $P < 0.05$ was regarded as statistically significant.

RESULTS

Adipocyte AMPK Regulating Mitochondrial Biogenesis and Structural Integrity Was Required for Cold-Induced Adaptive Thermogenesis in Inguinal White Adipose Tissue

One of the important functions of brown and beige fat is defending against hypothermia in cold environments through adaptive thermogenesis, which is crucial for maintaining whole-body energy homeostasis (Harms and Seale, 2013). Cold exposure stimulates β-adrenergic signaling via regulating norepinephrine (NE) secretion from sympathetic nerves, which indirectly activates AMPK signaling by inducing lipolysis and mitochondrial uncoupling in the adipose tissue of rodents (Gauthier et al., 2008). It has been reported that in response to cold acclimation, different adipose tissue depots play diverse roles in metabolic remodeling, displaying enhanced thermogenic activity in BAT and contributing to browning in iWAT and in eWAT to a lesser extent (Jia et al., 2016). We wondered whether the sensitivity of AMPK activation in response to short-term

cold exposure varied among different fat pads. To probe the role of AMPK signaling in cold-induced adaptive thermogenesis in different adipose depots, 9-week-old male C57BL/6J mice were housed at room temperature (RT) or challenged with cold temperature (4°C) for 24 h, and the expression levels of proteins reflecting AMPK activation and thermogenic capacity in various adipose depots, including interscapular BAT, inguinal white adipose tissue (iWAT), and epididymal white adipose tissue (eWAT), were examined by western blot analysis. AMPK was significantly activated by cold exposure in iWAT, as evidenced by increased AMPKα phosphorylation (Thr172), but was unaffected in BAT and eWAT (**Figure 1A** and Supplementary Figure 1A). Similarly, the expression of the thermogenic protein UCP1 was up-regulated by cold in iWAT, but not in BAT and eWAT (**Figure 1A** and Supplementary Figures 1A,B), suggesting a depot-specific positive correlation between AMPK activation and adaptive thermogenesis in iWAT.

To investigate the physiological effects of adipocyte AMPKα on whole-body energy metabolism, we generated adipose tissue-specific AMPKα knockout (referred to as AKO) mice by crossing Adiponectin-Cre mice with double AMPK α1/α2-floxed mice (referred to as floxed mice). Western blot analyses of AMPKα1 and AMPKα2 expression in different fat pads and liver were performed to examine the knockout efficiency of AKO mice. The expression of both AMPKα1 and AMPKα2 and the mRNA levels of their encoding genes (*Prkaa1* and *Prkaa2*) in iWAT, eWAT, and BAT were substantially reduced in AKO mice; in contrast, that in the liver was not different between the genotypes (**Figure 1B** and Supplementary Figures 1C,D,I–L), indicating that the deletion of AMPKα was specific to adipose tissue. Because AMPKα function as an indispensable subunit of the heterotrimeric complex (Fentz et al., 2015), we examined the expression levels of its regulatory subunits β and γ. Surprisingly, expression of subunit AMPKβ1, AMPKβ2, AMPKγ1, and AMPKγ2 were significantly decreased in adipose tissue of AKO mice, but not in liver (**Figure 1B** and Supplementary Figures 1E–H). However, the mRNA levels of genes encoding subunit β (*Prkab1* and *Prkab2*) and subunit γ (*Prkag1* and *Prkag2*) were unaltered between genotypes (Supplementary Figures 1I–L), which suggests that the presence of AMPKα might be critical for protein stability of β subunits and γ subunits. These data indicate that efficient adipocyte-specific deletion of AMPK was achieved.

First, chow-fed male AKO mice and age-matched floxed littermates were challenged with cold exposure at 4°C for 8 h to assess the cold tolerance of both genotypes. During the cold challenge, the rectal temperature of AKO mice decreased more rapidly than that of floxed mice (**Figure 1C**), indicating that the capacity of adaptive thermogenesis in AKO mice was impaired. To determine the adaptive thermogenic activity of different adipose pads, cold exposure was extended to 48 h. The content and integrity of mitochondria affect its function of oxidation metabolism and cellular energy status during thermogenesis process (Bal et al., 2017a). The total number of mitochondria in different adipose pads was determined by assessing mitochondrial DNA copy number. The mitochondria number was reduced in iWAT and BAT of AKO mice compared to that of floxed mice, whereas that in eWAT did not differ in these two genotypes (Supplementary Figure 1M), suggesting that AMPK deletion likely inhibited mitochondrial biogenesis in iWAT and BAT, both of which contribute to adaptive thermogenesis during prolonged cold exposure. Next, the mitochondrial morphology in iWAT and BAT were assessed by using transmission electron microscopy. Accordingly, the mitochondria number per micrograph was decreased in iWAT and BAT of AKO mice by approximately 66 and 43%, respectively (**Figures 1D,E,G,H**). The mitochondrial structure was altered in iWAT and BAT of AKO mice after cold adaption and the disrupted cristae were increased by approximately 146 and 170%, respectively (**Figures 1D,F,G,I**). These observations indicate that adipocyte AMPK deficiency impaired both the structural integrity of mitochondria and mitochondrial biogenesis.

In addition, the expression of thermogenesis-related genes and proteins responding to cold acclimation was detected by Quantitative RT-PCR. The mRNA levels of thermogenesis-related genes, including *Ucp1*, *Ppargc1a*, *Dio2*, *Elovl3*, *Prdm16*, *Cidea*, *Cox7a1*, *Cox8b,* and *Cox5b*, and fatty acid oxidation (FAO)-related genes, such as *Ppargc1b*, *Cpt1b,* and *Lcad*, were dramatically reduced in the iWAT of the AKO mice after cold exposure (**Figure 1J**), but were unchanged in eWAT (Supplementary Figure 1P). In agreement of this result, the expression levels of the thermogenic protein UCP1 and of PGC-1α, a master coregulatory factor for mitochondrial biogenesis (Wu et al., 1999), were significantly reduced by genetic deletion of adipocyte AMPKα (**Figure 1L** and Supplementary Figure 1N), indicating that cold-induced browning was severely impaired in the iWAT of AKO mice. In addition to the thermogenic remodeling of iWAT, BAT-mediated adaptive thermogenesis is also highly responsive to cold stimulation (Rosen and Spiegelman, 2014). We then examined the expression pattern of thermogenic genes and proteins in the BAT of cold-acclimated AKO mice and floxed mice. In line with the reduced content and disrupted cristae of mitochondria, the expression of *Ppargc1a* and FAO-related genes, including *Ppargc1b* and *Lcad*, were decreased in BAT of AKO mice. However, the expression of thermogenic genes, such as *Ucp1*, *Ppargc1a*, *Dio2*, *Elovl3*, *Prdm16*, *Cidea*, *Cox7a1*, *Cox8b,* and *Cox5b*, were not significantly altered in the BAT of AKO mice (**Figure 1K**). Western blot analysis showed that the expression of UCP1 and PGC-1α in the BAT of the AKO mice was comparable with that of the floxed mice (**Figure 1M** and Supplementary Figure 1O), denoting that BAT-mediated adaptive thermogenesis was not readily perturbed by adipocyte AMPKα deletion *in vivo*. Moreover, the knockdown of AMPKα by using Cre-expressing adenovirus in differentiated stromal vascular fraction (SVF) cells isolated from the iWAT of AMPK α1/α2-floxed mice inhibited NE-induced thermogenic gene induction (Supplementary Figure 2), indicating that AMPK may serve as an important modulator of thermogenesis in a cell-autonomous manner. Together, these data demonstrate that the abrogation of AMPKα in adipose tissue impairs mitochondrial integrity and function and suppresses cold-induced adaptive thermogenesis and the browning of white adipocytes in iWAT, which may contribute to cold intolerance of AKO mice.

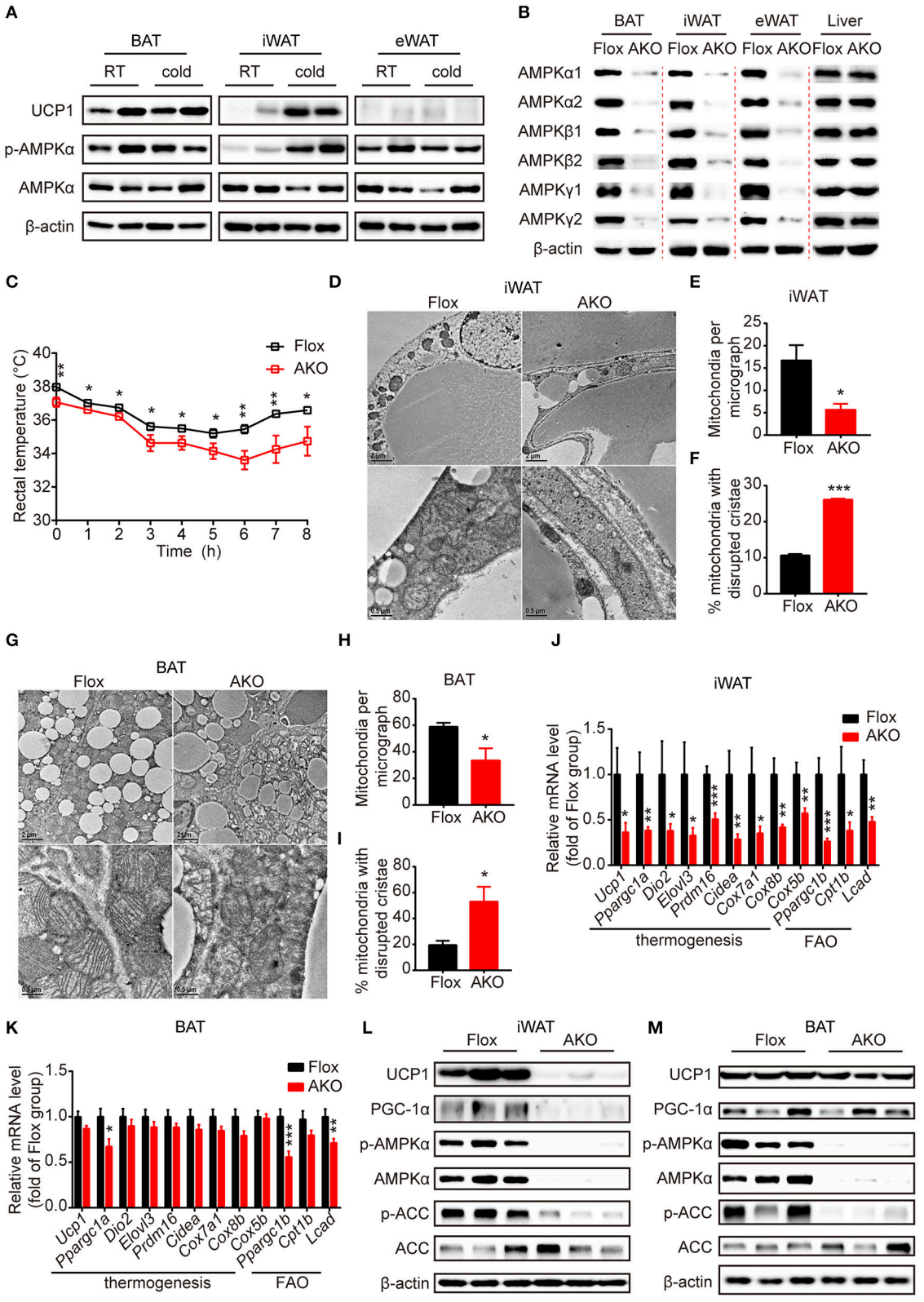

FIGURE 1 | Adipose AMPK deficiency impaired cold tolerance and suppressed cold-induced thermogenesis specifically in inguinal white adipose tissue. **(A)** Western blot analysis of UCP1, p-AMPKα (T172) and AMPKα protein levels in the interscapular brown adipose tissue (BAT), inguinal white adipose tissue (iWAT) and epididymal

(Continued)

FIGURE 1 | white adipose tissue (eWAT) of 9-week-old male wild-type (WT) mice housed at RT or 4°C for 24 h. β-actin was used as a loading control. $n = 4$. **(B)** Western blot analysis of AMPKα1, α2, β1, β2, γ1, γ2 protein expression levels in the BAT, iWAT, eWAT and liver of 10-week-old male AKO mice and age-matched floxed littermates. β-actin was used as a loading control. $n = 3$. **(C)** Rectal temperature of 8-week-old chow-fed AKO and floxed mice at 4°C for 8 h. $n = 9$. **(D–M)** 8-week-old male chow-fed AKO mice and floxed mice were housed at 4°C for 48 h. Representative transmission electronic microscopy images of iWAT **(D)** and BAT **(G)**, total number of mitochondria per micrograph in iWAT **(E)** and BAT **(H)** and the percentage of mitochondria with disrupted cristae over total mitochondria in iWAT **(F)** and BAT **(I)** from AKO mice and floxed mice were shown. $n = 3$. Scale bar: 2 μm in low magnification (×5,000, upper) and 0.5 μm in high magnification (×20,000, bottom). The relative mRNA levels of thermogenic genes and fatty acid oxidation (FAO)-related genes in the iWAT **(J)** and BAT **(K)** of AKO mice and floxed mice were analyzed by quantitative RT-PCR (normalized to *36b4*). $n = 8$–9. The expression levels of AMPKα, p-AMPKα (T172), ACC, p-ACC (S79), UCP1 and PGC-1α in the iWAT **(L)** and BAT **(M)** of AKO mice and floxed mice were determined by western blot analysis. Data are presented as the means ± SEM. Student's *t*-test. $^{*}P < 0.05$, $^{**}P < 0.01$, $^{***}P < 0.001$ compared with the indicated control group.

Adipocyte AMPK Protected against Diet-Induced Obesity and Related Metabolic Dysfunction

To investigate the metabolic effects of adipocyte AMPK ablation in response to a HFD, 8-week-old male AKO mice and age-matched floxed littermates were fed either a chow diet or a HFD for 34 weeks. Beginning at 29 weeks of age, the chow-fed AKO mice gained more weight than their counterparts, and the HFD challenge exacerbated the weight gain caused by the deletion of adipocyte AMPK, as evidenced by the earlier appearance (at 25 weeks of age) of more severe obesity in HFD-fed AKO mice (**Figure 2A**). Accordingly, the AKO mice were visually bigger and more obese than the HFD-fed or chow-fed floxed mice (**Figure 2B**). Although adipocyte AMPKα deletion did not affect food intake in mice fed a chow diet or a HFD (Supplementary Figure 3), chow- and HFD-fed AKO mice exhibited greater adiposity than the floxed mice, as evidenced by a higher fat mass in the AKO groups (**Figure 2C**). The relative iWAT weight was increased in AKO mice fed a chow diet or a HFD, but the weight of perirenal WAT (pWAT) was increased only in the HFD-fed AKO mice, while relative weights of eWAT and liver were unchanged (**Figure 2D**). Interestingly, the relative weight of BAT was decreased in the chow- and HFD-fed AKO mice, probably due to the inhibition of brown adipogenesis during early BAT development by the deletion of AMPKα (Yang et al., 2016). Moreover, glucose tolerance was impaired in the AKO mice fed a chow diet or a HFD, as shown by an increased area under the curve (AUC) in this group (**Figure 2E**). Defects in insulin sensitivity were also observed in the AKO mice fed a chow diet or a HFD (**Figure 2F**). Notably, the plasma levels of insulin and leptin, an adipokine that positively correlates to obesity and fat mass (Considine et al., 1996), were markedly elevated in both chow- and HFD-fed mice, while as an important adipose-derived hormone, adiponectin, the level of which is closely associated with insulin resistance and negatively correlated with adiposity (Yamauchi et al., 2001), was decreased by 36 and 32% in chow- and HFD-fed AKO mice, respectively (**Table 1**). The plasma level of glucagon, acting as a counterregulatory hormone for insulin (Jiang and Zhang, 2003), was reduced in both chow- and HFD-fed mice (**Table 1**), which may be a consequence of increased insulin level in AKO mice. Furthermore, the plasma levels of triglyceride (TG) and total cholesterol (TC) were significantly increased by 34 and 39% in HFD-fed AKO mice, respectively, but not in chow-fed AKO mice (**Table 1**), indicating that adipocyte AMPK deletion aggravated the development of hyperlipidemia under HFD stress. However, there were no significant changes in the levels of low-density lipoprotein cholesterol (LDL-C), high-density lipoprotein cholesterol (HDL-C) and nonesterified fatty acid (NEFA) between genotypes fed with a chow-diet or a HFD (**Table 1**). Collectively, these results suggest that adipocyte AMPK play a vital role in combating HFD-induced obesity, dysregulated glucose homeostasis and insulin resistance.

Effects of Adipocyte AMPKα Deficiency on the Morphology of Adipocytes in Different Depots *in Vivo*

Since the AKO mice were prone to HFD-induced obesity, we further investigate the effect of adipocyte AMPKα deletion on the morphology of different adipose depots. H&E staining showed that adipocyte size in the iWAT of chow- or HFD-fed AKO mice were notably larger than that in the floxed mice, as indicated by increased adipocyte area in the iWAT (**Figures 3A,B**). However, the adipocyte size in the eWAT of chow- and HFD-fed mice was not influenced by adipocyte AMPKα deletion (**Figures 3A,C**). The lipid droplets in the BAT of chow- or HFD-fed AKO mice were obviously larger than those of the floxed mice (**Figures 3A,D**), which may be owing to diminished expression of FAO-related gene in the BAT (**Figure 1K**). As mentioned above, adipocyte AMPKα deficiency specifically affected the expression of thermogenesis- and FAO-related genes and proteins in iWAT, which may hinder lipid mobilization and contribute to the increased adipocyte size and weight of inguinal adipose tissue.

Adipocyte AMPKα Deficiency Reduced Basal and β3-Adrenergic-Activated Energy Expenditure

Since the development of obesity and obesity-related metabolic dysfunction is generally due to an imbalance between energy intake and energy expenditure, we continued to evaluate the effect of adipocyte AMPKα deletion on energy expenditure under basal conditions and in response to acute β3-adrenergic receptor (AR) activation. Under basal conditions or after i.p. injections with β3-AR activator CL 316,243, the O_2 consumption and energy expenditure (EE) of chow- and HFD-fed AKO mice were significantly reduced during the 12-h light-dark cycle (**Figures 4A–D**), but locomotor activity was unchanged (Supplementary Figures 4B,D). Additionally, the basal respiration exchange ratio (RER) was unaltered in the AKO mice fed a chow diet or a HFD (Supplementary Figures 4A,C), but the CL 316,243-stimulated RER was slightly decreased in

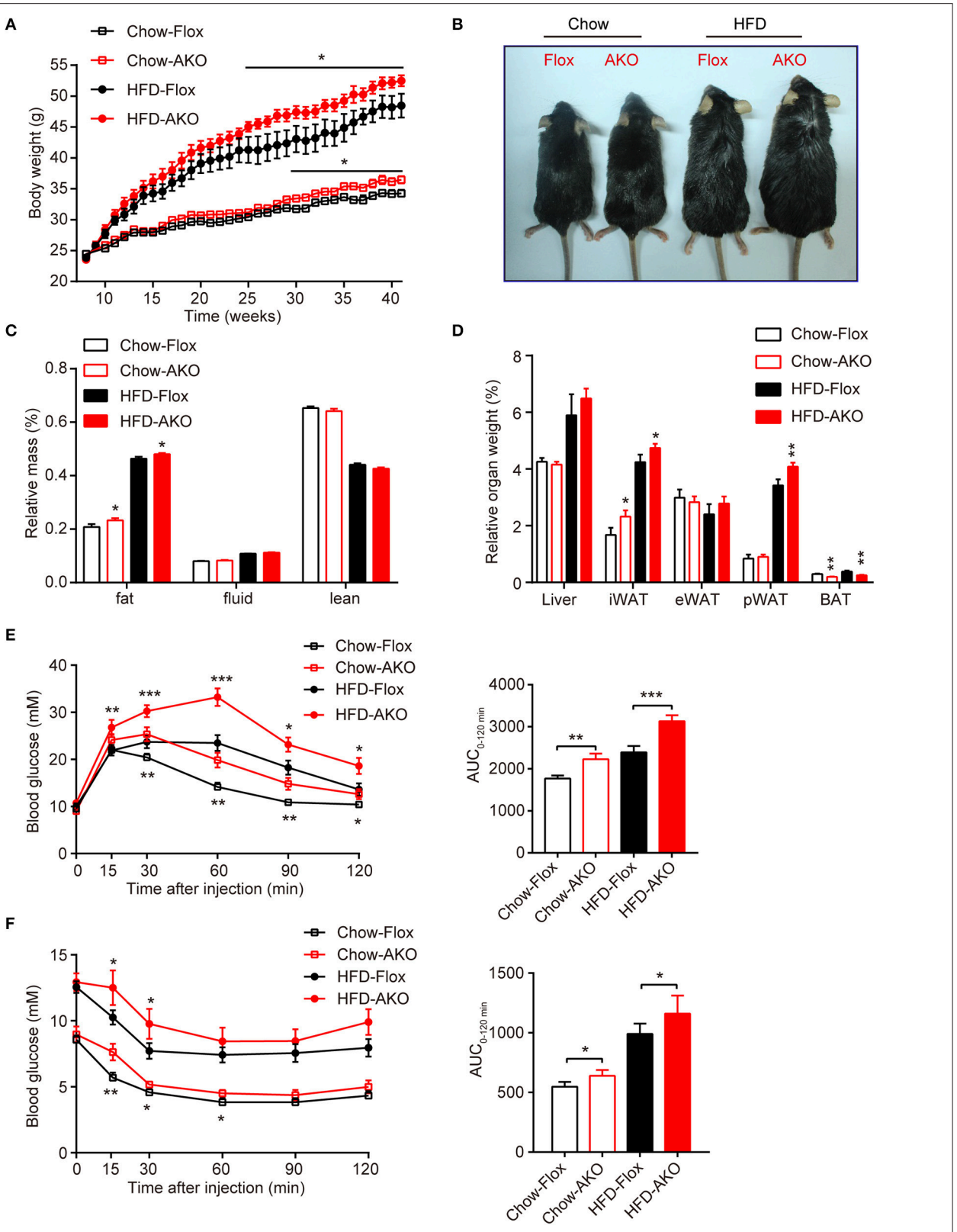

FIGURE 2 | Adipose-specific AMPKα deletion exacerbated high-fat diet (HFD)-induced adiposity and glucose intolerance. **(A)** Change in body weight of AKO mice and age-matched floxed littermates during the indicated period. **(B)** Representative images of 41-week-old male AKO mice and age-matched flox/flox mice. **(C)** Fat

(Continued)

FIGURE 2 | mass, fluid mass and lean mass relative to the total body weight of 40-week-old mice. **(D)** Relative weight of the liver, iWAT, eWAT, pWAT, and BAT to the total body weight of mice. **(E)** Blood glucose levels from the intraperitoneal glucose tolerance test (ipGTT) of 20-week-old mice following a single injection of glucose (2 g/kg) (left). The area under the curve (AUC) of the ipGTT during the indicated times was calculated as the blood glucose multiplied by the time (mM*min) (right). **(F)** Blood glucose levels of 30-week-old mice following a single injection of insulin (0.75 U/kg) in the intraperitoneal insulin tolerance test (ITT) (left). The AUC of the ITT is shown (right). Chow-Flox: AMPK α1/α2-floxed mice fed a chow diet, Chow-AKO: adipose tissue-specific AMPK α1/α2 KO mice fed a chow diet, HFD-Flox: AMPK α1/α2-floxed mice fed a HFD, HFD-AKO: adipose tissue-specific AMPK α1/α2 KO mice fed a HFD. Data are presented as the means ± SEM. $n = 11–15$. Student's *t*-test. $^*P < 0.05$, $^{**}P < 0.01$, $^{***}P < 0.001$ compared with the corresponding Flox group.

TABLE 1 | Plasma metabolic variables in floxed mice and AKO mice fed with a chow diet or a HFD.

Parameters	Chow-Flox	Chow-AKO	HFD-Flox	HFD-AKO
TC (mM)	1.97 ± 0.13	2.01 ± 0.17	4.2 ± 0.47	5.84 ± 0.27**
LDL-C (mM)	1.49 ± 0.04	1.60 ± 0.05	2.67 ± 0.21	3.23 ± 0.16
HDL-C (mM)	0.92 ± 0.04	0.84 ± 0.06	1.56 ± 0.11	1.65 ± 0.04
LDL-C/HDL-C	1.65 ± 0.07	1.77 ± 0.06	1.92 ± 0.07	1.81 ± 0.09
TG (mM)	0.70 ± 0.05	0.69 ± 0.05	0.41 ± 0.04	0.55 ± 0.04**
NEFA (mEq/L)	0.83 ± 0.06	0.86 ± 0.06	0.54 ± 0.06	0.53 ± 0.03
Insulin (ng/ml)	3.04 ± 0.39	4.34 ± 0.53*	20.08 ± 3.56	29.31 ± 3.59*
Leptin (ng/ml)	3.40 ± 0.62	5.74 ± 0.81*	45.97 ± 4.53	57.08 ± 2.19*
Irisin (ng/ml)	55.05 ± 1.74	47.47 ± 5.49	34.64 ± 1.5	33.21 ± 2.13
Adiponectin (μg/ml)	15.20 ± 2.72	9.78 ± 0.88*	14.63 ± 1.52	9.99 ± 0.99*
Glucagon (pg/ml)	231.67 ± 20.24	147.10 ± 32.72*	119.09 ± 15.19	77.18 ± 16.28*
Epinephrine (pg/ml)	234.30 ± 40.59	263.74 ± 35.51	235.32 ± 24.75	208.48 ± 30.08
NE (pg/ml)	541.40 ± 5.97	532.86 ± 13.41	501.83 ± 10.87	502.49 ± 11.95

*Values are expressed as the means ± SEM. n = 7–8. Student's t-test. *P < 0.05, **P < 0.01 compared with the corresponding Flox group. TC, total cholesterol; NEFA, nonesterified fatty acid; HDL-C, high-density lipoprotein cholesterol; LDL-C, low-density lipoprotein cholesterol; TG, triglycerides; NE, norepinephrine.*

the AKO mice fed the chow diet (Supplementary Figure 4A). The plasma levels of catecholamines, including epinephrine and norepinephrine, and irisin were unaltered between genotypes (**Table 1**), which excludes the effects of circulating hormones on energy metabolism of AKO mice. Overall, these data signify that the impaired energy expenditure due to adipocyte AMPKα ablation results in obesity and that adipocyte AMPK is important for the regulation of whole-body energy homeostasis.

Lack of Adipocyte AMPKα Promoted the Development of Liver Steatosis and Fibrosis

As it was previously shown that deletion of adipocyte AMPK β1/β2 subunits induces hepatic lipid accumulation and liver insulin resistance (Mottillo et al., 2016), we then examined the effect of loss of adipocyte AMPKα on hepatic metabolism in our genotypes. H&E staining showed that hepatocytes in AKO mice displayed more lipid accumulation with enlarged lipid droplets (**Figures 5A,B**), additionally evidenced by the increased liver content of TG and TC in HFD-fed AKO mice (**Figures 5D,E**). Sirus Red staining indicated that liver fibrosis area was augmented in AKO mice fed with a chow diet or HFD (**Figures 5A,C**) and liver hydroxyproline (main component of collagen) level was significantly increased in HFD-fed AKO mice (**Figure 5F**), suggesting appearance of severe fibrosis in the liver of HFD-fed AKO mice. In addition, the expression levels of lipogenesis-related genes, such as glucose kinase (*Gck*), malic enzyme (*Me1*), fatty acid synthase (*Fasn*) and acetyl-CoA carboxylase 1 (*Acc1*), and fibrosis-related genes including smooth muscle actin alpha 2 (Acta2, encoding α smooth muscle actin), collagen type I alpha 1 chain (Col1a1), connective tissue growth factor (*Ctgf*), matrix metallopeptidase 2 (*Mmp2*) and tissue inhibitor of metalloproteinases 1 (*Timp1*) were up-regulated in AKO mice especially fed with a HFD (**Figures 5G,H**). Despite unchanged relative weight of liver between genotypes (**Figure 2D**), the absolute liver weight was obviously increased in HFD-fed AKO mice (**Figure 5I**). We further explored the status of insulin resistance in the liver of HFD-fed floxed and AKO mice by detecting the endogenous activity of insulin signaling. The phosphorylation levels of insulin receptor (IR) tyrosine-1162 (IR^{Y1162}) and serine/threonine kinase (AKT) serine-473 (AKT^{S473}) were dramatically repressed in HFD-fed AKO mice (**Figures 5J–L**), indicating impairment in insulin sensitivity in the liver after adipocyte AMPKα deletion. Moreover, the plasma levels of alanine aminotransferase (ALT) and aspartate transaminase (AST) were significantly increased in HFD-fed AKO mice (**Figures 5M,N**), verifying that hepatic lipotoxicity trended to be more severe in AKO mice. Taken together, these results demonstrated that adipocyte AMPKα ablation induced hepatic lipid accumulation and eventually exacerbated the development of liver steatosis and even fibrosis.

Chronic Treatment with the AMPK Activator A-769662 Alleviated HFD-Induced Obesity, Glucose, and Lipid Metabolic Disorders

AMPK activity has been reported to be reduced in both the BAT and WAT of obese animal models (Ruderman et al., 2010). Consistent with these reports, we also demonstrated that mice with adipocyte AMPKα ablation were predisposed to HFD-induced obesity. To assess the anti-obesity efficacy of chronic AMPK activation *in vivo*, we investigated the effect of the administration of A-769662, an AMPK allosteric activator, in chow- and HFD-fed mice. A-769662 (30 mg/kg/day) was administered q.d. for 6 weeks. During treatment, A-769662 did not affect food intake in either chow-fed or HFD-fed mice (**Figure 6B**). In chow-fed mice, body weight gain was generally unchanged by A-769662 treatment. Meanwhile, in HFD-fed mice, body weight gain was significantly decreased (by 49%) during the 6 weeks of A-769662 treatment (**Figure 6A**). A-769662 did not alter WAT or liver weight in chow-fed mice, but in HFD-fed mice, the weight of the liver, iWAT and pWAT was reduced by 15, 23, and 13%, respectively, but the eWAT

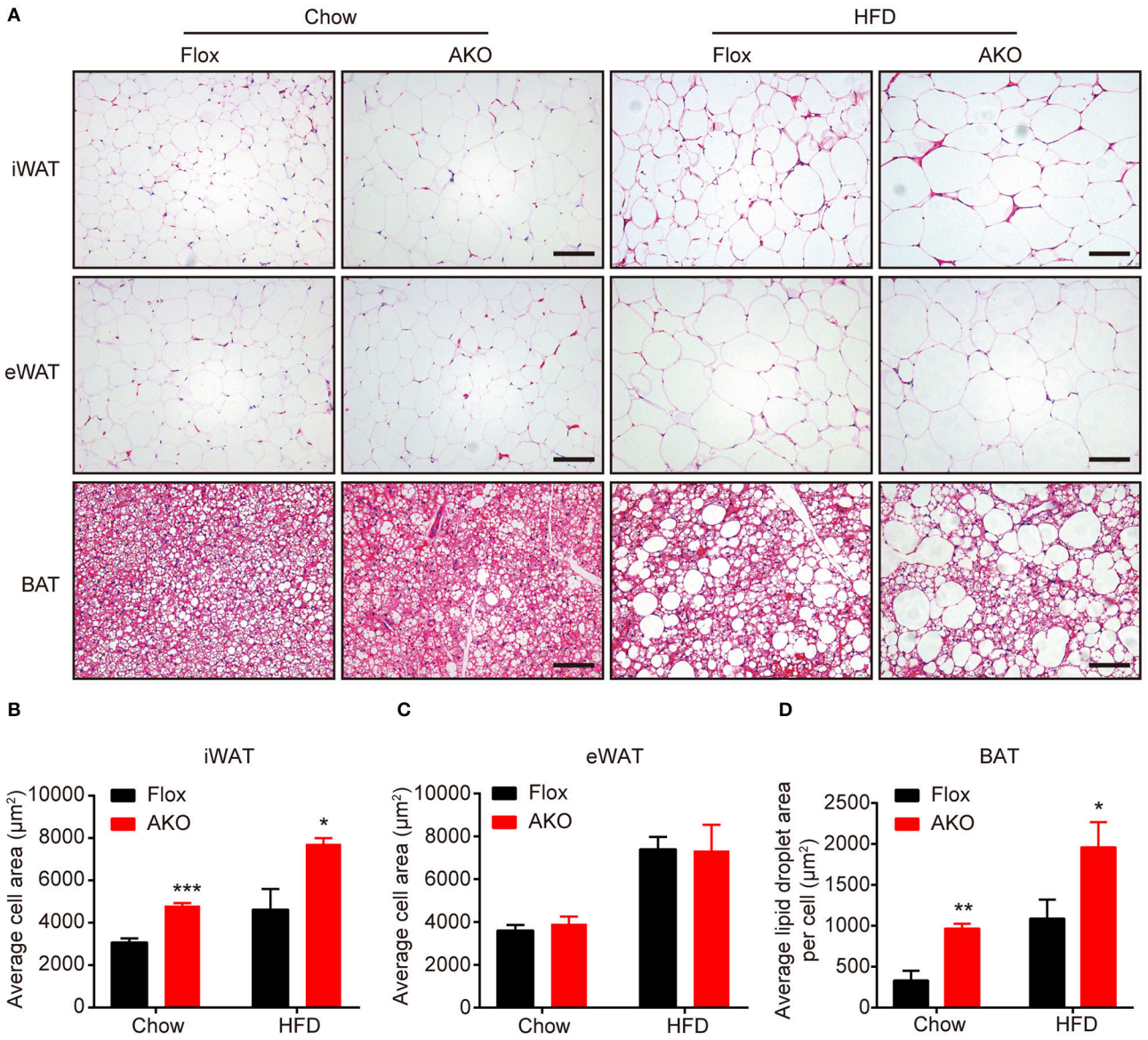

FIGURE 3 | Lack of adipocyte AMPKα increased adipocyte size in inguinal white adipose tissue. **(A)** Representative H&E stained images of iWAT, eWAT, and BAT in AKO mice and age-matched floxed littermates fed a chow diet (left) or a HFD (right). Scale bar = 100 μm. **(B–D)** Average adipocyte area in iWAT **(B)** and eWAT **(C)** and average lipid droplet area in the BAT **(D)** in AKO mice and floxed littermates fed a chow diet or a HFD. Data are presented as the means ± SEM. $n = 5$-7. Student's *t*-test. $^{*}P < 0.05$, $^{**}P < 0.01$, $^{***}P < 0.001$ compared with the corresponding Flox group.

weight was unchanged (**Figure 6C**). Accordingly, the content of TG and TC in liver were significantly decreased by A-769662 treatment in HFD-fed mice (**Figures 6D,E**). The fasting blood glucose level was not affected by A-769662 treatment in chow-fed mice or HFD-fed mice (**Figure 6F**). Nevertheless, A-769662 improved glucose tolerance in HFD-fed mice, as evidenced by the approximately 12% decrease in the AUC (**Figures 6G,H**), while had no effect on chow-fed mice. Insulin tolerance test showed that A-769662 treatment did not improve insulin sensitivity in HFD-fed mice (**Figures 6I,J**). In chow-fed mice, the plasma parameters were not significantly changed by A-769662 treatment (**Table 2**). However, in HFD-fed mice, the plasma levels of TG, TC and low-density lipoprotein cholesterol (LDL-C) were decreased by 27, 36, and 27% (**Table 2**), respectively. In addition, the insulin and leptin levels were also decreased by 41 and 56% (**Table 2**), respectively. Together, these results revealed that A-769662 had anti-obesity and anti-hyperlipidemic effects, and this agonist improved glucose tolerance in HFD-fed mice but not in chow-fed mice, indicating that chronic AMPK activation might be specifically effective in the obese mouse model and have negligible adverse effects in normal lean mice.

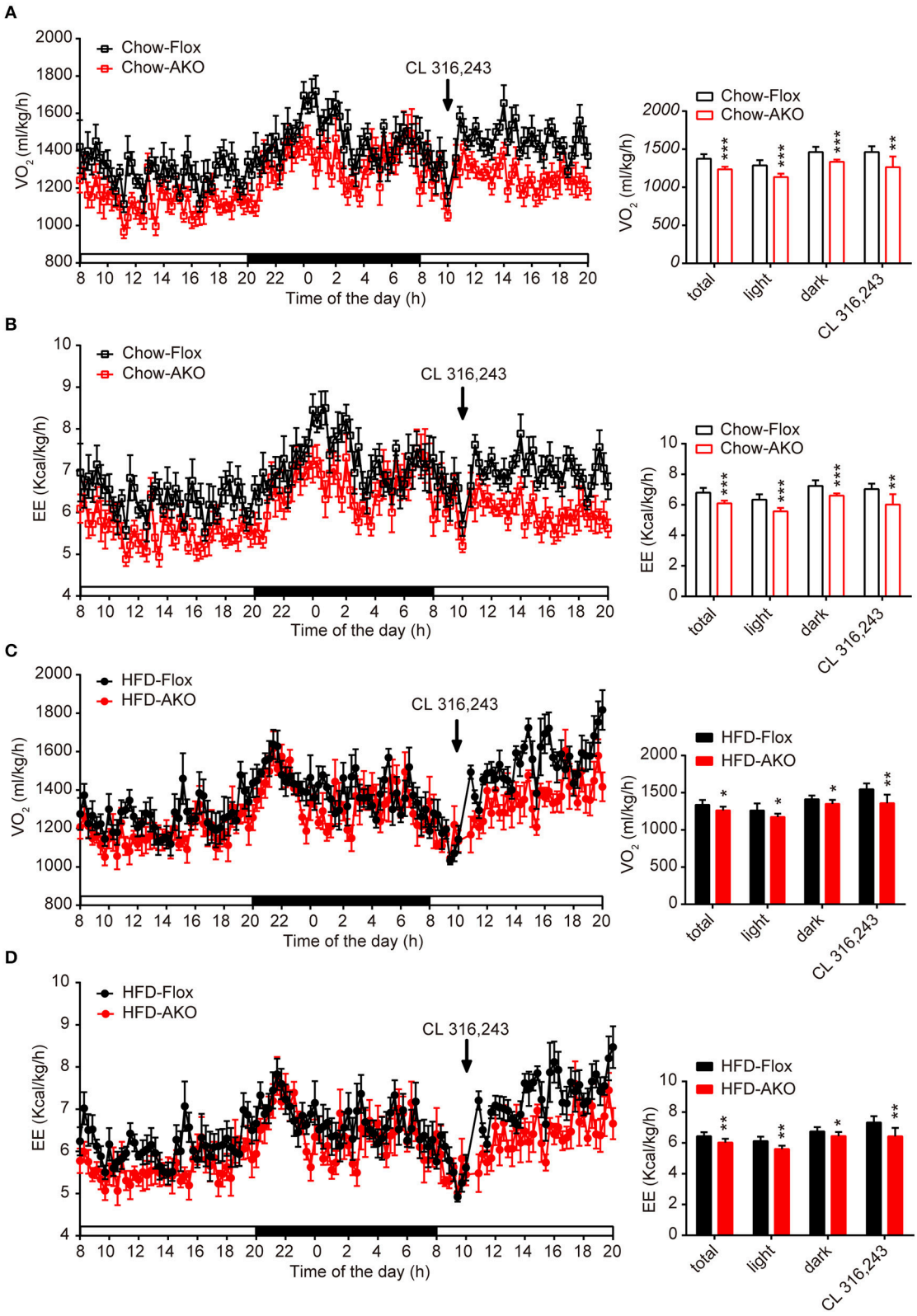

FIGURE 4 | Deletion of adipocyte AMPKα reduced basal and β3-adrenergic-activated energy expenditure in chow- and HFD-fed mice. **(A–D)** Metabolic cage analyses of 40-week-old AKO and floxed mice fed a chow or a HFD were performed. **(A)** The O_2 consumption of chow-fed mice during a 12-h light-dark cycle and

(Continued)

FIGURE 4 | after an injection of CL 312,643 (1 mg/kg) (left). Average basal and CL 312,643-stimulated O_2 consumption of chow-fed mice (right). **(B)** The energy expenditure (EE) of chow-fed mice during a 12-h light-dark cycle and after an injection of CL 312,643 (1 mg/kg) (left). Average basal and CL 312,643-stimulated EE of chow-fed mice (right). **(C)** The O_2 consumption of HFD-fed mice during a 12-h light-dark cycle and after an injection of CL 312,643 (1 mg/kg) (left). Average basal and CL 312,643-stimulated VO_2 consumption of HFD-fed mice (right). **(D)**The EE of HFD-fed mice during a 12-h light-dark cycle and after an injection of CL 312,643 (1 mg/kg) (left). Average basal and CL 312,643-stimulated EE of HFD-fed mice (right). Data are presented as the means ± SEM. $n = 8$. Student's *t*-test. $^*P < 0.05$, $^{**}P < 0.01$, $^{***}P < 0.001$ compared with the corresponding Flox group.

A-769662 Promoted Energy Expenditure in HFD-Fed Mice

After observing the anti-obesity effects of A-769662 on HFD-fed mice, we further investigated the effect of A-769662 treatment on whole-body energy expenditure of HFD-fed mice at 4th week of treatment by using indirect calorimetry. The last administration was given 4 h before the experiment. The animals were monitored for O_2 consumption, EE and locomotor activity for 24 h. A-769662 increased the total and dark-phase O_2 consumption and EE in HFD-fed mice (**Figures 7A,B**), but did not induce any significant changes in RER or locomotor activity (Supplementary Figures 5A,B). Additionally, A-769662-treated group exhibited a higher body temperature during the 120–200 min after cold exposure at 4°C (**Figure 7C**), suggesting that A-769662 protected against hypothermia via enhanced adaptive thermogenesis. Meanwhile, the O_2 consumption and EE of chow-fed mice were unchanged by A-769662 treatment (data not shown). These results suggest that the anti-obesity effects of A-769662 on HFD-fed mice might be due to increased energy expenditure.

A-769662 Induced Browning Signature in the iWAT of HFD-Fed Mice

Brown and beige fat specialize in energy expenditure through thermogenesis (Harms and Seale, 2013). Since we observed an increase in EE and resistance to cold exposure following A-769662 treatment in HFD-fed mice, we further investigated the cellular and molecular mechanism of A-769662-induced thermogenesis *in vivo*. The weight (**Figure 6C**) and histological morphology (**Figures 8A,D**) of BAT and the expression of thermogenesis-related genes in the BAT (Supplementary Figure 6A) were all unchanged by A-769662 treatment. In accordance with the reduced iWAT weight induced by A-769662 treatment, the adipocyte area in iWAT was reduced by approximately 57% (**Figures 8A,B**). And mitochondria content in iWAT, but not in eWAT or BAT, was elevated by A-769662 treatment (**Figure 8E**), suggesting that AMPK activation enhanced mitochondrial biogenesis in iWAT. Moreover, the mRNA levels of the BAT-specific marker *Ucp1* and other thermogenesis-related genes, including *Cidea*, *Cox8b*, *Cox7a1,* and *Ppargc1a*, in iWAT were significantly up-regulated by A-769662 treatment, and most of the brown-selective markers, such as *Oplah*, *Fbxo31*, *Acot2*, *Hspb7,* and *Slc29a1* (Wu et al., 2012), were also increased (**Figure 8F**), indicating a genetic conversion of iWAT into beige adipose induced by A-769662. We also detected the expression of the general adipogenic marker *aP2*, and it was unaffected by treatment (**Figure 8F**), implying that A-769662 may have no impact on the differentiation of inguinal adipocytes. However, the adipocyte area and expression of thermogenesis-related genes in the eWAT were unaltered (**Figures 8A,C**, Supplementary Figure 6B). After observing an increase in the expression of thermogenic genes in iWAT, we further investigated the expression levels of thermogenic proteins. We found that the protein levels of UCP-1 and PGC-1α were markedly increased in iWAT (**Figures 8G,H**). Simultaneously, AMPK signaling in iWAT was activated by A-769662 treatment, as evidenced by the increased phosphorylation of AMPKα and its downstream substrate ACC (**Figures 8G,H**), which suggests that chronic AMPK activation by A-769662 induced iWAT browning in diet-induced obese mice. Taken together, these results indicate that A-769662 specifically promote browning in the iWAT of HFD-fed mice.

A-769662 Facilitated Thermogenesis *in Vitro* through AMPK Signaling Pathway

To explore the effect of A-769662-induced AMPK activation on differentiated adipocytes in a cell-autonomous manner, SVF cells from iWAT were induced to differentiate into beige adipocytes and were treated with DMSO or A-769662 at the indicated concentration on day 7. The expression of thermogenesis-related genes, such as *Ucp1*, *Cidea*, *Cox8b*, *Cox7a1,* and *Ppargc1a*, was significantly increased by A-769662 treatment in a concentration-dependent manner (**Figure 9A**). Importantly, similar to the *in vivo* results, the expression of thermogenic protein UCP1 and of PGC-1α was also remarkably increased in differentiated iWAT-SVF cells, which was concomitant with the activation of AMPK signaling by A-769662 treatment (**Figures 9B,C**). In addition, the basal and uncoupled O_2 consumption rates (OCRs) were both up-regulated by A-769662 treatment in differentiated iWAT-SVF cells (**Figure 9D**). To confirm whether the effect of A-769662 on promoting thermogenesis was dependent on AMPK activation, primary SVF cells isolated from iWAT of the floxed mice were induced to differentiate into beige adipocytes, followed by adding Cre lentivirus at day 6 of differentiation to knockdown AMPKα expression, and were then treated with A-769662 at indicated concentration on day 8. As a result, the expression of genes encoding AMPKα1 and AMPKα2 (*Prkaa1* and *Prkaa2*, respectively) and total AMPKα in iWAT-SVF cells were significantly reduced and the activation of AMPK signaling by A-769662 was successfully blocked after Cre lentivirus infection (**Figures 9E–G**). Importantly, A-769662 treatment up-regulated the expression of thermogenesis marker *Ucp1* and *Ppargc1a* and their encoding products, which were remarkably blunted after AMPKα knockdown (**Figures 9E–G**), suggesting that AMPK activation was required for A-769662-facilitated thermogenesis. These data indicate that A-769662 promotes

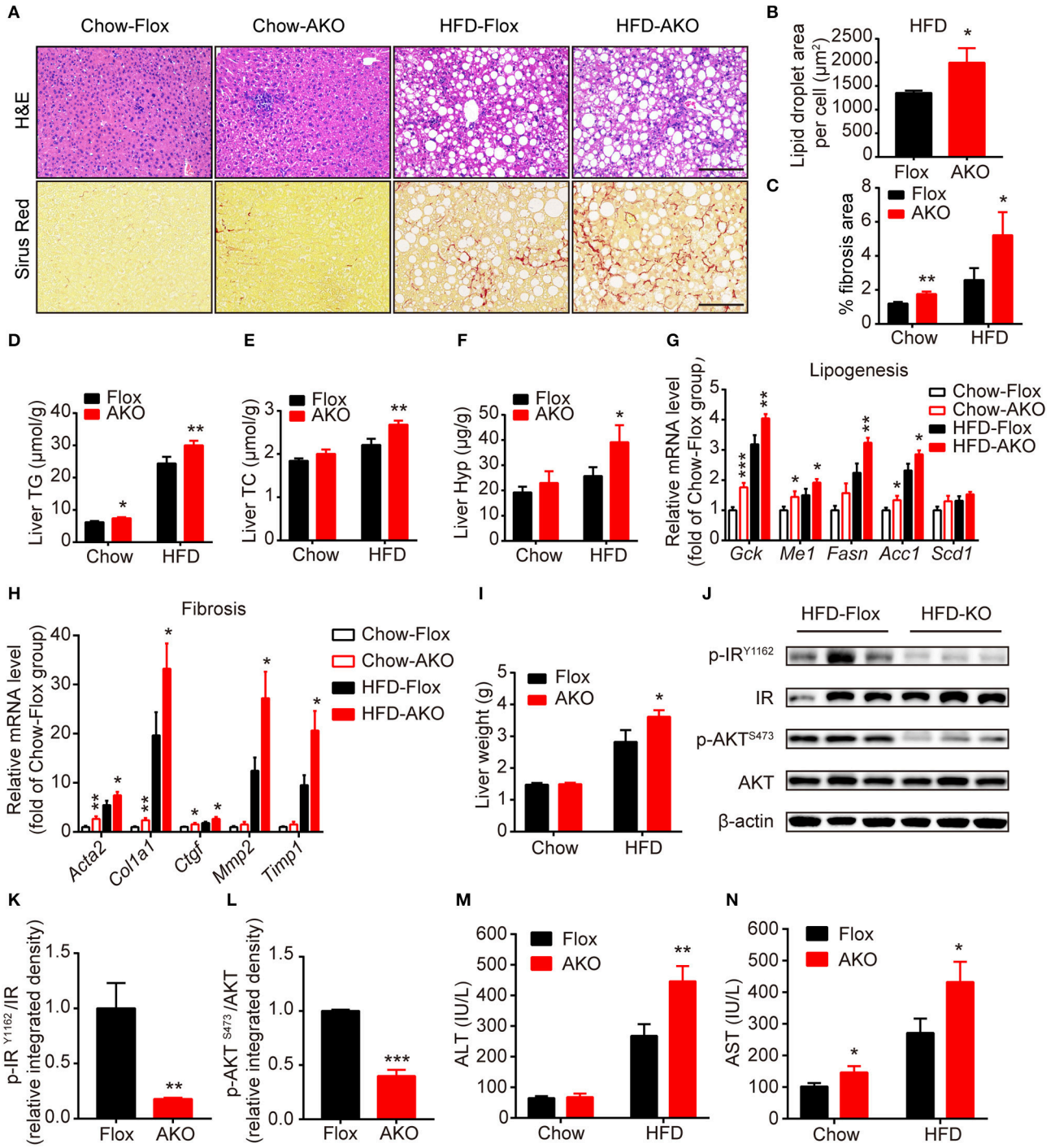

FIGURE 5 | Adipocyte AMPK deficiency promoted the development of liver steatosis and fibrosis. **(A)** Representative H&E stained (top) and Sirius red stained (bottom) images of liver in AKO mice and age-matched floxed littermates fed with a chow diet (left) or a HFD (right). Scale bar = 100 μm. **(B)** Average lipid droplet area per cell in liver in AKO mice and floxed littermates fed with a chow diet or a HFD. **(C)** Fibrosis area in liver were evaluated in chow- or HFD-fed AKO mice and floxed littermates. **(D,E)** Liver TG **(D)** and TC (**E**) levels in chow- or HFD-fed AKO mice and floxed littermates. **(F)** Liver hydroxyproline level in chow- or HFD-fed AKO mice and floxed littermates. **(G,H)** The relative mRNA levels of lipogenesis genes **(G)** and fibrosis-related genes **(H)** in the liver of in chow- or HFD-fed AKO mice and floxed littermates were analyzed by quantitative RT-PCR (normalized to *Actb*). $n = 8$–9. **(I)** Absolute liver weight in chow- or HFD-fed AKO mice and floxed littermates. **(J)** The expression levels of AKT, p-AKT (S473), IR, p-IR (Y1162) in the liver of HFD-fed AKO mice and floxed littermates were determined by western blot analysis. (**K,L**) Relative phosphorylation levels of AKT and IR were determined by densitometric quantification of the immunoblots shown in **(J)**. $n = 3$. **(M,N)** Plasma ALT and AST levels in chow- or HFD-fed AKO mice and floxed littermates. Data are presented as the means ± SEM. Student's *t*-test. $^{*}P < 0.05$, $^{**}P < 0.01$, $^{***}P < 0.001$ compared with the corresponding Flox group.

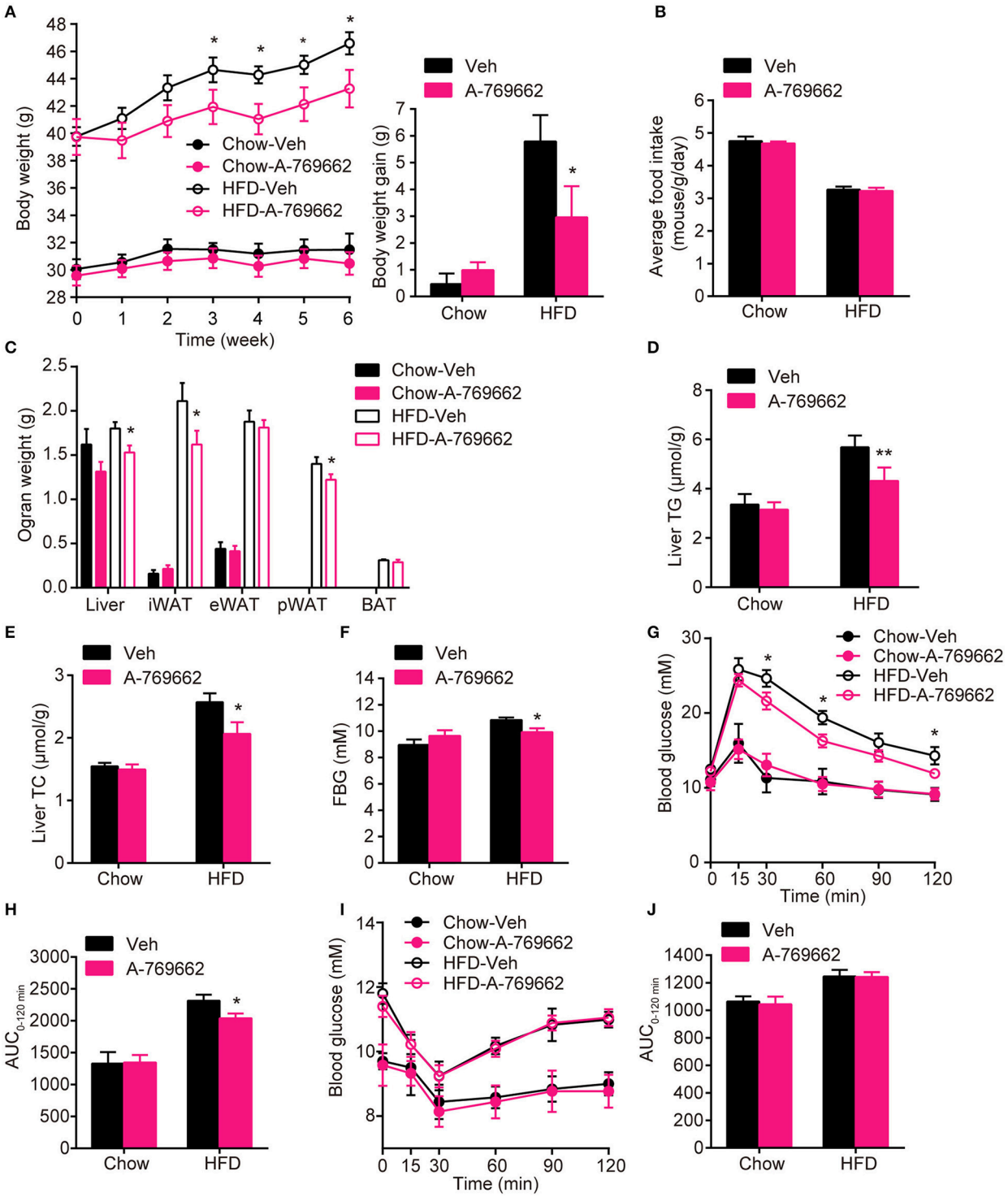

FIGURE 6 | Chronic AMPK activation by A-769662 protected against HFD-induced obesity and dysregulated glucose metabolism **(A)** Body weight (left) and average body weight gain (right) of chow- and HFD-fed mice during the 6-week treatment period. **(B)** Average food intake of chow- and HFD-fed mice during the 6-week treatment period. **(C)** Absolute weights of the liver, iWAT, eWAT, pWAT and BAT of chow- and HFD-fed mice after 6-week treatment. **(D,E)** Liver TG **(D)** and TC (**E**) levels of chow- and HFD-fed mice after 6-week treatment. **(F)** Fasting blood glucose was measured during the 4th week of treatment. **(G,H)** Intraperitoneal glucose tolerance tests of chow- and HFD-fed mice were conducted at week 4 of treatment **(G)**. The AUC from 0 to 120 min was calculated **(H)**. (**I,J**) Insulin tolerance test of chow- and HFD-fed mice were conducted at week 5 of treatment **(I)**. The AUC from 0 to 120 min was calculated **(J)**. Chow-Veh: mice fed a chow diet and treated with vehicle, Chow-A-769662: mice fed a chow diet and treated with A-769662, HFD-Veh: mice fed a HFD and treated with vehicle, HFD-A-769662: mice fed a HFD and treated with A-769662. Data are presented as the means ± SEM. $n = 5$–9. Student's t-test. $^{*}P < 0.05$, $^{**}P < 0.01$ compared with the indicated control group.

TABLE 2 | Chronic effects of A-769662 on plasma metabolic variables in chow-fed mice and HFD-fed mice.

Parameters	Chow-Veh	Chow-A-769662	HFD-Veh	HFD-A-769662
TC (mM)	3.58 ± 0.37	3.64 ± 0.47	8.04 ± 0.52	5.12 ± 0.56***
LDL-C (mM)	0.66 ± 0.08	0.57 ± 0.03	1.66 ± 0.11	1.21 ± 0.16*
HDL-C (mM)	0.44 ± 0.04	0.45 ± 0.07	0.58 ± 0.04	0.54 ± 0.07
LDL-C/HDL-C	1.47 ± 0.08	1.29 ± 0.24	3.09 ± 0.37	2.70 ± 0.45
TG (mM)	0.50 ± 0.04	0.53 ± 0.06	0.46 ± 0.02	0.34 ± 0.03**
NEFA (mEq/L)	0.62 ± 0.06	0.64 ± 0.09	0.52 ± 0.05	0.45 ± 0.03
Insulin (ng/ml)	1.51 ± 0.13	1.67 ± 0.04	4.64 ± 0.79	2.74 ± 0.32*
Leptin (ng/ml)	1.99 ± 0.56	2.10 ± 0.33	68.42 ± 7.07	30.31 ± 5.05***
Irisin (ng/ml)	108.85 ± 6.21	102.52 ± 4.06	109.04 ± 3.28	106.59 ± 4.40

*Values are expressed as the means ± SEM. n = 6–10. Student's t-test. *p < 0.05, **p < 0.01, ***p < 0.001 compared with the corresponding vehicle group.*

thermogenesis *in vitro* via AMPK signaling pathway, which may contribute to A-769662-induced browning in iWAT *in vivo*.

DISCUSSION

Since obesity has become a global health problem and efforts to reduce energy intake show either limited effectiveness or unacceptable side effects (James et al., 2010), therapeutic strategies aimed at increasing EE are an attractive approach for combatting obesity (Tam et al., 2012). Approaches attempting to enhance the thermogenic activity of brown and beige fat may be beneficial for obesity therapy because the activity of brown and beige fat have been shown to be inversely correlated with BMI and fat mass and positively related to EE in humans (Saito et al., 2009; van Marken Lichtenbelt et al., 2009). Reduced adipose tissue AMPK activity is generally observed in many obese and diabetic animal models as well as in obese humans with insulin resistance (Yu et al., 2004; Ruderman et al., 2010; Gauthier et al., 2011; Xu et al., 2012). The physiological relevance of lowered AMPK activity in adipose tissue to whole-body adiposity remains ambiguous. Here, we found that ablation of adipocyte AMPKα impaired adaptive thermogenesis and EE in response to cold exposure or β3-adrenergic stimulation, and predisposed HFD-fed mice to obesity, glucose intolerance and insulin resistance. Importantly, the lack of adipocyte AMPKα selectively blunted cold-induced thermogenic protein expression in iWAT, resulting in reduced energy utilization and increased adipocyte size, indicating that adipocyte AMPKα is required for browning in iWAT. In contrast, A-769662-induced direct AMPK activation promoted browning in iWAT, which may contribute to the reduced adiposity and improved glucose and lipid metabolism observed in A-769662-treated HFD-fed mice. In summary, these findings indicate that reduced AMPK activity in adipose tissue might be an important pathogenic factor in obesity and the related metabolic syndrome, and the chronic activation of AMPK by A-769662 protects from HFD-induced adiposity and metabolic dysfunction.

Since both catalytic subunits AMPK α1 and α2 exist in adipose tissue and the deletion of a single subunit often leads to the up-regulated activity of the other subunit (Bauwens et al., 2011), we generated AKO mice by crossing Adiponectin-Cre mice with AMPK α1/α2-foxed mice in order to investigate the metabolic role of adipocyte AMPKα. The Adiponectin-driven Cre recombinase is supposed to be expressed at the beginning during the early stage of BAT development (Cohen et al., 2014). When fed a chow diet, AKO mice started to gain more weight than age-matched floxed littermates at 29 weeks of age, however, when fed a HFD, this difference occurred, at 25 weeks of age, indicating that the loss of adipocyte AMPKα accelerates the development of obesity in response to a HFD. These phenotypes were analogous to the inducible mouse model with adipocyte AMPK β1/β2 deletion (iβ1β2AKO) after 8 weeks of age previously reported by Mottillo et al. (2016). The iβ1β2AKO mice had defects not only in the browning of WAT but also in BAT-mediated thermogenesis due to impaired mitochondrial integrity and function but not mitochondrial biogenesis. Intriguingly, we observed that there were not only defects in mitochondrial structure but also reduced total number of mitochondria in iWAT and BAT of AKO mice. However, the thermogenic capacity of BAT from the AKO mice in our study was normal compared with that of the floxed mice, suggesting that AMPK might play different roles in BAT function at different ages and that the unaffected thermogenesis of BAT in AKO mice might be remedied through an unknown mechanism. In addition, both hepatic steatosis and fibrosis were developed in HFD-fed AKO mice, which is more severe than that in iβ1β2AKO mice. This may be attributed to AMPK deletion at earlier stage and longer period of HFD challenge in AKO mice compared to that of iβ1β2AKO mice (Mottillo et al., 2016). It is well-established that adipose tissue-liver crosstalk plays a vital role in regulating systemic glucose and lipid metabolism (Stern et al., 2016). Adiponectin ameliorates liver ectopic lipid accumulation by inhibiting hepatic lipogenesis and enhancing β-oxidation. The plasma level of adiponectin was reduced in chow- and HFD-fed AKO mice, which may intensify the development of hepatic steatosis and even fibrosis. Accumulative evidence have shown that leptin plays a crucial role in the development of liver fibrosis (Marra, 2002). The plasma level of leptin increased along with increased fat mass in AKO mice, which partially explains the aggravating progression of liver fibrosis in AKO mice. Besides, another study reported by Sun-Joong *et al.* showed that adipose tissue-specific AMPK α1/α2 KO mice using Adiponectin-Cre or aP2-Cre model displayed a lean phenotype due to enhanced lipolysis in adipose tissue (Kim et al., 2016). The Adiponectin-Cre model is known to have better efficiency and specificity for adipocytes than the aP2-Cre model (Jeffery et al., 2014), so Adiponectin-Cre model is more suitable for the study of adipose tissue. After comparing the phenotypes of the adiponectin-driven AMPK α1/α2 KO mice used in our study and that by Sun-Joong et al., several difference were found. The adiponectin-driven AMPK α1/α2 KO mice in their study started to gain less body weight and fat mass at 10 weeks of age, while the body weights of our mice showed no significant change between genotypes, and the fat mass was not determined at that time point (**Figure 2A**). In addition, the body weight change in adiponectin-driven AMPK α1/α2 KO mice after 12 weeks of age was not shown,

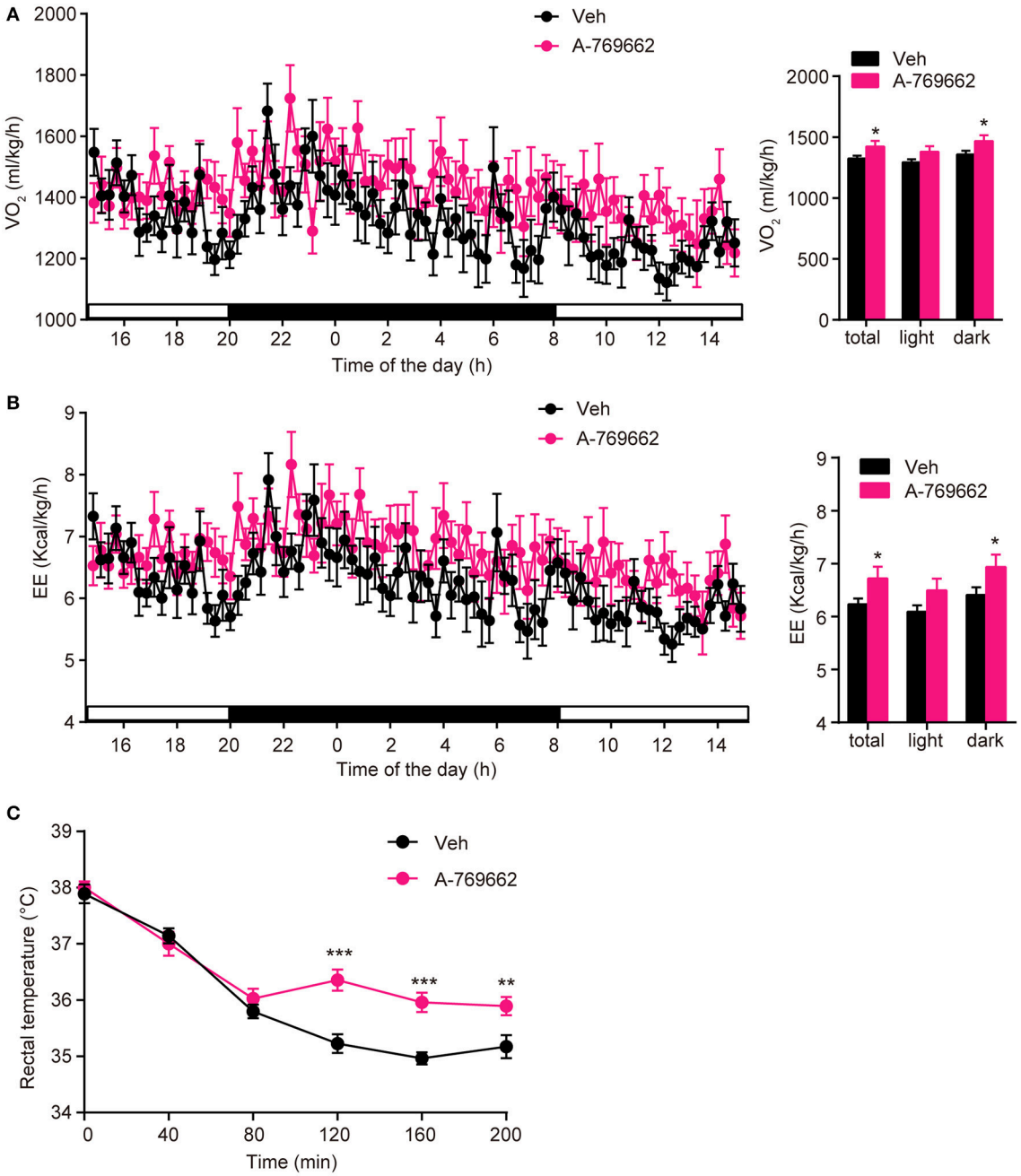

FIGURE 7 | A-769662 promoted energy expenditure and cold tolerance in HFD-fed mice. **(A,B)** During the 4th week of chronic administration, indirect calorimetry was used to investigate the energy metabolism of HFD-fed mice. Mice were dosed with vehicle or A-769662 (30 mg/kg) and then acclimated to the chamber for 12 h. Change of O_2 consumption (**A** left), EE (**B** left) during the indicated periods and average O_2 consumption (**A** right), EE (**B** right) during the whole period of measurement were assessed. $n = 8$. **(C)** Change in body temperature of HFD-fed mice after cold exposure at 4°C. $n = 11$–12. Data are presented as the means ± SEM. Student's *t*-test. $^*P < 0.05$, $^{**}P < 0.01$, and $^{***}P < 0.001$ compared with the indicated control group.

and the long-term effects of adipocyte AMPK deletion on whole-body metabolism remained unknown in their study. However, despite unaltered body weight, defective adaptive thermogenesis and cold tolerance were observed in the AKO mice in our study at 8 weeks of age, which may lead to reduced EE and accumulated adiposity during aging and in response to the HFD challenge. One possible reason for the differences in the phenotypes of their study and ours might be that the mice used in the experiments were at different ages.

AMPK signaling is indirectly activated by catecholamine secretion in response to cold or β-adrenergic stimulation (Gauthier et al., 2008). We also showed that the sensitivity of

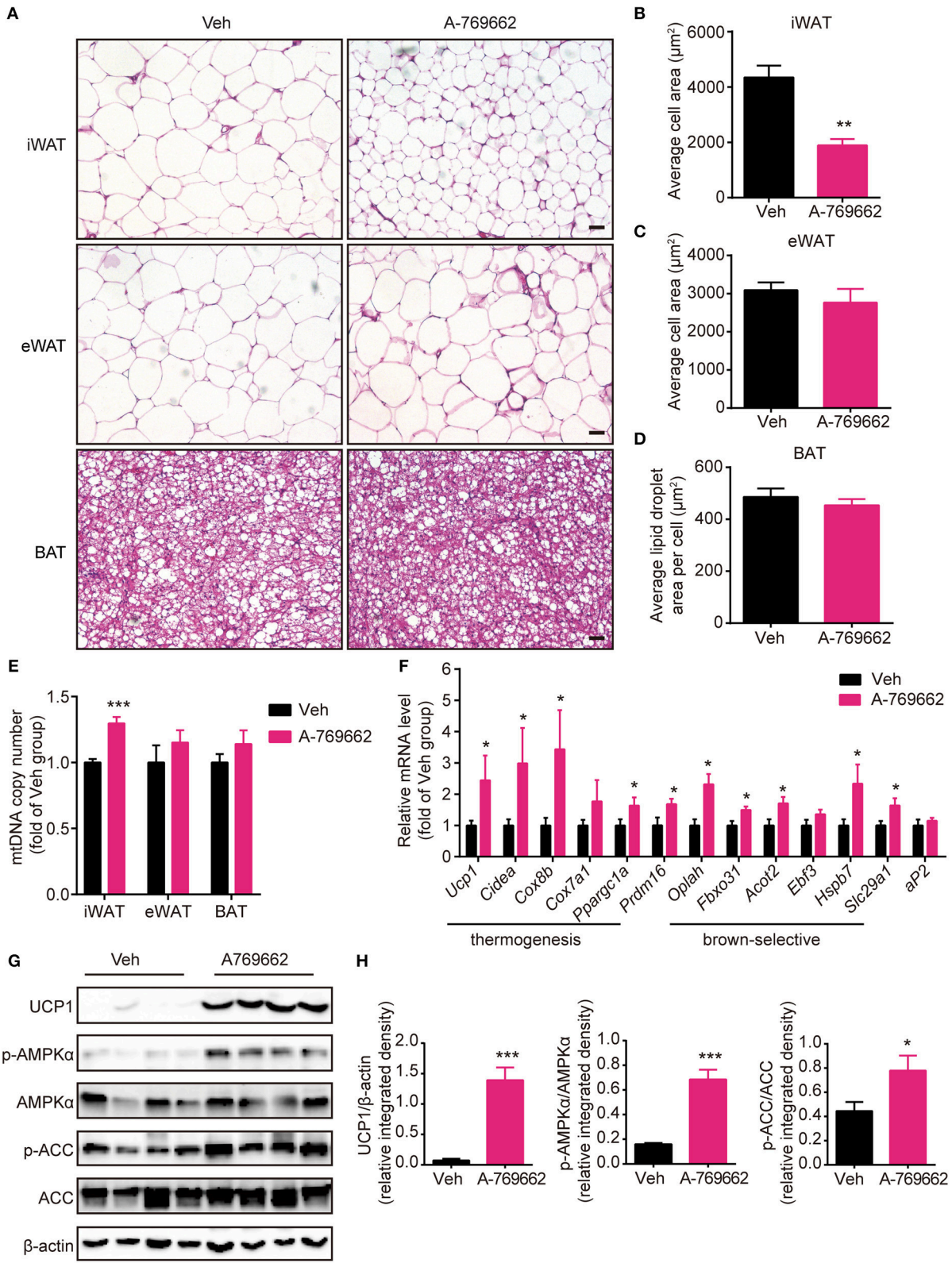

FIGURE 8 | A-769662 induced browning in the inguinal WAT of HFD-fed mice. **(A)** Representative H&E-stained images of the iWAT, eWAT and BAT of HFD-fed mice. Scale bar = 100 μm. **(B–D)** Average adipocyte area in the iWAT **(B)** and eWAT **(C)** and average lipid droplet area in the BAT **(D)** of HFD-fed mice. $n = 4$–6. **(E)**

(Continued)

FIGURE 8 | Mitochondrial DNA copy number of iWAT, eWAT, and BAT in HFD-fed mice. **(F)** Relative mRNA levels of thermogenic genes and brown-selective genes in the iWAT of HFD-fed mice after 6 weeks of treatment. $n = 6$–8. **(G)** Western blot analysis of UCP1, AMPKα, p-AMPKα (T172), ACC, and p-ACC (S79) expression levels in the iWAT of HFD-fed mice after 6 weeks of treatment. β-actin was used as a loading control. **(H)** Relative protein expression level of UCP1 and the relative phosphorylation levels of AMPKα and ACC were determined by densitometric quantification of the immunoblots shown in **(G)**. $n = 4$. Data are presented as the means ± SEM. Student's *t*-test. $^{*}P < 0.05$, $^{**}P < 0.01$, $^{***}P < 0.001$ compared with the indicated control group.

AMPK activation and UCP1 expression in different fat depots were diverse, with iWAT being the most responsive to cold exposure, and eWAT and BAT being less responsive to the cold stimulation (**Figure 1A** and Supplementary Figure 1A). Ablation of adipocyte AMPKα specially impaired mitochondria quality control and biogenesis in iWAT and BAT but not in eWAT (**Figures 1J–M** and Supplementary Figure 1M). Accordingly, the adipocyte size in the iWAT and BAT of AKO mice was increased while that in eWAT were unchanged (**Figures 3A–D**). Nonetheless, the expression of the thermogenesis-related protein was markedly reduced in iWAT but not in BAT of AKO mice. In addition, chronic AMPK activation by A-769662 treatment selectively promoted browning in the iWAT of HFD-fed mice but not in eWAT or BAT (**Figures 8A–H** and Supplementary Figures 6A,B). Our observations are in line with previous reports that eWAT is more "resistant" to browning than iWAT fat depots, while iWAT has greater plasticity and ability to modulate metabolic function upon stimulation, as evidenced by the up-regulation of brown-selective marker genes in response to cold or β-adrenergic stimulation (Bartelt and Heeren, 2014). Despite the unique structural and molecular characteristics of different fat depots that cause these depot-specific differences, our findings suggest that the high sensitivity of AMPK activation in iWAT may contribute to its plasticity in adaptation to various environmental and hormonal cues.

A previous study reported that the improvement in blood glucose level from A-769662 treatment was mainly due to targeting liver tissue, and A-769662 treatment reduced food intake in a 14-day study with *ob/ob* mice (Fullerton et al., 2013). In this study, we also observed that A-769662 ameliorated glucose and lipid disorders in HFD-fed mice (**Figure 6** and **Table 2**). However, in our model, food consumption was unchanged during the 6 weeks of study, ruling out the disturbance of energy intake differences in the anti-obesity effect of A-769662. Besides liver, WAT is another target tissue of A-769662, as evidenced by the tissue weight, morphology, related gene expression and UCP-1 protein level. Moreover, there was a considerable amount of A-769662 distribution in the adipose tissue of HFD-fed mice (Supplementary Figure 7), suggesting a direct effect of A-769662 on adipose tissue. In this study, we observed that A-769662 treatment augmented whole-body EE and enhanced adaptive thermogenesis in HFD-fed mice, and these effects were not driven by increased locomotor activity (**Figures 7A,B** and Supplementary Figure 5B). BAT activity plays a primary role in cold-induced adaptive thermogenesis and EE in rodents (Tam et al., 2012). However, in our study, the mRNA levels of thermogenesis-related genes were not up-regulated by A-769662 in the BAT (Supplementary Figure 6A). These results seem to rule out the possibility that BAT plays a predominant role in the A-769662-induced enhancement of EE and adaptive thermogenesis. Skeletal muscle, as a large organ and major site of facultative thermogenesis, also contributes to EE (Zurlo et al., 1990), but the gene expression of *Ppargc1a*, an AMPK downstream substrate and key regulator of mitochondrial biogenesis and oxidative phosphorylation (OXPHOS) (Arany, 2008), was not changed by A-769662 in the skeletal muscle of HFD-fed mice (Supplementary Figure 8). Meanwhile, the mRNA levels of *Ppargc1a* and other thermogenic genes, and the protein level of UCP1 were increased by A-769662 in iWAT; in contrast, the expression levels of cold-induced UCP1 and PGC-1α protein were remarkably reduced in iWAT with adipocyte AMPK deletion. Therefore, it is possible that the A-769662-induced improvement of metabolic disorders in obese mice is at least partly due to increased EE through the browning of iWAT.

There are also studies suggesting that long-term AICAR treatment promotes energy dissipation in chow-fed rat models (Gaidhu et al., 2009, 2011) and improves glucose homeostasis and insulin resistance in diabetic mouse models (Buhl et al., 2002; Song et al., 2002). AICAR treatment also had an inhibitory effect on food consumption in these chronic studies. In our study with long-term A-769662 treatment, the chow-fed mice exhibited no effect on food intake, EE or fat metabolism, which may be due to variations in species, treatment duration, dosage and injection frequency in different animal models. Actually, it was reported that no detectable distribution of A-769662 into the brain of *ob/ob* mice (1 h after a single injection at a dose of 30 mg/kg; Cool et al., 2006), which suggests that the absence of effect of A-769662 on food intake may be owing to no exposure of A-769662 into the brain. Although AICAR and A-769662 are both AMPK activators, they have different mechanisms. AICAR activates AMPK by being taken up into cells and converted into an AMP mimetic, ZMP (Hardie, 2011). Similar to AMP, A-769662 allosterically activates AMPK and inhibits the dephosphorylation of AMPK (Thr-172). However, AMPK activation by A-769662 is exclusively dependent on the existence of glycogen binding domain within the β1 subunit, but not the γ subunit to which AMP binding (Sanders et al., 2007). The absence of effect on chow-fed mice is also consistent with the study conducted by Cool et al. (2006). In our study, the pro-browning effect of A-769662 only existed in the HFD-fed mice, and this may be owing to differences in metabolism and energy status of HFD-fed and chow-fed mice. This result suggests that in mouse models, the anti-obesity effect of chronic AMPK activation is more sensitive and responsive in diet-induced obese mice.

Beige adipocytes have been reported to arise from two alternative processes: *de novo* differentiation from progenitor cells and trans-differentiation from white adipocytes (Bartelt and Heeren, 2014). In general, the differentiation of brown

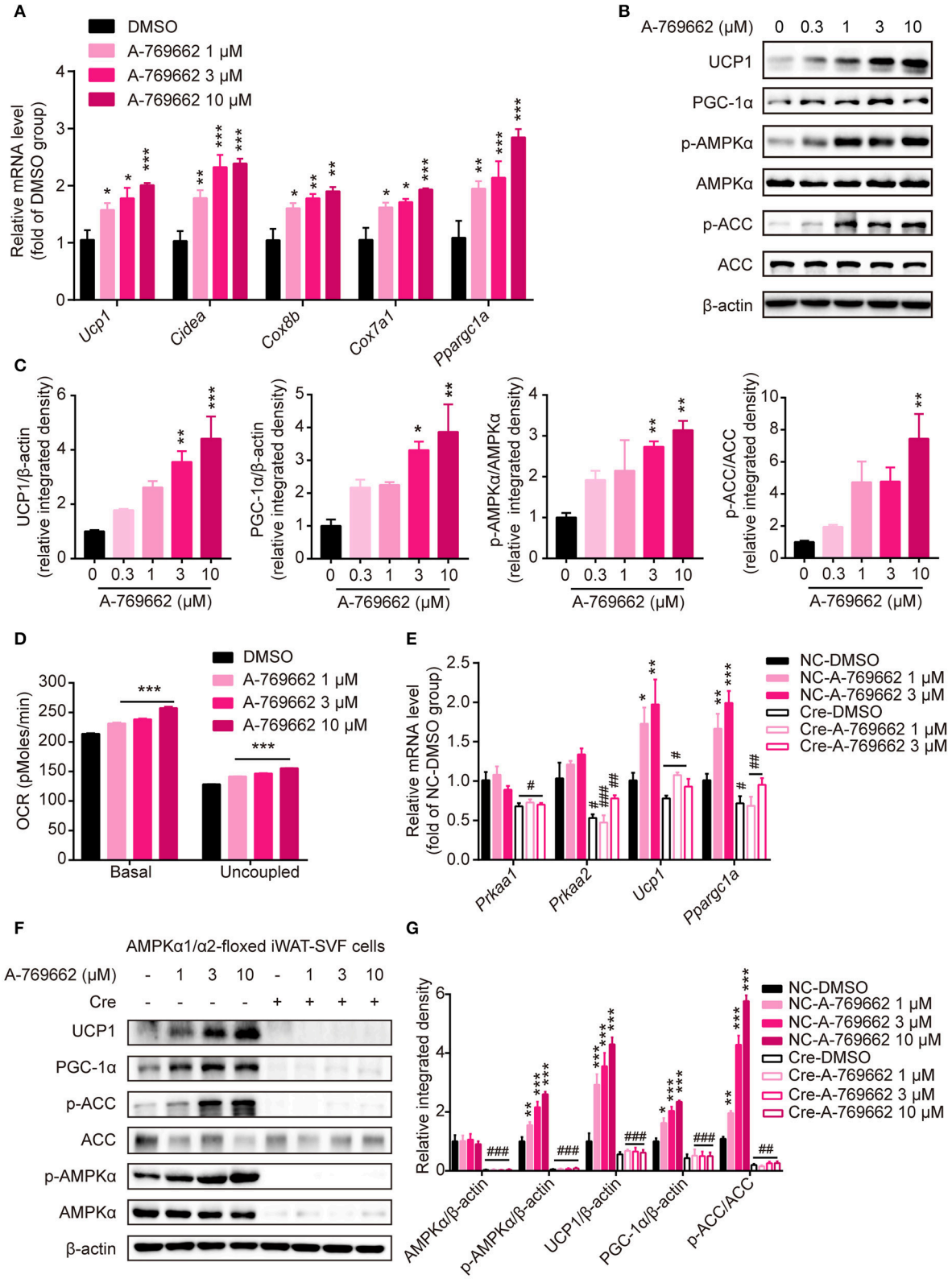

FIGURE 9 | A-769662 facilitated thermogenesis in differentiated iWAT-SVF cells through AMPK signaling pathway. **(A–D)** iWAT-SVF cells were induced to differentiation toward brown-like adipocytes and were treated with the indicated compounds on day 7. **(A)** Relative mRNA levels of thermogenic genes in differentiated

(Continued)

FIGURE 9 | iWAT-SVF cells treated with the indicated compounds for 6 h were analyzed by quantitative RT-PCR. $n = 4$. **(B)** Western blot analysis of UCP1, PGC-1α, p-AMPKα (T172), AMPKα, p-ACC (S79), and ACC expression levels in differentiated iWAT-SVF cells treated with indicated compounds on day 7 for 24 h. **(C)** Relative protein expression levels of UCP1 and PGC-1α and the relative phosphorylation levels of AMPKα and ACC were determined by densitometric quantification of the immunoblots shown in (**B**). n = 3. **(D)** Basal and uncoupled oxygen consumption rate (OCR) of differentiated iWAT-SVF cells treated with NE (10 μM) for 3 h or with DMSO or A-769662 at different concentrations on day 7 for 12 h. $n = 4$. **(E–G)** iWAT-SVF cells were isolated from iWAT of 5-week-old AMPK α1/α2-floxed mice and induced to differentiate toward beige adipocytes. Cells were infected with NC and Cre lentivirus on day 6 to knockdown AMPKα expression and were treated with the indicated compounds on day 8. **(E)** Relative mRNA levels of the indicated genes in differentiated iWAT-SVF cells treated with the indicated compounds for 6 h on day 8 were analyzed by quantitative RT-PCR. $n = 4$. **(F)** Western blot analysis of UCP1, PGC-1α, p-AMPKα (T172), AMPKα, p-ACC (S79), and ACC expression levels in differentiated iWAT-SVF cells treated with indicated compounds on day 8 for 24 h. **(G)** Relative protein expression levels of UCP1 and PGC-1α and the relative phosphorylation levels of AMPKα and ACC were determined by densitometric quantification of the immunoblots shown in **(F)**. $n = 3$. Data are presented as the means ± SEM. One-way ANOVA. $^{*}P < 0.05$, $^{**}P < 0.01$, $^{***}P < 0.001$ compared with the indicated DMSO group; $^{\#}P < 0.05$, $^{\#\#}P < 0.01$, $^{\#\#\#}P < 0.001$ compared with the indicated NC group.

adipocytes shares most of the transcriptional regulation pathways with beige adipocytes (Inagaki et al., 2016). Some studies have reported that AMPK plays a positive role in brown adipocyte differentiation and brown fat development in murine cell lines and animal models (Vila-Bedmar et al., 2010). AMPK activation by AICAR treatment in human adipose-derived mesenchymal stem cells (hADMSCs) from pericardial adipose tissue is reported to induce a morphological change similar to beige adipocytes, but without an actual change of metabolic function (Abdul-Rahman et al., 2016). The restricted effect of AICAR on inducing beige adipogenesis might due to the differences in species or original depots of cells and basal activity/expression level of AMPK or the intrinsic specificity of AICAR. However, the indirect activation of AMPK by berberine has been demonstrated to promote WAT browning by enhancing thermogenesis in mature beige adipocytes via the AMPK-PGC-1α pathway (Zhang et al., 2014). Similarly, direct AMPK activation by A-769662 did not induce the differentiation of iWAT-SVF cells toward beige adipocytes *in vitro* (data not shown) and had no effect on the expression of the adipogenic marker *aP2* in iWAT *in vivo* (**Figure 8F**). Alternatively, A-769662 enhanced thermogenesis in differentiated iWAT-SVF cells, as detected by the increased expression of thermogenic genes and proteins and the up-regulated O_2 consumption, which is directly reliant on the activation of AMPK signaling (**Figures 9A–G**). Moreover, we further determined the plasma level of irisin, which has been reported to stimulate the browning of WAT through specific actions on the beige preadipocyte population (Tseng et al., 2008); the plasma irisin level was not affected by A-769662 treatment (**Table 2**), and the *Fndc5* mRNA level in skeletal muscle was also influenced (Supplementary Figure 8). These results indicate that the browning of WAT in HFD-fed mice by A-769662 is not due to the direct modulation of SVF cell differentiation, but may derive from direct trans-differentiation of mature adipocytes in iWAT.

In summary, our results demonstrated that the ablation of adipocyte AMPKα impairs adaptive thermogenesis and energy expenditure in response to cold and β-adrenergic stimulation, leading to a predisposition for HFD-induced obesity and metabolic dysfunction. Moreover, pharmacological chronic AMPK activation by A-769662 alleviated diet-induced obesity via promoting browning in inguinal WAT. Overall, our findings indicate that AMPK plays a vital role in modulating WAT browning in response to thermal, nutritional and pharmacological cues, supporting chronic AMPK activation as a potentially effective approach for the treatment of obesity and related metabolic diseases through increasing thermogenesis.

AUTHOR CONTRIBUTIONS

LW, LZ, and BL contributed to study design, data analyzing, discussion and preparation of the manuscript. LW, LZ, BL, HJ, YD, ZX, and LS contributed to conducting the experiments. JYL and JL contributed to study design, discussion, reviewing and editing the manuscript.

FUNDING

This work was supported by a grant from National Key Research and Development (2016YFC1305500), the National Natural Science Foundation of China (81673493, 81673489), the Shanghai Commission of Science and Technology (14431902800,16JC1405000, 16430711700).

ACKNOWLEDGMENTS

We thank Dr. Jiqiu Wang from Ruijin Hospital, Shanghai Jiaotong University School of Medicine, for discussion and the guidance for SVFs isolation and differentiation.

SUPPLEMENTARY MATERIAL

The Supplementary Material for this article can be found online at: https://www.frontiersin.org/articles/10.3389/fphys.2018.00122/full#supplementary-material

REFERENCES

Abdul-Rahman, O., Kristóf, E., Doan-Xuan, Q. M., Vida, A., Nagy, L., Horváth, A., et al. (2016). AMP-activated kinase (AMPK) activation by AICAR in human white adipocytes derived from pericardial white adipose tissue stem cells induces a partial beige-like phenotype. *PLoS ONE* 11:e0157644. doi: 10.1371/journal.pone.0157644

Arany, Z. (2008). PGC-1 coactivators and skeletal muscle adaptations in health and disease. *Curr. Opin. Genet. Dev.* 18, 426–434. doi: 10.1016/j.gde.2008.07.018

Bagchi, M., Kim, L. A., Boucher, J., Walshe, T. E., Kahn, C. R., and D'Amore, P. A. (2013). Vascular endothelial growth factor is important for brown adipose tissue development and maintenance. *FASEB J.* 27, 3257–3271. doi: 10.1096/fj.12-221812

Bal, N. C., Maurya, S. K., Pani, S., Sethy, C., Banerjee, A., Das, S., et al. (2017a). Mild cold induced thermogenesis: are BAT and skeletal muscle synergistic partners? *Biosci. Rep.* 37:BSR20171087. doi: 10.1042/BSR20171087

Bal, N. C., Maurya, S. K., Sopariwala, D. H., Sahoo, S. K., Gupta, S. C., Shaikh, S. A., et al. (2012). Sarcolipin is a newly identified regulator of muscle-based thermogenesis in mammals. *Nat. Med.* 18, 1575–1579. doi: 10.1038/nm.2897

Bal, N. C., Singh, S., Reis, F. C. G., Maurya, S. K., Pani, S., Rowland, L. A., et al. (2017b). Both brown adipose tissue and skeletal muscle thermogenesis processes are activated during mild to severe cold adaptation in mice. *J. Biol. Chem.* 292, 16616–16625. doi: 10.1074/jbc.M117.790451

Bartelt, A., and Heeren, J. (2014). Adipose tissue browning and metabolic health. *Nat. Rev. Endocrinol.* 10, 24–36. doi: 10.1038/nrendo.2013.204

Bauwens, J. D., Schmuck, E. G., Lindholm, C. R., Ertel, R. L., Mulligan, J. D., Hovis, I., et al. (2011). Cold tolerance, cold-induced hyperphagia, and nonshivering thermogenesis are normal in alpha(1)-AMPK(-/-) mice. *Am. J. Physiol. Regul. Integr. Comp. Physiol.* 301, R473–R83. doi: 10.1152/ajpregu.00444.2010

Berry, D. C., Stenesen, D., Zeve, D., and Graff, J. M. (2013). The developmental origins of adipose tissue. *Development* 140, 3939–3949. doi: 10.1242/dev.080549

Bordicchia, M., Liu, D., Amri, E. Z., Ailhaud, G., Dessì-Fulgheri, P., Zhang, C., et al. (2012). Cardiac natriuretic peptides act via p38 MAPK to induce the brown fat thermogenic program in mouse and human adipocytes. *J. Clin. Invest.* 122, 1022–1036. doi: 10.1172/JCI59701

Boström, P., Wu, J., Jedrychowski, M. P., Korde, A., Ye, L., Lo, J. C., et al. (2012). A PGC1-alpha-dependent myokine that drives brown-fat-like development of white fat and thermogenesis. *Nature* 481, 463–468. doi: 10.1038/nature10777

Buhl, E. S., Jessen, N., Pold, R., Ledet, T., Flyvbjerg, A., Pedersen, S. B., et al. (2002). Long-term AICAR administration reduces metabolic disturbances and lowers blood pressure in rats displaying features of the insulin resistance syndrome. *Diabetes* 51, 2199–2206. doi: 10.2337/diabetes.51.7.2199

Carling, D. (2004). The AMP-activated protein kinase cascade–a unifying system for energy control. *Trends Biochem. Sci.* 29, 18–24. doi: 10.1016/j.tibs.2003.11.005

Carling, D., Thornton, C., Woods, A., and Sanders, M. J. (2012). AMP-activated protein kinase: new regulation, new roles? *Biochem. J.* 445, 11–27. doi: 10.1042/BJ20120546

Carling, D., Zammit, V. A., and Hardie, D. G. (1987). A common bicyclic protein kinase cascade inactivates the regulatory enzymes of fatty acid and cholesterol biosynthesis. *FEBS Lett.* 223, 217–222. doi: 10.1016/0014-5793(87)80292-2

Carlson, C. A., and Kim, K. H. (1973). Regulation of hepatic acetyl coenzyme A carboxylase by phosphorylation and dephosphorylation. *J. Biol. Chem.* 248, 378–380.

Cohen, P., Levy, J. D., Zhang, Y., Frontini, A., Kolodin, D. P., Svensson, K. J., et al. (2014). Ablation of PRDM16 and beige adipose causes metabolic dysfunction and a subcutaneous to visceral fat switch. *Cell* 156, 304–316. doi: 10.1016/j.cell.2013.12.021

Collins, S. (2011). beta-Adrenoceptor Signaling Networks in Adipocytes for Recruiting Stored Fat and Energy Expenditure. *Front. Endocrinol. (Lausanne).* 2:102. doi: 10.3389/fendo.2011.00102

Considine, R. V., Sinha, M. K., Heiman, M. L., Kriauciunas, A., Stephens, T. W., Nyce, M. R., et al. (1996). Serum immunoreactive-leptin concentrations in normal-weight and obese humans. *N. Engl. J. Med.* 334, 292–295. doi: 10.1056/NEJM199602013340503

Cool, B., Zinker, B., Chiou, W., Kifle, L., Cao, N., Perham, M., et al. (2006). Identification and characterization of a small molecule AMPK activator that treats key components of type 2 diabetes and the metabolic syndrome. *Cell Metab.* 3, 403–416. doi: 10.1016/j.cmet.2006.05.005

Corton, J. M., Gillespie, J. G., Hawley, S. A., and Hardie, D. G. (1995). 5-aminoimidazole-4-carboxamide ribonucleoside. A specific method for activating AMP-activated protein kinase in intact cells? *Eur. J. Biochem.* 229, 558–565.

Dagon, Y., Avraham, Y., and Berry, E. M. (2006). AMPK activation regulates apoptosis, adipogenesis, and lipolysis by eIF2alpha in adipocytes. *Biochem. Biophys. Res. Commun.* 340, 43–47. doi: 10.1016/j.bbrc.2005.11.159

Day, E. A., Ford, R. J., and Steinberg, G. R. (2017). AMPK as a therapeutic target for treating metabolic diseases. *Trends Endocrinol. Metabol.* 28, 545–560. doi: 10.1016/j.tem.2017.05.004

Fentz, J., Kjøbsted, R., Birk, J. B., Jordy, A. B., Jeppesen, J., Thorsen, K., et al. (2015). AMPKalpha is critical for enhancing skeletal muscle fatty acid utilization during *in vivo* exercise in mice. *FASEB J.* 29, 1725–1738. doi: 10.1096/fj.14-266650

Finucane, M. M., Stevens, G. A., Cowan, M. J., Danaei, G., Lin, J. K., Paciorek, C. J., et al. (2011). National, regional, and global trends in body-mass index since 1980: systematic analysis of health examination surveys and epidemiological studies with 960 country-years and 9.1 million participants. *Lancet* 377, 557–567. doi: 10.1016/S0140-6736(10)62037-5

Folch, J., Lees, M., and Sloane Stanley, G. H. (1957). A simple method for the isolation and purification of total lipides from animal tissues. *J. Biol. Chem.* 226, 497–509.

Fullerton, M. D., Galic, S., Marcinko, K., Sikkema, S., Pulinilkunnil, T., Chen, Z. P., et al. (2013). Single phosphorylation sites in Acc1 and Acc2 regulate lipid homeostasis and the insulin-sensitizing effects of metformin. *Nat. Med.* 19, 1649–1654. doi: 10.1038/nm.3372

Gaidhu, M. P., Fediuc, S., Anthony, N. M., So, M., Mirpourian, M., Perry, R. L., et al. (2009). Prolonged AICAR-induced AMP-kinase activation promotes energy dissipation in white adipocytes: novel mechanisms integrating HSL and ATGL. *J. Lipid Res.* 50, 704–715. doi: 10.1194/jlr.M800480-JLR200

Gaidhu, M. P., Frontini, A., Hung, S., Pistor, K., Cinti, S., and Ceddia, R. B. (2011). Chronic AMP-kinase activation with AICAR reduces adiposity by remodeling adipocyte metabolism and increasing leptin sensitivity. *J. Lipid Res.* 52, 1702–1711. doi: 10.1194/jlr.M015354

Gauthier, M. S., Miyoshi, H., Souza, S. C., Cacicedo, J. M., Saha, A. K., Greenberg, A. S., et al. (2008). AMP-activated protein kinase is activated as a consequence of lipolysis in the adipocyte - Potential mechanism and physiological relevance. *J. Biol. Chem.* 283, 16514–16524. doi: 10.1074/jbc.M708177200

Gauthier, M. S., O'Brien, E. L., Bigornia, S., Mott, M., Cacicedo, J. M., Xu, X. J., et al. (2011). Decreased AMP-activated protein kinase activity is associated with increased inflammation in visceral adipose tissue and with whole-body insulin resistance in morbidly obese humans. *Biochem. Biophys. Res. Commun.* 404, 382–387. doi: 10.1016/j.bbrc.2010.11.127

Habinowski, S. A., and Witters, L. A. (2001). The effects of AICAR on adipocyte differentiation of 3T3-L1 cells. *Biochem. Biophys. Res. Commun.* 286, 852–856. doi: 10.1006/bbrc.2001.5484

Hardie, D. G. (2011). Sensing of energy and nutrients by AMP-activated protein kinase. *Am. J. Clin. Nutr.* 93, 891S-6. doi: 10.3945/ajcn.110.001925

Harms, M., and Seale, P. (2013). Brown and beige fat: development, function and therapeutic potential. *Nat. Med.* 19, 1252–1263. doi: 10.1038/nm.3361

Hoffman, N. J., Parker, B. L., Chaudhuri, R., Fisher-Wellman, K. H., Kleinert, M., Humphrey, S. J., et al. (2015). Global phosphoproteomic analysis of human skeletal muscle reveals a network of exercise-regulated kinases and AMPK substrates. *Cell Metab.* 22, 922–935. doi: 10.1016/j.cmet.2015.09.001

Inagaki, T., Sakai, J., and Kajimura, S. (2016). Transcriptional and epigenetic control of brown and beige adipose cell fate and function. *Nat. Rev. Mol. Cell Biol.* 17, 480–495. doi: 10.1038/nrm.2016.62

Jager, S., Handschin, C., Pierre, J., and Spiegelman, B. M. (2007). AMP-activated protein kinase (AMPK) action in skeletal muscle via direct phosphorylation of PGC-1 alpha. *Proc. Natl. Acad. Sci. U.S.A.* 104, 12017–12022. doi: 10.1073/pnas.0705070104

James, W. P., Caterson, I. D., Coutinho, W., Finer, N., Van Gaal, L. F., Maggioni, A. P., et al. (2010). Effect of sibutramine on cardiovascular outcomes in overweight and obese subjects. *N. Engl. J. Med.* 363, 905–917. doi: 10.1056/NEJMoa1003114

Jeffery, E., Berry, R., Church, C. D., Yu, S., Shook, B. A., Horsley, V., et al. (2014). Characterization of Cre recombinase models for the study of adipose tissue. *Adipocyte* 3, 206–211. doi: 10.4161/adip.29674

Jia, R., Luo, X. Q., Wang, G., Lin, C. X., Qiao, H., Wang, N., et al. (2016). Characterization of cold-induced remodelling reveals depot-specific differences across and within brown and white adipose tissues in mice. *Acta Physiol.* 217, 311–324. doi: 10.1111/apha.12688

Jiang, G., and Zhang, B. B. (2003). Glucagon and regulation of glucose metabolism. *Am. J. Physiol. Endocrinol. Metab.* 284, E671–E678. doi: 10.1152/ajpendo.00492.2002

Kajimura, S., Spiegelman, B. M., and Seale, P. (2015). Brown and beige fat: physiological roles beyond heat generation. *Cell Metab.* 22, 546–559. doi: 10.1016/j.cmet.2015.09.007

Kim, S. J., Tang, T., Abbott, M., Viscarra, J. A., Wang, Y., and Sul, H. S. (2016). AMPK Phosphorylates desnutrin/ATGL and hormone-sensitive lipase to regulate lipolysis and fatty acid oxidation within adipose tissue. *Mol. Cell. Biol.* 36, 1961–1976. doi: 10.1128/MCB.00244-16

Lee, P., Linderman, J. D., Smith, S., Brychta, R. J., Wang, J., Idelson, C., et al. (2014). Irisin and FGF21 are cold-induced endocrine activators of brown fat function in humans. *Cell Metab.* 19, 302–309. doi: 10.1016/j.cmet.2013.12.017

Marra, F. (2002). Leptin and liver fibrosis: a matter of fat. *Gastroenterology* 122, 1529–1532. doi: 10.1053/gast.2002.33369

Mihaylova, M. M., and Shaw, R. J. (2011). The AMPK signalling pathway coordinates cell growth, autophagy and metabolism. *Nat. Cell Biol.* 13, 1016–1023. doi: 10.1038/ncb2329

Mottillo, E. P., Desjardins, E. M., Crane, J. D., Smith, B. K., Green, A. E., Ducommun, S., et al. (2016). Lack of adipocyte AMPK exacerbates insulin resistance and hepatic steatosis through brown and beige adipose tissue function. *Cell Metab.* 24, 118–129. doi: 10.1016/j.cmet.2016.06.006

O'Neill, H. M., Holloway, G. P., and Steinberg, G. R. (2013). AMPK regulation of fatty acid metabolism and mitochondrial biogenesis: implications for obesity. *Mol. Cell. Endocrinol.* 366, 135–151. doi: 10.1016/j.mce.2012.06.019

Parlee, S. D., Lentz, S. I., Mori, H., and MacDougald, O. A. (2014). Quantifying size and number of adipocytes in adipose tissue. *Meth. Enzymol.* 537, 93–122. doi: 10.1016/B978-0-12-411619-1.00006-9

Rosen, E. D., and Spiegelman, B. M. (2014). What we talk about when we talk about fat. *Cell* 156, 20–44. doi: 10.1016/j.cell.2013.12.012

Rowland, L. A., Bal, N. C., Kozak, L. P., and Periasamy, M. (2015). Uncoupling protein 1 and sarcolipin are required to maintain optimal thermogenesis, and loss of both systems compromises survival of mice under cold stress. *J. Biol. Chem.* 290, 12282–12289. doi: 10.1074/jbc.M115.637603

Ruderman, N. B., Xu, X. J., Nelson, L., Cacicedo, J. M., Saha, A. K., Lan, F., et al. (2010). AMPK and SIRT1: a long-standing partnership? *Am. J. Physiol. Endocrinol. Metab.* 298, E751–E760. doi: 10.1152/ajpendo.00745.2009

Saito, M., Okamatsu-Ogura, Y., Matsushita, M., Watanabe, K., Yoneshiro, T., Nio-Kobayashi, J., et al. (2009). High incidence of metabolically active brown adipose tissue in healthy adult humans: effects of cold exposure and adiposity. *Diabetes* 58, 1526–1531. doi: 10.2337/db09-0530

Sanders, M. J., Ali, Z. S., Hegarty, B. D., Heath, R., Snowden, M. A., and Carling, D. (2007). Defining the mechanism of activation of AMP-activated protein kinase by the small molecule A-769662, a member of the thienopyridone family. *J. Biol. Chem.* 282, 32539–32548. doi: 10.1074/jbc.M706543200

Schaffer, B. E., Levin, R. S., Hertz, N. T., Maures, T. J., Schoof, M. L., Hollstein, P. E., et al. (2015). Identification of AMPK phosphorylation sites reveals a network of proteins involved in cell invasion and facilitates large-scale substrate prediction. *Cell Metab.* 22, 907–921. doi: 10.1016/j.cmet.2015.09.009

Sellayah, D., Bharaj, P., and Sikder, D. (2011). Orexin is required for brown adipose tissue development, differentiation, and function. *Cell Metab.* 14, 478–490. doi: 10.1016/j.cmet.2011.08.010

Song, X. M., Fiedler, M., Galuska, D., Ryder, J. W., Fernström, M., Chibalin, A. V., et al. (2002). 5-Aminoimidazole-4-carboxamide ribonucleoside treatment improves glucose homeostasis in insulin-resistant diabetic (ob/ob) mice. *Diabetologia* 45, 56–65. doi: 10.1007/s125-002-8245-8

Stern, J. H., Rutkowski, J. M., and Scherer, P. E. (2016). Adiponectin, leptin, and fatty acids in the maintenance of metabolic homeostasis through adipose tissue crosstalk. *Cell Metab.* 23, 770–784. doi: 10.1016/j.cmet.2016.04.011

Tam, C. S., Lecoultre, V., and Ravussin, E. (2012). Brown adipose tissue: mechanisms and potential therapeutic targets. *Circulation* 125, 2782–2791. doi: 10.1161/CIRCULATIONAHA.111.042929

Tseng, Y. H., Kokkotou, E., Schulz, T. J., Huang, T. L., Winnay, J. N., Taniguchi, C. M., et al. (2008). New role of bone morphogenetic protein 7 in brown adipogenesis and energy expenditure. *Nature* 454, 1000–1004. doi: 10.1038/nature07221

van Marken Lichtenbelt, W. D., Vanhommerig, J. W., Smulders, N. M., Drossaerts, J. M., Kemerink, G. J., Bouvy, N. D., et al. (2009). Cold-activated brown adipose tissue in healthy men. *N. Engl. J. Med.* 360, 1500–1508. doi: 10.1056/NEJMoa0808718

Vila-Bedmar, R., Lorenzo, M., and Fernández-Veledo, S. (2010). Adenosine 5'-monophosphate-activated protein kinase-mammalian target of rapamycin cross talk regulates brown adipocyte differentiation. *Endocrinology* 151, 980–992. doi: 10.1210/en.2009-0810

Wang, J., Liu, R., Wang, F., Hong, J., Li, X., Chen, M., et al. (2013). Ablation of LGR4 promotes energy expenditure by driving white-to-brown fat switch. *Nat. Cell Biol.* 15, 1455–1463. doi: 10.1038/ncb2867

Whittle, A. J., Carobbio, S., Martins, L., Slawik, M., Hondares, E., Vázquez, M. J., et al. (2012). BMP8B increases brown adipose tissue thermogenesis through both central and peripheral actions. *Cell* 149, 871–885. doi: 10.1016/j.cell.2012.02.066

Wu, J., Boström, P., Sparks, L. M., Ye, L., Choi, J. H., Giang, A. H., et al. (2012). Beige adipocytes are a distinct type of thermogenic fat cell in mouse and human. *Cell* 150, 366–376. doi: 10.1016/j.cell.2012.05.016

Wu, Z., Puigserver, P., Andersson, U., Zhang, C., Adelmant, G., Mootha, V., et al. (1999). Mechanisms controlling mitochondrial biogenesis and respiration through the thermogenic coactivator PGC-1. *Cell* 98, 115–124. doi: 10.1016/S0092-8674(00)80611-X

Xu, X. J., Gauthier, M. S., Hess, D. T., Apovian, C. M., Cacicedo, J. M., Gokce, N., et al. (2012). Insulin sensitive and resistant obesity in humans: AMPK activity, oxidative stress, and depot-specific changes in gene expression in adipose tissue. *J. Lipid Res.* 53, 792–801. doi: 10.1194/jlr.P022905

Yamauchi, T., Kamon, J., Waki, H., Terauchi, Y., Kubota, N., Hara, K., et al. (2001). The fat-derived hormone adiponectin reverses insulin resistance associated with both lipoatrophy and obesity. *Nat. Med.* 7, 941–946. doi: 10.1038/90984

Yang, Q., Liang, X., Sun, X., Zhang, L., Fu, X., Rogers, C. J., et al. (2016). AMPK/alpha-ketoglutarate axis dynamically mediates DNA demethylation in the Prdm16 promoter and brown adipogenesis. *Cell Metab.* 24, 542–554. doi: 10.1016/j.cmet.2016.08.010

Ye, L., Kleiner, S., Wu, J., Sah, R., Gupta, R. K., Banks, A. S., et al. (2012). TRPV4 is a regulator of adipose oxidative metabolism, inflammation, and energy homeostasis. *Cell* 151, 96–110. doi: 10.1016/j.cell.2012.08.034

Yu, X., McCorkle, S., Wang, M., Lee, Y., Li, J., Saha, A. K., et al. (2004). Leptinomimetic effects of the AMP kinase activator AICAR in leptin-resistant rats: prevention of diabetes and ectopic lipid deposition. *Diabetologia* 47, 2012–2021. doi: 10.1007/s00125-004-1570-9

Zhang, B. B., Zhou, G., and Li, C. (2009). AMPK: an emerging drug target for diabetes and the metabolic syndrome. *Cell Metab.* 9, 407–416. doi: 10.1016/j.cmet.2009.03.012

Zhang, Z., Zhang, H., Li, B., Meng, X., Wang, J., Zhang, Y., et al. (2014). Berberine activates thermogenesis in white and brown adipose tissue. *Nat. Commun.* 5:5493. doi: 10.1038/ncomms6493

Zhou, Y., Wang, D., Zhu, Q., Gao, X., Yang, S., Xu, A., et al. (2009). Inhibitory effects of A-769662, a novel activator of AMP-activated protein kinase, on 3T3-L1 adipogenesis. *Biol. Pharm. Bull.* 32, 993–998. doi: 10.1248/bpb.32.993

Zurlo, F., Larson, K., Bogardus, C., and Ravussin, E. (1990). Skeletal muscle metabolism is a major determinant of resting energy expenditure. *J. Clin. Invest.* 86, 1423–1427. doi: 10.1172/JCI114857

Conflict of Interest Statement: The authors declare that the research was conducted in the absence of any commercial or financial relationships that could be construed as a potential conflict of interest.

The handling Editor declared a shared affiliation, though no other collaboration, with the authors HJ and YD.

frontiers in Physiology

TECHNOLOGY REPORT
published: 20 February 2018
doi: 10.3389/fphys.2018.00085

AdipoCount: A New Software for Automatic Adipocyte Counting

Xuhao Zhi[1,2], *Jiqiu Wang*[3], *Peng Lu*[4], *Jue Jia*[5], *Hong-Bin Shen*[1,2]* *and Guang Ning*[3]*

[1] *Institute of Image Processing and Pattern Recognition, Shanghai Jiao Tong University, Shanghai, China,* [2] *Key Laboratory of System Control and Information Processing, Ministry of Education of China, Shanghai, China,* [3] *Department of Endocrinology and Metabolism, China National Research Center for Metabolic Diseases, Ruijin Hospital, Shanghai Jiao Tong University School of Medicine, Shanghai, China,* [4] *Laboratory of Endocrinology and Metabolism, Shanghai Institutes for Biological Sciences, University of Chinese Academy of Sciences, Chinese Academy of Sciences, Shanghai, China,* [5] *Affiliated Hospital of Jiangsu University, Zhenjiang, China*

Obesity has spread worldwide and become a common health problem in modern society. One typical feature of obesity is the excessive accumulation of fat in adipocytes, which occurs through the following two physiological phenomena: hyperplasia (increase in quantity) and hypertrophy (increase in size) of adipocytes. In clinical and scientific research, the accurate quantification of the number and diameter of adipocytes is necessary for assessing obesity. In this study, we present a new automatic adipocyte counting system, AdipoCount, which is based on image processing algorithms. Comparing with other existing adipocyte counting tools, AdipoCount is more accurate and supports further manual correction. AdipoCount counts adipose cells by the following three-step process: (1) It detects the image edges, which are used to segment the membrane of adipose cells; (2) It uses a watershed-based algorithm to re-segment the missing dyed membrane; and (3) It applies a domain connectivity analysis to count the cells. The outputs of this system are the labels and the statistical data of all adipose cells in the image. The AdipoCount software is freely available for academic use at: http://www.csbio.sjtu.edu.cn/bioinf/AdipoCount/.

Keywords: cell counting, obesity, adipocytes, image segmentation, software validation, cellularity, AdipoCount

OPEN ACCESS

Edited by:
Gabriele Giacomo Schiattarella, University of Naples Federico II, Italy

Reviewed by:
Carles Bosch, Eurecat, Spain
Meredith Emily Kennedy Calvert, University of California, San Francisco, United States
Nicolas Heck, Université Pierre et Marie Curie, France

***Correspondence:**
Hong-Bin Shen
hbshen@sjtu.edu.cn
Guang Ning
gning@sibs.ac.cn

Specialty section:
This article was submitted to Clinical and Translational Physiology, a section of the journal Frontiers in Physiology

Received: *07 November 2017*
Accepted: *25 January 2018*
Published: *20 February 2018*

Citation:
Zhi X, Wang J, Lu P, Jia J, Shen H-B and Ning G (2018) AdipoCount: A New Software for Automatic Adipocyte Counting. Front. Physiol. 9:85. doi: 10.3389/fphys.2018.00085

INTRODUCTION

Cell counting is a very common and fundamental task in research and clinical practice. For instance, accurate cell counting is very important in the study of cell proliferation. When pathologists make diagnostic decisions, they want to refer to the number of cells (Kothari et al., 2009).

In the past, one common way to perform this task was to count cells manually with the help of tools such as a counting chamber. However, manual examination and counting is very time-consuming and highly dependent on the skills of operators. With the increasing demand for cellular analysis, labor-intensive manual analysis was gradually replaced by automatic cell counting methods (Landini, 2006; Han et al., 2012). Among the automatic methods, one of the most powerful and versatile methods for cellular analysis is computer image analysis using image processing algorithms.

Many algorithms have been developed for cell segmentation and counting. There exist diversity and specificity among cell morphologies, microscopes and stains; however, most algorithms

are specifically designed for one or several types of cells (Di Rubeto et al., 2000; Liao and Deng, 2002; Refai et al., 2003). It is necessary but difficult to develop a generally applicable cell segmentation method (Meijering, 2012). Common cell segmentation approaches are mainly divided into intensity thresholding (Wu et al., 2006), feature detection (Liao and Deng, 2002; Su et al., 2013), morphological filtering (Dorini et al., 2007), deformable model fitting (Yang et al., 2005; Nath et al., 2006), and neural-network-based segmentation (Ronneberger et al., 2015). The most predominant and widely used approach for cell segmentation is intensity thresholding (Wu et al., 2010). In addition, software programs that target biological images have been developed, such as Fiji (Schindelin et al., 2012), CellProfiler (Lamprecht et al., 2007), and Cell Image Analyzer (Baecker and Travo, 2006).

Software programs have developed for semi-automatic or automatic adipose cell counting (Chen and Farese, 2002; Björnheden et al., 2004; Galarraga et al., 2012; Osman et al., 2013; Parlee et al., 2014). For instance, Adiposoft (Galarraga et al., 2012), which is one of the best adipocyte counting software programs, has been developed as a plug-in for Fiji (Schindelin et al., 2012). The process of Adiposoft is very straightforward: First, the red channel of the input image is processed by thresholding. Second, a watershed algorithm is used to segment the adipose cells. In general, most adipocyte counting systems require images to be of high quality, and noise in the image will result in reduced counting accuracy. However, in the production of adipose slices and microscopy imaging, noise is inevitable, and staining quality is mixed. Therefore, the most common way of detecting the proliferation (change in quantity) and hypertrophy (change in diameter) of adipocytes is still manual counting. In contrast to other existing automatic adipose cell counting tools, AdipoCount uses not only gray information but also gradient information to segment the membrane in an adipocyte image. In addition, AdipoCount has a pre-processing step for eliminating noise and correcting illumination and uses a series of post-processing steps to improve the segmentation result. We also develop a re-segmentation step in AdipoCount for dealing with missing dyed membrane and improving the counting accuracy, which is an innovation in adipose cell counting software. Additionally, the segmentation result can be manually corrected by adding or erasing lines on it.

Most cells are cytoplasm-stained or nucleus-stained and the cells are blob-like, which makes it easy to perform intensity thresholding and ellipse fitting. Unlike most cell images, adipose cell images are membrane-stained, which results in large differences in the adipose cell segmentation approach, compared to methods for segmenting other types of cells. To detect all the adipose cells, the stained membrane should be segmented first, which can be used to estimate the interior of each adipose cell. After the segmentation of cells, a connected domain analysis algorithm is executed to count the cells.

The staining quality of slices will affect the accuracy of cell counting. For slices with high staining quality, the segmentation algorithm is very reliable and its counting accuracy is high. However, for poorly stained adipose tissue images, there could be noise due to a minced membrane and miss-staining is common, so it is necessary to use a pre-processing step to eliminate noise and a re-segmentation process to complete missing areas of the membrane. To address uneven stain quality, we design the adipose cell counting system with three modules: an illumination correction module, a pre-processing module for eliminating noise, and a re-segmentation module for completing missing dyed areas of the membrane. The outputs of this system are statistical data for all cells and a visualized counting result (labeled adipose cell image). Based on the statistical data and the visualized counting result, further manual correction can be efficiently performed.

METHODS

For a given stained adipose tissue image, as illustrated in **Figure 1**, the first step is graying, which outputs a grayscale image. The graying process ignores the color information and retains the intensity information, which is used for further thresholding and edge detection.

As shown in **Figure 2**, the AdipoCount system contains the following three modules: (1) a membrane segmentation module, (2) a re-segmentation module, and (3) a cell counting module.

The input of the membrane segmentation module is a grayscale image, and there are two parallel processes, namely, thresholding and edge detection. The outputs of these two processes are combined to generate the final membrane segmentation result. Before thresholding and edge detection,

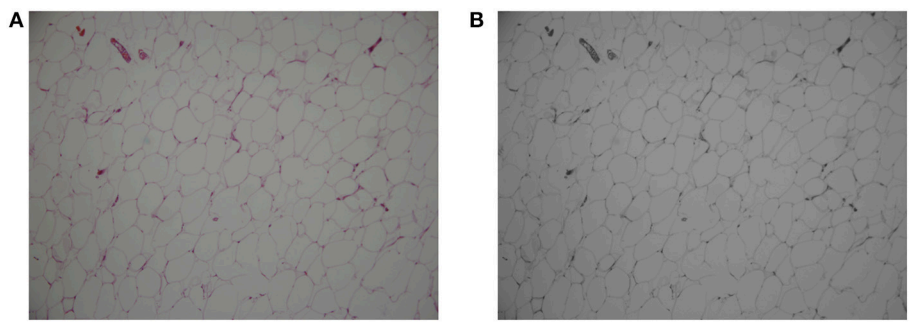

FIGURE 1 | Original color image of adipose cells **(A)** and its grayscale image **(B)**.

an image enhancement step is performed: for thresholding, illumination correction is carried out on the grayscale image; for edge detection, histogram equalization is performed on the grayscale image.

The input of the re-segmentation module is the membrane segmentation result that was generated by the membrane segmentation module. With the membrane image, first, a post-process is implemented to eliminate noise and estimate the interiors of adipose cells. Second, a watershed-based algorithm is used for further image segmentation, which can complete some missing dyed areas of the membrane to improve the final accuracy of cell counting.

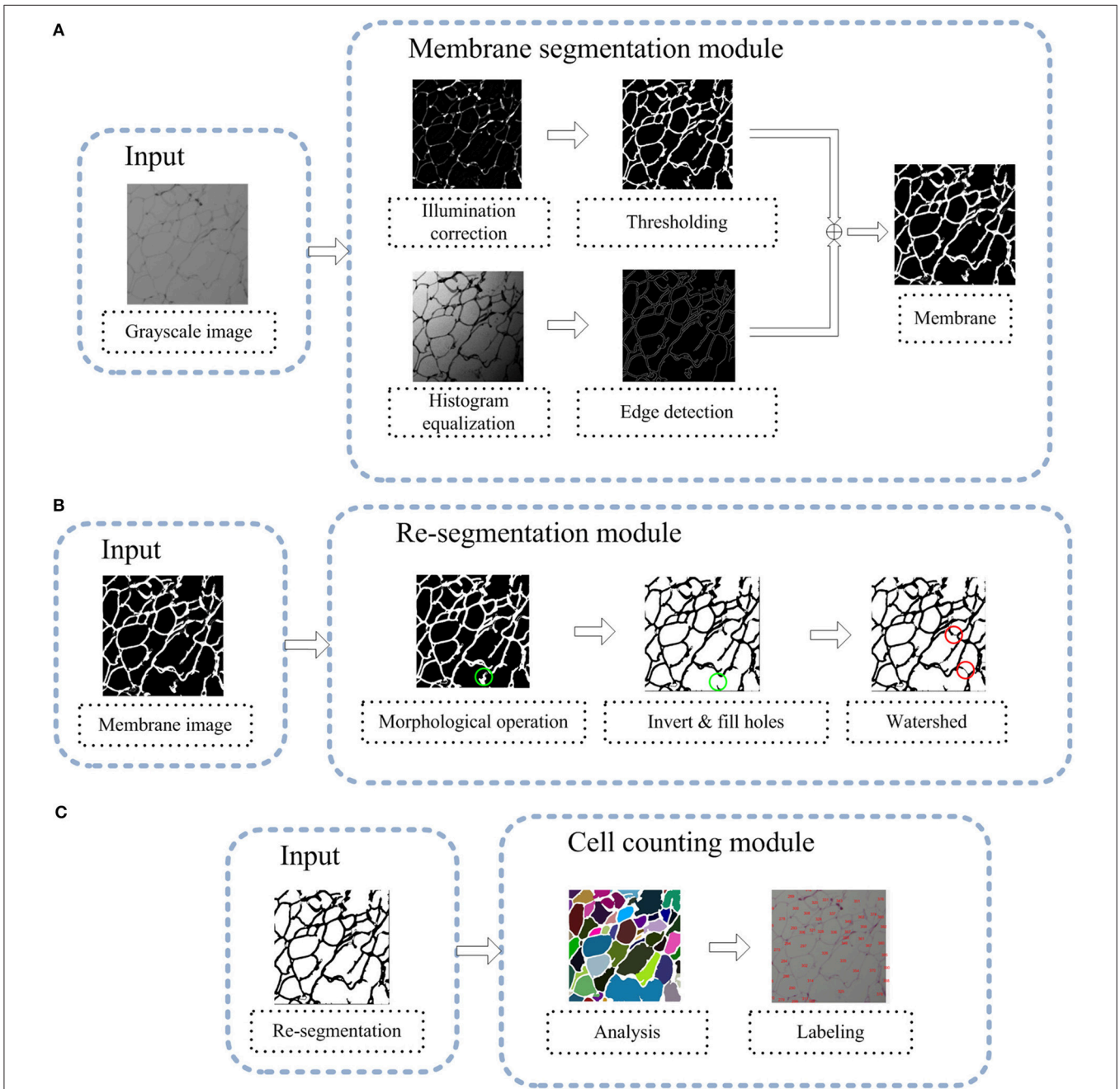

FIGURE 2 | (A) Flowchart of the membrane segmentation module. The input is a grayscale image, and the output is a segmented membrane. The binary image that is generated by thresholding and the edge detection result are combined to generate the final membrane segmentation output. **(B)** Flowchart of the re-segmentation module. The input is a segmented membrane image. The morphological operation can fill holes in the membrane and make the segmentation of the membrane more reliable. Then, we invert the image and fill holes inside the cell area; as illustrated by the green circle, the separated and short segments of the membrane are eliminated. Then, a watershed-based algorithm is used, and as indicated by the red circle, some missing dyed areas of the membrane are detected. **(C)** Flowchart of the cell counting module. The input of this module is a re-segmentation image and the image is labeled using a connected-domain analysis method.

The input of the cell analysis module is the re-segmentation result from the re-segmentation module. To perform cell counting, a connected domain analysis method is applied to detect all adipose cells. The final results of the AdipoCount system are statistical data on all adipose cells and the labeled image, which provides a basis for manual verification.

Membrane Segmentation

Because the adipose cells are membrane-stained, the entire membrane should be segmented to detect cell interiors. As shown in **Figure 2A**, in the membrane segmentation module, there are two separate processes: thresholding and edge detection. Thresholding is membrane segmentation according to the pixel intensity, through which the input grayscale image is converted into a binary image. Before thresholding, an illumination correction process is necessary (Leong et al., 2003), because the input image may have uneven illumination since corner areas of an image are always darker than the center area. To implement illumination correction, we define two Gaussian filters, which are denoted as g_1 and g_2, as follows:

$$g_\sigma(x, y) = \frac{1}{\sqrt{2\,\pi\,\sigma^2}}\exp(-\frac{(x-\mu)^2+(y-\mu)^2}{2\sigma^2})(-H < x, y < H) \tag{1}$$

where μ is set to zero; σ is the standard deviation of the distribution, which is set to 0.5 for g_1 and 30 for g_2; H is the kernel size, which is set to 3 for g_1 and 60 for g_2; and (x, y) is the position relative to the center of the window. Then, illumination correction is implemented as follows:

$$I_c = I^*(g_2 - g_1) \tag{2}$$

where * stands for convolution, I is the input grayscale image and I_c is the illumination-corrected image, as illustrated in **Figure 3A**. g_1 is a Gaussian filter with a small kernel size, and an image that is blurred by g_1 has some noise filtered out and retains most of the information from the original image. g_2 has a much bigger kernel size than g_1. When using g_2 for convolution, the pixels inside its kernel are blurred, which can make the illumination more equalized. An image that is blurred by g_2 only retains low-frequency information. By the subtraction operation, we can filter the low-frequency information and keep the high-frequency information, such as the membrane.

After the above process, the illumination is much more even. Then, an adaptive thresholding method, namely, OTSU, is used. OTSU (Otsu, 1979) is a classic thresholding method, which can find a threshold that separates foreground from background with maximum intensity variance.

Some areas of the membrane are stained too weakly and the intensity is not strong enough for segmentation by thresholding. Thus, edge detection is also used to ensure that the entire stained membrane can be segmented. Before edge detection, as shown in **Figure 4**, a histogram equalization process is implemented to enhance the contrast of the image, so the edge can be easily

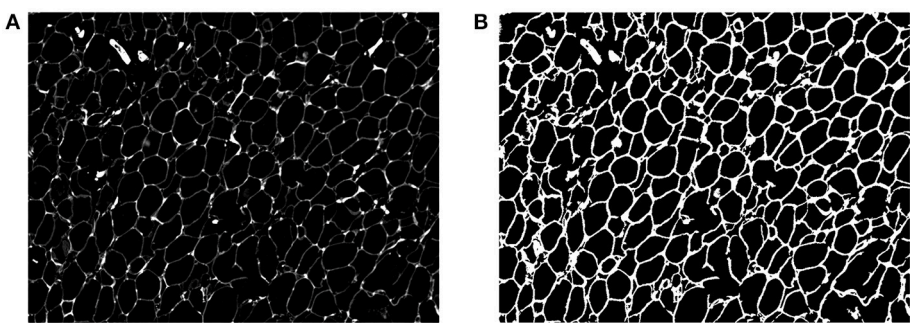

FIGURE 3 | (A) The image after illumination correction. **(B)** Binary image after thresholding.

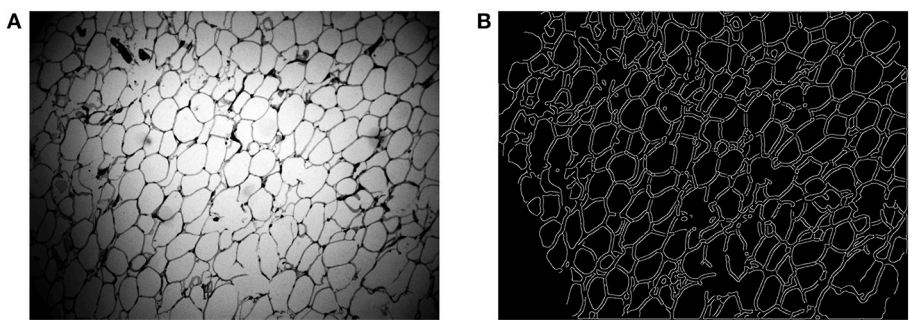

FIGURE 4 | (A) The histogram equalization image. **(B)** Membrane edge.

detected. Then, we use the Canny edge detection algorithm (Canny, 1986) to detect the membrane. After thresholding and edge detection, we can obtain the binary image (**Figure 3B**) and the edge image (**Figure 4B**). Then, we add those two images together to generate the membrane.

Re-segmentation

During the processes of slicing and dyeing adipose tissue, minced membrane and other tissues may occur as noise. To address this problem, we develop a post-process for eliminating noise.

As shown in **Figure 2B**, the input of this module is a binary image of the membrane. As is well known, in the adipose tissue, adipose cells are closely packed. Thus, in a binary image of the membrane, all membrane segments should be combined into a single connected domain. The noise is always isolated in a small domain, which can be removed by a morphological operation. Specifically, we first detect the entire connected domain and eliminate all subdomains with areas that are smaller than T, where T is a defined area threshold. Then, an opening operation, a closing operation and a dilation operation are

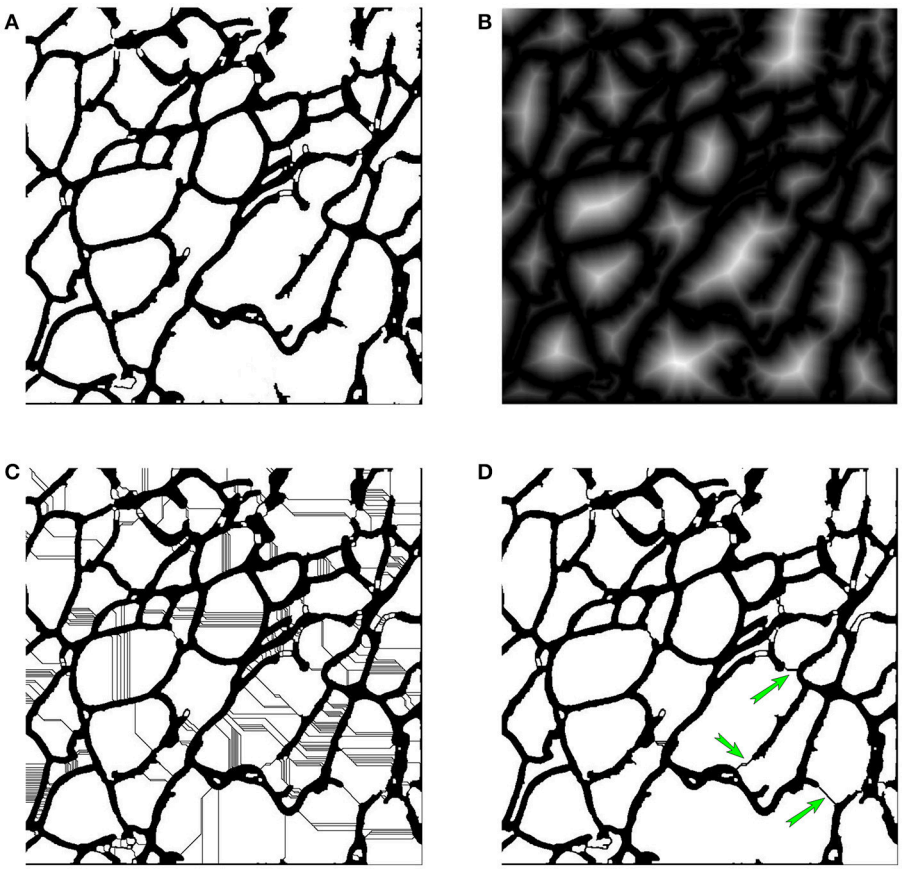

FIGURE 5 | (A) The post-processed image. **(B)** Distance map. **(C)** Watershed-transformed image. **(D)** Re-segmented image, where green arrows show the detected missing dyed membrane.

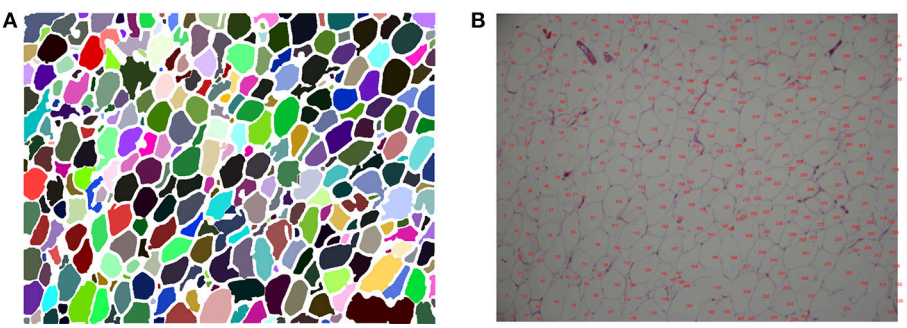

FIGURE 6 | (A) Visualized segmentation result, in which each adipose cell is labeled with a different color. **(B)** Labeled image with cell numbers.

applied sequentially. Next, an intensity reversal operation is applied to invert the background and foreground. Then, we fill the holes inside the cell area, to remove the separated and short membrane areas. The post-processed image is shown in **Figure 5A**.

After the post-process, some noise can be eliminated, but there remain missing dyed membrane areas, which will lead to inaccurate detection of adipose cells. To estimate the membrane, a watershed-based algorithm is applied for further image segmentation. The watershed algorithm was proposed by Beucher (Beucher and Lantuéjoul, 1979), improved by Vincent and Soille (1991), and has become a popular image segmentation method.

The watershed algorithm stimulates a flooding process. A grayscale image is identified with a topographical surface, in which every point's altitude equals the intensity of the corresponding pixel. Before the watershed transform, we first compute the distance map (Meyer and Fernand, 1994), in which every pixel's value is the distance from the nearest zero-point. The distance map is shown in **Figure 5B**. Then, we use watershed algorithm to perform further image segmentation on the distance map. Through the watershed transform, many watersheds are generated, as illustrated in **Figure 5C**, which is over-segmented.

To detect the membrane, we develop a judgement criterion for filtering false-positive watersheds and choose the most-probable watersheds as membrane areas. In our protocol, we consider watershed w as a membrane of domain D, and split D into two sub-domains, which are denoted as D_1 and D_2, if it satisfies both of the following conditions:

$$L < L_T \tag{3}$$

$$\frac{A_1}{A_2} < R_a \tag{4}$$

where L is the length of w and L_T is the threshold, which can filter long watersheds since missing dyed membrane segments are more likely to be short. A_1 and A_2 are the areas of D_1 and D_2 ($A_1 > A_2$), and R_a is the area ratio threshold, which ensures that the sub-domains have similar area. After this filtering process, we can obtained the most-probable missing dyed membrane segments, as illustrated in **Figure 5D**, which are shown with green arrows.

Cell Counting

After re-segmentation, adipose cells are segmented, so cell counting and analysis can be implemented; the flowchart is shown in **Figure 2C**. Each adipose cell is a connected domain in the image, so we first detect all the connected domains using the region-growing method (Adams and Bischof, 1994). After this process, we can obtain every cell's position, area and diameter. Then, we label every cell's number at the corresponding position on the original color image; the visualized results are shown in **Figure 6**. With the statistical data and the labeled image, further correction can be easily performed manually.

We use F1-score to evaluate the counting result. The F1-score is calculated by:

$$P = \frac{TP}{GT} \tag{5}$$

$$R = \frac{TP}{EN} \tag{6}$$

$$F = 2^* \frac{P^* R}{P + R} \tag{7}$$

where P is precision, R is recall rate, and F is F1-score.

EXPERIMENTS AND DISCUSSION

To test the robustness of AdipoCount, we selected a batch of stained adipose tissue images. These images have different dyeing qualities. Images with high quality have clear membranes; those with low quality may have large amounts of noise and many blurred membrane areas. The results show that our system achieves high counting accuracy on high-dyeing-quality images. For low-dyeing-quality images, AdipoCount eliminates most noise and recovers some missing dyed membrane areas, which improves the overall segmentation results.

Due to the constraints of the dyeing process, missing dyed membrane areas are inevitable, so the re-segmentation process is necessary. **Figure 7A** is the segmentation result without a re-segmentation process and **Figure 7B** is the segmentation result with a re-segmentation process. Some missing dyed membrane areas are detected by the re-segmentation module (e.g., in

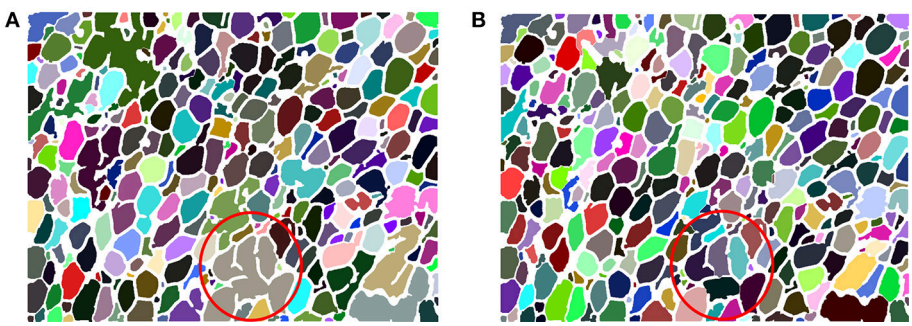

FIGURE 7 | (A) AdipoCount's segmentation result without re-segmentation. The number of detected cells is 303. **(B)** AdipoCount's segmentation result with re-segmentation. The number of detected cells is 335.

Figure 7A, the brown region inside the red circle is segmented into 6 different cells, as shown in **Figure 7B**). Therefore, more adipose cells can be segmented, which can improve the counting results.

As shown in **Figures 8A–C**, our segmentation results for high-quality stained images are satisfactory. Nearly the entire membrane is segmented and most adipose cells are correctly detected. For an image with a blurred membrane, as shown in **Figure 8D**, our system still detects the blurred membrane, which is thicker than a clear membrane. For images with dense adipose cells, such as that shown in **Figure 8E**, which are usually small, our system detects them with high accuracy.

We further compared our AdipoCount with Adiposoft, which can be download at http://imagej.net/Adiposoft. We used 5

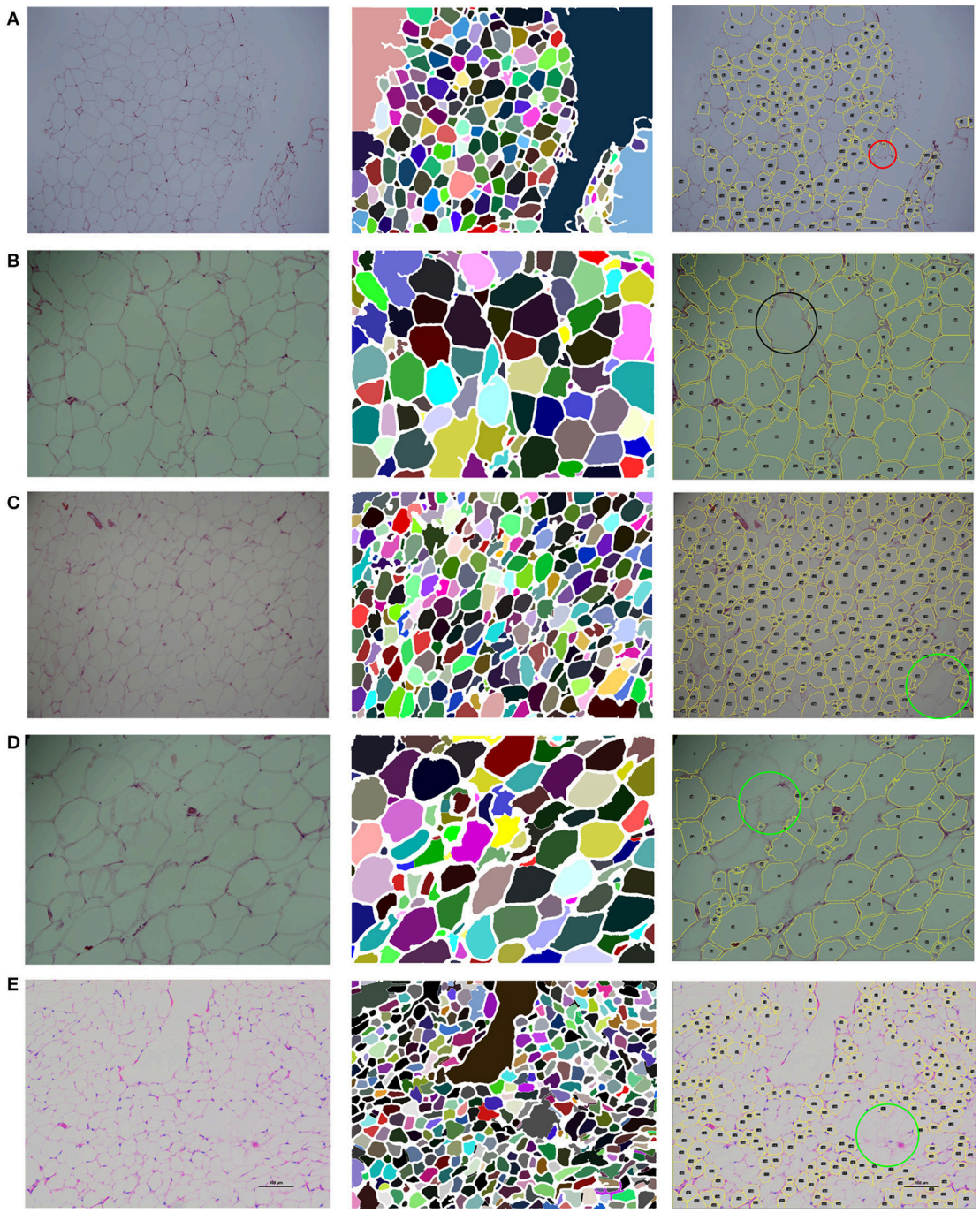

FIGURE 8 | Segmentation of five test images. The segmentation results in the second column are generated by AdipoCount. The segmentation results in the third column are generated by Adiposoft. **(A–C)** Three high-quality stained images and their segmentation results. **(D)** An image with a blurred membrane and its segmentation results. **(E)** An image with dense adipose cells and its segmentation results.

adipocyte images to evaluate the counting accuracies of these two software programs, and the counting results are listed in **Table 1**. Based on these results, AdipoCount outperforms Adiposoft. As shown in **Figure 8**, cells are commonly missed during counting in segmentation results that are generated by Adiposoft, some cells with small size (e.g., the region inside the red circle in **Figure 8A**) or large size (e.g., the region inside the black circle in **Figure 8B**) are not detected, and cells with blurred membrane are not detected (e.g., the region inside the green circle in **Figures 8C–E**). We also compare the computation times of these two software programs. As shown in **Table 2**, our AdipoCount is more efficient than Adiposoft.

As shown in **Figure 9**, AdipoCount supports manual correction, such as adding or deleting membrane segments in the segmentation result. In addition, manual correction is convenient to implement. We can select two points in the segmentation result (**Figure 9A**) and draw a line between them to create a new membrane. If we want to delete a membrane, we can draw a rectangle on top of the segmentation result and eliminate the membrane inside it. By manual correction, AdipoCount can add missing membrane segments and delete false membrane segments, which results in improved counting accuracy.

TABLE 1 | Cell counting results of 5 test images[a].

Test image	Method	GT	EN	FP	FN	TP	F1-score (%)
Figure 8A	AdipoCount	266	255	5	16	250	96.0
	Adiposoft		169	12	109	157	72.2
Figure 8B	AdipoCount	128	126	6	8	120	94.5
	Adiposoft		116	12	24	104	85.3
Figure 8C	AdipoCount	354	335	6	25	329	95.5
	Adiposoft		302	45	97	257	78.4
Figure 8D	AdipoCount	120	113	5	12	108	92.7
	Adiposoft		90	14	44	76	72.4
Figure 8E	AdipoCount	475	447	25	53	422	91.5
	Adiposoft		209	27	293	182	53.2

[a]*GT, ground-truth manual-counting cell number; EN, estimated number of cells that are segmented by the method; FP, false-positive detection; FN, false-negative detection; TP, true-positive detection.*

TABLE 2 | Computation times of 5 test images[a].

Test Image	Figure 8A	Figure 8B	Figure 8C	Figure 8D	Figure 8E
AdipoCount	4.56 s	2.96 s	8.15 s	5.53 s	6.75 s
Adiposoft	12.26 s	10.56 s	11.13 s	11.83 s	7.15 s

[a]*Hardware: all the experiments were carried out on a PC Intel (R) Core (TM) i7-4790 processor with a clock speed of 3.60 GHz and 8 GB of RAM.*

CONCLUSIONS

Adipose cell counting is an important task in obesity research. Multiple software programs have been developed for biological image processing, such as Fiji, which can aid biologists in manual adipose cell counting. In addition, researchers have developed automatic adipose cell counting tools, such as Adiposoft, which can process images and generate counting results. However, the counting accuracy and usability of these tools need to be improved. We have developed a fully automatic adipose cell counting system, namely, AdipoCount, which contains three modules: a membrane segmentation module, a re-segmentation module and a cell counting module. The membrane segmentation module can segment the membrane, the re-segmentation module can estimate missing dyed membrane areas and improve the segmentation result, and the cell counting module can detect, count and label the cells in the image. Comparing with other automatic adipose cell counting software programs, AdipoCount uses more image attributes, such as color intensity and gradient information, to generate accurate segmentation results and a watershed re-segmentation method is implemented to address missing dyed membrane areas. The segmentation results can be further corrected manually. AdipoCount has been tested on a batch of adipose tissue images with different dyeing qualities and our results show that AdipoCount outperforms existing software and can provide reliable counting results for reference in clinical studies. However, when applying our system on images with low signal-to-noise ratio (SNR) or many missing dyed membrane areas, the counting results have much room for improvement.

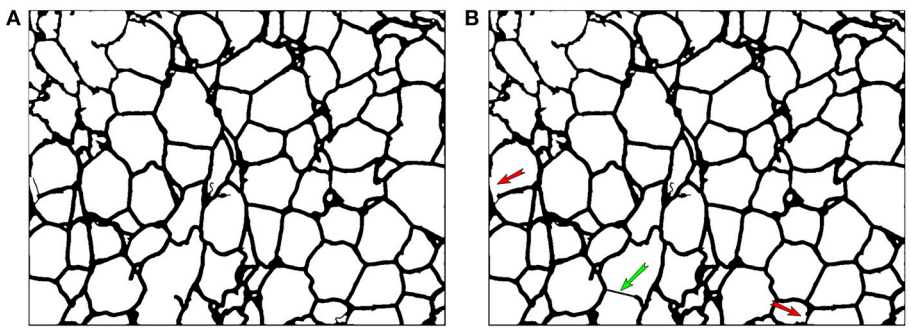

FIGURE 9 | Manual correction of segmentation result. **(A)** The segmentation result before manual correction. **(B)** The manual correction result, where the green arrow shows an added membrane segment, and the red arrows show deleted membrane segments.

In future work, we will add more noise elimination engines, try to improve AdipoCount's robustness and efficiency, and enhance its interactive functions to make it more powerful on challenging images.

AUTHOR CONTRIBUTIONS

XZ, JW, PL, JJ, H-BS, and GN discussed the project idea. XZ and H-BS designed and developed the method. XZ, JW, PL, JJ, and GN discussed and verified the tested data. Under H-BS and GN instructions, XZ did the experiments, and the paper was written by XZ, JW, and H-BS.

ACKNOWLEDGMENTS

This work was supported by the National Natural Science Foundation of China (No. 61671288, 61725302, 91530321, 61603161, 81500351) and the Science and Technology Commission of Shanghai Municipality (No. 16JC1404300, 17JC1403500).

REFERENCES

Adams, R., and Bischof, L. (1994). Seeded region growing. *IEEE Trans. Pattern Anal. Mach. Intell.* 16, 641–647. doi: 10.1109/34.295913

Baecker, V., and Travo, P. (2006). "Cell image analyzer - A visual scripting interface for ImageJ and its usage at the microscopy facility Montpellier RIO Imaging," in *Proceedings of the ImageJ User and Developer Conference*, 105–110.

Beucher, S., and Lantuéjoul, C. (1979). "Use of watersheds in contour detection," in *International Workshop on Image Processing, Real-time Edge and Motion Detection* (Rennes), 391–396.

Björnheden, T., Jakubowicz, B., Levin, M., Odén, B., Edén, S., Sjöström, L., et al. (2004). Computerized determination of adipocyte size. *Obes. Res.* 12, 95–105. doi: 10.1038/oby.2004.13

Canny, J. (1986). A computational approach to edge detection. *IEEE Trans. Pattern Anal. Mach. Intell.* 8, 679–698. doi: 10.1109/TPAMI.1986.4767851

Chen, H. C., and Farese, R. V. (2002). Determination of adipocyte size by computer image analysis. *J. Lipid Res.* 43, 986–989.

Di Rubeto, C., Dempster, A., Khan, S., and Jarra, B. (2000). "Segmentation of blood images using morphological operators," in IEEE *Proceedings 15th International Conference on Pattern Recognition* (Barcelona), 397–400.

Dorini, L. B., Minetto, R., and Leite, N. J. (2007). "White blood cell segmentation using morphological operators and scale-space analysis," in *IEEE XX Brazilian Symposium on Computer Graphics and Image Processing, SIBGRAPI 2007* (IEEE), 294–304.

Galarraga, M., Campión, J., Muñoz-Barrutia, A., Boqué, N., Moreno, H., Martínez, J. A., et al. (2012). Adiposoft: automated software for the analysis of white adipose tissue cellularity in histological sections. *J. Lipid Res.* 53, 2791–2796. doi: 10.1194/jlr.D023788

Han, J. W., Breckon, T. P., Randell, D. A., and Landini, G. (2012). The application of support vector machine classification to detect cell nuclei for automated microscopy. *Mach. Vis. Appl.* 23, 15–24. doi: 10.1007/s00138-010-0275-y

Kothari, S., Chaudry, Q., and Wang, M. D. (2009). "Automated cell counting and cluster segmentation using concavity detection and ellipse fitting techniques," in *IEEE International Symposium on Biomedical Imaging: From Nano to Macro, 2009. ISBI'09* (Boston, MA), 795–798. doi: 10.1109/ISBI.2009.5193169

Landini, G. (2006). Quantitative analysis of the epithelial lining architecture in radicular cysts and odontogenic keratocysts. *Head Face Med.* 2, 1–9. doi: 10.1186/1746-160X-2-4

Leong, F. J., Brady, M., and McGee, J. O. (2003). Correction of uneven illumination (vignetting) in digital microscopy images. *J. Clin. Pathol.* 56, 619–621. doi: 10.1136/jcp.56.8.619

Liao, Q., and Deng, Y. (2002). "An accurate segmentation method for white blood cell images," in *IEEE International Symposium on Biomedical Imaging, 2002. Proceedings. 2002* (Washington, DC), 245–248.

Meijering, E. (2012). Cell segmentation: 50 years down the road [life sciences]. *IEEE Signal Process. Mag.* 29, 140–145. doi: 10.1109/MSP.2012.2204190

Meyer, and Fernand (1994). Topographic distance and watershed lines. *Signal Proces.* 38, 113–125. doi: 10.1016/0165-1684(94)90060-4

Lamprecht, M., R., Sabatini, D. M., and Carpenter, A. E. (2007). CellProfiler: free, versatile software for automated biological image analysis. *BioTechniques* 42, 71–75. doi: 10.2144/000112257

Nath, S. K., Palaniappan, K., and Bunyak, F. (2006). "Cell segmentation using coupled level sets and graph-vertex coloring," in *International Conference on Medical Image Computing and Computer-Assisted Intervention* (Berlin; Heidelberg; Copenhagen: Springer), 101–108.

Osman, O. S., Selway, J. L., KäPczyåSka, M. G. A., Stocker, C. J., OåDowd, J. F., Cawthorne, M. A., et al. (2013). A novel automated image analysis method for accurate adipocyte quantification. *Adipocyte* 2, 160–164. doi: 10.4161/adip.24652

Otsu, N. (1979). A threshold selection method from gray-level histograms. *IEEE Trans. Syst. Man Cybern.* 9, 62–66. doi: 10.1109/TSMC.1979.4310076

Parlee, S. D., Lentz, S. I., Mori, H., and MacDougald, O. A. (2014). Quantifying size and number of adipocytes in adipose tissue. *Meth. Enzymol.* 537, 93–122. doi: 10.1016/B978-0-12-411619-1.00006-9

Refai, H., Li, L., Teague, T. K., and Naukam, R. (2003). "Automatic count of hepatocytes in microscopic images," in *IEEE Proceedings International Conference on Image Processing. ICIP 2003* (Barcelona), II–1101.

Ronneberger, O., Fischer, P., and Brox, T. (2015). "U-net: convolutional networks for biomedical image segmentation," in *International Conference on Medical Image Computing and Computer-Assisted Intervention* (Munich; Cham: Springer), 234–241.

Schindelin, J., Arganda-Carreras, I., Frise, E., Kaynig, V., Longair, M., Pietzsch, T., et al. (2012). Fiji: an open-source platform for biological-image analysis. *Nat. Methods* 9, 676–682. doi: 10.1038/nmeth.2019

Su, H., Yin, Z., Huh, S., and Kanade, T. (2013). Cell segmentation in phase contrast microscopy images via semi-supervised classification over optics-related features. *Med. Image Anal.* 17, 746–765. doi: 10.1016/j.media.2013.04.004

Vincent, L., and Soille, P. (1991). Watersheds in digital spaces: an efficient algorithm based on immersion simulations. *IEEE Trans. Pattern Anal. Mach. Intell.* 13, 583–598. doi: 10.1109/34.87344

Wu, J., Zeng, P., Zhou, Y., and Olivier, C. (2006). "A novel color image segmentation method and its application to white blood cell image analysis," in *Signal Processing, 2006 8th International Conference on: IEEE* (Beijing).

Wu, Q., Merchant, F., and Castleman, K. (2010). *Microscope Image Processing.* Amsterdam; Boston, MA: Academic Press.

Yang, F., Mackey, M., Ianzini, F., Gallardo, G., and Sonka, M. (2005). "Cell segmentation, tracking, and mitosis detection using temporal context," in *Medical Image Computing and Computer-Assisted Intervention–MICCAI 2005* (Berlin; Heidelberg: Springer), 302–309.

Conflict of Interest Statement: The authors declare that the research was conducted in the absence of any commercial or financial relationships that could be construed as a potential conflict of interest.

frontiers in Physiology

ORIGINAL RESEARCH
published: 23 January 2018
doi: 10.3389/fphys.2018.00014

Discovery of Phosphatidic Acid, Phosphatidylcholine, and Phosphatidylserine as Biomarkers for Early Diagnosis of Endometriosis

Jingjie Li[1†], Yue Gao[2†], Lihuan Guan[2], Huizhen Zhang[2], Jiahong Sun[2], Xiao Gong[3], Dongshun Li[2], Pan Chen[4], Zheng Ma[5], Xiaoyan Liang[1], Min Huang[2] and Huichang Bi[2]*

[1] Center of Reproductive Medicine, The Sixth Affiliated Hospital, Sun Yat-sen University, Guangzhou, China, [2] School of Pharmaceutical Sciences, Sun Yat-sen University, Guangzhou, China, [3] School of Public Health, Guangdong Pharmaceutical University, Guangzhou, China, [4] Department of Pharmacy, The First Affiliated Hospital, Sun Yat-sen University, Guangzhou, China, [5] Institute of Population Research, Peking University, Beijing, China

The sensitivity and specificity of clinical diagnostic indicators and non-invasive diagnostic methods for endometriosis at early stage is not optimal. Previous studies demonstrated that abnormal lipid metabolism was involved in the pathological development of endometriosis. Our cross-sectional study included 21 patients with laparoscopically confirmed endometriosis at stage I–II and 20 infertile women who underwent diagnostic laparoscopy combined with hysteroscopy from January 2014 to January 2015. Eutopic endometrium was collected by pipelle endometrial biopsy. Lipid metabolites were quantified by ultra-high performance liquid chromatography coupled with electrospray ionization high-resolution mass spectrometry (UHPLC-ESI-HRMS). Lipid profiles of endometriosis patients at early stage (I–II) was characterized by a decreased concentration of phosphatidylcholine (18:1/22:6), (20:1/14:1), (20:3/20:4), and phosphatidylserine (20:3/23:1) and an increased concentration of phosphatidic acid (25:5/22:6) compared with control. The synthesized predicting strategy with 5 biomarkers has a specificity of 75.0% and a sensitivity of 90.5%. Lipid profile of eutopic endometrium in endometriosis was effectively characterized by UHPLC-ESI-HRMS-based metabolomics. Our study demonstrated the alteration of phosphatidic acid, phosphatidylcholine, phosphatidylserine metabolites in endometriosis and provided potential biomarkers for semi-invasive diagnose of endometriosis at early stage.

Keywords: endometriosis, lipid profiling, UHPLC-ESI-HRMS, eutopic endometrium, early diagnosis

OPEN ACCESS

Edited by:
Dechun Feng,
National Institute on Alcohol Abuse and Alcoholism, United States

Reviewed by:
Jianbo Wan,
University of Macau, China
Grace L. Guo,
Rutgers University, The State University of New Jersey, United States

***Correspondence:**
Huichang Bi
bihchang@mail.sysu.edu.cn

[†]*Co-first authors.*

Specialty section:
This article was submitted to Clinical and Translational Physiology, a section of the journal Frontiers in Physiology

Received: *20 November 2017*
Accepted: *08 January 2018*
Published: *23 January 2018*

Citation:
Li J, Gao Y, Guan L, Zhang H, Sun J, Gong X, Li D, Chen P, Ma Z, Liang X, Huang M and Bi H (2018) Discovery of Phosphatidic Acid, Phosphatidylcholine, and Phosphatidylserine as Biomarkers for Early Diagnosis of Endometriosis. Front. Physiol. 9:14. doi: 10.3389/fphys.2018.00014

INTRODUCTION

The prevalence of endometriosis is estimated as 2–10% in the general female population and up to 40% in women with subfertility (Eskenazi and Warner, 1997; Ozkan et al., 2008; Dunselman et al., 2014), which significantly compromises quality of life in women and adolescents and causes a substantial societal economic burden (Gao et al., 2006; Nnoaham et al., 2011; Soliman et al., 2016). Currently, diagnosis of endometriosis is extremely challengeable due to similar symptoms to other gynecological and gastrointestinal diseases. Since endometriosis at early stage lacks specific imaging features, the reliable way to diagnose endometriosis, especially at early

stage, is surgical laparoscopy. As the common diagnostic indicator, cancer antigen 125 (CA125) has been shown to be more beneficial for diagnosing advanced stages (III–IV) than stages I and II (Hirsch et al., 2016). Therefore, diagnosis of endometriosis is typically delayed up to 8–10 years from the initial appearance of symptoms (Greene et al., 2009; Nnoaham et al., 2011; Hudelist et al., 2012). It is urgent to development novel diagnostic biomarkers and non-invasive methods for endometriosis diagnosis. In this study, we investigated alterations of lipid profile in eutopic endometrium of endometriosis patients at stage I–II by ultra-high performance liquid chromatography coupled with electrospray ionization high-resolution mass spectrometry (UHPLC-ESI-HRMS)-based metabolomics, which provided potential markers for early diagnosis of this disease.

MATERIALS AND METHODS

Study Design and Sample Source

A cross-sectional study was performed on stored samples prospectively collected from women who participated in a previous metabonomic study. Participants were recruited from Reproductive Medicine Research Center, Sixth Hospital of Sun Yat-sen University from June 2014 to January 2015, who underwent diagnostic laparoscopy and hysteroscopy for infertility. This study was approved by institutional review board from sixth Hospital of Sun Yat-sen University, and written informed consent was taken from all participants (approval number: G2012021). All participants had regular menstrual cycles (28 ± 7 days) without hormonal treatment in 3 months prior to sample collection. Women laparoscopic and hysteroscopic diagnosed with endometriosis at stage I–II were further visually confirmed the presence of endometriosis according to American Society of Reproductive Medicine revised system (American Society for Reproductive Medicine, 1997). Patients who were diagnosed as endometriosis by transvaginal ultrasonography or had the history of abnormally increased CA125 previously were excluded from this study. Endometrial polyp, endometritis, submucous myoma, and hydrosalpinx were also excluded. Eutopic endometrium samples were collected by pipelle endometrial biopsy on day 3–5 after the end of menstrual bleeding during laparoscopy and hysteroscopy or within 3 months after surgery.

Sample Preparation for Lipidomics

Endometrial tissues were obtained from 20 infertile women (Control) and 21 women with endometriosis. Lipids extraction was performed according to methyl-tert-butyl ether (MTBE) method (Matyash et al., 2008). 0.01 g endometrium samples were thawed and then homogenized in 200 μL PBS using Precellys 24 homogenizer (Bertin, France). Then 150 μL of homogenate was added to 1.2 mL chilled mixture of methanol/MTBE/water (4:5:5, v/v/v). Samples were incubated on ice for 1 h and vortexed for 1 min every 15 min. Following centrifugation (2,000 rpm, 5 min), 200 μL supernatant of each sample was transferred to new tubes and dried under nitrogen flow at room temperature. Samples were re-suspended in 500 μL mixture of methanol/isopropanol (1:1, v/v) and centrifuged at 18,000 × g for 5 min at 4°C Finally, 2 μL of supernatant was injected for UHPLC-ESI-HRMS (Thermo Scientific, San Jose, CA) analysis. Three microliter of each sample was mixed to be quality control (QC) samples (Zhang et al., 2017).

UHPLC-ESI-HRMS Measurement of Endometrial Tissues

Samples were separated using an Ascentis Express C18 2.7 μm column (100 × 2.1 mm, Sigma-Aldrich, St. Louis, MO) on a Thermo Scientific Dionex Ultimate 3000 UHPLC system. Flow rate was 0.3 mL/min while column temperature was 45°C. The mobile phases consisted of (A) 5% acetonitrile in isopropanol with 10 mM ammonium formate and 0.1% formic acid and (B) 50% water in acetonitrile with 10 mM ammonium formate and 0.1% formic acid. Linear gradient was as follows: 0–0.5 min remaining at 20% A, linearly increasing to 50% A at 7.5 min, then linearly decreasing to 20% A at 10 min, following increasing to 100% A at 20 min, holding at 100% A until 21.9 min, then linearly increasing to 80% B at 22 min and equilibrating until 25 min. Mass spectrometry was performed with a Thermo Scientific Q ExactiveTM benchtop Orbitrap mass spectrometer equipped with heated ESI source in ESI positive and negative modes (Thermo Scientific, San Jose, CA). The main parameters for MS/MS included AGC target 1e5; maximum IT 65 ms; isolation window 1.2 *m/z*; normalized collision energy 25, 35 eV in positive mode and 20, 30, and 40 eV in negative mode; apex trigger 5–10 s; and dynamic exclusion 10.0 s. Ionization conditions were operated at spray voltage 3.5 kV and capillary temperature 300°C (Yu et al., 2016).

Lipidomic Data Processing

The acquired total ion chromatograms (TIC) and mass spectra from UHPLC-ESI-HRMS were exported as raw files by Xcalibur (Thermo Scientific, San Jose, CA). Three-dimensional data set including *m/z*-values, retention times, and peak areas were extracted by LipidSearch software (Thermo Scientific, San Jose, CA) to perform lipids identification and evaluate matching degrees by A, B, C, D four grades. Orthogonal projection to latent structures discriminant analysis (OPLS-DA) in positive and negative modes were carried out by SIMCA-P 13.0 Software (Umetrics, Kinnelon, NJ) to visualize differences of lipid metabolites between endometriosis patients and control. S-plots were generated in OPLS-DA mode and potential markers were selected on the basis of a variable importance in the projection (VIP) with threshold of 1.0 (Dutta et al., 2016). A logistic regression analysis was used to assessing the strength of association between lipid metabolites and minimal-mild endometriosis. The receiver operating characteristic (ROC) curve was plotted and the area under the curve (AUC) was calculated. The optimal point on ROC curve provided the best trade-off between sensitivity and specificity. Shapiro–Wilk test was used to evaluate the normality of distribution, then statistical significance was calculated using Student's *t*-test and non-parametric Mann–Whitney U-test, with $p < 0.05$ as statistical significance level. Statistical test was carried out by SPSS 20.0 software (IBM Analytics, USA).

RESULTS

The endometriosis group was composed of 14 patients at stage I and 7 patients at stage II. None of patients in this group was confirmed with ovarian endometriomas by laparoscopy. The control group consisted of 20 participants. Two groups were balanced in terms of age, BMI, and AMH level (**Table 1**).

A total of 468 ions in positive mode and 253 ions in negative mode were observed. The comparison of TIC can be seen in the mirror plots (**Figure 1**). Multiple differences in peak intensities detected at the same retention time, indicates different lipid spectrums between endometriosis patients and control. OPLS-DA models with acceptable R^2Y and Q^2 revealed a trend of separation between two groups (**Figures 2A,B**), indicating distinct lipid profiles of endometriosis patients. The alteration of lipids was identified by VIP >1.0 and then validated at an univariate level by Student's *t*-test or Mann–Whitney U-test, with $p < 0.05$ set as the level of statistical significance. Lipid identification was performed using LipidSearch software to directly identify lipid species from accurate precursor *m/z* and MS/MS raw data with the reference of large-scale database. As shown in **Figures 2C,D**, PC (18:1/22:6), PC (20:1/14:1), PC (20:3/20:4), PA (25:5/22:6), and PS (20:3/23:1) were selected as potential markers and details were summarized in **Table 2**. Apparently, levels of PC (18:1/22:6), PC (20:1/14:1), PC (20:3/20:4), and PS (20:3/23:1) were significantly decreased in endometriosis group, which have previously been to involve in the progress of endometriosis (Vouk et al., 2016). However, PA (25:5/22:6) level was much higher in endometriosis group compared to control (**Figure 3**), which could be a novel marker of endometriosis and further facilitated to the mechanism studies of the disease. The multivariable regression model for early stage endometriosis included five independent predictors: PC (18:1/22:6), PC (20:1/14:1), PC (20:3/20:4), PS (20:3/23:1), and PA (25:5/22:6). The apparent AUC of ROC curve for the complete model predicting early endometriosis was 0.871 with a sensitivity of 0.905 and specificity of 0.750 (**Figure 4**).

DISCUSSION

Quantitative tracing of lipid metabolism under pathophysiological stimuli, environmental or genetic modifications has been successfully used as a diagnostic tool to monitor disease and develop new treatment strategies. In order to optimize lipidomics system, lipids extraction was performed according to MTBE method in this study. Compared to traditional methods, such as Bligh&Dyer method and Folch method, MTBE method delivers similar or better recoveries and performs better extraction efficiency, especially for PC, TG, and SM. Furthermore, MTBE is noncorrosive and chemically stable without forming peroxides during storage, which presents no danger to degrade labile lipids (Matyash et al., 2008). Previous studies reported alterations of lipid profile in serum, peritoneal fluid, follicular fluid, and endometrium of endometriosis patients (Vouk et al., 2012, 2016; Cordeiro et al., 2015; Chagovets et al., 2017). However, it is has not been investigated the alteration of lipid metabolism in endometrium.

This is the first time to report alterative levels of phosphatidic acid (PA), phosphatidylcholine (PC), and phosphatidylserine (PS) in eutopic endometrium of endometriosis patients at early stage. Instead of peripheral blood or urine, endometrium might contain various information to indicate the presence of endometriosis, using the direct source of the disease is perhaps logical to identify biomarkers for endometriosis (Ahn et al., 2017). Besides, pipelle biopsy is minimally invasive and suitable for outpatient. Hence, eutopic endometrium is ideal to analyze lipid profile of endometriosis for identifying potential biomarkers. We collected samples strictly on day 3–5 after menstrual cessation, which ensured all samples obtained in early follicle phase. The time to collect samples was chosen according to hysteroscopic surgical requirements and patient compliance. Unfortunately, we did not collect enough data on patients with advanced endometriosis because few patients in stage III–IV in our center met the inclusion criteria (exposure to hormonal drugs within 3 months).

In this study, we observed PA (25:5/22:6) was significantly higher in endometriosis patients compared to control group. It is the first to report PA is involved in the pathophysiology of endometriosis. PA is a phospholipid consisting out of a glycerol backbone with two fatty acids and one phosphate group attached, which is a central intermediate for the synthesis and storage of membrane lipids (Castro-Gomez et al., 2015). It has been implicated in various cellular signaling pathways, including in cell growth, proliferation, cell motility, and reactive oxygen species (ROS) production (Wang et al., 2006). PA has not only been shown to exert anti-apoptotic effects (Wang et al., 2006), but also has been identified as a mitogenic activator of the mammalian target of rapamycin signaling pathway to promote cell proliferation and generate survival signals (Chen, 2004), which might contribute to active proliferative capacity of endometriosis. Moreover, PA is related to cell motility (O'Luanaigh et al., 2002; Su et al., 2006), which may promote endometrium migration and invasion. PA is also responsible for the production of ROS via activating NADPH oxidase (Palicz et al., 2001). Excessive release of ROS plays an essential role in the inflammation process, which is involved in the pathogenesis of endometriosis by inducing endometrial fragment adhesion, proliferation, and neovascularization (Donnez et al., 2016). In addition, previous evidences suggested prostaglandin

TABLE 1 | Characteristics of participant.

	Endometriosis patients ($n = 21$)	Control group ($n = 20$)	*P*
Age (years)	29.71 ± 3.117	30.45 ± 3.034	0.4487
BMI (kg/m^2)	20.76 ± 1.716	21.24 ± 2.882	0.5198
AMH (ng/ml)	4.417 ± 2.990	6.117 ± 5.079	0.2189
Endometriosis stage			
I stage	14	N/A	
II stage	7	N/A	
Ovarian endometriomas	N/A	N/A	

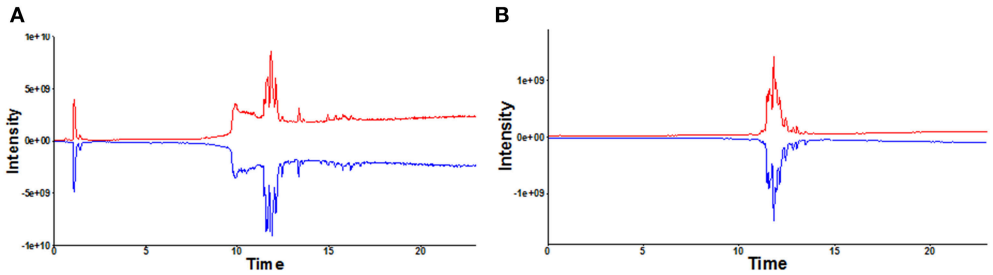

FIGURE 1 | Mirror plot of representative total ion chromatograms (TIC) under positive **(A)** and negative mode **(B)**. TIC in red: healthy controls; TIC in blue: endometriosis patients.

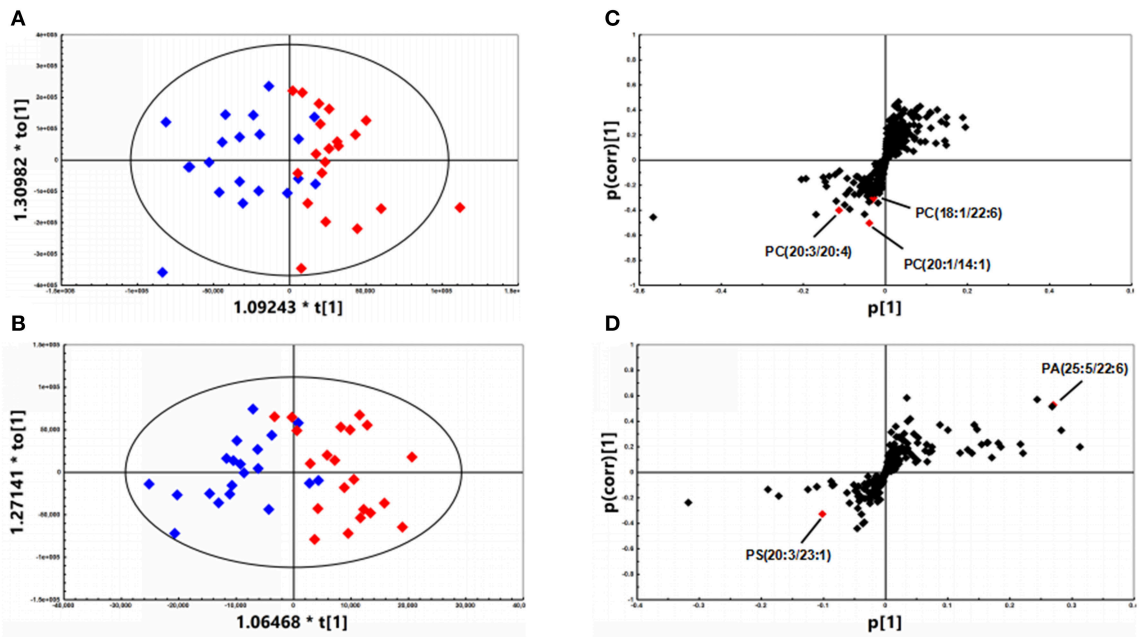

FIGURE 2 | OPLS-DA plots of patients with endometriosis ($n = 21$, *red diamonds*) and healthy controls ($n = 20$, *blue diamonds*) under **(A)** positive ($R^2Y = 0.712$; $Q^2 = 0.412$) mode and **(B)** negative ($R^2Y = 0.728$; $Q^2 = 0.602$) mode. **(C)** S-plot under positive mode with selected PCs highlighted in red. **(D)** S-plot under negative mode with selected PE and PA highlighted in red.

TABLE 2 | Detailed information of significantly changed lipids between endometriosis patients and healthy controls.

Lipid molecular	Molecular formula	Adduct	*m/z*	t_R (min)	*P*-values	VIP-values	Fold change
POSITIVE MODE							
PC(18:1/22:6)	$C_{48}H_8O_8N_1P_1$	M+H	832.5815	11.7155	0.012	1.1382	1.1120
PC(20:1/14:1)	$C_{42}H_{80}O_8N_1P_1$	M+H	758.5690	12.7660	0.005	1.0215	1.6466
PC(20:3/20:4)	$C_{48}H_{82}O_8N_1P_1$	M+H	832.5851	11.4469	0.03	2.8718	1.4716
NEGATIVE MODE							
PA(25:5/22:6)	$C_{50}H_{77}O_8P_1$	M–H	835.5275	11.9538	0.037	3.7783	1.6479
PS(20:3/23:1)	$C_{49}H_{88}O_{10}N_1P_1$	M–H	880.6049	11.7765	0.028	2.1203	1.2424

E2 (PGE2) and cyclooxygenase-2 (COX-2) in pathophysiology and pathogenesis of endometriosis (Wu et al., 2007; Banu et al., 2008; Machado et al., 2010). Lysophosphatidic acid (LPA) signaling stimulates PGE2 production and COX-2 expression in endometrial cells (Lin et al., 2008; Woclawek-Potocka et al., 2009). LPA is considered as potential factor for endometriosis (Ye and Chun, 2010), which is as the main source of PA. In this study, no significant difference of LPA was detected in endometrium.

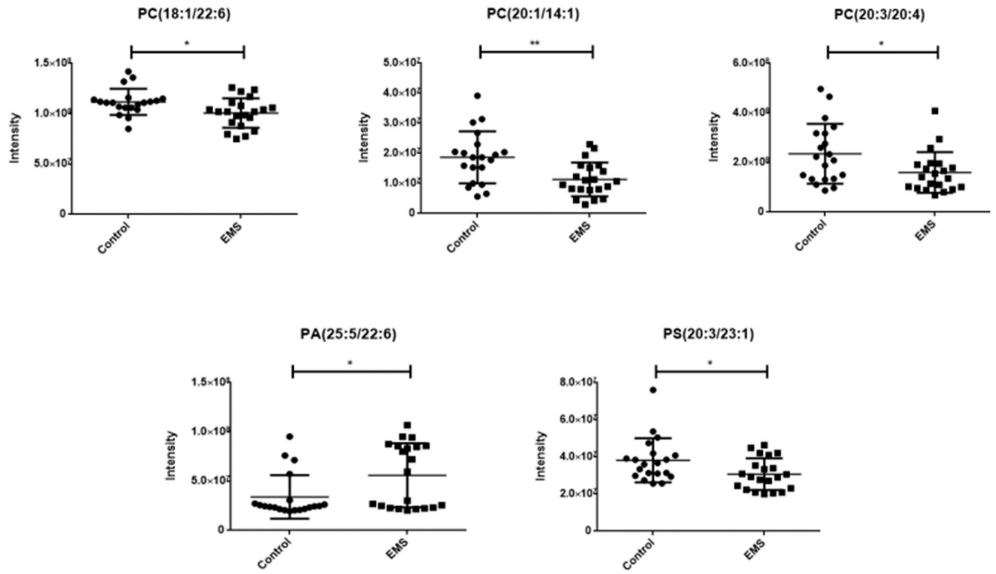

FIGURE 3 | Scatter diagram of five selected lipids. PCs and PS in endometriosis patients were significant decreased compared to healthy controls, while PA in endometriosis patients was higher than healthy controls. Data are expressed as mean ± SD. $^{*}p < 0.05$, $^{**}p < 0.01$, endometriosis patients (EMS, $n = 21$) vs. healthy controls (Control, $n = 20$).

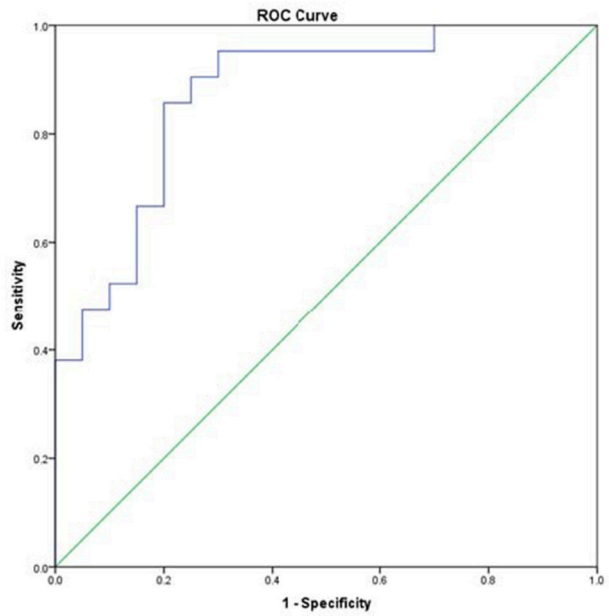

FIGURE 4 | Receiver operating characteristic curves for endometriosis at minimal-mild stage.

We speculated that PA alteration occurs earlier compared to LPA in the development of endometriosis, which might be used as a novel predictor of endometriosis at early stage.

Eutopic endometrium contributed to pathogenesis of endometriosis due to the increase of proliferation, migration, and invasion of ectopic endometrium (Joshi et al., 2015; Laudanski et al., 2015). We detected PS (20:3/23:1) decreased significantly in endometriosis group in this study. Only one study mentioned PS level was observed lower in follicular fluid in endometriosis patients previously (Cordeiro et al., 2015). Phospholipids are maintained asymmetrically in the eukaryotic plasma membrane in health cells. PS exposure on the cell surface shows an apoptotic signal for phagocytes (Segawa and Nagata, 2015; Nagata et al., 2016). Lower PS (20:3/23:1) levels may be due to reduced endometrial apoptotic cells in endometriosis patients. Three unsaturated PC (20:3/20:4), PC (18:1/22:6), PC (20:1/14:1) were significantly decreased in eutopic endometrium of endometriosis patients. Our results are consistent with previous studies (Vouk et al., 2012, 2016; Cordeiro et al., 2015). PC is one of the major sources of polyunsaturated fatty acids, that are the precursors of eicosanoids and has numerous biological activities (van der Veen et al., 2017). Evidence has accrued that PC contribute to both proliferative growth and programmed cell death (Ridgway, 2013). PC synthesis is increased in response to fatty acid and fatty acid-derived substrates, which is frequently observed in cancer cells (Ridgway, 2013). Unlike malignancy, PC markedly decreased in endometrium in endometriosis. This difference can be used to distinguish between endometriosis and malignancy. PC serves as a source for sphingomyelins and production of prostaglandins that may lead to decreased PC levels in endometrial tissue in this study. Sphingomyelins are abundant in endometriosis, which promotes cell survival in response to apoptotic stimuli (Vouk et al., 2012). Prostaglandins mediate inflammation in pathophysiology of endometriosis (Banu et al., 2008). Meanwhile, PC itself is also closely related to inflammation process (Drobnik et al., 2003; Ganna et al., 2014). Thus, PC has been correlated as a potential biomarker for endometriosis.

CONCLUSION

This is the first report that PA, PC, and PS alterations in eutopic endometrium of endometriosis at stage I–II by UHPLC-ESI-HRMS-based metabolomics. These findings provide potential biomarkers for semi-invasive diagnose of endometriosis at early stages in clinical practice. However, a large sample size study on endometriosis lipidolomics analysis is needed to validate the implications of these individual lipids in the pathophysiology of endometriosis. Our findings also provide potential targets for therapeutic approach of this disease.

AUTHOR CONTRIBUTIONS

JL: conceived of study, wrote the manuscript and supervised patient recruitment. YG, LG, HZ and DL: contributed to the study execution, analysis, and interpretation of data. XG: performed data analysis and interpretation. JS and PC: reviewed manuscript. HB, MH, ZM and XL: supervised patient recruitment, data collection, data evaluation, drafting, editing, and approving the final version of this paper for submission.

ACKNOWLEDGMENTS

This study was financially supported by the National Natural Science Foundation of China (No. 81601347, 81503156, 81320108027), Natural Science Foundation of Guangdong Province (No. 2014A030310096), and Public Welfare Research and Capacity Building Fund of Guangdong (No. 2016A020218006).

REFERENCES

Ahn, S. H., Singh, V., and Tayade, C. (2017). Biomarkers in endometriosis: challenges and opportunities. *Fertil. Steril.* 107, 523–532. doi: 10.1016/j.fertnstert.2017.01.009

American Society for Reproductive Medicine (1997). Revised American Society for Reproductive Medicine classification of endometriosis: 1996. *Fertil. Steril.* 67, 817–821.

Banu, S. K., Lee, J., Speights, V. O. Jr., Starzinski-Powitz, A., and Arosh, J. A. (2008). Cyclooxygenase-2 regulates survival, migration, and invasion of human endometriotic cells through multiple mechanisms. *Endocrinology* 149, 1180–1189. doi: 10.1210/en.2007-1168

Castro-Gomez, P., Garcia-Serrano, A., Visioli, F., and Fontecha, J. (2015). Relevance of dietary glycerophospholipids and sphingolipids to human health. *Prostaglandins Leukot. Essent. Fatty Acids* 101, 41–51. doi: 10.1016/j.plefa.2015.07.004

Chagovets, V. V., Wang, Z., Kononikhin, A. S., Starodubtseva, N. L., Borisova, A., Salimova, D., et al. (2017). Endometriosis foci differentiation by rapid lipid profiling using tissue spray ionization and high resolution mass spectrometry. *Sci. Rep.* 7, 2546. doi: 10.1038/s41598-017-02708-x

Chen, J. (2004). Novel regulatory mechanisms of mTOR signaling. *Curr. Top. Microbiol. Immunol.* 279, 245–257. doi: 10.1007/978-3-642-18930-2_14

Cordeiro, F. B., Cataldi, T. R., Perkel, K. J., do Vale Teixeira da Costa, L., Rochetti, R. C., Stevanato, J., et al. (2015). Lipidomics analysis of follicular fluid by ESI-MS reveals potential biomarkers for ovarian endometriosis. *J. Assist. Reprod. Genet.* 32, 1817–1825. doi: 10.1007/s10815-015-0592-1

Donnez, J., Binda, M. M., Donnez, O., and Dolmans, M. M. (2016). Oxidative stress in the pelvic cavity and its role in the pathogenesis of endometriosis. *Fertil. Steril.* 106, 1011–1017. doi: 10.1016/j.fertnstert.2016.07.1075

Drobnik, W., Liebisch, G., Audebert, F. X., Frohlich, D., Gluck, T., Vogel, P., et al. (2003). Plasma ceramide and lysophosphatidylcholine inversely correlate with mortality in sepsis patients. *J. Lipid Res.* 44, 754–761. doi: 10.1194/jlr.M200401-JLR200

Dunselman, G. A., Vermeulen, N., Becker, C., Calhaz-Jorge, C., D'Hooghe, T., De Bie, B., et al. (2014). ESHRE guideline: management of women with endometriosis. *Hum. Reprod.* 29, 400–412. doi: 10.1093/humrep/det457

Dutta, M., Anitha, M., Smith, P. B., Chiaro, C. R., Maan, M., Chaudhury, K., et al. (2016). Metabolomics reveals altered lipid metabolism in a mouse model of endometriosis. *J. Proteome Res.* 15, 2626–2633. doi: 10.1021/acs.jproteome.6b00197

Eskenazi, B., and Warner, M. L. (1997). Epidemiology of endometriosis. *Obstet. Gynecol. Clin. North Am.* 24, 235–258. doi: 10.1016/S0889-8545(05)70302-8

Ganna, A., Salihovic, S., Sundstrom, J., Broeckling, C. D., Hedman, A. K., Magnusson, P. K., et al. (2014). Large-scale metabolomic profiling identifies novel biomarkers for incident coronary heart disease. *PLoS Genet.* 10:e1004801. doi: 10.1371/journal.pgen.1004801

Gao, X., Outley, J., Botteman, M., Spalding, J., Simon, J. A., and Pashos, C. L. (2006). Economic burden of endometriosis. *Fertil. Steril.* 86, 1561–1572. doi: 10.1016/j.fertnstert.2006.06.015

Greene, R., Stratton, P., Cleary, S. D., Ballweg, M. L., and Sinaii, N. (2009). Diagnostic experience among 4,334 women reporting surgically diagnosed endometriosis. *Fertil. Steril.* 91, 32–39. doi: 10.1016/j.fertnstert.2007.11.020

Hirsch, M., Duffy, J., Davis, C. J., Nieves Plana, M., Khan, K. S., International Collaboration to Harmonise, O., et al. (2016). Diagnostic accuracy of cancer antigen 125 for endometriosis: a systematic review and meta-analysis. *BJOG* 123, 1761–1768. doi: 10.1111/1471-0528.14055

Hudelist, G., Fritzer, N., Thomas, A., Niehues, C., Oppelt, P., Haas, D., et al. (2012). Diagnostic delay for endometriosis in Austria and Germany: causes and possible consequences. *Hum. Reprod.* 27, 3412–3416. doi: 10.1093/humrep/des316

Joshi, N. R., Su, R. W., Chandramouli, G. V., Khoo, S. K., Jeong, J. W., Young, S. L., et al. (2015). Altered expression of microRNA-451 in eutopic endometrium of baboons (*Papio anubis*) with endometriosis. *Hum. Reprod.* 30, 2881–2891. doi: 10.1093/humrep/dev229

Laudanski, P., Charkiewicz, R., Tolwinska, A., Szamatowicz, J., Charkiewicz, A., and Niklinski, J. (2015). Profiling of selected microRNAs in proliferative eutopic endometrium of women with ovarian endometriosis. *Biomed. Res. Int.* 2015:760698. doi: 10.1155/2015/760698

Lin, C. I., Chen, C. N., Huang, M. T., Lee, S. J., Lin, C. H., Chang, C. C., et al. (2008). Lysophosphatidic acid upregulates vascular endothelial growth factor-C and tube formation in human endothelial cells through LPA(1/3), COX-2, and NF-kappaB activation- and EGFR transactivation-dependent mechanisms. *Cell. Signal.* 20, 1804–1814. doi: 10.1016/j.cellsig.2008.06.008

Machado, D. E., Berardo, P. T., Landgraf, R. G., Fernandes, P. D., Palmero, C., Alves, L. M., et al. (2010). A selective cyclooxygenase-2 inhibitor suppresses the growth of endometriosis with an antiangiogenic effect in a rat model. *Fertil. Steril.* 93, 2674–2679. doi: 10.1016/j.fertnstert.2009.11.037

Matyash, V., Liebisch, G., Kurzchalia, T. V., Shevchenko, A., and Schwudke, D. (2008). Lipid extraction by methyl-tert-butyl ether for high-throughput lipidomics. *J. Lipid Res.* 49, 1137–1146. doi: 10.1194/jlr.D700041-JLR200

Nagata, S., Suzuki, J., Segawa, K., and Fujii, T. (2016). Exposure of phosphatidylserine on the cell surface. *Cell Death Differ.* 23, 952–961. doi: 10.1038/cdd.2016.7

Nnoaham, K. E., Hummelshoj, L., Webster, P., d'Hooghe, T., de Cicco Nardone, F., de Cicco Nardone, C., et al. (2011). Impact of endometriosis on quality of life and work productivity: a multicenter study across ten countries. *Fertil. Steril.* 96, 366–373 e368. doi: 10.1016/j.fertnstert.2011.05.090

O'Luanaigh, N., Pardo, R., Fensome, A., Allen-Baume, V., Jones, D., Holt, M. R., et al. (2002). Continual production of phosphatidic acid by phospholipase D is essential for antigen-stimulated membrane ruffling in cultured mast cells. *Mol. Biol. Cell* 13, 3730–3746. doi: 10.1091/mbc.E02-04-0213

Ozkan, S., Murk, W., and Arici, A. (2008). Endometriosis and infertility: epidemiology and evidence-based treatments. *Ann. N. Y. Acad. Sci.* 1127, 92–100. doi: 10.1196/annals.1434.007

Palicz, A., Foubert, T. R., Jesaitis, A. J., Marodi, L., and McPhail, L. C. (2001). Phosphatidic acid and diacylglycerol directly activate NADPH oxidase by interacting with enzyme components. *J. Biol. Chem.* 276, 3090–3097. doi: 10.1074/jbc.M007759200

Ridgway, N. D. (2013). The role of phosphatidylcholine and choline metabolites to cell proliferation and survival. *Crit. Rev. Biochem. Mol. Biol.* 48, 20–38. doi: 10.3109/10409238.2012.735643

Segawa, K., and Nagata, S. (2015). An apoptotic 'Eat Me' signal: phosphatidylserine exposure. *Trends Cell Biol.* 25, 639–650. doi: 10.1016/j.tcb.2015.08.003

Soliman, A. M., Yang, H., Du, E. X., Kelley, C., and Winkel, C. (2016). The direct and indirect costs associated with endometriosis: a systematic literature review. *Hum. Reprod.* 31, 712–722. doi: 10.1093/humrep/dev335

Su, W., Chardin, P., Yamazaki, M., Kanaho, Y., and Du, G. (2006). RhoA-mediated phospholipase D1 signaling is not required for the formation of stress fibers and focal adhesions. *Cell. Signal.* 18, 469–478. doi: 10.1016/j.cellsig.2005.05.027

van der Veen, J. N., Kennelly, J. P., Wan, S., Vance, J. E., Vance, D. E., and Jacobs, R. L. (2017). The critical role of phosphatidylcholine and phosphatidylethanolamine metabolism in health and disease. *Biochim Biophys Acta* 1859(9 Pt B), 1558–1572. doi: 10.1016/j.bbamem.2017.04.006

Vouk, K., Hevir, N., Ribic-Pucelj, M., Haarpaintner, G., Scherb, H., Osredkar, J., et al. (2012). Discovery of phosphatidylcholines and sphingomyelins as biomarkers for ovarian endometriosis. *Hum. Reprod.* 27, 2955–2965. doi: 10.1093/humrep/des152

Vouk, K., Ribic-Pucelj, M., Adamski, J., and Rizner, T. L. (2016). Altered levels of acylcarnitines, phosphatidylcholines, and sphingomyelins in peritoneal fluid from ovarian endometriosis patients. *J. Steroid Biochem. Mol. Biol.* 159, 60–69. doi: 10.1016/j.jsbmb.2016.02.023

Wang, X., Devaiah, S. P., Zhang, W., and Welti, R. (2006). Signaling functions of phosphatidic acid. *Prog. Lipid Res.* 45, 250–278. doi: 10.1016/j.plipres.2006.01.005

Woclawek-Potocka, I., Kondraciuk, K., and Skarzynski, D. J. (2009). Lysophosphatidic acid stimulates prostaglandin E2 production in cultured stromal endometrial cells through LPA1 receptor. *Exp. Biol. Med.* 234, 986–993. doi: 10.3181/0901-RM-36

Wu, M. H., Shoji, Y., Chuang, P. C., and Tsai, S. J. (2007). Endometriosis: disease pathophysiology and the role of prostaglandins. *Expert Rev. Mol. Med.* 9, 1–20. doi: 10.1017/S146239940700021X

Ye, X., and Chun, J. (2010). Lysophosphatidic acid (LPA) signaling in vertebrate reproduction. *Trends Endocrinol. Metab.* 21, 17–24. doi: 10.1016/j.tem.2009.08.003

Yu, T., Wang, Y., Zhang, H., Johnson, C. H., Jiang, Y., Li, X., et al. (2016). Metabolomics reveals mycoplasma contamination interferes with the metabolism of PANC-1 cells. *Anal. Bioanal. Chem.* 408, 4267–4273. doi: 10.1007/s00216-016-9525-9

Zhang, H., Gao, Y., Sun, J., Fan, S., Yao, X., Ran, X., et al. (2017). Optimization of lipid extraction and analytical protocols for UHPLC-ESI-HRMS-based lipidomic analysis of adherent mammalian cancer cells. *Anal. Bioanal. Chem.* 409, 5349–5358. doi: 10.1007/s00216-017-0483-7

Conflict of Interest Statement: The authors declare that the research was conducted in the absence of any commercial or financial relationships that could be construed as a potential conflict of interest.

frontiers in Physiology

ORIGINAL RESEARCH
published: 23 January 2018
doi: 10.3389/fphys.2018.00015

Astragaloside IV Inhibits Adipose Lipolysis and Reduces Hepatic Glucose Production *via* Akt Dependent PDE3B Expression in HFD-Fed Mice

Qun Du[1], *Shuihong Zhang*[2], *Aiyun Li*[3], *Imran S. Mohammad*[4], *Baolin Liu*[2] *and Yanwu Li*[1]*

[1] *Pi-Wei Institute, Guangzhou University of Chinese Medicine, Guangzhou, China,* [2] *Jiangsu Key Laboratory of TCM Evaluation and Translational Research, Department of Pharmacology of Chinese Materia Medica, China Pharmaceutical University, Nanjing, China,* [3] *Experiment Center for Science and Technology, Shanghai University of Traditional Chinese Medicine, Shanghai, China,* [4] *Department of Pharmaceutics, China Pharmaceutical University, Nanjing, China*

Objective: This study aims to investigate the effect of astragaloside IV on adipose lipolysis and hepatic gluconeogenesis.

Methods: High-fat diet (HFD) feeding induced adipose dysfunction with enhanced endogenous glucose production in mice. The effects of Astragaloside IV on lipolysis and hepatic glucose production were investigated.

Results: HFD feeding induced cAMP accumulation through reducing PDE3B expression and activity in adipose tissue. As a result, HFD feeding increased adipose lipolysis in mice. Astragaloside IV enhanced Akt phosphorylation and promoted Akt binding to PDE3B to preserve PDE3B content, resultantly reducing adipose cAMP accumulation. Knockdown of Akt1/2 diminished the effect of astragaloside IV on PDE3B induction, indicative of the role of Akt in astragaloside IV action. As a result from blocking of cAMP/PKA signaling, astragaloside IV suppressed hormone-sensitive lipase (HSL) activation and inhibited inflammation-associated adipose lipolysis. Moreover, astragaloside IV reduced ectopic fat deposition in the liver and inhibited FoxO1 activation *via* regulation of Akt, resultantly restraining excess hepatic glucose production.

Conclusion: We showed that preserving PDE3B content by Akt is a key regulation to prevent lipolysis. Astragaloside IV inhibited lipolysis by reducing cAMP accumulation *via* regulation of Akt/PDE3B, contributing to limiting hepatic lipid deposition and restraining excessive hepatic glucose production.

Keywords: astragaloside IV, Akt, PDE3B, lipolysis, gluconeogenesis

OPEN ACCESS

Edited by:
Xinran Ma,
East China Normal University, China

Reviewed by:
Bin-Nan Wu,
Kaohsiung Medical University, Taiwan
Yu-Chiang Lai,
University of Dundee, United Kingdom

***Correspondence:**
Yanwu Li
liyanwu@gzucm.edu.cn

Specialty section:
This article was submitted to Clinical and Translational Physiology, a section of the journal Frontiers in Physiology

Received: *26 October 2017*
Accepted: *08 January 2018*
Published: *23 January 2018*

Citation:
Du Q, Zhang S, Li A, Mohammad IS, Liu B and Li Y (2018) Astragaloside IV Inhibits Adipose Lipolysis and Reduces Hepatic Glucose Production via Akt Dependent PDE3B Expression in HFD-Fed Mice. Front. Physiol. 9:15. doi: 10.3389/fphys.2018.00015

INTRODUCTION

In obesity, the adipose tissue frequently represents inflammation, endoplasmic reticulum (ER) stress and dysregulation of adipokine expression, which contribute to diabetes and insulin resistance through various mechanisms (Yuan et al., 2001; Greenberg and Obin, 2006; Wang et al., 2016). Adipose tissue serves as a site for fat storage, where fatty acids stored as triacylglycerols in

adipocytes, constitute the primary energy reserves. Meanwhile, the stored triacylglycerols could be hydrolyzed by lipases, such as adipose triglyceride lipase (ATGL) and HSL, leading to the release of glycerol and free fatty acids (FFAs). The increased free FFAs flux from adipose tissue to non-adipose tissue promotes ectopic fat deposits and increases lipid accumulation in liver and skeletal muscle, leading to insulin resistance (Perry et al., 2015; Ritter et al., 2015; Wang et al., 2016). Dysregulation of adipose lipolysis increases the release of FFAs into the circulation, and consistent with this, elevated levels of circulating FFAs are often observed in individuals subjected to insulin resistance and diabetes (Coppack et al., 1992).

It was noted that, the several hormones and effectors can induce lipolysis in adipose tissue by the activation of cAMP-dependent protein kinase A (PKA). As a second messenger for cellular responses, cAMP is formatted by adenylate cyclase and constantly degraded by phosphodiesterase (PDEs). In response to cAMP accumulation, PKA activation initiates lipolysis cascade through activation of HSL and perilipin, which break triglycerides (TGs), resulting in the release of glycerol and FFAs (Belfrage et al., 1980; Strålfors and Belfrage, 1983). As cAMP signaling is located at the upstream of lipolysis cascades, the regulation of cAMP is a key determinant in the control of the downstream lipolysis process. PDEs are the enzymes that degrade cAMP or cGMP by breaking the phosphodiester bond and PDE3B is proposed to be the predominant isoform of PDEs in adipose tissue, capable of cAMP degradation (Nilsson et al., 2006; Degerman et al., 2011). Insulin inhibits lipolysis and regulation of PDE3B is a key step in its action (Kitamura et al., 1999; Frühbeck et al., 2014). In contrast, proinflammatory cytokine TNF-α increases cAMP accumulation by suppression of PDE3B, and thus induces lipolysis (Rahn Landström et al., 2000; Zhang et al., 2002), indicative of the involvement of inflammation in lipolysis.

Astragaloside IV is a saponin and main active component in the medicinal plant *Astragalus membranaceus*, which widely used in traditional Chinese medicine for the treatment of metabolic disorders. Astragaloside IV exerts anti-diabetic effects (Lv et al., 2010), improves metabolic parameters in fructose-fed mice and ameliorates adipose dysfunction (Jiang et al., 2008; Zhang et al., 2011), well-demonstrating its action in the improvement of metabolism. It is generally accepted that insulin inhibits lipolysis through PI3K/Akt signaling (Kitamura et al., 1999). However, this knowledge has been challenged by recent published studies, which showed that Akt is dispensable for insulin to suppress lipolysis (Frühbeck et al., 2014; Koren et al., 2015). Similarly, Akt is also proposed to be dispensable for insulin to suppress hepatic gluconeogenesis (Lu et al., 2012; Titchenell et al., 2015). These findings raise question whether pharmacological activation of Akt could inhibit adipose lipolysis and hepatic glucose production is independent on insulin. Astragaloside IV protects cardiac function through regulation of PI3K/Akt and Akt/GSK-3β signaling, indicative of its positive effect on Akt activation (He et al., 2012; Jia et al., 2014). Therefore, it is tempting to know if astragaloside IV could inhibit adipose lipolysis *via* regulation of Akt. To address this issue, we investigated the effect of astragaloside IV on lipolysis in the adipose tissue of high-fat diet (HFD)-fed mice and found that astragaloside IV could inhibit lipolysis by reducing cAMP accumulation *via* regulation of Akt/PDE3B, contributing to limiting hepatic lipid deposition and restraining excessive hepatic glucose production. This finding provides novel mechanistic insights regarding the protective effects of astragaloside IV on metabolic homeostasis and contributes to the design of new strategies for the management of metabolic diseases.

MATERIALS AND METHODS

Materials

Astragaloside IV (purity ≥ 98%) was obtained from Shanghai Forever Biotech Co., Ltd. (Shanghai, China). Astragaloside IV was dissolved in DMSO to prepare 10 mM stock solution and then was diluted at 1,000-fold in culture medium to generate a working concentration at 10 μM. 0.1% DMSO as a solvent control was run concurrently with the experiments. Palmitate (PA, Sinopharm, Shanghai, China) was dissolved in ethanol to prepare 200 mM stock solution and then further diluted with medium containing 10% FFA-free BSA at the ratio of 1:19 to obtain a concentration of 10 mM before use. Metformin was obtained from Sino-American Shanghai Squibb Pharma (Shanghai, China). Akt inhibitor triciribine, MK2206 and AZD5363 was from Apex Bio (Houston, USA). Isoproterenol was from Shanghai Harvest Pharmaceutical Co., Ltd. (Shanghai, China). TNF-α was from R&D Systems.

Animals

Male ICR mice (6–8 weeks of age) were purchased from the Laboratory Animal Center of Nanjing Qinglongshan and were acclimatized in facility with a constant temperature (22 ± 1°C) and a 12-h light-dark cycle with free access to water and food. All experiments were approved by Animal Ethics Committee of China Pharmaceutical University.

Mice were fed with normal chow diet or HFD containing 10% lard, 10% yolk, 1% cholesterol, 0.2% cholate, and 78.8% standard diet simultaneously with oral administration of astragaloside IV (50, 100 mg/kg) or metformin (200 mg/kg) daily for 2 weeks. While, control mice were received the vehicle only. Mice body weight and food intake were measured and recorded daily. Two weeks later, after 12 h fasting, blood samples were collected from orbital sinus to examine total cholesterol (TC), TG, glucose, FFAs, and glycerol concentrations in the serum using commercial kits. Meanwhile, the epididymis adipose tissue was rapidly isolated and stored at −80°C for further assay.

Cell Culture

3T3-L1 cells (a cell line of preadipocytes, Cell Bank of Chinese Academy of Sciences, Shanghai, China) were grown in Dulbecco's Minimum Essential Medium (DMEM, Gibco, USA) containing 10% FBS, 100 μg/mL of streptomycin and 100 U/mL of penicillin. At 80–90% of confluence, the culture medium were replaced with fresh DMEM supplemented with 10% FBS, isobutylmethylxanthine (0.5 M), dexamethasone (1 μM), and insulin (10 μg/mL) for next 48 h. Then, change the medium with

DMEM containing 10% FBS and insulin (10 μg/mL) for another 8–10 days for differentiation.

Measurement of Glycerol and FFAs Release

The normal mice or the HFD-fed mice were sacrificed by cervical dislocation. The epididymal adipose tissue was isolated and chopped into small pieces immediately. After incubation in DMEM for 24 h, FFAs and glycerol concentrations in the medium were determined by commercial kits (Jiancheng Bioengineering Institute, Nanjing, China). The contents of FFAs and glycerol in the serum were also determined with the commercial kits (Jiancheng Bioengineering Institute, Nanjing, China) according to the manufacturers' instructions. For isoproterenol or TNF-α stimulation, the epididymis adipose tissue of normal mice was stimulated with isoproterenol (1 μM) or TNF-α (20 ng/mL) for 2 or 16 h, respectively, in the presence of indicated agents.

Determination of cAMP, AMP, and Cytokines in the Adipose Tissue

Adipose tissue were rinsed and homogenized in cold lysis buffer to prepare 10% adipose homogenate. After centrifuged at 12,000 g for 15 min at 4°C, the supernatant was collected to measure the concentration of cAMP (USCN, Wuhan, China) and AMP (Chengbin Biotech, Shanghai, China) using the corresponding commercial assay kits, while TNF-α and IL-6 contents were measured using ELISA Kits (Cusabio Biotech, Wuhan, China), respectively. For isoproterenol treatment, the isolated adipose tissue of normal mice was incubated with isoproterenol (1 μM) for 2 h in the presence of indicated agents.

Measurement of PDE Activity in Adipose Tissue

Epididymis adipose tissue was isolated from HFD-fed mice and homogenized in double-distilled water. The supernatant was desalted by gel filtration and then measured using a PDE activity assay kit (Colorimetric) (ab139460; Abcam, Cambridge, MA).

Determination of Hepatic Triglyceride and Acetyl CoA

The liver was isolated from HFD-fed mice and homogenized in ice-cold RIPA lysis buffer. The homogenates were then centrifuged and the supernatants was collected for the detection of TG and acetyl CoA concentrations using commercial kits (Shuojia, Shanghai, China) according to the manufacturer's instructions.

Glucose and Pyruvate Tolerance Tests

For pyruvate or glucagon tolerance test, fasted HFD-fed mice were treated with oral administration of astragaloside IV (50, 100 mg/kg) or metformin (200 mg/kg). Then after 2 h, mice were intraperitoneally injected with pyruvate (2 g/kg) for pyruvate tolerance test, or orally administrated with glucose (2.0 g/kg) for glucose tolerance test. Blood samples were collected from the orbital sinus at regular intervals for the assay of glucose using a commercial Kit. Blood glucose area under curve (AUC) was calculated as the follows: $0.5 \times [Bg0 + Bg0.5]/2 + 0.5 \times [Bg0.5 + Bg1.0]/2 + [Bg1 + Bg2]/2$ (Bg0, Bg0.5, Bg1.0, and Bg2.0 referred to the blood glucose content at 0, 0.5, 1.0, and 2.0 h).

Hepatic Glucose Production

The fasted mice (over 18 h) were sacrificed by cervical dislocation and liver was perfused in situ with Hank's Balanced Salt Solution, followed by digestion with collagenase IV. The collected hepatocytes were resuspended and cultured for further treatment in DMEM supplemented with 10% FBS and incubated at 37°C in an atmosphere of 5% CO_2. For glucose production, hepatocytes were pretreated with indicated treatment and cultured in glucose-free media supplemented with 10 mM pyruvate for 6 h. Then the Glucose contents in the medium were assayed.

Small Interfering RNA Transfection

3T3-L1 cells were cultured with small interfering RNA (siRNA) duplexes specific Akt (Santa Cruz Biotechnology, CA, USA) or a noncoding siRNA using transfection reagents for 7 h. After the transfection, the culture medium was replaced with DMEM containing 10% FBS for 48 h for experiments.

Immunoprecipitation

For immunoprecipitation, differentiated 3T3-L1 cells were pre-treated with astragaloside IV (10 μM) for 0.5 h and then incubated with 100 μM of PA for 4 h. Then, adipocytes were washed and lysed on ice for 15 min. Next, the lysate was centrifuged at 12,000 g for 20 min and the cleared fractions were collected. Cleared fractions were incubated with anti-PDE3B antibody overnight at 4°C, following by incubation with protein A+G agarose beads (Beyotime Institute of Biotechnology, Shanghai, China) for 2 h. After washed five times with the lysis buffer, immunoprecipitates were boiled in 1% SDS loading buffer and used to be immunoblotted. For immunoprecipitation of the liver of HFD mice, the protein was collected and immunoprecipitated by using anti-FoxO1 antibody (Cell Signaling, Danvers, MA).

Western Blot Analysis

Total proteins were extracted from the adipose tissue, liver or adipocytes using cold RIPA buffer (Beyotime Institute of Biotechnology, Nanjing, China) with 1% phenylmethanesulfonyl fluoride. Protein concentration was determined using a Pierce™ BCA Protein Assay Kit (Beyotime Institute of Biotechnology, Nanjing, China). To analysis the expression of protein, aliquots containing 60 μg of protein were electrophoresed by SDS-PAGE, then transferred to a polyvinylidene fluoride membrane. After blocking with TBST supplemented with 5% nonfat milk powder at room temperature for 2 h, membranes were incubated with primary antibodies, including PDE3B (Bioworld Technology, St. Paul, MN, USA), p-PKA substrate (Cell Signaling Technology, Beverly, MA, USA), p-HSL (S565–S660) (Cell Signaling Technology), HSL (Cell Signaling Technology), p-JNK(Bioworld Technology), JNK (Bioworld Techology), p-Akt (S473) (Cell Signaling Technology), Akt

(Cell Signaling Technology), PAS (Cell Signaling Technology), p-PDH (E1-alpha) (phospho S293) (Abcam), PDH (Abcam), PC [EPR7365] (Abcam), and GAPDH (Bioworld Techology) for overnight at 4°C. Then, the membranes were washed for three times and incubated with the secondary antibody at room temperature for 2 h. The immunoblots were visualized by ECL Western Blot Detection System and quantized by Image-ProPlus 6.0 software. The relative intensities of each band were calculated by the mean intensity of four independent experiments.

Quantitative Real-Time PCR

Total RNA was isolated from the liver or adipose of HFD-fed mice. RNA obtained was reversely transcribed into cDNA by using the HieffTM First Strand cDNA Synthesis Super Mix for RT-qPCR+gDNA wiper system (Yeasen). The relative gene expression was relatively quantified by HieffTM qPCR SYBR Green Master Mix (No Rox Plus) kit (Yeasen) with CFX96TM realtime system (BIO-RAD, USA). Primer sequences were shown below: PEPCK, F: GTGCTGGAGTGGATGTTCGG, R: CTGGC TGATTCTCTGTTTCAGG; G6PaseF: ACTGTGGGCATCAAT CTCCTC, R: CGGGACAGACAGACGTTCAGC; PDE3B, F: A AAGCGCAGCCGGTTACTAT, R: CACCACTGCTTCAAGTC CCAG; β-actin, F: GGGAAATCGTGCGTGAC, R: AGGCTGGA AAAGAGCCT. The results of mRNA level were calculated with the $2^{-\Delta\Delta Ct}$ method.

Immunofluorescence

After treatment, differentiated 3T3-L1 cells were fixed with 4% paraformaldehyde for 20 min, and permeabilized with 0.2% Triton X-100 for 10 min at room temperature. After blocking with 3% BSA, specimens were then labeled with specific primary antibodies (anti-PDE3B, anti-p-Akt) overnight at 4°C, followed by incubation with fluorescent secondary antibodies for 1 h at 37°C. After washing, specimens were examined with a confocal scanning microscope (Zeiss LSM 700).

Statistical Analysis

All data were expressed as mean ± SD. Results were analyzed using Student's *t*-test and one-way analysis of variance (ANOVA) followed by Student-Newman-Keuls multiple comparison test. Values of $p < 0.05$ were considered statistically significant.

RESULTS

Astragaloside IV Prevented Lipolysis in Adipose Tissue of HFD-Fed Mice

To investigate the effects of astragaloside IV on adipose dysfunction, we first observed the regulation of lipolysis in the freshly isolated epididymal adipose tissue from HFD-fed mice, and found that oral administration of astragaloside IV at concentrations of 50 and 100 mg/kg significantly reduced FFAs and glycerol release (**Figures 1A,B**). Similar to astragaloside IV, anti-diabetic agent metformin also reduced FFAs, and glycerol release from adipose tissue (**Figures 1A,B**). Consistent with what observed in adipose tissue, astragaloside IV, and metformin effectively reduced the elevated levels of blood FFAs and glycerol in HFD-fed mice (**Figures 1C,D**), while the contents of TC, triacylglycerol and glucose in the blood were not affected (**Figures 1E–G**). These results showed that astragaloside IV inhibited lipolysis in HFD-fed mice.

Astragaloside IV Reduced cAMP Accumulation in Adipose Tissue

As a second messenger, cAMP is a key regulator responsible for the initiation of lipolysis in adipose tissue. HFD feeding induced cAMP accumulation in adipose tissue along with the reduction of AMP levels, whereas astragaloside IV as well as metformin reversed the alterations in adipose tissue (**Figures 2A,B**). PDE3B, a member of PDEs, predominantly expresses in the adipose tissue, exerting the ability to degrade cAMP. We observed that HFD feeding significantly attenuated PDE3B gene and protein expression and meanwhile inhibited PDE enzymatic activity (**Figures 2C,D**) in adipose tissue. Astragaloside IV as well as metformin normalized PDE3B gene and protein expression and preserved PDE enzymatic activity in the adipose tissue of HFD-fed mice, suggesting the possibility to prevent cAMP accumulation by preserving PDE3B content by promoting its gene expression, at least in part.

Akt activation is documented to regulate PDE3B activity (Kitamura et al., 1999). In the adipose tissue, astragaloside IV prevented HFD-induced Akt impairment by preserving phosphorylation (**Figure 2E**). We isolated epididymal adipose tissue from normal mice and treat with isoproterenol to measure cAMP contents and FFAs release. We noted that astragaloside IV significantly decreased isoproterenol-induced cAMP and reduced FFAs release in isolated adipose tissue, but this action was blocked by co-treatment with Akt inhibitor triciribine (**Figures 2F,G**). Moreover, pro-inflammatory cytokine TNF-α impaired PDE3B both gene and protein expression in adipose tissues (**Figure 2H**), indicative of the involvement of inflammation in lipolysis. Similarly, the protective effect of astragaloside IV on PDE3B gene and protein expression was also abolished by Akt inhibitor triciribine (**Figure 2H**). To avoid unexpected off-target effects, we chose another two specific Akt inhibitors: MK2206 and AZD5363 and observed that both of this two inhibitors could abolished the protective effect of astragaloside IV on PDE3B gene and protein expression (**Figure 2H**), further confirming the involvement of Akt on PDE3B regulation. These results suggested that Akt was involved in Astragaloside IV action to prevent cAMP accumulation in adipose tissue.

Astragaloside IV Preserved PDE3B Content *via* Regulation of Akt

Next, we examined the regulation of Akt in differentiated 3T3-L1 cells and found that astrgaloside IV increased Akt phosphorylation in a concentration-dependent manner (from 0.1 to 10 μM) (**Figure 3A**). The result of the time course showed that astragaloside IV enhanced Akt phosphorylation in the early period and reached the highest expression at 4 h (**Figure 3B**). To identify whether PDE3B could be phosphorylated by Akt,

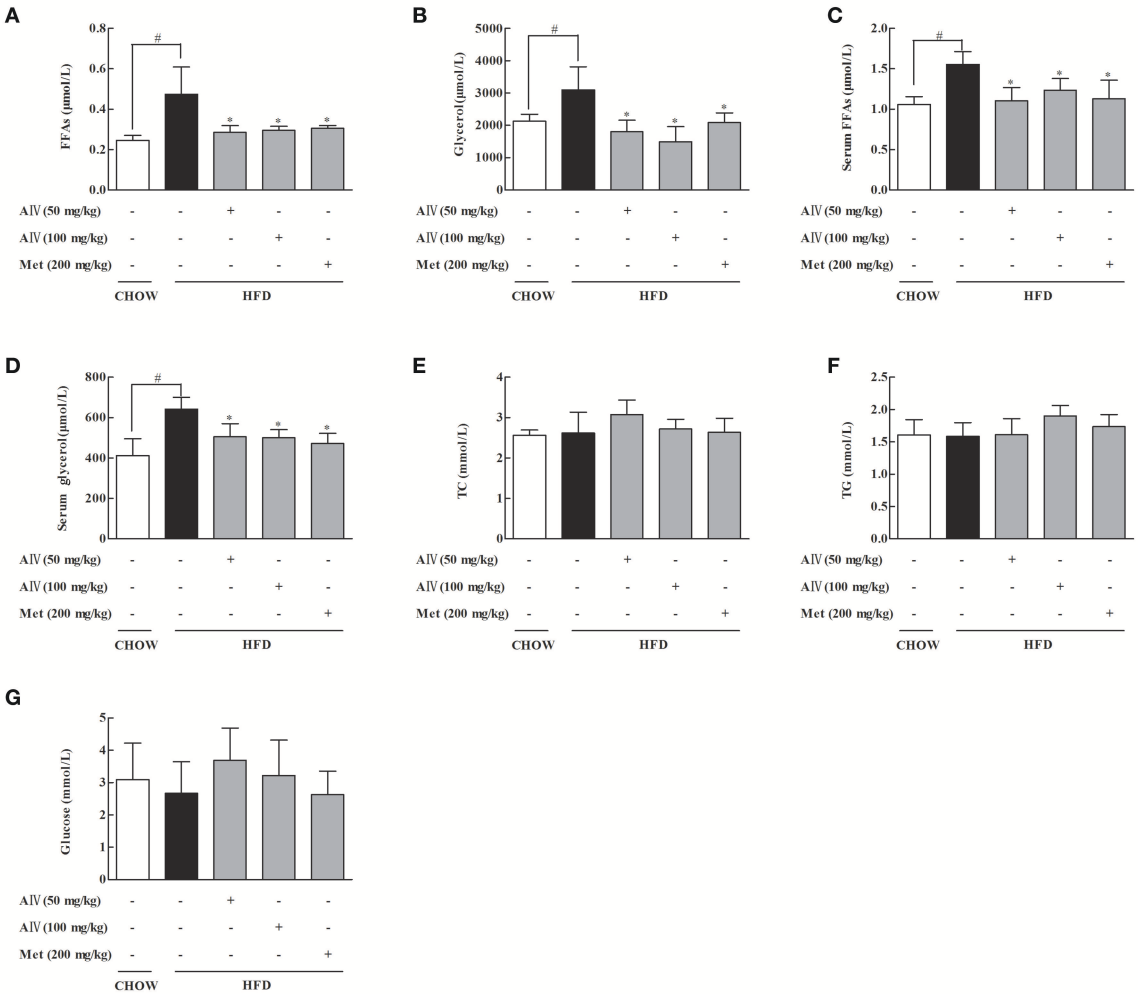

FIGURE 1 | Astragaloside IV prevented lipolysis in adipose tissue of HFD-fed mice. Mice were fed with high fat diet (HFD) for 2 weeks and simultaneously administrated with astragaloside IV (AIV, 50 and 100 mg/kg) and metformin (Met, 200 mg/kg) by gavage. **(A,B)**, Free fatty acids (FFAs) and glycerol contents in the adipose tissues; **(C,D)**, Free fatty acids (FFAs) and glycerol contents in the blood. **(E–G)**, Total cholesterol (TC), triglyceride (TG), and glucose in the blood. Data were expressed as the mean ± SD ($n = 6$). $^{*}p < 0.05$ vs. model; $^{\#}p < 0.05$ vs. control.

complete amino-acid sequences of PDE3B were scanned by the Scansite databases. Search result revealed that mice PDE3B contains Akt consensus phosphorylation sites (**Figure 3C**), suggesting that the involvement of Akt in PDE3B phosphorylation. Then immunoprecipitation examination showed that phosphorylated Akt consensus sequence (PAS) presented in PDE3B and astrgaloside IV treatment increased PAS expression when cells were exposed to PA (**Figure 3D**), confirming the regulation of PDE3B by Akt. Meanwhile, we found that astrgaloside IV increased total Akt and p-Akt expression in PDE3B protein (**Figure 3D**). Consistently, immunofluorescent staining further revealed that astrgaloside IV promoted PDE3B and p-Akt co-localization against PA insults, indicating that astrgaloside IV promoted Akt translocation to PDE3B (**Figure 3E**). In 3T3-L1 cells, astragaloside IV preserved PDE3B protein expression, while knockdown of Akt1/2 with siRNA diminished the effect of astragaloside IV (**Figure 3F**), providing evidence that Akt was required for astragaloside IV to preserve PDE3B protein expression.

Astragaloside IV Suppressed Lipolysis Signaling and Inflammation in Adipose Tissue of HFD-Fed Mice

PKA activation is a downstream signaling of cAMP regulation in adipose tissue. In response to cAMP accumulation, PKA 62 KD substrate phosphorylation increased in adipose tissue, a result indicating PKA activation. Astragaloside IV and metformin administration inhibited PKA activation by dephosphorylation of PKA 62 KD substrate (**Figure 4A**). Hormone-sensitive lipase (HSL) hydrolyzes intracellular diacylglycerol to monoacylglycerol, leading to the release of FFAs and glycerol. HSL activation is regulated by phosphorylation modification. Phosphorylation of Ser 660 activates HSL, while

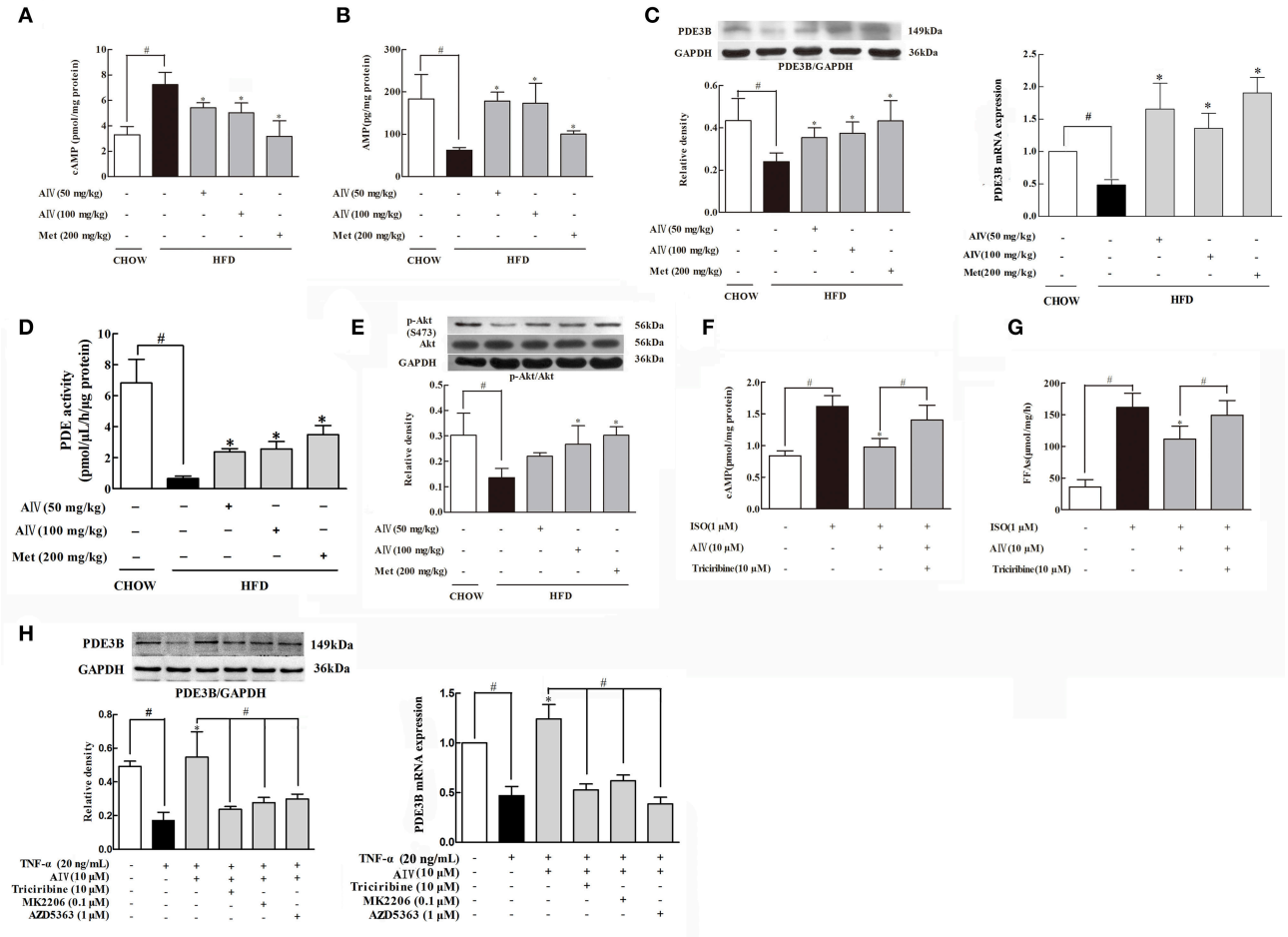

FIGURE 2 | Astragaloside IV reduced cAMP accumulation in adipose tissue. **(A,B)**, The contents of cAMP and AMP in the adipose tissues of HFD-fed mice ($n = 6$); **(C)**, PDE3B gene and protein expression in the adipose tissue of HFD-fed mice was examined by Western blot ($n = 4$); **(D)**, PDE activity in the adipose tissue of HFD-fed mice was measured using a PDE activity assay kit ($n = 6$); **(E)**, The phosphorylation of Akt in the adipose tissue of HFD-fed mice was examined by Western blot. The epididymal adipose tissue of normal mice was incubated with isoprenaline (ISO) in the presence of astragaloside IV (AIV) or Akt inhibitor triciribine for 2 h. The contents of cAMP **(F)** and FFAs **(G)** were assayed by commercial kits ($n = 6$); **(H)**, Isolated epididymal adipose tissue was pretreated with astragaloside IV (AIV) or three Akt inhibitors triciribine, MK2206 and AZD5363, and then stimulated with TNF-α for 16 h. PDE3B gene and protein expression was detected ($n = 4$), (Astragaloside IV, AIV; Metformin, Met). The results were expressed as the mean ± SD. $^{*}p < 0.05$ vs. model; $^{\#}p < 0.05$ vs. control.

phosphorylation at the residue 565 is proposed to inhibit HSL activation (Djouder et al., 2010). In adipose tissue, HFD feeding increased HSL phosphorylation at Ser 660 and attenuated the phosphorylation at 565 residue, whereas these alterations were reversed by oral administration of astragaloside IV (**Figures 4B,C**), demonstrating its inhibitory effect on HSL activation. Similarly, metformin also effectively inhibited HSL activation.

As is known, inflammation is involved in adipose lipolysis (Rahn Landström et al., 2000; Zhang et al., 2002). In adipose tissue, HFD feeding induced JNK activation by enhancing phosphorylation and increased proinflammatory cytokine TNF-α and IL-6 production. Oral administration of astragaloside IV inactivated JNK by dephosphorylation and reduced TNF-α and IL-6 production, demonstrating its action in suppression of inflammation in adipose tissue (**Figures 4D–F**). Metformin also inactivated lipolysis signaling and inhibited inflammatory response in adipose tissue.

Astragaloside IV Reduced Hepatic Lipid Deposition in HFD-Fed Mice

Astragaloside IV inhibited adipose lipolysis and decreased the elevated levels of circulating FFAs, and this regulation should prevent ectopic lipid deposition. Indeed, astragaloside IV as well as metformin reduced hepatic lipid deposit, evidenced by reduced hepatic TG contents (**Figure 5A**). HE staining showed that astragaloside IV and metformin reduced hepatocellular vacuolation with respect to the control (**Figure 5B**). Since acetyl CoA is an end product of fatty acid oxidation, the reduced acetyl CoA by astragaloside should be a result from reduced fatty acid entry and oxidation (**Figure 5C**). Previously, the acetyl CoA is proposed to inhibit pyruvate dehydrogenase (PDH)

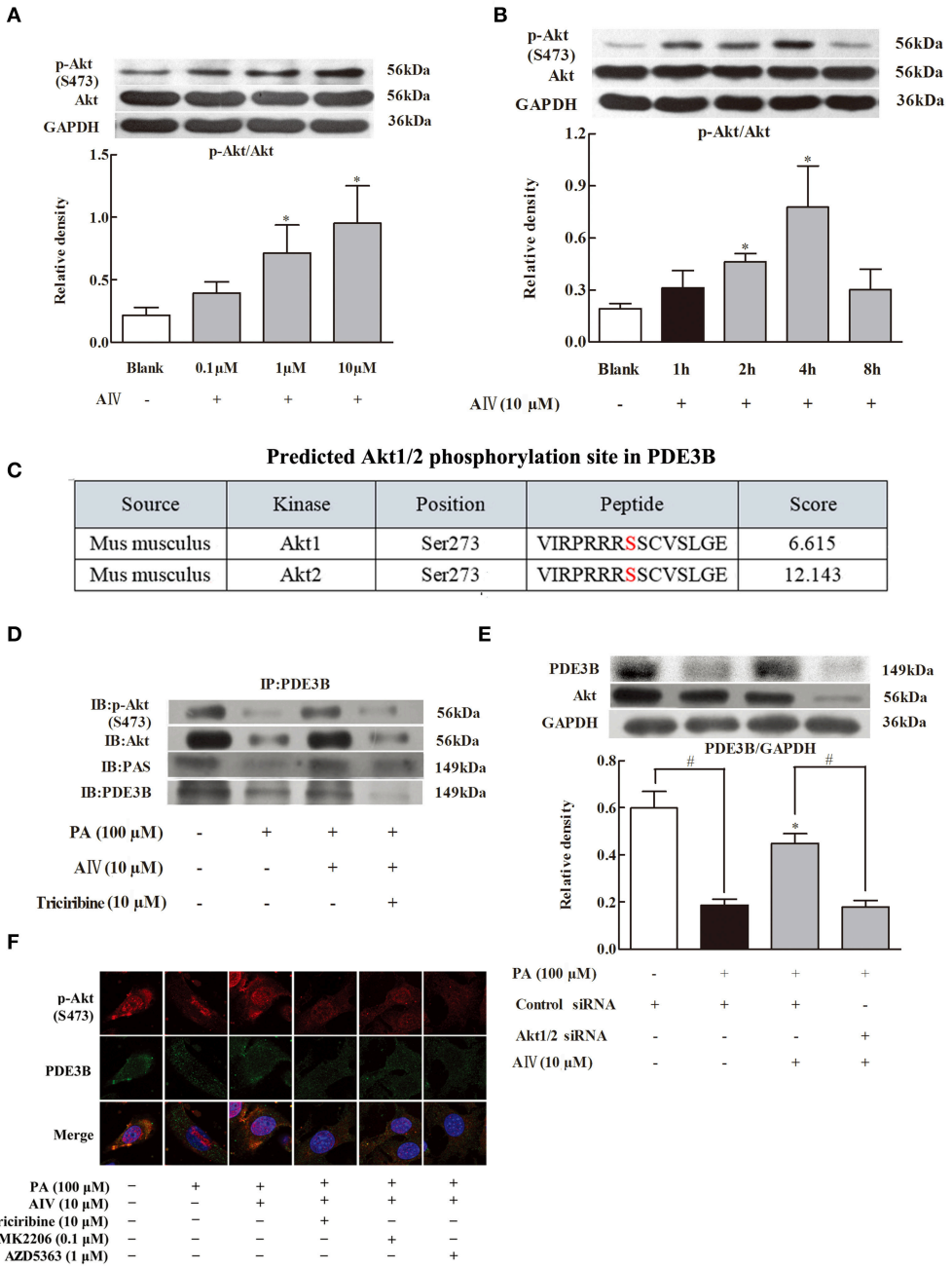

FIGURE 3 | Astragaloside IV preserved PDE3B *via* regulation of Akt. **(A,B)**, Akt phosphorylation in differentiated adipocytes were examined by Western blot; **(C)**, Akt1/2 phosphorylation site in PDE3B predicted by GPS 3.0; **(D)**, p-Akt, Akt, or PAS in PDE3B in differentiated adipocytes were determined with immunoprecipitation and Western blot; **(E)**, Confocal images of PDE3B and p-Akt co-localization was observed by immunofluorescent staining. Scale bar: 10 μm; **(F)**, 3T3-L1 preadipocytes were transfected with Akt1/2 or control siRNA to silence Akt and then incubated with palmitate (PA) for 4 h. The expression of PDE3B was detected with Western blot, (Astragaloside IV, AIV; Palmitate, PA). The results were expressed as the mean ± SD ($n = 4$). $^{*}p < 0.05$ vs. model; $^{\#}p < 0.05$ vs. control.

activity (Sugden and Holness, 2003) with pyruvate carboxylase (PC) induction (Adina-Zada et al., 2012), contributing to gluconeogenesis. As expected, astragaloside IV improved PDH activity by dephosphorylation (**Figure 5D**) and reduced PC protein expression (**Figure 5E**) in the liver of HFD-fed mice.

Astragaloside IV Regulated Akt and FoxO1 in the Liver of HFD-Fed Mice

Astragaloside IV administration preserved Akt phosphorylation in the liver of HFD-fed mice (**Figure 6A**). FoxO1 is a transcription factor encoding genes for gluconeogenesis,

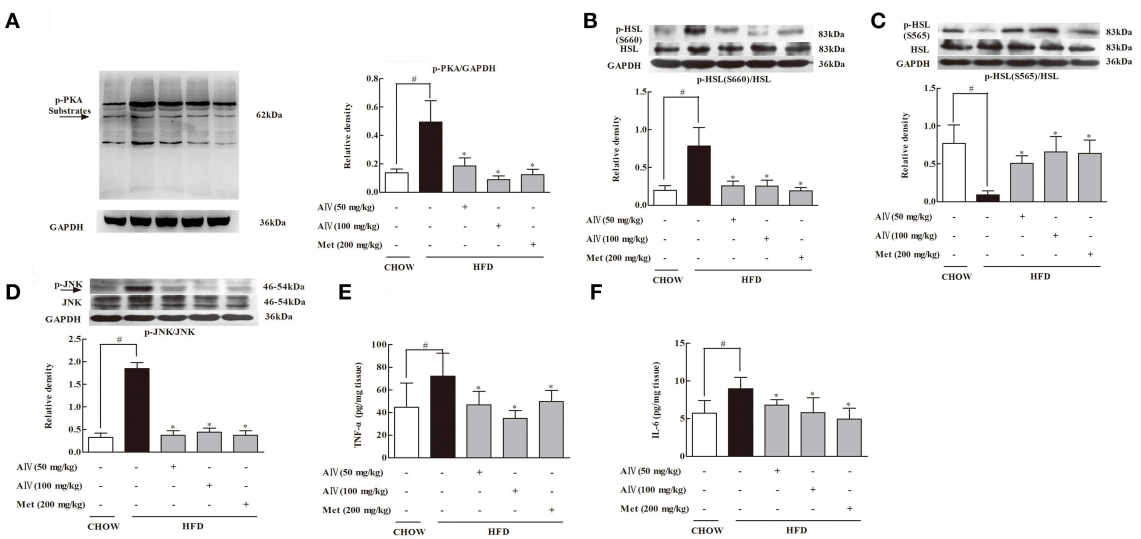

FIGURE 4 | Astragaloside IV surpressed PKA/HSL signaling and inflammation in adipose tissue of HFD-fed mice. **(A)**, PKA, **(B)**, HSL(S660), and **(C)** HSL(S565) protein expressions in the adipose tissue of HFD-fed mice were examined by Western blot ($n = 4$). Arrow points to 62kDa. **(D)**, JNK protein expression in the adipose tissue of HFD-fed mice was examined by Western blot ($n = 4$). **(E,F)**, The levels of TNF-α and IL-6 in the adipose tissue of HFD-fed mice were assayed by ELISA kits ($n = 6$). (Astragaloside IV, AIV; Metformin, Met). The results were expressed as the mean ± SD. $^{*}p < 0.05$ vs. model; $^{\#}p < 0.05$ vs. control.

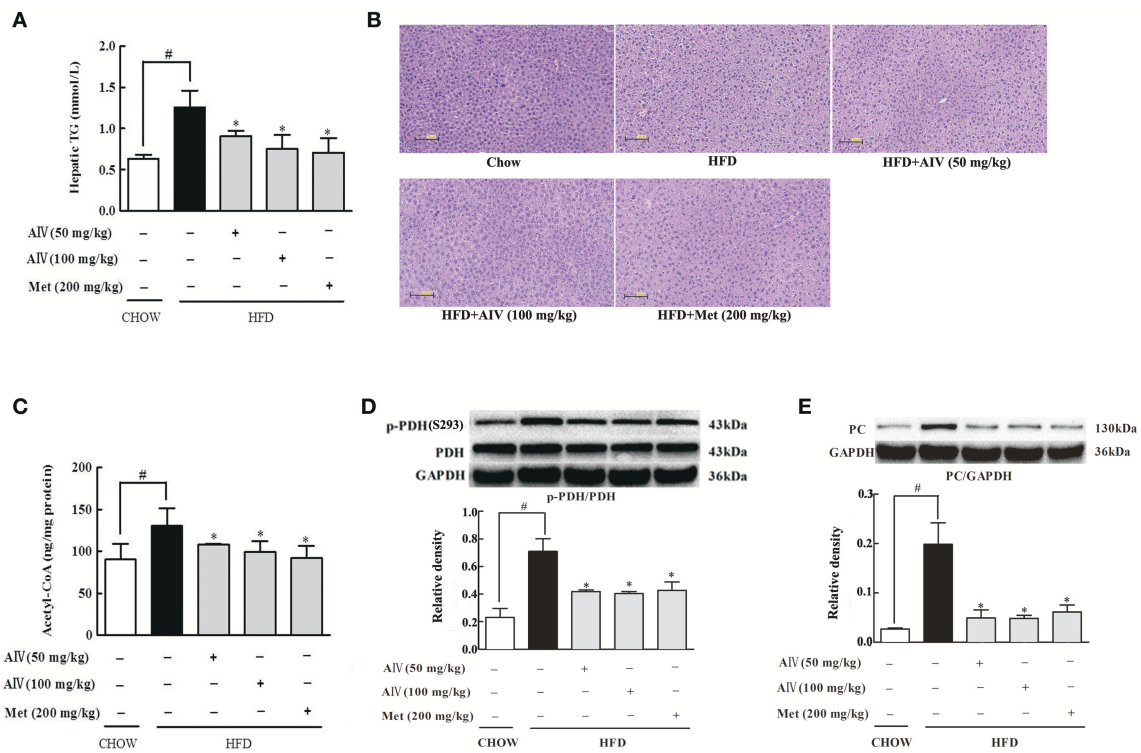

FIGURE 5 | Astragaloside IV ameliorated hepatic lipid deposition in HFD-fed mice. **(A)**, Triglyceride (TG) concentration in the liver ($n = 6$). **(B)**, Hepatic H&E satining ($n = 4$). **(C)**, Acetyl CoA levels in the liver ($n = 6$). PDH phosphorylation **(D)** and PC **(E)** protein expression in the liver of HFD-fed mice was examined by Western blot ($n = 4$). (Astragaloside IV, AIV; Metformin, Met). The results were expressed as the mean ± SD. $^{*}p < 0.05$ vs. model; $^{\#}p < 0.05$ vs. control.

and its activation is modulated by phosphorylation (Ozcan et al., 2012). HFD feeding increased hepatic FoxO1 protein expression with attenuated phosphorylation, indicative of FoxO1 activation, but these alternations were reversed by astragaloside IV (**Figure 6B**). Consistent with this, when FoxO1 protein was immunoprecipitated and then blotted using p-Akt

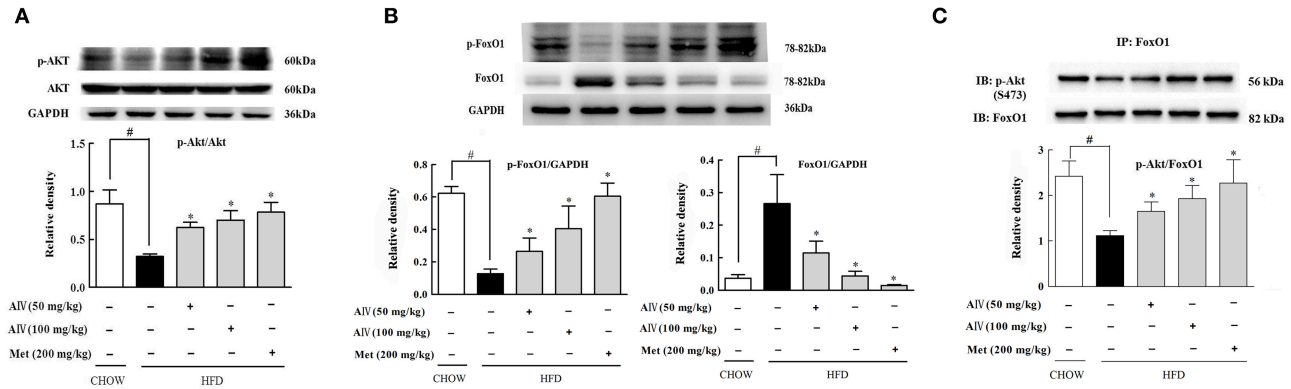

FIGURE 6 | Astragaloside IV regulated Akt and FoxO1 in the liver of HFD-fed mice. **(A)**, The phosphorylation of Akt in the liver of HFD-fed mice was examined by Western blot ($n = 4$). **(B)**, p-FoxO1 and FoxO1 protein expression in the liver of HFD-fed mice was examined by Western blot ($n = 4$). **(C)**, p-Akt in FoxO1 was determined with immunoprecipitation and Western blot ($n = 4$). (Astragaloside IV, AIV; Metformin, Met). The results were expressed as the mean ± SD. $^{*}p < 0.05$ vs. model; $^{\#}p < 0.05$ vs. control.

(Ser473) antibody, astragaloside IV increased phosphorylated Akt expression in FoxO1, indicating the direct interaction between Akt and FoxO1 (**Figure 6C**). These results suggested that astragaloside IV suppressed FoxO1 activation *via* regulation of Akt.

Astragaloside IV Reduced Hepatic Gluconeogenesis

Phosphoenolpyruvate carboxykinase (PEPCK) and glucose 6-phosphatase (G6Pase) are gluconeogenic genes responsible for hepatic glucose production. HFD feeding induced PEPCK and G6Pase gene expression in the liver, indicative of enhanced gluconeogenesis (**Figures 7A,B**). Astragaloside IV suppressed gene expressions for PEPCK and G6Pase in the liver of HFD-fed mice, demonstrating the action to restrain hepatic gluconeogenesis (**Figures 7A,B**). As expected, astragaloside IV reduced pyruvate-driven glucose production in primary hepatocytes (**Figure 7C**), but the action was attenuated by Akt inhibitor triciribine. Pyruvate tolerance is employed for hepatic glucose output, because pyruvate provides the substrate for hepatic glucose production. Concordant with the inhibitory effect on hepatic gluconeogenic gene induction, astragaloside IV reduced blood glucose rise in response to pyruvate load in HFD-fed mice (**Figure 7D**). These results indicated that astragaloside IV restrained excessive endogenous glucose production in HFD-fed mice. Meanwhile, astragaloside IV also improved glucose tolerance in HFD-fed mice (**Figure 7E**).

DISCUSSION

Insulin inhibits adipose lipolysis through PI3K/Akt signaling. In the present study, we showed that astragaloside IV preserved PDE3B content and reduced cAMP accumulation *via* regulation of Akt in an insulin independent manner, thereby inhibiting inflammation-associated lipolysis. In view of the association of adipose dysfunction with metabolic disorder diseases (Perry et al., 2015; Ritter et al., 2015), this finding provides a mechanical explanation for the beneficial effects of astragaloside IV on the regulation of metabolic homeostasis.

In the basal state, the triacylglyceride (TG) pool in adipocytes is kept at a balance between non-esterified free fatty acids (NFFAs) release from TG and re-esterification of non-esterified fatty acids to produce TG, depending on energy demands. In obesity and diabetes, the balance is disturbed due to adipose dysfunction, leading to increased lipolysis (Greenberg et al., 2011). Indeed, we observed that adipose lipolysis increased in HFD-fed mice. Lipolysis cascade is initiated by cAMP/PKA signaling in adipose tissue. As a second messenger in response to cellular stress, cAMP is synthesized by adenylate cyclase. In adipose tissue, astragaloside IV reduced cAMP accumulation with increased AMP contents. Adenosine nucleosides are proposed to inhibit adenylate cyclase activity in fat cells (Fain et al., 1972), and consistent with this, metformin is documented to inhibit adenylate cyclase activity and reduced cAMP by elevating the levels of AMP in the liver (Miller et al., 2013). In addition, metformin has also been known to activate PDE4B in hepatocyte, contributing to the decrease of cAMP with increase of AMP level, as AMP itself is a byproducts of PDE (Johanns et al., 2016). Similar to metformin, astragaloside IV reduced cAMP generation with increased AMP contents in the adipose tissue of HFD-fed mice, suggesting that astragaloside IV could inhibit cyclase activity *via* upregulation of AMP, a regulation relative with reducing energy charge. Reduced cellular energy charge (increased AMP/ATP ratio) can induce AMPK activation. Astragaloside IV enhances AMPK activity in endothelial cells (Zhao et al., 2015), suggesting its potential to reduce cellular energy charge. In addition to the inhibition of adenylate cyclase activity by upregulation of AMP.

In adipocytes, PDE3B prevented cAMP accumulation by degradation and this regulation is influenced by the modulation of PDE3B activity. It is believed that Akt mediates the anti-lipolytic effect of insulin *via* phosphorylation of PDE3B (Kitamura et al., 1999; Frühbeck et al., 2014). In spite that Akt

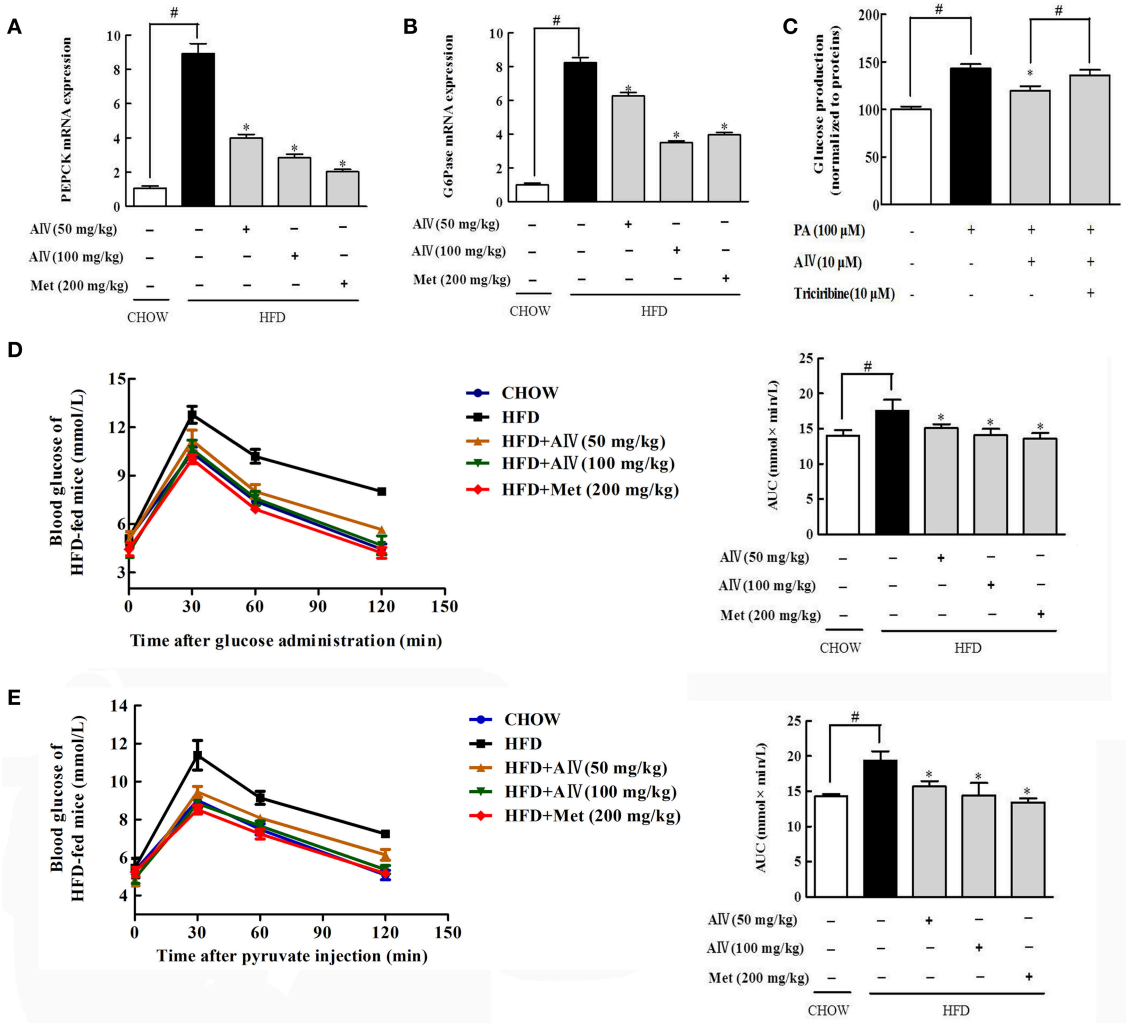

FIGURE 7 | Astragaloside IV reduced hepatic gluconeogenesis. Phosphoenolpyruvate carboxykinase (PEPCK) **(A)** and glucose 6-phosphatase (G6Pase) **(B)** gene expression in the liver was examined by qPCR ($n = 4$). **(C)** Glucose production in primary hepatocytes ($n = 6$). Pyruvate tolerance test with the AUC **(D)** and glucose tolerance test with the AUC **(E)** in HFD-fed mice ($n = 6$). The results were expressed as the mean ± SD. (Astragaloside IV, AIV; Metformin, Met). $^{*}p < 0.05$ vs. model; $^{\#}p < 0.05$ vs. control.

is proposed to be dispensable for the suppression of lipolysis by insulin (DiPilato et al., 2015; Koren et al., 2015), there is a PAS in PDE3B, indicating the potency to be regulated by Akt. Moreover, Akt exerts the ability to increase PDE3B activity by phosphorylation of PDE3B (Kitamura et al., 1999; Frühbeck et al., 2014). Therefore, it is possible that Akt could directly regulate PDE3B in an insulin independent manner. Akt traverses the cell interior with regulated localization. In response to palmitate challenge, PDE3B protein expression was reduced. Astragaloside IV promoted Akt translocation to PDE3B and induced PAS induction in PDE3B with the preserved PDE3B expression. Knockdown of Akt1/2 blocked the action of astragaloside IV to preserve PDE3B content in adipocytes when exposed to palmitate challenge, indicating that astragaloside IV protected PDE3B content in Akt dependent manner. Inflammatory molecules could impair PDE3B activity in adipose tissue and liver (Rahn Landström et al., 2000; Ke et al., 2015). In this context, the regulation of Akt dependent PDE3B activation should contribute to ameliorating adipose dysfunction inflammation involved. In the present study, pro-inflammatory cytokine TNF-α impaired PDE3B activity in the adipose tissue, indicative of the impact of inflammatory on lipolysis. Akt inhibitors diminished the protective effect of astragaloside IV on PDE3B gene and protein content, provided evidence to support the conclusion.

In response to cAMP accumulation, PKA activation modulates HSL phosphorylation to induce FFAs release. Phosphorylation of HSL occurs on multiple sites, including Ser-660, which stimulates catalytic activity, and Ser-565, which is believed to inactivate HSL (Djouder et al., 2010). As a downstream regulation from blocking cAMP/PKA signaling, astragaloside IV inactived HSL by dephosphorylation of HSL Ser-660. Meanwhile, Astragaloside IV also restored HSL

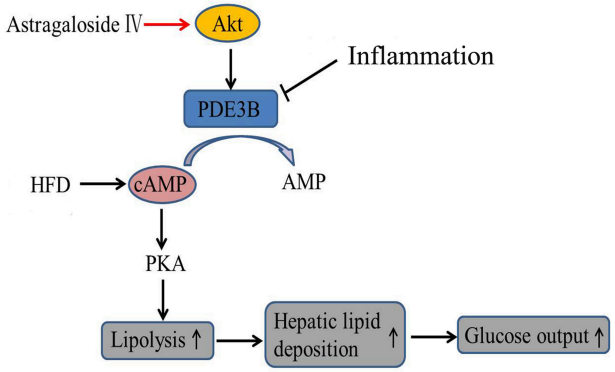

FIGURE 8 | The proposed regulatory pathway for astragaloside IV action in inhibition of adipose lipolysis. Astragaloside IV (AIV) activated Akt and prevented cAMP accumulation in adipose tissue by protecting PDE3B induction from inflammation- associated impairment, and thereby inhibited lipolysis *via* blocking cAMP/PKA activation and decreased hepatic glucose production *via* reducing hepatic lipid deposition.

phosphorylation at Ser-565, and this action should contribute to suppression of HSL activation. Inflammation is involved in adipose dysfunction, contributing to enhance lipolysis (Rahn Landström et al., 2000). Pro-inflammatory cytokine TNF-α and inflammatory signaling induce adipose lipolysis (Rahn Landström et al., 2000; Zhang et al., 2002). Astragaloside IV inactivated JNK by dephosphorylation and reduced TNF-α and IL-6 production, well demonstrating its anti-inflammatory effects. Astragaloside IV inhibited inflammation and this action should be involved in the blockage of lipolysis signaling. The anti-inflammatory effects of astragaloside IV have been well-documented (Zhang and Frei, 2015; Dong et al., 2017), our work provides evidence that the anti-inflammatory action is involved in the amelioration of adipose dysfunction.

Increased adipose lipolysis can induce ectopic fat deposits, and fat accumulation in muscle is shown to induce insulin resistance (Xiao et al., 2017b), while hepatic fat deposition enhances glucagon response to increase glucose output (Xiao et al., 2017a). Astragaloside IV decreased circulating FFAs by inhibiting adipose lipolysis, and thereby effectively prevented lipid deposition in the liver of HFD-fed mice. As a result from limited FFAs uptake by hepatocyte, astragaloside IV reduced acetyl CoA production from fatty acid oxidation, More than a metabolic intermediate, acetyle CoA is involved in the regulation of cellular metabolism (Pietrocola et al., 2015). Consistent with this, we observed increased PDH phosphorylation and PC protein expression in the liver of HFD-fed mice, a regulation likely due to acetyle CoA accumulation (Sugden and Holness, 2003; Adina-Zada et al., 2012). Pyruvate is generated in the cytoplasm through glycolysis and imported into mitochondria through mitochondrial pyruvate carrier. Mitochondrial pyruvate is converted to acetyl CoA by PDH for oxidation, or to oxaloacetate by PC for gluconeogenesis (Jeoung et al., 2014). In the present study, when HFD feeding impaired PDH activity by phosphorylation, it is reasonable to speculate that more mitochondrial pyruvate would be shifted from oxidation to gluconeogenesis pathway. Astragaloside IV improved PDH activity by dephosphorylation with suppression of PC, and this regulation should contribute to reduce hepatic glucose production by blocking substrate supply for gluconeogenesis.

Meanwhile, we also found that Astragaloside IV preserved Akt phosphorylaiton and downregulated FoxO1 protein expression with restoration of phosphorylation, indicative of FoxO1 inactivation. Astragaloside IV promoted phosphorylated Akt binding to FoxO1, providing support to the suppression of FoxO1 by Akt. As a transcription factor, FoxO1 upregulates gluconeogenic gene expression. It is well-established that Akt inactivates FoxO1 by phosphorylation to reduce hepatic glucose production. Astragaloside IV improved pyruvate intolerance in HFD-fed mice and reduced pyruvate-driven glucose production in hepatocytes, well-demonstrating the inhibitory effects of excess glucose production associated with lipid disorders. In addition to the inhibition of lipolysis *via* Akt dependent PDE3B activation in adipose tissue, these results further showed that astragaloside IV restrained hepatic gluconeogenesis through Akt-mediated FoxO1 inactivation.

In conclusion, astragaloside IV enhanced Akt phosphorylation and suppressed inflammation-associated lipolysis *via* reducing cAMP accumulation in adipose tissue, and thereby reduced hepatic lipid fat deposition and restrained excess hepatic glucose production. The proposed regulatory pathway was shown in **Figure 8**. This finding not only elucidated a previously unrecognized role of astragaloside IV to improve adipose function, but also suggested that PDE3B activity in adipose tissue might be therapeutically targeted to ameliorate adipose dysfunction and inhibit hepatic gluconeogenesis in metabolic disorders.

AUTHOR CONTRIBUTIONS

YL: Designed the research; QD: Performed experiments, analyzed data, and drafted the manuscript; SZ and AL: Collected data and reviewed the manuscript; BL: Contributed to the discussion and review of the manuscript. All authors approved the final version of the paper.

FUNDING

This work was supported in part by the National Natural Science Foundation of China (No. 81373798).

REFERENCES

Adina-Zada, A., Zeczycki, T. N., St Maurice, M., Jitrapakdee, S., Cleland, W. W., and Attwood, P. V. (2012). Allosteric regulation of the biotin-dependent enzyme pyruvate carboxylase by acetyl CoA. *Biochem. Soc. Trans.* 40, 567–572. doi: 10.1042/BST20120041

Belfrage, P., Fredrikson, G., Nilsson, N. O., and Strålfors, P. (1980). Regulation of adipose tissue lipolysis: phosphorylation of hormones sensitive lipase in

intact rat adipocytes. *FEBS Lett.* 111, 120–124. doi: 10.1016/0014-5793(80)80775-7

Coppack, S. W., Evans, R. D., Fisher, R. M., Frayn, K. N., Gibbons, G. F., Humphreys, S. M., et al. (1992). Adipose tissue metabolism in obesity: lipase action *in vivo* before and after a mixed meal. *Metab. Clin. Exp.* 41, 264–272. doi: 10.1016/0026-0495(92)90269-G

Degerman, E., Ahmad, F., Chung, Y. W., Guirguis, E., Omar, B., Stenson, L., et al. (2011). From PDE3B to the regulation of energy homeostasis. *Curr. Opin. Pharmacol.* 11, 676–682. doi: 10.1016/j.coph.2011.09.015

DiPilato, L. M., Ahmad, F., Harms, M., Seale, P., Manganiello, V., and Birnbaum, M. J. (2015). The role of PDE3B phosphorylation in the inhibition of lipolysis by insulin. *Mol. Cell. Biol.* 35, 2752–2760. doi: 10.1128/MCB.00422-15

Djouder, N., Tuerk, R. D., Suter, M., Salvioni, P., Thali, R. F., Scholz, R., et al. (2010). PKA phosphorylates and inactivates AMPKalpha to promote efficient lipolysis. *EMBO J.* 29, 469–481. doi: 10.1038/emboj.2009.339

Dong, Z., Zhou, J., Zhang, Y., Chen, Y., Yang, Z., Huang, G., et al. (2017). Astragaloside-IV alleviates heat-induced inflammation by inhibiting endoplasmic reticulum stress and autophagy. *Cell. Physiol. Biochem.* 42, 824–837. doi: 10.1159/000478626

Fain, J. N., Pointer, R. H., and Ward, W. F. (1972). Effects of adenosine nucleosides on adenylate cyclase, phosphodiesterase, cyclic adenosine monophosphate accumulation, and lipolysis in fat cells. *J. Biol. Chem.* 247, 6866–6872.

Frühbeck, G., Méndez-Giménez, L., Fernández-Formoso, J. A., Fernández, S., and Rodríguez, A. (2014). Regulation of adipocyte lipolysis. *Nutr. Res. Rev.* 27, 63–93. doi: 10.1017/S095442241400002X

Greenberg, A. S., Coleman, R. A., Kraemer, F. B., McManaman, J. L., Obin, M. S., Puri, V., et al. (2011). The role of lipid droplets in metabolic disease in rodents and humans. *J. Clin. Invest.* 121, 2102–2110. doi: 10.1172/JCI46069

Greenberg, A. S., Obin, M. S. (2006). Obesity and the role of adipose tissue ininflammation and metabolism. *Am. J. Clin. Nutr.* 83, 461S−465S.

He, Y., Xi, J., Zheng, H., Zhang, Y., Jin, Y., and Xu, Z. (2012). Astragaloside-IV inhibits oxidative stress-induced mitochondrial permeability transition pore opening by inactivating GSK-3β *via* nitric oxide in H9c2 cardiac cells. *Oxid. Med. Cell. Longev.* 2012:935738. doi: 10.1155/2012/935738

Jeoung, N. H., Harris, C. R., and Harris, R. A. (2014). Regulation of pyruvate metabolism in metabolic-related diseases. *Rev. Endocr. Metab. Disord.* 15, 99–110. doi: 10.1007/s11154-013-9284-2

Jia, Y., Zuo, D., Li, Z., Liu, H., Dai, Z., Cai, J., et al. (2014). Astragaloside IV inhibits doxorubicin-induced cardiomyocyte apoptosis mediated by mitochondrial apoptotic pathway *via* activating the PI3K/Akt pathway. *Chem. Pharm. Bull.* 62, 45–53. doi: 10.1248/cpb.c13-00556

Jiang, B., Yang, Y., Jin, H., Shang, W., Zhou, L., Qian, L., et al. (2008). Astragaloside IV attenuates lipolysis and improves insulin resistance induced by TNFalpha in 3T3-L1 adipocytes. *Phytother. Res.* 22, 1434–1439. doi: 10.1002/ptr.2434

Johanns, M., Lai, Y. C., Hsu, M. F., Jacobs, R., Vertommen, D., Van Sande, J., et al. (2016). AMPK antagonizes hepatic glucagon-stimulated cyclic AMP signalling *via* phosphorylation-induced activation of cyclic nucleotide phosphodiesterase 4B. *Nat. Commun.* 7:10856. doi: 10.1038/ncomms10856

Ke, B., Zhao, Z., Ye, X., Gao, Z., Manganiello, V., Wu, B., et al. (2015). Inactivation of NF-κB p65 (RelA) in liver improves insulin sensitivity and inhibits cAMP/PKA pathway. *Diabetes* 64, 3355–3362. doi: 10.2337/db15-0242

Kitamura, T., Kitamura, Y., Kuroda, S., Hino, Y., Ando, M., Kotani, K., et al. (1999). Insulin-induced phosphorylation and activation of cyclic nucleotide phosphodiesterase 3B by the serine-threonine kinase Akt. *Mol. Cell. Biol.* 19, 6286–6296. doi: 10.1128/MCB.19.9.6286

Koren, S., DiPilato, L. M., Emmett, M. J., Shearin, A. L., Chu, Q., Monks, B., et al. (2015). The role of mouse Akt2 in insulin-dependent suppression of adipocyte lipolysis *in vivo*. *Diabetologia* 58, 1063–1070. doi: 10.1007/s00125-015-3532-9

Lu, M., Wan, M., Leavens, K. F., Chu, Q., Monks, B. R., Fernandez, S., et al. (2012). Insulin regulates liver metabolism *in vivo* in the absence of hepatic Akt and Foxo1. *Nat. Med.* 18, 388–395. doi: 10.1038/nm.2686

Lv, L., Wu, S. Y., Wang, G. F., Zhang, J. J., Pang, J. X., Liu, Z. Q., et al. (2010). Effect of astragaloside IV on hepatic glucose-regulating enzymes in diabetic mice induced by a high-fat diet and streptozotocin. *Phytother. Res.* 24, 219–224. doi: 10.1002/ptr.2915

Miller, R. A., Chu, Q., Xie, J., Foretz, M., Viollet, B., and Birnbaum, M. J. (2013). Biguanides suppress hepatic glucagon signalling by decreasing production of cyclic AMP. *Nature* 494, 256–260. doi: 10.1038/nature11808

Nilsson, R., Ahmad, F., Swärd, K., Andersson, U., Weston, M., Manganiello, V., et al. (2006). Plasma membrane cyclic nucleotide phosphodiesterase 3B (PDE3B) is associated with caveolae in primary adipocytes. *Cell. Signal.* 18, 1713–1721. doi: 10.1016/j.cellsig.2006.01.010

Ozcan, L., Wong, C. C., Li, G., Xu, T., Pajvani, U., Park, S. K., et al. (2012). Calcium signaling through CaMKII regulates hepatic glucose production in fasting and obesity. *Cell Metab.* 15, 739–751. doi: 10.1016/j.cmet.2012.03.002

Perry, R. J., Camporez, J. P., Kursawe, R., Titchenell, P. M., Zhang, D., Perry, C. J., et al. (2015). Hepatic acetyl CoA links adipose tissue inflammation to hepatic insulin resistance and type 2 diabetes. *Cell* 160, 745–758. doi: 10.1016/j.cell.2015.01.012

Pietrocola, F., Galluzzi, L., Bravo-San Pedro, J. M., Madeo, F., and Kroemer, G. (2015). Acetyl coenzyme A: a central metabolite and second messenger. *Cell Metab.* 21, 805–821. doi: 10.1016/j.cmet.2015.05.014

Rahn Landström, T., Mei, J., Karlsson, M., Manganiello, V., and Degerman, E. (2000). Down-regulation of cyclic-nucleotide phosphodiesterase 3B in 3T3-L1 adipocytes induced by tumour necrosis factor alpha and cAMP. *Biochem. J.* 346 (Pt 2), 337–343. doi: 10.1042/0264-6021:3460337

Ritter, O., Jelenik, T., and Roden, M. (2015). Lipid-mediated muscle insulin resistance: different fat, different pathways? *J. Mol. Med.* 93, 831–843. doi: 10.1007/s00109-015-1310-2

Strålfors, P., and Belfrage, P. (1983). Phosphorylation of hormone-sensitive lipase by cyclic AMP-dependent protein kinase. *J. Biol. Chem.* 258, 15146–15152.

Sugden, M. C., and Holness, M. J. (2003). Recent advances in mechanisms regulating glucose oxidation at the level of the pyruvate dehydrogenase complex by PDKs. *Am. J. Physiol. Endocrinol. Metab.* 284, E855–E862. doi: 10.1152/ajpendo.00526.2002

Titchenell, P. M., Chu, Q., Monks, B. R., and Birnbaum, M. J. (2015). Hepatic insulin signaling is dispensable for suppression of glucose output by insulin *in vivo*. *Nat. Commun.* 6:7078. doi: 10.1038/ncomms8078

Wang, L., Zhang, B., Huang, F., Liu, B., and Xie, Y. (2016). Curcumin inhibits lipolysis *via* suppression of ER stress in adipose tissue and prevents hepaticinsulin resistance. *J. Lipid Res.* 57, 1243–1255. doi: 10.1194/jlr.M067397

Xiao, N., Lou, M. D., Lu, Y. T., Yang, L. L., Liu, Q., Liu, B., et al. (2017a). Ginsenoside Rg5 attenuates hepatic glucagon response *via* suppression of succinate-associated HIF-1α induction in HFD-fed mice. *Diabetologia* 60, 1084–1093. doi: 10.1007/s00125-017-4238-y

Xiao, N., Yang, L. L., Yang, Y. L., Liu, L. W., Li, J., Liu, B., et al. (2017b). Ginsenoside Rg5 inhibits succinate-associated lipolysis in adipose tissue and prevents muscle insulin resistance. *Front. Pharmacol.* 8:43. doi: 10.3389/fphar.2017.00043

Yuan, M., Konstantopoulos, N., Lee, J., Hansen, L., Li, Z. W., Karin, M., et al. (2001). Reversal of obesity- and diet-induced insulin resistance with salicylates or targeted disruption of Ikkbeta. *Science* 293, 1673–1677. doi: 10.1126/science.1061620

Zhang, H. H., Halbleib, M., Ahmad, F., Manganiello, V. C., and Greenberg, A. S. (2002). Tumor necrosis factor-alpha stimulates lipolysis in differentiated human adipocytes through activation of extracellular signal-related kinase and elevation of intracellular cAMP. *Diabetes* 51, 2929–2935. doi: 10.2337/diabetes.51.10.2929

Zhang, N., Wang, X. H., Mao, S. L., and Zhao, F. (2011). Astragaloside IV improves metabolic syndrome and endothelium dysfunction in fructose-fed rats. *Molecules* 16, 3896–3907. doi: 10.3390/molecules16053896

Zhang, W. J., and Frei, B. (2015). Astragaloside IV inhibits NF-κB activation and inflammatory gene expression in LPS-treated mice. *Med. Inflamm.* 2015:274314. doi: 10.1155/2015/274314

Zhao, Y., Li, Q., Zhao, W., Li, J., Sun, Y., Liu, K., et al. (2015). Astragaloside IV and cycloastragenol are equally effective in inhibition of endoplasmic reticulum stress-associated TXNIP/NLRP3 inflammasome activation in the endothelium. *J. Ethnopharmacol.* 169, 210–218. doi: 10.1016/j.jep.2015.04.030

Conflict of Interest Statement: The authors declare that the research was conducted in the absence of any commercial or financial relationships that could be construed as a potential conflict of interest.

frontiers in Physiology

MINI REVIEW
published: 08 January 2018
doi: 10.3389/fphys.2017.01122

Commensal Homeostasis of Gut Microbiota-Host for the Impact of Obesity

Pengyi Zhang[1,2*†], *Xiangjing Meng*[3†], *Dongmei Li*[2], *Richard Calderone*[2], *Dewei Mao*[1] and *Bo Sui*[1]

[1] Sport Science Research Center, Shandong Sport University, Jinan, China, [2] Department of Microbiology & Immunology, Georgetown University Medical Center, Washington, DC, United States, [3] Shandong Academy of Pharmaceutical Science, Jinan, China

Gut microbiota and their metabolites have been linked to a series of chronic diseases such as obesity and other metabolic dysfunctions. Obesity is an increasingly serious international health issue that may lead to a risk of insulin resistance and other metabolic diseases. The relationship between gut microbiota and the host is both interdependent and relatively independent. In this review, the causality of gut microbiota and its role in the pathogenesis and intervention of obesity is comprehensively presented to include human genotype, enterotypes, interactions of gut microbiota with the host, microbial metabolites, and energy homeostasis all of which may be influenced by dietary nutrition. Diet can enhance, inhibit, or even change the composition and functions of the gut microbiota. The metabolites they produce depend upon the dietary substrates provided, some of which have indispensable functions for the host. Therefore, diet is a key factor that maintains or not a healthy commensal relationship. In addition, the specific genotype of the host may impact the phylogenetic compositions of gut microbiota through the production of host metabolites. The commensal homeostasis of gut microbiota is favored by a balance of microbial composition, metabolites, and energy. Ultimately the desired commensal relationship is one of mutual support. This article analyzes the clues that result in patterns of commensal homeostasis. A deeper understanding of these interactions is beneficial for developing effective prevention, diagnosis, and personalized therapeutic strategies to combat obesity and other metabolic diseases. The idea we discuss is meant to improve human health by shaping or modulating the beneficial gut microbiota.

Keywords: gut microbiota, enterotypes, interactions, commensal homeostasis, obesity, diet

OPEN ACCESS

Edited by:
Nuo Sun,
National Heart Lung and Blood Institute (NIH), United States

Reviewed by:
Lingdi Wang,
National Institutes of Health (NIH), United States
Pu Gao,
Institute of Biophysics (CAS), China

***Correspondence:**
Pengyi Zhang
pz102@georgetown.edu

†These authors have contributed equally to this work.

Specialty section:
This article was submitted to Clinical and Translational Physiology, a section of the journal Frontiers in Physiology

Received: *06 November 2017*
Accepted: *19 December 2017*
Published: *08 January 2018*

Citation:
Zhang P, Meng X, Li D, Calderone R, Mao D and Sui B (2018) Commensal Homeostasis of Gut Microbiota-Host for the Impact of Obesity. Front. Physiol. 8:1122. doi: 10.3389/fphys.2017.01122

INTRODUCTION

Gut microbiota is identified as a relatively new and key player in the treatment of obesity. Changes in the gut microbiota, have been shown to not only correlate with good health but, conversely, lead to the pathogenesis of obesity and various metabolic diseases. It is hoped that a defined composition of gut microbiota can prevent or even cure obesity and related diseases. Interactions of the gut microbiota and host, or metabolites they produce, are still under investigation. Gut microbiota represents a large number and complex community of microorganisms and their genetic material

living in the intestines of humans and other animals. The gut microbiota has been linked with a number of chronic diseases such as obesity, diabetes, and other metabolic diseases (Zhao, 2013). As known, obesity is an increasingly serious international health issue that can increase the risk of the insulin resistance and other metabolic syndromes (Frayling et al., 2007; Perry et al., 2016). In this review, the causality between the composition of the gut microbiota and its role in the pathogenesis of obesity and obesity-related metabolic disorders are critically described, based on metagenome analysis of the microbiota, microbe-microbe, and microbiota-host interactions, and the specific metabolites produced by microbiota and host (Musso et al., 2010).

HOMEOSTASIS OF ENTEROTYPE AND HOST

The gut microbiota has a collective metabolic activity, which impacts and responds to the host as an integrated virtual organ. Some components of the "organ" can be negative factors and contribute to the pathogenesis of various metabolic diseases. The adverse effect can be reversed by modulating one's diet to build a helpful commensal community. The mechanisms that the gut microbiota has on metabolic homeostasis and immune responses are currently being unraveled (O'Hara and Shanahan, 2006). Depending on the species and functional composition of the human gut microbiota, the host can be classified as enterotypes (species) which represent a highly aggregated microbial community structure in multidimensional space (Arumugam et al., 2011; Ding and Schloss, 2014). Based on the proportion of genera/species, their abundance, specific metabolites, and collective functions, the phylogenetic compositions of gut microbiota from individuals living in these environments have been analyzed. The results indicate that the gut microbiota can be mainly arranged as four enterotypes: *Bacteroides*, *Prevotella*, *Rminococcus,* and *Firmicutes* (Gill et al., 2006; Kurokawa et al., 2007; Zoetendal et al., 2008; Jensen et al., 2009). The enterotypes have different dominant classifications, pathways, functions, and correlations in abundance of co-occurring genera. The enterotype of *Bacteroides* has the potential to metabolize carbohydrates and proteins through the enzymes involved in glycolysis and pentose phosphate pathways (Martens et al., 2009). Enterotype *Prevotella* is able to act on the gut mucin oligosaccharide synergistically (Wright et al., 2000). In spite of the degradation of mucin, enterotype *Ruminococcus* also promotes the transport and uptake of monosaccharides by enriching in the membrane and binding mucin for hydrolysis (Derrien et al., 2004). Enterotype *Firmicutes* interacts positively with fiber but negatively with fat (Wu et al., 2011). The enterotypes use different strategies to acquire energy from the substrates available in the gut ecosystem. The specific compositions of enterotypes respond to the special metabolic mechanisms for carbohydrate, amino acids, and fatty acid metabolism. These strategies determine the incidence of obesity and related metabolic diseases (Devaraj et al., 2013). Thus, the gut microbiota provides an important contribution to the health status of individuals. The studies of enterotypes could be utilized to assess and diagnose the numerous human metabolic disorder syndromes, for instance obesity and complications such as diabetes and cardiovascular pathologies.

The formation of enterotypes is closely related to individual long-term diets or drug intake. Even for short-term changes in the microbiota, the enterotypes can still remain relatively stable. But the human gut microbiota can change rapidly, for example, within one day to cope with the drastic changes in diet and medical therapies as a result of disease intervention (Wu et al., 2011). A high-fat diet could promote changes in the gut microbiota composition, as described with the replacement of the *Bacteroidetes* enterotype by both *Firmicutes* and *Proteobacteria* (Hildebrandt et al., 2009). These types of changes are characteristic of a well-balanced host-microbial symbiosis due to diet and responses to medications. Understanding the roles of particular enterotypes and changes will be helpful to an intervention in the pathogenesis of obesity and related diseases and to personalize therapies.

HOMESTASIS OF GUT MICROBIOTA-HOST INTERACTIONS

The diversity and specificity of human gut microbiota closely correlated to the host genotype, diet, and metabolites mediating this interaction (Nicholson et al., 2012). The host genotype can impact the physical status of the human body by regulating the gut microbiota. Metagenome analysis of gut microbiota in lean and obese individuals indicated significant differences in genotype and its richness. It allowed these investigators to analyze a few bacterial markers to distinguish the level of individual microbial species and genotype richness (Le Chatelier et al., 2013). In turn, the genotype richness could predict the risk of obesity, our understanding of the commensal relationship, and identify potential therapeutic targets (Goodrich et al., 2014). One species of a little-known intestinal bacterium was identified through a study of twins. It is highly inheritable and more common and personified in slender people. In this study, 1,000 fecal samples were collected from 416 pairs of twins and the microorganisms were identified by gene sequencing. Compared to the dizygotic twins, the gut microbiota of monozygotic twins who have the complete same genome is more concordant, especially in the family *Christensenellaceae* which was the most heritable taxon and enriched in individuals with low body mass index (BMI). A similar observation of weight loss was noted in fecal transplanted, germ-free mice (Goodrich et al., 2014). Thus, the human genome has a profound effect on the composition of gut microbiota. Increasing the abundance of *Christensenellaceae* could help individuals prevent obesity. The gut microbiota just described would be a new approach for obesity treatment. Personalized therapy with probiotics could be built on the foundation of individual genomes. According to this study, these specific intestinal bacteria are inheritable, and their diversity mainly depends on the host genotype but not other environment impact factors. The same result was also found in the gut microbiota transplanted experiment from four pairs of obese and lean human twins to germ-free mice respectively

(Ridaura et al., 2013; Cox et al., 2014). Mice transplanted with microbiota from the obese one of the twins also exhibited an increase in weight and adiposity despite given the same diet. Interestingly, obesity was reduced when the obese and lean mice lived together to share and change their gut microbiomes.

Furthermore, diet modulates the activity of host and gut microbiota synchronously to influence their interaction. A high-fat diet enhanced gene expressions of both the host and microbiota. The genes whose expression increased included a colonic goblet, cell-specific gene (RELMβ) of the host, and genes for bacterial chemotaxis and flagellar assembly in the gut microbiota (Hildebrandt et al., 2009). In the obese mice, a high triglyceride-derived fatty acid intake was commonly accompanied with hyperexpression of the enzymes that digest polysaccharides and lipoproteins by the gut microbiota (Bäckhed et al., 2004). *Bacteroides thetaiotaomicron* is identified as an emerging obesity-associated gut microbial species. It alleviated diet-induced body-weight gain and adiposity by altering circulating amino acids (Liu et al., 2017). The gut microbiota and host could communicate with each other by the universal language "eukaryotic signaling molecule." Thus, *N*-acyl amides produced by gut microbiota could interact with GPR119, G-protein coupled receptor (GPCR), to regulate metabolic hormones and glucose homeostasis (Cohen et al., 2017). Perhaps GPR119 might be the potential target molecule in the treatment of obesity and diabetes.

Interestingly, germ-free mice or mice treated with antibiotics to reduce the gut microbiome showed a better glucose tolerance and insulin sensitivity, and could maintain a low BMI. The germ-free mice had less food intake and more energy expenditure than normal mice (Turnbaugh et al., 2006). Even under a high-fat diet, the germ-free mice remained slim and also produced more beige fat when the normal mice become obese (Suárez-Zamorano et al., 2015). Meanwhile, antibiotic treatment in early life changed the gut microbial composition and the activity of genes associated with carbohydrate and lipid metabolism, as well as the level of special hormones, leading to the obesity (Cho et al., 2012). The MHC-II-mediated protection from type I diabetes was significantly affected due to the destruction of gut microbiota homeostasis (Silverman et al., 2017). Therefore, short-term and low doses of antibiotics had a long-term effect on young rats, altering the microbiome-host metabolic interactions, leading to the obesity in their middle age. These data suggest that the gut microbiota in the early stages of life may affect the formation of metabolic signaling pathways in the host (Cox et al., 2014).

EXOGENOUS AND ENDOGENOUS EFFECTORS TO DYNAMIC BALANCE OF GUT MICROBIOTA

The gut microbiota is able to modulate multiple host metabolic pathways, interactive host-microbiota metabolism and signal transmission, and microbiome-gut-brain axis reactions (Nicholson et al., 2012). The dietary fiber-derived short chain fatty acids (SCFAs) and their receptors are recognized as one set of important mediator links of diet to gut microbiota-host homeostasis (Turnbaugh et al., 2006). SCFAs activate GPR41 and GPR43, two SCFA-specific GPCRs, to induce satiety and energy expenditure by promoting the secretion of the gut hormone peptide YY (PYY), and induce insulin secretion and adiposity reduction in obese individuals by significantly enhancing PYY and glucagon-like peptide-1 (GLP-1) secretion, respectively (Samuel et al., 2008; Thomas et al., 2009; Tolhurst et al., 2012; Chambers et al., 2015; Li et al., 2017). Especially, the acetate was shown to be the key factor leading to obesity. An altered gut microbiota increased the production of acetate in rats, which increased the risk of the activation of the parasympathetic nervous system, promoted pancreatic β cells to increase glucose-stimulated insulin secretion (GSIS), triggered ghrelin secretion, led to hyperphagia, obesity, insulin resistance, and other related syndromes. Finally, the complete process of rodent obesity caused by the gut microbiota disbalance was established. The results demonstrated increased acetate production due to the nutrient-gut microbiota and the subsequent parasympathetic activation could be developed as potential therapeutic targets for obesity (Perry et al., 2016). SCFAs and correlate cascade signal pathways unraveled a novel strategy to achieve the gut microbiota-host commensal homeostasis. Simultaneously, this efficient dietary intervention is also conducive to create a well-developed therapy and to prevent obesity and energy metabolic syndromes (Khan et al., 2014). Meanwhile, a recent study showed that omega-3 fatty acids were closely related to gut microbiota diversity. It also reduced the oxidative stress of intestines by inducing the production of N-carbamylglutamate (NCG) (Menni et al., 2017). In addition to the exogenous effectors described above, a α-MSH mimetic bacterial protein ClpB identified as an endogenous effector from *E. coli* K12 during exponential growth, was involved in the gut microbiota-brain signal pathway. By promoting PYY and GLP-1 secretion, activating c-Fos in hypothalamic proopiomelanocortin (POMC) neurons, the host reduced hunger and increased satiety. Thus, the mediator expressed during the nutrient-induced *E. coli* growth could be used as the signal to terminate eating since it had an impact on the diet process (Breton et al., 2016).

In the patients with severe disbalance of gut microbiota due to antibiotic treatment, prebiotics and probiotics were heavily consumed and significantly decreased. Short-term, randomized controlled trials showed that prebiotics and probiotics were beneficial to insulin sensitivity, postprandial incretins, and glucose tolerance (Musso et al., 2010). Prebiotics, inulin-typefructans (ITF), and arabinoxylan-oligosaccharides (AXOS) restored the balance of gut microbiota and increased the number of *Bifidobacteria* and butyrate-producing colon bacteria (Broekaert et al., 2011). The proportion of the latter in the intestinal microbiome was a key marker in the protection against obesity and type II diabetes, which indicated that the structure of the intestinal microbial community can be used as an effective environmental factor to prevent and diagnose these chronic metabolic diseases. Based on the metagenome analysis, different intestinal microbiome markers were screened and selected to establish the prediction model of obesity and type II diabetes for Chinese and Europeans, respectively (Qin et al., 2012; Karlsson et al., 2013; Cai et al., 2015;

Rivière et al., 2016). A return to a healthy state occurs when the proportion of "hunger" microbes and the proportion of microbes that cause "satiety" in the gut microbiota are in a dynamic equilibrium state (Rooks and Garrett, 2016). A deeper understanding of these functions will be beneficial for establishing effective therapeutic strategies to combat obesity and correlate diseases, and improve health by modulating the gut microbiota.

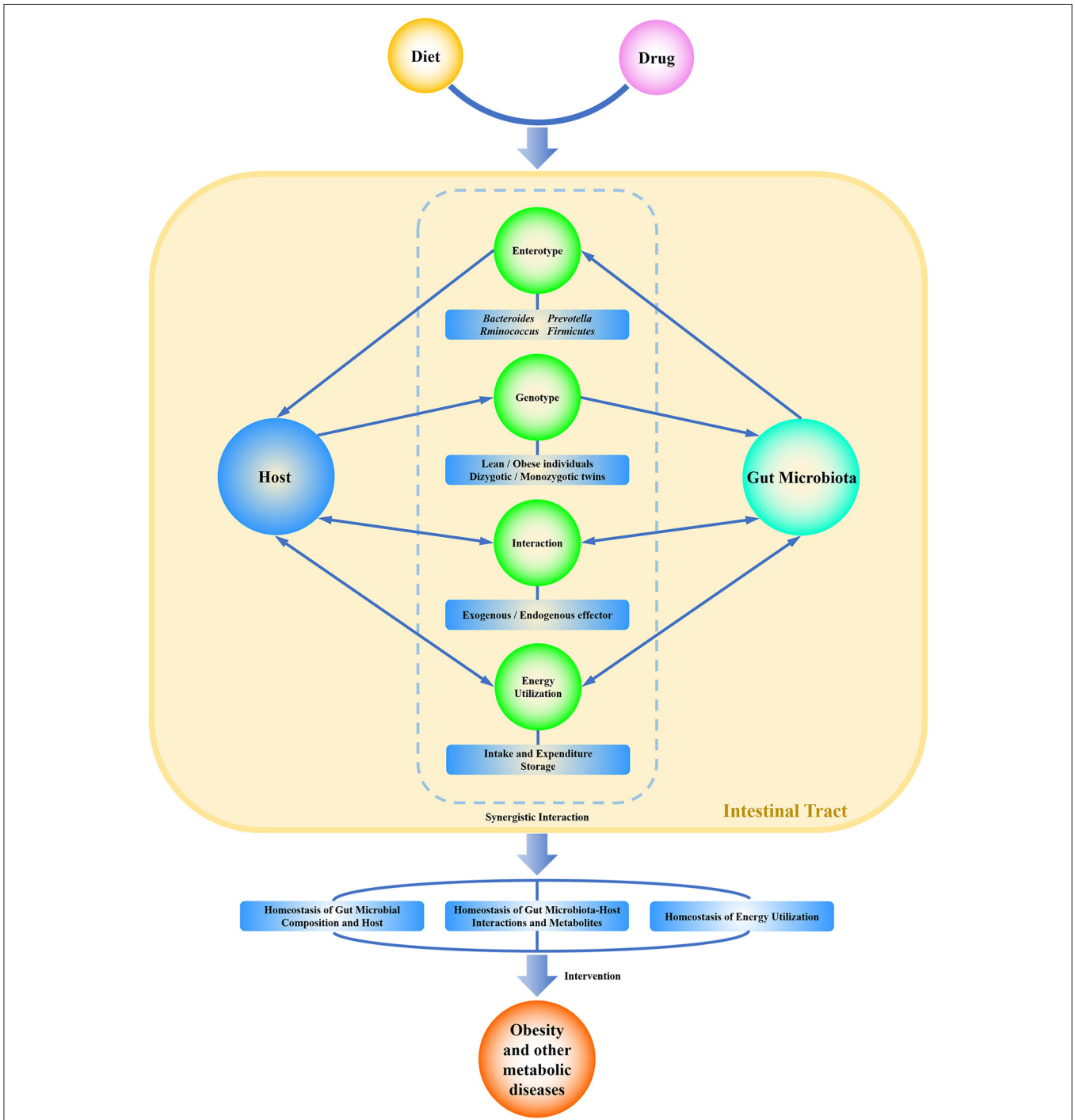

FIGURE 1 | Graphical representation of the commensal homeostasis of gut microbiota-host under the intervention of diet and drugs. Diet and drugs can be digested, absorbed, and metabolized by the host and gut microbiota. The host and gut microbiota can interact synergistically to impact the physiological status of the human body. They not only support themselves directly by using nutritional substrates but also impact each other indirectly by enterotype, genotype, metabolites, and related functions. Ultimately, the host and gut microbiota achieve a commensal homeostasis of composition, interactions, metabolites, and energy utilization.

ENERGY HOMEOSTASIS UNDER DIET INTERVENTION

The prevalence of obesity is tightly linked to excessive energy availability and sedentariness. The gut microbiota could induce or modulate the signal transmission directly or indirectly to affect energy homeostasis (Rosenbaum et al., 2015). The quali-/quantitative changes in gut microbiota composition affect both energy balance (intake and expenditure) and energy storage which would lead to the development of obesity in the dysfunctional state (Scarpellini et al., 2010; Kobyliak et al., 2016). The obese gut microbiota changes the abundance of the two dominant enterotypes, the *Bacteroidetes* and the *Firmicutes*, to gain more energy production (Turnbaugh et al., 2006). This study which was carried out in the adult female monozygotic and dizygotic twins, and their mothers, indicated that the gut microbiota could be shared among the family members, but with variation among individuals. Some of the metabolites generated by enterotypes closely correlate with energy acquisition and subsequently lead to a risk of obesity in the host. These enterotypes enhanced the efficiency of energy extraction and fat storage via enzymes related to fermentation (Tilg and Kaser, 2011). Germ-free mice fed different combinations of saturated fat and high-fiber food revealed a transmissible, rapid, and modifiable effect of diet by gut microbiota (Turnbaugh et al., 2009; Ridaura et al., 2013). The investigation of diet intervention conducted in the obese and overweight individuals found that the abundance of gut microbiota was increased by high-fiber and low-fat diet, which improved the clinical symptoms associated with obesity (Cotillard et al., 2013). The Life Lines-DEEP project analyzed the relationship of the gut microbiota and 126 exogenous and intrinsic host factors, including 60 dietary factors, 18.7% of which was associated with the variation in human gut microbiota composition (Zhernakova et al., 2016). A group of "core microbiome" genes was identified and shared among 154 individuals, which was associated with obesity at phylum-level changes. The obesity reversely reduced the microbial diversity, altered the gene expression and metabolic pathways and ultimately the energy harvest (Turnbaugh and Gordon, 2009). The Flemish Gut Flora Project analyzed the effect of various factors on the intestinal microbial diversity. It revealed a 14-genera core microbiota and sixty-nine covariates associated to microbiota variation (Falony et al., 2016). In addition, the association of microbial communities and dietary patterns was also elucidated by use of a mathematical model in clinical trials, which tried to create the universal rules of the molecular mechanism of intestinal microbial interaction and predict the responses of different patients to the modified diet (Qin et al., 2010). Compared to the host genotype, diet played a more important role on the variation of the individual gut microbiota, which showed a definite dose-dependent relationship with the response to diet. Subtle changes in diet might cause changes in gut microbiota compositions (Carmody et al., 2015).

CONCLUSION

The focus of this review was developed from research on the structure and function of gut microbiota as well as the integration of gut microbiota-host interactions at a higher dimension. The commensal pattern of gut microbiota will be made clearer through gene sequencing, metagenome analysis, gut microbiota-host responses, and verification in gnotobiotic animals. The diet intake and the specific metabolites produced by the host and the microbiota can be utilized to change or recover the ecosystem of intestinal homeostasis either in health or pathologic conditions (Scarpellini et al., 2010). Modulation of gut microbiota could be a useful and alternative method to block and even cure obesity and other metabolic syndromes. A healthy lifestyle, including the reasonable composition of dietary nutrition and the avoidance of excessive energy intake, may establish a friendly gut microbiota-host homeostasis. The commensal homeostasis of gut microbiota is favored by a balance of microbial composition, metabolites, and energy (**Figure 1**). In turn, this ideal relationship may have positive effects on the prevention and therapy of obesity and other related metabolic diseases.

AUTHOR CONTRIBUTIONS

PZ and XM: contributed to conception, design and manuscript writing; DL, RC, DM, and BS: all contributed substantially to the writing and revision of the manuscript and approved its final version.

ACKNOWLEDGMENTS

We thank the Natural Science Foundation of Shandong Province, China (ZR2017LC013), the Higher Education Priority Academic Talent Development Program of Shandong Province to support PZ. This work was also supported by the Key research and development plan of Shandong Province, China (2016GSF122009, 2016GSF122015).

REFERENCES

Arumugam, M., Raes, J., Pelletier, E., Le Paslier, D., Yamada, T., Mende, D. R., et al. (2011). Enterotypes of the human gut microbiome. *Nature* 473, 174–180. doi: 10.1038/nature09944

Bäckhed, F., Ding, H., Wang, T., Hooper, L. V., Koh, G. Y., Nagy, A., et al. (2004). The gut microbiota as an environmental factor that regulates fat storage. *Proc. Natl. Acad. Sci. U.S.A.* 101, 15718–15723. doi: 10.1073/pnas.0407076101

Breton, J., Tennoune, N., Lucas, N., Francois, M., Legrand, R., Jacquemot, J., et al. (2016). Gut commensal, *E. coli* proteins activate host satiety pathways following nutrient-induced bacterial growth. *Cell Metab.* 23, 324–334. doi: 10.1016/j.cmet.2015.10.017

Broekaert, W. F., Courtin, C. M., Verbeke, K., Van de Wiele, T., Verstraete, W., and Delcour, J. A. (2011). Prebiotic and other health-related effects of cereal-derived arabinoxylans, arabinoxylan-oligosaccharides, and xylooligosaccharides. *Crit. Rev. Food Sci. Nutr.* 51, 178–194. doi: 10.1080/10408390903044768

Cai, L., Wu, H., Li, D., Zhou, K., and Zou, F. (2015). Type 2 diabetes biomarkers of human gut microbiota selected via iterative sure independent screening method. *PLoS ONE* 10:e0140827. doi: 10.1371/journal.pone.0140827

Carmody, R. N., Gerber, G. K., Luevano, J. J., Gatti, D. M., Somes, L., Svenson, K. L., et al. (2015). Diet dominates host genotype in shaping the murine gut microbiota. *Cell Host Microbe* 17, 72–84. doi: 10.1016/j.chom.2014.11.010

Chambers, E. S., Viardot, A., Psichas, A., Morrison, D. J., Murphy, K. G., Zac-Varghese, S. E., et al. (2015). Effects of targeted delivery of propionate to the human colon on appetite regulation, body weight maintenance and adiposity in overweight adults. *Gut* 64, 1744–1754. doi: 10.1136/gutjnl-2014-307913

Cho, I., Yamanishi, S., Cox, L., Methé, B. A., Zavadil, J., Li, K., et al. (2012). Antibiotics in early life alter the murine colonic microbiome and adiposity. *Nature* 488, 621–626. doi: 10.1038/nature11400

Cohen, L. J., Esterhazy, D., Kim, S. H., Lemetre, C., Aguilar, R. R., Gordon, E. A., et al. (2017). Commensal bacteria make GPCR ligands that mimic human signalling molecules. *Nature* 549, 48–53. doi: 10.1038/nature23874

Cotillard, A., Kennedy, S. P., Kong, L. C., Prifti, E., Pons, N., Le Chatelier, E., et al. (2013). Dietary intervention impact on gut microbial gene richness. *Nature* 500, 585–588. doi: 10.1038/nature12480

Cox, L. M., Yamanishi, S., Sohn, J., Alekseyenko, A. V., Leung, J. M., Cho, I., et al. (2014). Altering the intestinal microbiota during a critical developmental window has lasting metabolic consequences. *Cell* 158, 705–721. doi: 10.1016/j.cell.2014.05.052

Derrien, M., Vaughan, E. E., Plugge, C. M., and de Vos, W. M. (2004). *Akkermansia muciniphila* gen. nov., sp. nov., a human intestinal mucin-degrading bacterium. *Int. J. Syst. Evol. Microbiol.* 54, 1469–1476. doi: 10.1099/ijs.0.02873-0

Devaraj, S., Hemarajata, P., and Versalovic, J. (2013). The human gut microbiome and body metabolism: implications for obesity and diabetes. *Clin. Chem.* 59, 617–628. doi: 10.1373/clinchem.2012.187617

Ding, T., and Schloss, P. D. (2014). Dynamics and associations of microbial community types across the human body. *Nature* 509, 357–360. doi: 10.1038/nature13178

Falony, G., Joossens, M., Vieira-Silva, S., Wang, J., Darzi, Y., Faust, K., et al. (2016). Population-level analysis of gut microbiome variation. *Science* 352, 560–564. doi: 10.1126/science.aad3503

Frayling, T. M., Timpson, N. J., Weedon, M. N., Zeggini, E., Freathy, R. M., Lindgren, C. M., et al. (2007). A common variant in the FTO gene is associated with body mass index and predisposes to childhood and adult obesity. *Science* 316, 889–894. doi: 10.1126/science.1141634

Gill, S. R., Pop, M., Deboy, R. T., Eckburg, P. B., Turnbaugh, P. J., Samuel, B. S., et al. (2006). Metagenomic analysis of the human distal gut microbiome. *Science* 312, 1355–1359. doi: 10.1126/science.1124234

Goodrich, J. K., Waters, J. L., Poole, A. C., Sutter, J. L., Koren, O., Blekhman, R., et al. (2014). Human genetics shape the gut microbiome. *Cell* 159, 789–799. doi: 10.1016/j.cell.2014.09.053

Hildebrandt, M. A., Hoffmann, C., Sherrill-Mix, S. A., Keilbaugh, S. A., Hamady, M., Chen, Y. Y., et al. (2009). High-fat diet determines the composition of the murine gut microbiome independently of obesity. *Gastroenterology* 137, 1716–1724.e1–2. doi: 10.1053/j.gastro.2009.08.042

Jensen, L. J., Kuhn, M., Stark, M., Chaffron, S., Creevey, C., Muller, J., et al. (2009). STRING 8–a global view on proteins and their functional interactions in 630 organisms. *Nucleic Acids Res.* 37, D412–D416. doi: 10.1093/nar/gkn760

Karlsson, F. H., Tremaroli, V., Nookaew, I., Bergström, G., Behre, C. J., Fagerberg, B., et al. (2013). Gut metagenome in european women with normal, impaired and diabetic glucose control. *Nature* 498, 99–103. doi: 10.1038/nature12198

Khan, M. T., Nieuwdorp, M., and Bäckhed, F. (2014). Microbial modulation of insulin sensitivity. *Cell Metab.* 20, 753–760. doi: 10.1016/j.cmet.2014.07.006

Kobyliak, N., Conte, C., Cammarota, G., Haley, A. P., Styriak, I., Gaspar, L., et al. (2016). Probiotics in prevention and treatment of obesity: a critical view. *Nutr. Metab.* 13:14. doi: 10.1186/s12986-016-0067-0

Kurokawa, K., Itoh, T., Kuwahara, T., Oshima, K., Toh, H., Toyoda, A., et al. (2007). Comparative metagenomics revealed commonly enriched gene sets in human gut microbiomes. *DNA Res.* 14, 169–181. doi: 10.1093/dnares/dsm018

Le Chatelier, E., Nielsen, T., Qin, J., Prifti, E., Hildebrand, F., Falony, G., et al. (2013). Richness of human gut microbiome correlates with metabolic markers. *Nature* 500, 541–546. doi: 10.1038/nature12506

Li, X., Shimizu, Y., and Kimura, I. (2017). Gut microbial metabolite short-chain fatty acids and obesity. *Biosci. Microbiota Food Health* 36, 135–140. doi: 10.12938/bmfh.17-010

Liu, R., Hong, J., Xu, X., Feng, Q., Zhang, D., Gu, Y., et al. (2017). Gut microbiome and serum metabolome alterations in obesity and after weight-loss intervention. *Nat. Med.* 23, 859–868. doi: 10.1038/nm.4358

Martens, E. C., Koropatkin, N. M., Smith, T. J., and Gordon, J. I. (2009). Complex glycan catabolism by the human gut microbiota: the *Bacteroidetes* Sus-like paradigm. *J. Biol. Chem.* 284, 24673–24677. doi: 10.1074/jbc.R109.022848

Menni, C., Zierer, J., Pallister, T., Jackson, M. A., Long, T., Mohney, R. P., et al. (2017). Omega-3 fatty acids correlate with gut microbiome diversity and production of N-carbamylglutamate in middle aged and elderly women. *Sci. Rep.* 7:11079. doi: 10.1038/s41598-017-10382-2

Musso, G., Gambino, R., and Cassader, M. (2010). Obesity, diabetes, and gut microbiota: the hygiene hypothesis expanded? *Diabetes Care* 33, 2277–2284. doi: 10.2337/dc10-0556

Nicholson, J. K., Holmes, E., Kinross, J., Burcelin, R., Gibson, G., Jia, W., et al. (2012). Host-gut microbiota metabolic interactions. *Science* 336, 1262–1267. doi: 10.1126/science.1223813

O'Hara, A. M., and Shanahan, F. (2006). The gut flora as a forgotten organ. *EMBO Rep.* 7, 688–693. doi: 10.1038/sj.embor.7400731

Perry, R. J., Peng, L., Barry, N. A., Cline, G. W., Zhang, D., Cardone, R. L., et al. (2016). Acetate mediates a microbiome-brain-beta-cell axis to promote metabolic syndrome. *Nature* 534, 213–217. doi: 10.1038/nature18309

Qin, J., Li, R., Raes, J., Arumugam, M., Burgdorf, K. S., Manichanh, C., et al. (2010). A human gut microbial gene catalogue established by metagenomic sequencing. *Nature* 464, 59–65. doi: 10.1038/nature08821

Qin, J., Li, Y., Cai, Z., Li, S., Zhu, J., Zhang, F., et al. (2012). A metagenome-wide association study of gut microbiota in type 2 diabetes. *Nature* 490, 55–60. doi: 10.1038/nature11450

Ridaura, V. K., Faith, J. J., Rey, F. E., Cheng, J., Duncan, A. E., Kau, A. L., et al. (2013). Gut microbiota from twins discordant for obesity modulate metabolism in mice. *Science* 341:1241214. doi: 10.1126/science.1241214

Rivière, A., Selak, M., Lantin, D., Leroy, F., and De Vuyst, L. (2016). Bifidobacteria and butyrate-producing colon bacteria: importance and strategies for their stimulation in the human gut. *Front. Microbiol.* 7:979. doi: 10.3389/fmicb.2016.00979

Rooks, M. G., and Garrett, W. S. (2016). Gut microbiota, metabolites and host immunity. *Nat. Rev. Immunol.* 16, 341–352. doi: 10.1038/nri.2016.42

Rosenbaum, M., Knight, R., and Leibel, R. L. (2015). The gut microbiota in human energy homeostasis and obesity. *Trends Endocrinol. Metab.* 26, 493–501. doi: 10.1016/j.tem.2015.07.002

Samuel, B. S., Shaito, A., Motoike, T., Rey, F. E., Backhed, F., Manchester, J. K., et al. (2008). Effects of the gut microbiota on host adiposity are modulated by the short-chain fatty-acid binding G protein-coupled receptor, Gpr41. *Proc. Natl. Acad. Sci. U.S.A.* 105, 16767–16772. doi: 10.1073/pnas.0808567105

Scarpellini, E., Campanale, M., Leone, D., Purchiaroni, F., Vitale, G., Lauritano, E. C., et al. (2010). Gut microbiota and obesity. *Intern. Emerg. Med.* 5, 53–56. doi: 10.1007/s11739-010-0450-1

Silverman, M., Kua, L., Tanca, A., Pala, M., Palomba, A., Tanes, C., et al. (2017). Protective major histocompatibility complex allele prevents type 1 diabetes by shaping the intestinal microbiota early in ontogeny. *Proc. Natl. Acad. Sci. U.S.A.* 114, 9671–9676. doi: 10.1073/pnas.1712280114

Suárez-Zamorano, N., Fabbiano, S., Chevalier, C., Stojanović, O., Colin, D. J., Stojanović, A., et al. (2015). Microbiota depletion promotes browning of white adipose tissue and reduces obesity. *Nat. Med.* 21, 1497–1501. doi: 10.1038/nm.3994

Thomas, C., Gioiello, A., Noriega, L., Strehle, A., Oury, J., Rizzo, G., et al. (2009). TGR5-mediated bile acid sensing controls glucose homeostasis. *Cell Metab.* 10, 167–177. doi: 10.1016/j.cmet.2009.08.001

Tilg, H., and Kaser, A. (2011). Gut microbiome, obesity, and metabolic dysfunction. *J. Clin. Invest.* 121, 2126–2132. doi: 10.1172/JCI58109

Tolhurst, G., Heffron, H., Lam, Y. S., Parker, H. E., Habib, A. M., Diakogiannaki, E., et al. (2012). Short-chain fatty acids stimulate glucagon-like peptide-1 secretion via the G-protein-coupled receptor FFAR2. *Diabetes* 61, 364–371. doi: 10.2337/db11-1019

Turnbaugh, P. J., and Gordon, J. I. (2009). The core gut microbiome, energy balance and obesity. *J. Physiol.* 587, 4153–4158. doi: 10.1113/jphysiol.2009.174136

Turnbaugh, P. J., Hamady, M., Yatsunenko, T., Cantarel, B. L., Duncan, A., Ley, R. E., et al. (2009). A core gut microbiome in obese and lean twins. *Nature* 457, 480–484. doi: 10.1038/nature07540

Turnbaugh, P. J., Ley, R. E., Mahowald, M. A., Magrini, V., Mardis, E. R., and Gordon, J. I. (2006). An obesity-associated gut microbiome with increased capacity for energy harvest. *Nature* 444, 1027–1031. doi: 10.1038/nature05414

Wright, D. P., Rosendale, D. I., and Robertson, A. M. (2000). Prevotella enzymes involved in mucin oligosaccharide degradation and evidence for a small operon of genes expressed during growth on mucin. *FEMS Microbiol. Lett.* 190, 73–79. doi: 10.1111/j.1574-6968.2000.tb09265.x

Wu, G. D., Chen, J., Hoffmann, C., Bittinger, K., Chen, Y. Y., Keilbaugh, S. A., et al. (2011). Linking long-term dietary patterns with gut microbial enterotypes. *Science* 334, 105–108. doi: 10.1126/science.1208344

Zhao, L. (2013). The gut microbiota and obesity: from correlation to causality. *Nat. Rev. Microbiol.* 11, 639–647. doi: 10.1038/nrmicro3089

Zhernakova, A., Kurilshikov, A., Bonder, M. J., Tigchelaar, E. F., Schirmer, M., Vatanen, T., et al. (2016). Population-based metagenomics analysis reveals markers for gut microbiome composition and diversity. *Science* 352, 565–569. doi: 10.1126/science.aad3369

Zoetendal, E. G., Rajilic-Stojanovic, M., and de Vos, W. M. (2008). High-throughput diversity and functionality analysis of the gastrointestinal tract microbiota. *Gut* 57, 1605–1615. doi: 10.1136/gut.2007.133603

Conflict of Interest Statement: The authors declare that the research was conducted in the absence of any commercial or financial relationships that could be construed as a potential conflict of interest.

The reviewer LW and handling Editor declared their shared affiliation.

frontiers in Physiology

ORIGINAL RESEARCH
published: 04 January 2018
doi: 10.3389/fphys.2017.01117

Obesity or Overweight, a Chronic Inflammatory Status in Male Reproductive System, Leads to Mice and Human Subfertility

Weimin Fan[1,2†], Yali Xu[1†], Yue Liu[1†], Zhengqing Zhang[3], Liming Lu[4] and Zhide Ding[1*]*

[1] *Shanghai Key Laboratory for Reproductive Medicine, Department of Histology Embryology, Genetics and Developmental Biology, School of Medicine, Shanghai Jiao Tong University, Shanghai, China,* [2] *Reproductive Medicine Center, Shanghai Ruijin Hospital, School of Medicine, Shanghai Jiao Tong University, Shanghai, China,* [3] *The Laboratory of Clinical Medicine, Shanghai No.9 People's Hospital, School of Medicine, Shanghai Jiao Tong University, Shanghai, China,* [4] *Laboratory of Immune Regulation, Shanghai Institute of Immunology, Shanghai Jiao Tong University School of Medicine, Shanghai, China*

OPEN ACCESS

Edited by:
Dechun Feng,
National Institute on Alcohol Abuse and Alcoholism, United States

Reviewed by:
Xingxing Zang,
Albert Einstein College of Medicine, United States
Aijuan Qu,
Capital Medical University, China

***Correspondence:**
Liming Lu
lulunew2003@163.com
Zhide Ding
zding@shsmu.edu.cn

† These authors have contributed equally to this work.

Specialty section:
This article was submitted to Clinical and Translational Physiology, a section of the journal Frontiers in Physiology

Received: *24 October 2017*
Accepted: *18 December 2017*
Published: *04 January 2018*

Citation:
Fan W, Xu Y, Liu Y, Zhang Z, Lu L and Ding Z (2018) Obesity or Overweight, a Chronic Inflammatory Status in Male Reproductive System, Leads to Mice and Human Subfertility. Front. Physiol. 8:1117. doi: 10.3389/fphys.2017.01117

Obesity is frequently accompanied with chronic inflammation over the whole body and is always associated with symptoms that include those arising from metabolic and vascular alterations. On the other hand, the chronic inflammatory status in the male genital tract may directly impair spermatogenesis and is even associated with male subfertility. However, it is still unclear if the chronic inflammation induced by obesity damages spermatogenesis in the male genital tract. To address this question, we used a high fat diet (HFD) induced obese mouse model and recruited obese patients from the clinic. We detected increased levels of tumor necrosis factor (TNF-α), interleukin-6 (IL-6), and NOD-like receptor family pyrin domain containing-3 (NLRP3) in genital tract tissues including testis, epididymis, seminal vesicle, prostate, and serum from obese mice. Meanwhile, the levels of immunoglobulin G (IgG) and corticosterone were significantly higher than those in the control group in serum. Moreover, signal factors regulated by TNF-α, i.e., p38, nuclear factor-κB (NF-κB), Jun N-terminal kinase (JNK), extracellular signal-regulated kinase (ERK), and their phosphorylated status, and inflammasome protein NLRP3 were expressed at higher levels in the testis. For overweight and obese male patients, the increased levels of TNF-α and IL-6 were also observed in their seminal plasma. Furthermore, there was a positive correlation between the TNF-α and IL-6 levels and BMI whereas they were inversely correlated with the sperm concentration and motility. In conclusion, impairment of male fertility may stem from a chronic inflammatory status in the male genital tract of obese individuals.

Keywords: inflammation, reproductive system, overweight and obesity, male, subfertility

INTRODUCTION

Obesity is a global health problem and the prevalence of obesity has risen substantially in the past three decades. For instance, the number of overweight and obese individuals increased from 857 million in 1980, to 2.1 billion in 2013. Worldwide, the proportion of men who were overweight increased from 28.8% in 1980, to 36.9% in 2013 (Ng et al., 2014).

Generally, obesity is a metabolic disease resulting from behavior and heritable causes. Meanwhile, it is also associated with a number of chronic states including metabolic syndrome, hyperlipidemia, type-2 diabetes, cancer, cardiovascular disease, and infertility (An et al., 2017). Besides these associations between obesity and disease, studies over the past years indicate there are important signaling pathways connecting this metabolic syndrome with the immune system (Tilg and Moschen, 2006). These interactions between metabolism and immune system seem to be orchestrated by several mediators derived from immune cells, adipocytes, and systemic inflammation that are induced by obesity (Wellen and Hotamisligil, 2005). One of the sources of these mediators may be dysfunctional adipocytes (Esser et al., 2014).

There is substantive evidence supporting the notion that obesity is correlated with a chronic inflammatory response based on the identification of abnormal cytokines such as TNF-α and IL-6, along with the activation of pro-inflammatory signaling pathways (Wellen and Hotamisligil, 2005). Many studies found that adipocytes can directly express TNF-α in rodents. This finding formed the basis for suggesting that adipocytes have crucial role in inducing chronic inflammatory responses in obesity. Interestingly, these findings were consistent with a human study showing increased TNF-α production in the adipose tissue of obese individuals, which declined TNF-α production after weight loss (Kern et al., 1995). Moreover, it has been reported recently that the NOD-like receptor family pyrin domain containing-3 (NLRP3), one of the inflammasomes, is associated with obesity and contributes to obesity-induced inflammation (Vandanmagsar et al., 2011).

On the other hand, there is much evidence showing that obesity reduces sperm quality and then impairs male fertility (Teerds et al., 2011; Hammiche et al., 2012; Liu and Ding, 2017), whereas metabolic syndrome, hyperlipidemia, and a pro-inflammatory state are independently linked with male subfertility (Klöting and Blüher, 2014). However, it is unclear how obesity elicits its effects on sperm morphology or function. Namely, it needs to be clarified if it occurs as a consequence of increases in obesity and/or is an indirect associated complication of this condition.

We report here on the use of a Male obese mouse model which was successfully induced by being fed a high fat diet (HFD). In parallel, 272 semen samples from healthy, overweight and obese human males were collected and then analyzed. This endeavor had two goals: (1) To determine if obesity can either induce inflammatory responses or increase the expression of pro-inflammation cytokines in the male genital tract and serum; (2) To determine if the proinflammatory cytokines had effects on relevant signaling pathways mediating control of testicular spermatogenesis or on sperm function in the caudal epididymis.

MATERIALS AND METHODS

Animals and Obese Model Establishment

Animal experiments were conducted according to the International Guiding Principles for Biomedical Research Involving Animals, as promulgated by the Society for the Study of Reproduction. This research program was approved by the Ethics Committee of Shanghai Jiao Tong University School of Medicine (NO. A2015-034). C57BL/6 mice (Male: aged 3 weeks) were purchased from Shanghai Laboratory Animal Center, and acclimated in the Animal Center of Jiao Tong University Medical School at least for 1 week prior to experimentation. Male mice were divided in two groups every time: 10 mice were continuously fed a high-fat diet (HFD) containing 23.3% casein, 0.3% L-cysteine, 8.5% corn starch, 11.7% maltodextrin, 20.1% sucrose, 5.8% cellulose, 2.9% soybean oil, 20.7% lard, 5.2% mineral mix, 1.2% vitamin mix, and 0.3% choline bitartrate, and 10 control mice fed a normal diet including 19% casein, 0.2% L-cysteine, 29.9% corn starch, 3.3% maltodextrin, 33.2% sucrose, 4.7% cellulose, 2.4% soybean oil, 1.9% lard, 4.3% mineral mix, 0.9% vitamin mix, and 0.2% choline bitartrate in subsequent 10 weeks. Body weight of all animals and food intake were measured every week.

Mice Serum Lipids and Apolipoprotein (Apo)

The mice serum lipids, such as cholesterol (CHOL), triglycerides (TGL), high density lipoprotein (HDL), and low density lipoprotein (LDL), as well as apolipoprotein including ApoB and ApoE were measured at 14 weeks. Precise levels of these lipids were detected using a Roche COBAS c 311 auto biochemistry analyzer (Roche Diagnostics, Mannheim, Germany).

Histological Analysis

Tissues from both HFD mice and control diet (CD) mice were taken for histological evaluation. Mice testes and a small piece of liver were fixed in Bouin's solution for 24 h, and then stored in 70% ethanol for 2 h. Tissues were embedded in paraffin, then sliced into 5 μm thick sections and mounted on glass slides, followed by dewaxing and rehydration. The specimens were then stained with hematoxylin and eosin (H&E), finally observed using a microscope (Nikon, ECLIPSE E600, Japan).

mRNA Quantification by Real-Time qRT-PCR

Mice testes, epididymal caput and cauda, prostate, and seminal vesicle were homogenized in the TRIzol reagent (Invitrogen, US). cDNA was prepared from 1 μg RNA using PrimeScript RT Master Mix (TaKaRa, Japan). SYBR green-based quantification real-time PCR was applied to measure IL-6, TNF-α, and NLRP3 expression in testes, epididymal caput and cauda, prostates, and seminal vesicles from both HFD mice and CD mice. The sequences of the primers were as follows: IL-6, forward 5′-TTCT TGGGACTGATGCTGGT-3′, reverse 5′-CCTCCGACTTGTGA AGTGGT-3′; TNF-α, forward 5′-ACGGCATGGATCTCAAAG AC-3′, reverse 5′-GTGGGTG-AGGAGCACGTAGT-3′; NLRP3, forward 5′-CATCAATGCTGCTTCGACAT-3′, reverse 5′-TCA GTCCCACACACAGCAAT-3′. Real-Time PCR was performed on an ABI 7500 (Applied Biosystems, US) using SYBR Premix Ex Taq II (TaKaRa, Japan) according to the manufacturer's protocol. The expression levels of genes were normalized against β-actin and a segment of β-actin was amplified with the forward primer

5′-GGGAATGGGTCAGAAGGACT-3′ and reverse primer 5′-C TTCTCCATGTCG-TCCCAGT-3′.

Mice Serum Analyses by ELISA

Testosterone, estradiol, progesterone, corticosterone, IgG, IgM, TNF-α, and IL-6 levels in mice sera were measured at the age of 14 weeks. Testosterone (R&D Systems, USA), estradiol (Cayman Chemical, USA), progesterone (Cayman Chemical, USA), corticosterone (ALPCO, USA), IgG (ICL, USA), IgM (ICL, USA), TNF-α (Anogen, Canada), IL-6 (Anogen, Canada) in sera were detected, respectively, by using the immunoassay kits according to the manufacturer's protocol.

Protein Sample Preparation from Testes

Mice testes were homogenized in RIPA lysis buffer (Thermo Fisher Scientific, USA) containing protease inhibitor (Thermo Fisher Scientific, USA) on ice for 30 min. Then the tissue lysates were centrifuged at 12,000 × g, 10 min, 4°C. The testicular proteins in the supernatant were collected and the concentrations were determined by the BCA Protein Assay Kit (Thermo Fisher Scientific, USA).

Western Blot Analysis

Protein samples (20 μg) were separated by using 12% denaturing polyacrylamide gels, then transferred to polyvinylidene difluoride (PVDF) membranes (Millipore, Germany) using a semi-dry transfer apparatus (Bio-Rad, Hercules, CA, USA). Membranes were blocked with 5% bovine serum albumin (BSA) for 1 h at room temperature and immunoblotting was performed overnight at 4°C with the antibodies: p38 (Cell Signaling Technology, 1:1000), p-p38 (phospho T180 + Y182, Abcam, 1:1000), NF-κB (p65, Cell Signaling Technology, 1:1000), p-NF-κB p65 (phospho S536, Abcam, 1:1000), JNK (SAPK/JNK, Cell Signaling Technology, 1:1000), p-JNK (phospho T183 + Y185, Cell Signaling Technology, 1:1000), ERK1/2 (p44/42, Cell Signaling Technology, 1:1000), p-ERK (p-p44/42, phospho T202 + Y204, Cell Signaling Technology, 1:1000), and NLRP3 (Abcam, 1:2000), followed by incubation with secondary antibody conjugated to HRP (Abgent, San Diego, CA, USA, 1:10000 dilution). Meanwhile, β-actin (Cell Signaling Technology, 1:1000) was used to validate protein loading equivalence simultaneously. Signals were generated by enhanced chemiluminescence (Millipore, Germany) according to the manufacturer's protocol and detected by a Luminescent Image Analyzer (Image Quant LAS 4000, GE imagination at work, USA).

Semen Specimens

Human semen specimens were obtained from Reproductive Medicine Center, Ruijin Hospital, Shanghai Jiao Tong University, School of Medicine. Use of the semen samples was approved by the Ethics Committee of this institution and all experiments were performed in accordance with relevant guidelines and regulations.

All semen specimens, both from normal and obese or overweight donors (20 to 35 years old), were collected and the donors gave written informed consent for the use of their leftover semen samples when all IVF treatments finished. Notably, individuals having a history of long-term medication, varicocoele, and infection as indicated by a large number of leukocytes in the semen were excluded from the study. Furthermore, samples that were hyperviscous and necrozoospermic (sperm viability <70%) were also excluded from the study. A computer assisted semen analyzer (CASA, Hamilton-Thorn Research, Beverly, MA, USA) then evaluated semen specimen quality based on parameters described in the World Health Organization guidelines (WHO, 2010).

Semen Samples Preparation and Seminal Plasma ELISA

Fresh human semen specimens were centrifuged (800 g, 10 min, 4°C) and the supernatant containing seminal plasma proteins were stored immediately at −80°C until further use. TNF-α, IL-6 in seminal plasma were detected using the related immunoassay kits (Anogen, Canada) according to the manufacturer's protocol.

Statistical Analysis

All data were analyzed using SAS 8.2 software, and results are presented as mean ± SD. Comparisons between two groups were made using student's *t*-test appropriately. One-way analysis of variance (ANOVA) test was used assuming a two-tail hypothesis with $P < 0.05$. Differences were considered statistically different when $P < 0.05$.

RESULTS

Food Intake, Body Weight, and Hepatic Morphology

Male C57BL/6 mice consumed a high-fat diet for 10 weeks and gained significantly more weight in comparison to that of age-matched littermates fed a normal diet (31.63 ± 1.96 g vs. 26.29 ± 1.05 g, $n = 30$, $P < 0.05$). The differences in body weight between these two groups persisted for 6 weeks (**Figure 1A**). The food intake by the HFD group per week was always less than that of normal diet group (**Figure 1B**), but the high-fat diet contains much more calories. Besides, liver morphological analysis clearly indicated that the high-fat diet fed mice had a serious hepatic steatosis and fat vacuoles were evident in almost every hepatic cell (**Figure 1C**). Then, mice fed a high-fat diet for 10 weeks were placed in the obese group whereas those fed a normal diet were assigned to the control group.

Serum Lipid and Hormone Profiles

Male mice fed with HFD had higher levels of cholesterol (CHOL) (4.36 ± 0.47 mmol/L vs. 2.30 ± 0.65 mmol/L, $n = 10$, $P < 0.01$), HDL (2.16 ± 0.30 mmol/L vs. 1.47 ± 0.25 mmol/L, $n = 10$, $P < 0.01$) and LDL (0.47 ± 0.11 mmol/L vs. 0.26 ± 0.11 mmol/L, $n = 10$, $P < 0.01$) than those in the control group, but there was no difference in their triglyceride (TGL) concentration (1.19 ± 0.40 mmol/L vs. 1.16 ± 0.28 mmol/L, $n = 10$, $P > 0.05$) between the two groups (**Figure 2A**). Besides, in obese mice, ApoB and ApoE levels were significantly elevated compared to those in

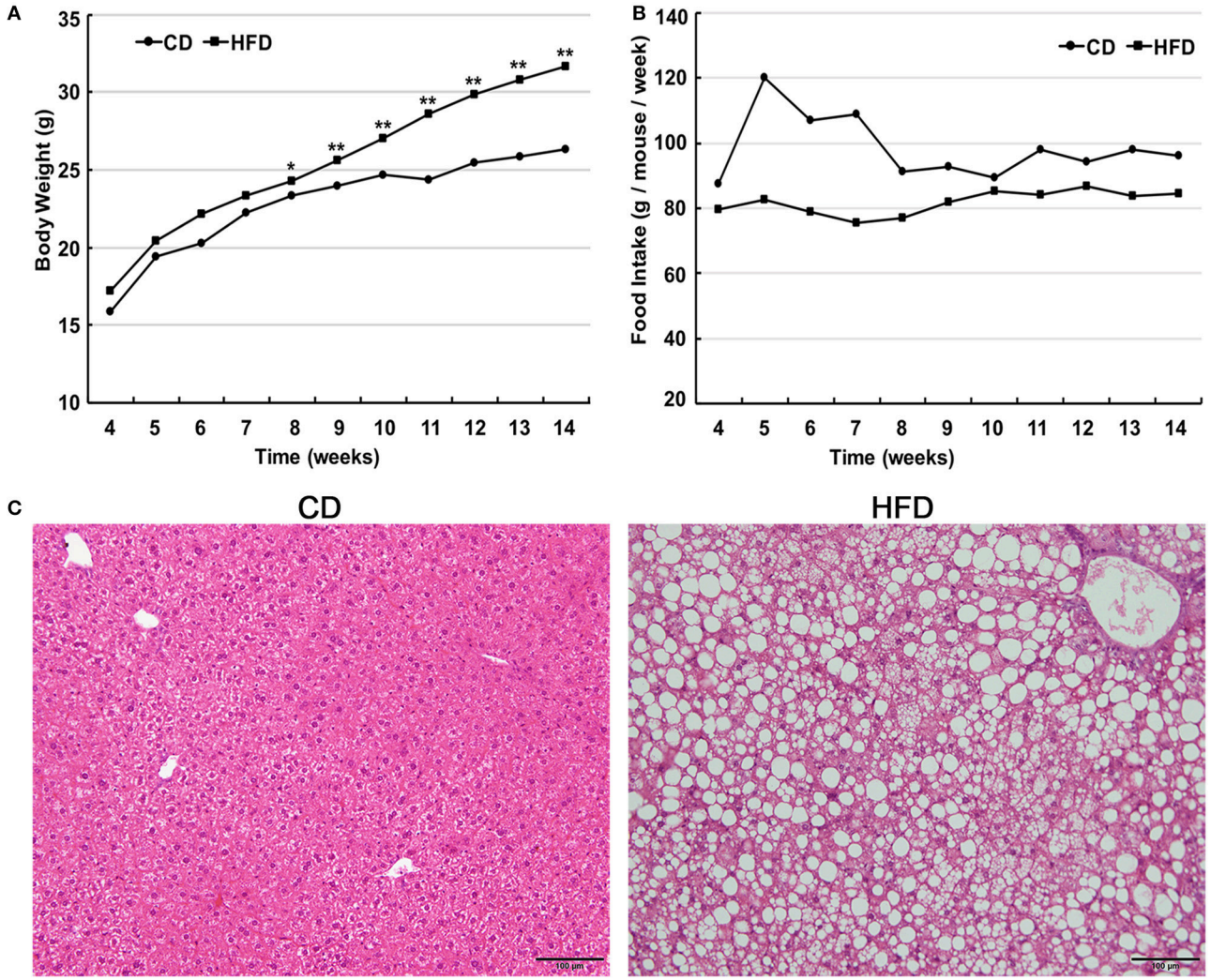

FIGURE 1 | High fat diet feeding establishes obese mouse model. **(A)** Comparison of time-dependent increases in body weight between CD ($n = 30$) and HFD groups ($n = 30$), showed that the body weight gain of the HFD group was significantly greater than that of the CD group (*$P < 0.05$, **$P < 0.01$). **(B)** Weekly food intake on control diet (CD) and high-fat diet (HFD). **(C)** Hematoxylin and eosin-stained hepatic sections from mice fed either CD or HFD showed a serious hepatic steatosis in HFD fed mice. Scale bar = 100 μm.

control mice (0.08 ± 0.03 g/L vs. 0.05 ± 0.007 g/L, 5.18 ± 0.86 mg/dl vs. 2.46 ± 1.00 mg/dl, $n = 10$, $P < 0.01$; **Figures 2B,C**).

Serum estradiol level was much higher in obese mice than that in the control group (16.74 ± 1.06 pg/ml vs. 9.14 ± 2.58 pg/ml, $n = 10$, $P < 0.01$), and inversely, serum testosterone (4.58 ± 1.44 ng/ml vs. 7.95 ± 0.80 ng/ml, $n = 10$, $P < 0.01$) and progesterone (10.38 ± 1.43 pg/ml vs. 12.76 ± 1.62 pg/ml, $n = 10$, $P < 0.05$) levels significantly decreased in obese mice compared to those in the control group (**Figures 2D–F**).

Effects of High-Fat Diet on Testicular Morphological Structure

Morphological analysis of the testes indicated that obese mice had an abnormal testicular structure compared with that of normal mice (**Figure 3**). The seminiferous epithelia were atrophied in high-fat diet mice and cell adhesion between spermatogenic cells and Sertoli cells were impaired and loosely arranged.

Levels of Pro-inflammatory Cytokines, Corticosterone, IgG, and IgM in Sera

The serous levels of IL-6, TNF-α, corticosterone, IgG, and IgM were measured by ELISA. The results demonstrated that obesity induced significantly higher expression levels of IL-6 and TNF-α in sera. In obese mice, IL-6 and TNF-α levels were obviously higher than those in the control group (IL-6: 9.50 ± 1.54 pg/ml vs. 5.37 ± 0.72 pg/ml, TNF-α: 30.91 ± 5.74 pg/ml vs. 18.18 ± 1.46 pg/ml, $n = 10$, $P < 0.01$, **Figures 4A,B**). On the other hand, the corticosterone level was significantly higher in obese mice than

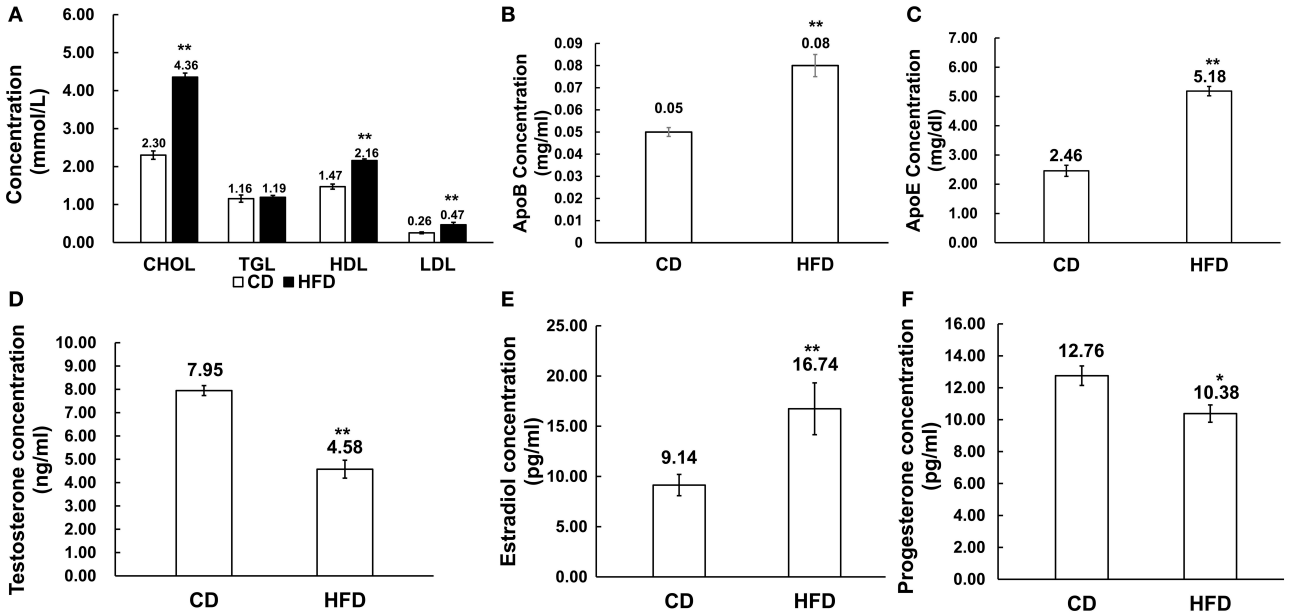

FIGURE 2 | Alteration of serum lipid and sex hormone level profiles in HFD mice. **(A)** Comparison of serum lipid level profiles in CD and HFD groups; CHOL: total cholesterol, TGL, triglycerides; HDL, high density lipoprotein; LDL, low density lipoprotein. **(B,C)** Comparison of ApoB and ApoE profiles in CD and HFD mice. **(D–F)** Comparison of serum sex hormone profiles between CD and HFD groups, including testosterone, estradiol and progesterone. $^{*}P < 0.05$, $^{**}P < 0.01$.

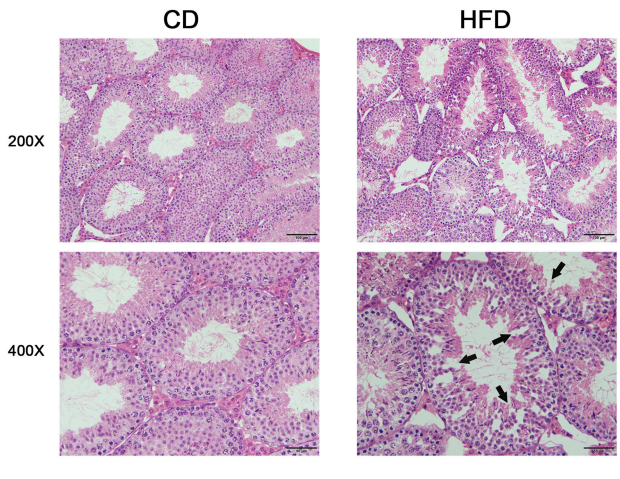

FIGURE 3 | Comparison of testicular morphology in CD and HFD mice. Hematoxylin and eosin-stained testicular sections, both imaged with 20× and 40× objectives, revealed loosely arranged spermatogenic cells (arrows) on the seminiferous epithelium in HFD mice. Scale bar = 50 or 100 μm.

that in the control group (165.75 ± 37.01 ng/ml vs. 115.93 ± 37.74 ng/ml, $n = 10$, $P < 0.01$, **Figure 4C**). Meanwhile, the level of IgG was much higher in high-fat diet mice than that in control group (6227.40 ± 2256.22 μg/ml vs. 3620.39 ± 1390.46 μg/ml, $n = 10$, $P < 0.01$, **Figure 4D**), whereas the IgM concentration in serum was unchanged between high-fat diet and normal-diet mice (185.51 ± 78.65 μg/ml vs. 181.73 ± 80.31 μg/ml, $n = 10$, $P > 0.05$, **Figure 4E**).

mRNA Expression of Pro-inflammatory Cytokines and Inflammasome in Mice Genital Tract Tissues

The mRNA levels of IL-6, TNF-α, and NLRP3 in testis, epididymal caput, epididymal cauda, prostate, and seminal vesicle tissues were measured to assess the inflammatory alteration in male genital tract from obese mice. The results of Real-Time PCR showed that the mRNA levels of IL-6, TNF-α, and NLRP3 remarkably increased in obese male genital tract. In testis, the mRNA expressions of IL-6, TNF-α, and NLRP3 were 3.7 ± 0.83, 2.24 ± 0.50, and 2.42 ± 0.51 folds higher in obese mice, respectively, than those in the normal group ($n = 10$, $P < 0.05$, **Figure 5A**). In the epididymal caput, the mRNA expression levels of IL-6, TNF-α, and NLRP3 were 3.05 ± 0.79, 1.90 ± 0.17, and 1.51 ± 0.16-folds higher, respectively, than those in the normal group ($n = 10$, $P < 0.05$, **Figure 5B**). In the epididymal cauda, the mRNA expression levels of IL-6 TNF-α, NLRP3 were 3.85 ± 0.71, 2.80 ± 0.61, and 2.45 ± 0.20-folds higher, respectively, than those in the normal group ($n = 10$, $P < 0.05$, **Figure 5C**). In the prostate, the mRNA expression levels of IL-6, TNF-α, and NLRP3 were about 6.56 ± 0.58, 4.23 ± 0.54, and 5.44 ± 0.88-folds higher, respectively, than those in the normal group ($n = 10$, $P < 0.05$, **Figure 5D**). Besides, in the seminal vesicle, the mRNA expression levels of IL-6, TNF-α, and NLRP3 were 8.75 ± 1.53, 4.41 ± 0.77, and 5.71 ± 1.30-folds higher in obese mice, respectively, than those in the normal group ($n = 10$, $P < 0.05$, **Figure 5E**). These results further validated that obesity can indeed induce a chronic inflammatory status in the male mice genital tract.

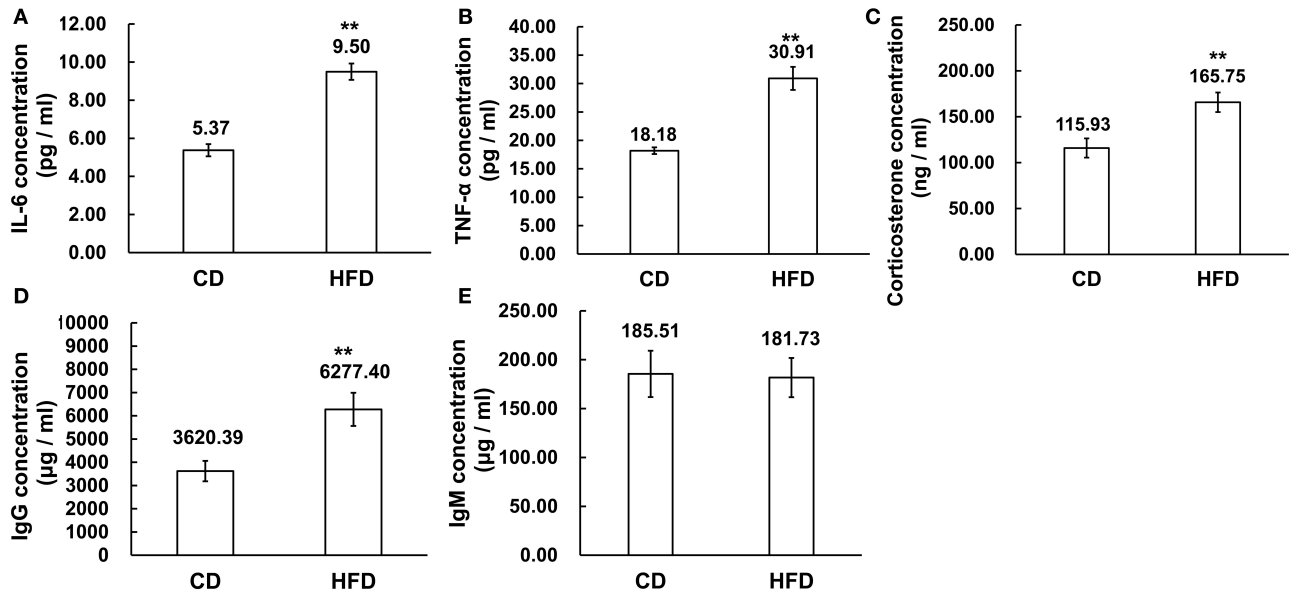

FIGURE 4 | Alteration of inflammation related cytokines in sera. **(A,B)** Pro-inflammatory cytokines IL-6 and TNF-α expression levels were significantly higher in sera of mice fed a HFD than a CD. **(C)** Corticosterone concentration was higher in sera of mice fed a HFD than a CD. **(D,E)** Immunoglobulins, IgG, and IgM concentration, was significantly higher level of IgG in sera of mice fed a HFD than a CD while the IgM concentrations were unchanged in the CD and HFD mice sera $^{**}P < 0.01$.

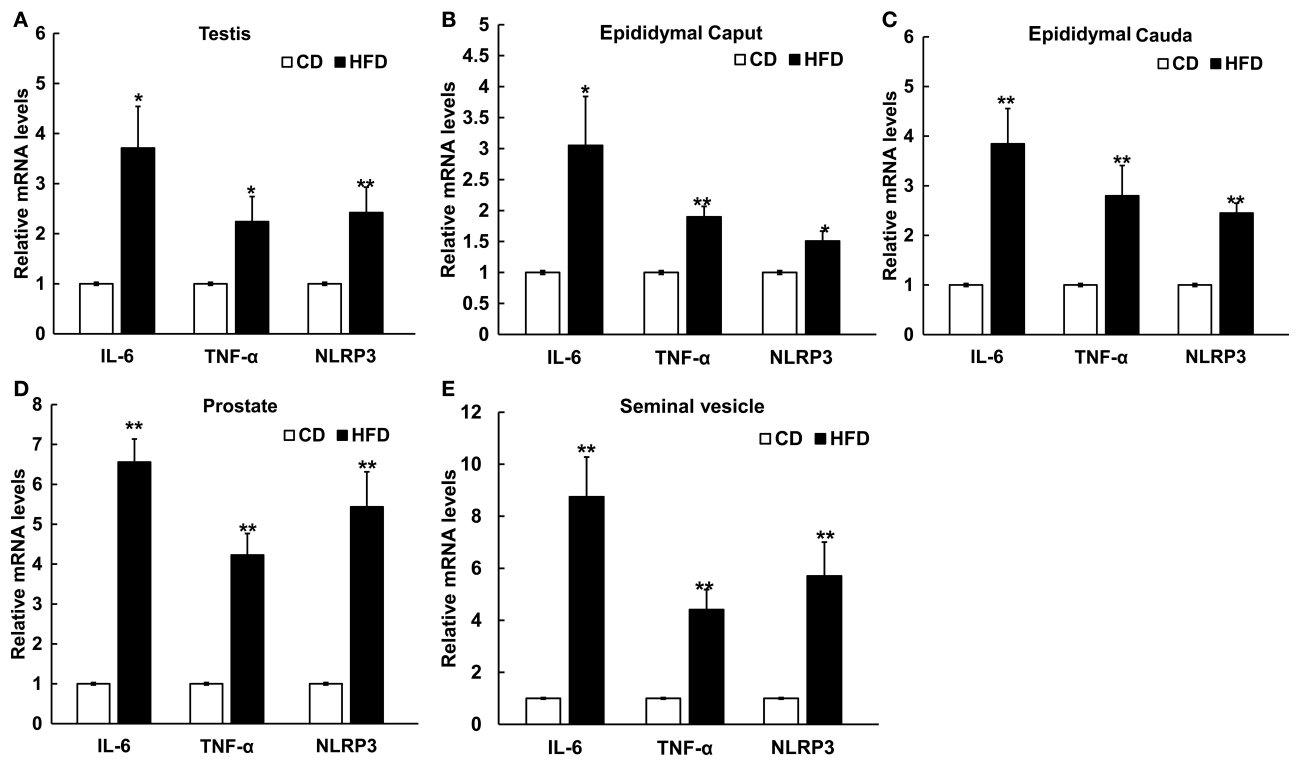

FIGURE 5 | Differential expressions of pro-inflammatory cytokines and NLRP3 inflammasome protein in male genital tract. IL-6, TNF-α and NLRP3 mRNA levels in: **(A)** testis, **(B)** epididymal caput, **(C)** epididymal cauda, **(D)** prostate, and **(E)** seminal vesicle, and in all of these tissues mRNA levels significantly increased in HFD mice. $^{*}P < 0.05$, $^{**}P < 0.01$.

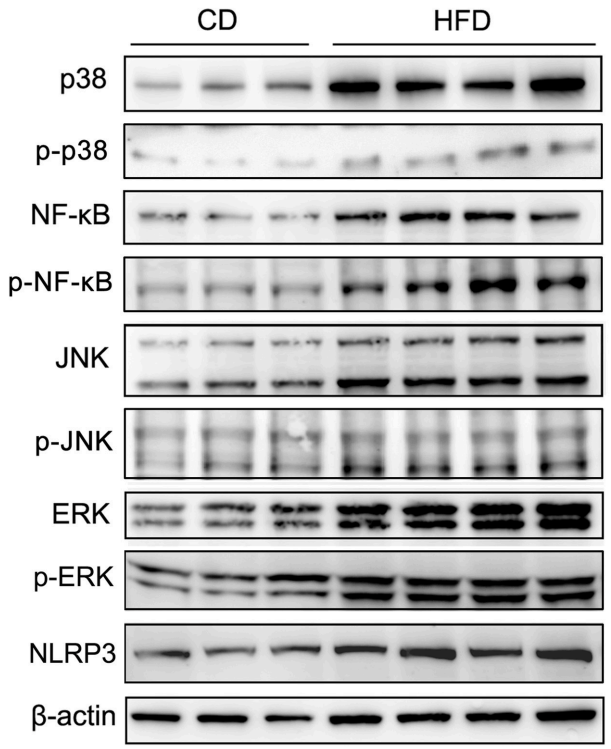

FIGURE 6 | Alteration of testicular inflammation related protein levels. Western blot analyses of representative downstream signaling proteins mediating inflammation, include p38 MAPK, phosphorylated p38 (p-p38), NF-κB, phosphorylated NF-κB p65 (p-NF-κB), JNK, phosphorylated JNK (p-JNK), ERK1/2, phosphorylated ERK1/2 (p-ERK) and inflammasome protein NLRP3, showed that the levels of these inflammation related proteins in testes significantly increased in mice fed a HFD. β-actin expression invariance confirmed protein loading equivalence and normalized aforementioned expression levels.

Expression of p38, NF-κB, JNK, ERK, and Their Phosphorylated Status, and NLRP3 in Testis in High Fat Diet Fed Mice

To evaluate the effects of TNF-α expression rises on signaling pathway mediators in obese mice, we determined their effects on some key representatives. They included p38, NF-κB (p65), JNK, ERK1/2 (p44/42), phosphorylated p38 (p-p38), phosphorylated NF-κB p65 (p-NF-κB), phosphorylated JNK (p-JNK), phosphorylated ERK1/2 (p-ERK), and NLRP3 in testes. The results of Western blots showed that all of these effectors were upregulated in response to high-fat treatment (**Figure 6**).

Expression Levels of IL-6 and TNF-α in Seminal Plasma of Normal, Overweight, and Obese Human Males

To confirm that chronic inflammation existed in the genital tract of overweight and obese males, 272 semen samples from normal weight, overweight and obese human males were collected and then analyzed accordingly. The CASA analyses of spermatozoa from both normal, overweight and obese males revealed that the sperm concentration and motility were inversely reverse correlated with BMI ($n = 272$, $P < 0.01$, **Figures 7A,B**). Especially, the sperm concentration and motility from overweight (sperm concentration: 87.11 ± 64.12 million sperm/ml and sperm motility: 56.77 ± 24.33%, $n = 150$, $P < 0.01$) and obese males (sperm concentration: 76.30 ± 47.73 million sperm/ml and sperm motility: 57.52 ± 26.78%, $n = 40$, $P < 0.01$) greatly decreased in comparison to those from the normal donors (sperm concentration: 113.35 ± 47.19 million sperm/ml and sperm motility: 80.25 ± 10.13%, $n = 82$, $P < 0.01$, **Figures 7E,F**). Simultaneously, the expression levels of IL-6 and TNF-α in seminal plasma measured by ELISA were also significantly correlated with BMI ($n = 272$, $P < 0.01$, **Figures 7C, D**). The results showed that IL-6 expression in the seminal plasma from overweight (25.89 ± 21.45 pg/ml, $n = 150$, $P < 0.01$) and obese males (37.73 ± 27.52 pg/ml, $n = 40$, $P < 0.01$) was obviously up-regulated in comparison to that from the normal males (13.08 ± 11.44 pg/ml, $n = 82$, **Figure 7G**). Meanwhile, TNF-α levels in seminal plasma from obese males (14.35 ± 10.83 pg/ml, $n = 40$, $P < 0.01$) was markedly elevated compared with that from normal males (8.91 ± 5.54 pg/ml, $n = 82$, **Figure 7H**).

DISCUSSION

Chronic inflammation is relevant to increases in adipose tissue content, which occurs along with the expression of abnormal adipocytokines, including several interleukins and tumor necrosis factor (Kaur, 2014). Moreover, high-fat diet feeding is known to induce increases in the secretion of intestinal pro-inflammatory cytokines and large increases in intestinal permeability (Li et al., 2008; Liu et al., 2012). In our previous findings, the male obese mouse model induced by high-fat diet can develop a remarkable impairment of sperm function, including reduced sperm motility, decreased acrosome reaction and fertility rate, and abnormal sperm morphology (Fan et al., 2015). Similar to male obesity, the pro-inflammatory state in males induced by chronic infection, smoking, and environmental toxins is also associated with subfertility phenotypes (Bachir and Jarvi, 2014). Thus, in the present study, our aim was to determine if there is a correlation between male obesity and chronic inflammation and elucidate its underlying mechanism.

Initially, an obese mouse model was successfully established by feeding a HFD which leads to development of an obese phenotype that includes significant increases in body weight, prominent rises in total cholesterol in, LDL, HDL, and apolipoprotein levels in the serum and serious hepatic steatosis. Besides, a remarkable endocrine dysregulation was detected in obese mice. Such defects were accompanied by very notable abnormal sex hormone expression patterns that included increased estradiol and decreased testosterone and progesterone levels.

Sex steroid hormones, such as estradiol, testosterone, and progesterone, regulate a considerable number of functions including reproduction, cell proliferation, and apoptosis as well as the responses to microbial or viral infections (Edwards, 2005). Sex steroid hormones can significantly modulate the

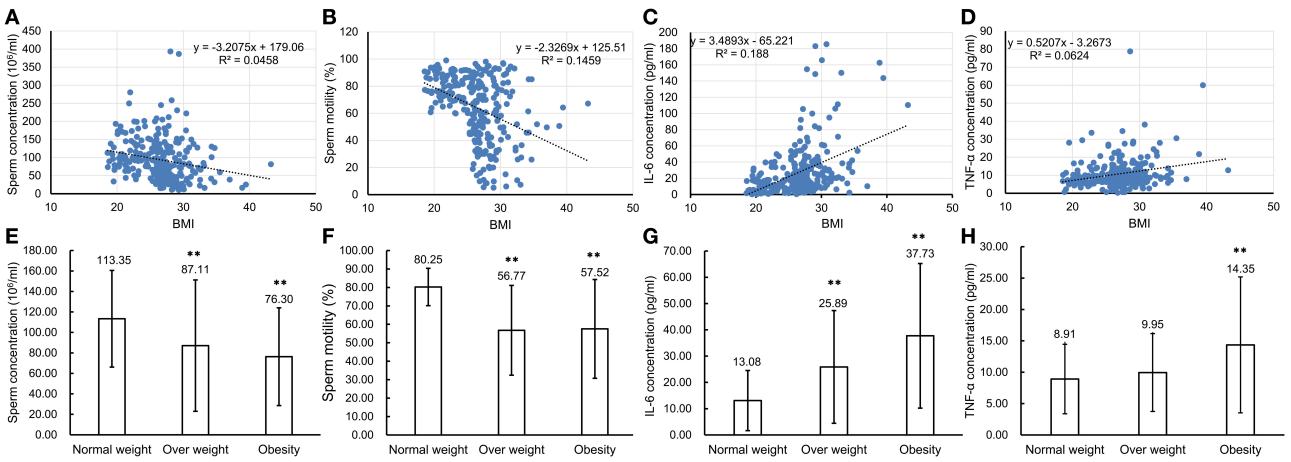

FIGURE 7 | Comparison of parameter values used to assess sperm health and pro-inflammatory cytokine levels in seminal plasma of normal weight, overweight and obese males. **(A–D)** Correlations between BMI of the total 272 males and sperm concentration **(A)**, sperm motility **(B)**, IL-6 concentration **(C)** and TNF-α concentration **(D)**. Pearson r correlation calculations evaluated the association between BMI, sperm parameters and seminal plasma cytokine levels. **(E–H)** Comparison of sperm concentration **(E)**, sperm motility **(F)** with levels of IL-6 **(G)**, and TNF-α **(H)** in seminal plasma of normal weight, overweight and obese males. $^{**}P < 0.01$.

activity of immune cells, i.e., as a protective factor, testosterone appears to suppress the activation and production of pro-inflammatory cytokines such as TNF-α, γ-interferon, and IL-6, in macrophages, lymphocytes, and vascular smooth muscle cells (McKay and Cidlowski, 1999; Malkin et al., 2003). On the other hand, estrogens can enhance both cellular and humoral immune responses and contribute to the resistance against infections through stimulating the synthesis of pro-inflammation cytokines including IL-6 and TNF-α (Vegeto et al., 1999; Straub, 2007). Moreover, it is well established that progesterone is an immunosuppressive agent that can blunt NF-κB activation (Su et al., 2009). Therefore, these previous reports concur with our present results, namely; the higher IL-6, TNF-α, and NF-κB levels detected in male genital tract tissues which may suppress testosterone and progesterone levels along with upregulating estradiol.

It is apparent that obesity can induce testicular inflammation through activating several different signaling pathways. In the male genital tract, testicular macrophages along with some proinflammatory cytokines such as IL-6 produced by Leydig and Sertoli cells contribute to the development of chronic inflammation (Maegawa et al., 2002). On the other hand, some immune regulatory factors can be secreted by Leydig and Sertoli cells in the testis. All of these factors contribute to regulating spermatogenesis and other testicular cell functions (Fraczek and Kurpisz, 2015). In addition, other proinflammatory cytokines as well as different immune regulatory factors are also produced in the epididymis and seminal vesicles (Huleihel and Lunenfeld, 2004; Seshadri et al., 2009). Actually, increases in the cytokines expression levels are indeed one of the first signals released by the innate host defense to counteract genital tract inflammation (Fraczek and Kurpisz, 2015). Consistent with this notion, our data shows that a prolonged high-fat diet could lead to increases in NLRP3 inflammasome and proinflammatory cytokine expression level such as IL-6 and TNF-α in the testis, epididymal caput, epididymal cauda, prostate, and seminal vesicle. Meanwhile, significant increases also occurred in IL-6 and TNF-α levels in sera. Besides, compared with the control group, corticosterone, and IgG concentrations were higher in obese mice sera. Notably, corticosterone, which acutely increases in response to inflammation through the hypothalamic–pituitary–adrenal (HPA) axis, has potent immunosuppressive and anti-inflammatory effects that are essential for regulating inflammation (Hueston and Deak, 2014). Such control is manifested by IgG which is the major antibody isotype in serum expressed by B lymphocytes and plasma cells. It provides immunity to inflammation, whereas IgM antibodies, have broad spectrum nonspecific effects because they recognize diverse microbial determinants and autoantigens. They are crucial for early protection against infection from viruses, bacteria, protozoa, fungi, and helminths, and control of autoimmunity. In addition, IgM exerts an important homeostatic function by clearing dead cells (Panda and Ding, 2015; Chistiakov et al., 2016; Pleass et al., 2016). Indeed we found that increases in corticosterone and IgG but not IgM in obese mice serum link obesity to chronic inflammation rather than infection or autoimmunity. Furthermore, our results clearly show that obesity can lead to systemic inflammation that includes a regional inflammatory reaction in the male genital tract, which is a crucial site for supporting sperm production, maturation, and sustaining its function.

Inflammation can harm the male genital tract by increasing reactive oxygen species (ROS) generation (Keck et al., 1998). In turn, excessive ROS levels must be continuously inactivated by seminal plasma antioxidants to maintain normal cell function. When free radicals become excessive, they overwhelm the genital tract antioxidant defense system. Such a scenario is indicative of an oxidative stress condition (Agarwal et al., 2003). Some previous reports indicated that seminal oxidative stress was negatively correlated with either sperm concentration, motility,

or progressive motility (Kemal Duru et al., 2000). On the other hand, TNF-α levels were reported to increase in some tissues isolated from obese human populations and rodents showing such rises play a crucial role in obesity-induced inflammation (Tilg and Moschen, 2006). TNF-α can also inhibit tumorigenesis and viral replication through inducing apoptosis (Kruglov et al., 2008). Several studies have revealed that TNF-α is one of the major cytokines produced and released by macrophages and other mononuclear phagocytes. It plays an essential role in the development of inflammation and the activation of other molecules in signaling pathways. They include p38, NF-κB, JNK1/2, and ERK1/2 (Azenabor et al., 2015). In the testis, most of the germ cells undergo spontaneous degeneration during spermatogenesis and TNF-α determines the size of the germ cell population in the seminiferous epithelium by inducing germ cell apoptosis and disrupting Sertoli cell junctions as well as inhibiting steroidogenesis in Leydig cells (Lysiak, 2004). The high concentration TNF-α can alter intracellular Ca^{2+} homeostasis by decreasing plasma membrane permeability to Ca^{2+} (Carrasquel et al., 2013), whereas Ca^{2+} signaling mediated responses are one of the main factors regulating sperm function (Publicover et al., 2007). Many studies reported that Ca^{2+} signaling is involved in the regulation of dynein activity in mice sperm flagella (Lesich et al., 2012). Consequently, higher TNF-α levels are associated with reduced sperm motility and abnormal morphology (Perdichizzi et al., 2007; Pascarelli et al., 2016). Additionally, TNF-α is a NF-κB activator which is a transcription factor having multiple critical roles in the regulation of the immune responses. There is accumulating evidence to show that NF-κB can regulate male germ cell apoptosis. Meanwhile, apoptotic cell death is essential for limiting germ cell population expansion during spermatogenesis and its dysregulation may directly cause male infertility (Pentikäinen et al., 2002). In our experiments, we found that higher TNF-α and NF-κB expression was prominent in the testicular male genital tracts of mice on a high-fat diet. We also found that their spermatozoa function was impaired based on significant declines in motility, progressive, and acrosome reaction. Moreover, a remarkable lower pregnancy rate was evident in mated normal female mice (Fan et al., 2015).

Blood-testis barrier (BTB) is one of the most protective blood-tissue barriers in mammals. Meiosis I and II, spermiogenesis, and spermiation all occur in a specialized microenvironment behind these highly resistant shields (Cheng and Mruk, 2012). It is reported that the BTB function can be disrupted by cytokines such as TGF-β, IL-1, and TNF-α, but instead enhanced by testosterone (Lie et al., 2013). TNF-α upregulated FAS expression and triggered increases in apoptosis through the NF-κB pathway which ultimately disrupted the BTB in mouse Sertoli cells (Starace et al., 2005). These TNF-α effects agree with those induced by recombinant TNF-α which compromised the tight junctional integrity of cultured *in vitro* Sertoli cells (Siu et al., 2003). Besides, mitogen-activated protein kinase (MAPK) cascade activation is associated with testicular BTB disassembly (Wong and Cheng, 2005; Li et al., 2006). The MAPK cassette consists of the p38, ERK1/2, c-Jun N-terminal kinase (JNK), or ERK5 pathways that can undergo activation leading to testicular dysfunction in mice fed a HFD (Lie et al., 2013). In the present study, testicular morphological analysis revealed that the seminiferous epithelia were atrophied in obese mice. Furthermore, the continuity of cell adhesions between spermatogenic cells and Sertoli cells was severely compromised. All of these disruptive effects may be induced by excessive increases in proinflammatory cytokine expression levels. We showed that disruptive effects of increases in proinflammatory cytokines on the testicular microenvironment are attributable to increases in the expression levels and phosphorylation status of testicular p38, NF-κB, ERK, JNK, and NLRP3 as well as some inflammation related signaling proteins. Such effects suggest that they are potentially related to the male fertility declines stemming from perturbing hormonal biosynthesis, germ cell development as well as disrupting BTB integrity. Such effects agree with our previous study in which we showed that cell junction related proteins such as clathrin, ZO-1 and occludin expression was remarkably down-regulated in obese mice.

More important, in order to verify the correlation between being overweight or obese and sperm parameters as well as proinflammatory cytokine levels in semen plasma, semen samples were collected from 272 donors, including 82 normal weight, 150 overweight, and 40 obese individuals respectively. Based on the sperm parameters measured by CASA, we found a negative relationship between sperm concentration, motility, and BMI, which indicated that both overweight and obese males were associated with low sperm counts and declines in sperm motility. Moreover, the concentrations of IL-6 and TNF-α were measured in the semen plasma and the results clearly showed that their levels significantly increased in the semen plasma from obese or overweight males compared with that of normal body weight individuals. These observations further demonstrated that obesity or overweight can indeed up-regulate cytokine concentrations in the male genital tract and impair sperm quality. These changes are consistent with those occurring in mice on a HFD. These results confirm previous data showing that there is a negative correlation between cytokine levels in the semen plasma and semen quality based on declines in sperm concentration (Furuya et al., 2003; Sanocka et al., 2003), motility, and progressive motility (Matalliotakis et al., 2006).

In conclusion, this study demonstrates that excessive body weight and obesity in humans is associated with development of an inflammatory status in the male genital tract. This condition constitutes one of the risk factors leading to male infertility. It stems from increases in proinflammatory cytokine levels that can impair male fertility via inducing germ cell apoptosis and compromising testicular BTB integrity. Such effects eventually adversely impair the biological functions of mature gametes. Furthermore, in parallel with this study, our clinical experiments also indicate that in comparison to males who have normal body weight, the obese or overweight individuals had poor semen quality combined with higher levels of IL-6 and TNF-α in the semen plasma. This close correspondence between the clinical signs and functional changes seen in obese mice on a HFD with those in overweight and obese human males suggest that reducing chronic testicular inflammation provides a novel therapeutic option to reduce male infertility in humans.

AUTHOR CONTRIBUTIONS

WF, YX, and YL collected and prepared clinical samples and data, and conducted experiments, data generation and analysis, and manuscript preparation. ZZ performed experiments and collected data. LL and ZD was responsible for the conception and design, supervision of all aspects of the laboratory experiments, data analysis and the preparation, and final approval of the manuscript.

FUNDING

This research project was supported by National Natural Science Foundation of China (No.81370752, No.81571487, No.81701503, No.81671579, and No.31370904), the Science and Technology Commission of Shanghai Municipality (No.16ZR1418600, No.15401900500, and No.14140901600), the Shuguang Planning of Shanghai Municipal Education Commission (16SG14), The National Key Research and Development Program (2017YFA0104500).

ACKNOWLEDGMENTS

We thank Ms. Yangqin Hu (Shanghai Key Laboratory for Reproductive Medicine) for her technical assistance. We are also grateful to Prof. Peter Reinach for editorial assistance. The authors declare that there is no conflict of interest that would prejudice the impartiality of this work.

REFERENCES

Agarwal, A., Saleh, R. A., and Bedaiwy, M. A. (2003). Role of reactive oxygen species in the pathophysiology of human reproduction. *Fertil. Steril.* 79, 829–843. doi: 10.1016/S0015-0282(02)04948-8

An, R., Ji, M., and Zhang, S. (2017). Global warming and obesity: a systematic review. *Obes. Rev*. doi: 10.1111/obr.12624. [Epub ahead of print].

Azenabor, A., Ekun, A. O., and Akinloye, O. (2015). Impact of Inflammation on male reproductive tract. *J. Reprod. Infertil*. 16, 123–129.

Bachir, B. G., and Jarvi, K. (2014). Infectious, inflammatory, and immunologic conditions resulting in male infertility. *Urol. Clin. North Am*. 41, 67–81. doi: 10.1016/j.ucl.2013.08.008

Carrasquel, G., Camejo, M. I., Michelangeli, F., and Ruiz, M. C. (2013). Effect of tumor necrosis factor-α on the intracellular Ca^{2+} homeostasis in human sperm. *Am. J. Reprod. Immunol*. 70, 153–161. doi: 10.1111/aji.12106

Cheng, C. Y., and Mruk, D. D. (2012). The blood-testis barrier and its implications for male contraception. *Pharmacol Rev*. 64, 16–64. doi: 10.1124/pr.110.002790

Chistiakov, D. A., Orekhov, A. N., and Bobryshev, Y. V. (2016). Immune-inflammatory responses in atherosclerosis: role of an adaptive immunity mainly driven by T and B cells. *Immunobiology* 221, 1014–1033. doi: 10.1016/j.imbio.2016.05.010

Edwards, D. P. (2005). Regulation of signal transduction pathways by estrogen and progesterone. *Annu. Rev. Physiol*. 67, 335–376. doi: 10.1146/annurev.physiol.67.040403.120151

Esser, N., Legrand-Poels, S., Piette, J., Scheen, A. J., and Paquot, N. (2014). Inflammation as a link between obesity, metabolic syndrome and type 2 diabetes. *Diabetes Res. Clin. Pract*. 105, 141–150. doi: 10.1016/j.diabres.2014.04.006

Fan, Y., Liu, Y., Xue, K., Gu, G., Fan, W., Xu, Y., et al. (2015). Diet-induced obesity in male C57BL/6 mice decreases fertility as a consequence of disrupted blood-testis barrier. *PLoS ONE* 14:e0120775. doi: 10.1371/journal.pone.0120775

Fraczek, M., and Kurpisz, M. (2015). Cytokines in the male reproductive tract and their role in infertility disorders. *J. Reprod. Immunol*. 108, 98–104. doi: 10.1016/j.jri.2015.02.001

Furuya, Y., Akashi, T., and Fuse, H. (2003). Soluble Fas and interleukin-6 and interleukin-8 levels in seminal plasma of infertile men. *Arch. Androl*. 49, 449–452. doi: 10.1080/01485010390219926

Hammiche, F., Laven, J. S., Twigt, J. M., Boellaard, W. P., Steegers, E. A., and Steegers-Theunissen, R. P. (2012). Body mass index and central adiposity are associated with sperm quality in men of subfertile couples. *Hum. Reprod*. 27, 2365–2372. doi: 10.1093/humrep/des177

Hueston, C. M., and Deak, T. (2014). The inflamed axis: the interaction between stress, hormones, and the expression of inflammatory-related genes within key structures comprising the hypothalamic-pituitary-adrenal axis. *Physiol. Behav*. 124, 77–91. doi: 10.1016/j.physbeh.2013.10.035

Huleihel, M., and Lunenfeld, E. (2004). Regulation of spermatogenesis by paracrine/autocrine testicular factors. *Asian J. Androl*. 6, 259–268.

Kaur, J. (2014). A comprehensive review on metabolic syndrome. *Cardiol. Res. Pract*. 2014:943162. doi: 10.1155/2014/943162

Keck, C., Gerber-Schäfer, C., Clad, A., Wilhelm, C., and Breckwoldt, M. (1998). Seminal tract infections: impact on male fertility and treatment options. *Hum. Reprod. Update* 4, 891–903. doi: 10.1093/humupd/4.6.891

Kemal Duru, N., Morshedi, M., and Oehninger, S. (2000). Effects of hydrogen peroxide on DNA and plasma membrane integrity of human spermatozoa. *Fertil Steril*. 74, 1200–1207. doi: 10.1016/S0015-0282(00)01591-0

Kern, P. A., Saghizadeh, M., Ong, J. M., Bosch, R. J., Deem, R., and Simsolo, R. B. (1995). The expression of tumor necrosis factor in human adipose tissue. Regulation by obesity, weight loss, and relationship to lipoprotein lipase. *J. Clin. Invest*. 95, 2111–2119. doi: 10.1172/JCI117899

Klöting, N., and Blüher, M. (2014). Adipocyte dysfunction, inflammation and metabolic syndrome. *Rev. Endocr. Metab. Disord*. 13, 277–287. doi: 10.1007/s11154-014-9301-0

Kruglov, A. A., Kuchmiy, A., Grivennikov, S. I., Tumanov, A. V., Kuprash, D. V., and Nedospasov, S. A. (2008). Physiological functions of tumor necrosis factor and the consequences of its pathologic overexpression or blockade: mouse models. *Cytokine Growth Factor Rev*. 19, 231–244. doi: 10.1016/j.cytogfr.2008.04.010

Lesich, K. A., Kelsch, C. B., Ponichter, K. L., Dionne, B. J., Dang, L., and Lindemann, C. B. (2012). The calcium response of mouse sperm flagella: role of calcium ions in the regulation of dynein activity. *Biol. Reprod*. 86, 105. doi: 10.1095/biolreprod.111.094953

Li, H., Lelliott, C., Håkansson, P., Ploj, K., Tuneld, A., Verolin-Johansson, M., et al. (2008). Intestinal, adipose, and liver inflammation in diet-induced obese mice. *Metabolism* 57, 1704–1710. doi: 10.1016/j.metabol.2008.07.029

Li, M. W., Xia, W., Mruk, D. D., Wang, C. Q., Yan, H. H., Siu, M. K., et al. (2006). Tumor necrosis factor α reversibly disrupts the blood-testis barrier and impairs Sertoli-germ cell adhesion in the seminiferous epithelium of adult rat testes. *J. Endocrinol*. 190, 313–329. doi: 10.1677/joe.1.06781

Lie, P. P., Cheng, C. Y., and Mruk, D. D. (2013). Signalling pathways regulating the blood-testis barrier. *Int. J. Biochem. Cell Biol*. 45, 621–625. doi: 10.1016/j.biocel.2012.12.009

Liu, Y., and Ding, Z. (2017). Obesity, a serious etiologic factor for male subfertility in modern society. *Reproduction* 154, 123–131. doi: 10.1530/REP-17-0161

Liu, Z., Brooks, R. S., Ciappio, E. D., Kim, S. J., Crott, J. W., Bennett, G., et al. (2012). Diet-induced obesity elevates colonic TNF-α in mice and is accompanied by an activation of Wnt signaling: a mechanism for obesity-associated colorectal cancer. *J. Nutr. Biochem*. 23, 1207–1213. doi: 10.1016/j.jnutbio.2011.07.002

Lysiak, J. J. (2004). The role of tumor necrosis factor-alpha and interleukin-1 in the mammalian testis and their involvement in testicular torsion and autoimmune orchitis. *Reprod. Biol. Endocrinol*. 2:9. doi: 10.1186/1477-7827-2-9

Maegawa, M., Kamada, M., Irahara, M., Yamamoto, S., Yoshikawa, S., Kasai, Y., et al. (2002). A repertoire of cytokines in human seminal plasma. *J. Reprod. Immunol*. 54, 33–42. doi: 10.1016/S0165-0378(01)00063-8

Malkin, C. J., Pugh, P. J., Jones, R. D., Jones, T. H., and Channer, K. S. (2003). Testosterone as a protective factor against atherosclerosis–immunomodulation and influence upon plaque development and stability. *J. Endocrinol.* 178, 373–380. doi: 10.1677/joe.0.1780373

Matalliotakis, I. M., Cakmak, H., Fragouli, Y., Kourtis, A., Arici, A., and Huszar, G. (2006). Increased IL-18 levels in seminal plasma of infertile men with genital tract infections. *Am. J. Reprod. Immunol.* 55, 428–433. doi: 10.1111/j.1600-0897.2006.00380.x

McKay, L. I., and Cidlowski, J. A. (1999). Molecular control of immune/inflammatory responses: interactions between nuclear factor-kappa B and steroid receptor-signaling pathways. *Endocr. Rev.* 20, 435–459.

Ng, M., Fleming, T., Robinson, M., Thomson, B., Graetz, N., Margono, C., et al. (2014). Global, regional, and national prevalence of overweight and obesity in children and adults during 1980-2013: a systematic analysis for the Global Burden of Disease Study 2013. *Lancet* 384, 776–781. doi: 10.1016/S0140-6736(14)60460-8

Panda, S., and Ding, J. L. (2015). Natural antibodies bridge innate and adaptive immunity. *J. Immunol.* 194, 13–20. doi: 10.4049/jimmunol.1400844

Pascarelli, N. A., Fioravanti, A., Moretti, E., Guidelli, G. M., Mazzi, L., and Collodel, G. (2016). The effects *in vitro* of TNF-α and its antagonist 'etanercept' on ejaculated human sperm. *Reprod. Fertil. Dev.* 29, 1169–1177. doi: 10.1071/RD16090

Pentikäinen, V., Suomalainen, L., Erkkilä, K., Martelin, E., Parvinen, M., Pentikäinen, M. O., et al. (2002). Nuclear factor-kappa B activation in human testicular apoptosis. *Am. J. Pathol.* 160, 205–218. doi: 10.1016/S0002-9440(10)64364-7

Perdichizzi, A., Nicoletti, F., La Vignera, S., Barone, N., D'Agata, R., and Vicari, E. (2007). Effects of tumour necrosis factor-α on human sperm motility and apoptosis. *J. Clin. Immunol.* 27, 152–162. doi: 10.1007/s10875-007-9071-5

Pleass, R. J., Moore, S. C., Stevenson, L., and Hviid, L. (2016). Immunoglobulin M: restrainer of inflammation and mediator of immune evasion by *Plasmodium falciparum* malaria. *Trends Parasitol.* 32, 108–119. doi: 10.1016/j.pt.2015.09.007

Publicover, S., Harper, C. V., and Barratt, C. (2007). $[Ca^{2+}]$i signalling in sperm–making the most of what you've got. *Nat. Cell Biol.* 9, 235–242. doi: 10.1038/ncb0307-235

Sanocka, D., Jedrzejczak, P., Szumała-Kaekol, A., Fraczek, M., and Kurpisz, M. (2003). Male genital tract inflammation: the role of selected interleukins in regulation of pro-oxidant and antioxidant enzymatic substances in seminal plasma. *J. Androl.* 24, 448–455. doi: 10.1002/j.1939-4640.2003.tb02693.x

Seshadri, S., Bates, M., Vince, G., and Jones, D. I. (2009). The role of cytokine expression in different subgroups of subfertile men. *Am. J. Reprod. Immunol.* 62, 275–282. doi: 10.1111/j.1600-0897.2009.00736.x

Siu, M. K., Lee, W. M., and Cheng, C. Y. (2003). The interplay of collagen IV, tumor necrosis factor-α, gelatinase B (matrix metalloprotease-9), and tissue inhibitor of metalloproteases-1 in the basal lamina regulates Sertoli cell-tight junction dynamics in the rat testis. *Endocrinology* 144, 371–387. doi: 10.1210/en.2002-220786

Starace, D., Riccioli, A., D'Alessio, A., Giampietri, C., Petrungaro, S., Galli, R., et al. (2005). Characterization of signaling pathways leading to Fas expression induced by TNF-alpha: pivotal role of NF-kappaB. *FASEB J.* 19, 473–475. doi: 10.1096/fj.04-2726fje

Straub, R. H. (2007). The complex role of estrogens in inflammation. *Endocr. Rev.* 28, 521–574. doi: 10.1210/er.2007-0001

Su, L., Sun, Y., Ma, F., Lü, P., Huang, H., and Zhou, J. (2009). Progesterone inhibits Toll-like receptor 4-mediated innate immune response in macrophages by suppressing NF-kappaB activation and enhancing SOCS1 expression. *Immunol. Lett.* 125, 151–155. doi: 10.1016/j.imlet.2009.07.003

Teerds, K. J., de Rooij, D. G., and Keijer, J. (2011). Functional relationship between obesity and male reproduction: from humans to animal models. *Hum. Reprod. Update* 17, 667–683. doi: 10.1093/humupd/dmr017

Tilg, H., and Moschen, A. R. (2006). Adipocytokines: mediators linking adipose tissue, inflammation and immunity. *Nat. Rev. Immunol.* 6, 772–783. doi: 10.1038/nri1937

Vandanmagsar, B., Youm, Y. H., Ravussin, A., Galgani, J. E., Stadler, K., and Mynatt, R. L. (2011). The NLRP3 inflammasome instigates obesity-induced inflammation and insulin resistance. *Nat. Med.* 17, 179–188. doi: 10.1038/nm.2279

Vegeto, E., Pollio, G., Pellicciari, C., and Maggi, A. (1999). Estrogen and progesterone induction of survival of monoblastoid cells undergoing TNF-alpha-induced apoptosis. *FASEB J.* 13, 793–803.

Wellen, K. E., and Hotamisligil, G. S. (2005). Inflammation, stress, and diabetes. *J. Clin. Invest.* 115, 1111–1119. doi: 10.1172/JCI25102

WHO (2010). *Laboratory Manual for the Examination and Processing of Human Semen.* Geneva: World Health Organization.

Wong, C. H., and Cheng, C. Y. (2005). Mitogen-activated protein kinases, adherens junction dynamics, and spermatogenesis: a review of recent data. *Dev. Biol.* 286, 1–15. doi: 10.1016/j.ydbio.2005.08.001

Conflict of Interest Statement: The authors declare that the research was conducted in the absence of any commercial or financial relationships that could be construed as a potential conflict of interest.

frontiers in Physiology

REVIEW
published: 19 December 2017
doi: 10.3389/fphys.2017.01047

Links between Dietary Protein Sources, the Gut Microbiota, and Obesity

Lise Madsen[1, 2, 3]*, *Lene S. Myrmel*[1], *Even Fjære*[1], *Bjørn Liaset*[1] and *Karsten Kristiansen*[2, 3]

[1] National Institute of Nutrition and Seafood Research, Bergen, Norway, [2] Laboratory of Genomics and Molecular Biomedicine, Department of Biology, University of Copenhagen, Copenhagen, Denmark, [3] BGI-Shenzhen, Shenzhen, China

The association between the gut microbiota and obesity is well documented in both humans and in animal models. It is also demonstrated that dietary factors can change the gut microbiota composition and obesity development. However, knowledge of how diet, metabolism and gut microbiota mutually interact and modulate energy metabolism and obesity development is still limited. Epidemiological studies indicate an association between intake of certain dietary protein sources and obesity. Animal studies confirm that different protein sources vary in their ability to either prevent or induce obesity. Different sources of protein such as beans, vegetables, dairy, seafood, and meat differ in amino acid composition. Further, the type and level of other factors, such as fatty acids and persistent organic pollutants (POPs) vary between dietary protein sources. All these factors can modulate the composition of the gut microbiota and may thereby influence their obesogenic properties. This review summarizes evidence of how different protein sources affect energy efficiency, obesity development, and the gut microbiota, linking protein-dependent changes in the gut microbiota with obesity.

Keywords: gut microbiota, obesity, dietary proteins, diet, protein source, mouse models, metabolism, dietary fats

OPEN ACCESS

Edited by:
Xinran Ma,
East China Normal University, China

Reviewed by:
Ilana Kolodkin-Gal,
Weizmann Institute of Science, Israel
Abdel Qawasmeh,
Charles Sturt University, Australia
Yu-Chiang Lai,
University of Dundee, United Kingdom

***Correspondence:**
Lise Madsen
lise.madsen@nifes.no

Specialty section:
This article was submitted to Clinical and Translational Physiology, a section of the journal Frontiers in Physiology

Received: *01 September 2017*
Accepted: *30 November 2017*
Published: *19 December 2017*

Citation:
Madsen L, Myrmel LS, Fjære E, Liaset B and Kristiansen K (2017) Links between Dietary Protein Sources, the Gut Microbiota, and Obesity. Front. Physiol. 8:1047. doi: 10.3389/fphys.2017.01047

INTRODUCTION

The importance of the gut microbiota in obesity is well documented (Villanueva-Millan et al., 2015; Sonnenburg and Backhed, 2016; reviewed in Baothman et al., 2016). Still, lifestyle and diet are closely linked to obesity, and increased consumption of energy-dense food with a concomitant increase in total energy intake is probably a major driver of the obesity epidemic (Swinburn et al., 2011; Romieu et al., 2017). In humans dietary patterns play important roles in shaping the gut microbiota (De Filippo et al., 2010; Muegge et al., 2011; Yatsunenko et al., 2012; David et al., 2014; Schnorr et al., 2014; Carmody et al., 2015; Graf et al., 2015) as well as in the development of obesity (Bellissimo and Akhavan, 2015).

High protein diets are reported to promote weight loss and weight maintenance in humans (Westerterp-Plantenga et al., 2009, 2012; Pesta and Samuel, 2014; Pasiakos, 2015), but a systematic review revealed that the long-term effects of high-protein diets are neither consistent nor conclusive (Lepe et al., 2011). The results from rodent trials are more consistent, and a number of studies has demonstrated that a high protein: carbohydrate ratio prevents high fat diet induced obesity (Lacroix et al., 2004; Marsset-Baglieri et al., 2004; Morens et al., 2005; Pichon et al., 2006; Madsen et al., 2008; Ma et al., 2011; Freudenberg et al., 2012, 2013; Hao et al., 2012; McAllan et al., 2014).

Importantly, the notion that the obesogenic potential of high fat diets in rodents is attenuated by increasing the protein:carbohydrate ratio is largely based on studies using casein or whey as the protein source. However, there is little knowledge as to how different protein sources may modulate the response to high protein intake. Recently, we demonstrated that feeding obesity-prone C57BL/6J mice a high fat, high protein diet using casein, soy, or filets of cod, beef, chicken (skinless) or pork as protein sources led to striking differences in obesity development at thermoneutral conditions. Casein was the most efficient protein source preventing weight gain and accretion of adipose mass, whereas mice fed high protein diets based on "white meat" (lean pork or chicken filets) had the highest increase in feed efficiency and adipose tissue mass (Liisberg et al., 2016b). Epidemiological studies also indicate that intake of dairy and vegetarian protein sources is associated with protection against obesity, whereas a high intake of meat, in particular red meat, predicts higher weight gain (Fogelholm et al., 2012; Smith et al., 2015; Mozaffarian, 2016). To what extent intake of red meat protein affects the composition and function of the gut microbiota in humans remains to be established.

It has been suggested that dietary patterns are associated with distinct bacterial communities in the human gut (Wu et al., 2011). It is further well known that dietary characteristics, such as the content of fat, whole grain, fruits and nuts, as well as high fiber diets in general, influence the gut microbiota (De Filippo et al., 2010; Muegge et al., 2011; David et al., 2014; Schnorr et al., 2014; Carmody et al., 2015; Graf et al., 2015; Eid et al., 2017). However, it is still not established which food constituents specifically promote growth and function of beneficial bacteria in the intestine. Recently, differences in profiles of gut bacteria between rats fed proteins from red meat (beef and pork), chicken, and fish (here defined as white meat) and other sources (casein and soy) were reported (Zhu et al., 2015, 2016). Still, very little is known about the effect of protein source and quality on the regulation of energy balance.

An undoubtedly important factor determining protein quality is the amino acid composition (Millward et al., 2008). Different protein sources provide different amino acids (AAs) that differ in properties and effects on body functions. In addition to the amino acid composition, different protein sources vary in the content of micro- and macronutrients as well as undesirable compounds. For instance, legumes are rich in fibers, red meat is generally rich in saturated fat and iron, dairy products are generally high in calcium, whereas fatty fish may contain polychlorinated biphenyls (PCBs) in addition to omega-3 fatty acids and vitamin D. Additionally, the absorption rate of protein rich food items may vary and is likely to affect postprandial energy metabolism (Boirie et al., 1997; Soucy and Leblanc, 1998; Stanstrup et al., 2014; Aadland et al., 2015, 2016; Vincent et al., 2017). To further complicate the picture, the effects of protein rich food on energy metabolism is strongly influenced by the background diet, i.e., the complemental part of the meal that also varies in micro- and macronutrients depending on food habits and culture. Finally, the gut microbiota may directly determine to what extent dietary proteins are converted into other metabolically active compounds such as short-chain fatty acids, branched chain fatty acids, or different nitrogen containing compounds (Lin et al., 2017).

Here, we summarize evidence of how different protein sources affect energy efficiency, obesity development and the gut microbiota in humans and mice. The overall phylum level composition in mouse gut is quite similar to that of the human gut microbiome, with Firmicutes, Bacteroidetes, and Proteobacteria comprising more than 70% of the gut microbiota (Xiao et al., 2015). Although only 4.0% of the mouse gut microbial genes are shared with those of the human gut microbiome, the mouse and human gut microbiome are functionally similar sharing 95.2% of their KEGG orthologous groups (Xiao et al., 2015). Of note, introduction of fecal microbes from human adult female twin pairs discordant for obesity into germ-free mice fed low-fat mouse chow induced an obese phenotype in chow fed mice receiving fecal bacteria from the obese twin (Ridaura et al., 2013). Vice versa, *Christensenella minuta*, a cultured member of the *Christensenellaceae* taxa known to be enriched in humans with low body mass index, led to reduced adiposity when transplanted to germ free mice together with an obese-associated microbiome (Goodrich et al., 2014). The reduced abundance of *Bacteroides thetaiotamicron* in obese humans is correlated with an increase in plasma glutamate, and interestingly, gavaging normal SPF C57BL/6 with *B. thetaiotaomicron* reduced diet-induced obesity in mice and diminished plasma glutamate levels (Liu et al., 2017). Hence, adiposity related phenotypes can be transmissible from humans to mice. We here review how different protein sources affect energy efficiency, obesity development and the gut microbiota. Finally, we discuss the possible importance of different amino acids, fatty acid composition and persistent organic pollutants (POPs). Different protein sources will also contain different amount of other food components, including micronutrients, trace elements, and vitamins. Their impact on the gut microbiota was recently reviewed (Roca-Saavedra et al., 2017), but since their possible roles on obesity development remain to be established, this will not be further described here.

PROTEIN SOURCES, GUT MICROBIOTA, AND OBESITY

High protein diets represent a popular dietary approach to induce weight loss in humans. Data from numerous convincing rodent trials demonstrate strong attenuation or total prevention of high fat diet-induced obesity when the diet contains a high protein:carbohydrate ratio (Lacroix et al., 2004; Marsset-Baglieri et al., 2004; Morens et al., 2005; Pichon et al., 2006; Madsen et al., 2008; Ma et al., 2011; Freudenberg et al., 2012, 2013; Hao et al., 2012; McAllan et al., 2014). Still, review of human trials has revealed that the long-term effects of high-protein diets on obesity are neither consistent nor conclusive (Lepe et al., 2011; Astrup et al., 2015). In mice, we have demonstrated that long term high fat, high protein feeding limits obesity development and prevents the reduction in survival observed in mice fed a high fat, high sucrose diet compared to low fat fed mice (Kiilerich et al.,

2016). In humans aged 50–65, results from the study of Levine et al. suggest that a high protein intake may be associated with increased overall mortality. However, this was not observed if the proteins were plant derived. It was suggested that the intake of animal proteins was a main factor driving the increase in overall mortality, highlighting the importance of the protein source (Levine et al., 2014) and the type of dietary protein would most likely modulate the (anti)-obesogenic effect of high protein diets also in humans.

The gut microbiota may also convert components from different protein sources into compounds that may be linked to development of disease. Well-known examples are L-carnitine and phosphatidylcholine, present in red meats and egg, which can be metabolized to trimethylamine and trimethylamine oxide (TMAO). In humans, circulating TMAO levels are reported to be associated with increased risk for atherosclerosis development (Koeth et al., 2013; Tang et al., 2013) and recently also linked to obesity (Dumas et al., 2017). However, fish and seafood, known to protect against cardiovascular disease contain high amounts of TMAO (Cho et al., 2017; Landfald et al., 2017). It is speculated that free TMAO from seafood may act as an electron acceptor for facultative anaerobic bacteria able to respire with the aldehydes resulting from the TMA elimination reactions of choline and carnitine (Cho et al., 2017).

Both diet composition (Arumugam et al., 2011; Graf et al., 2015; Kiilerich et al., 2016; Xiao et al., 2017) and the state of obesity (Ley et al., 2005, 2006) are important factors determining the gut microbial diversity in both animals and humans. As mentioned above, epidemiological studies have linked food groups and dietary patterns to obesity. Still, the linkage between diet, obesity, and gut microbiota is not elucidated. Vegetarian diets, whole grain products, fruits and nuts, vegetables, and legumes, as well as food constituents such as fat, protein, phytochemicals and fibers impact the gut microbiota in humans (Graf et al., 2015). The latter may be of particular importance as non-digestible carbohydrates or fibers represent a primary energy source for many gut microbes. Hence, bacterial fermentation, total bacterial numbers and species composition are affected. Further, fibers reduce the energy density of the diet, and microbial fermentation results in production of short chain fatty acids (SCFAs) that apart from a multitude of effects on host physiology may influence directly on metabolism (Flint, 2012; Koh et al., 2016; Sawicki et al., 2017). Accumulating evidence suggests the gut microbiota as a link between the dietary impact and host metabolism. The diet-induced response of the gut microbiota has been divided into; (1) a rapid gut response upon large dietary changes, (2) long-term dietary habits as a dominant factor for gut microbiota composition and (3) different responses upon dietary change due to individualized gut microbiota (reviewed in Sonnenburg and Backhed, 2016).

It has been reported that a high-protein low carbohydrate diet when given in combination with caloric restriction in obese humans resulted in an increase in branched-chain fatty acids, a decrease in butyrate, and a decrease in the abundance of the *Roseburia/Eubacterium rectale* group of bacteria in the gut (Russell et al., 2011). Concomitantly, the levels of metabolites associated with protection from cancer decreased whereas the levels of several metabolites assumed to be hazardous increased. Unfortunately, the protein sources in these diets were not described. Using casein as the protein source, we have demonstrated that in mice fed high fat diets with high or low protein:sucrose ratio, the dietary fat content, and not the protein:sucrose ratio, was the major driver of the composition of the gut microbiota (Kiilerich et al., 2016). Distinct changes in the gut microbiome composition were also observed over time, suggesting that host age in mice (Kiilerich et al., 2016) as well as in humans (Claesson et al., 2012) is also an important factor in defining the gut microbiome.

We have investigated the effect of a high fat, high protein diet using casein, soy, or filets of cod, beef, chicken (skinless) or pork as protein sources in C57BL/6J mice (Liisberg et al., 2016b). Of note, among the protein sources tested, casein was the only protein that actually prevented development of obesity and the mice fed casein had significantly lower fat mass than mice fed a high fat, high sucrose (HF/HS) reference diet (**Figure 1**; Liisberg et al., 2016b). Fat masses in mice fed a high proportion of soy, cod and beef were comparable to those fed HF/HS diet (**Figure 1**). Strikingly, compared with mice fed the HF/HS reference diet, mice fed diets with high content of proteins from chicken and pork had significantly more fat mass (**Figure 1**), also verified by dissection of different adipose tissue depots (Liisberg et al., 2016b). Mice fed proteins from pork exhibited a "whitening" of the classic brown adipose tissue, whereas the mice fed casein maintained a classic brown adipocyte morphology. The casein fed mice further exhibited an upregulated expression of genes related to futile cycling in brown adipose tissue. Of note, differences in obesity development could not be explained by differences in feed intake or digestibility of protein or fat (Liisberg et al., 2016b). Compared with mice fed a low fat reference diet and mice fed a high proportion of casein or soy, the pork and chicken fed mice also had reduced lean mass (**Figure 1**).

So far, very little is known on how different protein sources affect the gut microbiota. But recently, the composition of gut bacteria in the caecum of rats fed proteins from red meat (beef and pork), white meat (chicken and fish) as well as casein and soy was determined (Zhu et al., 2015). In this study, the meat proteins had been extracted from animal muscles and the animal feed contained regular amount (20%) of protein and was low (7%) in fat. Marked inter- and intra-group variation in the composition of the cecal microbiota was observed, with a more tight microbiota clustering of rats fed the non-meat proteins casein and soy, indicating that the composition of the gut microbiota diverged between rats fed feed based on meat proteins and non-meat proteins (Zhu et al., 2015). Young rats fed a diet with proteins from chicken (17.7%) for 14 days had an increased relative abundance in the genus *Lactobacillus*. However, the opposite pattern was demonstrated in middle-aged rats (Zhu et al., 2016).

Animal studies from our laboratories suggest that proteins from seafood are less obesogenic than proteins from terrestrial animals. C57BL/6J mice fed a Western diet containing a mixture of lean seafood (ling, rosefish, cod, wolf fish, and muscle from

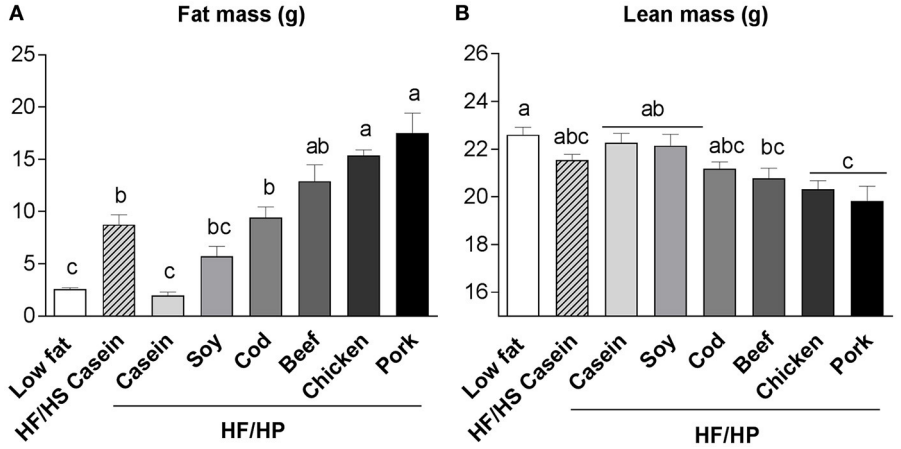

FIGURE 1 | Fat mass **(A)** and lean mass **(B)** of male C57BL/6J mice fed high fat, high protein diets with different protein sources; casein, soy, cod, beef, chicken, or pork for 11 weeks at thermoneutral conditions. Mice fed a low fat and high fat, high sucrose diet based on casein were used as references. Diet composition and analyses are described in Liisberg et al. (2016b). Data represent mean ± SEM ($n = 9$). Different letters above the bars denote significant differences between the groups ($p < 0.05$), using 1-way ANOVA followed by Tukey's multiple comparison.

Canadian scallop) for 12 weeks accumulated less fat mass than mice fed a Western diet containing a mixture of skinless chicken breast, pork tenderloin, and beef sirloin (Holm et al., 2016). Comparison of the gut microbiomes of mice fed the two Western diets revealed significant differences in the relative abundance of operational taxonomic units belonging to the orders *Bacteroidales* and *Clostridiales*, with genes involved in metabolism of aromatic amino acids exhibiting higher relative abundance in the microbiomes of mice fed the seafood Western diet (Holm et al., 2016). Whether these differences in the abundance of microbial genes were of physiological relevance is still not clear. In a similar dietary setting, obesity development was attenuated in mice by exchanging lean pork meat with cod (Liisberg et al., 2016a). Further, intake of lean seafood such as white crab meat, scallop, and a mixture of cod and scallops has been demonstrated to attenuate diet-induced obesity and hepatic steatosis in mice (Tastesen et al., 2014a,b).

As discussed above, rodent studies clearly demonstrate that the protein source modulates the obesogenic effect of high protein diets and that casein is a rather unique protein source. However, the anti-obesogenic properties of casein may also extend to other milk-derived proteins, such as whey, and may be of relevance in humans. Epidemiological studies indicate that a high intake of low-fat dairy products is associated with protection against obesity (Fogelholm et al., 2012; Mozaffarian, 2016). Additionally, some human intervention studies using a dairy protein source with 80% casein and 20% whey have shown promising effects on weight loss (Zemel et al., 2004; Faghih et al., 2011). Still a meta-analysis of randomized controlled trials suggests that dairy intake only increases weight loss in combination with energy restriction (Chen et al., 2012).

To our knowledge, data on the potential of casein and/or whey to induce weight loss in obese animals is lacking. When present in the diet in regular amounts we have demonstrated that casein has an anti-obesogenic effect when compared with meat proteins from terrestrial animals and seafood (Ibrahim et al., 2011; Tastesen et al., 2014b). However, data from us and others suggest that whey is slightly more efficient than casein (Lillefosse et al., 2014; McAllan et al., 2015; Tranberg et al., 2015). Of note, concomitant with reduced weight gain, mice fed whey protein isolate had lower stomach weight and intestinal length (McAllan et al., 2015). In a study where mice were fed a high fat diet with either casein or a lactoperoxidase and lactoferrin-enriched whey protein isolate (WPI) at different doses, WPI specifically increased *Lactobacillaceae/Lactobacillus* and decreased *Clostridiaceae/Clostridium* in high fat diet-fed mice (McAllan et al., 2015). Further, Shi et al. have shown that replacing 5, 50, or 100% of the dietary casein-derived energy content with WPI caused a proportional suppression of body weight gain in high fat diet fed mice (Shi et al., 2011). It has been demonstrated that in comparison to casein, whey protein intake increased levels of *Lactobacilli* and *Bifidobacteria* in a rat model of colitis (Sprong et al., 2010). Still, whether the observed changes in the gut microbiota can be linked to differences in the anti-obesogenic effects of casein and whey remain to be investigated. It should be mentioned that some strains of *Bifidobacteria* are reported to have anti-obesogenic properties in rodents (An et al., 2011; Wang et al., 2015; Li et al., 2016). Increased proportions of *Lactobacillus* have been observed in high fat diet fed mice (Clarke et al., 2013). However, certain species of *Lactobacillus,* such as *Lactobacillus plantarum* (Isokpehi et al., 2017) were recently associated with weight-loss in humans. Further, supplementation with *Lactobacillus curvatus HY7601* and *L. plantarum KY1032* in diet-induced obese mice was associated with gut microbial changes and reduction in obesity (Park et al., 2013). The two probiotic strains *L. plantarum* KY1032 and *L. curvatus* HY7601 have also been demonstrated to reduce adipose tissue mass in diet-induced obese mice (Yoo et al., 2013).

In line with epidemiological studies indicating that a high intake of proteins from vegetarian sources and dairy is associated with protection against obesity (Fogelholm et al., 2012; Mozaffarian, 2016), rats receiving soy as the protein source

were demonstrated to gain less body weight than rats receiving beef, pork, or turkey (Brandsch et al., 2006). A few human studies have investigated differences between omnivores and vegetarians but the results from these studies are not consistent (Graf et al., 2015). Human and animal studies investigating the effect of soy on the microbiota were recently reviewed, and in general, consumption of soy foods appeared to increase the levels of *Bifidobacteria* and *Lactobacilli* and alter the ratio between Firmicutes and Bacteroidetes (Huang et al., 2016). Although challenged, a decreased Bacteroidetes-to-Firmicutes ratio has been associated with obesity in both humans and animals (Ley et al., 2005; Turnbaugh et al., 2006). Further, as demonstrated with certain strains of *Lactobacillus* (see above), also some strains of *Bifidobacteria* have been associated with protection against diet-induced obesity in rodents (An et al., 2011; Wang et al., 2015; Li et al., 2016). Still, further studies are required to establish a causal relationship.

BRANCHED CHAIN AMINO ACIDS

Beyond the needs required for protein synthesis, amino acids participate in numerous pathways and certain amino acids may be directly involved in regulating metabolism. The impact on metabolism can be directly proportional to dietary intake. For instance, dietary intake of tryptophan or phenylalanine affects appetite regulation, intake of arginine alters nitric oxide production, and intake of branched chain amino acids (BCAAs) activates mammalian target of rapamycin complex 1. Casein and whey have a high content of the BCAAs; valine, leucine, and isoleucine. Of note, the chronic elevated levels of BCAAs in mice with disrupted mitochondrial branched chain aminotransferase were associated with increased energy expenditure (She et al., 2007). In rats fed a high fat diet, inclusion of BCAAs also attenuated obesity (Newgard et al., 2009). The relative high amounts of BCAAs in casein and whey, may hence contribute to the anti-obesogenic effect of dairy proteins. Studies by Freudenberg et al. have demonstrated that increasing leucine content in a high fat diet with regular protein content to a level matching a diet with high whey content attenuated obesity development (Freudenberg et al., 2012, 2013). Of note, BCAA-supplementation in mice delayed age-associated changes in the gut microbiota (Yang et al., 2016). In addition, BCAA supplemented mice had higher abundance of *Akkermansia* and *Bifidobacterium* in the gut. This may be of importance as *Akkermansia muciniphilia* has been associated with protection against diet-induced obesity (Everard et al., 2013; Shin et al., 2014), and the same has been reported for some strains of *Bifidobacteria* (An et al., 2011; Wang et al., 2015; Li et al., 2016). Still, the finding that equimolar supplementation with alanine decreased body fat mass gain in a short-term mouse experiment similarly as leucine (Freudenberg et al., 2013; Petzke et al., 2014), suggests that at least some of the observed effects are not specifically related to leucine, but due to increased amino nitrogen consumption. Thus, emphasizing that the effect of BCAA on metabolism is complex and far from fully understood.

TAURINE

Compared to terrestrial protein sources, seafood protein is characterized by high levels of taurine (Spitze et al., 2003). Supplementation of taurine to the diet or drinking water has been shown to prevent diet-induced weight gain, adiposity, and steatosis in rodents (Nakaya et al., 2000; Chang et al., 2011; Nardelli et al., 2011). In mice, it has been demonstrated that taurine supplementation reduced the abundance of Proteobacteria, especially *Helicobacter* and led to increased SCFA content in feces (Yu et al., 2016). SCFA, mainly acetate, propionate and butyrate are produced from non-digestible carbohydrates and may enter the systemic circulation and directly affect metabolism. Thus, SCFAs generally have been reported to counteract obesity in both rodents and humans (Canfora et al., 2015). However, a recent study revealed that increased acetate production led to hyperphagia and obesity in mice (Perry et al., 2016).

We have demonstrated that in mice fed an obesogenic diet with varying taurine concentrations, i.e., chicken, cod, crab, and scallop, for 7 weeks, the intake of taurine and glycine correlated negatively with body mass and total fat mass gain (Tastesen et al., 2014a). Further, rats fed diets with fish protein hydrolysate, rich in taurine and glycine exhibited reduced adiposity, possibly via increased bile acid concentration in plasma (Liaset et al., 2009, 2011). Primary bile acids are synthesized in the liver from cholesterol where they are conjugated to glycine or taurine in a species-dependent manner, and metabolized into secondary bile acids in the gut by the microbiota. Bile acids are ligands for the nuclear receptor farnesoid X receptor (FXR) and intestinal FXR is required for the development of obesity in response to a high-fat diet (Li et al., 2013). In addition, bile acids may also by binding and activating TGR5 increase energy expenditure (Watanabe et al., 2006; Broeders et al., 2015; Zietak and Kozak, 2016). In rodents, it has been proposed that the gut microbiota, in addition to regulating secondary bile acid metabolism, also inhibits bile acid synthesis in the liver by alleviating FXR inhibition in the ileum via reduced production of tauro-beta-muricholic acid (Sayin et al., 2013). Further, it is demonstrated that the gut microbiota promoted weight gain in an FXR-dependent manner, and the bile acid profiles and composition of fecal microbiota differed between $Fxr^{-/-}$ and wild-type mice (Parseus et al., 2017). Hence, whether the amino acid composition in protein rich food is able to influence obesity development via effects on bile acid metabolism in the microbiota warrants further investigation.

FATTY ACID COMPOSITION

In addition to the amino acid composition, different protein sources vary in other macronutrients. Regarding obesity development, the type and amount fat may be of particular importance. Meat from terrestrial sources, in particular red and processed meats, is rich in saturated fatty acids (SFAs), whereas meat from seafood, such as mackerel, halibut and salmon contains marine *n*-3 polyunsaturated fatty acids. The dietary fatty acid composition may influence obesity development directly,

as well as via their reported influence on the gut microbiota. Animal studies have shown that intake of diets rich in SFAs resulted in increased adiposity and lower metabolic rate, relative to a polyunsaturated fatty acid (PUFA)-rich diet (Matsuo et al., 1995; Takeuchi et al., 1995). Data from an intervention study with abdominally obese humans also showed that intake of SFAs, as compared to *n*-6 PUFAs, promoted hepatic fat deposition (Bjermo et al., 2012). In an overeating study with young healthy adults, intake of SFAs induced hepatic and visceral fat gain as compared to intake of *n*-6 PUFAs (Rosqvist et al., 2014). Thus, consumption of SFAs is likely to induce fat gain relative to *n*-6 PUFAs. We recently demonstrated that the fatty acid composition in salmon filet may be of importance. Replacement of marine oils in salmon feed with vegetable oils, soybean oil in particular, profoundly increased the *n*-6:*n*-3 ratio in fish filets and in red blood cells (RBCs) collected from mice consuming the salmon (Alvheim et al., 2013; Midtbo et al., 2013). Of note, the increased *n*-6:*n*-3 ratio in the RBC of the mice was accompanied with increased obesity (Alvheim et al., 2013; Midtbo et al., 2013, 2015). Although the results from rodent studies are more convincing than results from human trials (Madsen and Kristiansen, 2012), *n*-3 fatty acids are reported to increase weight loss also in humans (Thorsdottir et al., 2007).

It is well-known that the gut microbiota of high-fat diet-induced obese mice differs from that of lean mice (Serino et al., 2012; Xiao et al., 2015; Kiilerich et al., 2016), and we recently demonstrated that high-fat feeding rather than obesity drives taxonomical and functional changes in the gut microbiota in mice (Xiao et al., 2017). The dietary fatty acid composition is also reported to change the gut bacteria profile. Compared with *n*-6 or *n*-3 PUFAs, feeding mice diets rich in SFAs, over a 14-week period decreased the proportion of Bacteroidetes species and hence, the SFA-rich diet resulted in significantly greater decreases in Bacteroidetes-to-Firmicutes ratio than did either of the PUFA-rich diets (Liu et al., 2012). Mice fed fish oil are also reported to have increased levels of *A. muciniphila* (Caesar et al., 2015), which has been shown to reduce fat mass gain, and white adipose tissue macrophage infiltration, and to improve gut barrier function and glucose metabolism when administered to mice with diet-induced obesity. Further, antibiotic-treated mice receiving gut microbiota from a lard-fed donor showed increased adiposity and inflammation, whereas enrichment of *Akkermansia* co-occurred with partial protection against adiposity in mice transplanted with microbiota from fish oil fed mice (Caesar et al., 2015).

The different fatty acids have different capacities to activate the Toll-like receptors. In the study mentioned above, saturated lipids from lard were suggested to induce metabolic inflammation through Toll-like receptor signaling mediated by the gut microbiota (Caesar et al., 2015). By contrast, in another study on middle-aged rats, fish oil feeding was demonstrated to increase the relative abundances of the phylum Proteobacteria and the genus *Desulfovibrio*, concurrent with induced inflammation compared to rats receiving diets with soy bean oil or lard (Li et al., 2017). The innate pathogen receptors, a part of the first line of defense against infectious agents, including Toll-like receptors, nucleotide oligomerization domain containing proteins, and inflammasomes, have been pointed out as a link between the gut microbiota and host metabolism (Jin and Flavell, 2013). Inflammasome-deficiency-dependent modulation of the gut microbiota may be associated with abnormalities related to the metabolic syndrome and obesity in mouse models (Henao-Mejia et al., 2012). Further, changes in gut permeability may be affected through the interaction between diet, host and gut microbiota, augmenting access for proinflammatory molecules and activating inflammation, thereby affecting obesity development (reviewed in Tremaroli and Backhed, 2012).

It has been demonstrated that inclusion of lean fish in low energy diets was as efficient as inclusion of fatty fish or fish oil supplement in accelerating weight loss in humans (Thorsdottir et al., 2007). The total content of *n*-3 PUFAs is far lower in lean than in fatty seafood, but in lean seafood the majority of the fatty acids are present in the phospholipid (PL) fraction (Lie and Lambertsen, 1991). The bioavailability of eicosapentaenoic acid (EPA) and docosahexaenoic acid (DHA) is reported to be higher when they are PL-bound than triacylglycerol (TAG)-bound (Murru et al., 2013). Of note, the anti-obesogenic effects of PL-bound *n*-3 PUFAs are superior to TAG-bound *n*-3 PUFAs in mice (Rossmeisl et al., 2012). The high biological activity of PL-bound PUFAs is suggested to include effects mediated via the endocannabinoid signaling system (Batetta et al., 2009; Rossmeisl et al., 2012).

The endocannabinoid signaling system may link the gut microbiota to adipogenesis, as CB_I receptors are reported to control gut permeability through interactions with the gut microbiota (Muccioli et al., 2010). Further, changes in the composition of the gut microbiota during obesity induce gut-barrier dysfunction, which may lead to leakage from the gut of components from Gram-negative bacteria and metabolic endotoxemia triggering the onset of metabolic disorders associated with obesity (Cani et al., 2016). Conversely, administration of the intestinal bacterium *A. muciniphila* to high-fat diet fed mice led to an increase in intestinal levels of the endocannabinoids, 2-arachidonoylglycerol, 2-oleoylglycerol and 2-palmitoylglycerol, along with improved gut-barrier function and decreased metabolic endotoxemia (Everard et al., 2013). The molecular mechanisms that link gut microorganisms and the synthesis of endocannabinoids or other bioactive lipids are still unknown, and it is not known to what extent such molecules play significant roles in obesity development or metabolic dysfunctions associated with obesity.

PERSISTENT ORGANIC POLLUTANTS

Importantly, food is also the primary route of exposure to pollutants from numerous chemical classes. Actually, food contributes more than 90 % to the total current exposure of POPs, especially food of animal origin such as fish, dairy products, or meat (Li et al., 2006; Malisch and Kotz, 2014). During the last decade increasing attention has been paid to the possible relationship between POP exposure and the current obesity epidemic. Studies have reported an association between obesity

and plasma levels of certain polychlorinated biphenyls (PCBs) and pesticides (Dhooge et al., 2010; Ronn et al., 2011; Lee et al., 2012; Roos et al., 2013). Thus, concern about the possible connection between exposure to environmental contaminants and the epidemics of obesity has been raised (Lee et al., 2014). However, a causal relationship between POP exposure and obesity development has not yet been demonstrated, and inverse relationships between obesity and plasma levels of POPs, in particular highly chlorinated PCBs, are also reported (Nawrot et al., 2002; Dirinck et al., 2011). A direct causal link between POP exposure and obesity in humans is difficult to establish, but repeated injections of PCB-153 (Wahlang et al., 2013) and PCB-77 (Arsenescu et al., 2008) are reported to exacerbate obesity in mice. We have previously observed that POPs of marine origin accumulate in adipose tissue concomitant with obesity development in mice fed farmed Atlantic salmon (Ibrahim et al., 2011). However, mice fed high levels of POPs from whale meat were leaner than control casein fed mice, despite a high accumulation of POPs in adipose tissue (Ibrahim et al., 2012). In a recent study we reduced the levels of PCBs and DDTs by 50% in salmon filets by partial replacement of fish oil with vegetable oils in aquatic feed leading to aggravated insulin resistance and hepatic lipid accumulation, despite a reduction in the levels of PCBs and DDTs (Midtbo et al., 2013).

The relationship between the gut bacteria and environmental pollutants is bidirectional (Parks et al., 2013). First, POP exposure

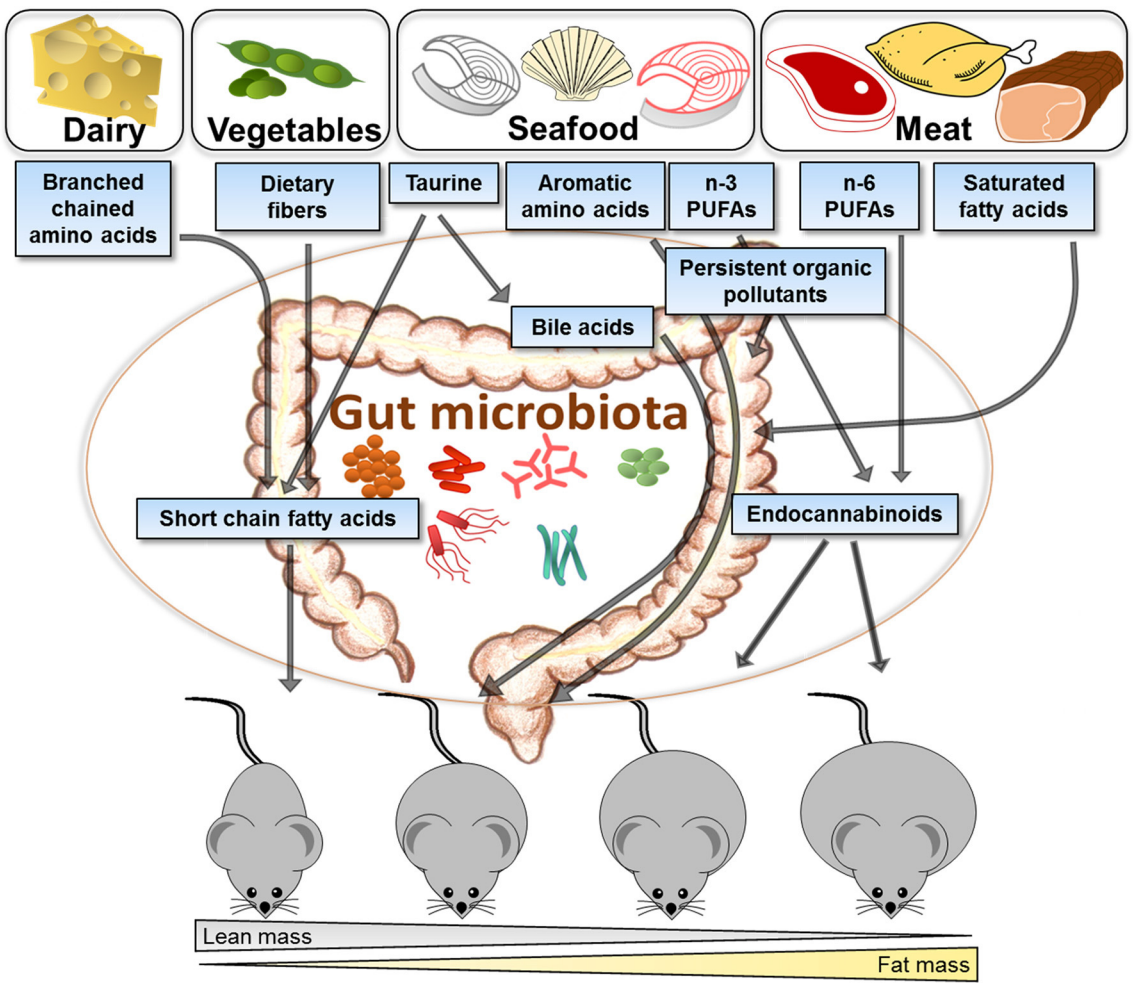

FIGURE 2 | Illustration of how different protein sources vary in their efficiency to attenuate obesity development and suggested links with the gut microbiota. Proteins derived from different food sources contain varying amounts of amino acids, fatty acids, and pollutants, which may interact with the gut microbiota and change the host metabolism, and further impact on obesity development. Casein and other dairy products have a high content of branched chain amino acids and are efficient protein sources for attenuating obesity development in rodents. Proteins from vegetarian sources contribute to high fiber content in the diet and have been demonstrated to protect against obesity. Compared to animal protein sources, seafoods contain high amounts of taurine, aromatic amino acids, *n*-3 polyunsaturated fatty acids (PUFAs) and persistent organic pollutants, which further may impact on the gut microbiota, production of bile acids or endocannabinoids. Different sources of meat contribute with saturated fatty acids, n-6 PUFAs and persistent organic pollutants. Generally, intake of proteins from meat has been demonstrated to be more obesogenic than intake of proteins from seafood or vegetables. It remains to be established to what extent such differences between proteins reflect direct metabolic effects in the host or to what extent the microbiota plays a causal role.

alters the composition of the gut microbiota in mice. It has been demonstrated that gavage with a high dose of a mixture of PCB congeners found in meat and fatty fish for 2 days diminished the overall abundance of bacteria (Choi et al., 2013). Of note, exercise prevented these changes (Choi et al., 2013). Further, it has been reported that exposure to 2,3,7,8 tetrachlorodibenzofuran, TCDF, alters the gut microbiome by shifting the ratio of Firmicutes to Bacteroidetes (Zhang et al., 2015), which as mentioned earlier has been associated with obesity (Ley et al., 2005; Turnbaugh et al., 2006). Secondly, the gut microbiota can affect body burden of POPs by a number of mechanisms. The bacteria may metabolize the POPs and alter absorption and excretion as well as influence the host detoxification capacity and the enterohepatic circulation of environmental chemicals (Claus et al., 2016; Spanogiannopoulos et al., 2016). Last, we have provided evidence that the dietary composition of macronutrients profoundly modulates accumulation of four environmental relevant POPs in adipose tissue and liver in C57BL/6 mice (Myrmel et al., 2016). Thus, understanding the potential roles of the gut microbiota in the metabolism and toxicity of environmental pollutants could provide valuable knowledge for targeted approaches in reducing the detrimental health impact of environmental pollution.

CONCLUSION

The efficiency of different proteins to attenuate obesity in both human and animal trials varies depending on the protein source as illustrated in **Figure 2**. Different food groups and dietary patterns are linked to obesity and disease development, and to distinct gut microbiota composition. However, the association between diet, obesity and gut microbiota is not established. Here we have reviewed data from several different studies in order to illustrate how different protein sources may affect the gut microbiota, linking protein-dependent changes in the gut microbiota with metabolism. The varying amounts of amino acids, fatty acid composition, and POPs derived from different protein sources, such as dairy, vegetarian sources, seafood and meat, are discussed in light of their impact on gut microbiota and obesity. Casein and other dairy proteins stand out as the most efficient protein sources in preventing obesity, having a high content of BCAAs with possible impact on gut microbiota and obesity. The distinct impacts of lean seafood and meat are suggested to involve differences in the content of amino acids, such as aromatic amino acids, glycine and taurine, possibly affecting the bile acids with further impact on energy expenditure and the gut microbiota. The *n*-3 PUFAs may affect the metabolism through the endocannabinoid system and the gut microbiota composition, but the molecular mechanisms linking the gut microorganisms to the synthesis of endocannabinoids or other bioactive lipids are still largely unexplored. As dietary sources will inevitably lead to exposure of pollutants, their impact on metabolism may also contribute to the varying impact of different protein sources. Knowledge of the mutually reciprocal interactions between the gut microbiota and environmental pollutants present in different food sources and the combined effects on whole body metabolism could provide new modalities involving targeted dietary approaches reducing the detrimental health impact of environmental pollution.

AUTHOR CONTRIBUTIONS

LM: Researched data and wrote the article; KK, LSM, EF, and BL: Contributed to discussion of the content, illustration, revised, and/or edited the manuscript before submission.

REFERENCES

Aadland, E. K., Graff, I. E., Lavigne, C., Eng, O., Paquette, M., Holthe, A., et al. (2016). Lean seafood intake reduces postprandial C-peptide and lactate concentrations in healthy adults in a randomized controlled trial with a crossover design. *J. Nutr.* 146, 1027–1034. doi: 10.3945/jn.115.229278

Aadland, E. K., Lavigne, C., Graff, I. E., Eng, O., Paquette, M., Holthe, A., et al. (2015). Lean-seafood intake reduces cardiovascular lipid risk factors in healthy subjects: results from a randomized controlled trial with a crossover design. *Am. J. Clin. Nutr.* 102, 582–592. doi: 10.3945/ajcn.115.112086

Alvheim, A. R., Torstensen, B. E., Lin, Y. H., Lillefosse, H. H., Lock, E. J., Madsen, L., et al. (2013). Dietary linoleic acid elevates endogenous 2-arachidonoylglycerol and anandamide in Atlantic salmon (*Salmo salar* L.) and mice, and induces weight gain and inflammation in mice. *Br. J. Nutr.* 109, 1508–1517. doi: 10.1017/S0007114512003364

An, H. M., Park, S. Y., Lee, D. K., Kim, J. R., Cha, M. K., Lee, S. W., et al. (2011). Antiobesity and lipid-lowering effects of *Bifidobacterium* spp. in high fat diet-induced obese rats. *Lipids Health Dis.* 10:116. doi: 10.1186/1476-511X-10-116

Arsenescu, V., Arsenescu, R. I., King, V., Swanson, H., and Cassis, L. A. (2008). Polychlorinated biphenyl-77 induces adipocyte differentiation and proinflammatory adipokines and promotes obesity and atherosclerosis. *Environ. Health Perspect.* 116, 761–768. doi: 10.1289/ehp.10554

Arumugam, M., Raes, J., Pelletier, E., Le Paslier, D., Yamada, T., Mende, D. R., et al. (2011). Enterotypes of the human gut microbiome. *Nature* 473, 174–180. doi: 10.1038/nature09944

Astrup, A., Raben, A., and Geiker, N. (2015). The role of higher protein diets in weight control and obesity-related comorbidities. *Int. J. Obes.* 39, 721–726. doi: 10.1038/ijo.2014.216

Baothman, O. A., Zamzami, M. A., Taher, I., Abubaker, J., and Abu-Farha, M. (2016). The role of Gut Microbiota in the development of obesity and Diabetes. *Lipids Health Dis.* 15:108. doi: 10.1186/s12944-016-0278-4

Batetta, B., Griinari, M., Carta, G., Murru, E., Ligresti, A., Cordeddu, L., et al. (2009). Endocannabinoids may mediate the ability of (n-3) fatty acids to reduce ectopic fat and inflammatory mediators in obese Zucker rats. *J. Nutr.* 139, 1495–1501. doi: 10.3945/jn.109.104844

Bellissimo, N., and Akhavan, T. (2015). Effect of macronutrient composition on short-term food intake and weight loss. *Adv. Nutr.* 6, 302S−308S. doi: 10.3945/an.114.006957

Bjermo, H., Iggman, D., Kullberg, J., Dahlman, I., Johansson, L., Persson, L., et al. (2012). Effects of n-6 PUFAs compared with SFAs on liver fat, lipoproteins, and inflammation in abdominal obesity: a randomized controlled trial. *Am. J. Clin. Nutr.* 95, 1003–1012. doi: 10.3945/ajcn.111.030114

Boirie, Y., Dangin, M., Gachon, P., Vasson, M. P., Maubois, J. L., and Beaufrere, B. (1997). Slow and fast dietary proteins differently modulate postprandial protein accretion. *Proc. Natl. Acad. Sci. U.S.A.* 94, 14930–14935. doi: 10.1073/pnas.94.26.14930

Brandsch, C., Shukla, A., Hirche, F., Stangl, G. I., and Eder, K. (2006). Effect of proteins from beef, pork, and turkey meat on plasma and liver lipids of rats compared with casein and soy protein. *Nutrition* 22, 1162–1170. doi: 10.1016/j.nut.2006.06.009

Broeders, E. P., Nascimento, E. B., Havekes, B., Brans, B., Roumans, K. H., Tailleux, A., et al. (2015). The bile acid chenodeoxycholic acid increases human brown adipose tissue activity. *Cell Metab.* 22, 418–426. doi: 10.1016/j.cmet.2015.07.002

Caesar, R., Tremaroli, V., Kovatcheva-Datchary, P., Cani, P. D., and Backhed, F. (2015). Crosstalk between gut microbiota and dietary lipids aggravates WAT inflammation through TLR signaling. *Cell Metab.* 22, 658–668. doi: 10.1016/j.cmet.2015.07.026

Canfora, E. E., Jocken, J. W., and Blaak, E. E. (2015). Short-chain fatty acids in control of body weight and insulin sensitivity. *Nat. Rev. Endocrinol.* 11, 577–591. doi: 10.1038/nrendo.2015.128

Cani, P. D., Plovier, H., Van Hul, M., Geurts, L., Delzenne, N. M., Druart, C., et al. (2016). Endocannabinoids–at the crossroads between the gut microbiota and host metabolism. *Nat. Rev. Endocrinol.* 12, 133–143. doi: 10.1038/nrendo.2015.211

Carmody, R. N., Gerber, G. K., Luevano, J. M. Jr., Gatti, D. M., Somes, L., Svenson, K. L., et al. (2015). Diet dominates host genotype in shaping the murine gut microbiota. *Cell Host Microbe* 17, 72–84. doi: 10.1016/j.chom.2014.11.010

Chang, Y. Y., Chou, C. H., Chiu, C. H., Yang, K. T., Lin, Y. L., Weng, W. L., et al. (2011). Preventive effects of taurine on development of hepatic steatosis induced by a high-fat/cholesterol dietary habit. *J. Agric. Food Chem.* 59, 450–457. doi: 10.1021/jf103167u

Chen, M., Pan, A., Malik, V. S., and Hu, F. B. (2012). Effects of dairy intake on body weight and fat: a meta-analysis of randomized controlled trials. *Am. J. Clin. Nutr.* 96, 735–747. doi: 10.3945/ajcn.112.037119

Cho, C. E., Taesuwan, S., Malysheva, O. V., Bender, E., Tulchinsky, N. F., Yan, J., et al. (2017). Trimethylamine-N-oxide (TMAO) response to animal source foods varies among healthy young men and is influenced by their gut microbiota composition: a randomized controlled trial. *Mol. Nutr. Food Res.* 61:1600324. doi: 10.1002/mnfr.201600324

Choi, J. J., Eum, S. Y., Rampersaud, E., Daunert, S., Abreu, M. T., and Toborek, M. (2013). Exercise attenuates PCB-induced changes in the mouse gut microbiome. *Environ. Health Perspect.* 121, 725–730. doi: 10.1289/ehp.1306534

Claesson, M. J., Jeffery, I. B., Conde, S., Power, S. E., O'connor, E. M., Cusack, S., et al. (2012). Gut microbiota composition correlates with diet and health in the elderly. *Nature* 488, 178–184. doi: 10.1038/nature11319

Clarke, S. F., Murphy, E. F., O'sullivan, O., Ross, R. P., O'toole, P. W., Shanahan, F., et al. (2013). Targeting the microbiota to address diet-induced obesity: a time dependent challenge. *PLoS ONE* 8:e65790. doi: 10.1371/journal.pone.0065790

Claus, S. P., Guillou, H., and Ellero-Simatos, S. (2016). The gut microbiota: a major player in the toxicity of environmental pollutants? *NPJ Biofilms Microb.* 2:16003. doi: 10.1038/npjbiofilms.2016.3

David, L. A., Maurice, C. F., Carmody, R. N., Gootenberg, D. B., Button, J. E., Wolfe, B. E., et al. (2014). Diet rapidly and reproducibly alters the human gut microbiome. *Nature* 505, 559–563. doi: 10.1038/nature12820

De Filippo, C., Cavalieri, D., Di Paola, M., Ramazzotti, M., Poullet, J. B., Massart, S., et al. (2010). Impact of diet in shaping gut microbiota revealed by a comparative study in children from Europe and rural Africa. *Proc. Natl. Acad. Sci. U.S.A.* 107, 14691–14696. doi: 10.1073/pnas.1005963107

Dhooge, W., Den Hond, E., Koppen, G., Bruckers, L., Nelen, V., Van De Mieroop, E., et al. (2010). Internal exposure to pollutants and body size in Flemish adolescents and adults: associations and dose-response relationships. *Environ. Int.* 36, 330–337. doi: 10.1016/j.envint.2010.01.005

Dirinck, E., Jorens, P. G., Covaci, A., Geens, T., Roosens, L., Neels, H., et al. (2011). Obesity and persistent organic pollutants: possible obesogenic effect of organochlorine pesticides and polychlorinated biphenyls. *Obesity* 19, 709–714. doi: 10.1038/oby.2010.133

Dumas, M. E., Rothwell, A. R., Hoyles, L., Aranias, T., Chilloux, J., Calderari, S., et al. (2017). Microbial-host co-metabolites are prodromal markers predicting phenotypic heterogeneity in behavior, obesity, and impaired glucose tolerance. *Cell Rep.* 20, 136–148. doi: 10.1016/j.celrep.2017.06.039

Eid, H. M., Wright, M. L., Anil Kumar, N. V., Qawasmeh, A., Hassan, S. T. S., Mocan, A., et al. (2017). Significance of microbiota in obesity and metabolic diseases and the modulatory potential by medicinal plant and food ingredients. *Front. Pharmacol.* 8:387. doi: 10.3389/fphar.2017.00387

Everard, A., Belzer, C., Geurts, L., Ouwerkerk, J. P., Druart, C., Bindels, L. B., et al. (2013). Cross-talk between Akkermansia muciniphila and intestinal epithelium controls diet-induced obesity. *Proc. Natl. Acad. Sci. U.S.A.* 110, 9066–9071. doi: 10.1073/pnas.1219451110

Faghih, S., Abadi, A. R., Hedayati, M., and Kimiagar, S. M. (2011). Comparison of the effects of cows' milk, fortified soy milk, and calcium supplement on weight and fat loss in premenopausal overweight and obese women. *Nutr. Metab. Cardiovasc. Dis.* 21, 499–503. doi: 10.1016/j.numecd.2009.11.013

Flint, H. J. (2012). The impact of nutrition on the human microbiome. *Nutr. Rev.* 70(Suppl. 1), S10–S13. doi: 10.1111/j.1753-4887.2012.00499.x

Fogelholm, M., Anderssen, S., Gunnarsdottir, I., and Lahti-Koski, M. (2012). Dietary macronutrients and food consumption as determinants of long-term weight change in adult populations: a systematic literature review. *Food Nutr. Res.* 56:19103. doi: 10.3402/fnr.v56i0.19103

Freudenberg, A., Petzke, K. J., and Klaus, S. (2012). Comparison of high-protein diets and leucine supplementation in the prevention of metabolic syndrome and related disorders in mice. *J. Nutr. Biochem.* 23, 1524–1530. doi: 10.1016/j.jnutbio.2011.10.005

Freudenberg, A., Petzke, K. J., and Klaus, S. (2013). Dietary L-leucine and L-alanine supplementation have similar acute effects in the prevention of high-fat diet-induced obesity. *Amino Acids* 44, 519–528. doi: 10.1007/s00726-012-1363-2

Goodrich, J. K., Waters, J. L., Poole, A. C., Sutter, J. L., Koren, O., Blekhman, R., et al. (2014). Human genetics shape the gut microbiome. *Cell* 159, 789–799. doi: 10.1016/j.cell.2014.09.053

Graf, D., Di Cagno, R., Fak, F., Flint, H. J., Nyman, M., Saarela, M., et al. (2015). Contribution of diet to the composition of the human gut microbiota. *Microb. Ecol. Health Dis.* 26:26164. doi: 10.3402/mehd.v26.26164

Hao, Q., Lillefosse, H. H., Fjaere, E., Myrmel, L. S., Midtbo, L. K., Jarlsby, R. H., et al. (2012). High-glycemic index carbohydrates abrogate the antiobesity effect of fish oil in mice. *Am. J. Physiol. Endocrinol. Metab.* 302, E1097–E1112. doi: 10.1152/ajpendo.00524.2011

Henao-Mejia, J., Elinav, E., Jin, C., Hao, L., Mehal, W. Z., Strowig, T., et al. (2012). Inflammasome-mediated dysbiosis regulates progression of NAFLD and obesity. *Nature* 482, 179–185. doi: 10.1038/nature10809

Holm, J. B., Ronnevik, A., Tastesen, H. S., Fjaere, E., Fauske, K. R., Liisberg, U., et al. (2016). Diet-induced obesity, energy metabolism and gut microbiota in C57BL/6J mice fed Western diets based on lean seafood or lean meat mixtures. *J. Nutr. Biochem.* 31, 127–136. doi: 10.1016/j.jnutbio.2015.12.017

Huang, H., Krishnan, H. B., Pham, Q., Yu, L. L., and Wang, T. T. (2016). Soy and gut microbiota: interaction and implication for human health. *J. Agric. Food Chem.* 64, 8695–8709. doi: 10.1021/acs.jafc.6b03725

Ibrahim, M. M., Fjaere, E., Lock, E. J., Froyland, L., Jessen, N., Lund, S., et al. (2012). Metabolic impacts of high dietary exposure to persistent organic pollutants in mice. *Toxicol. Lett.* 215, 8–15. doi: 10.1016/j.toxlet.2012.09.022

Ibrahim, M. M., Fjaere, E., Lock, E. J., Naville, D., Amlund, H., Meugnier, E., et al. (2011). Chronic consumption of farmed salmon containing persistent organic pollutants causes insulin resistance and obesity in mice. *PLoS ONE* 6:e25170. doi: 10.1371/journal.pone.0025170

Isokpehi, R. D., Simmons, S. S., Johnson, M. O., and Payton, M. (2017). Genomic evidence for bacterial determinants influencing obesity development. *Int. J. Environ. Res. Public Health* 14:345. doi: 10.3390/ijerph14040345

Jin, C., and Flavell, R. A. (2013). Innate sensors of pathogen and stress: linking inflammation to obesity. *J. Allergy Clin. Immunol.* 132, 287–294. doi: 10.1016/j.jaci.2013.06.022

Kiilerich, P., Myrmel, L. S., Fjaere, E., Hao, Q., Hugenholtz, F., Sonne, S. B., et al. (2016). Effect of a long-term high-protein diet on survival, obesity development, and gut microbiota in mice. *Am. J. Physiol. Endocrinol. Metab.* 310, E886–E899. doi: 10.1152/ajpendo.00363.2015

Koeth, R. A., Wang, Z., Levison, B. S., Buffa, J. A., Org, E., Sheehy, B. T., et al. (2013). Intestinal microbiota metabolism of L-carnitine, a nutrient in red meat, promotes atherosclerosis. *Nat. Med.* 19, 576–585. doi: 10.1038/nm.3145

Koh, A., De Vadder, F., Kovatcheva-Datchary, P., and Backhed, F. (2016). From dietary fiber to host physiology: short-chain fatty acids as key bacterial metabolites. *Cell* 165, 1332–1345. doi: 10.1016/j.cell.2016.05.041

Lacroix, M., Gaudichon, C., Martin, A., Morens, C., Mathe, V., Tome, D., et al. (2004). A long-term high-protein diet markedly reduces adipose tissue without major side effects in Wistar male rats. *Am. J. Physiol. Regul. Integr. Comp. Physiol.* 287, R934–R942. doi: 10.1152/ajpregu.00100.2004

Landfald, B., Valeur, J., Berstad, A., and Raa, J. (2017). Microbial trimethylamine-N-oxide as a disease marker: something fishy? *Microb. Ecol. Health Dis.* 28:1327309. doi: 10.1080/16512235.2017.1327309

Lee, D. H., Lind, L., Jacobs, D. R. Jr., Salihovic, S., Van Bavel, B., and Lind, P. M. (2012). Associations of persistent organic pollutants with abdominal obesity in the elderly: the Prospective Investigation of the Vasculature in Uppsala Seniors (PIVUS) study. *Environ. Int.* 40, 170–178. doi: 10.1016/j.envint.2011.07.010

Lee, D. H., Porta, M., Jacobs, D. R. Jr., and Vandenberg, L. N. (2014). Chlorinated persistent organic pollutants, obesity, and type 2 diabetes. *Endocr. Rev.* 35, 557–601. doi: 10.1210/er.2013-1084

Lepe, M., Bacardi Gascon, M., and Jimenez Cruz, A. (2011). Long-term efficacy of high-protein diets: a systematic review. *Nutr. Hosp.* 26, 1256–1259. doi: 10.3305/nh.2011.26.6.5353

Levine, M. E., Suarez, J. A., Brandhorst, S., Balasubramanian, P., Cheng, C. W., Madia, F., et al. (2014). Low protein intake is associated with a major reduction in IGF-1, cancer, and overall mortality in the 65 and younger but not older population. *Cell Metab.* 19, 407–417. doi: 10.1016/j.cmet.2014.02.006

Ley, R. E., Backhed, F., Turnbaugh, P., Lozupone, C. A., Knight, R. D., and Gordon, J. I. (2005). Obesity alters gut microbial ecology. *Proc. Natl. Acad. Sci. U.S.A.* 102, 11070–11075. doi: 10.1073/pnas.0504978102

Ley, R. E., Turnbaugh, P. J., Klein, S., and Gordon, J. I. (2006). Microbial ecology: human gut microbes associated with obesity. *Nature* 444, 1022–1023. doi: 10.1038/4441022a

Li, F., Jiang, C., Krausz, K. W., Li, Y., Albert, I., Hao, H., et al. (2013). Microbiome remodelling leads to inhibition of intestinal farnesoid X receptor signalling and decreased obesity. *Nat. Commun.* 4:2384. doi: 10.1038/ncomms3384

Li, H., Zhu, Y., Zhao, F., Song, S., Li, Y., Xu, X., et al. (2017). Fish oil, lard and soybean oil differentially shape gut microbiota of middle-aged rats. *Sci. Rep.* 7:826. doi: 10.1038/s41598-017-00969-0

Li, Q. Q., Loganath, A., Chong, Y. S., Tan, J., and Obbard, J. P. (2006). Persistent organic pollutants and adverse health effects in humans. *J. Toxicol. Environ. Health Part A* 69, 1987–2005. doi: 10.1080/15287390600751447

Li, Z., Jin, H., Oh, S. Y., and Ji, G. E. (2016). Anti-obese effects of two Lactobacilli and two Bifidobacteria on ICR mice fed on a high fat diet. *Biochem. Biophys. Res. Commun.* 480, 222–227. doi: 10.1016/j.bbrc.2016.10.031

Liaset, B., Hao, Q., Jorgensen, H., Hallenborg, P., Du, Z. Y., Ma, T., et al. (2011). Nutritional regulation of bile acid metabolism is associated with improved pathological characteristics of the metabolic syndrome. *J. Biol. Chem.* 286, 28382–28395. doi: 10.1074/jbc.M111.234732

Liaset, B., Madsen, L., Hao, Q., Criales, G., Mellgren, G., Marschall, H. U., et al. (2009). Fish protein hydrolysate elevates plasma bile acids and reduces visceral adipose tissue mass in rats. *Biochim. Biophys. Acta* 1791, 254–262. doi: 10.1016/j.bbalip.2009.01.016

Lie, O., and Lambertsen, G. (1991). Fatty acid composition of glycerophospholipids in seven tissues of cod (Gadus morhua), determined by combined high-performance liquid chromatography and gas chromatography. *J. Chromatogr.* 565, 119–129. doi: 10.1016/0378-4347(91)80376-N

Liisberg, U., Fauske, K. R., Kuda, O., Fjaere, E., Myrmel, L. S., Norberg, N., et al. (2016a). Intake of a Western diet containing cod instead of pork alters fatty acid composition in tissue phospholipids and attenuates obesity and hepatic lipid accumulation in mice. *J. Nutr. Biochem.* 33, 119–127. doi: 10.1016/j.jnutbio.2016.03.014

Liisberg, U., Myrmel, L. S., Fjaere, E., Ronnevik, A. K., Bjelland, S., Fauske, K. R., et al. (2016b). The protein source determines the potential of high protein diets to attenuate obesity development in C57BL/6J mice. *Adipocyte* 5, 196–211. doi: 10.1080/21623945.2015.1122855

Lillefosse, H. H., Clausen, M. R., Yde, C. C., Ditlev, D. B., Zhang, X., Du, Z. Y., et al. (2014). Urinary loss of tricarboxylic acid cycle intermediates as revealed by metabolomics studies: an underlying mechanism to reduce lipid accretion by whey protein ingestion? *J. Proteome Res.* 13, 2560–2570. doi: 10.1021/pr500039t

Lin, R., Liu, W., Piao, M., and Zhu, H. (2017). A review of the relationship between the gut microbiota and amino acid metabolism. *Amino Acids* 49, 2083–2090. doi: 10.1007/s00726-017-2493-3

Liu, R., Hong, J., Xu, X., Feng, Q., Zhang, D., Gu, Y., et al. (2017). Gut microbiome and serum metabolome alterations in obesity and after weight-loss intervention. *Nat. Med.* 23, 859–868. doi: 10.1038/nm.4358

Liu, T., Hougen, H., Vollmer, A. C., and Hiebert, S. M. (2012). Gut bacteria profiles of Mus musculus at the phylum and family levels are influenced by saturation of dietary fatty acids. *Anaerobe* 18, 331–337. doi: 10.1016/j.anaerobe.2012.02.004

Ma, T., Liaset, B., Hao, Q., Petersen, R. K., Fjaere, E., Ngo, H. T., et al. (2011). Sucrose counteracts the anti-inflammatory effect of fish oil in adipose tissue and increases obesity development in mice. *PLoS ONE* 6:e21647. doi: 10.1371/journal.pone.0021647

Madsen, L., and Kristiansen, K. (2012). Of mice and men: factors abrogating the antiobesity effect of omega-3 fatty acids. *Adipocyte* 1, 173–176. doi: 10.4161/adip.20689

Madsen, L., Pedersen, L. M., Liaset, B., Ma, T., Petersen, R. K., Van Den Berg, S., et al. (2008). cAMP-dependent signaling regulates the adipogenic effect of n-6 polyunsaturated fatty acids. *J. Biol. Chem.* 283, 7196–7205. doi: 10.1074/jbc.M707775200

Malisch, R., and Kotz, A. (2014). Dioxins and PCBs in feed and food–review from European perspective. *Sci. Total Environ.* 491–492, 2–10. doi: 10.1016/j.scitotenv.2014.03.022

Marsset-Baglieri, A., Fromentin, G., Tome, D., Bensaid, A., Makkarios, L., and Even, P. C. (2004). Increasing the protein content in a carbohydrate-free diet enhances fat loss during 35% but not 75% energy restriction in rats. *J. Nutr.* 134, 2646–2652.

Matsuo, T., Sumida, H., and Suzuki, M. (1995). Beef tallow diet decreases beta-adrenergic receptor binding and lipolytic activities in different adipose tissues of rat. *Metab. Clin. Exp.* 44, 1271–1277. doi: 10.1016/0026-0495(95)90028-4

McAllan, L., Skuse, P., Cotter, P. D., O'connor, P., Cryan, J. F., Ross, R. P., et al. (2014). Protein quality and the protein to carbohydrate ratio within a high fat diet influences energy balance and the gut microbiota in C57BL/6J mice. *PLoS ONE* 9:e88904. doi: 10.1371/journal.pone.0088904

McAllan, L., Speakman, J. R., Cryan, J. F., and Nilaweera, K. N. (2015). Whey protein isolate decreases murine stomach weight and intestinal length and alters the expression of Wnt signalling-associated genes. *Br. J. Nutr.* 113, 372–379. doi: 10.1017/S0007114514004024

Midtbo, L. K., Borkowska, A. G., Bernhard, A., Ronnevik, A. K., Lock, E. J., Fitzgerald, M. L., et al. (2015). Intake of farmed Atlantic salmon fed soybean oil increases hepatic levels of arachidonic acid-derived oxylipins and ceramides in mice. *J. Nutr. Biochem.* 26, 585–595. doi: 10.1016/j.jnutbio.2014.12.005

Midtbo, L. K., Ibrahim, M. M., Myrmel, L. S., Aune, U. L., Alvheim, A. R., Liland, N. S., et al. (2013). Intake of farmed Atlantic salmon fed soybean oil increases insulin resistance and hepatic lipid accumulation in mice. *PLoS ONE* 8:e53094. doi: 10.1371/journal.pone.0053094

Millward, D. J., Layman, D. K., Tome, D., and Schaafsma, G. (2008). Protein quality assessment: impact of expanding understanding of protein and amino acid needs for optimal health. *Am. J. Clin. Nutr.* 87, 1576S−1581S.

Morens, C., Keijzer, M., De Vries, K., Scheurink, A., and Van Dijk, G. (2005). Effects of high-fat diets with different carbohydrate-to-protein ratios on energy homeostasis in rats with impaired brain melanocortin receptor activity. *Am. J. Physiol. Regul. Integr. Comp. Physiol.* 289, R156–R163. doi: 10.1152/ajpregu.00774.2004

Mozaffarian, D. (2016). Dietary and policy priorities for cardiovascular disease, diabetes, and obesity: a comprehensive review. *Circulation* 133, 187–225. doi: 10.1161/CIRCULATIONAHA.115.018585

Muccioli, G. G., Naslain, D., Backhed, F., Reigstad, C. S., Lambert, D. M., Delzenne, N. M., et al. (2010). The endocannabinoid system links gut microbiota to adipogenesis. *Mol. Syst. Biol.* 6:392. doi: 10.1038/msb.2010.46

Muegge, B. D., Kuczynski, J., Knights, D., Clemente, J. C., Gonzalez, A., Fontana, L., et al. (2011). Diet drives convergence in gut microbiome functions across mammalian phylogeny and within humans. *Science* 332, 970–974. doi: 10.1126/science.1198719

Murru, E., Banni, S., and Carta, G. (2013). Nutritional properties of dietary omega-3-enriched phospholipids. *Biomed Res. Int.* 2013:965417. doi: 10.1155/2013/965417

Myrmel, L. S., Fjaere, E., Midtbo, L. K., Bernhard, A., Petersen, R. K., Sonne, S. B., et al. (2016). Macronutrient composition determines accumulation of persistent organic pollutants from dietary exposure in adipose tissue of mice. *J. Nutr. Biochem.* 27, 307–316. doi: 10.1016/j.jnutbio.2015.09.019

Nakaya, Y., Minami, A., Harada, N., Sakamoto, S., Niwa, Y., and Ohnaka, M. (2000). Taurine improves insulin sensitivity in the Otsuka Long-Evans Tokushima Fatty rat, a model of spontaneous type 2 diabetes. *Am. J. Clin. Nutr.* 71, 54–58.

Nardelli, T. R., Ribeiro, R. A., Balbo, S. L., Vanzela, E. C., Carneiro, E. M., Boschero, A. C., et al. (2011). Taurine prevents fat deposition and ameliorates plasma

lipid profile in monosodium glutamate-obese rats. *Amino Acids* 41, 901–908. doi: 10.1007/s00726-010-0789-7

Nawrot, T. S., Staessen, J. A., Den Hond, E. M., Koppen, G., Schoeters, G., Fagard, R., et al. (2002). Host and environmental determinants of polychlorinated aromatic hydrocarbons in serum of adolescents. *Environ. Health Perspect.* 110, 583–589. doi: 10.1289/ehp.02110583

Newgard, C. B., An, J., Bain, J. R., Muehlbauer, M. J., Stevens, R. D., Lien, L. F., et al. (2009). A branched-chain amino acid-related metabolic signature that differentiates obese and lean humans and contributes to insulin resistance. *Cell Metab.* 9, 311–326. doi: 10.1016/j.cmet.2009.02.002

Park, D. Y., Ahn, Y. T., Park, S. H., Huh, C. S., Yoo, S. R., Yu, R., et al. (2013). Supplementation of *Lactobacillus curvatus* HY7601 and *Lactobacillus plantarum* KY1032 in diet-induced obese mice is associated with gut microbial changes and reduction in obesity. *PLoS ONE* 8:e59470. doi: 10.1371/journal.pone.0059470

Parks, B. W., Nam, E., Org, E., Kostem, E., Norheim, F., Hui, S. T., et al. (2013). Genetic control of obesity and gut microbiota composition in response to high-fat, high-sucrose diet in mice. *Cell Metab.* 17, 141–152. doi: 10.1016/j.cmet.2012.12.007

Parseus, A., Sommer, N., Sommer, F., Caesar, R., Molinaro, A., Stahlman, M., et al. (2017). Microbiota-induced obesity requires farnesoid X receptor. *Gut* 66, 429–437. doi: 10.1136/gutjnl-2015-310283

Pasiakos, S. M. (2015). Metabolic advantages of higher protein diets and benefits of dairy foods on weight management, glycemic regulation, and bone. *J. Food Sci.* 80(Suppl. 1), A2–A7. doi: 10.1111/1750-3841.12804

Perry, R. J., Peng, L., Barry, N. A., Cline, G. W., Zhang, D., Cardone, R. L., et al. (2016). Acetate mediates a microbiome–brain–β-cell axis to promote metabolic syndrome. *Nature* 534, 213–217. doi: 10.1038/nature18309

Pesta, D. H., and Samuel, V. T. (2014). A high-protein diet for reducing body fat: mechanisms and possible caveats. *Nutr. Metab.* 11:53. doi: 10.1186/1743-7075-11-53

Petzke, K. J., Freudenberg, A., and Klaus, S. (2014). Beyond the role of dietary protein and amino acids in the prevention of diet-induced obesity. *Int. J. Mol. Sci.* 15, 1374–1391. doi: 10.3390/ijms15011374

Pichon, L., Huneau, J. F., Fromentin, G., and Tome, D. (2006). A high-protein, high-fat, carbohydrate-free diet reduces energy intake, hepatic lipogenesis, and adiposity in rats. *J. Nutr.* 136, 1256–1260.

Ridaura, V. K., Faith, J. J., Rey, F. E., Cheng, J., Duncan, A. E., Kau, A. L., et al. (2013). Gut microbiota from twins discordant for obesity modulate metabolism in mice. *Science* 341:1241214. doi: 10.1126/science.1241214

Roca-Saavedra, P., Mendez-Vilabrille, V., Miranda, J. M., Nebot, C., Cardelle-Cobas, A., Franco, C. M., et al. (2017). Food additives, contaminants and other minor components: effects on human gut microbiota-a review. *J. Physiol. Biochem.* doi: 10.1007/s13105-017-0564-2. [Epub ahead of print].

Romieu, I., Dossus, L., Barquera, S., Blottiere, H. M., Franks, P. W., Gunter, M., et al. (2017). Energy balance and obesity: what are the main drivers? *Cancer Causes Control* 28, 247–258. doi: 10.1007/s10552-017-0869-z

Ronn, M., Lind, L., Van Bavel, B., Salihovic, S., Michaelsson, K., and Lind, P. M. (2011). Circulating levels of persistent organic pollutants associate in divergent ways to fat mass measured by DXA in humans. *Chemosphere* 85, 335–343. doi: 10.1016/j.chemosphere.2011.06.095

Roos, V., Ronn, M., Salihovic, S., Lind, L., Van Bavel, B., Kullberg, J., et al. (2013). Circulating levels of persistent organic pollutants in relation to visceral and subcutaneous adipose tissue by abdominal MRI. *Obesity* 21, 413–418. doi: 10.1002/oby.20267

Rosqvist, F., Iggman, D., Kullberg, J., Cedernaes, J., Johansson, H. E., Larsson, A., et al. (2014). Overfeeding polyunsaturated and saturated fat causes distinct effects on liver and visceral fat accumulation in humans. *Diabetes* 63, 2356–2368. doi: 10.2337/db13-1622

Rossmeisl, M., Jilkova, Z. M., Kuda, O., Jelenik, T., Medrikova, D., Stankova, B., et al. (2012). Metabolic effects of n-3 PUFA as phospholipids are superior to triglycerides in mice fed a high-fat diet: possible role of endocannabinoids. *PLoS ONE* 7:e38834. doi: 10.1371/journal.pone.0038834

Russell, W. R., Gratz, S. W., Duncan, S. H., Holtrop, G., Ince, J., Scobbie, L., et al. (2011). High-protein, reduced-carbohydrate weight-loss diets promote metabolite profiles likely to be detrimental to colonic health. *Am. J. Clin. Nutr.* 93, 1062–1072. doi: 10.3945/ajcn.110.002188

Sawicki, C. M., Livingston, K. A., Obin, M., Roberts, S. B., Chung, M., and McKeown, N. M. (2017). Dietary fiber and the human gut microbiota: application of evidence mapping methodology. *Nutrients* 9:125. doi: 10.3390/nu9020125

Sayin, S. I., Wahlstrom, A., Felin, J., Jantti, S., Marschall, H. U., Bamberg, K., et al. (2013). Gut microbiota regulates bile acid metabolism by reducing the levels of tauro-beta-muricholic acid, a naturally occurring FXR antagonist. *Cell Metab.* 17, 225–235. doi: 10.1016/j.cmet.2013.01.003

Schnorr, S. L., Candela, M., Rampelli, S., Centanni, M., Consolandi, C., Basaglia, G., et al. (2014). Gut microbiome of the Hadza hunter-gatherers. *Nat. Commun.* 5:3654. doi: 10.1038/ncomms4654

Serino, M., Luche, E., Gres, S., Baylac, A., Berge, M., Cenac, C., et al. (2012). Metabolic adaptation to a high-fat diet is associated with a change in the gut microbiota. *Gut* 61, 543–553. doi: 10.1136/gutjnl-2011-301012

She, P., Reid, T. M., Bronson, S. K., Vary, T. C., Hajnal, A., Lynch, C. J., et al. (2007). Disruption of BCATm in mice leads to increased energy expenditure associated with the activation of a futile protein turnover cycle. *Cell Metab.* 6, 181–194. doi: 10.1016/j.cmet.2007.08.003

Shi, J., Tauriainen, E., Martonen, E., Finckenberg, P., Ahlroos-Lehmus, A., Tuomainen, A., et al. (2011). Whey protein isolate protects against diet-induced obesity and fatty liver formation. *Int. Dairy J.* 21, 513–522. doi: 10.1016/j.idairyj.2011.03.006

Shin, N. R., Lee, J. C., Lee, H. Y., Kim, M. S., Whon, T. W., Lee, M. S., et al. (2014). An increase in the *Akkermansia* spp. population induced by metformin treatment improves glucose homeostasis in diet-induced obese mice. *Gut* 63, 727–735. doi: 10.1136/gutjnl-2012-303839

Smith, J. D., Hou, T., Ludwig, D. S., Rimm, E. B., Willett, W., Hu, F. B., et al. (2015). Changes in intake of protein foods, carbohydrate amount and quality, and long-term weight change: results from 3 prospective cohorts. *Am. J. Clin. Nutr.* 101, 1216–1224. doi: 10.3945/ajcn.114.100867

Sonnenburg, J. L., and Backhed, F. (2016). Diet-microbiota interactions as moderators of human metabolism. *Nature* 535, 56–64. doi: 10.1038/nature18846

Soucy, J., and Leblanc, J. (1998). Effects of beef steak and cod fillet on plasma glucose, insulin, amino acids and energy metabolism in normal subjects. *Nutr. Res.* 18, 1113–1123. doi: 10.1016/S0271-5317(98)00093-1

Spanogiannopoulos, P., Bess, E. N., Carmody, R. N., and Turnbaugh, P. J. (2016). The microbial pharmacists within us: a metagenomic view of xenobiotic metabolism. *Nat. Rev. Microbiol.* 14, 273–287. doi: 10.1038/nrmicro.2016.17

Spitze, A. R., Wong, D. L., Rogers, Q. R., and Fascetti, A. J. (2003). Taurine concentrations in animal feed ingredients; cooking influences taurine content. *J. Anim. Physiol. Anim. Nutr.* 87, 251–262. doi: 10.1046/j.1439-0396.2003.00434.x

Sprong, R. C., Schonewille, A. J., and Van Der Meer, R. (2010). Dietary cheese whey protein protects rats against mild dextran sulfate sodium-induced colitis: role of mucin and microbiota. *J. Dairy Sci.* 93, 1364–1371. doi: 10.3168/jds.2009-2397

Stanstrup, J., Schou, S. S., Holmer-Jensen, J., Hermansen, K., and Dragsted, L. O. (2014). Whey protein delays gastric emptying and suppresses plasma fatty acids and their metabolites compared to casein, gluten, and fish protein. *J. Proteome Res.* 13, 2396–2408. doi: 10.1021/pr401214w

Swinburn, B. A., Sacks, G., Hall, K. D., McPherson, K., Finegood, D. T., Moodie, M. L., et al. (2011). The global obesity pandemic: shaped by global drivers and local environments. *Lancet* 378, 804–814. doi: 10.1016/S0140-6736(11)60813-1

Takeuchi, H., Matsuo, T., Tokuyama, K., Shimomura, Y., and Suzuki, M. (1995). Diet-induced thermogenesis is lower in rats fed a lard diet than in those fed a high oleic acid safflower oil diet, a safflower oil diet or a linseed oil diet. *J. Nutr.* 125, 920–925.

Tang, W. H., Wang, Z., Levison, B. S., Koeth, R. A., Britt, E. B., Fu, X., et al. (2013). Intestinal microbial metabolism of phosphatidylcholine and cardiovascular risk. *N. Engl. J. Med.* 368, 1575–1584. doi: 10.1056/NEJMoa1109400

Tastesen, H. S., Keenan, A. H., Madsen, L., Kristiansen, K., and Liaset, B. (2014a). Scallop protein with endogenous high taurine and glycine content prevents high-fat, high-sucrose-induced obesity and improves plasma lipid profile in male C57BL/6J mice. *Amino Acids* 46, 1659–1671. doi: 10.1007/s00726-014-1715-1

Tastesen, H. S., Ronnevik, A. K., Borkowski, K., Madsen, L., Kristiansen, K., and Liaset, B. (2014b). A mixture of cod and scallop protein reduces adiposity and

improves glucose tolerance in high-fat fed male C57BL/6J mice. *PLoS ONE* 9:e112859. doi: 10.1371/journal.pone.0112859

Thorsdottir, I., Tomasson, H., Gunnarsdottir, I., Gisladottir, E., Kiely, M., Parra, M. D., et al. (2007). Randomized trial of weight-loss-diets for young adults varying in fish and fish oil content. *Int. J. Obes.* 31, 1560–1566. doi: 10.1038/sj.ijo.0803643

Tranberg, B., Madsen, A. N., Hansen, A. K., and Hellgren, L. I. (2015). Whey-reduced weight gain is associated with a temporary growth reduction in young mice fed a high-fat diet. *J. Nutr. Biochem.* 26, 9–15. doi: 10.1016/j.jnutbio.2014.07.009

Tremaroli, V., and Backhed, F. (2012). Functional interactions between the gut microbiota and host metabolism. *Nature* 489, 242–249. doi: 10.1038/nature11552

Turnbaugh, P. J., Ley, R. E., Mahowald, M. A., Magrini, V., Mardis, E. R., and Gordon, J. I. (2006). An obesity-associated gut microbiome with increased capacity for energy harvest. *Nature* 444, 1027–1031. doi: 10.1038/nature05414

Villanueva-Millan, M. J., Perez-Matute, P., and Oteo, J. A. (2015). Gut microbiota: a key player in health and disease. A review focused on obesity. *J. Physiol. Biochem.* 71, 509–525. doi: 10.1007/s13105-015-0390-3

Vincent, A., Savolainen, O. I., Sen, P., Carlsson, N. G., Almgren, A., Lindqvist, H., et al. (2017). Herring and chicken/pork meals lead to differences in plasma levels of TCA intermediates and arginine metabolites in overweight and obese men and women. *Mol. Nutr. Food Res.* 61. doi: 10.1002/mnfr.201600400

Wahlang, B., Falkner, K. C., Gregory, B., Ansert, D., Young, D., Conklin, D. J., et al. (2013). Polychlorinated biphenyl 153 is a diet-dependent obesogen that worsens nonalcoholic fatty liver disease in male C57BL6/J mice. *J. Nutr. Biochem.* 24, 1587–1595. doi: 10.1016/j.jnutbio.2013.01.009

Wang, J., Tang, H., Zhang, C., Zhao, Y., Derrien, M., Rocher, E., et al. (2015). Modulation of gut microbiota during probiotic-mediated attenuation of metabolic syndrome in high fat diet-fed mice. *ISME J.* 9, 1–15. doi: 10.1038/ismej.2014.99

Watanabe, M., Houten, S. M., Mataki, C., Christoffolete, M. A., Kim, B. W., Sato, H., et al. (2006). Bile acids induce energy expenditure by promoting intracellular thyroid hormone activation. *Nature* 439, 484–489. doi: 10.1038/nature04330

Westerterp-Plantenga, M. S., Lemmens, S. G., and Westerterp, K. R. (2012). Dietary protein - its role in satiety, energetics, weight loss and health. *Br. J. Nutr.* 108(Suppl. 2), S105–S112. doi: 10.1017/S0007114512002589

Westerterp-Plantenga, M. S., Nieuwenhuizen, A., Tome, D., Soenen, S., and Westerterp, K. R. (2009). Dietary protein, weight loss, and weight maintenance. *Annu. Rev. Nutr.* 29, 21–41. doi: 10.1146/annurev-nutr-080508-141056

Wu, G. D., Chen, J., Hoffmann, C., Bittinger, K., Chen, Y. Y., Keilbaugh, S. A., et al. (2011). Linking long-term dietary patterns with gut microbial enterotypes. *Science* 334, 105–108. doi: 10.1126/science.1208344

Xiao, L., Feng, Q., Liang, S., Sonne, S. B., Xia, Z., Qiu, X., et al. (2015). A catalog of the mouse gut metagenome. *Nat. Biotechnol.* 33, 1103–1108. doi: 10.1038/nbt.3353

Xiao, L., Sonne, S. B., Feng, Q., Chen, N., Xia, Z., Li, X., et al. (2017). High-fat feeding rather than obesity drives taxonomical and functional changes in the gut microbiota in mice. *Microbiome* 5:43. doi: 10.1186/s40168-017-0258-6

Yang, Z., Huang, S., Zou, D., Dong, D., He, X., Liu, N., et al. (2016). Metabolic shifts and structural changes in the gut microbiota upon branched-chain amino acid supplementation in middle-aged mice. *Amino Acids* 48, 2731–2745. doi: 10.1007/s00726-016-2308-y

Yatsunenko, T., Rey, F. E., Manary, M. J., Trehan, I., Dominguez-Bello, M. G., Contreras, M., et al. (2012). Human gut microbiome viewed across age and geography. *Nature* 486, 222–227. doi: 10.1038/nature11053

Yoo, S. R., Kim, Y. J., Park, D. Y., Jung, U. J., Jeon, S. M., Ahn, Y. T., et al. (2013). Probiotics, *L. plantarum* and *L. curvatus* in combination alter hepatic lipid metabolism and suppress diet-induced obesity. *Obesity* 21, 2571–2578. doi: 10.1002/oby.20428

Yu, H., Guo, Z., Shen, S., and Shan, W. (2016). Effects of taurine on gut microbiota and metabolism in mice. *Amino Acids* 48, 1601–1617. doi: 10.1007/s00726-016-2219-y

Zemel, M. B., Thompson, W., Milstead, A., Morris, K., and Campbell, P. (2004). Calcium and dairy acceleration of weight and fat loss during energy restriction in obese adults. *Obes. Res.* 12, 582–590. doi: 10.1038/oby.2004.67

Zhang, L., Nichols, R. G., Correll, J., Murray, I. A., Tanaka, N., Smith, P. B., et al. (2015). Persistent organic pollutants modify gut microbiota-host metabolic homeostasis in mice through aryl hydrocarbon receptor activation. *Environ. Health Perspect.* 123, 679–688. doi: 10.1289/ehp.1409055

Zhu, Y., Li, H., Xu, X., Li, C., and Zhou, G. (2016). The gut microbiota in young and middle-aged rats showed different responses to chicken protein in their diet. *BMC Microbiol.* 16:281. doi: 10.1186/s12866-016-0895-0

Zhu, Y., Lin, X., Zhao, F., Shi, X., Li, H., Li, Y., et al. (2015). Meat, dairy and plant proteins alter bacterial composition of rat gut bacteria. *Sci. Rep.* 5:15220. doi: 10.1038/srep15220

Zietak, M., and Kozak, L. P. (2016). Bile acids induce uncoupling protein 1-dependent thermogenesis and stimulate energy expenditure at thermoneutrality in mice. *Am. J. Physiol. Endocrinol. Metab.* 310, E346–E354. doi: 10.1152/ajpendo.00485.2015

Conflict of Interest Statement: The authors declare that the research was conducted in the absence of any commercial or financial relationships that could be construed as a potential conflict of interest.

frontiers in Physiology

ORIGINAL RESEARCH
published: 25 October 2017
doi: 10.3389/fphys.2017.00853

Branched-Chain Amino Acid Negatively Regulates KLF15 Expression via PI3K-AKT Pathway

Yunxia Liu†, Weibing Dong†, Jing Shao, Yibin Wang, Meiyi Zhou and Haipeng Sun**

Key Laboratory of Cell Differentiation and Apoptosis of Chinese Ministry of Education, Department of Pathophysiology, Shanghai Jiao Tong University School of Medicine, Shanghai, China

Recent studies have linked branched-chain amino acid (BCAA) with numerous metabolic diseases. However, the molecular basis of BCAA's roles in metabolic regulation remains to be established. KLF15 (Krüppel-like factor 15) is a transcription factor and master regulator of glycemic, lipid, and amino acids metabolism. In the present study, we found high concentrations of BCAA suppressed KLF15 expression while BCAA starvation induced KLF15 expression, suggesting KLF15 expression is negatively controlled by BCAA.Interestingly, BCAA starvation induced PI3K-AKT signaling. KLF15 induction by BCAA starvation was blocked by PI3K and AKT inhibitors, indicating the activation of PI3K-AKT signaling pathway mediated the KLF15 induction. BCAA regulated KLF15 expression at transcriptional level but not post-transcriptional level. However, BCAA starvation failed to increase the KLF15-promoter-driven luciferase expression, suggesting KLF15 promoter activity was not directly controlled by BCAA. Finally, fasting reduced BCAA abundance in mice and KLF15 expression was dramatically induced in muscle and white adipose tissue, but not in liver. Together, these data demonstrated BCAA negatively regulated KLF15 expression, suggesting a novel molecular mechanism underlying BCAA's multiple functions in metabolic regulation.

Keywords: BCAA, Klf15, PI3K, Akt, regulation

OPEN ACCESS

Edited by:
Dechun Feng,
National Institute on Alcohol Abuse and Alcoholism, United States

Reviewed by:
Zlyi Liu,
National Institutes of Health (NIH), United States
Liming Yang,
Harbin Medical University, China

****Correspondence:***
Haipeng Sun
sun.haipeng@yahoo.com
Meiyi Zhou
xiaozhoutongzhi@163.com

† These authors have contributed equally to this work.

Specialty section:
This article was submitted to Clinical and Translational Physiology, a section of the journal Frontiers in Physiology

Received: *03 September 2017*
Accepted: *12 October 2017*
Published: *25 October 2017*

Citation:
Liu Y, Dong W, Shao J, Wang Y, Zhou M and Sun H (2017) Branched-Chain Amino Acid Negatively Regulates KLF15 Expression via PI3K-AKT Pathway. Front. Physiol. 8:853. doi: 10.3389/fphys.2017.00853

INTRODUCTION

Branched chain amino acid (BCAA), including leucine, isoleucine, and valine, are essential amino acids. In addition to building proteins, numerous metabolic functions of BCAA have been investigated (Nair and Short, 2005). BCAA modulates insulin and glucagon secretion in pancreas (Meijer and Dubbelhuis, 2004). Increasing BCAA intake was often associated with positive effects on body weight and glucose homeostasis, attenuating obesity and type 2 diabetes mellitus T2DM (Lynch and Adams, 2014). BCAA regulates protein synthesis and degradation in various tissues. In addition, BCAA influences brain function by participating in synthesis and transport of glutamate, an important excitatory neurotransmitter, and by modifying large, neutral amino acid transport at the blood–brain barrier (Joshi et al., 2006).

Branched chain amino acid (BCAA) has recently been linked with numerous diseases. Elevated circulating levels of BCAA have been associated with an increased risk of T2DM and insulin resistance in humans (Newgard et al., 2009; Huang et al., 2011; Melnik, 2012; Lu et al., 2013; Lynch and Adams, 2014). Defect of BCAA catabolism promotes heart failure progression and

associated with cardiovascular diseases (Shah et al., 2010; Sun et al., 2016). Impaired BCAA transportation and metabolism is associated with autism (Novarino et al., 2012; Târlungeanu et al., 2016). Elevated plasma BCAA levels have been found in early pancreatic ductal adenocarcinoma patients, supporting formation of non–small cell lung carcinoma and growth of pancreatic ductal adenocarcinoma (Mayers et al., 2014, 2016; Dey et al., 2017). The novel roles of BCAA in metabolic, cardiovascular, neurological diseases, and cancer are being investigated.

Little is known about the molecular basis of BCAA's function in cells. BCAA, especially leucine, is one key regulator of target of rapamycin complex 1 (TORC1) signaling, which is the central component of a complex signaling network of cell growth and metabolism (Saxton and Sabatini, 2017). Recently, SESN2 has been reported to be a cytoplasmic leucine sensor to activate TORC1 (Saxton et al., 2016; Wolfson et al., 2016). It has been implicated that BCAA enhanced TORC1 activation and contributed to insulin resistance (Newgard et al., 2009). In Maple Syrup Urine Disease and heart failure, branched-chain alpha keto acid (BCKA), the intermediate metabolite of BCAA catabolism, suppressed mitochondrial respiration and induced oxidative stress in cells (Funchal et al., 2006; Ribeiro et al., 2007; Sun et al., 2016). Other than these observations, the molecular basis of BCAA's roles in metabolic regulation remains to be fully explored.

KLF15 (Krüppel-like factor 15) is a transcription factor and a master regulator of metabolism. KLF15-deficient mice have impaired ability to catabolize muscle BCAAs as fuel for gluconeogenic flux during fasting (Gray et al., 2007). In addition, during sustained aerobic exercise, KLF15-deficient mice fail to augment muscle lipid utilization and consequently have impaired endurance exercise capacity (Haldar et al., 2012; Prosdocimo et al., 2014). During adipocyte differentiation, KLF15 is dramatically induced and indispensable for the differentiation (Mori et al., 2005). Under fasting condition, KLF15 is induced and inhibits the expression of SREBP-1C in liver, suppressing lipogenesis (Takeuchi et al., 2016). KLF15 regulates the insulin-sensitive glucose transporter GLUT4 expression (Gray et al., 2002). KLF15 is one key regulator of circadian homeostasis and controls the homeostasis of amino acids during circadian cycle (Jeyaraj et al., 2012; Zhang et al., 2015). In addition, KLF15 controlled the circadian homeostasis of bile acid synthesis. KLF15 deficient mice produced much less bile acids that slowed down the absorption of lipid and other nutrients (Han et al., 2015). Thus, KLF15 is a master regulator of circadian and metabolic regulation of bile acid, glycemic, lipid, and amino acids.

In an effort to understand molecular basis of BCAA's function in cells, we examined the gene expression profiles in mouse embryonic fibroblasts (MEF) in response to BCAA starvation and replenishment. Unexpectedly, KLF15 was among the dramatically regulated genes. In the present study, we investigated the KLF15 regulation by BCAA. The results demonstrated BCAA controls KLF15 expression through PI3K-AKT signaling pathway.

MATERIALS AND METHODS

Animals

Wildtype C57BL/6 mice were purchased from SLAC Laboratory Animals Company Limited, Shanghai, China. All animals were housed at with a 12-h light, 12-h dark cycle with free access to water and standard chow. This study was carried out in accordance with the guidelines of the Committee for Humane Treatment of Animals at Shanghai Jiao Tong University School of Medicine. The protocol was approved by the Committee for Humane Treatment of Animals at Shanghai Jiao Tong University School of Medicine.

Cell Culture

HepG2, NIH 3T3, and MEF cells were cultured in Dulbecco's modified Eagle's medium (Hyclone, Beijing) supplemented with 10% fetal bovine serum (FBS, Gibco BRL, Gaithersburg, MD), penicillin (100 IU/mL) and streptomycin (100 μg/mL) in a humidified 5% CO2-95% air incubator at 37°C. Custom BCAA-free DMEM was provided by Invitrogen. BCAA and BCKA chemicals were purchased from Sigma.

Plasmids, Transfection, and Luciferase Assays

The 3′UTR of mouse *KLF15* was identified using the UCSC Genome Browser (http://genome.ucsc.edu/) and cloned into the psiCHECK_2 plasmid (Promega) with XhoI and NotI sites, respectively. The 3'UTR fragment (921 bp) was located in the 3′ flanking region of the synthetic Renilla luciferase gene. Thus, Renilla luciferase expression can be regulated by the downstream 3′UTR activity. The promoter region of *Klf15* (−5 kb before the translation start site in the second exon) was cloned into PGL3 reporter vector (Promega) (Jeyaraj et al., 2012). Plasmids were transfected using lipofectimine2000 (Invitrogen) according to the manufacturer's protocol. The transfected cells were rinsed once with cold PBS and lysed with passive lysis buffer (Promega) after transfection for 24 h. Luciferase activity was measured using the GloMax-Multi Detection System (Promega) and the Dual-Luciferase Reporter Assay System (Promega). Renilla luciferase expression was normalized to the expression of firefly luciferase. Data are represented as means ± SE from three biological replicates representing three independent experiments.

RNA Extraction, Reverse Transcription and Real-Time PCR Analysis

Total RNA was extracted using the Trizol (Invitrogen) according to the manufacturer's instructions. Total RNA (2 μg) was reverse transcribed using random primers and MMLV (Promega). Each cDNA sample was analyzed in triplicate with the Applied Biosystems Prism7900HT Real-Time PCR System using Absolute SYBR Green (ABI) with the specific primers. The relative amount of specific mRNA was normalized by 18sRNA. Mouse KLF15 primer sequences are: forward, 5′-TCTCGTCACCGA

AATGCTCA-3′ and reverse, 5′-GAGTCAGGGCTGGCACAA GA-3′.

Western Blot Analysis

Proteins from tissue or cells were harvested in buffer (50 mM HEPES [pH7.4], 150 mM NaCl, 1% NP-40, 1 mM EDTA, 1 mM EGTA, 1 mM glycerophosphate, 2.5 mM sodium pyrophosphate 1 mM Na3VO4, 20 mM NaF, 1 mM phenylmethylsulfonyl fluoride, 1 μg/mL of aprotinin, leupeptin, and pepstatin). Samples were separated on 4–12% Bis-Tris gels (Invitrogen), and transferred onto a nitrocellulose blot (Amersham). The blot was probed with the indicated primary antibodies. Protein signals were detected using conjugated secondary antibodies and enhanced chemiluminescence (ECL) western blotting detection regents (Pierce). The BCKDK antibody (AV52131) was purchased from sigma. Phospho-Akt (#4051 for pAKT Ser473 and #2965 for pAKT Thr308) and total AKT (#9272 for AKT1,2,3) antibodies were purchased from Cell Signaling Technology. β-actin antibody was purchased from Sigma Chemical Co.

Determination of BCAA Concentration

Fifty microliter of plasma was precleared of protein by addition of an equal volume of methanol, followed by two rounds of centrifugation to precipitate protein. The supernatant (90% recovery) was lyophilized and resuspended in 45 μl dH_2O. Standards (L-valine, L-leucine, L-isoleucine, L-allo-isoleucine) were prepared from powder. 10 mM stocks were made in dH_2O and serial pooled dilutions prepared. A 250 μM stock of D3-Leucine was also prepared in dH_2O. 2 μl of standard or 2 μl of sample was diluted in 50 μl of butanolic HCL in 1.5 ml tube, heated to 60°C for 20 min and then speed vacuumed to dryness. The samples were resuspended in 200 ul of 50:50 dH_2O:acetonitrile containing 0.1% formic acid. The samples were analyzed by LC-MS/MS.

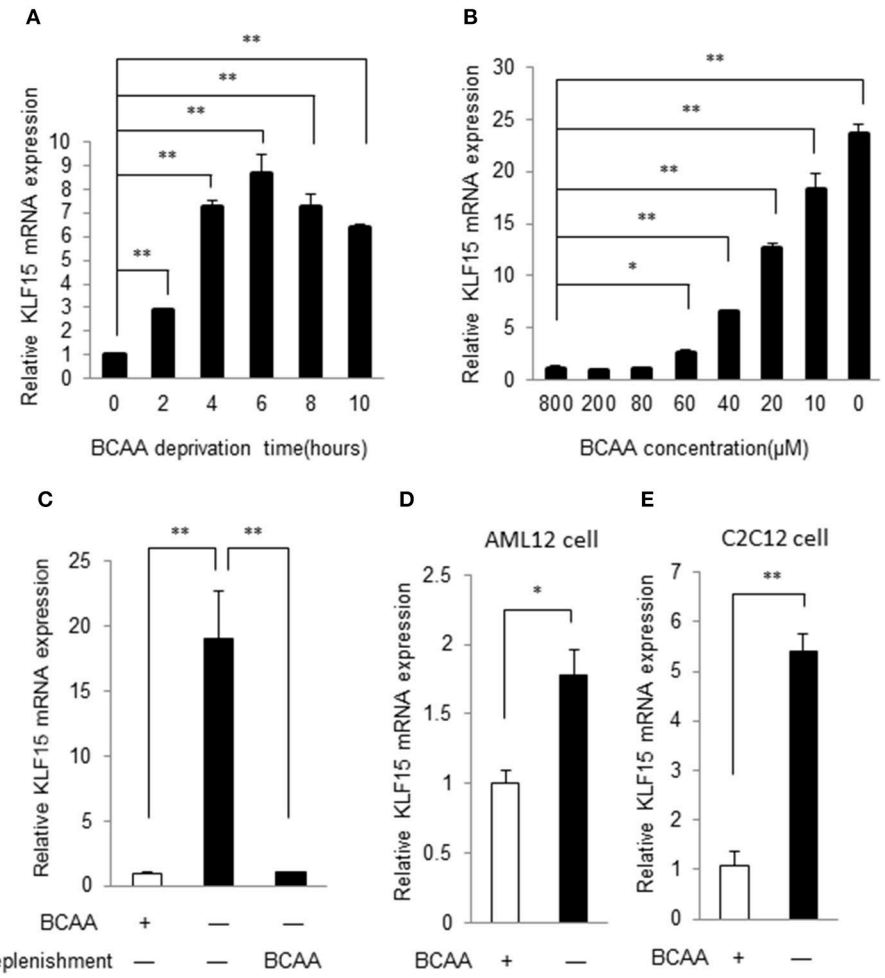

FIGURE 1 | BCAA negatively controls KLF15 expression. Quantitative PCR results of KLF15 in MEFs. **(A)** MEFs were cultured in BCAA-free DMEM for indicated time before harvesting. **(B)** MEFs were cultured with different concentrations of BCAAs for 6 h before harvesting. **(C)** MEFs were cultured without BCAA (–) for 4 h followed with or without (–) BCAA replenishment for extra 2 h before harvesting. **(D,E)**, AML12 liver cell line **(D)** and C2C12 muscle cell line **(E)** were cultured with (+) or without (–) BCAA for 4 h before harvesting. Data are means ± SE for three individual samples. *$p < 0.05$, **$p < 0.01$.

Statistical Analysis

Unless otherwise specified, statistical analyses were performed with Student's *t*-test (two groups) or one-way ANOVA (>2 groups) where appropriate. Data are calculated as the mean ± SE (standard error) unless otherwise indicated. A *p*-value of less than 0.05 was considered statistically significant.

RESULTS

KLF15 Expression Is Negatively Controlled by BCAAs

To verify the KLF15 regulation by BCAAs identified in gene expression profiles of MEF (data not shown), we examined the time course of KLF15 expression following BCAA deprivation. In commercial Dulbecco's Modified Eagle's Medium (DMEM), the BCAAs concentration is 800 μM. A customized DMEM containing all components except for BCAAs was used to deprive BCAA. In MEFs, KLF15 mRNA demonstrated a clear increase at 2 h after BCAA deprivation, and remained elevated for at least 10 h (**Figure 1A**). Further study showed that BCAA suppressed KLF15 expression in a dose-dependent way (**Figure 1B**). To further verify the suppression of BCAA on KLF15 expression, we starved the cells with BCAA-free DMEM and then replenished with BCAA. BCAA replenishment clearly inhibited the BCAA-deprivation-induced KLF15 expression (**Figure 1C**). KLF15 induction by BCAA starvation was also observed in other cell

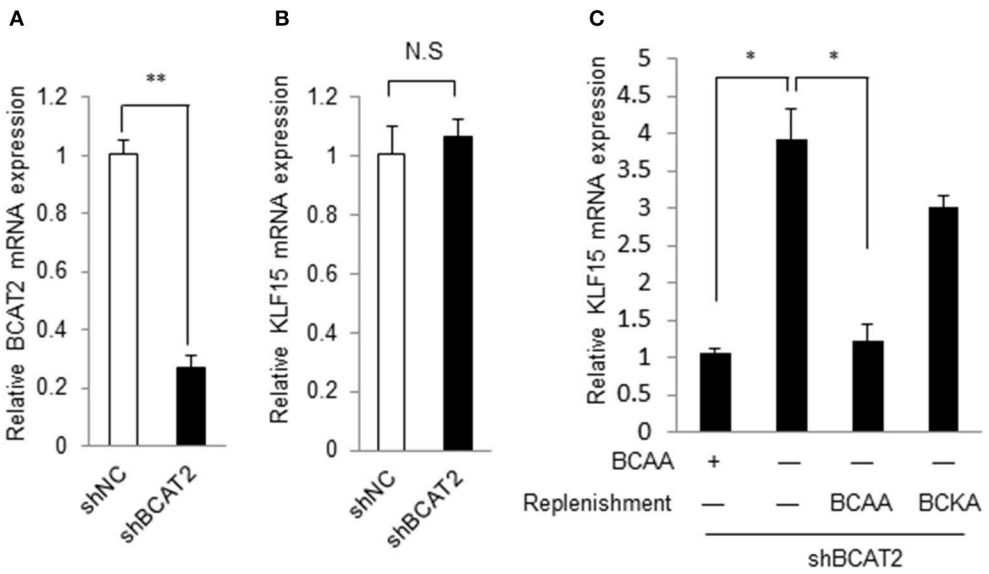

FIGURE 2 | BCAA but not their catabolites regulate KLF15 expression. **(A,B)** Quantitative PCR results of BCAT2 **(A)** or KLF15 **(B)** in MEFs with *Bcat2* silencing using shRNA. **(C)** Quantitative PCR results of KLF15 in MEFs with *Bcat2* silencing with or without BCKA (500 μM) or 800 μM BCAAs replenishment for 2 h after 4-h BCAA starvation (–). $^{*}p < 0.05$, $^{**}p < 0.01$.

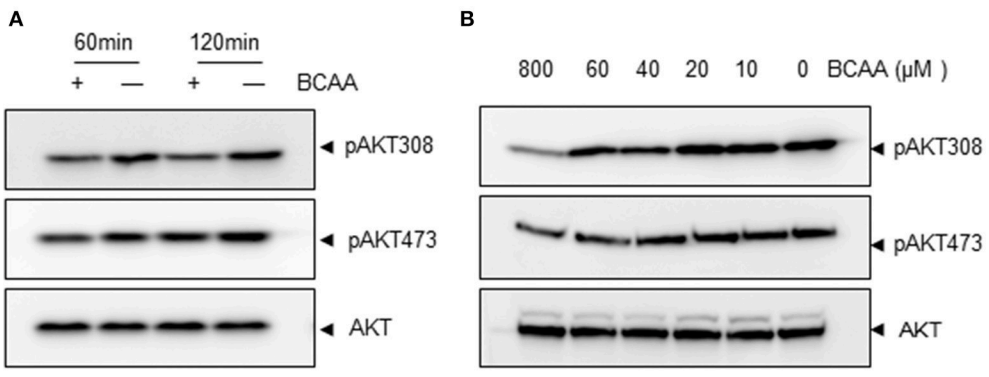

FIGURE 3 | BCAA starvation induces AKT phosphorylation. Measurements of Ser473 or Thr308 phosphorylation of AKT (pAKT) or total AKT (60KD band) using immunoblots. **(A)** MEF cells were treated with BCAA deprivation (–) for indicated time. **(B)** MEF cells were treated with different concentrations of BCAAs for 2 h. Data showed 1 experiment representative of 3.

types, such as liver (AML12) and muscle (C2C12) cell lines (**Figures 1D,E**).

BCAA but Not Their Catabolites Regulate KLF15

BCAA can be catabolized in cells. BCAA and their catabolites such as BCKA and 3-hydroxyisobutyrate exert various physiological and pathological functions (Lynch and Adams, 2014; Jang et al., 2016). We then explored whether BCAA or their catabolic intermediates affected the KLF15 expression. Branched-chain amino acid transaminase 2 (BCAT2) catalyzes the first reaction of BCAA catabolism. If the BCAT2 expression is abolished, BCAA can't be catalyzed into BCKA and other intermediates. When BCAT2 expression was silenced by siRNA in NIH-3T3 cell (**Figure 2A**), KLF15 expression was not affected (**Figure 2B**). Meanwhile, In the BCAT2 knockdown cell, KLF15 expression was induced by BCAA deprivation, which was inhibited by replenishing BCAA (**Figure 2C**). Thus, BCAA, but not BCKA or downstream catabolites, suppressed the expression of KLF15.

BCAA Starvation Activates PI3K-AKT Signaling Pathway

We then explored the signaling pathway(s) involved in KLF15 regulation by BCAA. A recent study showed that amino acid starvation activated PI3K/AKT signaling (Tato et al., 2011). PI3K is a key signaling molecule to transduce extracellular signals to regulate gene expression in a variety of cell types. AKT is a well-known downstream target of PI3K and its activation can be measured by phosphorylation at signature sites Ser473 or Thr308. To address whether BCAA deprivation activated PI3K pathway, we determined the AKT phosphorylation at Ser473 and Thr308 in response to BCAA starvation. BCAA deprivation caused significant AKT activation at 1 and 2 h (**Figure 3A**; **Figure S1**).

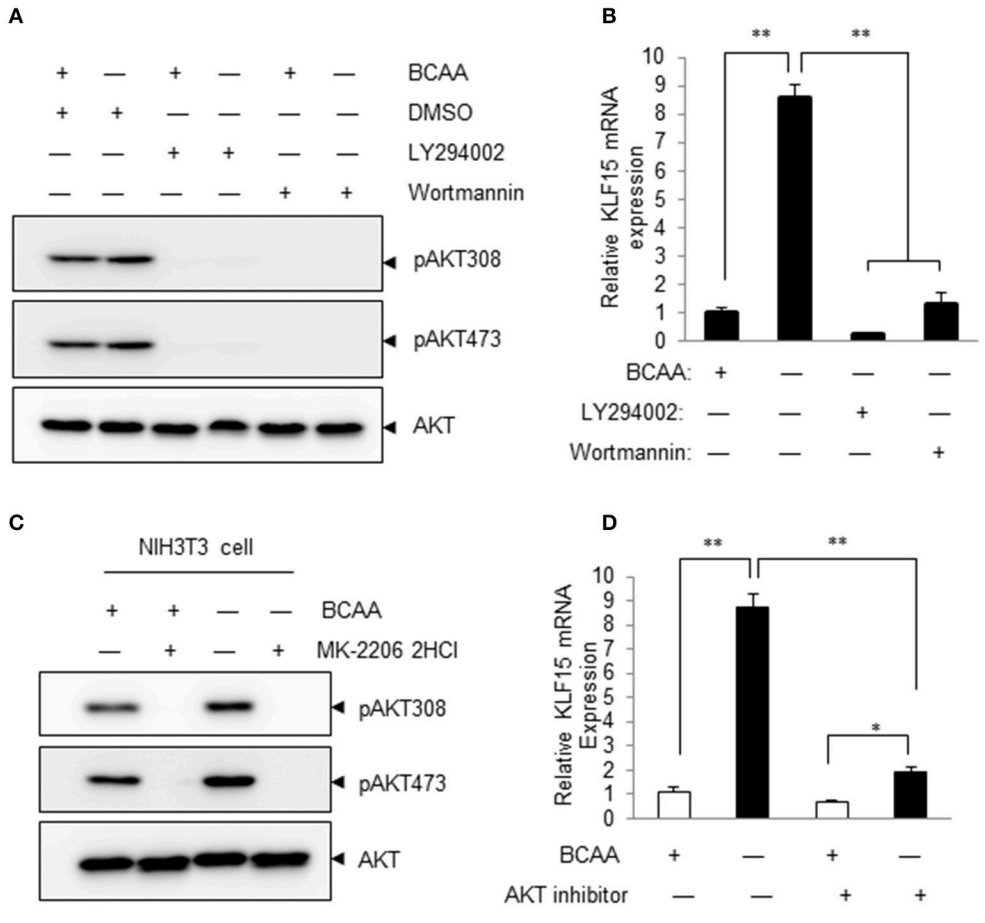

FIGURE 4 | Inhibitors of PI3K and AKT attenuate BCAA-starvation-induced KLF15 expression. **(A)** Measurements of Ser473 or Thr308 phosphorylation of AKT (pAKT) or total AKT (60KD band) using immunoblots. Cells were pretreated 60 min with 10 μM LY294002 or 1 μM Wortmannin before BCAA deprivation (–) for 2 h. Data showed 1 experiment representative of 3. **(B)** Cells were pretreated 60 min with 10 μM LY294002 or 1 μM Wortmannin before BCAA deprivation (–) for 4 h and then harvested for measurement of KLF15 mRNA by quantitative PCR. **(C)** Measurements of Ser473 or Thr308 phosphorylation of AKT (pAKT) or total AKT (60KD band) using immunoblots. Cells were pretreated 60 min with 10 μM AKT inhibitor MK-2206 before BCAA deprivation (–) for 2 h. Data showed 1 experiment representative of 3. **(D)** Cells were pretreated 60 min with 10 μM AKT inhibitor MK-220 before BCAA deprivation (–) for 4 h and then harvested for measurement of KLF15 mRNA by quantitative PCR. Data are means ± SE for three individual samples. $^{*}p < 0.05$, $^{**}p < 0.01$.

BCAAs deprivation induced AKT activation in a dose-dependent way (**Figure 3B**; **Figure S2**).

PI3K-AKT Signaling Mediates BCAA-Starvation-Induced KLF15 Expression

Pharmacological inhibitors of PI3K were then used to determine whether PI3K signaling pathway participated in BCAA-deprivation-induced KLF15 expression. The basal level and BCAA-starvation-induced Akt phosphorylation at Thr308 and Ser473 were blocked by LY294002 and Wortmannin, demonstrating a clear inhibition of PI3K signaling (**Figure 4A**; **Figure S3**). Both LY294002 and Wortmannin abolished BCAA-starvation-induced KLF15 expression (**Figure 4B**). Similarly, AKT inhibitor MK-2206 inhibited AKT activation (**Figure 4C**; **Figure S4**) and the KLF15 mRNA expression induced by BCAA starvation (**Figure 4D**). Together, these data support a critical role of PI3K-AKT signaling pathway in BCAA-starvation-induced KLF15 expression.

BCAA Regulates KLF15 Expression at Transcriptional Level

We then investigated whether BCAA starvation induced KLF15 expression at transcriptional or post-transcriptional level. Actinomycin D, an inhibitor of RNA synthesis, prevented KLF15 induction by BCAA starvation (**Figure 5A**), suggesting a transcriptional regulation. To investigate whether BCAAs affected KLF15 expression at post-transcriptional level, we cloned mouse KLF15 3'UTR fragments into the reporter vector p-siCHECK_2, where Renilla luciferase expression is regulated by downstream 3′UTR, and generated Luc-3′UTR reporters. After transfecting this reporter vector into cells, the luciferase activity was measured. The results showed that BCAA starvation did not affect the expression of the luciferase fused with mouse

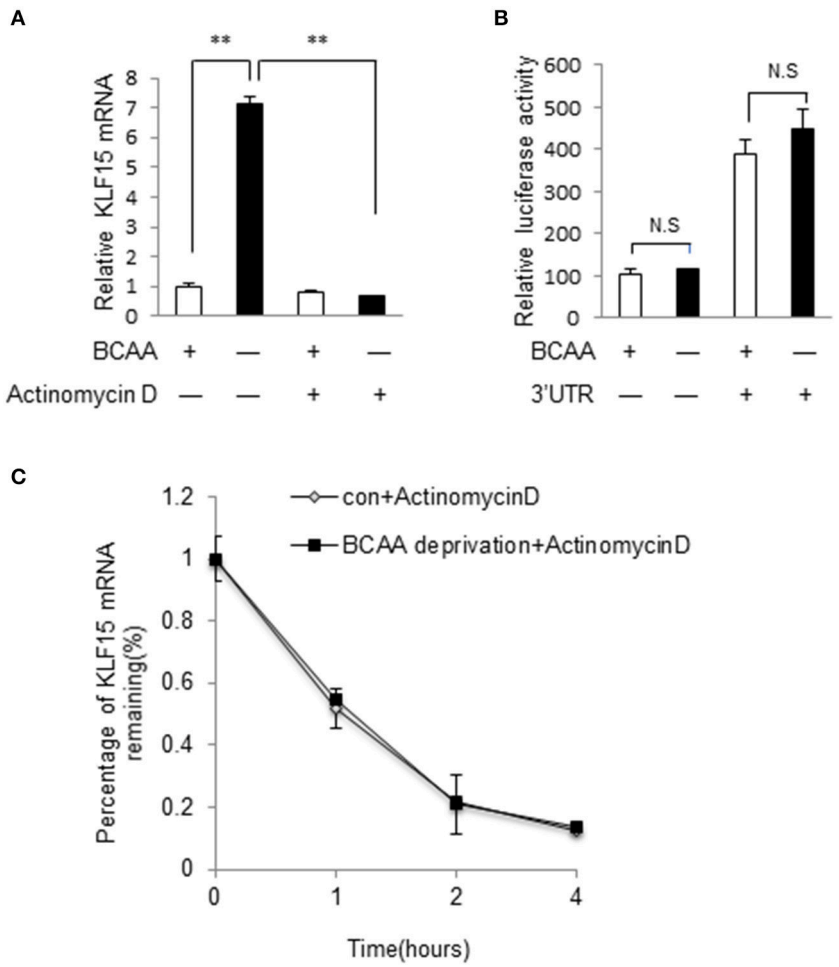

FIGURE 5 | BCAA regulates KLF15 expression at transcriptional level. **(A)** Quantitative PCR was performed to measure the mRNA level of KLF15 in cells pretreated with actinomycin D (5 μg/ml) or DMSO for 30 min before BCAA starvation (–) for 6 h. **(B)** Luciferase assay results from MEF cells transfected with luciferase reporter vectors with (+) or without (–) KLF15 3'UTR with (+) or without BCAA (–). **(C)** Quantitative PCR was performed to measure the relative mRNA level of KLF15 in cells treated with actinomycin D (5 μg/ml) for indicated time in the presence (con) or absence of BCAA (BCAA starvation). Data are means ± SE for three individual samples. $^{**}p < 0.01$.

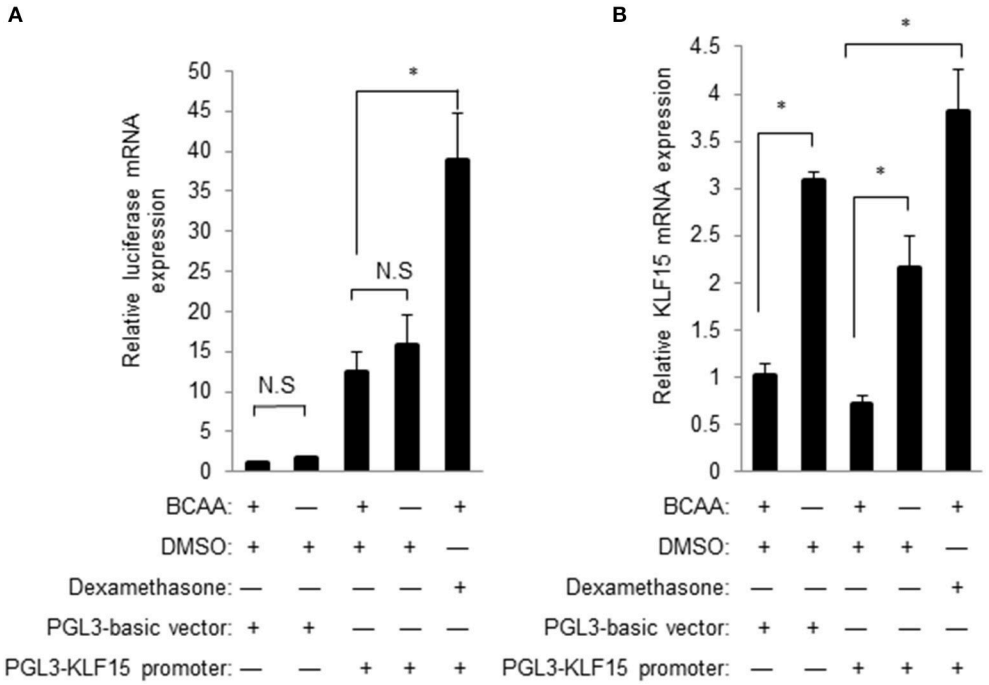

FIGURE 6 | BCAA does not directly affect KLF15 promoter activity. Quantitative PCR was performed to measure the mRNA level of luciferase **(A)** or KLF15 **(B)** in cells transfected with empty PGL3-basic or KLF15-promoter-driving luciferase constructs and treated with BCAA starvation (–) or dexamethasone for 24 h. Data are means ± SE for three individual samples. *$p < 0.05$.

KLF15 3'UTR (**Figure 5B**). Meanwhile, BCAA starvation failed to affect the half-life of KLF15 mRNA (**Figure 5C**). These data suggest that BCAA starvation affect the KLF15 expression at transcriptional but not post-transcriptional level.

BCAA Does Not Directly Regulate KLF15 Promoter Activity

A common mechanism of transcriptional regulation is promoter activation. A chimeric construct of luciferase gene under the control of KLF15 promoter was introduced into cells by transient transfection (Jeyaraj et al., 2012). KLF15-promoter contains a well-defined GRE for the transactivity by glucocorticoid receptor (Shimizu et al., 2011). Unexpectedly, BCAA starvation failed to increase the KLF15-promoter-driven luciferase activity (data not shown). Meanwhile, the KLF15-promoter-driven luciferase mRNA expression was also not induced by BCAA starvation (**Figure 6A**) even BCAA starvation induced endogens KLF15 mRNA expression (**Figure 6B**). On the other hand, activation of KLF15 promoter and mRNA were observed following dexamethasone treatment (**Figure 6**). Thus, BCAA starvation induced the KLF15 transcription without directly affecting KLF15 promoter activation.

BCAA Abundance Is Negatively Associated with KLF15 Expression *in Vivo*

We further investigated the relationship between BCAA and KLF15 expression *in vivo*. Plasma BCAA levels significantly decreased after 12-h fasting (**Figure 7A**). We measured the KLF15 expression in different tissues in fasted mice. KLF15 expression was significantly induced in muscle and white adipose tissue, but not in liver (**Figure 7B**). These data suggest that, *in vivo*, BCAA abundance was negatively associated with KLF15 expression.

DISCUSSION

Our data demonstrated that KLF15 expression is negatively controlled by BCAA. BCAA starvation induced KLF15 expression. The regulation occurs at transcriptional level although KLF15 promoter activity was not directly controlled by BCAA. Interestingly, BCAA starvation induced PI3K-AKT signaling that mediated KLF15 expression. In addition to the cellular studies, we further showed that BCAA abundance is negative associated with KLF15 expression *in vivo*. Considering the critical roles of KLF15 in numerous cellular functions, these data suggested BCAA could play roles in metabolic regulation through controlling KLF15 expression.

It has been well established that BCAA, particularly leucine, positively regulates mTOR activity. The mechanism was revealed only recently, showing leucine directly interacts with its sensor Sestrin2 and activates mTOR via numerous protein-protein interactions on the surface of lysosome (Saxton et al., 2016; Wolfson et al., 2016). In this way, BCAA, particularly leucine, positively regulates TORC1 activity independent of AKT activity. On the other hand, insulin and other growth factors induced mTOR via activating PI3K-AKT pathway (Saxton and Sabatini, 2017). In the present study, BCAA starvation reduced TORC1 activity (data not shown). Therefore, it is interesting to find

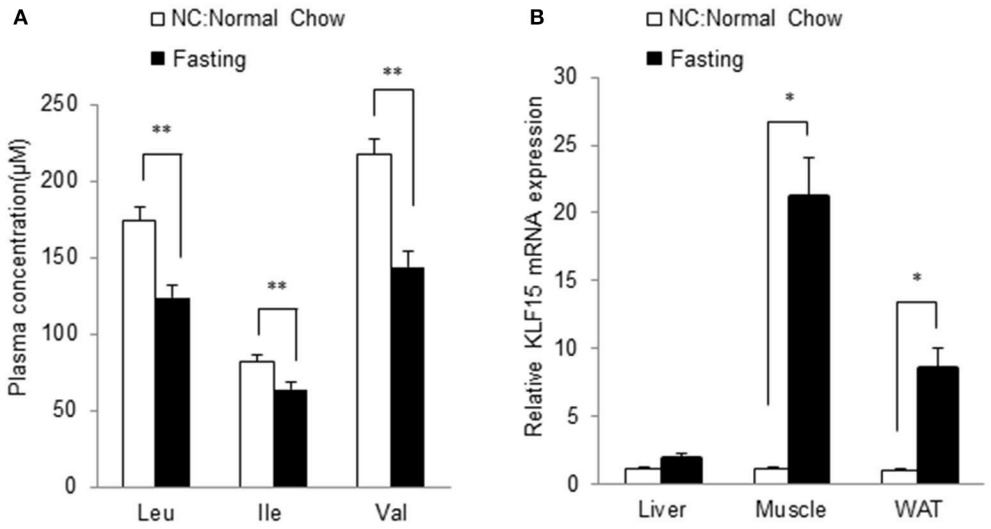

FIGURE 7 | Fasting leads to lower BCAA abundance and higher KLF15 expression *in vivo*. Mice at 10-week of age were fasted for 12 h. Plasma levels of BCAAs were measured (**A**, $n = 7$ in each group) and mRNA level of KLF15 in different tissues were analyzed with quantitative PCR (**B**, $n = 4$ in each group). $^{*}p < 0.05$, $^{**}p < 0.01$.

that BCAA starvation induced PI3K-AKT activity while reducing mTOR activity. Further investigations are warranted to elucidate how BCAA-regulated PI3K-AKT and Sestrin2 pathways crosstalk to determine the mTOR activity.

Our results showed that BCAA regulates KLF15 mRNA expression at transcriptional level, illustrated by the inhibition from actinomycin D and lack of activity by KLF15 3′UTR. However, the KLF15 promoter-driving luciferase expression was not affected by BCAA starvation even though the endogenous KLF15 mRNA is induced. The KLF15 promotor used in the current study has high GC content. It is possible that the structure of KLF15 promoter in the plasmid impaired the response to BCAA starvation. On the other hand, epigenetic changes induced by BAA starvation has been reported (Chaveroux et al., 2010). Amino acid starvation induces the transcription of numerous genes such as CHOP, ATF3, and TRB3, a process associated with modifications of histone acetylation and chromatin structure. The KLF15 promoter activation may require epigenetic changes, which remains to be further explored.

The KLF15 induction in response to BCAA starvation appears to be cell type specific. Among different cell types, liver cell line such as AML12 showed the weakest increase of KLF15 mRNA in response to BCAA starvation. The KLF15 mRNA in AML12 was induced ∼1.8-fold by BCAA deprivation, compared to more than 5-fold induction in other cell types (**Figure 1**). Similarly, in liver, the KLF15 expression showed a trend for increase in response to fasting, whereas the KLF15 induction was more significant in skeletal muscle and white adipose tissue. This cell-type-specific KLF15 induction indicated diverse BCAA sensing mechanisms and responses to BCAA nutrient in different cells and tissues.

In conclusion, our data showed that BCAA negatively regulate KLF15 expression. Dysfunctional BCAA homeostasis has been linked with metabolic, neurological, cancer, and cardiovascular diseases three regulation by BCAA strongly indicates a novel mechanism for BCAA's roles in different physiological processes.

ETHICS STATEMENT

All animal procedures were carried out in accordance with the guidelines and protocols approved by the Committee for Humane Treatment of Animals at Shanghai Jiao Tong University School of Medicine.

AUTHOR CONTRIBUTIONS

HS designed the research; MZ helped to design the overall study; WD, YL, and JS performed the research; MZ, YW, and HS analyzed the data; all authors contributed to the manuscript preparation.

ACKNOWLEDGMENTS

This work was supported by Ministry of Science and Technology of China (2012BAI02B05 and 2013YQ030923), National Natural Science Foundation of China (NSFC81570717 and 81522011), and Science and Technology Commission of Shanghai Municipality (13ZR1423300 and 16JC1404400). We thank Dr. Mukesh Jain at Case Western Reserve University for providing KLF15-promoter-luciferase constructs.

SUPPLEMENTARY MATERIAL

The Supplementary Material for this article can be found online at: https://www.frontiersin.org/articles/10.3389/fphys.2017.00853/full#supplementary-material

REFERENCES

Chaveroux, C., Lambert-Langlais, S., Cherasse, Y., Averous, J., Parry, L., Carraro, V., et al. (2010). Molecular mechanisms involved in the adaptation to amino acid limitation in mammals. *Biochimie* 92, 736–745. doi: 10.1016/j.biochi.2010.02.020

Dey, P., Baddour, J., Muller, F., Wu, C. C., Wang, H., Liao, W. T., et al. (2017). Genomic deletion of malic enzyme 2 confers collateral lethality in pancreatic cancer. *Nature* 542, 119–123. doi: 10.1038/nature21052

Funchal, C., Latini, A., Jacques-Silva, M. C., Dos Santos, A. Q., Buzin, L., Gottfried, C., et al. (2006). Morphological alterations and induction of oxidative stress in glial cells caused by the branched-chain α-keto acids accumulating in maple syrup urine disease. *Neurochem. Int.* 49, 640–650. doi: 10.1016/j.neuint.2006.05.007

Gray, S., Feinberg, M. W., Hull, S., Kuo, C. T., Watanabe, M., Sen-Banerjee, S., et al. (2002). The Kruppel-like factor KLF15 regulates the insulin-sensitive glucose transporter GLUT4. *J. Biol. Chem.* 277, 34322–34328. doi: 10.1074/jbc.M201304200

Gray, S., Wang, B., Orihuela, Y., Hong, E. G., Fisch, S., Haldar, S., et al. (2007). Regulation of gluconeogenesis by krüppel-like factor 15. *Cell Metab.* 5, 305–312. doi: 10.1016/j.cmet.2007.03.002

Haldar, S. M., Jeyaraj, D., Anand, P., Zhu, H., Lu, Y., Prosdocimo, D. A., et al. (2012). Kruppel-like factor 15 regulates skeletal muscle lipid flux and exercise adaptation. *Proc. Natl. Acad. Sci. U.S.A.* 109, 6739–6744. doi: 10.1073/pnas.1121060109

Han, S., Zhang, R., Jain, R., Shi, H., Zhang, L., Zhou, G., et al. (2015). Circadian control of bile acid synthesis by a KLF15-Fgf15 axis. *Nat. Commun.* 6, 7231. doi: 10.1038/ncomms8231

Huang, Y., Zhou, M., Sun, H., and Wang, Y. (2011). Branched-chain amino acid metabolism in heart disease: an epiphenomenon or a real culprit? *Cardiovasc. Res.* 90, 220–223. doi: 10.1093/cvr/cvr070

Jang, C., Oh, S. F., Wada, S., Rowe, G. C., Liu, L., Chan, M. C., et al. (2016). A branched-chain amino acid metabolite drives vascular fatty acid transport and causes insulin resistance. *Nat. Med.* 22, 421–426. doi: 10.1038/nm.4057

Jeyaraj, D., Scheer, F. A., Ripperger, J. A., Haldar, S. M., Lu, Y., Prosdocimo, D. A., et al. (2012). Klf15 orchestrates circadian nitrogen homeostasis. *Cell Metab.* 15, 311–323. doi: 10.1016/j.cmet.2012.01.020

Joshi, M. A., Jeoung, N. H., Obayashi, M., Hattab, E. M., Brocken, E. G., Liechty, E. A., et al. (2006). Impaired growth and neurological abnormalities in branched-chain Ĩ±-keto acid dehydrogenase kinase-deficient mice. *Biochem. J.* 400, 153–162. doi: 10.1042/BJ20060869

Lu, J., Xie, G., Jia, W., and Jia, W. (2013). Insulin resistance and the metabolism of branched-chain amino acids. *Front. Med.* 7, 53–59. doi: 10.1007/s11684-013-0255-5

Lynch, C. J., and Adams, S. H. (2014). Branched-chain amino acids in metabolic signalling and insulin resistance. *Nat. Rev. Endocrinol.* 10, 723–736. doi: 10.1038/nrendo.2014.171

Mayers, J. R., Wu, C., Clish, C. B., Kraft, P., Torrence, M. E., Fiske, B. P., et al. (2014). Elevation of circulating branched-chain amino acids is an early event in human pancreatic adenocarcinoma development. *Nat. Med.* 20, 1193–1198. doi: 10.1038/nm.3686

Mayers, J. R., Torrence, M. E., Danai, L. V., Papagiannakopoulos, T., Davidson, S. M., Bauer, M. R., et al. (2016). Tissue of origin dictates branched-chain amino acid metabolism in mutant Kras-driven cancers. *Science* 353, 1161–1165. doi: 10.1126/science.aaf5171

Meijer, A. J., and Dubbelhuis, P. F. (2004). Amino acid signalling and the integration of metabolism. *Biochem. Biophys. Res. Commun.* 313, 397–403. doi: 10.1016/j.bbrc.2003.07.012

Melnik, B. C. (2012). Leucine signaling in the pathogenesis of type 2 diabetes and obesity. *World J. Diabetes* 3, 38–53. doi: 10.4239/wjd.v3.i3.38

Mori, T., Sakaue, H., Iguchi, H., Gomi, H., Okada, Y., Takashima, Y., et al. (2005). Role of Kruppel-like factor 15 (KLF15) in transcriptional regulation of adipogenesis. *J. Biol. Chem.* 280, 12867–12875. doi: 10.1074/jbc.M410515200

Nair, K. S., and Short, K. R. (2005). Hormonal and signaling role of branched-chain amino acids. *J. Nutr.* 135, 1547S—1552S.

Newgard, C. B., An, J., Bain, J. R., Muehlbauer, M. J., Stevens, R. D., Lien, L. F., et al. (2009). A branched-chain amino acid-related metabolic signature that differentiates obese and lean humans and contributes to insulin resistance. *Cell Metab.* 9, 311–326. doi: 10.1016/j.cmet.2009.02.002

Novarino, G., El-Fishawy, P., Kayserili, H., Meguid, N. A., Scott, E. M., Schroth, J., et al. (2012). Mutations in BCKD-kinase lead to a potentially treatable form of autism with epilepsy. *Science* 338, 394–397. doi: 10.1126/science.1224631

Prosdocimo, D. A., Anand, P., Liao, X., Zhu, H., Shelkay, S., Artero-Calderon, P., et al. (2014). Kruppel-like factor 15 is a critical regulator of cardiac lipid metabolism. *J. Biol. Chem.* 289, 5914–5924. doi: 10.1074/jbc.M113.531384

Ribeiro, C. A., Sgaravatti, A. M., Rosa, R. B., Schuck, P. F., Grando, V., Schmidt, A. L., et al. (2007). Inhibition of brain energy metabolism by the branched-chain amino acids accumulating in maple syrup urine disease. *Neurochem. Res.* 33, 114–124. doi: 10.1007/s11064-007-9423-9

Saxton, R. A., Knockenhauer, K. E., Wolfson, R. L., Chantranupong, L., Pacold, M. E., Wang, T., et al. (2016). Structural basis for leucine sensing by the Sestrin2-mTORC1 pathway. *Science* 351, 53–58. doi: 10.1126/science.aad2087

Saxton, R. A., and Sabatini, D. M. (2017). mTOR signaling in growth, metabolism, and disease. *Cell* 168, 960–976. doi: 10.1016/j.cell.2017.02.004

Shah, S. H., Bain, J. R., Muehlbauer, M. J., Stevens, R. D., Crosslin, D. R., Haynes, C., et al. (2010). Association of a peripheral blood metabolic profile with coronary artery disease and risk of subsequent cardiovascular events. *Circ. Cardiovasc. Genet.* 3, 207–214. doi: 10.1161/CIRCGENETICS.109.852814

Shimizu, N., Yoshikawa, N., Ito, N., Maruyama, T., Suzuki, Y., Takeda, S., et al. (2011). Crosstalk between glucocorticoid receptor and nutritional sensor mTOR in skeletal muscle. *Cell Metab.* 13, 170–182. doi: 10.1016/j.cmet.2011.01.001

Sun, H., Olson, K. C., Gao, C., Prosdocimo, D. A., Zhou, M., Wang, Z., et al. (2016). Catabolic defect of branched-chain amino acids promotes heart failure. *Circulation* 133, 2038–2049. doi: 10.1161/CIRCULATIONAHA.115.020226

Takeuchi, Y., Yahagi, N., Aita, Y., Murayama, Y., Sawada, Y., Piao, X., et al. (2016). KLF15 Enables rapid switching between lipogenesis and gluconeogenesis during fasting. *Cell Rep.* 16, 2373–2386. doi: 10.1016/j.celrep.2016.07.069

Târlungeanu, D. C., Deliu, E., Dotter, C. P., Kara, M., Janiesch, P. C., Scalise, M., et al. (2016). Impaired amino acid transport at the blood brain barrier is a cause of autism spectrum disorder. *Cell* 167, 1481–1494.e1418. doi: 10.1016/j.cell.2016.11.013

Tato, I., Bartrons, R., Ventura, F., and Rosa, J. L. (2011). Amino acids activate mammalian target of rapamycin complex 2 (mTORC2) via PI3K/Akt signaling. *J. Biol. Chem.* 286, 6128–6142. doi: 10.1074/jbc.M110.166991

Wolfson, R. L., Chantranupong, L., Saxton, R. A., Shen, K., Scaria, S. M., Cantor, J. R., et al. (2016). Sestrin2 is a leucine sensor for the mTORC1 pathway. *Science* 351, 43–48. doi: 10.1126/science.aab2674

Zhang, L., Prosdocimo, D. A., Bai, X., Fu, C., Zhang, R., Campbell, F., et al. (2015). KLF15 establishes the landscape of diurnal expression in the heart. *Cell Rep.* 13, 2368–2375. doi: 10.1016/j.celrep.2015.11.038

Conflict of Interest Statement: The authors declare that the research was conducted in the absence of any commercial or financial relationships that could be construed as a potential conflict of interest.

frontiers in Physiology

ORIGINAL RESEARCH
published: 06 October 2017
doi: 10.3389/fphys.2017.00758

Inhibition of (pro)renin Receptor Contributes to Renoprotective Effects of Angiotensin II Type 1 Receptor Blockade in Diabetic Nephropathy

Lin Zhang[1†], Xiao-Fei An[2†], Xin Ruan[3], Dong-Dong Huang[3], Li Zhou[4], Hong Xue[4], Li-Min Lu[4] and Ming He[3*]*

[1] Department of Biochemistry and Molecular Cell Biology, Shanghai Jiao Tong University School of Medicine, Shanghai, China, [2] Department of Endocrinology, Jiangsu Province Hospital of Chinese Medicine, Affiliated Hospital of Nanjing University of Chinese Medicine, Nanjing, China, [3] Key Laboratory of Cell Differentiation and Apoptosis of Chinese Ministry of Education, Department of Pathophysiology, Shanghai Jiao Tong University School of Medicine, Shanghai, China, [4] Department of Physiology and Pathophysiology, Fudan University Shanghai Medical College, Shanghai, China

OPEN ACCESS

Edited by:
Xinran Ma,
East China Normal University, China

Reviewed by:
Hongbing Liu,
Tulane University, United States
Hui Sheng,
Tenth People's Hospital of Tongji University, China

***Correspondence:**
Li-Min Lu
lulimin@shmu.edu.cn
Ming He
heming@shsmu.edu.cn

[†] These authors have contributed equally to this work.

Specialty section:
This article was submitted to Clinical and Translational Physiology, a section of the journal Frontiers in Physiology

Received: 17 July 2017
Accepted: 19 September 2017
Published: 06 October 2017

Citation:
Zhang L, An X-F, Ruan X, Huang D-D, Zhou L, Xue H, Lu L-M and He M (2017) Inhibition of (pro)renin Receptor Contributes to Renoprotective Effects of Angiotensin II Type 1 Receptor Blockade in Diabetic Nephropathy. Front. Physiol. 8:758. doi: 10.3389/fphys.2017.00758

Aims: Renal renin-angiotensin system (RAS) plays a pivotal role in the development of diabetic nephropathy (DN). Angiotensin II (Ang II) type 1 receptor (AT_1R) blockade elevates (pro)renin, which may bind to (pro)renin receptor (PRR) and exert receptor-mediated, angiotensin-independent profibrotic effects. We therefore investigated whether PRR activation leads to the limited anti-fibrotic effects of AT_1R blockade on DN, and whether PRR inhibition might ameliorate progression of DN.

Methods: To address the issue, the expression of RAS components was tested in different stages of streptozotocin (STZ)-induced diabetic rats (6, 12, and 24 weeks) and 6-week AT_1R blockade (losartan) treated diabetic rats. Using the blocker for PRR, the handle region peptide (HRP) of prorenin, the effects of PRR on high glucose or Ang II-induced proliferative and profibrotic actions were evaluated by measurement of cell proliferation, matrix metalloproteinase-2 (MMP-2) activity, activation of extracellular signal-regulated kinase 1/2 (ERK1/2) and transforming growth factor-β1 (TGF-β1) expression in rat mesangial cells (MCs).

Results: PRR was downregulated in the kidneys of different stages of diabetic rats (6, 12, and 24 weeks). Moreover, 6-week losartan treatment further suppressed PRR expression via upregulating AT_2R, and ameliorated diabetic renal injury. HRP inhibited high glucose and Ang II-induced proliferative and profibrotic effects in MCs through suppressing TGF-β1 expression and activating MMP-2. Meanwhile, HRP enhanced losartan's anti-fibrotic effects through further inhibiting phosphorylation of ERK1/2 and

TGF-β1 expression. Moreover, the inhibitive effect of HRP on Ang II-induced TGF-β1 expression depended on the regulation of PRR expression by AT_2R.

Conclusions: Our findings suggest that inhibition of PRR contributes to renoprotection against diabetic nephropathy by AT_1R blockade.

Keywords: diabetic nephropathy, renin-angiotensin system, (pro)renin receptor, angiotensin II type 1 receptor, angiotensin II type 2 receptor

INTRODUCTION

Diabetic nephropathy (DN) is one of the most important long-term complications of diabetes and the major cause of end-stage renal disease and mortality in diabetic patients (Reidy et al., 2014). Activated renal tissue-localized renin-angiotensin system (RAS) plays an important role in the development of kidney disease in diabetes (Rahimi, 2016). Though multiple clinical trials have shown that angiotensin-converting enzyme inhibitors (ACEI) (Lewis et al., 1993) and Angiotensin II (Ang II) type 1 receptor (AT_1R) blockades (ARB) (Brenner et al., 2001) attenuate DN, these effects were limited and were unable to halt the progression of DN into end-stage organ failure (Zhang et al., 2011). One of the most remarkable changes during Ang II blockade treatment is the increased production of prorenin/renin in plasma and kidney (Gomez et al., 1990; Zhang et al., 2011). Increased plasma prorenin concentration is associated with microalbuminuria in patients with diabetes mellitus (Deinum et al., 1999). Moreover, in addition to produce Ang II, prorenin/renin had its receptor, (pro)renin receptor (PRR) (Nguyen et al., 2002). The binding of prorenin/renin to PRR exerts angiotensin-independent, receptor-mediated profibrotic effects through activating intracellular signal transductions such as extracellular-signal-regulated kinase (ERK) and p38MAPK (Nguyen et al., 2002). We hypothesize that PRR activation may limit the anti-fibrotic effects of angiotensin blockade in DN, and thus, PRR inhibition may enhance the therapeutic effects. In 2004, Ichihara et al. synthesized a decoy peptide, called "handle region peptide" (HRP), which serves as a PRR blocker (Ichihara et al., 2004). HRP prevented the development of glomerulosclerosis in human PRR transgenic rats (Kaneshiro et al., 2007). Our previous studies showed that both PRR siRNA and HRP inhibited mesangial cells (MCs) proliferation and reduced associated fibrotic factor release, including transforming growth factor-β1 (TGF-β1) and matrix metalloproteinase-2 (MMP-2) (He et al., 2009). However, the interaction between PRR and DN has not been well-studied.

In this study, we aim to investigate whether PRR plays a role during different stages of DN (from early to end stage) and during losartan (AT_1R blockade) treatment, especially in the setting of high glucose and Ang II-related renal fibrosis *in vivo* and *in vitro*. Our findings demonstrate that the kidney PRR is downregulated in diabetic rats and is further significantly suppressed after 6 weeks of losartan treatment. HRP inhibits high glucose and Ang II-induced proliferative and profibrotic effects in MCs through suppressing ERK1/2 activation, TGF-β1 expression and activating MMP-2. Co-treatment of HRP and losartan produced an additive anti-fibrotic effects through further inhibiting phosphorylation of ERK1/2 and TGF-β1 expression. HRP blunts Ang II-induced TGF-β1 expression through regulating PRR via AT_2R in MCs. Our findings highlight blockade of PRR as a possible new therapy for DN.

METHODS

Animals and Experimental Protocol

All animal procedures were carried out in accordance with the guidelines for the Care and Use of Laboratory Animals of Shanghai Jiao Tong University School of Medicine and approved by the Institutional Animal Care and Use Committee (Department of Laboratory Animal Science, Shanghai Jiao Tong University School of Medicine). Male Sprague-Dawley (SD) rats (150–200 g) were supplied by Shanghai SLAC Laboratory Animal Co. LTD (Shanghai, China). All animals were housed under standard laboratory conditions (12 h light/12 h dark, temperature 22–26°C, air humidity 55–60%) with *ad libitum* water and rat chow. The STZ-induced diabetic rat models in different stages were constructed as previously described (Tesch and Allen, 2007; He et al., 2010). Plasma level of glucose was measured using blood glucose kit assays (Jiancheng Bioengineering Company, Nanjing, China) 1 week after STZ administration. Rats with plasma glucose higher than 16.7 mM were used in the present study. The blood glucose, urine volume, urine protein excretion, and serum creatinine were measured as described previously (He et al., 2010).

For losartan treatment experiments, STZ-induced diabetic rats were further divided randomly into three groups: one was treated with losartan (gift of Hangzhou MSD Pharmaceutical Co. Ltd., Zhejiang, China) at a dose of 20 mg/kg body weight per day by gavage once daily ($n = 8$) for 6 weeks (beginning 1 week until 7 weeks after STZ administration); another group DM rats ($n = 8$) was given equal volume of water by gavage administration for 6 weeks. The third group, i.e., the non-diabetic rats, was used as the Control group ($n = 8$) and was given equal volume of water via gavage administration for 6 weeks. All the rats in these three groups were anesthetized and sacrificed after 6 weeks of losartan treatment to obtain the blood sample and kidney of each animal.

Histology and Immunohistochemistry

Rat kidneys collected from different groups were immediately fixed in 4% formaldehyde, and were then embedded in paraffin. Paraffin-embedded kidney sections (5 μm) were analyzed after hematoxylin & eosin (H&E) staining and periodic acid-Schiff (PAS) staining.

For immunohistochemistry, after deparaffinization and hydration through xylenes, slides were subjected to microwave

for antigen retrieval. Endogenous peroxidase activity was quenched and sections were incubated with rabbit serum for 20 min, followed by incubation overnight at 4°C with a 1:100 dilution of the primary antibody, rabbit anti- rat ATP6IP2/renin receptor antibody (Abcam, Cambridge, UK, 1:100 dilution). The PRR was then detected using a commercial immunoperoxidase staining kit (Boster ABC kit, Wuhan, China). Briefly, the sections were incubated with a 1:100 dilution of biotinylated secondary goat anti-rabbit antibody for about 30 min at 37°C, followed by avidin-biotin-peroxidase complex (ABC) reagent incubation for 30 min at 37°C. Bound antibody conjugates were visualized using 3,3′-diaminobenzidine (DAB) as a chromogen to develop a brown stain and mounted with glycerol gelatin. The sections were not counterstained with hematoxylin to better compare PRR expression (Deng et al., 2006).

Electron Microscopy Analysis

Rat kidneys were fixed in 2.5% glutaraldehyde in sodium cacodylate buffer. Samples were post-fixed in OsO4, dehydrated in ethanol, and embedded in resin. Ultrathin sections (50∼60 nm) were counterstained with uranyl acetate and lead citrate and examined with a Philips CM120 transmission electron microscope.

Measurements of the Components of RAS

For the determination of plasma renin activity, plasma AngII and kidney AngII, we treated the plasma and kidney as previously reported (He et al., 2009, 2010). Plasma renin activity was determined by the rate of angiotensin I (AngI) generation from angiotensinogen at a substrate concentration close to Km. Plasma renin activity was determined with Ang I radioimmunoassay kit (Beijing North Institute of biological technology, China) and plasma Ang II and kidney Ang II were determined with Ang II radioimmunoassay kit (Beijing North Institute of biological technology, China).

RNA Extraction and Real-time PCR

Total RNA of isolated renal cortexes or MCs was extracted using Trizol reagent (Invitrogen, Carlsbad, CA, USA) according to the manufacturer's instructions. Complementary DNA was synthesized with the Prime-Script RT reagent kit (Promega, Madison, WI). Real-time PCR was performed using SYBR Green PCR Master Mix (Applied Biosystems, CA) on an ABI 7900HT fast real-time PCR system (Applied Biosystems). Expression data were normalized to internal GAPDH and the relative expression levels were evaluated using the ΔΔCt method (He et al., 2010, 2013; Zhang et al., 2016). Primer sequences used in real-time PCR are shown in Table S1. The levels of target gene mRNA were calculated as a percentage of those in control MC or kidney. The data were expressed as average of triplicates ± SEM. The same experiments were repeated 3–5 times.

Western Blotting Analysis

Cell lysates were fractionated by sodium dodecyl sulfate (SDS)-polyacrylamide gelelectrophoresis and then transferred to nitrocellulose membrane (Axygen, Union City, CA). After blocking with 5% nonfat milk in Tris-buffered saline, the membranes were incubated with the antibodies against anti-ATP6IP2/renin receptor antibody (Abcam, Cambridge, UK, 1:1,000 dilution), anti-phosphorylation of ERK1/2 (Cell Signaling Technology, Beverly, MA, 1:1,000 dilution), anti-ERK1/2 (Cell Signaling Technology, Beverly, MA, 1:1,000 dilution) or anti-β-actin (Merck, Darmstadt, Germany, 1:5,000 dilution) followed by horseradish peroxidase (HRP)-linked secondary antibodies (KPL, Guildford, UK, 1:2,000 dilution) for 1 h at room temperature. The filter was finally washed three times and treated with enhanced chemiluminescent reagents, exposed to Kodak X-ray film for 1–20 min to detect the signals.

Cell Culture

The immortalized rat renal mesangial cell line was kindly provided by the Department of pathology of Fudan University, China (He et al., 2009). The cells were incubated in Dulbecco's modified Eagle medium (DMEM, Sigma-Aldrich, St. Louis, MO, USA) containing normal glucose concentration of 5.56 mM D-glucose and supplemented with 10% new bovine serum (NBS) in a humidified atmosphere of 95% air and 5% CO_2 at 37°C. To observe the effect of high glucose, D-glucose (Sigma-Aldrich) was added into the culture medium to increase the glucose concentration to 30 mM; and 24.44 mM mannitol (Sigma-Aldrich, St. Louis, MO, USA) was added instead of glucose to serve as osmolality control.

Fluorescence Microscopy Studies on Binding of HRP and PRR

To study the binding of HRP and PRR in MCs, we synthesized HRP labeled by FITC at the C terminal of the decapeptide, and its sequence is FITC-RILLKKMPSV-COOH (He et al., 2009). Treated with FITC-HRP for 5 min, MCs were washed by cold PBC twice, fixed, blocked, incubated with the anti-ATP6IP2/renin receptor antibody (Abcam, Cambridge, UK, 1:100 dilution), followed by 1 h of incubation at room temperature with Rhodamine (TRIC) labeled anti-goat antibody (rabbit polyclonal; 1:50; KPL, USA) in blocking buffer. Images were then obtained via the laser scanning confocal microscope (Leica, Germany). The co-localization was detected in a triple fluorescence photograph using View-sect software (Leica, Germany).

MMP-2 Activity Determination by Gelatin Zymography

The MMP-2 enzyme activity was determined by gelatin zymography as described previously (He et al., 2009).The ratio of the densities of active MMP-2 (68 kD) to total MMP-2 (the sum of 68 and 72 kD) represents the activity of MMP-2 in the culture medium. The experiment was performed in triplicate.

Cell Proliferation Assay

Cell proliferation of MCs was measured using a colorimetric 5-bromo-2′-deoxyuridine (BrdU) enzyme-linked immunosorbent assay (ELISA) (Roche Applied Science, USA.) according to the manufacturer's protocol. The developed color of the reaction product and thereby the absorbance values difference of 370 and 492 nm (A370–A492 nm) correlates directly to the amount

of DNA synthesis, and thus, cell proliferation. The experiments were performed in triplicate.

Statistical Analysis

All values are presented as mean ± SEM. The statistical significance of differences among groups was assessed by using one way-ANOVA, followed by Student-Newman-Keul test. A *P*-value of <0.05 was taken as statistically significant.

RESULTS

Renal Damage in the Different Stages of STZ-Induced Diabetic Duration

To investigate the role of PRR in DN, we constructed a STZ-induced diabetic rat model and the rats with blood glucose higher than 16.7 mM were included in this study. In the different stages of STZ-induced diabetic duration (6, 12, and 24 weeks after STZ administration), the urine protein excretion and metabolic indices, including blood glucose, body weight, and urine output of each group were collected (**Table 1**). After 6 or 12 weeks, the survival rates of both Control and diabetic mellitus (DM) group were 100% (7/7). But the survival rate of DM rats in 24 weeks was decreased to 75% (6/8), while no rats in Control group (7/7) died (**Table 1**). All of the DM rats in the three stages exhibited progressive increase in blood glucose level, urinary protein excretion, and kidney weight, but showed a decrease in body weight (**Figures 1A–C** and **Table 1**). Moreover, the urinary protein excretion in DM rats increased with time (2.74, 6.03, and 10.95-fold higher in DM than age-matched Control group at 6-, 12-, and 24-weeks). Renal pathological examination by H&E and PAS staining indicated glomerular hypertrophy, expansion of mesangium, and increased diffusely appearing deposits in the basement membranes of capillary loops of the glomeruli in DM rats (**Figures 1C,D**). Electron microscopy showed glomerular basement membrane thickening (**Figure 1E**), increase of mesangial matrix (**Figure 1F**), and extensive podocyte fusion in model groups (**Figure 1E**). The severity of renal morphological changes increased with time, approximating diffuse diabetic glomerulosclerosis at advanced DN stages. This series study provided a successful model for investigating the role of PRR in DN development.

Expression of PRR and the Other Components of RAS in the Kidney and Plasma of Diabetic Rat

We tested the components of RAS in kidneys of all groups. Plasma renin activity was significantly lower in DM rats than in the age-matched Control rats from early to end stage DN (at stages of 6-, 12-, and 24-week diabetic duration) (**Figure 2A**), but kidney (pro)renin mRNA was higher in DM rats (**Figure 2B**). Both PRR mRNA and protein levels in the renal cortex of DM rats were significantly lower than those of the Control group (**Figures 2C,D**). Meanwhile, DM rats showed a significant increase in plasma and kidney Ang II (**Figures 2E,F**).

Renal-Protective Effects of AT_1R Blockade (Losartan) in Diabetic Rats

AT_1R blockade losartan treatment (20 mg/kg body weight per day by gavage for 6 weeks) attenuated, but did not completely reverse hyperglycaemia, renal hypertrophy, polyuria, proteinuria and elevations of serum creatinine of DM rats (**Table 2**). Losartan had no effect on the body weight of DM rats. H&E (**Figure 3A**), PAS staining (**Figure 3B**), and electron microscopy (**Figures 3C,D**) showed that the changes of DN in 6 weeks, including glomerular hypertrophy, expansion of mesangium, mesangial matrix increase, glomerular basement membrane thickening and extensive podocyte fusion, were attenuated by losartan treatment. These data suggest that losartan exhibits a renoprotective effect in STZ-induced rats, but cannot completely halt the progression of DN into end-stage organ failure.

Effects of Losartan on the Expression of PRR and TGF-β1 Expression in Kidneys of Diabetic Rats

To investigate the roles of PRR in the protective effects of losartan in DN, we tested the renal levels of PRR, TGF-β1, and other components of RAS in the Control, DM and DM treated with losartan group (DM + losartan). DM rats exhibited a reduction of kidney PRR mRNA. Notably, 6-week DM + losartan rats had lower PRR mRNA expression compared with DM rats (**Figure 4A**). Immunohistochemical staining showed that PRR mainly localized in the glomeruli mesangium zone (**Figure 4B**). Moreover, the kidney positive staining for PRR of the DM + losartan group was significantly lower than that of

TABLE 1 | Blood glucose, kidney weight, urine volume, and urinary protein excretion in control rats (Control) and STZ-induced diabetic rats (DM).

	6W		12W		24W	
	Control ($n = 7$)	DM ($n = 7$)	Control ($n = 7$)	DM ($n = 7$)	Control ($n = 7$)	DM ($n = 6$)
Blood glucose (mmol/l)	7.2 ± 0.2	37.3 ± 1.9*	6.8 ± 0.2	30.3 ± 1.4*	6.9 ± 0.2	37.3 ± 1.1*
Body weight (g)	416.4 ± 9.1	345.6 ± 10.5*	548.9 ± 12.1	399.5 ± 14.3*	711.1 ± 22.2	430.8 ± 18.5*
Right kidney/body weight ($\times 10^{-3}$)	3.3 ± 0.1	5.8 ± 0.4*	2.9 ± 0.1	5.9 ± 0.3*	2.6 ± 0.1	6.6 ± 0.2*
Urine volume (ml/d)	21.2 ± 3.6	208.4 ± 13.6*	27.3 ± 3.4	275.3 ± 20.0*	30.3 ± 2.7	337.2 ± 22.1*
Urine protein excretion (mg/d)	32.6 ± 2.6	89.3 ± 6.2*	17.8 ± 1.3	107.3 ± 6.3*	17.4 ± 1.3	190.6 ± 13*

Data are expressed as mean ± SEM. $^*P < 0.05$ *compared with control rats in same time point.*

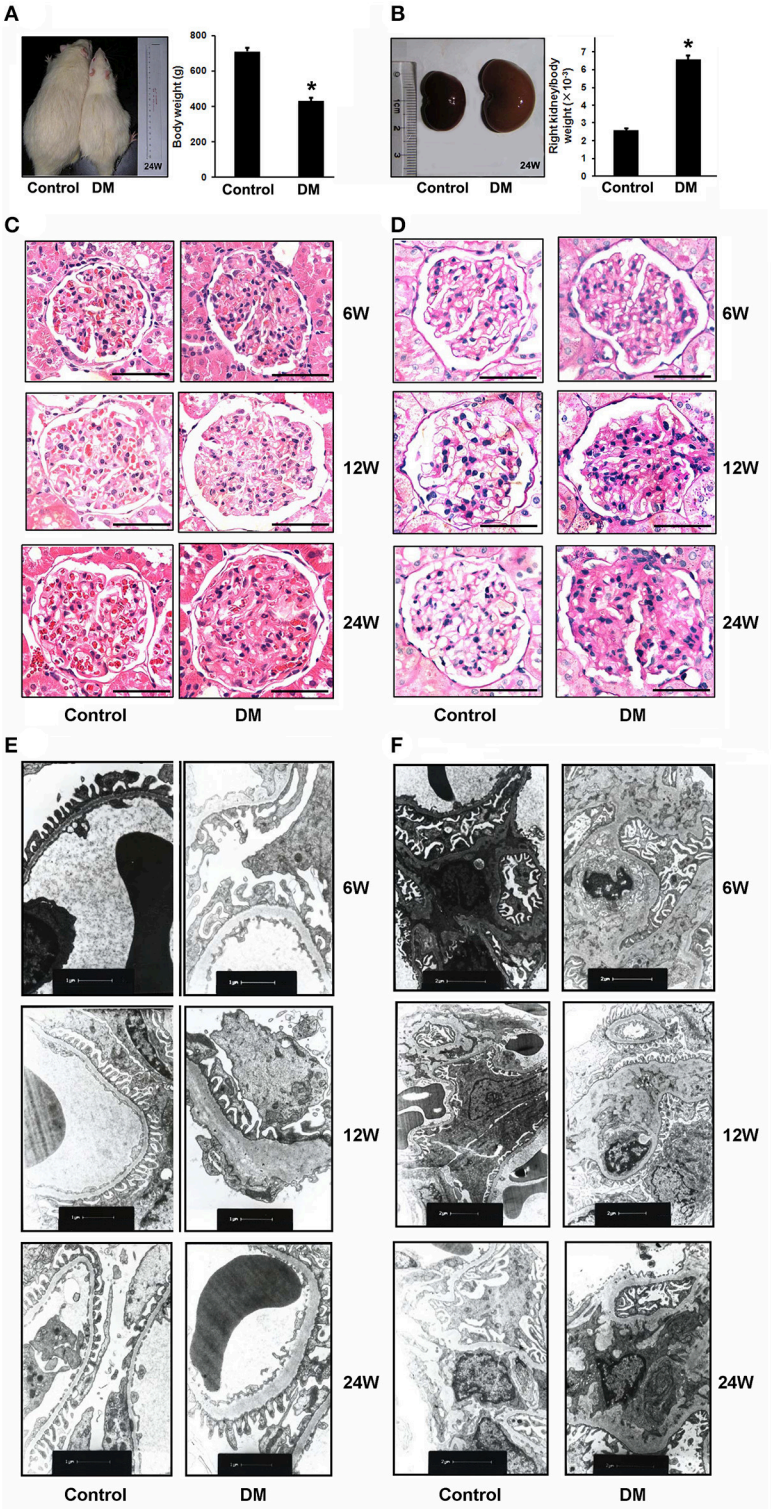

FIGURE 1 | Evidence for diabetic nephropathy (DN) in different stages of STZ-induced diabetic rats. **(A)** Body weight, **(B)** ratio of right kidney to body weight of the Control ($n = 7$) and diabetic rats (DM rats) ($n = 6$) in 24 weeks after STZ administration. The photographs are the representative for rats and kidneys. **(C)** Representative hematoxylin and eosin (H&E) staining and **(D)** periodic acid-Schiff (PAS) staining of glomeruli from Control and DM rats in the different diabetes stages (6, 12, and 24 weeks). Scale bar: 50 μm. **(E,F)** Electron microscopy of kidney sections from Control and DM rats in the different diabetes stages (6, 12, and 24 weeks after STZ administration). **(E)** Representative electron microscopy images of glomerular basement membranes and podocytes in glomeruli. Scale bar: 1 μm. **(F)** Representative electron microscopy images of mesangial areas in glomeruli. Scale bar: 2 μm. $^*P < 0.05$ Control vs. DM rats.

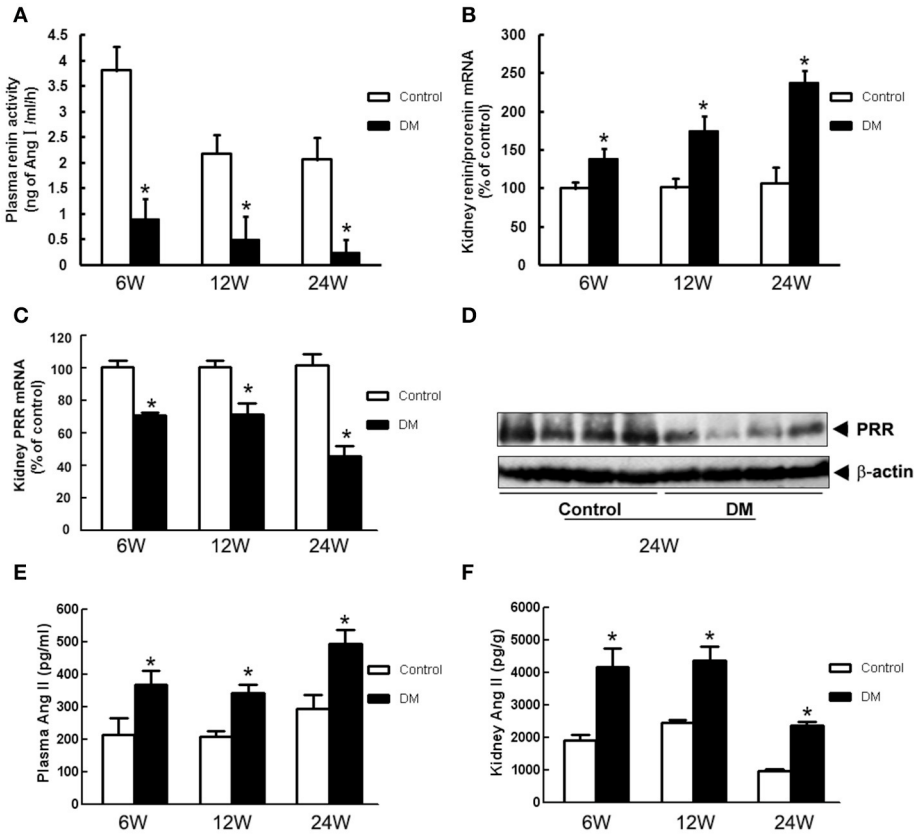

FIGURE 2 | RAS components in the plasma and kidney of Control and DM rats at the end of 6, 12, or 24 weeks after STZ induction. **(A)** Plasma renin activity measured by radioimmunoassay. **(B)** Kidney (pro)renin and **(C)** PRR mRNA level by real-time PCR. **(D)** Kidney PRR protein level by Western blotting. **(E)** Plasma and **(F)** kidney Ang II measured by radioimmunoassay. *$P < 0.05$ Control vs. DM rats in the same time point.

TABLE 2 | Effects of 6-week losartan treatment on blood glucose, kidney weight, urine protein excretion, and serum creatinine of STZ-induced diabetic rats.

Group	*n*	Blood glucose (mmol/l)	Body weight (g)	Right kidney/body weight ($\times 10^{-3}$)	Urine volume (ml/d)	Urine protein excretion (mg/d)	Serum creatintine (μmol/l)
Control	8	6.9 ± 0.2	465.1 ± 11.3	3.1 ± 0.1	20.6 ± 3.1	22.5 ± 2.6	61.5 ± 7.4
DM	8	25.3 ± 1.3*	348.1 ± 11.3*	6.7 ± 0.1*	208.3 ± 13.2*	64.1 ± 7.3*	85.4 ± 5.8*
DM+losartan	8	19.6 ± 2.8*#	362.3 ± 23.1*	5.7 ± 0.7*	145.8 ± 37.8*#	37.8 ± 7.5#	67.7 ± 5.2#

*Data are expressed as mean ± SEM. *$P < 0.05$ compared with control rats; #$P < 0.05$ for DM+losartan rats compared with DM rats.*

DM rats, similar to the real-time PCR results (**Figure 4A**). The increased kidney TGF-β1 mRNA of DM rats was attenuated by losartan, but the level was still higher than the Control group (**Figure 4C**). Meanwhile, the (pro)renin and AT_2R mRNA levels of DM rats were significantly increased after losartan treatment (**Figures 4D,F**). However, losartan had no effect on the kidney AT_1R level of DM rats (**Figure 4E**). These data suggest that AT_1R blockade may play renoprotective roles not only by blocking the AT_1R, but also by decreasing PRR.

Co-localization of HRP and PRR

Our previous study reported the existence of (pro)renin mRNA in MCs and renin activity in the cultured medium (He et al., 2009). HRP (10^{-6} M), the blocker of PRR, was used to identify the roles of PRR in the MCs *in vitro*. *In vivo*, PRR was observed mainly in the mesangium of cortical glomeruli (**Figure 4B**). In MCs, PRR mainly localized to the perinuclear zone and plasma membrane using immunofluorescence (**Figure 5Aa**). FITC-labeled HRP (FITC-HRP) was synthesized to observe the cellular distribution of the HRP-PRR complex. FITC-HRP translocated from culture medium into the cytoplasm within 30 s. Triple fluorescence photograph by confocal microscopy showed that the co-localization of PRR and FITC-HRP was mainly on the cell membrane and in the perinuclear zone of the cytoplasm in 5 min after FITC-HRP treatment (**Figures 5A,B**). These data further suggest that HRP may interact with PRR in MCs.

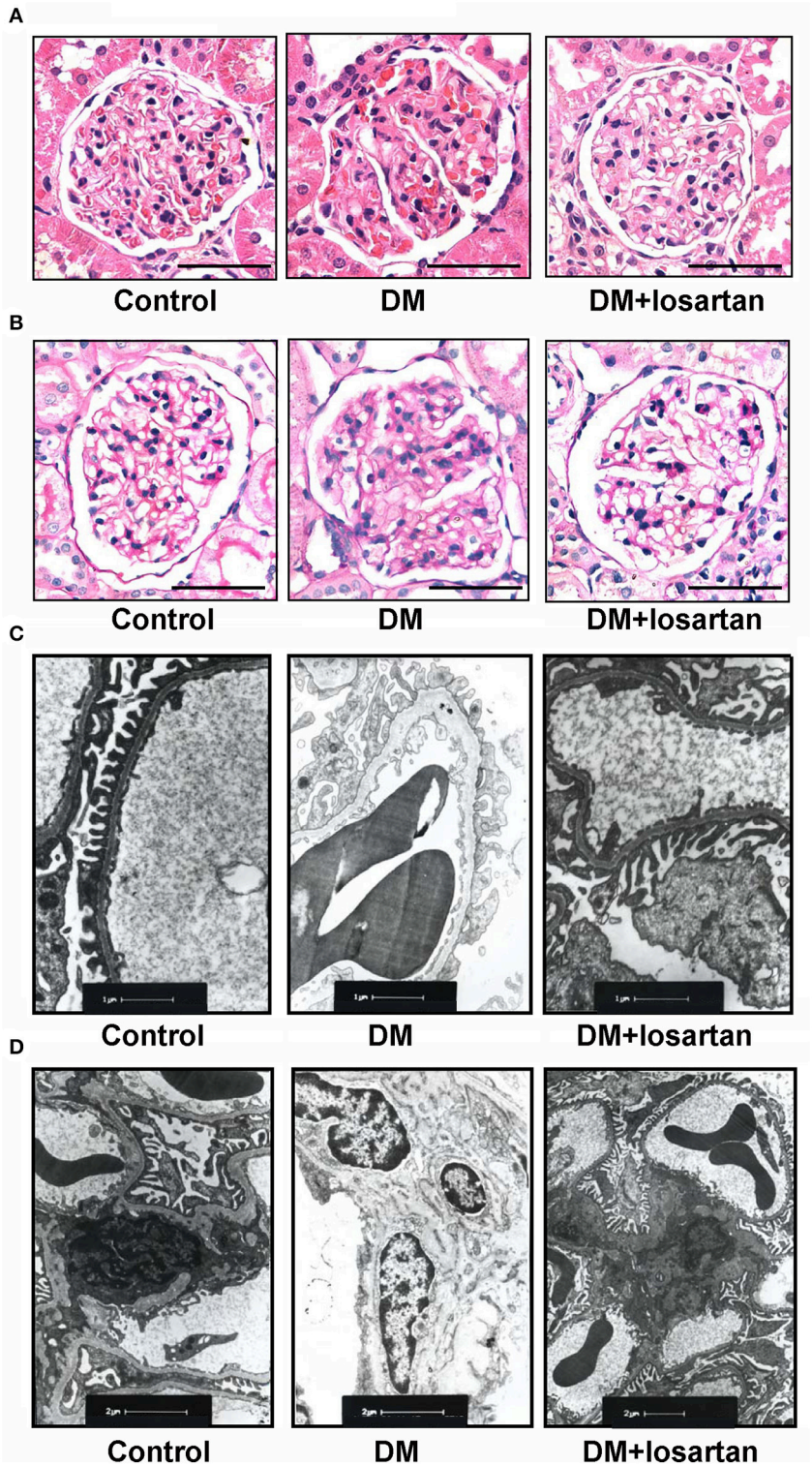

FIGURE 3 | Histology analysis of kidneys from Control, DM and losartan treated DM (DM + losartan) rats. **(A)** Representative H&E staining and **(B)** PAS staining of glomeruli from Control, DM and DM + losartan rats. Scale bar: 50 μm. **(C,D)** Electron microscopy of kidney sections. **(C)** Representative electron microscopy images of glomerular basement membranes and podocytes in glomeruli. Scale bar: 1 μm. **(D)** Representative electron microscopy images of mesangial areas of glomeruli. Scale bar: 2 μm.

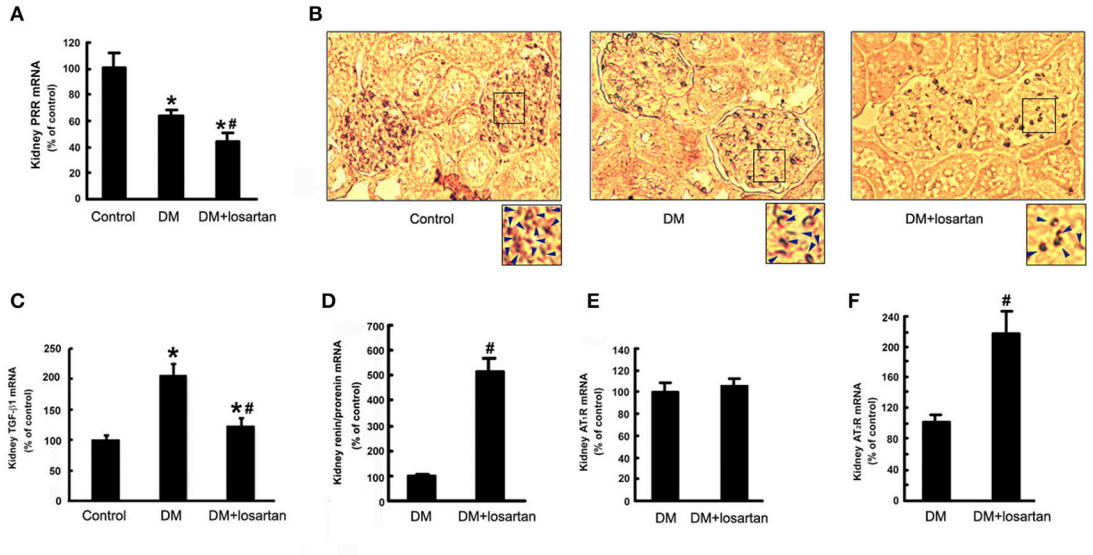

FIGURE 4 | Expression of the components of RAS and TGF-β1 in the kidney of Control, DM and DM + losartan rats. **(A)** Kidney PRR mRNA level by real-time PCR. **(B)** Immunohistochemical staining for PRR in the kidneys of Control ($n = 8$), DM ($n = 8$) and DM + losartan ($n = 8$) rats (not counterstained with hematoxylin to compare the PRR expression better). The arrows indicated the representative area of PRR expression in the renal tissues. **(C)** TGF-β1, **(D)** (pro)renin, **(E)** AT_1R, **(F)** AT_2R mRNA level in the kidneys of DM ($n = 8$) and DM + losartan ($n = 8$) rats by real-time PCR. *$P < 0.05$ compared with Control rats, $^{\#}P < 0.05$ compared with DM rats.

HRP Suppresses High Glucose-Induced Phosphorylation of ERK1/2, TGF-β1 Expression and MMP-2 Deactivation in MCs

Since it has been reported that PRR activation promotes the production of profibrotic factors through activating ERK signaling, we examined the effect of HRP on high glucose-induced phosphorylation of ERK1/2 and TGF-β1 expression, one of the most important fibrotic factors in DN (Nguyen et al., 2002). Treatment with high glucose caused a significant increase in phosphorylation of ERK1/2 (**Figure 6A**) and TGF-β1 mRNA expression (**Figure 6B**), while no significant change was observed in MCs treated with mannitol (as osmolarity control). HRP (10^{-6} M) attenuated high glucose-induced phosphorylation of ERK1/2 to control group level (**Figure 6A**). HRP (10^{-7} and 10^{-6} M) reversed the increased TGF-β1 mRNA expression to control level or even lower level than control (**Figure 6B**). High glucose also induced a decrease in MMP-2 activity of the MCs, while HRP (10^{-7} M and 10^{-6} M) reversed the decreased MMP-2 activity to control or mannitol group levels (**Figure 6C**). These data suggest that PRR is activated and involved in high glucose-induced proliferative and profibrotic effects and HRP may eliminate these effects through blocking the activation of PRR in MCs.

HRP Suppresses Ang II-Induced Cell Proliferation and MMP-2 Deactivation in MCs

Besides high glucose, Ang II is another pivotal factor in the pathogenesis of DN *in vivo* as shown in **Figure 2**. HRP (10^{-7} M and 10^{-6} M) eliminated high Ang II-induced cell proliferation as shown by BrdU incorporation (**Figure 6D**). In addition, the reduction of MMP-2 activity induced by Ang II (10^{-7} M) at 72 h was attenuated by HRP (**Figure 6E**). These data show HRP blunts Ang II-induced proliferative and profibrotic actions in MCs, suggesting that PRR may be involved in the Ang II signaling pathway.

Combined Treatment with HRP and Losartan Has an Additive Effect on Inhibiting Phosphorylation of ERK1/2 and TGF-β1 Expression in MCs

Ang II caused an increase in phosphorylation of ERK1/2 and a dose-dependent increase in TGF-β1 mRNA expression (**Figures 6F,G**). Losartan (10^{-6} M) or HRP (10^{-6} M) attenuated Ang II-induced phosphorylation of ERK1/2 and expression of TGF-β1 mRNA (**Figures 6F,H**). The level of phosphorylation of ERK1/2 and TGF-β1 expression in HRP or losartan individual treatment group is still higher than control group (**Figures 6F,H**). Notably, combined treatment with losartan and HRP led to a further reduction in phosphorylation of ERK1/2 (**Figure 6F**) and TGF-β1 expression (**Figure 6H**) to control level, suggesting that HRP may enhance losartan's anti-fibrotic effects on DN through further or fully inhibiting PRR.

Inhibitive Effects of HRP on the Ang II Signaling Pathway Depends on PRR Expression Regulated by AT_2R

As described in our previous studies (He et al., 2010), Ang II (10^{-7} M) or AT_2R agonist (CGP42112A) (10^{-6} M) decreased the expression of PRR mRNA, while AT_2R antagonist (PD123319)

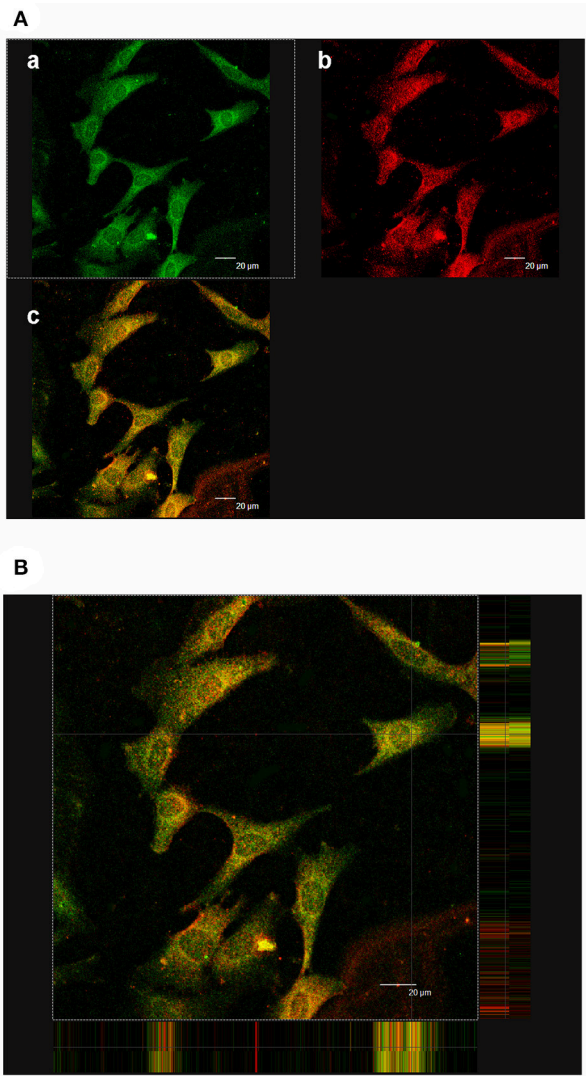

FIGURE 5 | Co-localization of PRR and FITC-HRP. **(Aa)** Immunofluorescence showing FITC-HRP was mainly located in the cytoplasm and membrane. **(b)** Immunofluorescence showing PRR was mainly located in the cytoplasm and membrane. **(c)** Analysis of the overlay of PRR and HRP. Yellow is the co-localization. **(B)** Triple fluorescence photograph with confocal microscopy reveals the co-localization of PRR and FITC-HRP (5 min). The co-localization (yellow staining) mainly focused in the membrane and cytoplasm. Scale bar: 20 μm.

(10^{-5} M) abolished the Ang II-induced repression of PRR expression (**Figure 6I**). HRP (10^{-6} M) did not affect the downregulation of PRR by AT_2R activation (**Figure 6I**). Ang II (10^{-7} M) stimulated TGF-β1 mRNA expression and CGP42112A (10^{-6} M) significantly reduced TGF-β1 mRNA expression after 24 h treatment (**Figure 6J**). HRP (10^{-6} M) suppressed the induction of TGF-β1 mRNA expression by combined treatment with Ang II (10^{-7} M) and PD123319 (10^{-5} M), but did not further reduce the expression of TGF-β1 induced by CGP42112A (10^{-6} M) (**Figure 6J**). These data indicate that Ang II-induced proliferative and profibrotic actions are mediated at least in part through PRR. Moreover, HRP inhibition on the Ang II signaling pathway is dependent on regulation of PRR expression by AT_2R.

DISCUSSION

A pivotal role for the RAS in the pathogenesis and development of DN is widely accepted, based largely on work showing the attenuation of DN by ACEI (Lewis et al., 1993; Zhang et al., 2011) and ARBs (Brenner et al., 2001; Zain and Awan, 2014). However, these agents cannot halt the progression of DN into end-stage organ failure, possibly because of insufficient suppression of the intrarenal RAS, especially the increased production of prorenin (Gomez et al., 1990). Prorenin, the inactive proenzyme form of renin, may contribute to kidney damage by binding to and activating PRR (Nguyen et al., 2002). On binding to PRR, pro(renin) induces direct (receptor-mediated, angiotensin-independent) proliferative and profibrotic effects by increasing phosphorylation of ERK1/2, and increasing TGF-β1 and MMP-2 expression (Nguyen et al., 2002; He et al., 2009). Therefore, PRR activation may limit therapeutic effects of ACEI and ARB on DN, and thus, a PRR blocker may enhance their anti-fibrotic effects.

In this study, DN models of different duration (6, 12, and 24 weeks) were constructed and metabolic indices, renal function, and kidney histological morphology suggested that the severity of renal damage increased with duration of STZ treatment. This series study provides a means for investigating the role of RAS in DN development. Plasma renin activity was suppressed and kidney (pro)renin mRNA expression was upregulated in DM rats, reflecting suppressed systemic RAS activity, possibly resulting from increased kidney-specific RAS activity (Price et al., 1999; Oshima et al., 2014). The expression of PRR mRNA and protein in the kidneys of DM rats was significantly downregulated in all three stages. These results are in agreement with our previous study showing the downregulation of PRR expression in the kidneys of early stage diabetic rats (1 and 3 weeks after STZ injection) (He et al., 2010). The regulation of kidney PRR expression during DM has not been consistently shown. Huang et al showed that the expression of rat kidney PRR was significantly increased 6 weeks after development of diabetes (Siragy and Huang, 2008). However, other reports showed no difference between the kidney PRR expression levels of nondiabetic and diabetic subjects (Konoshita et al., 2006). This difference may be caused by (1) different high glucose, Ang II and (pro)renin levels *in vivo*: we tested these parameters as shown in **Table 1** and **Figure 2**, but these were not shown in other reports; (2) mRNA and protein extracted from different regions of the renal tissues: our immunohistochemical staining showed PRR localized mainly to the glomeruli mesangium zone (**Figure 4B**), but other reports used whole kidney. The regulation of PRR in the different types of renal cells may be different.

The major interest of this study was focused on the roles of PRR in the renal-protective effects of AT_1R blockade on DN. We showed that losartan exhibited a protective effect on DN, suppressing phosphorylation of ERK1/2 and TGF-β1 expression, which also occurred in the previous observations in animals and patients (Siragy and Huang, 2008; Huang et al.,

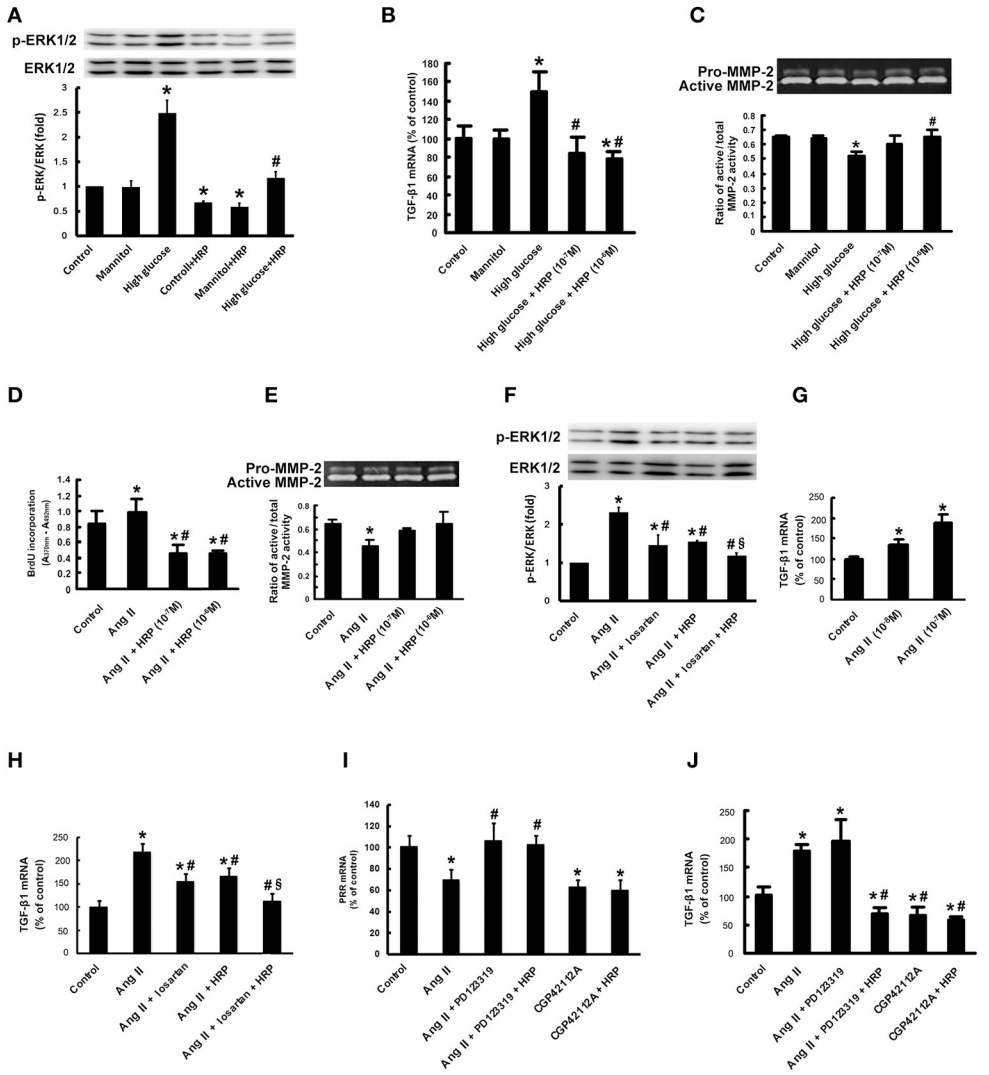

FIGURE 6 | HRP suppressed high glucose and Ang II-induced proliferative and fibrotic effects in MCs. Antagonistic action of HRP (10^{-7} M and 10^{-6} M) on high glucose-induced increase in phosphorylation of ERK1/2 **(A)** and TGF-β1 mRNA expression **(B)** by real-time PCR. **(C)** Abolition of the high glucose-induced decrease in MMP-2 activity by HRP by gelatin zymography. $^{*}P < 0.05$ compared with control; $^{\#}P < 0.05$ compared with high glucose group. **(D)** BrdU ELISA shows suppression of the Ang II-induced increase in proliferation of MCs by HRP (10^{-7} M and 10^{-6} M). **(E)** Abolition of the Ang II-induced decrease in MMP-2 activity by HRP (10^{-7} M and 10^{-6} M) by gelatin zymography. Co-treatment of HRP and losartan leads to a further reduction in phosphorylation of ERK1/2 **(F)** and TGF-β1 expressions **(H)** compared with losartan or HRP individual treatment. **(G)** Ang II causes a dose-dependent increase in TGF-β1 mRNA expression. **(I)** The suppressing effect of Ang II on PRR expression is induced by activation of AT_2R. HRP has no effect on the PRR expression. **(J)** Effects of AT_2R activation and PRR inhibition by HRP on TGF-β1 expressions in MCs by real-time PCR. $^{*}P < 0.05$ compared with control; $^{\#}P < 0.05$ compared with Ang II group; $^{\S}P < 0.05$ compared with individual treatment by losartan or HRP.

2011; Anbar et al., 2016). PRR activation by binding (pro)renin may activate ERK1/2 signaling, resulting in the production of profibrotic factors in diabetic nephropathy, such as TGF-β1 (Nguyen et al., 2002). Even PRR is suppressed (**Figure 6I**), HRP blunts high glucose and Ang II-induced phosphorylation of ERK1/2 (**Figures 6A,F**) and TGF-β1 expression (**Figures 6B,H**) through blocking the PRR. These suggest that PRR is activated and involved in diabetic nephropathy development even PRR is downregulated by high glucose and Ang II. Therefore, a clinically relevant finding in the present study is that losartan may further downregulate PRR. This maybe one of the mechanisms through which losartan exerts its renoprotective effects in DN besides blocking AT_1R. *In vivo*, losartan had a mild protective effect against diabetic glycemia (**Table 2**), which is similar to the findings of Murali and Goyal (Murali and Goyal, 2001). Meanwhile, kidney (pro)renin and AT_2R levels, but not AT_1R level, were significantly upregulated by losartan. So, increased tissue Ang II (**Figure 2F**) suppresses PRR expression via AT_2R

activation (**Figure 6I**), which is consistent with our previous studies (He et al., 2010). On the other hand, Schefe et al. reported that on the activation of PRR by (pro)renin, the direct interaction partner of PRR, promyelocytic leukemia zinc finger protein (PLZF) is translocated to the nucleus and repressed the transcription of the PRR itself (Schefe et al., 2006). The present results are in agreement with these findings: losartan-induced high (pro)renin levels suppressed PRR expression through a short negative-feedback loop, preventing excessive receptor activation. In addition, there is also evidence indicating that Ang II stimulation induces cytosolic PLZF to bind to AT_2R at the plasma membrane, driving PLZF to translocate into the nucleus in cardiac hypertrophy (Senbonmatsu et al., 2003). We observed the expression of PLZF mRNA in both the MCs and rat kidney (data not shown). Therefore, the possibility of the involvement of PLZF in regulation of PRR by AT_2R cannot be ruled out and we will further study the detailed mechanism.

On the basis of the available knowledge of PRR and present data, we hypothesize that in diabetic patients or animals, a high level of prorenin promotes renal MCs proliferation and fibrosis through binding to the PRR, which are further augmented by both high glucose and Ang II (via AT_1R). On the other hand, prorenin, as well as high glucose and Ang II lead to a downregulation of PRR expression, possibly through PLZF (Schefe et al., 2006) and AT_2R (Senbonmatsu et al., 2003; He et al., 2010), indicating a negative feedback mechanism (**Figure 7**). The final regulation and effects of PRR are determined by the balance of all of these factors. The activation of the downregulated PRR still involes in the diabetic nephropathy development. Besides blocking AT_1R, losartan exerts renoprotection through further downregulating PRR via upregulation of AT_2R (**Figure 7**). The present data suggest that downregulation of PRR plays an important adaptive and protective role in decreasing high glucose or Ang II induced renal fibrosis during diabetic condition.

HRP mimics the handle region of prorenin and binds competitively to PRR, thereby preventing receptor-mediated prorenin activation and intracellular signaling activation (Suzuki et al., 2003; Ichihara et al., 2004). In the present study, HRP eliminated the high glucose-induced profibrotic actions in MCs. Meanwhile, we firstly reported that HRP inhibited Ang II-induced MCs proliferation and MMP-2 deactivation, suggesting PRR is involved in Ang II-induced proliferative and profibrotic effects. The actions of Ang II are mainly via the signaling of AT_1 and AT_2 receptors (Senbonmatsu et al., 2003; Ding et al., 2016). Firstly, co-treatment of HRP and AT_1R blockade (losartan) showed an additive inhibitory effect on Ang II-induced phosphorylation of ERK1/2 and TGF-β1 expression (**Figure 6F**). Since losartan totally blocked the AT_1R, the effect of HRP cannot be explained on the basis of the suppression of local angiotensin generation, suggesting that HRP exerts beneficial effects in an Ang II-independent manner. This is consistent with the previous work showing that HRP inhibits the development of glomerulosclerosis in diabetic AT_{1A}-receptor-deficient mice (Ichihara et al., 2006). Therefore, therapeutically induced increases in (pro)renin play a role in the limited effectiveness of Ang II blockade, and PRR blockade maybe a good addition to AT_1R blockade for DN, especially for patients with high Ang II level (**Figure 7**). Secondly, HRP had no effect on the downregulationof PRR by activation of AT_2R. HRP suppressed Ang II and AT_2R blockade (PD123319)-induced increase of TGF-β1, but did not further reduce the decreased TGF-β1 expression by AT_2R agonist (CGP42112A). This result indicated that the inhbitive effects of HRP on Ang II-induced cell proliferation and fibrosis depended on the regulation of PRR by AT_2R.

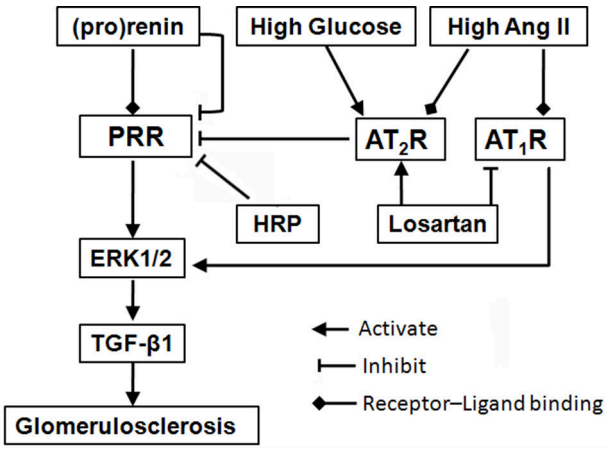

FIGURE 7 | Schematic diagram of a proposed mechanism for blockade of (pro)renin/PRR activation as a therapeutic strategy. Binding of (pro)renin and PRR activates ERK1/2 signaling, resulting in the production of profibrotic factors in diabetic nephropathy, such as TGF-β1. During diabetes development, high glucose and Ang II, as well as high level (pro)renin, lead to a downregulation of PRR expression, through the mediation of AT_2R (He et al., 2010) or PLZF (Schefe et al., 2006), indicating a negative feedback mechanism. But, the activation of the downregulated PRR still involes in the diabetic nephropathy development. Besides blocking AT_1R, losartan plays renoprotective roles through further suppressing PRR via upregulation of AT_2R. Moreover, HRP may enhance losartan's anti-fibrotic effects through further or fully inhibiting PRR. The present findings highlight blockade of PRR as a possible new addition therapy to AT_1R blockade for DN. Abbreviations: Ang II, angiotensin II; AT_1R, angiotensin II type 1 receptor; AT_2R, angiotensin II type 2 receptor; ERK1/2, extracellular signal-regulated kinases 1 and 2; HRP, handle region peptide (HRP) of prorenin; PLZF, promyelocytic zinc finger; PRR, (pro)renin receptor; TGF-β1, transforming growth factor-β1.

In summary, the present study suggests inhibition of PRR may play a protective role in decreasing high glucose or Ang II-induced renal fibrosis during diabetic condition (**Figure 7**). We demonstrated that kidney PRR was downregulated in different stages of diabetic rats and further suppressed after AT_1R blockade treatment. Importantly, HRP enhances losartan's therapeutic actions, confirming that PRR activation may be one of the reasons for limited anti-fibrotic effects of AT_1R blockade on DN and PRR blocker may be a possible new therapy for DN.

AUTHOR CONTRIBUTIONS

MH and LL contribute to conception and design, data analysis and manuscript writing. LinZ, XA, LiZ, and MH performed animal experiments and data acquisition. XR, DH, and HX performed experiments *in vitro* and analyzed the data. MH and XA performed the histology and immunostaining.

ACKNOWLEDGMENTS

This work was supported by grants from National Natural Science Foundation of China (81470841, 81170505, 81470591, and 81774248). Additionally, this work was sponsored by Shanghai Pujiang Program by Science and Technology Commission of Shanghai Municipality (16PJ1405400) and Jiangsu Province Natural Science Foundation (BK20141503). We would like to thank Yufei Liu of Stanford University, for the grammatical revision of this manuscript.

SUPPLEMENTARY MATERIAL

The Supplementary Material for this article can be found online at: https://www.frontiersin.org/articles/10.3389/fphys.2017.00758/full#supplementary-material

REFERENCES

Anbar, H. S., Shehatou, G. S., Suddek, G. M., and Gameil, N. M. (2016). Comparison of the effects of levocetirizine and losartan on diabetic nephropathy and vascular dysfunction in streptozotocin-induced diabetic rats. *Eur. J. Pharmacol.* 780, 82–92. doi: 10.1016/j.ejphar.2016.03.035

Brenner, B. M., Cooper, M. E., de Zeeuw, D., Keane, W. F., Mitch, W. E., Parving, H. H., et al. (2001). Effects of losartan on renal and cardiovascular outcomes in patients with type 2 diabetes and nephropathy. *N. Engl. J. Med.* 345, 861–869. doi: 10.1056/NEJMoa011161

Deinum, J., Ronn, B., Mathiesen, E., Derkx, F. H., Hop, W. C., and Schalekamp, M. A. (1999). Increase in serum prorenin precedes onset of microalbuminuria in patients with insulin-dependent diabetes mellitus. *Diabetologia* 42, 1006–1010. doi: 10.1007/s001250051260

Deng, H. X., Shi, Y., Furukawa, Y., Zhai, H., Fu, R., Liu, E., et al. (2006). Conversion to the amyotrophic lateral sclerosis phenotype is associated with intermolecular linked insoluble aggregates of SOD1 in mitochondria. *Proc. Natl. Acad. Sci. U.S.A.* 103, 7142–7147. doi: 10.1073/pnas.0602046103

Ding, D., Du, Y., Qiu, Z., Yan, S., Chen, F., Wang, M., et al. (2016). Vaccination against type 1 angiotensin receptor prevents streptozotocin-induced diabetic nephropathy. *J. Mol. Med.* 94, 207–218. doi: 10.1007/s00109-015-1343-6

Gomez, R. A., Chevalier, R. L., Everett, A. D., Elwood, J. P., Peach, M. J., Lynch, K. R., et al. (1990). Recruitment of renin gene-expressing cells in adult rat kidneys. *Am. J. Physiol.* 259, F660–F665.

He, M., Wang, Q. Y., Yin, Q. Q., Tang, J., Lu, Y., Zhou, C. X., et al. (2013). HIF-1alpha downregulates miR-17/20a directly targeting p21 and STAT3: a role in myeloid leukemic cell differentiation. *Cell Death Differ.* 20, 408–418. doi: 10.1038/cdd.2012.130

He, M., Zhang, L., Shao, Y., Wang, X., Huang, Y., Yao, T., et al. (2009). Inhibition of renin/prorenin receptor attenuated mesangial cell proliferation and reduced associated fibrotic factor release. *Eur. J. Pharmacol.* 606, 155–161. doi: 10.1016/j.ejphar.2008.12.050

He, M., Zhang, L., Shao, Y., Xue, H., Zhou, L., Wang, X. F., et al. (2010). Angiotensin II type 2 receptor mediated angiotensin II and high glucose induced decrease in renal prorenin/renin receptor expression. *Mol. Cell. Endocrinol.* 315, 188–194. doi: 10.1016/j.mce.2009.10.008

Huang, J., Matavelli, L. C., and Siragy, H. M. (2011). Renal (pro)renin receptor contributes to development of diabetic kidney disease through transforming growth factor-beta1-connective tissue growth factor signalling cascade. *Clin. Exp. Pharmacol. Physiol.* 38, 215–221. doi: 10.1111/j.1440-1681.2011.05486.x

Ichihara, A., Hayashi, M., Kaneshiro, Y., Suzuki, F., Nakagawa, T., Tada, Y., et al. (2004). Inhibition of diabetic nephropathy by a decoy peptide corresponding to the "handle" region for nonproteolytic activation of prorenin. *J. Clin. Invest.* 114, 1128–1135. doi: 10.1172/JCI21398

Ichihara, A., Suzuki, F., Nakagawa, T., Kaneshiro, Y., Takemitsu, T., Sakoda, M., et al. (2006). Prorenin receptor blockade inhibits development of glomerulosclerosis in diabetic angiotensin II type 1a receptor-deficient mice. *J. Am. Soc. Nephrol.* 17, 1950–1961. doi: 10.1681/ASN.2006010029

Kaneshiro, Y., Ichihara, A., Sakoda, M., Takemitsu, T., Nabi, A. H., Uddin, M. N., et al. (2007). Slowly progressive, angiotensin II-independent glomerulosclerosis in human (pro)renin receptor-transgenic rats. *J. Am. Soc. Nephrol.* 18, 1789–1795. doi: 10.1681/ASN.2006091062

Konoshita, T., Wakahara, S., Mizuno, S., Motomura, M., Aoyama, C., Makino, Y., et al. (2006). Tissue gene expression of renin-angiotensin system in human type 2 diabetic nephropathy. *Diabetes Care* 29, 848–852. doi: 10.2337/diacare.29.04.06.dc05-1873

Lewis, E. J., Hunsicker, L. G., Bain, R. P., and Rohde, R. D. (1993). The effect of angiotensin-converting-enzyme inhibition on diabetic nephropathy. The collaborative study group. *N. Engl. J. Med.* 329, 1456–1462. doi: 10.1056/NEJM199311113292004

Murali, B., and Goyal, R. K. (2001). Effect of chronic treatment with losartan on streptozotocin induced diabetic nephropathy. *Clin. Exp. Hypertens.* 23, 513–520. doi: 10.1081/CEH-100106822

Nguyen, G., Delarue, F., Burckle, C., Bouzhir, L., Giller, T., and Sraer, J. D. (2002). Pivotal role of the renin/prorenin receptor in angiotensin II production and cellular responses to renin. *J. Clin. Invest.* 109, 1417–1427. doi: 10.1172/JCI0214276

Oshima, Y., Morimoto, S., and Ichihara, A. (2014). Roles of the (pro)renin receptor in the kidney. *World J. Nephrol.* 3, 302–307. doi: 10.5527/wjn.v3.i4.302

Price, D. A., Porter, L. E., Gordon, M., Fisher, N. D., De'Oliveira, J. M., Laffel, L. M., et al. (1999). The paradox of the low-renin state in diabetic nephropathy. *J. Am. Soc. Nephrol.* 10, 2382–2391.

Rahimi, Z. (2016). The role of renin angiotensin aldosterone system genes in diabetic nephropathy. *Can. J. Diabetes* 40, 178–183. doi: 10.1016/j.jcjd.2015.08.016

Reidy, K., Kang, H. M., Hostetter, T., and Susztak, K. (2014). Molecular mechanisms of diabetic kidney disease. *J. Clin. Invest.* 124, 2333–2340. doi: 10.1172/JCI72271

Schefe, J. H., Menk, M., Reinemund, J., Effertz, K., Hobbs, R. M., Pandolfi, P. P., et al. (2006). A novel signal transduction cascade involving direct physical interaction of the renin/prorenin receptor with the transcription factor promyelocytic zinc finger protein. *Circ. Res.* 99, 1355–1366. doi: 10.1161/01.RES.0000251700.00994.0d

Senbonmatsu, T., Saito, T., Landon, E. J., Watanabe, O., Price, E. Jr., Roberts, R. L., et al. (2003). A novel angiotensin II type 2 receptor signaling pathway: possible role in cardiac hypertrophy. *EMBO J.* 22, 6471–6482. doi: 10.1093/emboj/cdg637

Siragy, H. M., and Huang, J. (2008). Renal (pro)renin receptor upregulation in diabetic rats through enhanced angiotensin AT1 receptor and NADPH oxidase activity. *Exp. Physiol.* 93, 709–714. doi: 10.1113/expphysiol.2007.040550

Suzuki, F., Hayakawa, M., Nakagawa, T., Nasir, U. M., Ebihara, A., Iwasawa, A., et al. (2003). Human prorenin has "gate and handle" regions for its non-proteolytic activation. *J. Biol. Chem.* 278, 22217–22222. doi: 10.1074/jbc.M302579200

Tesch, G. H., and Allen, T. J. (2007). Rodent models of streptozotocin-induced diabetic nephropathy. *Nephrology* 12, 261–266. doi: 10.1111/j.1440-1797.2007.00796.x

Zain, M., and Awan, F. R. (2014). Renin Angiotensin Aldosterone System (RAAS): its biology and drug targets for treating diabetic nephropathy. *Pak. J. Pharm. Sci.* 27, 1379–1391.

Zhang, J., Gu, C., Noble, N. A., Border, W. A., and Huang, Y. (2011). Combining angiotensin II blockade and renin receptor inhibition results in enhanced antifibrotic effect in experimental nephritis. *Am. J. Physiol. Renal Physiol.* 301, F723–732. doi: 10.1152/ajprenal.00271.2011

Zhang, L., An, X., Wang, Q., and He, M. (2016). Activation of cold-sensitive channels TRPM8 and TRPA1 inhibits the proliferative airway smooth muscle cell phenotype. *Lung* 194, 595–603. doi: 10.1007/s00408-016-9901-4

Conflict of Interest Statement: The authors declare that the research was conducted in the absence of any commercial or financial relationships that could be construed as a potential conflict of interest.

Advantages of publishing in Frontiers

OPEN ACCESS
Articles are free to read for greatest visibility and readership

FAST PUBLICATION
Around 90 days from submission to decision

HIGH QUALITY PEER-REVIEW
Rigorous, collaborative, and constructive peer-review

TRANSPARENT PEER-REVIEW
Editors and reviewers acknowledged by name on published articles

Frontiers
Avenue du Tribunal-Fédéral 34
1005 Lausanne | Switzerland

Visit us: www.frontiersin.org
Contact us: info@frontiersin.org | +41 21 510 17 00

REPRODUCIBILITY OF RESEARCH
Support open data and methods to enhance research reproducibility

DIGITAL PUBLISHING
Articles designed for optimal readership across devices

FOLLOW US
@frontiersin

IMPACT METRICS
Advanced article metrics track visibility across digital media

EXTENSIVE PROMOTION
Marketing and promotion of impactful research

LOOP RESEARCH NETWORK
Our network increases your article's readership